

WestminsterResearch

<http://www.westminster.ac.uk/research/westminsterresearch>

**Poly(3-Hydroxybutyrate), P(3HB) production and its
biomedical applications**

Everest Chukwuemeka Akaraonye

Faculty of Science and Technology

This is an electronic version of a PhD thesis awarded by the University of Westminster. © The Author, 2011.

This is an exact reproduction of the paper copy held by the University of Westminster library.

The WestminsterResearch online digital archive at the University of Westminster aims to make the research output of the University available to a wider audience. Copyright and Moral Rights remain with the authors and/or copyright owners.

Users are permitted to download and/or print one copy for non-commercial private study or research. Further distribution and any use of material from within this archive for profit-making enterprises or for commercial gain is strictly forbidden.

Whilst further distribution of specific materials from within this archive is forbidden, you may freely distribute the URL of WestminsterResearch:
(<http://westminsterresearch.wmin.ac.uk/>).

In case of abuse or copyright appearing without permission e-mail
repository@westminster.ac.uk

**POLY(3-HYDROXYBUTYRATE), P(3HB)
PRODUCTION AND ITS BIOMEDICAL
APPLICATIONS**

EVEREST CHUKWUEMEKA AKARAONYE

**A THESIS SUBMITTED IN PARTIAL FULFILMENT OF THE
REQUIREMENTS OF THE UNIVERSITY OF WESTMINSTER
FOR THE DEGREE OF DOCTOR OF PHILOSOPHY**

JUNE 2011

AUTHOR'S DECLARATION

I declare that the present work was carried out in accordance with the Guidelines and Regulations of the University of Westminster. The work is original except where indicated by special reference in the text.

The submission as a whole or part is not substantially the same as any that I previously or am currently making, whether in published or unpublished form, for a degree, diploma or similar qualification at any university or similar institution.

Until the outcome of the current application to the University of Westminster is known, the work will not be submitted for any such qualification at another university or similar institution.

Any views expressed in this work are those of the author and in no way represent those of the University of Westminster.

Signed:

Date: 22nd June, 2011

Abstract

In this project enhancement of poly(3-hydroxybutyrate), P(3HB) production using a Gram positive bacteria, *Bacillus cereus* SPV and sucrose as the main carbon source was successfully achieved. Different modes of fermentation including shaken flask, batch, fed-batch and two-stage fermentation were investigated in the study. A modified G-medium was formulated and used throughout the study. Potassium and sulphate were identified as the main limiting factor for P(3HB) accumulation in *Bacillus cereus* SPV. By limiting the potassium phosphate concentration to 0.5 g/L K_2HPO_4 in the production medium, the dry cell weight, P(3HB) yield and P(3HB) concentration improved to, 7.21 g/L, 82 % dcw and 5.95 g/L respectively (i.e. 236, 115.8 and 830 % increase in dry cell weight, P(3HB) yield and P(3HB) concentration respectively). In addition, economic production of P(3HB) using agricultural/industrial waste (molasses) as the main carbon substrate was achieved. The study was also carried out in both shaken flask and 2L fermenter. The maximum P(3HB) yield achieved was 61.07 % dcw in 1L shaken flask and 51.37 % dcw in 2L fermenter.

A novel wet cell PHA extraction was successfully developed in this project leading to high purity of the PHA produced with reduced crystallinity and efficient recovery. This is expected to save time, cost and enhanced continuous PHA production.

Furthermore, a novel inexpensive and sustainable 'compression moulding/particulate leaching' technique for tissue engineering scaffold fabrication was developed. The novel technique enabled the production of biodegradable composite scaffolds of P(3HB)/microfibrillated cellulose and magnetic P(3HB) nanocomposite for possible applications in cartilage and bone tissue engineering, respectively. Detailed studies on the 2D and 3D composites showed that the inclusion of microfibrillated cellulose into the P(3HB) matrix enhanced the mechanical properties, hydrophilicity, introduced microtopography features, enhanced surface chemistry and biocompatibility of the composite material while inclusion of magnetic nanoparticles and ferrofluid, in addition to the above features added magnetic properties and microhardness to the composite materials.

A unique controlled drug delivery system was developed with potential application in multiple drug delivery. The release study confirmed that the delivery system was able to control the release of BSA, a model protein.

Finally, composite magnetic microspheres were also produced and characterised for their efficient use in the delivery of cancer drug and analyses performed showed that the composite constructs have superparamagnetic properties which would be useful for targeted delivery.

Acknowledgements

First and foremost, I would like to thank God Almighty for His great Love, Intercession, Knowledge and Wisdom, without which the completion of this programme would not have been possible.

I wholeheartedly thank my director of study, Dr. Ipsita Roy, for her constant guidance, support, patience and encouragements, throughout my research. Her sincere and conscientious approach really inspired me to put in my possible best. I would like to extend my sincere regards to my second supervisor Prof. Taj Keshavarz, for his unalloyed support, guidance and encouragement. It is a great joy to have met such wonderful supervisors that gave me the opportunity to succeed in my academic pursuit.

I would like to thank my parents, Mr & Mrs Augustine Akaraonye for their wonderful inspirations, support and more especially for given me every opportunity I needed in life to be who I am today. I wouldn't have desired to have another parent other than them. May God continue to bless them and their efforts.

It is my pleasure to thank my fiancée, Miss Chinwe for her patience, encouragement and support throughout my period of study. Her understanding has been a great help.

My heartfelt gratitude goes to all the staffs and students of University of Westminster who have contributed in one way or the other to make my study a successful one.

I am highly indebted to the staffs of the Eastman Dental, University College London, more especially Prof. Jonathan Knowles for given me the opportunity to use the facilities in his lab for the characterisation of my samples. I remained indebted to Dr. Valid Salih, who supervised my cell biology study. I also remain grateful to the help of the following; Dr. Nicky Morgan, George, Muhammed and Graham, for their wonderful assistance in the material science aspects of my research. I sincerely, thank Dr. Mirka Safarikova for her help and provision of the magnetic materials I used in my study. I equally remain indebted to the staff of the Centre for Nanotechnology, Cheq Republic especially Dr. Jan Filip for assisting me in the characterisation of some of my samples.

Lastly but never the Least, I thank the University of Westminster and the Cavendish scholarship Committee for providing me the opportunity and means to have made all of this possible and help me actualize my dream.

List of abbreviations

2D	two dimensional
3D	three dimensional
3HB	3-hydroxybutyrate
3HV	3-hydroxyvalerate
%WA	water uptake/ water absorption
ΔH_f	heat of fusion
ALP	alkaline phosphatase
ATDC	Murine ATDC-5 cell line
CA	contact angle study
Ca	calcium
cm	centimetre
dcw	dry cell weight
DMA	dynamic mechanical analysis
DMAPAAmMel	rose bengal
DMEM	dulbecco's modified Eagle's medium
DSC	differential scanning calorimetry
E'	storage modulus
E	Young's modulus
E''	loss modulus
ECM	extracellular matrix
EDX	energy dispersive X-ray
emu	magnetic moment per unit mass
FBS	foetal bovine serum
FTIR	fourier transform infrared
G	10^9 (giga)
g	grams
h	hours
HA	hydroxyapatite
K	kelvin

L	litre
L-PLCL	poly(L-lactide-co-caprolactone)
LPS	lipopolysaccharides
M	10^6 (mega)
Mag-TE	emerging tissue engineering
mcl-PHA	medium chain length polyhydroxyalkanoate
MCLs	magnetic atomic liposomes
MFC	microfibrillated
min	minutes
mL	millilitre
mm	milimolar
mm	millimetre
MM	molecular weight
mol%	mole percent
n	10^{-9} (nano)
Na	sodium
NMR	nuclear magnetic resonance
°C	degree centigrade
O _e	Oerste
P	phosphorus
P(3HB)	poly(3-hydroxybutyrate)
P(3HB-co-3HHx)	poly(3-hydroxybutyrate-co-3-hydroxyhexanoate)
P(3HB-co-3HO)	poly(3-hydroxybutyrate-co-3-hydroxyoctanoate)
P(3HB-co-3HV)	poly(3-hydroxybutyrate-co-3-hydroxyvalerate)
P(3HB-co-4HB)	poly(3-hydroxybutyrate-co-4-hydroxybutyrate)
P(3HO-co-3HHx)	poly(3-hydroxyoctanoate-co-3-hydroxyhexanoate)
P(4HB)	poly(4-hydroxybutyrate)
Pa	pascal
PAANG	toluidine blue
PBS	phosphate buffer saline
PCL	poly(ϵ -caprolactone)
PDCHI	poly(dicyclohexaxylitaconate)

PDI	polydispersity index
PDLL	poly(DL-lactic acid)
PEG	polyethylene glycol
PGA	poly(glycolic acid)
PGTMC	poly(glycolide-co-trimethylene carbonate)
PHA	polyhydroxyalkanoates
PLA	poly(lactic acid)
ppm	parts per million
PTFE	polytetrafluorothylene
PVA	poly(vinyl alcohol)
RCM	residual cell mass
RMS	root mean square
rpm	revolutions per minute
SBF	simulated body fluid
scl-mcl-PHA	short chain length-medium chain length polyhydroxyalkanoate
scl-PHA	short chain length polyhydroxyalkanoate
SD	standard deviation
SEM	scanning electron microscope
SQUID	superconducting quantum interference device
T	Tesla
Tan δ	mechanical loss tangent
T _c	crystallisation temperature
TCP	tissue culture plastic
TE	tissue engineering
TEM	transmission electron microscope
T _g	glass transition temperature
T _m	melting temperature
TS	tensile strength
UTS	ultimate tensile strength
vol%	volume percent
wt%	weight percent
X _c	degree of crystallinity

XRD	x-ray diffraction
δ	delta
ϵ	epsilon
μ	10^{-6} (micro)
ρ	density
σ	sigma

Table of Contents

Abstract	I
Acknowledgement	II
List of abbreviations	III
List of contents	VII
List of tables	XX
List of figures	XXII

CHAPTER 1:- INTRODUCTION

1	Introduction	2
1.1	Biodegradable polymers	3
1.1.1	Polyhydroxyalkanoates, PHAs	4
1.1.1.1	PHAs and their structure	5
1.1.1.2	Types of PHAs and their physical properties	6
1.1.1.3	Biosynthesis and catabolism of intracellular PHA	10
1.1.1.4	Biodegradability and biocompatibility of PHAs	14
1.1.1.5	PHA production in specific bacteria	15
1.1.1.5.1	PHA production using wild type bacteria	15
1.1.1.5.2	PHA production using recombinant bacteria	20
1.1.1.5.3	PHA production using mixed or co-culture systems	21
1.1.1.6	Sustainable PHA production using inexpensive carbon sources	23
1.1.1.6.1	Use of whey as a cheap carbon source for PHA production	23
1.1.1.6.2	Use of wheat bran as cheap carbon sources for PHA production	24

1.1.1.6.3 Use of Rice bran as carbon source for PHA production	25
1.1.1.6.4 Use of starch as cheap carbon sources for PHA production	25
1.1.1.6.5 Use of molasses as cheap carbon sources for PHA production	26
1.1.1.6.6 The use of waste vegetable oil and plant oil as cheap carbon sources For PHA production	28
1.1.1.6.7 Use of wastewater as cheap material for PHA production	29
1.1.1.6.8 Use of CO ₂ and H ₂ as cheap carbon substrates for PHA production	30
1.1.1.6.9 Use of methanol as cheap substrate for PHA production	30
1.1.1.7 Production of PHAs in bioreactors	31
1.1.1.7.1 Batch fermentation	31
1.1.1.7.2 Fed-batch cultivation	32
1.1.1.7.3 Continuous cultivation	34
1.1.1.8 Uses of PHAs	35
1.1.2 Cellulose	39
1.2 Tissue Engineering	41
1.2.1 Bone tissue Regeneration	42
1.2.2 Cartilage tissue Regeneration	44
1.2.3 Scaffolds in Tissue Engineering of Bone and Cartilages	46
1.2.4 Biodegradable-polymer-based materials for tissue engineering scaffolds	49
1.3 Drug delivery	52
1.3.1 Polymeric P(3HB)-based material: A potential microparticulate delivery system for controlled release	53
1.3.2 P(3HB): A potential carrier for a multi-component delivery system	55
1.4 Objective of the thesis	56

CHAPTER 2:- MATERIALS AND METHODS

2.1	P(3HB) production, extraction and characterization	61
2.1.1	Materials	61
2.1.1.1	Medium composition (Kannan and Rehacek medium, (gL ⁻¹))	61
2.1.1.2	Medium composition (modified G-Medium, (gL ⁻¹))	61
2.1.1.3	Bacterial strain and maintenance	62
2.1.1.4	Seed culture preparation in nutrient broth	62
2.1.1.5	Seed culture preparation in modified G-medium	62
2.1.1.6	Kannan and Rehacek production medium preparation	63
2.1.2.1	P(3HB) production in shaken flasks	63
2.1.2.2	P(3HB) production in a fermenter (Batch production)	63
2.1.2.3	P(3HB) production in a fermenter (Fed-batch production)	64
2.1.2.4	P(3HB) production in a fermenter (Two-stage fermentation)	64
2.1.3	P(3HB) extraction	64
2.1.3.1	Dispersion method of P(3HB) extraction	65
2.1.3.2	Soxhlet extraction	65
2.1.3.3	Wet cell extraction	65
2.1.4	Quantification Analysis	66
2.1.4.1	Dry cell weight measurement	66
2.1.4.2	P(3HB) quantification	66
2.1.4.3	Gas chromatography-mass spectrometry (GC-MS)	66
2.1.4.4	Fourier transform-infrared spectroscopy (FT-IR)	67
2.1.4.5	X-ray diffraction (XRD)	67
2.1.4.6	Differential Scanning Calorimetry (DSC)	67

2.2.	Cellulose production	68
2.2.1	Materials	68
2.2.1.1	Medium composition (gL^{-1})	68
2.2.1.2	Bacterial strain and maintenance	68
2.2.2	Cellulose production in flasks	68
2.2.3	Cellulose extraction	69
2.2.4	Microfibrilated bacteria cellulose (MFC) production	69
2.2.5	Chemical modification of MFC	69
2.2.6	Determination of degree of acetylation	70
2.2.7	Quantification and Analysis	70
2.2.7.1	Cellulose dry weight measurement	70
2.2.7.2	Total viable counts	70
2.2.8	Characterization of modified microfibrilated cellulose	71
2.2.8.1	Infrared Spectroscopy (FTIR)	71
2.2.8.2	X-ray Diffraction Analysis	71
2.2.8.3	Scanning Electron Microscopy (SEM)	72
2.2.8.4	Dispersion Tests	72
2.3	P(3HB) composite preparation	73
2.3.1	P(3HB)/MFC nanocomposite film preparation	73
2.3.2	Preparation of composite scaffolds	73
2.3.3	Preparation of P(3HB)/MFC scaffold	73
2.3.4	Preparation of P(3HB)/Magnetic particles, and P(3HB)/Magnetic fluid composite scaffold	74
2. 4	P(3HB) composite characterization	75

2.4.1	Characterisation of P(3HB)/MFC films	75
2.4.1.1	Dynamic Mechanical Analysis (DMA)	75
2.4.1.2	Differential Scanning Calorimetry (DSC)	75
2.4.1.3	Contact angle study	76
2.4.1.4	Determination of surface charge	77
2.4.2	Characterization of P(3HB) Composite 3D scaffolds	77
2.4.2.1	Scanning electron microscopy (SEM)	77
2.4.2.2	Compression modulus measurement	77
2.4.2.3	Porosity measurements on the scaffolds	78
2.4.2.4	<i>In vitro</i> degradation study	78
2.4.2.5	SQUID Analysis	79
2.4.2.6	Protein adsorption study	79
2.4.2.7	Raman spectroscopy	80
2.5	<i>In vitro</i> biocompatibility study	81
2.5.1	Cell culture studies	81
2.5.2	Culturing and cyro-preservation of cell lines	82
2.5.3	Sample preparation	83
2.5.3.1	Sterilization of P(3HB)/MFC film samples	83
2.5.3.2	Sterilization of composite scaffold samples (P(3HB)/MFC; P(3HB)/Magnetic particles and P(3HB)/Magnetic fluid	83
2.5.4	Seeding of cells on P(3HB) composites	84
2.5.4.1	Cell seeding on P(3HB)/MFC film substrates	84
2.5.4.2	Seeding of ATDC cell lines on the P(3HB)/MFC composite scaffold samples	84
2.5.4.3	Seeding of MG-63 on the composite scaffold samples (P(3HB)/Magnetic	

particles, P(3HB)/Magnetic fluid	85
2.5.5 Cell proliferation assay	85
2.5.5.1 Alamar Blue assay of ATDC cell culture studies	85
2.5.5.2 Measurement of total protein production	86
2.5.6 Microstructural Analysis	86
2.5.6.1 Fixing of materials for SEM examinations	86
2.5.6.2 Scanning electron microscopy (SEM)	87
2.6 Drug delivery system	87
2.6.1 Preparation of particulate carriers	87
2.6.1.1 Preparation of magnetic microspheres containing drug	87
2.6.1.2 Preparation of microspheres containing encapsulated nanospheres	88
2.6.1.3 Preparation of microspheric scaffolds	90
2.6.2 Analysis and Assay	91
2.6.2.1 Determination of residual PVA content	91
2.6.3 Characterisation of microspheres	91
2.6.3.1 Particle size analysis using Dynamic Light scattering, DLS	91
2.6.3.2 Surface morphology and microstructure characterization using SEM	91
2.6.3.3 Determination of hydrophobicity of microspheres	92
2.6.3.4 In vitro BSA release from multipurpose microsphere	92
2.6.3.5 In vitro degradation of microsphere	93

CHAPTER 3:- ENHANCED AND ECONOMIC PRODUCTION OF PHAs

3.1.1 Introduction	95
--------------------	----

SECTION I: - P(3HB) production in *Bacillus cereus* SPV using Kannan and Rehacek medium and sucrose as carbon source

3.1.2	Results	97
3.1.2.1	P(3HB) production at the shaken flask level, using sucrose as the main carbon source in Kannan and Rehacek medium	97
3.1.2.2	P(3HB) production at 2L fermenter level, using sucrose as the main carbon source in Kannan and Rehacek medium	98
3.1.2.3	Comparison of dry cell weight, PHA concentration and PHA yield in shaken flask and 2L fermenter level	99
SECTION II: - Production of Poly(3-hydroxyalkanoate), P(3HB) by <i>Bacillus cereus</i> SPV using Modified G-medium and sucrose as the main Carbon Source		
3.2.1	Results	101
3.2.1.1	P(3HB) production by <i>Bacillus cereus</i> SPV using modified G-medium (MGM) supplemented with sucrose as the main carbon source in shaken flask	101
3.2.1.2	P(3HB) production by <i>Bacillus cereus</i> SPV using modified G-medium (MGM) supplemented with sucrose as the main carbon source in a 2L fermenter	102
3.2.1.3	Effect of increasing initial K_2HPO_4/KH_2PO_4 concentration in production medium on biomass and PHA accumulation by <i>Bacillus cereus</i> SPV	104
3.2.1.4	Effect of replacement of potassium phosphate buffer with 1.0 g/L KH_2PO_4 in MGM on biomass and P(3HB) accumulation by <i>Bacillus cereus</i> SPV	106
3.2.1.5	Effect of replacement of potassium phosphate buffer with 0.5 g/L KH_2PO_4 in MGM on biomass and P(3HB) accumulation by <i>Bacillus cereus</i> SPV	107
3.2.1.6	Effect of increasing yeast extract concentration in the MGM medium supplemented with sucrose as the main carbon source on <i>Bacillus cereus</i> SPV biomass and PHA accumulation	108
3.2.1.7	Effect of intermittent addition of sucrose solution to the growing	

<i>B. cereus</i> SPV culture in MGM production medium in a 2L fermenter	109
3.2.1.8 Production of P(3HB) by <i>Bacillus cereus</i> SPV using continuous feeding of sucrose as the main carbon source in modified G-medium in a 2L fermenter	111
3.2.1.8.1 Effect of replacement of potassium phosphate buffer in the production medium with 1.0 g/L KH_2PO_4 on the production of P(3HB) by <i>Bacillus cereus</i> SPV using a continuous feeding of sucrose as the main carbon source in a 5L fermenter	112
3.2.1.8.2 Effect of replacement of potassium phosphate buffer in the production medium with 0.5 g/L KH_2PO_4 on the production of P(3HB) by <i>Bacillus cereus</i> SPV using continuous feeding of sucrose in a 5L fermenter	113
3.2.1.9 Production of P(3HB) by <i>Bacillus cereus</i> SPV using Two-stage fermentation in 5L Fermenter	115
3.2.2 Development of a novel wet cell extraction to facilitate continuous PHA production	118
3.2.3 Characterisation of P(3HB)	119
3.2.3.1 Gas chromatography-Mass spectrometry	119
3.2.3.2 Nuclear Magnetic Resonance, NMR	121
3.2.3.3 Fourier Transfer – Infra Red (FTIR) Analysis	123
3.2.3.4 Differential Scanning Calorimetry, DSC Analysis	124
SECTION III:- Bioconversion of agricultural raw materials and waste (sugarcane molasses) into the highly valued-green material, P(3HB) by <i>Bacillus cereus</i> SPV	
3.3.1 Introduction	125
3.3.2 Results	126
3.3.2.1 Poly(3-hydroxybutyrate) production by <i>Bacillus cereus</i> SPV	

using sugarcane molasses as the main carbon source in a shaken flask	126
3.3.2.2 Poly(3-hydroxybutyrate) production by <i>Bacillus cereus</i> SPV using sugarcane molasses as the main carbon source in a 2L fermenter	127
3.3.2.3 Effect of reduced (NH ₄) ₂ PO ₄ concentration on biomass and P(3HB) accumulation by <i>Bacillus cereus</i> SPV, using sugarcane molasses as the main carbon source	128
3.3.2.4 Effect of continuous feeding of sugarcane molasses on biomass and P(3HB) accumulation by <i>Bacillus cereus</i> SPV	130
3.3.3 Characterization of the isolated PHAs	133
3.4 Discussion	135
3.5 Conclusions	143

CHAPTER 4:- BACTERIAL CELLULOSE PRODUCTION AND MODIFICATIONS

4.1 Introduction	145
4.2 Results	147
4.2.1 Production of bacterial cellulose from <i>Acetobacter xylinus</i>	148
4.2.2 Determination of the degree of acetylation	149
4.3 Characterisation of bacterial cellulose	150
4.3.1 Fourier Transform Infrared Spectroscopy (FTIR)	150
4.3.2 X-ray diffractometry	151
4.3.3 Dispersion of acetylated bacterial cellulose in chloroform	153
4.7 Discussion	154
4.8 Conclusion	156

CHAPTER 5:- POTENTIAL APPLICATION OF P(3HB)/MFC IN CARTILAGE REGENERATION

5.1 Introduction	159
------------------	-----

5.2	Results	160
5.2.1	Microstructural characterisation of P(3HB)/MFC composite film	161
5.2.2	Fourier Transfer-Infra Red (FT-IR) characterisation of P(3HB)/MFC composite	162
5.2.3	X-ray Diffraction Spectroscopy of P(3HB)/MFC composite	163
5.2.4	Thermal characterisation of P(3HB)/MFC composite	164
5.2.5	Dynamic mechanical analysis of P(3HB)/MFC composite films	166
5.2.6	Surface chemistry confirmation of P(3HB)/MFC composite film	168
5.2.7	Aqueous contact angle measurement	169
5.2.8	Water absorption test on neat P(3HB) and P(3HB)/MFC composite films	170
5.2.9	Weight loss of P(3HB)/MFC composite film during degradation studies in SBF	171
5.2.10	Total protein absorption analysis on the neat P(3HB) and P(3HB)/MFC composite films (2D structures)	172
5.3	Characterisation of the P(3HB)/MFC composite 3D scaffolds	173
5.3.1	Microstructural characterisation of P(3HB)/MFC composite 3D scaffolds	175
5.3.2	Compression testing	175
5.3.3	Protein absorption assay on P(3HB)/MFC composite 3D scaffold	177
5.4	Biodegradation	178
5.4.1	Weight loss measurement on P(3HB)/MFC composite 3D scaffold	179
5.4.2	Change in pH of the immersed SBF of the neat P(3HB) and (3HB)/MFC composite scaffolds	180
5.4.3	Raman Shift Spectroscopy	181
5.4.4	X-ray diffraction (XRD) analysis	182
5.4.5	Differential Scanning Calorimetry (DSC) analysis	183
5.5	Cytocompatibility study of P(3HB)/MFC composite materials using	

ATDC cell lines	185
5.5.1 Cell proliferation on P(3HB)/MFC composite material	185
5.5.2 Cell morphology	186
5.5.3 Total protein production by ATDC cells grown on P(3HB)/MFC composite	191
5.6 Discussion	192
5.7 Conclusion	202
 CHAPTER 6:- POTENTIAL APPLICATION OF P(3HB)/MNP AND P(3HB)/FF IN BONE REGENERATION	
6.1 Introduction	205
6.2 Results	206
6.2.1 Microstructural analysis of P(3HB)/MNP and P(3HB)/FF scaffolds	206
6.2.2 Morphology and structure of magnetic materials in the composite scaffolds	207
6.2.3 Magnetic properties of P(3HB)/MNP and P(3HB)/FF composite material	208
6.2.4 Mechanical and thermo-mechanical properties of P(3HB)/MNP and P(3HB)/FF composite	210
6.2.5 Fourier Transfer-Infra red, FT-IR Analysis	215
6.2.6 Hydrophilicity measurement on the composite materials	217
6.2.7 Total protein absorption on the P(3HB)/MNP and P(3HB)/FF composite films	217
6.3 Production of porous magnetic polymeric composite 3D scaffold for tissue engineering	218
6.3.1 Microstructure analysis of magnetic 3D composite scaffolds	218
6.3.2 Compressive mechanical test	219
6.4 <i>In vitro</i> degradation studies	221
6.4.1 Weight loss of the magnetic composite and pH change of the SBF solution	221

6.4.2	X-ray Diffraction, XRD analysis of P(3HB)/Magnetic nanoparticles immersed in SBF for 21 days	223
6.4.3	Raman Shift analysis of the degraded composite specimen	225
6.4.4	Thermal properties of the degrading composite	226
6.5	Cytocompatibility study of P(3HB)/MNP and P(3HB)/FF 2D and 3D composite structure using human osteosarcoma MG-63 cell line	230
6.5.1	Cell proliferation study	231
6.5.2	Whole protein production by human osteosarcoma MG-63 cell lines on the P(3HB)/MNP and P(3HB)/FF composites	233
6.5.3	Cell Morphology	234
6.6	Discussion	237
6.7	Conclusion	247

CHAPTER 7:- POTENTIAL APPLICATION OF P(3HB) IN DRUG DELIVERY SYSTEM

7.1	Introduction	251
-----	--------------	-----

SECTION I: - Potential application of P(3HB)/cellulose composites in multiple drug delivery system (encapsulation of cellulose nanospheres in P(3HB) microspheres)

7.1.2	Results	253
7.1.2.1	SEM examination	253
7.1.2.2	Particle size measurements using Dynamic Light Scattering, DLS	255
7.1.2.3	Surface chemistry measurement	256
7.1.2.4	Influence of organic solvent on the residual PVA on the microsphere surface	257
7.1.2.5	Influence of PVA concentration in the oil in water emulsion on the	

residual PVA associated with P(3HB) microspheres	257
7.1.2.6 <i>In vitro</i> BSA release analysis	258
7.1.2.7 <i>In-vitro</i> degradation studies	260
SECTION II: - Potential Application of P(3HB) in targeted drug delivery system	
7.2 Results	261
7.2.1 SEM characterisation of the morphology of P(3HB)/FF and P(3HB)/MNP	261
7.2.2 Effects of addition of different amounts of magnetic material on the shape and properties of microspheres produced	262
7.2.3 TEM characterisation of the internal structure of P(3HB)/FF and P(3HB)/MNP composite microspheres	263
7.2.4 Characterisation of the magnetic properties of P(3HB)/FF and P(3HB)/MNP composite microspheres	265
7.3 Discussion	267
7.4 Conclusion	273
CHAPTER 8:- CONCLUSIONS AND FUTURE WORK	
8.1 Conclusions	276
8.2 Future work	280
8.2.1 P(3HB) production	280
8.2.2 P(3HB)/MFC characterisation	280
8.2.3 P(3HB)/MNP and P(3HB)/FF	280
8.2.4 Biocompatibility study	281
8.2.5 Drug release kinetics	281
REFERENCES	283
PUBLICATIONS	316

List of Tables

- Table 1.1** Comparison of the physical properties of specific PHAs and two commonly used synthetic polymers
- Table 1.2** Comparison of the physical properties of scl-PHAs and mcl-PHAs with polypropylene,
- Table 1.3** Properties and features of Poly(3-hydroxybutyrate), P(3HB)
- Table 1.4** The accumulation of PHAs in *Bacillus spp.*
- Table 1.5** Comparison of PHA production in recombinant *E. coli*
- Table 1.6** PHA production in fed-batch cultivation reported for wild strain
- Table 1.7** Potential medical applications of P(3HB) and its copolymers in medicine.
- Table 2.1** Summary of analysis carried out on specific experiments.
- Table 3.1** Summary of the fermentation studies on the use of MGM medium and sucrose as the main carbon source for P(3HB) production in *Bacillus cereus* SPV.
- Table 3.2** Summary of the fermentation studies on the use of sugarcane molasses as a cheap carbon source for P(3HB) production in *Bacillus cereus* SPV
- Table 4.1** Comparison of the degree of acetylation of microfibrillated bacterial cellulose treated at different time points (0, 24, 48, 72 and 96) hours with acetyl anhydride and pyridine as a catalyst.
- Table 4.2** The crystallinity of native bacteria cellulose compared with the crystallinity of homogenised bacterial cellulose and acetylated bacteria cellulose.
- Table 5.1** Comparison of thermal properties for P(3HB)/MFC containing different amount of MFC per wt%
- Table 5.2** Comparison of mechanical properties of fabricated P(3HB)/MFC film with the mechanical properties of some skeletal tissue.
- Table 5.3** Summary of Dynamic Mechanical Analysis (DMA) carried out on the neat P(3HB) and P(3HB)/MFC composites

Table 5.4	Effect of degradation and bioactivity on the thermal properties of P(3HB)/MFC composite scaffold immersed in SBF for different time points
Table 5.5	Surface chemistries of the neat P(3HB) and P(3HB)/MFC composite
Table 6.1	Parameters of the hysteresis loops of neat P(3HB) and composite specimen containing different amount of MNP samples measured at a temperature of 300 K
Table 6.2	Mean and standard deviation of storage modulus (E'), and loss modulus (E'') for neat P(3HB), P(3HB)/MNP and P(3HB)/FF composite at different temperature
Table 6.3	Thermal properties for P(3HB)/Magnetic material composite containing different amount of Magnetic materials (Particles or fluid)
Table 6.4	Summary of Dynamic Mechanical Analysis (DMA) carried out on the neat P(3HB), P(3HB)/MNP and P(3HB)/FF composites
Table 6.5	Comparison of thermal properties (Melting temperature, T_m) for Magnetic polymeric composite scaffolds immersed in SBF for 30 days..
Table 6.6	Comparison of thermal properties (Crystallisation temperature, T_c) for P(3HB)/MNP and P(3HB)/FF composite scaffold immersed in SBF for 30 days.
Table 7.1	Parameters of the hysteresis loops of samples neat P(3HB) microsphere, P(3HB)/Magnetic particles composite microspheres containing 0.5, 1.0, and 1.5 mL magnetic particles suspension measured at a temperature of 300 K.

List of Figures

- Figure 1.1** Schematic representations of (A) Life cycle of production and degradation of biodegradable polymers from renewable sources and (B) Classification of Biodegradable polymers.
- Figure 1.2** The general structure of polyhydroxyalkanoates.
- Figure 1.3** SEM images of synthesized and intracellularly accumulated discrete granules of P(3HB) in bacteria.
- Figure 1.4** Chemical structures of PHAs currently under investigation for exploration in medicine and pharmacy.
- Figure 1.5** Diagram showing the metabolic pathways involved in the synthesis and degradation of Poly(3-hydroxybutrate) in *Ralstonia eutropha*
- Figure 1.6** Models of PHA granule formation.
- Figure 1.7** Classification of continuous processes based on the flow pattern
- Figure 1.8** Structure of Cellulose.
- Figure 1.9** schematic representations of processes of tissue engineering.
- Figure 1.10** Schematic representation of different mechanisms of drug release from a magnetic microspheres drug delivery system.
- Figure 1.11** Model for a multicomponent delivery system.
- Figure 1.12** Schematic representation of Experimental design
- Figure 2.1** Schematic representation of preparation of drug containing magnetic microspheres
- Figure 2.2** (a) Set up for goniometric measurement of contact angle of the P(3HB) composite materials, (b) an illustration of the sessile drop technique with a liquid droplet partially wetting a solid substrate (2D P(3HB) composite materials).
- Figure 2.2** Schematic representations of processes of preparation of microsphere containing nanospheres.

- Figure 3.1** A temporal profile of DCW (g/L), P(3HB) yield (% dcw), P(3HB) concentration (g/L) and RCM (g/L) produced by *Bacillus cereus* SPV in Kannan and Rehacek medium containing sucrose as the main carbon source in shaken flask cultivation.
- Figure 3.2** A temporal profile of DCW (g/L), P(3HB) yield (% dcw), P(3HB) concentration (g/L) and RCM (g/L) produced by *Bacillus cereus* SPV when sucrose was employed as the sole carbon source in batch fermentation using a 2L fermenter.
- Figure 3.3** Comparison of DCW (g/L), P(3HB) (g/L), and P(3HB) yield (% dcw), accumulated by *Bacillus cereus* SPV using sucrose as the main carbon source at shaken flask (1L) and fermenter (2L) levels.
- Figure 3.4** Temporal profile for DCW (g/L), P(3HB) yield (% dcw), P(3HB) concentration (g/L) and RCM (g/L) produced by *Bacillus cereus* SPV in MGM medium supplemented with sucrose in shake flask.
- Figure 3.5** Temporal profile for DCW (g/L), P(3HB) yield (% dcw), P(3HB) concentration (g/L) and RCM (g/L) produced by *Bacillus cereus* SPV in MGM medium supplemented with sucrose in 2 L fermenter.
- Figure 3.6** Temporal variation of DCW (g/L), P(3HB) yield, P(3HB) concentration (g/L) produced by *Bacillus cereus* SPV using MGM and sucrose as the main carbon source in a 2L fermenter and shake flask.
- Figure 3.7** A temporal profile of growth of *Bacillus cereus* SPV in MGM medium buffered with 0.25M K_2HPO_4/KH_2PO_4 and supplemented with sucrose in 2 L fermenter and recording of DCW, P(3HB) yield (% dcw), P(3HB) concentration and RCM (g/L) accumulated.
- Figure 3.8** Comparison of DCW (g/L), P(3HB) yield and P(3HB) concentration (g/L) achieved with initial 0.1M KH_2PO_4/KH_2PO_4 and 0.25M KH_2PO_4/KH_2PO_4 buffer present in the production medium.
- Figure 3.9** A temporal profile of DCW (g/L), P(3HB) yield (% dcw), P(3HB) concentration (g/L) and RCM (g/L) produced by *Bacillus cereus* SPV when

potassium phosphate buffer was replaced with 1.0 g/L of KH_2PO_4 in MGM medium in 5L fermenter.

Figure 3.10 A temporal profile of DCW, P(3HB) yield, P(3HB) concentration (g/L) and RCM (g/L) produced by *Bacillus cereus* SPV when potassium phosphate buffer was replaced with 0.5g/L of KH_2PO_4 in MGM medium in 5L fermenter.

Figure 3.11 Comparison of DCW (g/L), P(3HB) yield (% dcw), P(3HB) concentration (g/L) produced by *Bacillus cereus* SPV during batch fermentation with MGM media containing initial 1.0 g/L KH_2PO_4 and 0.5 KH_2PO_4 in a 5L fermenter.

Figure 3.12 A temporal profile of DCW (g/L), P(3HB) yield (% dcw), P(3HB) concentration (g/L) and RCM (g/L) produced by *Bacillus cereus* in a 2L Fermenter with an increased yeast extract concentration (4.5 g/L) in the production medium.

Figure 3.13 Temporal profile of DCW (g/L), P(3HB) yield, P(3HB) concentration (g/L) and RCM (g/L) produced by *Bacillus cereus* SPV during intermittent addition of sucrose in a 2L batch cultivation.

Figure 3.14 Temporal profile of DCW (g/L), P(3HB) yield, P(3HB) concentration (g/L) and RCM (g/L) produced by *Bacillus cereus* SPV during a continuous feeding of sucrose rich nutrient in a 2L fermenter containing MGM supplemented with 1.0 g/L KH_2PO_4 .

Figure 3.15 Temporal profile of DCW (g/L), P(3HB) yield, P(3HB) concentration (g/L) and RCM (g/L) produced by *Bacillus cereus* SPV during a continuous feeding of sucrose rich nutrient in 2L fermenter containing MGM supplemented with 0.5 g/L KH_2PO_4 .

Figure 3.16 Temporal variation of DCW (g/L), P(3HB) yield, P(3HB) concentration (g/L) produced by *Bacillus cereus* SPV during fed-batch fermentation with MGM media containing initial 1.0 g/L KH_2PO_4 and 0.5 KH_2PO_4 a 2L fermenter.

Figure 3.17 Temporal profile of DCW (g/L), P(3HB) yield, P(3HB) concentration and RCM (g/L) produced by *Bacillus cereus* SPV in a two- stage fermentation process in a 2L fermenter.

- Figure 3.18** Graph showing the amount of P(3HB), residual cell mass and percentage recovery achieved during a wet cell polymer isolation from *B. cereus* SPV.
- Figure 3.19** (a)The total ion chromatogram of the methanolysis products of the polymer isolated from *Bacillus cereus* SPV grown in MGM medium supplemented with sucrose as the main carbon substrate, (b) Mass spectra of the methyl ester of 3-hydroxybutyrate.
- Figure 3.20** (a) ^{13}C NMR spectrum of P(3HB), (b) ^1H NMR spectrum of isolated P(3HB) from *Bacillus cereus* SPV grown in MGM medium supplemented with sucrose as the main carbon source.
- Figure 3.21** FT-IR spectrum of P(3HB) isolated from *B. cereus* SPV grown in MGM medium supplemented with sucrose and P(3HB) from Sigma-Aldrich.
- Figure 3.22** DSC thermograms of P(3HB) accumulated by *B. cereus* SPV in MGM medium supplemented with sucrose and commercial P(3HB) purchased from Sigma-Aldrich.
- Figure 3.23** The temporal variation of DCW (g/L), P(3HB) yield, P(3HB) concentration (g/L) and RCM (g/L) produced by *Bacillus cereus* SPV in MGM medium supplemented with sugarcane molasses as the main carbon source in shaken flask culture.
- Figure 3.24** The temporal variation of DCW (g/L), P(3HB) yield, P(3HB) concentration (g/L) and RCM (g/L) produced by *Bacillus cereus* SPV using sugarcane molasses as the sole carbon source in batch fermentation using 2L fermenter.
- Figure 3.25** The temporal variation of DCW (g/L), P(3HB) yield, P(3HB) concentration (g/L) and RCM (g/L) produced by *Bacillus cereus* SPV in shaken flasks supplemented with sugarcane molasses as the main carbon source in MGM medium containing 1.0 g/L $(\text{NH}_4)_2\text{PO}_4$.
- Figure 3.26** The temporal variation of DCW (g/L), P(3HB) yield, P(3HB) concentration (g/L) and RCM (g/L) produced by *Bacillus cereus* SPV in a 2L fermenter with reduced $(\text{NH}_4)_2\text{PO}_4$.

- Figure 3.27** The temporal variation of DCW (g/L), P(3HB) yield, P(3HB) concentration (g/L) and RCM (g/L) produced by *Bacillus cereus* SPV during a continuous feeding of sugarcane molasses solution in 1L shaken flask cultures.
- Figure 3.28** The temporal variation of DCW (g/L), P(3HB) Yield (% dcw), P(3HB) concentration (g/L) and RCM g/L produced by *Bacillus cereus* SPV during a continuous feeding of sugarcane molasses solution in a 2L fermenter.
- Figure 3.29** ¹H-NMR spectrum of P(3HB) isolated from *Bacillus cereus* SPV, when sugarcane molasses was used as the main carbon source.
- Figure 3.30** FT-IR spectrum of (a) P(3HB) produced using *B. cereus* SPV grown in modified MGM media supplemented with sugarcane molasses and (b) Standard P(3HB) from Sigma-Aldrich.
- Figure 3.31** Comparison of DSC thermograms of P(3HB) accumulated by *B. cereus* SPV using sugar cane molasses and commercial P(3HB) purchased from Sigma-Aldrich.
- Figure 4.1** Flow chart for the production; chemical modification and characterisation of microfibrillated bacterial cellulose from *Acetobacter xylinus*.
- Figure 4.2** (A) Cell growth CFU mL⁻¹, pH, and bacterial cellulose yield of native and NaOH treated bacteria cellulose over different experimental time periods (B) SEM image of cellulose pellicle highlighting the mass of fibres.
- Figure 4.3** Chemical reaction of acetic anhydride with bacterial cellulose.
- Figure 4.4** FTIR spectra of Bacterial Cellulose with different levels of acetylation.
- Figure 4.5** XRD patterns of native bacteria cellulose, homogenised cellulose and acetylated cellulose.
- Figure 4.6** The stability of acetylated microfibrillated cellulose after one month of dissolution in chloroform.
- Figure 4.7** Schematic representation of summary of modified microfibrillated cellulose production.

- Figure 5.1** SEM micrographs of (a) Neat P(3HB) film, (b) 10 wt%, (c) 20 wt%, (d) 30 wt%, (e) 40 wt% and (f) 50 wt% MFC in P(3HB)/MFC Composite films.
- Figure 5.2** (a) FT-IR spectra of P(3HB)/MFC composite containing 40 wt% acetylated MFC (blue line); acetylated microfibrillated cellulose (red line), and FT-IR spectrum of P(3HB) (Black line); (b) Magnification of the FTIR spectra within the 2000 cm^{-1} and 750 cm^{-1} wave number.
- Figure 5.3** XRD spectra of (a) P(3HB)/MFC composite (black line), (b) acetylated cellulose and (c) neat P(3HB).
- Figure 5.4** DSC thermographs of neat P(3HB) and P(3HB)/MFC composite films (0-40 wt%) showing the melting temperature, T_m , crystallization temperature, T_c and glass transition temperature, T_g .
- Figure 5.5** The Stress-Strain curve of neat P(3HB) and P(3HB)/MFC composite films highlighting differences in the measured Young's moduli. Analysis was performed in triplicates.
- Figure 5.6** Moduli comparison of P(3HB)/MFC composite film containing different amounts of MFC.
- Figure 5.7** Images of neat P(3HB) and P(3HB)/MFC composite films with various MFC content stained with (a) Rose Bengal dye and (b) toluidine blue.
- Figure 5.8** Colour intensity of neat P(3HB) and P(3HB)/MFC composite films of various MFC content measured after staining with Rose Bengal and Toluidine blue dyes for 4 hours.
- Figure 5.9** Typical aqueous contact angle plot for P(3HB)/MFC composite film containing 50 wt% MFC.
- Figure 5.10** Relationship of Aqueous contact Angles and the weight percentage content of MFC in P(3HB)/MFC composite films.
- Figure 5.11** Comparison of percentage water absorption for neat P(3HB) and P(3HB)/MFC composite film (40 wt% MFC content) immersed in SBF for 28 days at 37 °C.

- Figure 5.12** Comparison of percentage weight loss of neat P(3HB) and P(3HB)/MFC composite film (40 wt% MFC content) and pH value of the immersed SBF after incubation for 28 days at 37 °C.
- Figure 5.13** Total protein adsorption on P(3HB)/MFC composite films using foetal bovine serum.
- Figure 5.14** (A) Digital images of different dimensions and type of scaffolds that can be produced using the compression moulding/particulate leaching techniques.
(B) Shows a digital image of scaffold prepared by incorporation of vitamin E and magnetic particles for bone regeneration
(C) Shows a digital image of scaffold prepared by incorporating cellulose microspheres in P(3HB) matrix
(D) SEM image showing the incorporation of microspheres containing drug and TFG- β 3 for sustainable nutrient/drug release during tissue regeneration;
(E) SEM image showing the arrangement of the microspheres around the pores of the scaffold for efficient content delivery;
(F) SEM image of the tightly bound microspheres on the walls of the pores.
- Figure 5.15** (a) Digital image of the P(3HB)/MFC scaffold after particulate leaching;
(b) SEM image of P(3HB)/MFC composite foam at lower magnification showing the microstructural pores in P(3HB)/MFC scaffold;
(c) SEM image of P(3HB)/MFC composite foam at higher magnification displaying the irregular pore structure with high interconnectivity.
- Figure 5.16** Typical stress-strain curves of neat P(3HB) and P(3HB)/MFC scaffolds of various MFC content under compression loading.
- Figure 5.17** Compressive modulus and yield strength for P(3HB)/MFC scaffolds with various MFC (wt%) content measured in air.
- Figure 5.18** Total protein adsorption study on P(3HB)/MFC composite scaffold using fetal bovine serum.
- Figure 5.19** Typical plot of percentage weight loss of P(3HB)/MFC composite scaffold and neat P(3HB) scaffold immersed in SBF for 7, 14 and 30 days.

- Figure 5.20** Change in pH of the SBF solution in which the neat P(3HB) and P(3HB)/MFC 3D scaffold were incubated.
- Figure 5.21** Raman Shift spectra performed on P(3HB)/MFC composite scaffold after immersion in SBF for 0, 7, 14, 21 and 30 days.
- Figure 5.22** X-ray diffraction spectra of P(3HB)/MFC scaffolds immersed in SBF for a period of 21 days.
- Figure 5.23** Normalised DSC (a) first heat scan (200 °C to -50 °C)
(b) Second heating curve (200 °C to -50 °C)
(c) Cooling curve (200 °C to -50 °C), obtained at a heating rate of 20 °C for P(3HB)/MFC composite scaffold immersed in SBF for various time points; 0, 7, 14, 21 and 30 days.
- Figure 5.24** Cell proliferation study using Alamar blue assay for P(3HB) and P(3HB)/MFC composite films on day 1,4 and 7.
- Figure 5.25** Cell proliferation relative to the control (neat P(3HB)) set at 100% for 1, 4 and 7 days growth, using Alamar Blue assay on P(3HB)/MFC Composite 3D Scaffold with different amount of MFC contents.
- Figure 5.26** SEM images of ATDC cells growing at day 1 on (A) Tissue culture plastic, (B) neat P(3HB) and (C) P(3HB)/MFC composite films shown at lower (x150) and higher (x500) magnifications.
- Figure 5.27** SEM images of ATDC cells growing at day 7 on (A) Tissue culture plastic, (B) neat P(3HB) and (C) P(3HB)/MFC composite films shown at lower (x150) and higher (x500) magnifications.
- Figure 5.28** SEM micrographs of ATDC cells grown on P(3HB)/MFC composite scaffold at Day 1; (a) ATDC cells growing on the pores in the scaffold;
(b) ATDC cells still in round shape adhering to the nanotopography walls of the pores in the scaffold;
(c) Cells growing filopodia after division and moving away for flattening;
(d) Group of cells growing in the pore of the scaffold material

(e) and (f) show a higher magnification of (d) for a clearer view of the cells adhering to one another and attaching themselves with their filopodia for communication.

Figure 5.29 SEM micrographs of ATDC cells growing on the pores in the P(3HB)/MFC 3D composite scaffold at Day 4.

(a) well spread ATDC cells extending their filopodia for cell-cell communications,

(b) A higher magnification of (a) Flattening and layering of ATDC cells on the polymeric composite 3D substrate;

(c) Densely growing ATDC cells inside the pore

(d) A higher magnification of (c) rounding up of cells for dividing and higher cell proliferation.

Figure 5.30 SEM micrographs of ATDC cells growing in the P(3HB)/MFC 3D composite scaffold at Day 7. The yellow arrows in (a) indicate the folding and withdrawal of filopodia, possibly for division and the red arrow highlights cells growing and bridging the pores.

(b) Well flattened cells on the polymeric 3D composite substrate, while the blue arrows in Figure (c) highlight rounded ATDC cells ready for division.

Figure 5.31 Whole Protein production by the ATDC cell line grown on tissue culture plate (control), P(3HB) and P(3HB)/MFC composite (40 wt% MFC) for 21 days.

Figure 5.32 Schematic representation of investigations and results achieved compared to neat P(3HB) 2D and 3D structures.

Figure 6.1 SEM image of (A1) neat P(3HB); (B1) P(3HB)/MNP; (C1) P(3HB)/FF at lower magnification (x150) and SEM Image of (A2) neat P(3HB); (B2) P(3HB)/MNP; P(3HB)/FF at higher magnification (x500).

Figure 6.2 TEM micrographs of (a) P(3HB)/MNP at lower concentration (14 mg), P(3HB)/MNP at higher concentration (54 mg), and (c) TEM micrograph of P(3HB)/FF (14 mg) composite scaffolds.

Figure 6.3 Electron diffraction patterns of (a) P(3HB)/MNP and (b) P(3HB)/FF composite scaffolds.

- Figure 6.4** Comparison of SQUID data of saturation of specific magnetization with an applied field of approximately 5000 Oe at 300 K for (a) neat P(3HB) and (b) P(3HB)/MNP composite scaffold containing different amounts of MNP (14, 27 and 54mg).
- Figure 6.5** Comparison of SQUID data of saturation of specific magnetization with an applied field of approximately 5000 Oe at 300 K for (a) P(3HB)/FF composite scaffold (12.5mg, average particle size, ca=10-15 nm), and P(3HB)/MNP composite scaffold (14 mg, ca=100 nm).
- Figure 6.6** Young's modulus (E) measurement for neat P(3HB), P(3HB)/MNP, and P(3HB)/FF composite containing 14 mg of either MNP or ferrofluid solution in 1g of P(3HB).
- Figure 6.7** Typical plot of Storage modulus and Loss modulus of neat P(3HB), P(3HB)/FF, and P(3HB)/MNP composite.
- Figure 6.8** Typical heat flow thermograph for (a) the first heating curve (b) the second heating curve from DSC analysis for the neat P(3HB) and P(3HB)/MNP composites.
- Figure 6.9** Typical heat flow thermograph for the cooling curve from DSC analysis for the neat P(3HB) and P(3HB)/MNP composites.
- Figure 6.10** FT-IR spectra of neat P(3HB), P(3HB)/MNP and P(3HB)/FF.
- Figure 6.11** Aqueous contact angles for neat P(3HB), P(3HB)/MNP and P(3HB)/FF composite films.
- Figure 6.12** Total protein adsorption study on P(3HB)/MNP and P(3HB)/FF films using fetal bovine serum (FBS).
- Figure 6.13** Typical (a) Digital image of P(3HB)/MNP composite scaffold, (b) SEM image of the composite scaffold revealing the interconnected pores, (c) SEM image of the pores reveal the magnetic nanoparticles (arrows) at lower magnification and at higher magnification.

- Figure 6.14** Typical stress-strain curves for (a) P(3HB)/MNP composites containing different amounts of MNP and (b) neat P(3HB) and P(3HB)/MNP and P(3HB)/FF composite scaffolds containing 14 mg of MNP or ferrofluid per 1g of P(3HB) under the same compression loading.
- Figure 6.15** Compressive modulus and stress strength for neat P(3HB), P(3HB)/MNP, and P(3HB)/FF composite scaffold containing 54 mg MNP and 54g ferrofluid respectively per 1g P(3HB), measured in air.
- Figure 6.16** Percentage weight loss by neat P(3HB), P(3HB)/MNP, and P(3HB)/FF immersed in SBF for 30 days.
- Figure 6.17** Change in pH of SBF with time of immersion of P(3HB), P(3HB)/MNP and P(3HB)/FF composite films.
- Figure 6.18** X-ray diffraction spectra for P(3HB), P(3HB)/FF composite scaffolds immersed in SBF for a period of 21 days.
- Figure 6.19** X-ray diffraction spectra for P(3HB), P(3HB)/MNP composite scaffolds immersed in SBF for a period of 21 days.
- Figure 6.20** Raman Shift spectra performed on P(3HB)/FF composite scaffold after immersion in SBF for 0, 7, 14, 21 and 30 days.
- Figure 6.21** Raman Shift spectra performed on P(3HB)/FF composite scaffold after immersion in SBF for 0, 7, 14, 21 and 30 days.
- Figure 6.22** Melting endotherm (a) first run and (b) second run for P(3HB)/MNP composite scaffold degrading in SBF solution for 30 days (Scanning rate 10 °C/min).
- Figure 6.23** DSC cooling exotherms (cooling rate of 10 °C/min) of P(3HB)/MNP at different time points of immersion in SBF solution.
- Figure 6.24** Melting endotherm (a) first run and (b) second run for P(3HB)/FF composite scaffold degrading in SBF solution for 30 days (Scanning rate 10 °C/min).
- Figure 6.25** DSC cooling exotherms (cooling rate of 10 °C/min) of P(3HB)/FF at different time points of immersion in SBF solution.

- Figure 6.26** Cell proliferation study using Alamar blue assay for neat P(3HB) and P(3HB)/MNP and P(3HB)/FF composite film performed on day 1, 3 and 6, and samples measured relative to the control set at 100%.
- Figure 6.27** Cell proliferation study using Alamar blue assay for P(3HB) and P(3HB)/MNP composite scaffold containing different amount of magnetic particle suspension performed on day 1, 4 and 7, and samples measured relative to the control set at 100%.
- Figure 6.28** Cell proliferations using Alamar blue assay for TCP, P(3HB) and P(3HB)/FF composite scaffold containing different amounts of ferrofluid performed on day 1, 4 and 7, and samples measured relative to the control set at 100%.
- Figure 6.30** Protein production by MG-63 cell lines on TCP, P(3HB), P(3HB)/MNP and P(3HB)/FF with normal growth media at different time points and measured relative to the control (TCP) set at 100%.
- Figure 6.31** SEM images of MG-63 cells growing on (A1) Tissue culture plastic; (B1) neat P(3HB); (C1) P(3HB)/MNP; and (D1) P(3HB)/FF film at Day 1. SEM images of MG-63 cells growing on (A2) Tissue culture plastic; (B2) neat P(3HB); (C2) P(3HB)/MNP; and (D2) P(3HB)/FF film at Day 7. Higher magnification of MG-63 cells growing at Day 7 revealing healthy cells that flattened out and attached on the materials and on each other forming monolayer on (A3) Tissue culture plastic; (B3) neat P(3HB); (C3) P(3HB)/MNP; and (D3) P(3HB)/FF films.
- Figure 6.32** SEM images of MG-63 cells growing at day 1 on (A) neat P(3HB) scaffold; (B) P(3HB)/MNP and P(3HB)/FF composite scaffolds at different magnifications shown on the top of the figure.
- Figure 6.33** SEM images of MG-63 cells growing at day 7 on (A) neat P(3HB) scaffold; (B) P(3HB)/MNP and (C) P(3HB)/FF composite scaffolds at different magnifications shown on the top of the figure.
- Figure 6.34** (a) Schematic model of a spherulite. Black arrows indicate direction of molecular alignment.

(b) Principle of lamellae formation during the crystallization of polymers.

Figure 6.35 Schematic representation of summary of investigations and results achieved compared to neat P(3HB).

Figure 7.1 Typical SEM image of cellulose nanospheres (a) at lower magnification (b) at higher magnifications (inset, magnified image revealing the surface topography of the cellulose nanospheres; (c) typical SEM image of a single P(3HB) microspheres containing cellulose nanospheres; (d) SEM image of cross section of P(3HB) microsphere displaying the cellulose nanospheres encapsulated within it.

Figure 7.2 Typical SEM image displaying the, almost, monodisperse P(3HB) microspheres containing cellulose nanospheres (a) at lower magnification, (b) at higher magnification.

Figure 7.3 Typical SEM image of a P(3HB) microsphere prepared with (a) 100 mg/mL and (b) 50 mg/mL chloroform.

Figure 7.4 The histogram of particle size distribution of microspheres measured using Dynamic Light Scattering, DLS technique.

Figure 7.5 Surface chemistry measurement of (A) cellulose nanospheres (B) P(3HB) microspheres with cellulose nanospheres, (C) P(3HB) microspheres without cellulose nanospheres using binding of Rose Bengal Blue.

Figure 7.6 Effect of organic solvent on % residual PVA associated with P(3HB) microspheres.

Figure 7.7 Determination of the effect of PVA concentration of the oil in water emulsion on the percentage residual PVA on the surface of microspheres.

Figure 7.8 standard curves for BSA concentration measurements. UV-visible spectroscopy measurements were carried out for known concentrations of BSA at the absorbance maximum of 280 nm

Figure 7.9 *In vitro* release of BSA for (A) Cellulose nanospheres loaded with BSA and encapsulated in P(3HB) microspheres, (B) Cellulose nanospheres and (C)

cellulose nanospheres loaded with BSA and encapsulated P(3HB) microspheres also loaded with BSA.

- Figure 7.10** Typical SEM image of degrading P(3HB) microspheres containing cellulose nanospheres after incubation for 14 days in a PBS solution containing lipase at 37 °C.
- Figure 7.11** Typical SEM image of P(3HB)/FF microsphere (a) at lower magnification and (b) at higher magnification.
- Figure 7.12** Typical SEM image of P(3HB)/MNP microsphere, inset is a magnified single microsphere highlighting the morphology of the microsphere
- Figure 7.13** Typical SEM image of (a) single P(3HB)/FF microsphere (b) cross section of a P(3HB)/FF microsphere displaying the non hollow morphology of the microsphere
- Figure 7.14** Typical SEM image of the P(3HB)/MNP microsphere revealing the internal structure of the microspheres at different amount of magnetic particles (a) 14 mg (b) 27 mg and (c) 40 mg of magnetic particles
- Figure 7.15** Transmission electron micrograph (TEM) of (a) P(3HB) microsphere (b) P(3HB)/FF microsphere, (c) P(3HB)/MNF composite microsphere containing lower concentration of MNP (14 mg MNP) and (d) P(3HB)/MNP composite microsphere containing higher concentration of MNP (27 mg MNP).
- Figure 7.16** Randomly oriented crystalline structure of (a) P(3HB)/FF and (b) P(3HB)/MNP composite microspheres.
- Figure 7.17** Comparison of SQUID data for (a) P(3HB), (b) P(3HB)/FF and (c) P(3HB)/MNP spheres saturation of specific magnetization with an applied field of approximately 5 000 Oe at 300K
- Figure 7.18** Schematic representation of summary of analysis and results achieved

Chapter 1

INTRODUCTION

Chapter 1

1 Introduction

In view of the innumerable applications of plastics, biodegradable polymers are urgently needed to reduce the adverse worldwide environmental and economic effects of conventional plastics. Also, since global petroleum reserves are finite, there is need for additional new sources of durable materials (Akaraonye *et al.*, 2010). Renewable materials from microorganisms can provide a source of sustainable alternative to petroleum derived chemicals including polymers. According to Bozell and Landucco, integrating renewable feed stocks into the economy could lower crude oil demand, thus limiting economic downturns in the chemical industry due to oil price volatility (Bozell and Landucco, 1993). It would also expand the options of the chemical industry by increasing feedstock flexibility and broadening the spectrum of potential chemical products. Hence, this would provide an acceptable answer to the current problems with petroleum-based chemicals. The development of biodegradable polyhydroxyalkanoates (PHAs) – an alternative to petroleum-based plastics, hence, has the potential to provide a permanent and global solution to solve the problems associated with synthetic plastics.

In spite of the potential applicability of PHAs, their introduction to the world-wide market is currently limited due to their higher production cost compared to their synthetic alternatives. Hence, to increase the economic viability of PHAs, there is a great need for the development of novel microbial processes for the production of PHAs with reduced production cost. Polyhydroxyalkanoates are being considered as potential materials for biomedical applications primarily in response, to emerging tissue engineering needs where a much wider range of biocompatible and biodegradable polymers are being sought for use as tissue engineering scaffolds. Consequently, the past few years have seen PHAs emerging as one of the leading biomaterials being studied for their biomedical applications because they can offer properties not available in synthetic absorbable polymers such as natural occurrence, proven biocompatibility as well as tailored bioabsorbability. The five major PHAs currently under intense investigations for their useful properties included poly(3-hydroxybutyrate), P(3HB), poly(4-hydroxybutyrate), P(4HB), poly(3-hydroxybutyrate-co-4-hydroxybutyrate),

P(3HB-co-4HB), poly(3-hydroxybutyrate-co-3-hydroxyvalerate), P(3HB-co-3HV), poly(3-hydroxyoctanoate-co-3-hydroxyhexanoates) and P(3HO-co-3HHx).

1.1 Biodegradable Polymers

In an environmental context, biodegradable polymers may be defined as those that undergo microbially induced chain scission, leading to mineralization, oxidation and hydrolysis, which can alter the polymer during the degradation process. In the same context, biodegradable polymers can also be described as a representation of those polymers which are capable of undergoing decomposition, primarily through enzymatic activities of microorganisms into CO₂, methane, inorganic compounds, or biomass, within a specified period of time (Mohanty *et al.*, 2002). In the medical context, biodegradability can be defined as the breakdown of solid polymeric materials due to macromolecular degradation with dispersion *in vivo* without proof of elimination from the body (Hutmacher *et al.*, 2000).

The challenge for the development of biodegradable polymers lies in the fact that such biopolymers should be stable during storage or usage and then degrade once disposed off after their intended lifetime. In contrast to the petroleum based plastics which result in the generation of toxic and recalcitrant waste, the production of biodegradable polymers involves aqueous processing environments during microbial cultivation, generation of non-toxic waste and the use of renewable non fossil feed stocks (Akaraonye *et al.*, 2010). Biodegradable polymers release carbon dioxide and water vapour into the air while undergoing biological decomposition, but, growing biomass during photosynthesis subsequently absorbs the released carbon dioxide (Figure 1.1A). Hence, the problems associated with conventional petroleum based plastics have brought biodegradable polymers to the forefront.

Biodegradable polymers (classified in Figure 1.1B) may be obtained from renewable resources or derived from petroleum-based chemicals. Through the blending of two or more biopolymers a new biodegradable polymer may be designed for specific requirements. Biodegradability is not only a function of the primary source of the polymer but also that of the degrading environment. Originally, biopolymers were intended to be used in packaging industries, farming, and other applications with minor strength requirements. However,

performance limitations and the high cost of biopolymers are major barriers for their widespread acceptance as a substitute for traditional non-biodegradable polymers. The high cost of biopolymers compared to traditional plastics is not only as a result of raw material costs for biopolymer synthesis; but also due to the low volume of production (Mohanty *et al.*, 2002). In the future, new and emerging applications for biopolymers will result in increased production.

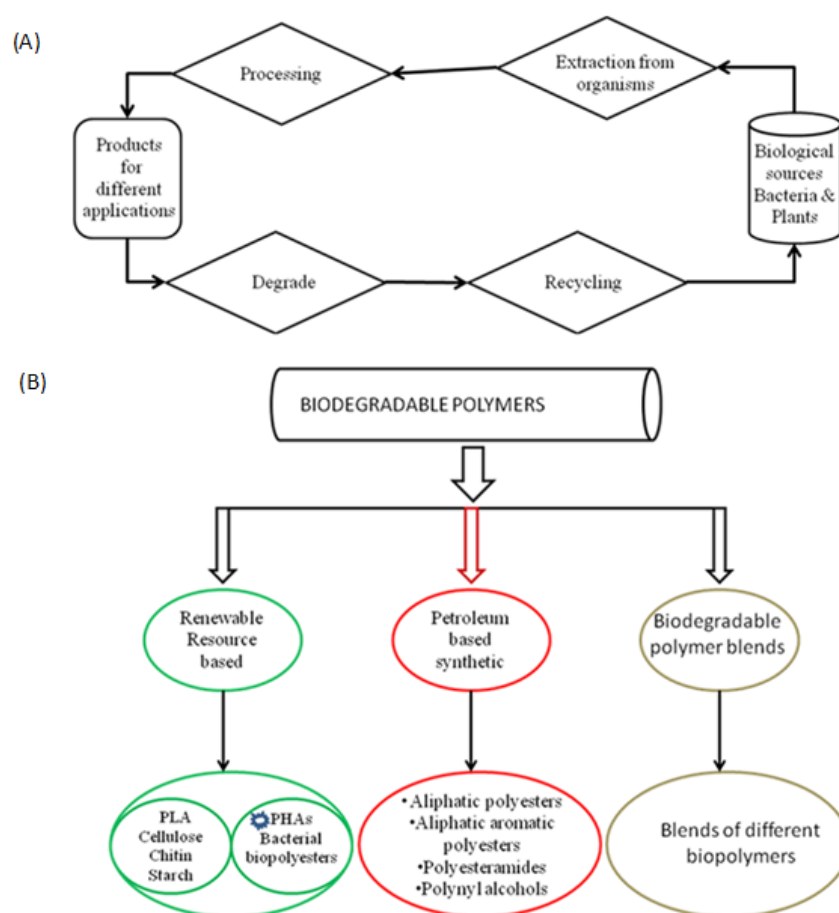


Figure 1.1 Schematic representations of (A) Life cycle of production and degradation of biodegradable polymers from renewable sources (B) Classification of biodegradable polymers (modified from Mohanty *et al.*, 2002).

1.1.1 Polyhydroxyalkanoates, PHAs

Currently, different types of biodegradable polymers are being investigated for different applications ranging from the production of every day used products to medical applications.

Various biodegradable polymers under investigations included polyhydroxyalkanoates (PHAs), polylactide (PLA), poly(ϵ -caprolactone) (PCL), poly(*p*-dioxanone) (PPDO) and poly(butylene succinate) (PBS). Other natural renewable polymers include porous sponges (from cellulose wood fibres), fibres (made from natural fibres), hydrogels, starch, cellulose, chitin, chitosan, lignin and proteins. Of all these, PHAs are one of the relatively newer families of biodegradable polymers that have a great potential in the future due to their variability in properties.

1.1.1.1 PHAs and their structure

PHAs are polyesters of hydroxyalkanoic acids with the general structure shown in Figure 1.2. The structure of PHAs produced by bacteria can be manipulated by genetic or physiological strategies (Steinbuechel, 1991). The pendant group (R in Figure 1.2) varies from methyl (C₁) to tridecyl (C₁₃). Within bacterial metabolism carbon substrates are converted into hydroxyacyl-CoA thioesters. The carboxylate group of one monomer forms an ester bond with the hydroxyl group of the neighbouring monomer and the reaction is catalysed by the host's PHA synthase. The molecular weight of PHAs varies in the range of $2 \times 10^5 - 3 \times 10^6$ Da, and this is dependent on the microorganism in which the polymer is produced and the growth conditions used (Byrom, 1994; Lee, 1995). The monomer HA units in these microbial polyesters are all in the R(-) configuration because of the stereospecificity of the PHA synthase (Philip *et al.*, 2007; Verlinden *et al.*, 2007). Hence, production of PHAs in bacteria guarantees stereospecific incorporation of the R(-) monomer which is essential for the biodegradability and biocompatibility of PHAs (Zinn and Hany, 2005). The length of the side chain and its functional group greatly influences the physical properties of the polymers such as melting point, glass transition temperature and crystallinity, which in turn determines their final application.

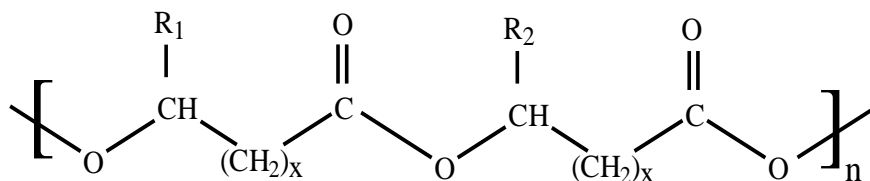


Figure 1.2 The general structure of polyhydroxyalkanoates (Philips *et al.*, 2007). (R₁/R₂ = alkyl groups C₁-C₁₃, X = 1-4, n = 100 – 30000)

PHAs are the most commonly encountered microbial storage polymer which functions in providing reserve carbon and energy to micro-organisms in which they are accumulated (Doi, 1990; Philips *et al.*, 2007). The polymers are accumulated as distinct intracellular granules (Figure 1.3).

In some organisms, PHAs play an additional role in spore and cyst formation. The PHAs synthesised by bacteria are stored in the form of insoluble inclusions in the cytoplasm (Steinbuechel, 1991). Because of their water-insolubility and the high molecular weight of PHAs, the internal osmotic pressure of the cell is only slightly affected by polymer accumulation thereby enabling the vital processes of the cell metabolism to function as normal. Accumulations of PHAs in some organisms usually occur under certain conditions that limit the growth of the micro-organism and the availability of high carbon source in the growth medium. The growth limiting conditions include the limitation of one of the following nutrients; nitrogen, phosphorus, potassium or oxygen.

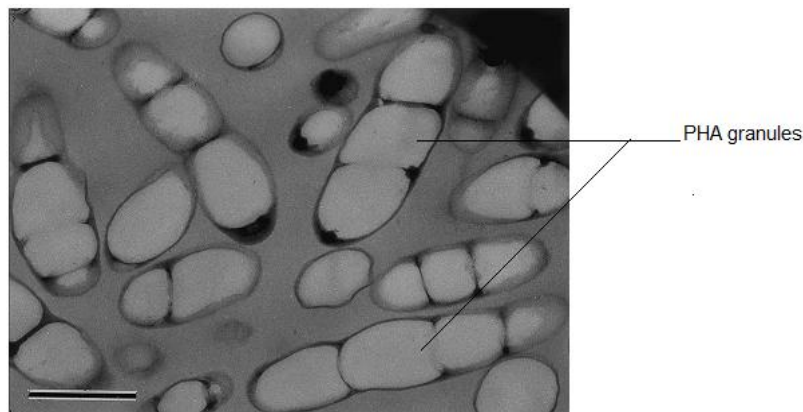


Figure 1.3 SEM images of synthesized and intracellularly accumulated discrete granules of P(3HB) in bacteria (Sudesh *et al.*, 2000).

1.1.1.2 Types of PHAs and their physical properties

PHAs are classified into two distinct groups based on the number of carbon atoms in the monomers. This include the short chain length (scl) polymers consisting of 3-5 carbon atom containing monomers, synthesized by numerous bacteria, including *Cuprivadus necator* and *Alcaligenes latus*. The other group is the medium chain length (mcl) polymers, consisting of 6-14 carbon atom containing monomers (Lee, 1996), also synthesized by bacteria including

Pseudomonas putida and *Pseudomonas mendocina*. Furthermore, copolymers of PHAs are found among the scl-PHAs e.g. poly(3-hydroxybutyrate-co-3-hydroxyvalerate), P(3HB-co-3HV), poly(3-hydroxybutyrate-co-4-hydroxyvalerate), P(3HB-co-4-HV) and mcl-PHAs e.g. poly(3-hydroxyhexanoate-co-3-hydroxyoctanoate), P(3HHx-co-3HO). A comparison of the properties of PHAs with conventional petrochemical based plastics such as polypropylene and polystyrene is shown in Table 1.1.

Table 1.1 Comparison of the physical properties of specific PHAs and two commonly used synthetic polymers

Polymer	T_m¹ (°C)	T_g² (°C)	Crystallinity³ (%)	Extension to break⁴ (%)	Tensile Strength⁵ (MPa)
P(3HB)	175-179	4	60-80	5-6	40
P(4HB)	53	-48	34	1000	104
P(3HB-co-16% 4HB)	150	-7	45	444	26
P(3HB-co-64 mol% 4HB)	50	-35	15	591	17
P(3HB-co-90 mol% 4HB)	50	-42	28	1080	65
P(3HB-co-3 mol% 3HV)	169-170	-1	69	-	35
P(3HB-co-14 mol% 3HV)	150	-1	56	-	30
P(3HB-co-20% 3HV)	145	-1	1.2	50	20
P(3HB-co-25 mol% 3HV)	137	-1	40	-	30
P(3HB-co-10% 3HHx)	127	-1	-	400	21
P(3HO-co-11 mol% 3HHx)	61	-36	30	300	10
P(3HB-co-6% 3HD)	130	-8	-	680	17
P(3HB-co-6 mol% 3HA)	133	-8	45	680	17
Polypropylene	176	-10	1.7	400	34.5
Polystyrene	240	100	3.1	-	50

(Adopted from Lee, 1995; Doi 1997; Borkenhagen *et al.*, 1998; Khanna and Srivastava, 2005; Tsuge, 2002)

¹Melting temperature is the temperature at which a polymer changes from solid to liquid state.

²Glass-transition temperature is the temperature at which the amorphous phase of the polymer is converted between rubbery and glassy states.

³Percent crystallinity is the ratio of crystalline material to total material (crystalline + amorphous)

⁴Extension to break represents the percent change in length at the material failure

⁵Tensile strength is the maximum stress a material subjected to the stretching load can withstand without tearing

Scl-PHAs such as P(3HB) and P(3HB-co-3HV) are crystalline polymers which are quite brittle and stiff, with high melting points and low glass transition temperatures. However, P(4HB), another scl-PHA is a strong, pliable thermoplastic polyester with a relatively simple structure (Figure 1.4) (Martin *et al.*, 2007). Some scl-PHAs have higher tensile strength compared to polypropylene and polystyrene as shown in Table 1.1. Mcl-PHAs on the other hand are thermoplastic elastomers with low crystallinity and tensile strength but high elongation to break. They have lower melting points and glass transition temperatures when compared to scl-PHAs and polypropylene as shown in Table 1.2.

Table 1.2 Comparison of the physical properties of scl-PHAs and mcl-PHAs with polypropylene

Properties	scl-PHAs	mcl-PHAs	Polypropylene
Crystallinity (%)	40-80	20-40	70
Melting Points (°C)	53 -180	30-80	176
Density (gcm ⁻³)	1.25	1.05	0.91
Tensile Strength (MPa)	43 -104	20	34
Glass transition temperature (°C)	-148 – 4	-40 – 150	-10
Extension to break (%)	6-1000	300-450	400
UV light resistant	Good	Good	Poor
Solvent resistant	Poor	Poor	Good
Biodegradability	Good	Good	None

(Adopted from Zinn and Hanny, 2005).

PHAs have attracted commercial interest as plastic materials because of their remarkable similarities in physical properties with synthetic polymers such as polypropylene. The major advantage of PHAs is that both the physical properties and the rate of degradation of PHAs can be altered by changing the bacterial source of the polymer and the corresponding fermentation conditions used. Special growth conditions of microorganisms allow inclusion of additional chiral monomers and functional groups to suit particular applications. Besides, the large diversity of monomers incorporated in PHAs provides a wide spectrum of polymers

with varying physical properties. These features help in placing PHAs at par with polypropylene and other petroleum-derived polymers (Madison and Huisman, 1999; Reddy *et al.*, 2003).

PHAs are optically active biological polyesters which are insoluble in water and exhibit a rather high degree of polymerisation that range from 10^5 to approximately 10^7 . The mechanical properties and biocompatibility of PHAs can be further improved by altering the physical properties through blending with other polymers, modifying the surface or combining PHA with other inorganic materials, thus, making them useful for a wider range of applications (Kang *et al.*, 2001; Scandola *et al.*, 1997).

P(3HB) is an isotactic polymer that exists in a fluid amorphous state within the cell (Lauzier, 1993). However, freeze-drying/organic solvent treatment during extraction from the bacteria irreversibly converts the polymer into a crystalline state (Hahn, 1995). The chemical structures of P(3HB) and copolymers of P(3HB) are summarised in Figure 1.4 while the material properties and features of poly(3-hydroxybutyrate), P(3HB) are summarised in Table 1.3

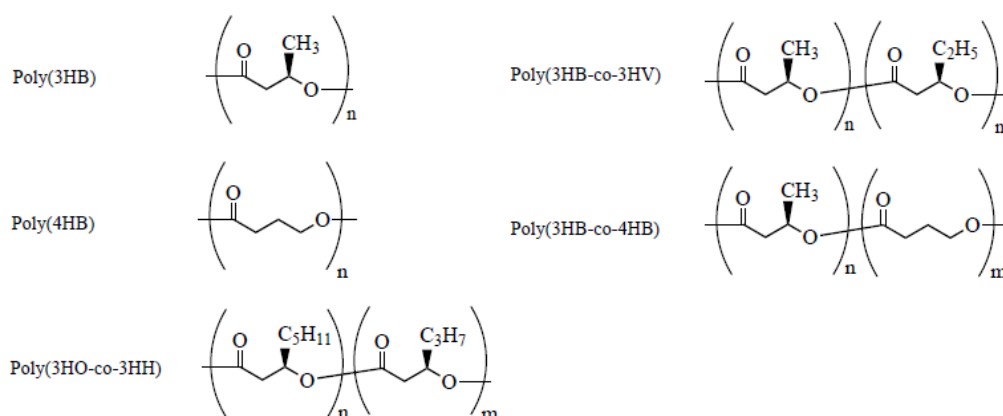


Figure 1.4 Chemical structures of PHAs currently under investigation for exploration in medicine and pharmacy.

Table 1.3 Properties and features of Poly(3-hydroxybutyrate), P(3HB)

-
1. Strong and malleable thermoplastic (ability to be moulded, made into films and fibres)
 2. Has tensile strength closely related to polyethylene
 3. Very low elongation to break (6%)
 4. Biodegradable (degradable into CO₂ and H₂O, aerobic; CH₄ and H₂O, anaerobic)
 5. Can be produced from naturally sustainable and bio-renewable agricultural feed stock
 6. Nontoxic to mammalian cells (biocompatible to various cell lines including osteoblast, epithelial cells and chondrocytes)
 7. Insoluble in water
 8. Highly crystalline
 9. Melting point is 180 °C.
 10. Enantiomeric and optically active
 11. Stereochemically regular in its repeating units
 12. High degree of polymerisation
 13. Possesses piezoelectric properties useful in osteoinduction.
-

1.1.1.3 Biosynthesis and Catabolism of intracellular PHA

Four pathways have been found to create PHAs in various bacteria (Khanna and Srivastava, 2005), For P(3HB) production, the main focus of this thesis, the pathways are catalyzed by three different enzymes, beta-ketothiolase, NADPH dependent reductase and P(3HB) synthase (Madison and Huisman, 1999). The first reaction involves the beta-ketothiolase, encoded by *phaA* gene. This enzyme promotes the condensation of two acetyl coenzyme A (acetyl-CoA) moieties in a reversible manner into acetoacetyl CoA. The second step involves the action of NADPH dependent reductase, encoded by the *phaB* gene, which reduces acetoacetyl-CoA to R-(-3)-hydroxybutyryl-CoA. The last reaction in the synthesis is catalysed by PHA synthase, encoded by the *phaC* gene, and polymerises the R-(3)-hydroxybutyryl-CoA to form P(3HB) (Anderson and Dawes, 1990; Poirier *et al.*, 1995; Lee, 1996; Huisman *et al.*, 1989) (Figure 1.5).

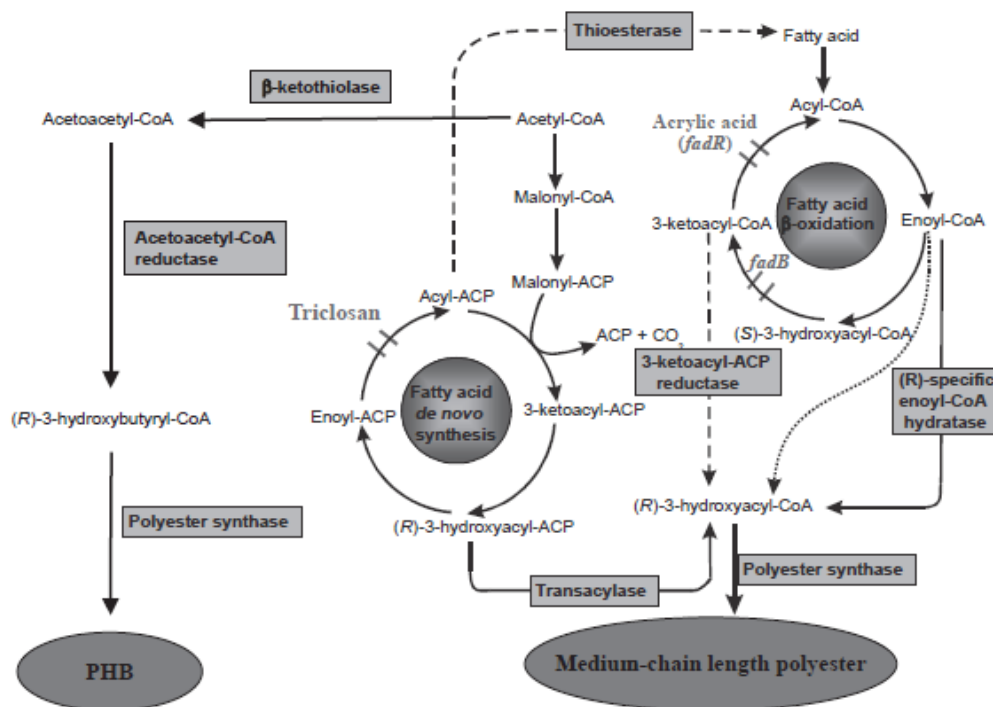


Figure 1.5 Diagram showing the metabolic pathways involved in the synthesis and degradation of Poly(3-hydroxybutyrate) in *Ralstonia eutropha* (Rehm, 2006).

Nevertheless, a different PHA biosynthetic pathway was found among *Pseudomonas* species belonging to rRNA homology group 1. *Pseudomonas oleovorans* and other *Pseudomonas* species accumulate PHA consisting of 3-hydroxyalkanoic acid of medium chain length when the cells are cultivated on alkanes, alkanols or alkanolic acids (Lagaveen *et al.*, 1988; Brandi *et al.*, 1988). Moreover, most of the rRNA homology group 1 *Pseudomonas*, except *P.oleovorans*, can also synthesize PHA containing medium chain length monomers from unrelated carbon sources such as carbohydrates. The bacteria are able to accumulate PHAs containing 3-hydrodecanoate (3HD) as the predominant monomer from different carbon sources ranging from gluconate, fructose, acetate, glycerol and lactate (Anderson and Dawes, 1990), while Huijberts *et al.* (1994) reported that the 3-hydroxyacyl monomers are derived from the *de novo* fatty acid biosynthesis pathway. There is another type of PHA biosynthetic pathway present in nearly all *Pseudomonas* species belonging to rRNA homology group II and the pathway involves the synthesis of copolyesters that are made up of the medium chain length 3HAs from acetyl-CoA. However, more research is currently being pursued in order to understand this pathway better (Shilpi and Ashok, 2004). Hence, for PHA synthesis, three

processes are involved, (Volva, 2004), a carbon source suitable for biosynthesis of a PHA must enter the cell from the environment; secondly, anabolic or catabolic reactions, or both, would have to convert the compound into a hydroxyacyl coenzyme A thioester (a substrate of the PHA synthase). Lastly, the PHA synthase uses these thioesters as a substrate and catalyzes the formation of the ester bond with the concomitant release of coenzyme A.

Availability of nutrients is a major key factor in regulating P(3HB) metabolism. There are usually high levels of CoA under balanced growth conditions. Thus, acetyl-CoA is metabolized in the tricarboxylic acid cycle resulting in the inhibition of P(3HB) synthesis. However, under nutrient limitation and presence of excess carbon, proteins can no longer be synthesized, hence, leading to the building up of NADH, a universal electron carrier in biosynthesis. NADH inhibits citrate synthase and consequently reduces the rate of oxidation of acetyl-CoA in the tricarboxylic acid cycle. This results to the accumulation of acetyl-CoA, which results in acetoacetyl-CoA formation leading to P(3HB) biosynthesis. The catabolism of intracellularly accumulated P(3HB) reserves is not initiated until all the available exogenous carbon and energy sources are virtually exhausted. During catabolism of P(3HB), acetyl-CoA is formed again and subsequently channelled into the tricarboxylic acid cycle to provide carbon and energy. Hence, P(3HB) metabolism occurs through a cyclic process with acetyl-CoA fulfilling the role of both precursor for P(3HB) formation and the product of P(3HB) catabolism. However, the conditions which favour PHA accumulation are likely to inhibit the degradation of accumulated PHA in order to prevent unrestricted cycling of polymer, by provision of excess carbon source that will discourage the reconversion of accumulated PHA into acetyl-CoA. However, interestingly Kawaguchi and Doi have reported the simultaneous accumulation and degradation of PHAs as they were formed (Kawaguchi and Doi, 1992).

PHA synthases and phasins are proteins that play important roles in PHA production. The PHA synthases play the central catalytic role in PHA synthesis and granule formation by catalyzing the polymerization of hydroxyacyl coenzyme A substrates to yield PHAs (Gerngross *et al.*, 1994). The synthesized PHAs in turn associate to form PHA granules (Rehm, 2007). Phasins are granule associated proteins found on the membranes of the PHA producing organisms (Gerngross and Martin, 1995; Madisson and Huisman, 1999). The phasin proteins play a role as structural proteins non-covalently attached to the polyester core

of PHA granules (Hanley *et al.*, 1999). Potter *et al.*, 2005, have shown that phasins promote PHA biosynthesis and their copy number has impact on PHA granules size. Jurasek and Marchessault, 2004 investigated the kinetics of self-assembly process of the PHA granules and observed phasins impact on the kinetics of granule formation by reduction in the lag phase. The amphiphilic PHA synthase–PHA complex attracts additional PHA synthase molecules and granules begin to grow from these initiation sites. The appearance of PHA in the cytoplasm stimulates the production of phasin molecules which attach themselves to the growing PHA granules. As the granules grow bigger, they begin to touch each other and move to optimize their packing. The phasin protein coat functions to prevent the granules from coalescing and this further help to increase the size of cells due to the growing PHA granules. Thus earlier production of phasin during PHA accumulation helps to protect the growing PHA granules and further the growth of the granules.

Tian and his colleagues (Tian *et al.*, 2005) have shown, through time course studies, that the early stage granules are not randomly distributed in the cytoplasm and are located close to the inner membrane. Rather, the emerging granules were found to arise exactly from the centre of the cell at unknown mediation. They suggested a new model for PHA granule formation, where the mediating elements provide the architectural scaffolds for the synthase as a site for the initiation of granule formation. This phenomenon of PHA formation and association to form granules has been described as the micelle model and budding model and illustrated in the Figure 1.6.

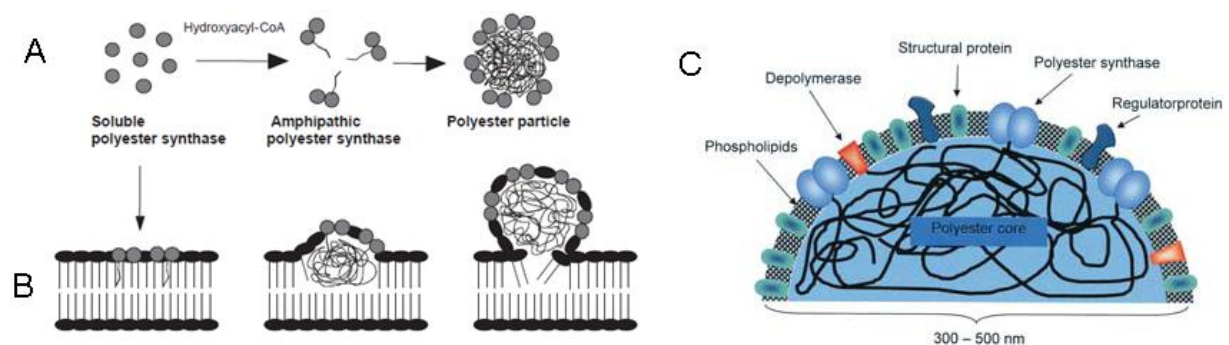


Figure 1.6 Models of PHA granule formation. (A) Micelle model showing soluble polyester synthase catalyzing the polymerization of hydroxyacyl coenzyme A substrates to yield PHAs and association of PHAs to form PHA granules. (B) Budding model showing granule formation at the cytoplasmic membrane (Rehm, 2007). (C) Schematic representation of a PHA granule with the associated (Rehm, 2003).

1.1.1.4 Biodegradability and Biocompatibility of PHAs

PHAs have attracted extensive attention due to their inherent biocompatibility and biodegradability (Wu *et al.*, 2008). PHAs can be completely degraded into harmless and naturally occurring molecules. They are naturally abundant in nature; they are part of the natural constituents of the soil, produced and degraded by a wide range of bacteria and fungi. Microorganisms in nature are able to degrade PHAs by using PHA depolymerases. Investigations by some researchers have described the isolation of bacteria that secrete specific depolymerase for P(3HB-co-3HV) (Muller and Jendrossek, 1993) or octanoate-based PHAs (Schirmer *et al.*, 1993). Although, both intracellular and extracellular depolymerases can degrade PHAs, the activities of these enzymes vary depending on the composition, crystallinity, additives and the surface area of the polymer. In addition, environmental conditions including temperature, moisture level and pH affect the rate of degradation. According to Doi, the extracellular depolymerases hydrolyze crystalline P(3HB), the intracellular depolymerases hydrolyse the amorphous phase of P(3HB) twenty times faster than the extracellular depolymerase. The extracellular PHA depolymerases hydrolyse the PHAs into water-soluble oligomers and monomers and subsequently utilise the resulting products as nutrients for biomass accumulation. The monomeric composition of PHAs also affects the degradation rate of the polymers. PHA copolymers containing the 4-hydroxybutyrate (4HB) monomer units degrade more rapidly than those with 3-hydroxybutyrate (3HB) or 3-hydroxyvalerate (3HV) monomer units. The end product of PHA degradation in an aerobic environment is carbon dioxide and water while in anaerobic condition is methane and water (Ojumu *et al.*, 2004).

In the context of medical applications, PHAs are established as biocompatible and biodegradable polymers. Besides, there have been reports of the presence of monomers of some of these polymers in the human body. Reusch and co-workers first identified P(3HB) in blood serum at a concentration of 0.6-18.2 mg L⁻¹ complexed with low-density lipoproteins, and with carrier protein albumin (Reusch *et al.*, 1992). The oligomers have also been detected in human aorta (Seebach *et al.*, 1994). In the human body, P(3HB), on degradation forms the innocuous 3-hydroxybutyric acid. The hydroxy acid is a ketone body, and is present at concentrations of 3-10 mg per 100 mL blood in healthy adults (Hocking and Marchessault, 1994).

In mammals, the hydrolysis of the polymer happens gradually (six months or more). This was shown as the result of six month's implantation of P(3HB) in mice which indicated a mass loss of less than 1.6% w/w (Pouton and Akhta, 1996). Various investigations have been carried out to assess the biocompatibility of PHAs. For example, Volova and co-workers have shown that P(3HB) and P(3HB-co-3HV) fibres have no toxic effects in living organisms (Volova *et al.*, 2003). Saito and colleagues have evaluated P(3HB) sheets in an inflammatory test using the chorioallantoic membrane of the developing egg and found that the polymer did not cause any inflammation (Saito *et al.*, 1991). The rate of *in vivo* (Korsatko *et al.*, 1983), and *in vitro* (Knowles, 1991) degradation were compared and the results indicated that degradation of P(3HB) *in vivo* is significantly faster than the hydrolysis in neutral buffer at body temperature (Korsatko *et al.*, 1983). Possibly, this is due to hydrolytic enzymes such as lipases present in the body which catalyse the *in vivo* degradation process. A detailed description of the biodegradability of PHAs is reviewed in Valappil *et al.*, 2006. Though, P(3HB) degradation is relatively slow. The rate of degradation can be further improved by employing specific processing conditions (Yasin *et al.*, 1990) or by treatment with γ -irradiation (Miller and Williams, 1987). Also, the rate of degradation of P(3HB) can be increased by blending P(3HB) with other biocompatible material to improve porosity, mechanical properties and surface area of the resulting composite material.

1.1.1.5 PHA production in specific bacteria

Many species of bacteria, synthesize PHAs. The list of such microorganisms is growing and currently contains more than 300 organisms (Ciesielski *et al.*, 2006; Berlanga *et al.*, 2006). Brief details of PHA production from different microorganisms are given below.

1.1.1.5.1 PHA production using wild type bacteria

PHA producing bacteria can be divided into two groups according to the culture conditions required for PHA synthesis. The first group requires the limitation of an essential nutrient(s) for the production of PHAs. Bacteria in this group include *Bacillus cereus*, *Cupriavidus necator*, *Rhodopseudomonas palustris* and *Methylobacterium organophilum*. The second

group synthesise PHAs alongside growth in the cultivation medium. Bacteria in this group include *Alcaligenes latus* and recombinant *E. coli* containing the PHA biosynthetic genes.

The genera *Bacillus* being identified as one of the first Gram-positive bacteria capable of PHA production, offers several advantages for PHA fermentation studies. These include chemoorganotrophic features, secretion of a large number of amylases and proteases. These features of *Bacillus* spp. explore the possibility of utilizing various agricultural raw materials as a carbon source for production of different metabolites. It is evident from literature that biomedical applications of PHAs frequently use commercially available polymers (Williams and Martin, 2002). However, literature reports show that the level of endotoxin in the commercial PHAs can reach up to 120 U/g (Lee *et al.*, 1999; Williams *et al.*, 1999). This can possibly be as a result of microbial cell debris containing lipopolysaccharides capable of causing negative reactions on cells in the *in vitro* systems and immunogenic reactions *in vivo* (Dufrene *et al.*, 1998; Rouxhet *et al.*, 2002). Lipopolysaccharides are found in the outer membranes of Gram-negative bacteria and play a major role in maintaining the structural integrity of bacteria and protection against certain type of chemical attacks. However, Gram positive bacteria, including the genus *Bacillus*, do not produce lipopolysaccharides, otherwise known as lipoglycans and therefore represent a preferred source of the polymer, especially for applications in medicine. Further, *Bacillus* represents a model system for the heterologous expression of foreign genes associated with PHA production and several fine chemicals too (they are capable of producing 20-25 g/L of extracellular enzymes of industrial importance) (Law *et al.*, 2003; Schallmey *et al.*, 2004). There has been a lot of work on the use of *Bacillus* for the production of a range of different PHAs by utilizing different carbon sources. These include incorporation of the tercopolymer of 3HB, 3HV, and 3HHx (3-hydroxy-hexanoate) utilizing β -caprolactone (Labuzek and Radecka, 2001), P(3HB-co-3HV) from glucose (Tajima *et al.*, 2003), P(3HB-co-3HV) from mahua flowers (Anil-Kumar *et al.*, 2007), from sucrose (Shamala *et al.*, 2003), and P(3HB) from soy molasses (Full *et al.*, 2006), sugarcane molasses, date syrup (Omar *et al.*, 2001) and corn steep liquor (Gouda *et al.*, 2001). The co-polymer synthesis from structurally unrelated carbon sources suggests that *Bacillus* has the potential for production of the PHA co-polymers using different substrates (Valappil *et al.*, 2007). However, in several cases the yield of PHA was considerably low on co-feeding with valerate (Valappil *et al.*, 2007).

Cupriavidus necator has been widely studied because of its potential in producing significant amount of P(3HB) from simple carbon substrates such as glucose, lactic acid and acetic acid (Ryu *et al.*, 1997). Also, olive oil, corn oil and palm oil have been used to produce approximately 80% dcw P(3HB) of dry cell mass from the organism (Futui and Doi, 1998). Poly(3-hydroxybutyrate-co-3-hydroxyvalerate), P(3HB-co-3HV), has been produced from the organism using odd numbered n-alkanoates as a carbon source (Futui and Doi, 1998) while terpolymers of poly(3-hydroxybutyrate-co-3-hydroxyvalerate-co-3-hydroxyhexanoate), P(3HB-co-3HV-co-3HHx) have been successfully produced using odd numbered alkanolic acids and a recombinant strain of *Cupriavidus necator* harbouring the PHA synthase gene of *Aeromonas caviae* (Futui, 1997).

Methylobacterium organophilum produces PHAs from the cheap carbon source, methanol. PHA recovery from the organism has been successfully carried out using a simple, efficient and environmentally friendly method. This method involves high-pressure homogenization in the presence of 5% (w/v) SDS detergent followed by centrifugation (Kim *et al.*, 1996). However, PHA production from glucose (53% dcw) and sucrose (40% dcw) gave better yield than when methanol (11% dcw) was utilised as the carbon source (Kim *et al.*, 1996).

Rhodopseudomonas palustris, a non-sulphur photosynthetic bacterium, has been extensively studied for its potential in producing P(3HB) and P(3HB-co-3HV) using different carbon and nitrogen sources. *Rhodospirillum* and *Rhodobacter* are two other non-sulphur photosynthetic bacterial genera that have been found to be particularly versatile in the production of the copolymer, P(3HB-co-3HV), using various carbon sources such as malate, acetic acid and n-alkanoic acid (Carlozzi and Sacchi, 2001).

A. latus is another organism that produces PHAs using carbon sources such as glucose, molasses and sucrose with good yields. PHA accumulation of approximately 88% dcw has been achieved after 8 hours of nitrogen limitation and 20 hours of total cultivation time from *A. latus* ATCC 29713, using sucrose as the sole carbon source (Wang and Lee, 1997). Investigations with different nitrogen sources have proven that *A. latus* are able to grow and produce PHAs with ammonium chloride and ammonium sulphate as nitrogen sources. However, ammonium nitrate and urea could not support PHA production in the organism (Grothe *et al.*, 1999). *A. latus* requires a temperature of 35°C, which makes P(3HB)

production from the organism economical by lowering the demand for cooling during fermentation. Interestingly, *A. latus* DSM 1123 requires only 5 hours in order to achieve an intracellular PHA concentration of 80% of dry cell weight, when grown on sucrose as the sole carbon source, a significant observation from the commercial production point of view. Also, PHA production in *A. latus* is growth associated; however, by employing nutrient limitation, PHA productivity in *A. latus* can be further enhanced. Optimum biomass and PHA accumulation can also be enhanced by feeding the organism with enriched medium.

Among the *Pseudomonas* species, *P. oleovorans* NRRL B-778 has been shown to accumulate mixtures of P(3HB) and mcl-PHAs such as P(3HO), when fed with mixtures of glucose and octanoic acid, while copolymers of P(3HB-co-3HV) were produced during growth with nonanoic acid (Ashby *et al.*, 2002). It has been observed that while media containing *n*-alkanoic acids, specifically from formate to decanoate as carbon sources, were able to support the growth of *P. oleovorans*, only hexanoate and higher *n*-alkanoic acids were able to support PHA accumulation in the organism (Brandl *et al.*, 1982). On the other hand, *Pseudomonas stutzeri* 1317 was found to synthesise a variety of PHAs when grown on glucose and fatty acids, either as separate carbon sources or mixtures of carbon sources in the production media (Guo-Qiang *et al.*, 2001). As expected, the monomeric structures of the PHAs produced by the organism are dependent on the structure of the fatty acids used as carbon sources. Therefore, the monomer percentage content in the PHA produced was adjusted by regulating the ratios of fatty acids fed to *P. stutzeri* 1317. Generally, *Pseudomonas putida* efficiently incorporates monomers in the range of C₈ - C₁₀. Long chain fatty acids such as oleate (C₁₈) are less efficiently utilised because of the need for the β -oxidation pathway leading to the production of C₈ and C₁₀ monomers that can then be incorporated into the PHA. Polymer yield per cell is often very high when medium-chain fatty acids are employed as sources of carbon. But, medium-chain fatty acids are very expensive and lead to an increase in the production cost. Table 1.4 provides a summary of different strains of *Bacillus* and the amounts of PHAs accumulated in them.

Table 1.4 The accumulation of PHAs in *Bacillus spp.*

Bacteria <i>(Bacillus spp)</i>	PHA content (% dcw)	Monomeric Units	Carbon Source	Reference
<i>Bacillus sp. JMa 5</i>	35.0	3HB	Molasses	Wu <i>et al.</i> , 2001
<i>B. circulans DMS 1529</i>	43.7	3HB	Acetate & 3-hydroxybutyrate	Chen <i>et al.</i> , 1991
	6.80	3HB, 3HV	Propionate	Chen <i>et al.</i> , 1991
<i>B. sphaericus</i>	30.2	3HB	Sucrose	Shamala <i>et al.</i> , 2003
<i>B. sphaericus DSM 28</i>	4.50	3HB, 3HV	Valerate	Chen <i>et al.</i> , 1991
<i>B. brevis</i>	32.1	3HB	Sucrose	Shamala <i>et al.</i> , 2003
<i>B. licheniformis DSM394</i>	25.8	3HB	Acetate & 3-hydroxybutyrate	Chen <i>et al.</i> , 1991
	6.20	3HB, 3HV	Propionate	Chen <i>et al.</i> , 1991
<i>B. amyloliquefaciens DSM7</i>	17.0	3HB	Acetate & 3-hydroxybutyrate	Chen <i>et al.</i> , 1991
	5.10	3HB, 3HV	Propionate	Chen <i>et al.</i> , 1991
<i>B. laterosporus DSM335</i>	29.5	3HB	Acetate & Propionate	Chen <i>et al.</i> , 1991
	5.00	3HB, 3HV	Propionate	Chen <i>et al.</i> , 1991
<i>B. macerans DSM7068</i>	40.5	3HB	Acetate & 3-hydroxybutyrate	Chen <i>et al.</i> , 1991
	4.70	3HB, 3HV	Propionate	Chen <i>et al.</i> , 1991
<i>B. subtilis DSM10</i>	33.5	3HB	Acetate & 3-hydroxybutyrate	Chen <i>et al.</i> , 1991
	6.60	3HB, 3HV	Valerate	Chen <i>et al.</i> , 1991
<i>B. thuringiensis DSM2046</i>	47.6	3HB	Acetate & 3-hydroxybutyrate	Chen <i>et al.</i> , 1991
	7.20	3HB, 3HV	Propionate	Chen <i>et al.</i> , 1991
<i>B. mycoides DSM2048</i>	44.7	3HB	Acetate & 3-hydroxybutyrate	Chen <i>et al.</i> , 1991
	7.50	3HB, 3HV	Propionate	Chen <i>et al.</i> , 1991
<i>B. mycoides RLJB0-107</i>	69.4	3HB	Sucrose	Borah <i>et al.</i> , 2002

Table 1.4 continued

<i>B. megaterium</i> DSM90	47.2	3HB	Acetate & 3-hydroxybutyrate	Chen <i>et al.</i> , 1991
	8.20	3HB, 3HV	Propionate	Chen <i>et al.</i> , 1991
<i>B. cereus</i> DMS31	41.4	3HB	Acetate & 3-hydroxybutyrate	Chen <i>et al.</i> , 1991
	7.30	3HB, 3HV	Propionate	Chen <i>et al.</i> , 1991
<i>B. cereus</i> UW85	8.90	3HB, 3HV, 6HHx	β -caprolactone & Glucose	Labuzek and Radeck, 2001
<i>Bacillus</i> sp. INT005	18.8	3HB, 3HV	Valerate	Tajima <i>et al.</i> 2003
	32.9	3HB, 3HHx	Hexanoate or Glucose	
	96.5	3HB, 4HB, 3HHx	4-hydroxybutyrate	
	97.3	3HB, 3HHx, 6HHx	ϵ -caprolactone	
<i>B. cereus</i> ATCC14579	2.20	3HB, 3HHx	Hexanoate	Caballero <i>et al.</i> , 1995

1.1.1.5.2 PHA production using recombinant bacteria

Recombinant organisms have been developed for increased PHA production. *E. coli* has been one of the most favoured hosts since growth related PHA production is possible. Also, the ability to grow fast, to achieve high cell density from several inexpensive carbon sources e.g. molasses and whey and high yield of the polymer are other positive features (Hahn, 1995; Fidler and Dennis, 1992). Hence, in addition, with the vast knowledge of *E. coli* genetics and its metabolic pathways, *E. coli* is expected to continue to play a significant part in the commercial production of PHAs.

Recombinant *E. coli* harbouring the *Cupriavidus necator* PHA biosynthetic genes were able to accumulate P(3HB) with an yield of 80-90% dcw in fed-batch cultivation while a P(3HB) content of 76% dcw was obtained in a pH-stat fed-batch culture (Kim, 1992). Liu and co-workers, achieved a P(3HB) concentration of 80% dcw when recombinant *E. coli* containing the *Cupriavidus necator* PHA biosynthetic genes was grown on molasses (a cheap carbon source) (Liu *et al.*, 1998). Studies have also proven that recombinant *E. coli* with the *Aeromonas hydrophila* biosynthetic genes (*orf1*) produced terpolymers of P(3-

hydroxybutyrate-co-3-hydroxyvalerate-co-3-hydroxyhexanoate) using decanoate and odd-chain fatty acids as carbon sources (Park *et al.*, 2001). Table 1.5 shows a comparison of the various examples of PHA production in *E. coli*.

Table 1.5 Comparison of PHA production in recombinant *E. coli*

Strain	Culture mode	Source of PHA biosynthetic genes	Type of PHA	Major substrate	Cell conc. (g L ⁻¹)	PHA content (%)	Productivity (g L ⁻¹ h ⁻¹)	Reference
<i>Escherichia coli</i> XL1-Blue	Fed-batch	<i>Alcaligenes latus</i>	P(3HB)	Glucose	194.1	73	4.63	De Groot <i>et al.</i> , 1997
<i>Escherichia coli</i> HMS174	Fed-batch	<i>Cupriavidus necator</i>	P(3HB)	Molasses	39.5	80	1	Chu <i>et al.</i> , 1997
<i>Escherichia coli</i> GCSC4401	Cell recycle fed-batch	<i>Alcaligenes latus</i>	P(3HB)	Whey (lactose)	194	87	4.6	Fine <i>et al.</i> , 1994
<i>Escherichia coli</i> XL1-Blue	Fed-batch	<i>Alcaligenes latus</i>	P(3HB-co-3HV)	Glucose propanoic acid; oleic acid supplementation	203.1	78.2	2.88	Fine <i>et al.</i> , 1994
<i>Escherichia coli</i> XL1-Blue	Fed-batch	<i>Cupriavidus necator</i> , <i>Clostridium kluyveri</i>	P(4HB)	Glucose, 4-hydroxybutyrate	12.6	36	0.07	Futui <i>et al.</i> , 1997
<i>Escherichia coli</i> RS3097	Fed-batch	<i>Pseudomonas aeruginosa</i>	PHAMCL	Decanoic acid	2.6	38	0.06	Ramada <i>et al.</i> , 2009

(Adopted from Li *et al.*, 2007)

1.1.1.5.3 PHA production using mixed or co-culture systems

Mixed or co-culture systems have also been shown to be effective for PHA production (Tanaka *et al.*, 1995). *Cupriavidus necator* is unable to metabolise sugars, molasses, whey or starchy waste. Consequently, mixed cultures of lactic acid producing bacteria such as

Lactobacillus lactis, *Propionibacterium* and *Lactobacillus delbruecki* and *Cupriavidus necator* (Tanaka *et al.*, 1995; Tohyama, 2002; Patnaik, 2005), have been used in a single-stage fermentation system. The original sugar substrates were converted into lactic acid first, which was later taken up by *Cupriavidus necator* to produce PHAs (Patnaik, 2005). In a two-stage system, xylose was first converted to lactate using *Lacticoccus lactis*. The lactate was further converted to P(3HB) by *Cupriavidus necator*. In another investigation, *Lactobacillus delbrueckii* was used to convert glucose to lactate which was later converted to P(3HB) by *Cupriavidus necator* (Tohyama and Shimizu, 1999; Tohyama, 2000).

Furthermore, the use of open mixed cultures, such as activated sludge has been investigated by many groups. By employing anaerobic conditions, Ueno and co-workers showed that 17% sludge dry weight of PHA can be produced from activated sludge (Ueno, 1993). PHA accumulation was further enhanced to 36% sludge dry weight by employing aerobic conditions. Satoh and his group further demonstrated that the use of anaerobic-aerobic sludge system could enhance the formation of 3-hydroxyvalerate-rich PHA while at the same time yield energy for the waste treatment (Satoh *et al.*, 1992). The group was able to achieve a PHA content of 20% sludge dry weight under anaerobic condition while the PHA content was further increased to 33% sludge dry weight by employing aerobic conditions. PHA accumulation was further enhanced by introduction of a microaerophilic-aerobic process (oxygen limitation). To induce microaerophilic-aerobic conditions, limited amount of oxygen was introduced into the anaerobic zone of the anaerobic-aerobic system. A PHA content of 62% sludge dry weight was produced using an acclimatised microaerophilic-aerobic process. From the results of these investigations, it was concluded that the use of open cultures can contribute to a decrease in the cost of production and hence, increase the market potential of PHAs (Patnaik, 2005). Liu and co-workers have also shown using undefined media and a mixed culture that the cost of production of PHAs can be further reduced by using activated sludge under non-aseptic condition. Their investigation resulted in the reduction of the production cost of PHA by 30~40% (Liu *et al.*, 2008).

1.1.1.6 Sustainable PHA production using inexpensive carbon sources.

There has been a considerable interest in the use of inexpensive cheap carbon substrates for PHA production since the cost of the carbon source accounts for almost 50% of the production costs (Kim, 2000). Hence, agricultural or food industry waste materials are being explored as cheap sources of carbon and nitrogen. Recycling of wastes generated from agriculture based industries for PHA production is not only crucial for reduction in production costs of the polymer but also for waste management. Process economics have revealed that the use of inexpensive and renewable carbon substrates as PHA carbon feedstock can contribute to as much as 40-50% reduction in the overall production cost (Marangoni *et al.*, 2002). The various cheap carbon sources that have been evaluated for PHA production include whey, wastewater from olive mills, molasses, corn steep liquor, starchy wastewater and palm oil mill effluent (Marangoni *et al.*, 2002; Lapointe *et al.*, 2002; Pozo *et al.*, 2002).

1.1.1.6.1 Use of whey as a cheap carbon source for PHA production

Recently, wastes produced by food processing industries are being developed as biorefinery feedstock for value-added-products (Di Donato, 2009). Whey is an example of such a food industry waste. It is the main by-product from the manufacture of cheese and casein. It represents about 80% - 90% of the volume of processed milk. Only about half of the whey produced is converted into useful products such as human and animal feed while the rest is disposed as waste causing environmental problems due to its high oxygen demand. Koller and co-workers have found that hydrolysed whey can be used by *Pseudomonas hydrogenovora* to accumulate up to 5 g/L biomass containing 1.27 g/L and 12% dcw P(3HB) monomers (Koller *et al.*, 2008). Wong and Lee evaluated PHA accumulation by a recombinant *Escherichia coli* strain GCSC 6576, harbouring a high copy plasmid containing *Cupriavidus necator* genes for PHA synthesis and the *E. coli ftsZ* gene for cell division, on whey powder as the main carbon source. They used whey powder in a pH-stat fed-batch fermentation and obtained a dry cell weight and P(3HB) concentration of 109 g/L and 50 g/L respectively in 47 hours. Further, with the same organism and using pH-stat fed-batch culture and concentrated whey solution containing 210 g/L lactose as nutrient feed, a dry cell

weight of 87 g/L and P(3HB) concentration of 69 g/L containing 87% dcw P(3HB) were achieved by Wong and Lee, 1998. Nikel and colleagues successfully produced 70.1 g/L biomass containing 51.1 g/L P(3HB) and 72.9 % dcw of P(3HB) in a pH controlled fed-batch fermentation at pH of 7.20 with whey and corn steep liquor as carbon and nitrogen sources respectively. The organism evaluated was a recombinant strain of *E. coli* K24K harbouring the *phaC* biosynthetic genes from *Azotobacter* sp. strain FA8 (Nikel *et al.*, 2006). P(3HB) was also efficiently produced when a recombinant *E. coli* strain (K24K) harbouring the *phaC* gene from *Azotobacter* sp. FA8 was grown aerobically in fed-batch cultures. The medium used was a semi synthetic medium supplemented with concentrated and deproteinated whey solution containing 25% (w/v) lactose. A total biomass and P(3HB) content of 58.2 g/L and 46.9% dcw respectively, were achieved. The successful use of whey as a carbon source for PHA production is certainly a step forward towards the reduction of the cost of PHA production.

1.1.1.6.2 Use of wheat bran as cheap carbon sources for PHA production

Wheat is a worldwide cultivated grass. In 2007, world production of wheat was estimated at 607 million tons, making it the third most-produced cereal after maize (784 millions) and rice (651 million tons). The ranking of top five world producers of wheat in 2009 were European Union (138.6 million tons), China (111 million tons), India (77.6 million tons), United States (55.1 million tons) and Russia (25.9 million tons) (Nikel *et al.*, 2006). Bran is the hard outer layer of grain and consists of combined aleurone and pericarp. Along with germ, bran is an integral part of whole wheat grain. It is a by-product of milling in the production of refined grain. Wheat bran is particularly rich in dietary fiber (50%), carbohydrates (15%), proteins (14%) and fats (6%) and significant quantities of vitamins and dietary minerals (FAO report, 2009). Although, bran is unlikely to create any negative environmental impact on the site of disposal, there is always reduction in oxygen concentration at the site of disposal of either wheat or rice bran. This is usually due to accumulation of microorganisms degrading the waste.

Many researchers have evaluated the used of wheat bran as a good accessible carbon feedstock in the production of biodegradable polyhydroxyalkanoates. In shaken flask study,

Van-Thuoc *et al.*, successfully grew *Halomonas boliviensis* LC1 on wheat bran hydrolysate to produce a total biomass of 3.19 g/L, a P(3HB) concentration of 1.08 g/L and a P(3HB) content of 33.8% dcw (Van-Thuoc *et al.*, 2008).

1.1.1.6.3 Use of Rice bran as a carbon source for PHA production

The world's estimated highest rice producers for the fiscal year 2009 were: China (193 million tons), India (148.4 million tons) and Bangladesh (46.5 millions) (Rice policy-IRRI report, 2009). Because of this high amount of production, there is usually a corresponding high amount of waste in the form of rice bran and its associated environmental impact. However, many researchers have shown that this can be transformed into environmentally friendly PHA. Huang *et al.*, have successfully used inexpensive extruded rice bran and corn starch in PHA production from *Haloferax mediterranei* (Huang *et al.*, 2006). A total biomass, PHA accumulation and PHA content of 140 g/L, 77.8 g/L and 55.6% dcw respectively were achieved from *Haloferax mediterranei* by employing extruded rice and extruded corn starch in the ratio of 1:8 in a pH-stat fed-batch fermentation.

1.1.1.6.4 Use of starch as cheap carbon sources for PHA production

Starch is readily available in large amount from plant sources and has been recently utilized as a carbon feedstock in PHA production (Huang *et al.*, 2006; Chen *et al.*, 2006). Because of its complex nature, the use of starch as a carbon source in PHA production requires enzymatic hydrolysis (Halami, 2008). Unfortunately, not all organisms can produce α -amylase, the enzyme responsible for the hydrolysis of starch. Hence, in order to be able to utilise starch, an exogenous source of α -amylase such as glycanases is required by these organisms (Huang *et al.*, 2006).

Chen and co-workers have successfully produced P(3HB-co-3HV) from *Haloferax mediterranei* with enzymatic extruded starch in a pH-stat with an initial pH of 7.0 in a fed-batch fermentation. A total biomass of 1.14 g/L with P(3HB-co-3HV) concentration and content of 0.84 g/L and 43% dcw respectively were accumulated by *Haloferax mediterranei*

when an extruded starch/yeast extract solution feed was maintained in the ratio of 1/1.7 g/g (Chen *et al.*, 2006). Furthermore, Quillaguaman *et al.*, achieved accumulation of 56% dcw P(3HB) and 1.2 g/L biomass in shaken flask cultures of *Halomonas boliviensis* when starch hydrolysate was used as the sole carbon source. The group observed that the amount of P(3HB) accumulated reduced to 35% dcw when the organism was grown in batch fermentation with optimum oxygen supply (Quillaguaman *et al.*, 2005). With reduced oxygen supply below optimum requirement for growth, P(3HB) yield was increased to 41% dcw. Thus, oxygen limitation during active cell growth enhances P(3HB) production in *Halomonas boliviensis*, but has adverse effect on biomass accumulations. *Bacillus cereus* CFR06 has also proven to be a good candidate for the utilization of soluble starch as the main carbon source in PHA production with an accumulation of 48% dcw PHA and 1g/L biomass in batch fermentation (Halami, 2008). Haas *et al.*, have observed that saccharified waste potato starch can be used as a viable alternative carbon source in high cell density P(3HB) production. A total biomass of 179 g/L and P(3HB) concentration of 94 g/L containing 55% dcw of P(3HB) were achieved in a fed-batch fermentation with *Ralstonia eutropha* NCIM 5149 (Haas *et al.*, 2008). The saccharification of starch helped to hydrolyze the starch to more acceptable simple sugars which were readily available to the organism.

1.1.1.6.5 Use of molasses as cheap carbon sources for PHA production

Molasses is a viscous by-product of the processing of sugar cane or sugar beets into sugar. There are two types of molasses, sulphured molasses and unsulphured molasses. Sulphured molasses are formed during the extraction of sugar from green unripe sugar cane when sulphur dioxide is added as a preservative during the sugar extraction process. Unsulphured molasses is derived from mature sugar cane which does not require treatment with sulphur. Cane molasses contains significant amount of vitamins and minerals and are a cheap source of calcium, magnesium, potassium and iron which are regarded as impurities in raw sugar. The sugar content of beet molasses is approximately 50% where sucrose is the predominant sugar, along with a significant amount of glucose and fructose. The non sugar components include calcium, potassium, oxalate and chloride ions. Also, beet molasses contain limited

amount of biotin (vitamin H or B₇) which is vital for bacterial cell growth. The limitation in biotin content can act as an inducer for PHA production.

Molasses are unpalatable and are a low value product. Hence, it is mainly used as an additive to animal feed supplement or as fermentation feedstock especially in yeast propagation (Wang *et al.*, 1979). Accumulation of molasses during sugar processing results in a negative environmental impact. Furthermore, about 1L fusel oil is produced per 100 kg of processed molasses, the disposal of which is a problem. Thus, the use of molasses as carbon feedstock for PHA production is a good alternative for the disposal of molasses as well as bioconversion of waste to an economically valuable product.

A reasonable amount of investigation has been carried out into the utilization of molasses for PHA production. Albuquerque *et al.*, have observed the production of 30% dcw P(3HB-co-3HV) with a highest cell concentration of 3.5 g/L, from a mixed bacterial culture using sugar cane molasses. A sequencing batch reactor (SBR) operated under aerobic dynamic feeding (ADF) (feast and famine) was used (Albuquerque *et al.*, 2007). Also, cane molasses was found to be an excellent substrate for the growth of *Bacillus sp* COLI/A6 and for subsequent PHA production by Santimano *et al.* A total biomass and PHA content of 6 g/L and 54.68% dcw respectively were achieved using cane molasses as the main carbon source in the production medium in batch fermentation (Santimano *et al.* 2009). Omar and co-workers have also observed successful production of P(3HB) by *Bacillus megaterium* from beet molasses (Omar *et al.*, 2001). A cell concentration of 3 g/L and P(3HB) content of 50% dcw were achieved when 5% (w/v) of beet molasses was supplemented in the production medium. Further, Solaiman *et al.*, successfully utilised soy molasses for the production of medium-chain-length PHA using *Pseudomonas corrugate*. A cell density of 3.4 g/L and a total PHA content of 5-17% dcw were achieved when 5% (w/v) soy molasses was added to the E-medium. The mcl-PHA produced was poly(3-hydroxydodecanoate-co-3-hydroxyoctanoate-co-3-hydroxytetradecenoate), P(3HDD-3HO-3HTDE) (Solaiman *et al.*, 2006).

1.1.1.6.6 The use of waste vegetable oil and plant oil as cheap carbon sources for PHA production

Production of waste vegetable oil has increased as a result of industrial activities and development of alternative sources of energy. It is estimated that more than 11 billion litres of waste vegetable oil is being produced annually in USA, mainly from industrial deep fryers in potato processing plants, snack food factories and fast food restaurants. While most of the waste vegetable oil produced does not have immediate toxic effects on wildlife, spills are potentially dangerous due to the physical damage caused to the ecosystem. Improper disposal of the waste vegetable oil leads to an increase in the biological oxygen demand (BOD) and chemical oxygen demand (COD), which in turn leads to the deoxygenation of water, an infiltration into soil sediments and aquifer contamination. These waste vegetable oils can be utilised as inexpensive carbon sources for PHA production. This will not only help in converting waste to a useful material but also aid in the waste disposal management of the waste vegetable oil.

Bhubalan *et al.*, have demonstrated that *Cupriavidus necator* can accumulate biomass and P(3HB) up to 7.9 g/L and 79% dcw respectively when grown on palm kernel oil (Bhubalan *et al.*, 2008). Also, Lee and colleagues have observed the production of 80% dcw P(3HB-co-3HV) by *Cupriavidus necator* H16 when grown on plant oils such as palm kernel oil. Simon-Colin and co-workers in their work achieved production of 63% dcw of the copolymer, P(3HO-co-3HD-co-3HDD) using *P. guezenei biovar tikehau*, when coprah oil was used as the main carbon substrate (Simon-Colin, 2008). Also, Fukui and Doi found that the wild type strain of *Ralstonia metallidurans* (*Alcaligenes eutrophus* H16) was able to accumulate 79% dcw, 81% dcw, 79% dcw and 82% dcw of P(3HB) on olive oil, corn oil, palm oil and oleic acid respectively. Also, a recombinant strain of *Ralstonia metallidurans* (a PHA-negative mutant), harbouring the *Aeromonas caviae* PHA synthase gene, *phaC_{AC}*, was shown to accumulate high amounts of the copolymer P(3HB-co-3HHx) with different %mol ratios of HHx (Fukui and Doi, 1998).

Although there are some good producers of PHAs, on an average the PHA accumulations are still low. Hence, more improvement is required to enhance growth and PHA production using plant oils in some organisms. For example, the growth of *Pseudomonas putida* KT2442 strain

KTT2 on olive oil waste water (alpechin) only produces a maximum PHA concentration and PHA content of 0.1 g/L and 3.59% dcw respectively with a corresponding biomass accumulation of 4.2 g/L. With another strain of *Pseudomonas putida* KT2442 (strain KT1) only 1.3 g/L of biomass and PHA concentration and content of 0.02 g/L and 1.6% dcw respectively, were achieved when grown on olive oil waste water (Ribera, 2001). Thus, more research on the development of superior vegetable oil-utilising strains and improved fermentation technology for the utilization of waste vegetable oils and other plant oils is needed to further enhance growth and PHA accumulation using these substrates.

1.1.1.6.7 Use of wastewater as cheap material for PHA production

Wastewater comprises of liquid waste discharged by domestic residences, commercial properties, and/or agricultural activities. It can drain directly into major watersheds with minimal or no treatment leading to serious impacts on the quality of the environment as well as health of the people. Wastewater contains a lot of pathogens which can cause a variety of illness. Also, some chemicals found in wastewater can pose health risks even at very low concentrations and can remain as a threat for a long period of time because of bioaccumulations in animal or human tissue.

Wastewater can be converted to useful material during treatment to remove the organic pollutants. Apart from gases like methane and hydrogen, PHA production can be achieved by the mixed bacterial culture. Cho *et al.*, successfully achieved the accumulation of 37% dcw P(3HB-co-3HV) and a cell concentration of 1.17 g/L using *Azotobacter vinelandii* UWD when grown on undiluted swine wastewater. A twofold dilution of swine wastewater with distilled water improved biomass accumulation to 2.02 g/L but reduced the amount of P(3HB-co-3HV) accumulation to 34% dcw. Further dilution of the swine wastewater resulted in decreased cell growth and PHA accumulation. Supplementation of the swine wastewater with 20 g/L glucose led to cell growth and P(3HB-co-3HV) production to be 4.6 and 8.6 times higher respectively, confirming that PHA production using swine wastewater can be increased by supplementing swine wastewater with carbon rich material such as food processing waste (Choi and Lee, 1999). Bengtsson and Werker successfully produced P(3HB-co-3HV) with an yield of 48.3% dcw from activated sludge, using paper mill

wastewater (Bengtsson *et al.*, 2007). Yan and colleagues achieved a PHA yield of 43% dcw of suspended solids using pulp and paper wastewater sludge, when acetate was used as an additional carbon substrate supplement (Yan *et al.*, 2006).

1.1.1.6.8 Use of CO₂ and H₂ as cheap carbon substrates for PHA production

Extensive research has begun on the use of CO₂ as ultimate feedstock for PHA production. Khanna and Srivastava have demonstrated that *Cupriavidus necator* has the ability to accumulate a high amount of P(3HB) when CO₂ was employed as a carbon source for PHA production (Khanna and Srivastava, 2005). In the absence of light energy, it has been proven that *Cupriavidus necator* can assimilate CO₂ but with the oxidation of hydrogen to produce PHA (Ishizaki *et al.*, 2001). *Cupriavidus necator* being a chemolithoautotrophic bacterium is able to grow using a mixture of hydrogen, oxygen and carbon dioxide as substrates for biomass and polymer accumulation, in a recycle-gas, closed-circuit culture system. The maximum P(3HB) concentration and yield achieved using *Cupriavidus necator* and CO₂ as carbon substrate were 56.4 g/L and 81.4% dcw respectively, the highest quoted value among the chemolithoautotrophic bacteria. *Cynobacterium synecoccus* MA19 has also been shown by Nishioka *et al.*, to be able to accumulate up to 55% dcw of P(3HB) and reach a cell density of 4.4 g/L under optimized conditions, when grown on CO₂ as the carbon substrate (Nishioka *et al.*, 2001).

1.1.1.6.9 Use of Methanol as cheap substrate for PHA production

Methanol is another readily available cheap carbon source that is utilised in the production of PHAs. It is a non-food substrate produced by the anaerobic digestion of woody materials and organic substrates. *Methylobacterium sp* GW2 has been found to readily utilise methanol for polymer production with a maximum P(3HB) yield of 40% dcw. The P(3HB) accumulation in the organism is growth associated thereby removing the need for a two-stage fermentation (Yezza *et al.*, 2006). Further, Bourque *et al.* used *Methylobacterium extorquens* to produce the homopolymer P(3HB) from methanol using a 2-L fed-batch fermentation. Using a mixture of methanol and valerate, the organism was able to accumulate copolymer of P(3HB-

co-20-mol% 3HV). A total biomass of 9 g/L and PHB content of 30-33% dcw were achieved (Bourque *et al.* 1992).

1.1.1.7 Production of PHAs in bioreactors

Although a large number of PHAs have been produced, only some of these have been produced in large amounts including P(3HB), P(3HB-co-3HV), P(3HV), P(4HB), P(3HB-co-3HHx) and P(3HHx-co-3HO). Many physiologically and taxonomically different bacteria possess the ability to produce large amount of PHAs, however, the full potential of these bacteria, in terms of PHA production, have not yet been fully harnessed. To increase PHA accumulation by these organisms, production strategies are being optimised to encourage large amounts of polymer accumulation by the organisms within a shorter time span. Also, the substrate ranges provided to the bacteria are being widened, exploring the utilization of novel carbon sources available from varied sources in large amounts and at very low cost. Varied types of fermentations have been used for the optimisation of PHA yield. These will be discussed in detail.

1.1.1.7.1 Batch Fermentation

Batch fermentation has been used in the production of short chain length PHAs from bacteria such as *Bacillus cereus* SPV. Valappil and co-workers produced P(3HB) using this organism in a batch fermentation with the Kannan and Rehacek medium and glucose as the primary carbon source (Valappil *et al.*, 2007). The initial pH of the medium was 6.8 and was not controlled during the fermentation. A maximum P(3HB) concentration of 29% dcw was obtained.

Batch cultures have also been employed in the investigation and optimisation of functionalized medium-chain-length polyhydroxyalkanoates (mcl-PHAs). Hartmann *et al.*, 2005 investigated the batch production of tailored olefinic mcl-PHA production from mixtures of octanoic acid (58 mol %) and 10-undecenoic acid (42 mol %) using *Pseudomonas putida* GPo1 (ATCC 29347). The molar fraction of each monomer in the mcl-

PHAs produced varied in the polymer produced during exponential growth phase as compared to that produced during stationary phase. This indicated different utilisation kinetics for the two carbon substrates used (Zinn *et al.*, 2004). The organism was found to accumulate more PHA during the initiation of nitrogen limitation. Preusting and co-workers observed that *Pseudomonas oleovorans* loses its viability after the onset of nitrogen limitation in batch cultures with a resultant death of the cells during the PHA accumulation stage (Preusting *et al.*, 1993). Thus, batch fermentation is not ideal for the production of PHAs, especially from organisms that cannot grow in nitrogen limiting conditions.

1.1.1.7.2 Fed-batch Cultivation

Fed-batch fermentation is one of the best methods of achieving a high cell density containing the highest possible amount of PHA. However, cell growth and PHA accumulation need to be balanced to avoid incomplete PHA accumulation or premature termination of the fermentation at low cell concentration. For instance, by using two different feeding strategies (DO-stat and nitrogen limitation) in the fed-batch production of PHA from *Alcaligenes latus*, a maximum specific growth rate of 0.265 h^{-1} was achieved compared to 0.075 h^{-1} achieved during batch fermentation with the same organism. A DO-stat feeding strategy was employed during the active growth phase without any nitrogen limitation. Nitrogen limitation was introduced later to enhance PHA production (Katrırcıođlu, 2003). Previously, Valappil and co-workers had observed a cell concentration and P(3HB) content of 3.0 g/L and 38.0 % dcw when *Bacillus cereus* SPV was grown in a fed-batch fermentation using a semi complex medium (Kannan and Rehacek medium) and glucose as the primary carbon source (Valappil *et al.*, 2007).

Although, fed-batch fermentation usually enhances high cell density and PHA accumulation, single stage fed-batch fermentations that are nitrogen limited do not always results in large PHA accumulation in some organisms. Sun *et al.*, found that *Pseudomonas putida* KT2440 could only accumulate biomass of 46.1 g/L, 27% dcw mcl-PHA and productivity of $1.01 \text{ g l}^{-1} \text{ h}^{-1}$ when nitrogen limiting conditions were employed in a fed-batch mode using nonanoic acid as the sole carbon source (Sun *et al.*, 2007). However, high biomass and PHA accumulation could be enhanced by regulating the supply of nutrients to the organism.

Supplying nonanoic acid to the organism at a specific growth rate of $\mu=0.15 \text{ h}^{-1}$ during exponential growth improved both cell concentration (70 g/L) and PHA content (75% dcw). Hence, the optimal strategy for fed-batch fermentation is to feed the growth limiting substrates at the same rate as the rate of substrate utilisation by the organism. This ensures that by-products that are generally related to the presence of high concentrations of the substrate are avoided by limiting its quantity to the amount that is required for the production of the product of interest. High concentrations of the substrate can lead to the production of more than one product of interest, thus, reducing the efficacy of the carbon flux towards PHA production.

Table 1.6 PHA production in fed-batch cultivation reported for wild strain

Strains	PHAs	Carbon Source	Culture Time (h)	DCW (g/L)	PHA Content (wt %)	PHA Con. (g/L)	Reference
<i>A.latus</i>	P(3HB)	Sucrose	18	143	50	71.5	Yamane <i>et al.</i> , 1996
<i>A.latus</i>	P(3HB)	Sucrose	20	112	88	98.7	Wang and lee 1997
<i>B.cereus SPV</i>	P(3HB)	Sucrose	20	112	88	8.34	This work
<i>B.cereus SPV</i>	P(3HB)	Sucrose	17	4.9	50.5	2.48	This work
<i>B.cereus SPV</i>	P(3HB)	Glucose	72	3.0	38	0.89	Valappil <i>et al.</i> , 2007
<i>C.necator</i>	P(3HB)	Glucose	50	164	76	121	Kim <i>et al.</i> , 1994
<i>C.necator</i>	P(3HB-co-3HV)	Glucose + Propionic acid	46	158	74	117	Kim <i>et al.</i> , 1994
<i>C.necator</i>	P(3HB)	Tapioca	59	106	58	61.5	Kim <i>et al.</i> , 1995
<i>C.necator</i>	P(3HB)	Soybean oil	96	126	76	95.8	Kahar <i>et al.</i> , 2004
<i>H.boliviensis</i>	P(3HB)	Glucose	33	44	81	35.4	Quillaguaman <i>et al.</i> , 2008
<i>H.boliviensis</i>	P(3HB)	Glucose	40	62	68.5	42.5	Guzman <i>et al.</i> , 2009
<i>P.extorquens</i>	P(3HB)	Methanol	170	233	64	149	Suzuki <i>et al.</i> , 1986

1.1.1.7.3 Continuous Cultivation

As a fermentation strategy, continuous fermentation is of interest because of the possibility of achieving high productivity, especially from strains with a high maximum specific growth rate (Braunegg, 1995). Continuous fermentation can be operated as a single or multiple-stage process (Figure 1.7). In a single-stage continuous fermentation, the biomass was found to increase while PHA content was found to decrease with an increase in dilution rate. A compromise between PHA content, cell concentration, and productivity is required in a single-stage continuous process if a reasonable PHA content is to be attained in the biomass. An early induction of nutrient limitation could result in less biomass accumulation and high PHA content while late introduction of nutrient limitation could result in high biomass accumulation but less PHA production. Hence, a two-stage continuous process is preferred. Using different dilution rates, 0.21 h^{-1} for cell growth (1st stage) and 0.16 h^{-1} for PHA-accumulation (second stage), a maximum overall productivity of $1.06 \text{ g L}^{-1} \text{ h}^{-1}$ and P(3HB) content of 63% dcw was achieved in a fed-batch cultivation of *Pseudomonas oleovorans* (Jung *et al.*, 2001).

Hartmann and co-workers have employed the strategy of different dilution rates in the production of tailored olefinic mcl-PHAs, with mixtures of octanoic acid (58%) and 10-undecenoic acid (42 mol %), using *P. putida GP01 (ATCC 29347)* in a chemostat. They found that the monomeric composition of the mcl-PHA produced depended on the dilution rate of the feed medium. The fraction of aliphatic monomers was slightly lower at high dilution rates and increased towards low dilution rates, indicating different kinetics for the incorporation of the two carbon substrates in *P. putida GP01* (Hartmann *et al.*, 2001). Zinn and colleagues have established in their work that dual (C, N) limited growth offers a new approach in producing PHAs with tailor-made properties (Zinn *et al.*, 2003; 2004). This strategy has been used for the production of tailored PHA, especially from toxic carbon sources such as carboxylic acids. Since growth is not affected when the substrate is fully metabolised, the toxic substance can be maintained at a threshold level of concentration (Zinn *et al.*, 2004).

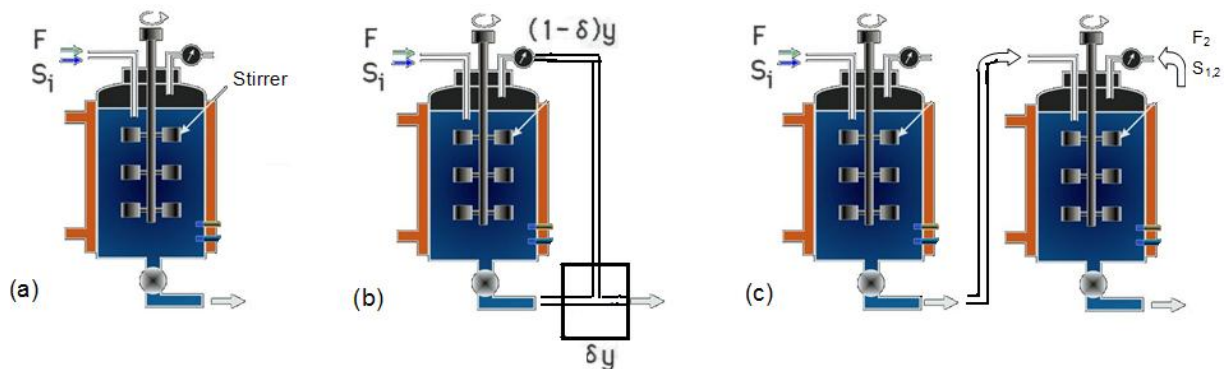


Figure 1.7 Classification of continuous processes based on the flow pattern (a) Single stage; (b) Single stage with recirculation; (c) Two stage with optional two stream medium

1.1.1.8 Uses of PHAs

Interest in the use of polyhydroxyalkanoates (PHAs) for packaging, medical, agricultural and fisheries applications has recently increased (Chen, 2005). Thus, PHAs can be a replacement for many conventional petrochemical products in application including moulded goods, paper coatings, performance additives, foils, films and diaphragms (Lauzier *et al.*, 1999; Chen, 2005). PHAs can also be used for manufacturing disposable everyday articles such as shampoo bottles and cosmetic materials (Hocking and Marchessault, 1994). In fact, the first commercial application of P(3HB-co-3VB) under the trade name, Biopol™ was in packaging personal hygiene products such as shampoo bottles. Over the years, the applications of Biopol™ have been extended to ranges of materials including toiletries, disposable razors, containers for biodegradable automobile oils etc. Despite the high cost, the use of Biopol™ as a raw material for packaging have been desired to increase the sale of other products due to the ‘green’ image. Besides, the products opened markets to applications which require biodegradability for functional reasons: bags for refuse disposal, golf trees which degrades when lost, fishing nets and materials dumped into the marine environments which have the potential to cause severe environmental problems if non degradable. PHAs can be used as hot-melt adhesives and non woven fabrics (Madison and Huisman, 1999; Steel and Norton-Berry, 1986). In 1993, EC legislation (Chapter 8.2) enhanced the applications of PHAs by demanding industries to be responsible to the management of waste generated out of the consumption of their products. Consequently, plastic materials, recycling which is

economically unattractive, have recently been made of biodegradable polymers. This is particularly true with the food industries and niche applications such as diapers and sanitary napkins. Also, PHAs can be used as sources for the synthesis of enantiomerically pure chemicals such as hydroxyalkanoic acids and as raw materials for the production of latex paints (Steinbüchel, 2001; Ren *et al.*, 2005; Williams, 1996; Scholz, 2000; Galego *et al.*, 2000). PHAs have promising uses as a new source for small molecules that have potential applications as biodegradable solvents and as carriers for long term slow release of nutrients, fertilizers, insecticides and herbicides (Lee, 1995; Galego, 2000). Further applications of PHAs in agriculture included their usefulness in biodegradable flower pots and mulch films.

Further applications of PHAs are within the medical and pharmaceutical industries and this is primarily due to their biodegradability and biocompatibility. Their *in vivo* biocompatibility has been reviewed in detail in Valappil *et al.*, 2007. Rigid P(3HB) because of their ability to stimulate fracture healing, have found applications in fixation and orthopaedic applications include sutures, meniscus regeneration devices, fixation rods, bone plates and bone fracture fixation (Martin and Williams, 2003). PHAs are also used in the production of repair patches, bone marrow scaffolds, ligament and tendon grafts, bone graft substitutes and bone dowels (Martin and Williams, 2003). PHAs can be used in the fabrication of three-dimensional, porous, biodegradable heart valve scaffolds (Sodian, 2000). Currently, EMPA is assessing the use of PHAs as a biopolymer for fibre production. Such fabric made from these fibres could be used in medical applications such as wound dressing. P(3HB) is also being considered for cartilage tissue engineering as scaffolds for the construction of a three-dimensional articular cartilage tissue for implantation (Freed *et al.*, 1998; Nehrer, 1997). Currently, the biomedical field is facing challenges in the need for tissue adhesives, tissue sealants and soft tissue fillers as a replacement for collagen and tissue adhesion preventives for the treatment of severe burns. PHAs and modified PHAs are being considered as solutions for the ever increasing biomedical challenges. To this effect, PHA composites containing collagen sponges and gels (Nehrer, 1997), polyglycolide (PGA) (Freed *et al.*, 1997), hyaluronic acid matrices (Freed *et al.*, 1993, Chu, 1997), polylactide (PLA) (Sittinger, 1996), poly(lactide-co-glycolide) (PLGA) (de Groot *et al.*, 1997), poly(L-lactide-co-caprolactone) (L-PLCL) and poly(glycolide-co-trimethylene carbonate) (PGTMC) (Fine, 1994) are currently being employed in regenerative medicine. Further, PHAs have also found application as a drug delivery system in the

management of different health problems. This is due to the ability of PHAs to yield normal mammalian metabolites which could be a feedstock for stereospecific drug industry. (R)-3-hydroxybutyrate is a natural component of human blood and could be used as a carbon source in intravenous infusion solutions in humans (Hiraide and Katayama, 1990). Tetrick and colleagues have also evaluated the use of (R)-3-hydroxybutyrate as intravenous administered energy source to piglets (Tetrick *et al.*, 1995). The monomer has been administered to obese patients undergoing therapeutic starvation to reduce protein loss (Pawan and Semple, 1983), while Chen and Chen, 1992 have reported interest in the use of this monomer as an irrigation solution to maintain the tissues during ocular surgery. The monomeric component of poly(4-hydroxybutyrate), poly(4HB), 4-hydroxybutyric acid is also another naturally occurring substance widely distributed in the mammalian body. Nelson and workers have reported the presence of this monomer in the brain, kidney, heart, liver, lung and muscle (Nelson *et al.*, 1981). As a result of the bioavailability of 4-hydroxybutyric acid, the monomer has been employed over the years as an intravenous agent for the induction of anaesthesia and long-term sedation (Entholzner *et al.*, 1995). Some of the major areas of application of P(3HB) and copolymer of P(3HB) in medicine are listed in Table 1.7.

Table 1.7 Potential medical applications of P(3HB) and its copolymers in medicine.

Type of Applications	Type of PHA	Products	References
Orthopaedic	P(3HB)	T-plate implants	Vainionpaa, 1986
	P(3HB)/HA	Reinforced composite	Doyle <i>et al.</i> , 1991
		Corticocancellous bone grafts	Galego <i>et al.</i> , 2000
	P(3HB), P(3HB-co-3HV)/HA	New bone formation	Misra <i>et al.</i> , 2009
	P(3HB)/Bioglass	New bone formation	Knowles 1991
	P(3HB-co-3HV)/Bioglass		
Wound Management	P(3HB)	Surgical repair of hernias	Baptist and Ziegler, 1965
		Gastrointestinal patch	Behrend <i>et al.</i> 1999
	P(3HB)	Absorbable sutures	Baptist and Ziegler, 1965
	P(3HB-co-3HV)	Suture coating	Wang and Lehmann, 1991
	P(3HB)		Holmes, 1985
	P(3HB), P(3HB-co-3HV)	Medical dusting powder	Webb and Adsetts, 1986
		Wound dressing	Steel and Norton-Berry, 1986
			Davies and Tighe, 1995

		Wound scaffold	Ishikawa, 1996
Urology	P(3HB) P(3HB-co-3HV)	Urethra repair Urethra reconstruction	Baptist and Ziegler, 1965 Bowald and Johansson, 1990
Nerve Repair	P(3HB)	Nerve repair	Aebischer <i>et al.</i> , 1988 Hazari <i>et al.</i> , 1999 Ljungberg <i>et al.</i> , 1999
Prodrugs	P(4HB)	Prodrug of 4-hydroxybutyrate	Williams and Martin, 2001 Sudesh <i>et al.</i> , 2000
Drug delivery	P(3HB)	Anticancer Anticancer antibiotics Delivery of two prodrugs Oral delivery of vaccine Delivery of progesterone	Bissery <i>et al.</i> , 1983, 1984 Juni <i>et al.</i> , 1985 Kawaguchi <i>et al.</i> , 1992 Kawaguchi <i>et al.</i> , 1992 Eldridge <i>et al.</i> , 1990 Gangrade and Price, 1991
	P(3HB-co-3HV) P(3HB)	Implants and Tablets	Korkusuz <i>et al.</i> , 2001 Hasirci <i>et al.</i> , 1998 Kharenko and Iordanskii 1999 Juni and Nakano, 1987
Cardiovascular	P(3HB)	Pericardial patch	Bowald and Johansson- Ruden, 1997, Duvernoy <i>et al.</i> , 1995 Nkere <i>et al.</i> , 1998
	P(3HB) P(4HB) P(3HB) P(3HB)	Artery Augmentation Atrial Septal defect repair Cardiovascular stents	Malm <i>et al.</i> , 1994 Stock <i>et al.</i> , 2000 Malm <i>et al.</i> , 1992 Behrend <i>et al.</i> , 2000 Behrend <i>et al.</i> , 1998 Unverdorben <i>et al.</i> , 1998 Schmitz and Behrend, 1997
	P(3HB-co-4HB)	Vascular Grafts	Noisshiki and Komatsuzaki 1995
Dental and Maxillofacial	P(3HB-co-3HV)	Guided Tissue Regeneration Guided Bone Regeneration	Galgut <i>et al.</i> , 1991 Leenstra <i>et al.</i> , 1995 Kostopoulos and Karring 1994a Kostopoulos and Karring 1994b
Nutritional uses	R-3-hydroxybutyrate	Human Nutrition	Veech, 1998, 2000 Martin <i>et al.</i> , 2000 Tasaki <i>et al.</i> , 1998 Brune and Niemann, 1977
	P(3HB) P(3HB), P(3HB-co-3HV)	Animal Nutrition	Holmes, 1988 Peoples <i>et al.</i> , 1999

1.1.2 Cellulose

Cellulose is a linear polymer made of glucose molecules linked by $\beta(1-4)$ glycosidic linkages. The structure of cellulose is shown in Figure 1.8. Cellulose is the most abundant natural biopolymer on earth and it is recognized as the major component of plant biomass and a representative of microbial extracellular polymers. Among the natural cellulose fibres, Bacterial cellulose (BC) - a biomaterial for tissue engineering, has become the latest emerging field of research in the present decade (Svensson *et al.*, 2005). Cellulose is synthesised by bacteria belonging to the genera of *Acetobacter*, *Rhizobium*, *Agrobacterium*, and *Sarcina*. However, the most efficient producers are Gram-negative, acetic acid bacteria, *Acetobacter xylinum* (reclassified as *Gluconobacter xylinus*, Yamanaka *et al.*, 2000). *Gluconobacter xylinus* is a non-pathogenic, rod-shaped, obligate aerobe notably known for its ability to produce extracellular cellulose with pure ultra-fine random fibre network with high crystallinity, water absorption and mechanical strength. The cellulose network produced by this organism is referred as pellicle. The formation of cellulose by laboratory bacterial cultures is an interesting and attractive biomimetic access to obtain pure cellulose for both organic and polymer chemists. Bacterial cellulose has been used for a variety of applications due to its potentially high mechanical properties. The high mechanical properties of bacterial cellulose, in turn, have been found to be due to high crystallinity, high orientation of the cellulose chains within the fibres, as well as pure cellulosic form of the polymer. Furthermore, the composition of bacterial cellulose has been found to be a combination of α and β allomorphs which are similar to those found in plant cellulose (Sugiyama *et al.*, 1991). According to Sugiyama *et al.*, the polymorph ratio of $I_{\alpha}:I_{\beta}$ is found to be of the order of 60:40 (in agitated culture) and to 70:30 in static culture (Sugiyama *et al.*, 1991). Despite their identical chemical composition, the structure (Figure 1.8) and mechanical properties of BC microfibrils differs from those of plant cellulose. BC microfibrils have high mechanical properties including tensile strength and modulus but also high water-holding capacity, mouldability, crystallinity and biocompatibility (Putra *et al.*, 2008). Despite the excellent mechanical properties of BC films (Nakagaito *et al.*, 2005), and BC composites (Gindl and Keckes, 2004), their Young's modulus values are far away from the possible values offered by the high modulus of microfibrils, estimated to be around 140 GPa in the longitudinal direction (Nakagaito *et al.*, 2005). For this reason, microstructural information is necessary for greater understanding of structure-mechanical property relationships and for applications both as a nanostructured material

itself but also as a composite combined with other materials. Cellulosic materials, in general, are expected to have a great potential since they are the most abundant renewable raw materials with multifunctional properties desirable in many areas of tissue engineering. Though, lots of interest in the isolation of cellulose and their used as reinforcement in polymers have been demonstrated (Nakagaito and yano 2004; Zimmermann *et al.*, 2005; Oksman and Sain 2005; Seydibeyoglu and Oksan 2008; Alemdar *et al.*, 2009; Jonoobi *et al.*, 2009), but, not much work has been carried out to incorporate these important biofibres into biodegradable P(3HB) composites in order to fabricate scaffolds for tissue regeneration. Hence, exploration of the potentials in P(3HB)/BC cellulose composite fabrication is one of the objectives of this thesis.

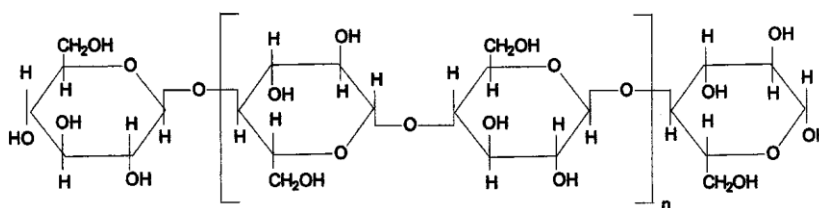


Figure 1.8 Structure of Cellulose (Mohanty *et al.*, 2002)

1.2 Tissue Engineering

Tissue engineering is one of the most upcoming research areas, involving the innovation of new biomaterials from both bioactive synthetic and natural resources using conventional technologies. As a multi-disciplinary field, tissue engineering combines biology, materials science, and surgical reconstruction with suitable biochemical and physico-chemical factors to provide living tissue products that restore, maintain, or improve tissue functions. Tissue engineering is closely associated with applications that repair or replace portions of or whole tissues (i.e. bone, cartilage, blood vessels, bladder, skin etc.). The need for this approach has increased primarily due to lack of donor organs and tissues. Hence, the approach offers the opportunities of researchers being able to expand the skills in repairing damaged tissues, develop improved surgical procedures, and significantly improve the qualities of life. Often, the tissues involved require certain mechanical and structural properties for proper functioning. By incorporating biofibres with biodegradable polymers, in three dimensional

scaffolds with appropriate porosity for mechanical support and tissue guidance, new tissues can be created while damaged ones could be regenerated within the shortest possible time. Tissue engineering also embraces the act of performing specific biochemical functions using cells within an artificially-created support system (e.g. an artificial pancreas or an artificial liver). Composite constructs are employed as carriers for growth factors to accelerate the healing process when placed *in vivo* (Ikada, 2006). Hence, tissue engineering is considered as a potential alternative to organ or tissue transplantation. Currently, three approaches are employed in the regeneration of tissues. These include infusion of isolated cells or cell substitution; use of tissue-inducing materials and implantation of cells seeded in scaffolds. These approaches are illustrated in Figure 1.9.

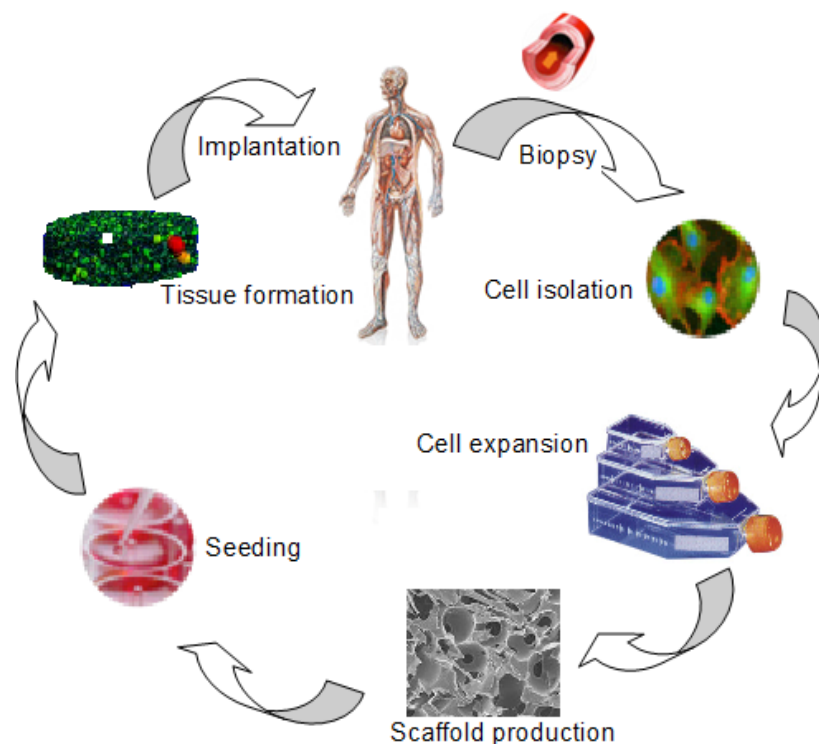


Figure 1.9 Schematic representation of the process of tissue engineering

1.2.1 Bone tissue engineering

Bone tissue regeneration is an emerging interdisciplinary field that seeks to address the needs by applying the principles of biology and engineering to the development of viable

substitutes that restore and maintain the function of human bone tissues (Hench *et al.*, 2002). Hence, the main aim of tissue engineering of bone is to obtain more functional cell-material constructs that could repair or regenerate damaged bones (Ignatius *et al.*, 2004). The dynamics of bone metabolism, a process of continuous remodelling throughout the life of the vertebrate, reside primarily within the activities of three cells which respond to the environment in association with the adjacent cells and circulating factors. The three cells include the osteoblast, osteocyte and osteoclast.

Osteoblasts synthesize and regulate the deposition and mineralization of the extracellular matrix of bone. Osteoblastic activities are regulated by the surrounding active hormones, growth factors, ions, lipid metabolites and steroids. The microenvironment of inorganic/organic bone matrix necessitates further specialization of the osteoblast. Osteocytes share similar lineage to osteoblasts. They are formed by the incorporation of osteoblasts into the bone matrix; hence, they are the most abundant bone cell among a group of highly differentiated cells. Osteocytes are highly differentiated cells with alkaline phosphatase activity, PTH receptors, and function as mechano-sensory cells. Osteocyte activation entails the processing of intracellular signalling molecules. The networks of osteocytes provide the cellular organization in the bone to respond to mechanical demands with either augmentation or reduction of bone apposition. Osteoclasts are multinucleated cells of hemopoietic cell origin involved in bone resorption. The complex unit that develops between the osteoclast and the dissolving bone surface is generated by the fusion of intracytoplasmic acidifying vesicles with the plasma membrane.

Bone defects result from trauma or diseases and in most cases; it is very difficult for the bone to regenerate on its own, more especially at old age. To solve the problem of new bone regenerations, many approaches have evolved which included standard drug therapy, the use of inserts to guide broken bones to heal and bone tissue engineering. Bone tissue engineering differs from the standard drug therapy or permanent implants in that the engineered bones becomes integrated within the patient and afford a potentially permanent and specific cure of the disease state.

Bone tissue engineering involves many approaches; however, all the approaches involve one or more of the following key ingredients: harvested cells, recombinant signalling molecules,

and three-dimensional (3D) matrices (Patrick *et al.*, 1998). One popular approach involves seeding cells in highly porous biodegradable matrices (or scaffolds), in the shape of the desired bone, with cells and signalling molecules (e.g., protein growth factors), then culturing and implanting the 3D matrixes (scaffolds) into the defect site to induce and direct the growth of new bone (Langer and Vacanti 1993; Hutmacher, 2000). The goal is for the cells to attach to the scaffold, multiply, differentiate (i.e., transform from a nonspecific or primitive state into cells exhibiting the bone-specific functions), and organize into normal, healthy bone as the scaffold degrades. The signalling molecules can be adhered to the scaffold or incorporated directly into the scaffold. The use of this approach to repair or regenerate new bones eliminates the problems of donor site scarcity, immune rejection and pathogen transfer (Xi *et al.*, 2008).

All bone tissue engineering techniques involve mimicking the natural milieu by placing the cells and growth factors in biodegradable scaffolds that can act as temporary extracellular matrixes (ECMs). Extracellular matrix is the part of the body that gives it form and shape. However, there are some variations in bone tissue engineering which depends on: the source of the cells (autologous, allogenic or xenograph), direct injection of cells and/or signalling molecules into the defected site (with or without scaffold), direct insertion of scaffolds seeded with cells or cells grown on scaffolds before implantation and the used of only signalling molecules without cells to initial bone regeneration. In all cases, no single approach or dosage of cells and growth factors will satisfy all clinical needs and the approach used in the regeneration of damaged bone will depend on situations. For example a young child bone will regenerate faster than an adult or diabetic patient and therefore different approached and care would have to be involved. Whilst, treatment concepts based on autogenic/tissue transplantation techniques eliminate the problems of donor site scarcity, immune rejection and pathogen transfers (Naughton *et al.*, 1995), many problems such as the recipient immune response have been reported in the case of allogenic bone regeneration (Bonfiglio *et al.*, 1972). Autografts are not limited by risks of disease transfer and histo-incompatibilities; however, the supply of autograft tissue is physically limited.

1.2.2 Cartilage tissue Regeneration

Cartilage is another expected target for tissue engineering; it differs from other tissues in its limited intrinsic potential for self-repair. The difficulty in the self-repair of cartilage seems to be due to lack of sufficient supply of healthy chondrocytes to the defective sites or to the low productivity of matrices in regenerated chondrocytes (Yamaoka *et al.*, 2006). The current treatments for cartilage repair rarely restore cartilages to full function or return the tissue to its native normal state (Tuli *et al.*, 2003). Cartilage repair techniques based on the use of autologous chondrocytes, either directly injected into the defect or further processed to engineer cartilaginous grafts, typically rely on the *ex vivo* expansion of the limited number of cells that can be obtained from a small biopsy. However, chondrocyte expansion is intrinsically associated with the well-known problem of cell de-differentiation (Benya and Shaffer, 1982; Binette *et al.*, 1998), and the redifferentiation capacity of expanded cells, especially if the source is of human origin, is rather limited (Bonaventure *et al.*, 1994).

However, cartilage tissue engineering could overcome such limitations by the use of several strategies including *ex vivo* culture techniques such as medium supplementation with specific growth factors (Jakob *et al.*, 2001, Barbero *et al.*, 2003; Malpeli *et al.*, 2004); cell growth on microcarrier beads (Malda *et al.*, 2003) or on collagen type II-coated substrates (Barbero *et al.*, 2006); and the use of supportive artificial materials. The general approach in the use of supportive artificial materials for the engineering of damage cartilage involves the use of biocompatible, structurally and mechanically sound scaffold, with an appropriate cell source, which is loaded with bioactive molecules that can promote cellular differentiation and/or maturation.

In principle, chondrocyte activities are maintained when they are housed in the proper 3D environment. During the development and growth of cartilage, the chondrocytes produce abundant matrices, encase themselves within cavities, and are eventually separated from each other (Kessel, 1998). In contrast, the chondrocytes deviated from the physiological 3D environment rapidly lose the typical phenotype and protein synthesis, which is termed dedifferentiation (von der Mark *et al.*, 1977). In cartilage tissue engineering, the chondrocytes isolated from their original tissues would be conditioned in a 3D environment, mimicking the

physiological situation with favourable scaffolds so as to reproduce their functions and enhance protein synthesis.

The progress towards successful cartilage regeneration has been extensively reviewed by Buckwalter and Mankin, 1997 and Newman, 1998. Their reports show that numerous clinical and basic scientific investigations have confirmed successful implantation of artificial matrices, growth factors, perichondrium and periosteum, can stimulate the formation of cartilaginous tissue in osteochondral and chondral defects in synovial fluids.

Several attempts have been made to utilize two types of scaffolds for cartilage tissue engineering. This includes the use of honeycomb, porous body, mesh, sponge, and unwoven fabric (Lu *et al.*, 2001). The advantages in the use of solid-type scaffolds above included the possibilities of shaping the macroscopic structure of regenerated tissues or supporting their mechanical strength. However, there are problems associated with the pore sizes in the scaffold matrices, the smaller the pore size, the more difficult it will be for the cells to infiltrate into the scaffold. In contrast, when the pore sizes of solid scaffolds are increased, the chondrocytes are attached to the walls of huge pores, but they are not placed in a 3D condition.

Another attempt reported in the use of porous scaffold for cartilage regeneration is the use of hydrogel. Various hydrogel materials derived from animals or plants have been utilized as porous scaffold for cartilage regeneration. Examples include collagen type I gel, fibrin glue, gelatin, agarose, or alginate (Chapinyo *et al.*, 2004; Ibusuki *et al.*, 2003; Steven *et al.*, 2004; Ting *et al.*, 1998; Gerard *et al.*, 2005). Although, the hydrogel lacks mechanical strength in itself, this type of material can be mixed with cells and can surround the seeded cells in all directions. The hydrogel type of scaffold could be used to reconstruct the 3D environment for the chondrocytes in cartilage tissue engineering. Many previous articles reported that those hydrogel materials were more effective in retaining chondrocyte functions or promoting matrix synthesis, when compared with monolayer culture (Yamaoka *et al.*, 2006). Despite the difficulties associated with the treatment of cartilages damaged by trauma or diseases, cartilage engineering *ex vivo* have proven promising in the regeneration of the affected cartilages. Researchers are further progressing towards developing new materials that could satisfy the present quest for lasting solutions to cartilage engineering.

1.2.3 Scaffolds in Tissue Engineering of Bone and Cartilages

Scaffolds are porous structures that provide matrices for cell adhesion, proliferation and differentiation (Chen *et al.*, 2006; Hutmacher, 2000). Scaffold materials for making matrices for bone tissue engineering include several classes of biomaterials: Native polymers, synthetic polymers, ceramics and composites. The principle of guided bone regeneration is that new bone formation will occur by providing a "passageway" for osteoblast lineage cells and osteoblasts. Precluding soft tissue prolapse into an osseous deficit provides the underpinning to guide bone, thereby preventing scar formation. Physiologically, fibroblasts are more likely to populate an intra osseous deficit than osteoblasts; therefore, by sustaining a zone for migration of osteoblast lineage cells, the clinical outcome should be bone and not connective tissue scar (Lin *et al.*, 2002). Hence, tissue engineering scaffolds play a central role in the provision of osteoconductive and osteoinductive (Murphy, 1999) environment for successful tissue engineering. The current synthetic polymers being used for hard tissue replacement include polymethylmethacrylate (PMMA) and polyhydroxyethylmethacrylate (PHEMA). PMMA/PHEMA is commercially prepared under the name hard tissue replacement (HTR-MFI) as blocks and particulates. The block format is for augmentation whereas particulates have periodontal applications to restore deficient alveolar bone (Lin *et al.*, 2002). Both polymers are synthetic and 'non degradable' - a property that have favoured extensive research in the use of native biodegradable and resorbable polymers (e.g. PHAs). Though synthetic polymers provide a wider range of properties such as mechanical and controllable degradation time (Griffith *et al.*, 2002), natural polymers are in general more favourable due to their biocompatibility that provides favourable physiological functions, such as cell attachment, differentiation and chemotaxis.

Apart from polymers, other biomaterials for bone and cartilage engineering include ceramic and hydroxyapatite. The most known use of ceramic in tissue engineering is dental applications; however, scientists are currently working actively towards the potentials of employing ceramics in bone tissue engineering. The most common ceramics often utilize in tissue engineering applications are Alumina (Al_2O_3) and hydroxyapatite (HA). Alumina has excellent corrosion resistance, good biocompatibility, high strength and high wear resistance. Hydroxyapatite on the other hand is a calcium-phosphate based ceramic. HA is a major component of the inorganic compartment of bone (Kumar *et al.*, 2007). HA prepared

commercially is biocompatible with biodegradability either absent or protracted (a timeline spanning years) (Lin *et al.*, 2002). The degradation of hydroxyapatite can be controlled by varying the chemical structure. Bioactive glasses (Bioglass[®]) have also been shown to bind to soft tissue and bone. These bioactive glasses contain different ratios of Na₂O-CaO-P₂O₅-SiO₂ (Misra *et al.*, 2007).

Cartilage repair is very difficult due to poor cartilage cell density and lack of vascularisation (Hunziker, 2001). Cartilage engineering scaffold, hence, provide the necessary support for cells to proliferate and maintain their differentiated function and by this means; the desired regeneration can be obtained. Architectural design of tissue engineering scaffolds defines the ultimate shape of the new cartilage. Thus, tissue engineering scaffolds provide characteristic extracellular matrix with porous structures which play an important role in permitting cell adhesion, proliferation and differentiation. Tissue engineering scaffolds can be designed as an open or closed construct depending on the need. In any case, for a material to serve as a biomaterial for bone and cartilage engineering the following conditions are necessary.

Biocompatibility: - In the production of 2D or 3D scaffold, it is desirable that starting point for the choice of a materials is compatibility. A biomaterial must be compatible with the host body. It must not enhance or encourage the elicitation of the host immune system. It must not contain clinically detectable primary or secondary foreign body reaction (Hutmacher, 1996).

Degradability: - To avoid the need for a post-surgical removal after performing its function in the body, a biomaterial scaffold must be degradable. In addition to degradability, a biomaterial must degrade at a rate that will permit complete repair or regeneration of the affected tissue. Also, the degradation product must not be toxic to the regenerating tissue. Thus, biomaterials are selected according to the intended function. For example, in bone regeneration, biomaterials like PGA and PDLA are not suitable as the sole material for bone tissue engineering scaffold (Thompson *et al.*, 1996). This is due to bulk degradation properties of this group of polymer. Their degradation commences a day after use which implies that the material may not be able to carry the load of the regenerating bone because of their high rate of degradation (Wong and Mooney, 1997). Rather, this group of polymer can be used in the form of a composite to obtain a controlled rate of degradation of their base material.

Chemically stable: - For a material to serve as a biomaterial for bone and cartilage regeneration, the material and its degradation products must be chemically stable. The degradation product should not affect the material or disturb the growing cells. For instance, the degradation product of PLA is lactic acid and at pH lower than 7.0, the degradation rate of the PLA increases. Hence, it is ideal that when polymers such as PLA is employed as a material for tissue engineering, the degradation product must be removed at the same rate at which they are produced, otherwise, both the spreading cells and the rate of degradation of the scaffold would be affected. However, PHAs such as P(3HB) undergo degradation leading to the formation of a hydroxy acid as the product of their degradation. Also, hydroxy acid is one of the constituents of blood. Hence, in the use of PHAs the product of degradation does not affect the stability of the scaffold.

Mechanically stable: - A bone tissue engineering scaffold must possess enough structural integrity during *in vitro* and *in vivo* remodelling processes. The scaffold must be able to provide enough support for the polymer/cell/tissue from the time of cell seeding up to the point where the hard tissue transplant is completely remodelled by the host tissue. The scaffold should possess sufficient strength and stiffness to function for a period until *in vivo* tissue growth has replaced the slowly degrading scaffold matrix (Hollinger and Chaudhari, 1992).

Interconnected pores: - Porosity and pore sizes are very important during fabrication of scaffolds for bone and cartilage tissue engineering applications. For efficient ingrowth of cells, vascularisation as well as diffusion of oxygen, nutrients and waste around the scaffold, it is important that the pores of a tissue engineering scaffold be highly connected with porosity level greater than 90%, with medium pore sizes ranging from 15 -35 μm and larger pore sizes greater than 200 μm (Whang *et al.*, 1999; Ma, 2004).

Apart from the features briefly discussed above, other important features that would be needed to be considered in the choice of a biomaterial for bone and cartilage scaffold production include, surface chemistry, ability to allow incorporation of materials such as growth factors, signalling molecules and drug and wettability which is very important in the initial cell adhesion and growth.

1.2.4 Biodegradable-polymer-based materials for tissue engineering scaffolds

Scientists have attempted to solve the problem of bone and cartilage defects in the past few years using synthetic grafts based on metals or ceramic such as hydroxyapatite and tricalcium phosphates. However, the synthetic materials have markedly differing mechanical properties when compared to the repairing bone and cartilage tissue. This always leads to incompatibility with consequent implant failure and need for urgent revision surgery (Lane *et al.*, 1999). Furthermore, due to long term implant instability, synthetic grafts routinely fail to meet the demands of an ageing, but still active population as they are fragile and lack the necessary flexibility. Hence, due to these limitations of bone grafts with synthetic materials, engineered native biodegradable polymers incorporated with growth factors have emerged as a conventional alternative treatment in bone and cartilage tissue repair and regeneration.

A lot of investigations on the exploration of biodegradable polymeric materials in porous, bioabsorbable tissue engineering scaffold fabrications have been reported. Such biodegradable polymers included collagen sponges and gels (Neher *et al.*, 1997), hyaluronic acid matrices (Aigner *et al.*, 1998), polyglycolide (PGA) (Freed *et al.*, 1993). Poly(L-lactide-co-caprolactone) (L-PLCL) (de Groot *et al.*, 1997), and poly(glycolide-co-trimethylene carbonate) (PGTMC) Fine *et al.*, 1994). In general, polymers of the poly(α -hydroxy acids) group undergo bulk degradation. The molecular weight of the polymer commences to decrease on day one (PGA, PDLA) or after a few weeks (PLLA), upon placement in an aqueous media (Wong and Mooney, 1997). However, the weight loss does not start until the molecular chains are reduced to a size which allows them to freely diffuse out of the polymer matrix (Kronenthal, 1975). This phenomenon has been studied in detail by a number of research groups including Agrawal *et al.*, 1997 and Garreau and Vert, 1990. The results of their investigations showed that hydrolysis of the polymers led to accelerated degradation and resorption kinetics until the physical integrity of polymer matrix is compromised. In addition, they found that the weight loss in the polymers was accompanied by a release of acidic by-products.

However, because of the urgent need for tailored biodegradable materials that are suitable for scaffolds in tissue engineering of bones and cartilages, the family of polyhydroxyalkanoates (PHAs) have emerged as prime candidates for the hard tissue engineering. Members of this group of biodegradable polymer are either thermoplastic or elastomeric polyesters and they

degrade slowly by surface erosion. Moreover, their physico-mechanical properties can be tailored during biosynthesis in bacteria. Besides, the mechanical and structural behaviour, degradation kinetics and bioactivity of PHAs can be further enhanced by incorporating other biocompatible and biodegradable materials to form composites (Navarro *et al.*, 2006).

Many *in vitro* and *in vivo* studies have been conducted on PHAs as biomaterials for both soft and hard tissue engineering (Avella *et al.*, 2000; Wang *et al.*, 2004). Results of investigations by different researchers have shown that porous PHA materials are good substrates for cell cultures (Rivard *et al.*, 1996; Gursel *et al.*, 2001). This is further supported by the result of evaluation carried out by Rivard *et al.*, 2006, which showed that cell proliferation rate on poly(3-hydroxybutyrate-*co*-3-hydroxyvalerate), P(3HB-*co*-3HV) matrix was similar to that observed in collagen sponges. However, Chen and Wang reported a number of problems encountered in their investigations with P(3HB-*co*-3HV) copolymers which included lack of bioactivity on the copolymer materials. They observed that new tissue could not bond tightly to the surface of the polymer (Chen and Wang, 2002). Thus, the development of composite materials containing a polymeric phase and a bioactive ceramic/magnetic material is regarded as a promising approach for preparing bioactive scaffolds for tissue engineering (Boccaccini *et al.*, 2002). Intensive research towards the incorporation of nanoparticles into the polymeric matrix with the prime objective of improving the mechanical properties as well as of incorporating nanotopographic features that mimic the nanostructure of natural bone is in progress (Hansen *et al.*, 2007; Torres *et al.*, 2007). In addition, the tailoring of roughness and topography of the pore surfaces is being explored due to the profound effect that surface roughness has on early cell attachment behaviour as well as subsequent cell adhesion, cytoskeletal organization and gene expression (Berry *et al.*, 2006). It is now accepted that the response of host tissue at the protein and cellular level to nanostructured surfaces is different than that observed to conventional (μm -size) surfaces (Liu *et al.*, 2007). Li *et al.*, have investigated the effect of incorporating bioactive glass to the biodegradable P(3HB-*co*-3HV) matrix and the result of their investigation confirmed that addition of bioactive glass not only further improved the mechanical properties of the resulting composite but added bioactivity to the composite (Li *et al.*, 2005). Furthermore, Misra, *et al.* have performed extensive investigations on the incorporation of Bioglass[®] to P(3HB) matrix. Based on their investigations, it was reported that the addition of nano sized Bioglass[®] had profound effect

in addition to nanotopographic features on the composite matrix. Furthermore, the group reported an increase in the wettability and protein adsorption on the composite, compared to the original neat P(3HB). In summary, the use of natural polymers such PHAs have been favoured by their inherent biocompatibility and ability to modulate their physico-mechanical properties through the addition of bioactive elements. With current pace of progress in the identification and utilization of abundant natural biomaterial, the tissue engineering will soon begin to benefit mankind.

1.3 Drug delivery

Drug delivery and sustained drug release are highly interesting for both academic purposes and clinical applications. In the past few decades, many drug-delivery tools or methods have been developed with the emphasis on non-viral vectors, especially synthetic polymers, as drug carriers. Besides, in the therapeutic treatment of some diseases (e.g. tumour), it is necessary that the release of drug molecules is guided and targeted towards the diseased cells and tissues; otherwise the healthy cells and tissues in the body could become casualties to the therapeutic treatment. To protect healthy cells and tissues, researchers have developed the use of technology to direct the delivery and release of drug molecules from the encapsulated polymeric material to the targeted site in the body.

Generally, three mechanisms have been predicted in the work of Glynn *et al.* for the release of the drug molecules from the polymeric microspheres into the blood vessels (Glynn *et al.*, 1976). These mechanism included diffusion, swelling, and degradation. Diffusion occurs as a result of a concentration gradient which results in the migration of drugs away from the microspheres into the surrounding body fluid. Swelling occurs when the drug encapsulated microspheres absorb fluid from the surrounding body fluid, which results in differential pressure and subsequent increase in the pore sizes. The increase in the pore sizes enables the drug molecules to migrate away from the spheres. Degradation occurs as a result of change in the physical parameters (such as change in temperature and pH), surrounding the microspheres which results in the hydrolysis of the polymeric material and subsequent release of the drug molecules. Also, degradation of the microspheres could result from the activities of surrounding enzymes on the polymeric materials of the microspheres. Apart from the three

mechanisms mentioned above, the internal and external parameters of the microspheres also play a role in the drug release kinetics of the polymeric materials. These parameters include the presence of hollow space in the microspheres, the formation of double walls, the presence of smooth or rough surfaces on the microspheres, the level of crystallinity of the polymeric materials, and the melting temperature of the polymeric materials. Figure 1.10 below, summarises the three mechanisms predicted for the release of drug molecules from a drug loaded polymeric releasing system.

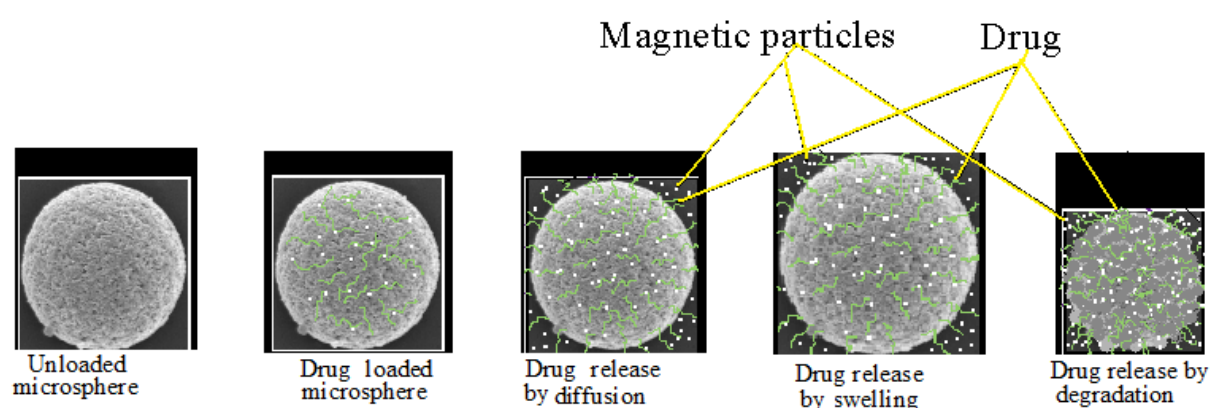


Figure 1.10 Schematic representation of different mechanisms of drug release from a magnetic microspheres drug delivery system.

1.3.1 Polymeric P(3HB)-based material: A potential microparticulate delivery System for controlled release

The potential use of P(3HB) as a microparticulate carrier has been evaluated in a number of studies. Studies have included investigations of these polymers for oral and intravenous drug delivery systems as well as the incorporation of magnetic materials for site directed therapeutic cure. One of the earliest investigations in the use of P(3HB) microspheres in drug delivery was performed by Bissery *et al.*, 1983 & 1984. They produced ^{14}C -labeled P(3HB) microspheres (1-12 μm) using a solvent evaporation technique. During their *in-vivo* studies, they discovered that the P(3HB) microspheres, administered intravenously in mice were located in the lungs of mice. However, when Lomustine [N-2-chloroethyl)-N'-cyclohexyl-N-nitrosourea; CCNU], were administered to Lewis lung carcinoma-bearing mice, little effect

was observed (Bissery *et al.*, 1985). The result of *in vitro* studies showed that the drug was completely released from the drug microspheres within 24 h compared with a release time of over 90 h when PLA microspheres were investigated (Bissery *et al.*, 1984). On the other hand, Brophy and Deasy, 1996 studied the release profile of sulphamethiozole from P(3HB) and P(3HB-*co*-3HV) of particles size (53-2000 μ m) formed by grinding a solvent-evaporated matrix of the components. They found that increasing the molecular weight of P(3HB) increases the rate of release of the drug. This observation was attributed to poor distribution of the drug in the highly crystalline polymer. Furthermore, they observed an increase in the rate of release of the drug as the size of the microspheres decreased. They attributed the effect to the increase in drug loading efficiency due to the large specific surface area of the P(3HB) microspheres. Brophy and Deasy also observed decrease in the release kinetics of the microspheres as the amount of valerate incorporated in P(3HB-*co*-3HV) copolymer chain increased. This was attributed to the increased distribution of the drug enhanced by the valerate component of the polymer chain. A sustained release of sulphamethiozole from P(3HB) microspheres (425-600 μ m) loaded at 50% have been used *in vivo* in dog. It was reported that the drug was completely released in about 24 hours when the drug was administered in dog which correlated with the *in vitro* studies.

Apart from anticancer drugs, several anticancer antibiotics, including doxorubicin, aclarubicin (Juni *et al.*, 1985), 2', 3'-diacyl-5-fluoro-2'-deoxyuridine (Kawaguchi *et al.*, 1992) have been similarly encapsulated. Juni *et al.*, observed *in vitro* release of 10% out of 13% aclarubicin HCl loaded in a P(3HB) microspheres with mean diameter of 170 μ m, over 5 days. Also, some researchers have suggested and proved that incorporation of polyesters in the drug-polymer complex could facilitate drug release by forming channels (interconnected pores) in P(3HB) matrix (Kubota *et al.*, 1988). On the other hand, Abe and colleagues reported faster release of an anticancer agent, lastet, from P(3HB) microspheres when acylglycerols were incorporated into the microspheres (Abe *et al.*, 1992). Kawaguchi and co-workers evaluated *in vivo*, release of two prodrugs of 5-fluoro-2'-deoxyurine from P(3HB) microsphere. The drugs were reported to induce higher antitumor effects against P388 leukaemia in mice, when compared with administration of the free prodrugs over five consecutive days (Kawaguchi *et al.*, 1992).

Apart from cancer related studies on the application of P(3HB) microspheres, P(3HB) microspheres have also been evaluated for its potential as a controlled release systems for the oral delivery of vaccines that could potentially protect vaccine antigens from digestion in the gut, and target delivery to Peyer's patches (Eldridge *et al.*, 1990). According to Eldridge *et al.*, a reasonable absorption of P(3HB) microspheres (of diameter <10µm) containing coumarin was observed in the Peyer's patch when a single dose of P(3HB) microsphere containing the drug was administered in mice.

1.3.2 P(3HB): A potential carrier for a multi-component delivery System

The ability to design biodegradable release devices that could generate impact on cosmetics, food industry and medicine would be of great help to further enhance sustainability in PHA applications. The drive to develop these bio-compatible surfaces for medical or pharmaceutical applications may lead to novel surfaces that could repel or combat bacterial adhesion and biofilm formation. Multicomponent delivery systems could be used to deliver active ingredients that do not normally mix well, such as water-soluble and fat-soluble drugs molecules and other ingredients, and release them simultaneously. This would enhance the stability and bioavailability of a wide range of drugs and nutrients; control their release characteristics and thus, prolong their residence time in the targeted site of delivery. Interestingly, two or more ingredients that would react with each other, through this device, can be separated and provided together, by placing one in the nanospheres and the other in the encapsulated microspheres. A typical example is folic acid and iron that work synergistically in the treatment of anaemia. These drugs can be encapsulated and delivered simultaneously using this device. Figure 1.11 shows a schematic illustration of the concept of a multiple drug delivery system. The nanospheres (green and pink) containing drug or any other active nutrient is encapsulated within the microspheres (yellow). Upon exposure to water or pH, the microsphere releases its contents, and over an extended period of time, the nanospheres release the encapsulated active ingredients through molecular diffusion, dissolution or enzymatic degradation by enzymes such as lipase. The surface properties of the

nanospheres can be altered to be bioadhesive or negatively or positively charged depending on the intended target site.

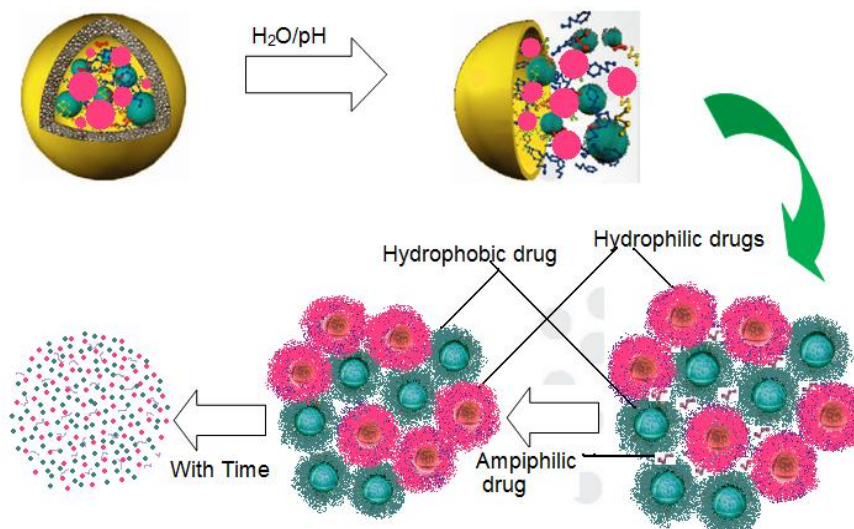


Figure 1.11 Model for a multicomponent delivery system.

Furthermore, the device can be of help in the oral delivery of drugs that have very repulsive taste on the taste bud. Unwanted taste can be masked by preventing interaction between the active molecule and the oral mucosal surface. To achieve this aim, the nanospheres can be prepared with a hydrophobic polymer material that can prevent bitter drugs encapsulated within their structures from going into solution and interacting directly with taste receptor. The system could consist of solid hydrophilic nanospheres composed of hydrophilic drugs or nutrients encapsulated in moisture-sensitive or pH-sensitive hydrophobic-drug containing microspheres or vice versa. The drugs or any other active ingredients in the nanospheres could be the same, or different from, those encapsulated in the microspheres. The materials for the nanospheres surface can include a moisture-sensitive bioadhesive material, such as starch derivatives, natural polymers, natural gums etc, making them capable of being bound to a biological membrane such as the oral cavity mucosa and retained on that membrane for an extended period of time. The nanospheres can be localised and the target drug or ingredients encapsulated within their structure to a particular region, or a specific site, thereby improving and enhancing the bioavailability of ingredients which have poor

bioavailability by themselves. It is expected that the microspheres would be able to release the nanospheres and its contents gradually once a favourable condition is encountered.

To prepare this device, it is necessary that a technology can generate nanospheres with a nano scale diameter is employed. The nanospheres after production and drug loading can be encapsulated in microspheres of about 10-20 μm in diameter. During the preparation of this device, it is necessary to ensure that the nanospheres are homogenously dispersed in the microspheres and not individually coated with the microsphere. This device can be used for maintaining bioavailability of certain nutrients that have poor bioavailability and high water solubility such as vitamin C. The nutrient could be loaded into the hydrophilic nanospheres and then encapsulated within the hydrophobic microspheres, such that slow release and bioavailability can be ensured. In the cosmetic industry, the device can find application in regulating the rate of releasing fragrance and scents thereby prolonging the life span of perfume and reduce their frequent applications.

1.4 Objective of the thesis

High cost of production is one of the limiting factors in the use of PHAs as a replacement for the existing petroleum based plastics. Reducing the cost of production and increasing the yield and productivity of PHAs is an important challenge for applied biotechnologists, since these would enhance the commercialization and applications of this polymer. The cost of carbon source alone account for about 50% of the production cost of PHAs (Kim, 2000; Mudliar *et al.*, 2008). Biologists have combined various micro-organisms with different carbon sources and production methods in order to produce different types of PHAs. Yet, sustainable production of these polymers through the utilization of cheaper available carbon sources and suitable PHA production medium has only partly been exploited.

Also, tailored biopolymer composites play an important role in the medical field such as surgical implant devices, drug delivery systems, and wound healing products. A biodegradable implant will not necessitate a second surgical event for removal; hence, it can be engineered to degrade at a rate that will slowly transfer load to a healing tissue and/or as the basis for a drug delivery system. Interestingly, all polyesters degrade eventually, with hydrolysis being the dominant mechanism. However, while aromatic polyesters such as PET

exhibit excellent material properties, they prove to be almost totally resistant to microbial attack. Aliphatic polyesters on the other hand are readily biodegradable, but usually lack good processability and mechanical performance due to their low molecular weight. Furthermore, most commercially available biodegradable composite polymers are petroleum-based. To avoid perturbation of the ecosystem, biodegradable composite polymers should be derived from renewable resources instead of oil reserves and their production needs to be performed in an environmentally friendly way.

Magnetic nanoparticles have been explored extensively for various biomedical applications. Some of these applications included their use as magnetofection to facilitate gene delivery (Scherer *et al.*, 2002), to induce hypothermia in response to an external alternating magnetic field to selectively destroy cancer cells (Johannsen *et al.*, 2005), as magnetically targeted carrier system in drug delivery applications (Lubbe *et al.*, 1996; Alexiou *et al.*, 2000). Ordinarily, micro and nanocarrier drug delivery systems, such as pure polymeric micro and nanoparticles, do not have the inherent imaging characteristics to monitor their distribution *in vivo*. Thus, for them to function in monitoring drug distribution, in the body, they will have to be incorporated with magnetic materials such as magnetic nanoparticles ferrofluid.

Innovative and smart P(3HB)-polymer carriers for drugs can help to reduce and even eliminate the side effects of drugs. With magnetic-biodegradable P(3HB) composites, the poor selectivity of drugs employed in many treatment methods such as chemotherapy can be avoided. Thus, P(3HB) can be employed as a carrier for smart materials in therapeutic drug delivery systems.

Hence, the prime objectives of the present investigation are:

(1) To investigate the economic production of poly(3-hydroxybutyrate). This would be done through formulation and optimisation of defined production medium that can increase the yield of P(3HB). Within this, different modes of fermentation studies such as shaken flask, batch fermentation, fed-batch and two-stage fermentation studies were carried out. Also, studies were performed on various cheap carbon sources to further increase yield in *Bacillus cereus* SPV. The polymers produced from various investigations were characterized for their monomeric composition, micro structural properties, thermal properties, mechanical properties, crystallinity and bioactivity.

(2) To utilize the P(3HB) produced above in the development of novel 2D and 3D biodegradable composite scaffolds with good processability and mechanical performance as well as sustainability, desired in the tissue engineering of bone and cartilages. The 2D and 3D scaffolds were characterized for their physico-mechanical properties as well as their bioactivity in order to assess their suitability in tissue engineering for bone and cartilage repair and regenerations.

(3) To further explore the potentials of producing bio-derived polymers in the development of novel constructs that could be utilized in multi-purpose delivery systems with excellent applications in medicine, cosmetics and nutrition. The delivery systems produced were characterized for their physico-chemical properties and *in vitro* degradation. The effectiveness of the composite construct in drug release was tested, *in vitro*, using BSA as a model drug.

(4) Finally, a magnetically responsive P(3HB) composite materials, “smart materials” with good applicability in magnetic drug targeting and magnetic fluid hyperthermia were designed and characterized.

The ultimate aim of this research is to extend the areas of applications of P(3HB) especially in medicine, and bring them in to the forefront of other commercially available polymers. Figure 1.12 depicts a schematic representation of the experimental design for this study.

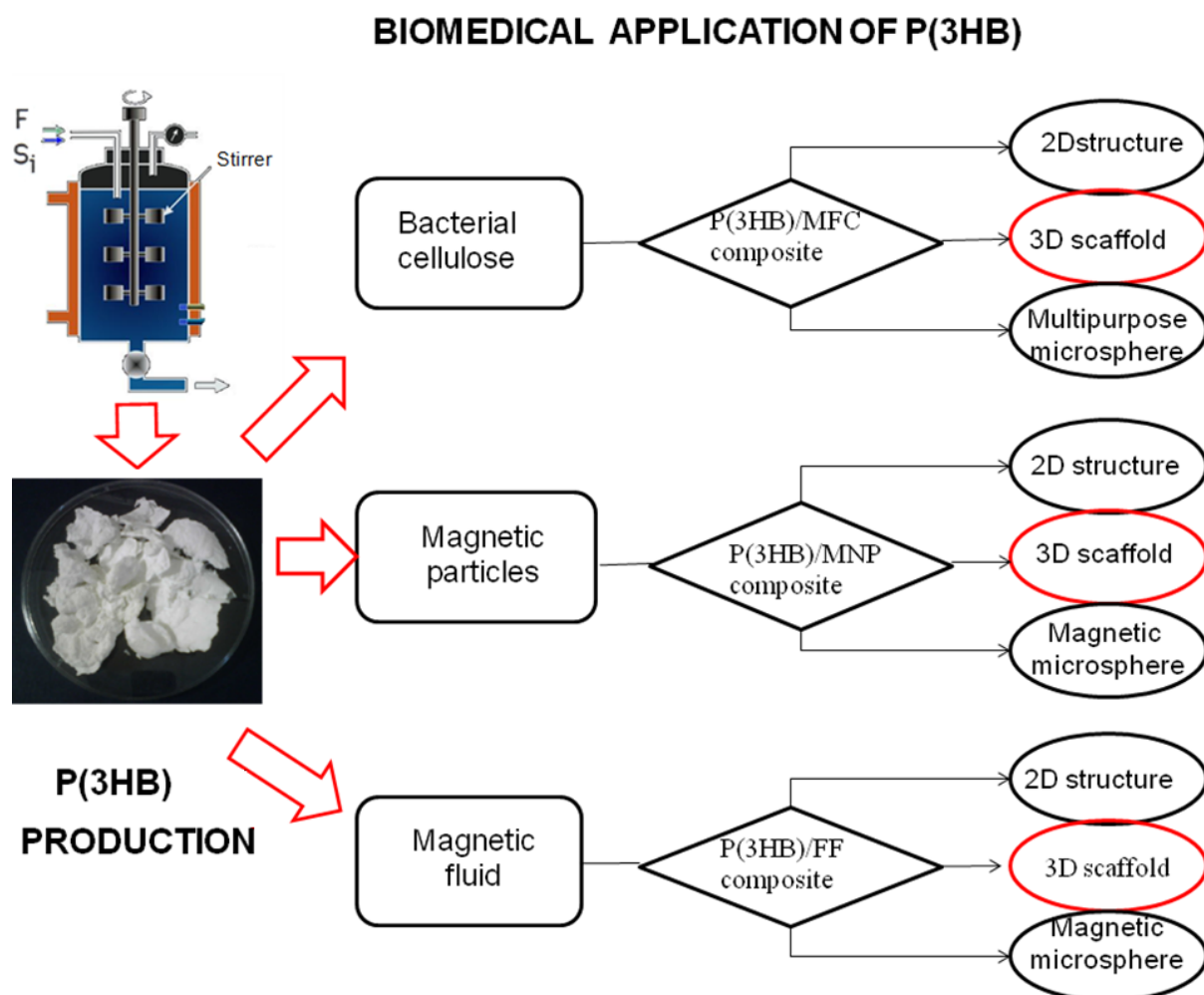


Figure 1.12 Schematic representation of Experimental design

Chapter 2

MATERIALS AND METHODS

Chapter 2

2.1 P(3HB) Production, Extraction and Characterization

2.1.1 Materials

All the chemicals used in P(3HB) production studies were purchased from Sigma-Aldrich Company Ltd (Dorset, England), however, yeast extract was purchased from DIFCO (BD UK Ltd., Oxford, UK). GC-MS analyses were performed using analytical grade reagents. HPLC water and deionised water were used where necessary. University of Westminster regulations and procedures on health and safety were followed. COSHH forms for each of the chemicals and instruments used were filled and signed while SOPs on each of the chemicals and instruments used for the study were read, signed and adhered to throughout the practical work

2.1.1.1 Medium Composition (Kannan and Rehacek medium, (gL⁻¹))

Water	1L
Sucrose	20
Yeast extract	2.5
KCl	3.0
(NH ₄) ₂ SO ₄	5.0
Defatted soybean dialysate	100 mL

2.1.1.2 Medium Composition (Modified G-Medium, (gL⁻¹))

Water	1L
FeSO ₄ .7H ₂ O	0.0005
CuSO ₄ .5H ₂ O	0.005
ZnSO ₄ .7H ₂ O	0.005
MnSO ₄ .7H ₂ O	0.05
MgSO ₄	0.2
CaCl ₂	0.05
(NH ₄) ₂ HPO ₄	2.0

(NH ₄) ₂ SO ₄	1.0
Sucrose	20.0
Ether-extracted yeast extracts	5.0
K ₂ HPO ₄	8.66
KH ₂ PO ₄	6.85

2.1.1.3 Bacterial Strain and maintenance

Bacillus cereus SPV used in this study was obtained from the culture collection of University of Westminster, London, UK. Stock cultures were grown at 30°C in nutrient broth (containing in (gL⁻¹): ‘Lab-Lemco’ powder 1.0; yeast extract, 2.0; peptone, 5.0; sodium chloride, 5.0) and maintained at 4°C on solid nutrient agar (containing in (gL⁻¹): ‘Lab-Lemco’ powder, 1.0; yeast extract, 2.0; peptone, 5.0; sodium chloride, 5.0; agar, 15.0).

2.1.1.4 Seed Culture preparation in Nutrient Broth

Cultures of *Bacillus cereus* SPV were grown at 30°C and 200 rpm for 14 h in nutrient broth (containing in (gL⁻¹): ‘Lab-Lemco’ powder 1.0; yeast extract, 2.0; peptone, 5.0; sodium chloride, 5.0). After 14 h growth, the culture was used to inoculate Kannan and Rehacek production medium (10% v/v) in either shaken flask or fermenter.

2.1.1.5 Seed Culture preparation in Modified G-medium

For P(3HB) production using defined medium, modified G-medium (MGM) containing the following nutrients in (gL⁻¹) of distilled water was used for preparation of the seed culture; FeSO₄·7H₂O, 0.0005; CuSO₄·5H₂O, 0.005; ZnSO₄·7H₂O, 0.005; MnSO₄·7H₂O, 0.05; MgSO₄, 0.2; CaCl₂, 0.05; potassium hydrogen phosphate (dibasic), 1.0; (NH₄)₂SO₄, 1.0; Sucrose, 20.0 and ether-extracted yeast extract, 4.0. The culture was allowed to grow at 30°C and 200 rpm for 10 h, after which 10% of the seed culture was used to inoculate the production medium in shaken flask or fermenter.

2.1.1.6. Kannan and Rehacek Production medium preparation.

Cultures of *Bacillus cereus* SPV were grown in a modified Kannan and Rehacek medium containing, (g^L⁻¹) sucrose, 20; yeast extract, 2.5; potassium chloride, 3; ammonium sulphate, 5.0 and 100 mL of defatted soybean dialysate (prepared from 10 g of defatted soybean meal in 1000 mL of distilled water for 24 h at 4°C).

2.1.2.1 P(3HB) production in Shaken flasks

Bacillus cereus SPV was grown at 30°C in 60 mL of nutrient broth in 250 mL flasks with rotary shaking at 200 rpm (Stuart orbital incubator 51500, UK). After about 10 h of growth, 15 ml of the culture broth was inoculated in 1-litre Erlenmeyer flasks containing 250 ml of the production medium. In all cases the pH was adjusted to 6.8 prior to cultivation. Samples were collected at defined time intervals during cultivation and analyzed for dry cell weight (dcw), P(3HB) content and residual cell mass (RCM).

2.1.2.2 P(3HB) production in a fermentor (Batch production)

For P(3HB) production in a fermentor, *Bacillus cereus* SPV was first grown at 30°C in 1-litre flasks containing 200 mL of the production medium (pH=6.8) and a defined carbon source, with shaking at 250 rpm (New Brunswick Scientific Classic Series, UK) for 10 h. This culture was used to inoculate a 2-litre fermentor vessel (electro lab, UK) containing production medium. Two drops of 1 mM antifoam (Down Corning, DB-110A) was added before inoculation of the fermenter with the seed culture and the pH was maintained at 6.8 using 0.5M HCl/NaOH where necessary. The air inflow rate and agitation speed were initially adjusted to 0.5 Lmin⁻¹ and 300 rpm, respectively, during the fermentation. When a decrease in dissolved oxygen was detected below 20%, the air inflow rate was increased to 1 Lmin⁻¹ to avoid oxygen limitation. Samples (ca. 10 mL) were collected at different time intervals for analysis.

2.1.2.3 P(3HB) production in a fermentor (Fed-Batch production)

For fed-batch P(3HB) production in a bioreactor, two methods of feeding was employed during the course of the study. In the first method, 1 g/mL of carbon source (stock solution) was prepared and aliquots of 10 mL were intermittently added to a 1.5 L culture broth at defined time intervals throughout the cultivation period.

In the second method, 0.5 g/mL carbon source (stock solution) was prepared and constantly fed to the culture at a feeding rate of 0.71 mL min⁻¹ after a reduction in OD₆₀₀ of the culture broth was noticed. This was performed to maintain excess carbon concentration and thus, promote P(3HB) accumulation in the organism.

2.1.2.4 P(3HB) production in a fermentor (Two-Stage fermentation)

For 2-stage fermentation, the production medium was prepared following the procedure described in Section 2.1.2.2. The same amount of nutrients was added except slight changes in chemicals which included (in g/L); (NH₄)₂HPO₄, 4.0, (NH₄)₂SO₄, 1.0, yeast extract, 5.0, K₂HPO₄/KH₂PO₄, 0.2M and 8 * 10⁻⁴M α-Picolinic acid. The same protocol in Section 2.1.2.2 was followed in the two-stage. However, after 30 h fermentation time, the first stage of the fermentation was stopped and the cells were harvested using sterilized jars. Aliquots of 350 mL of the culture broth were centrifuged at room temperature and 3000 rpm after which the cells were returned to the fermenter containing a fresh medium that was limited in some nutrients. The second medium contained (in g/L) (NH₄)₂HPO₄, 1.0, yeast extract, 2.5 g, FeSO₄.7H₂O, 0.0005, CuSO₄.5H₂O, 0.005, ZnSO₄.7H₂O, 0.005, MnSO₄.7H₂O, 0.05, MgSO₄, 0.2, CaCl₂, 0.05, sucrose, 20.0, K₂HPO₄, 0.5 and 6 * 10⁻⁴M α-Picolinic acid. Two drops of antifoam was added before the harvested cells were returned to the fermenter and the pH was maintained at 6.8 using 0.5M HCl/NaOH. The air inflow rate and agitation speed were adjusted to 0.5 Lmin⁻¹ and 300 rpm, respectively, during the fermentation. Samples (ca. 10 mL) were collected at different time intervals for analysis.

2.1.3 P(3HB) extraction

For P(3HB) extraction, three different methods were employed: dispersion, soxhlet extraction and wet cell extraction.

2.1.3.1 Dispersion method of P(3HB) extraction

For the extraction of P(3HB), the cells were harvested by centrifugation at 4600 rpm (12,000 g) (SORVALL[®] Legend RT Jenkons-PLC, UK) and then lyophilized. P(3HB) was extracted by treating 1 g of freeze-dried cells with a dispersion solution containing 50 mL of chloroform and 50 mL of a diluted (70%) sodium hypochlorite solution in water in an orbital shaker (Stuart orbital incubator 51500, UK), at 100 rev min⁻¹. The dispersion solution containing the dried cell was incubated at 37°C for 1 h. The mixture obtained was then centrifuged at 4600 rpm (12, 000 g) for 10 min, which resulted in three separate phases. The P(3HB) was recovered from the bottom phase, i.e. that of chloroform and precipitated using 10 volumes of ice-cold methanol.

2.1.3.2 Soxhlet extraction

The bacterial cells were harvested by centrifugation at 4600 rpm (12,000 g), and then lyophilized. The cell mass was then lysed in 16% sodium hypochlorite (pH 11) at 37°C for 1 h, centrifuged at 4600 rpm (12, 000 g), and the residue was washed twice each with water, acetone, ethanol and diethyl ether. Finally, the residue was dried and subjected to soxhlet extraction for 24 h using chloroform, and eventually P(3HB) was precipitated using ice cold methanol.

2.1.3.3 Wet cell extraction

For the wet cell P(3HB) extraction, the cells were harvested by centrifugation at 4600 rpm (12, 000 g) for 15 min and washed twice with water, acetone, ethanol and diethyl ether to remove media and proteins that bound to the cells. The washed bacterial cells were finally centrifuged for 30 min at 4600 rpm (12, 000 g). P(3HB) was extracted by treating 1 g of washed wet cells with a solution containing 50 mL of chloroform and 50 mL of a diluted (70%) sodium hypochlorite solution in water, in an orbital shaker (Stuart orbital incubator 51500, UK), at 100 rev min⁻¹. The wet cells were treated at 37°C for 3 h. The mixture obtained was then centrifuged at 4600 rpm (12, 000 g) for 10 min, which resulted in three separate phases. The P(3HB) was recovered from the bottom phase (i.e. that of chloroform), by precipitation using 10 volumes of ice-cold methanol.

2.1.4 Quantification Analysis

2.1.4.1 Dry cell weight measurement

Dry cell weight (dcw), was determined by centrifuging 3 mL of the culture samples at 2000 g for 15 min, the pellet washed twice with deionised water (milli-Q, Millipore, Billerica, MA, USA), and freeze dried until constant weight was obtained. The freeze dried cells were then weighed.

2.1.4.2 P(3HB) quantification

P(3HB) quantification was performed by employing the Law and Slepecky (1961) method, according to which the dried cell pellets containing intracellular P(3HB) were hydrolysed using concentrated sulphuric acid for 1 h to obtain crotonic acid, which was quantified by measuring absorbance at 235 nm (Hitachi- U2800A spectrophotometer, Lambda Advance Technology Ltd, UK) using a quartz cuvette. Samples were analysed in triplicates for both shaken flasks and fermentor.

2.1.4.3 Gas chromatography-mass spectrometry (GC-MS)

For the identification of the PHA, a slight modification of the gas chromatographic method of Huijberts *et al* (1994) was employed. The analysis was performed by mixing 1 mg mL⁻¹ of sample (dried cell) and 1 mg mL⁻¹ methyl benzoate solution in chloroform and the resultant mixture was added to a mixture of 2 mL of 15% sulphuric acid in methanol (ratio 1:1) and refluxed at 100°C for 5 h in a reflux apparatus. After the reaction, the tubes were cooled on ice for 5 min and 1.0 mL distilled water was added and the tubes vortexed for 1 min. After phase separation, the organic phase was collected and dried over anhydrous sodium sulphate. The analysis was performed using a Trace GC-MS (Thermo, San Jose, CA, USA). The Trace 2000 gas chromatograph was equipped with a ZB-5MS (Phenomenex, Torrance, CA, USA) column (30m length, 0.25 mm internal diameter, and 0.25 µm film thickness). The sample (1 µL), in chloroform, was injected with helium (1 mL min⁻¹) as the carrier gas. The injector temperature was 220°C and the column temperature was increased from 40°C to 320°C at 20°C min⁻¹ and held at the final temperature for 6 min.

For the quantification of the amount of the PHA and the relative mole fractions of each type of PHA, GC analysis was carried out. The PHA samples were methanolysed as described above and the analysis was carried out using a Sigma 3B gas chromatograph (Perkin Elmer, Waltham, MA, USA) equipped with a BP21 (SGE Europe Ltd, Kiln Farm, Milton Keynes, UK) column (50 m length, 0.25 mm internal diameter, and 0.25 μm film thickness). The sample (1 /A), in chloroform, was injected with helium (1 ml min⁻¹) as the carrier gas. The injector temperature was 225°C and the column temperature was increased from 40°C to 240°C at 20°C min⁻¹ and held at the final temperature for 10 min.

2.1.4.4 Fourier transform-infrared spectroscopy (FT-IR)

Freeze-dried, precipitated P(3HB) from *B. cereus* SPV was used to prepare KBr discs (sample:KBr, 1 : 100). An FT-IR spectrometer (Perkin Elmer) was used under the following conditions: spectral range, 4000-400 cm⁻¹; window material, CsI; 16 scans; resolution 4 cm⁻¹; the detector was a temperature-stabilized, coated FR-DTGS detector.

2.1.4.5 X-ray diffraction (XRD)

X-ray diffraction (XRD) analysis was performed on freeze-dried, precipitated P(3HB) from *B. cereus* SPV. Samples were analysed on a Brüker D8 Advance diffractometer in flat plate geometry, using Ni filtered Cu Ka, radiation. Data was collected from 10 to 100° with a primary beam slit size of 0.6 mm. A Brüker Lynx Eye silicon strip detector was used and a step size of 0.02° and a count time of 0.1 s per step.

2.1.4.6 Differential scanning calorimetry (DSC)

Thermal analysis of the samples (extracted and commercially available P(3HB)) was performed with a Perkin-Elmer Diamond DSC (Perkin-Elmer Instruments, USA). Samples in duplicates (4-6 mg) were encapsulated in standard aluminium pans and all tests were carried out under inert nitrogen. The samples were heated from -50 to 200°C at a heating rate of 20°C/min (first heating cycle). The samples were then brought to -50°C (cooling rate of 20°C/min) and further heated to 200°C with a heating rate of 10°C/min (second heating cycle).

2.2. Cellulose production

2.2.1 Materials

All the chemicals used for cellulose production were purchased from Sigma-Aldrich Company Ltd (Dorset, England) except for yeast extract which was purchased from DIFCO (BD UK Ltd., Oxford, UK).

2.2.1.1 Medium Composition (gL⁻¹)

CaCO ₃	12.0
Glucose	50
Yeast extract	5
Water	1L

2.2.1.2 Bacterial strain and maintenance

Acetobacter xylinum (JCM10150) used in this study was obtained from the culture collection of University of Westminster, London, UK. Stock cultures were grown at 27°C in a medium (containing in (gL⁻¹): Yeast extract, 5.0; calcium carbonate, 12.0; glucose, 50.0) and maintained at 4°C and pH 5.0.

2.2.2 Cellulose production in flasks

Acetobacter xylinum (JCM10150) cells were grown in a 20 mL universal tube containing 10 mL of production medium, under static conditions at 27°C for 24 h. After 24 h, 10 mL of the culture broth was aseptically transferred to 1.0 Litre Erlenmeyer flasks containing 300 mL of production medium. Incubations were performed at 27°C for 48, 72, 96 and 120 h under static conditions. The starting pH of the medium was 5.0.

2.2.3 Cellulose extraction

The resulting gel-like cellulose pellicle from *Acetobacter xylinum* (JCM10150) culture was collected from the air-water interface, washed with distilled water and treated with 2% sodium hydroxide at 80°C for 2 h. This was followed by rinsing with water.

2.2.4 Microfibrillated bacteria cellulose (MFC) production

Bacteria cellulose was harvested and treated with 2% sodium hydroxide for 1 h at 100°C to kill the *Acetobacter xylinum* cells, then washed several times with deionised water to remove the sodium hydroxide. The gel-like pellicles were first blended with a blender (Osterizer blender, Pulse matic, UK) to break the pellicles into smaller pieces and later homogenised using a homogenizer (Bucks Laboratory Mixer Emulsifier, UK) in order to produce microfibrillated bacterial cellulose.

2.2.5 Chemical Modification of MFC

The produced microfibrillated bacteria cellulose was acetylated to produce hydrophobic MFC. Acetylation reactions were performed on the microfibrillated cellulose produced in Section 2.2.4. The homogenised microfibrillated cellulose was centrifuged at 4600 rpm (12, 000 g) for 30 min, thrice, in order to remove the water contained in the cellulose solution. Then, Dimethylformamide (DMF) was subsequently added to the cellulose and the sample homogenised for 5 minutes in order to allow mixing with DMF and removal of water from the sample. The mixture was later centrifuged at 4600 rpm (12, 000 g) for 30 min. This process was repeated several times until all the water contained within the MFC was completely displaced by DMF. Each homogenization/redispersion step was carried out using a homogenizer (Bucks Laboratory Mixer Emulsifier, UK). Anhydrous acetic acid was later added to the MFC dispersed in DMF and homogenized for 5 min to remove any remaining water from the sample. The sample was then placed in a stoppered glass bottle containing a mixture of acetic acid, toluene and perchloric acid in a ratio of (200:250:1) mL, respectively. Stoppered flat bottom flask was used to avoid air from entering into the reaction. The mixture was homogenised for 2 min. Then a desired amount of acetic anhydride was added, the whole suspension was finally homogenized for an additional 2 min and introduced in the 2.5 L

stoppered flat bottom reaction flask and stirred under room temperature. Different reaction times were investigated, from 24 h to 72 h. At the end of the reaction, the suspension was centrifuged at 4600 rpm (12, 000 g) for 30 min. To eliminate all nonbonded chemicals (i.e. unreacted compounds and by-products formed), the modified MFC was subsequently washed three times with a toluene/ethanol/acetone mixture (4:1:1 by vol.), each washing included a homogenization and centrifugation step.

The degree of acetylation was determined using a standard saponification procedure.

2.2.6 Determination of degree of acetylation

To determine the degree of acetylation of the acetylated microfibrillated cellulose, 100 mg of freeze dried cellulose, collected at each time points of the acetylation reactions (24, 48, 72 h) was accurately weighed out and put into 40 mL of 75% ethanol in a glass bottle. The bottle, loosely stoppered, was heated to 50-60°C for 30 min for better swelling of the material. Then, 40 mL of 0.5N NaOH solution was added to the sample and the mixture was heated to 50-60°C for 15 min. The bottle was stoppered tightly and allowed to stand at room temperature for about 48 h. The excess alkali was then titrated with 0.5N HCl using phenolphthalein as an indicator.

2.2.7 Quantification and Analysis

2.2.7.1 Cellulose dry weight measurement

Whole pellicles were freeze dried (10°C, 0.006 mbar) and weighed on an analytical balance. Dry weights were determined as the average of at least three pellicles measured.

2.2.7.2 Total viable counts

The number of viable bacteria in the inoculum at the end of the fermentation was determined by the spread plate technique. The diluent used was peptone and the plating medium was solid nutrient agar (containing in (gL⁻¹): 'Lab-Lemco' powder, 1.0; yeast extract, 5.0; calcium

carbonate, 12.0; glucose, 50; agar, 15.0). Colonies were counted after 48, 72, 96 and 120 h of incubation at 27°C using an Omron H7EC digital colony counter (Applethorn, Australia).

2.2.8 Characterization of modified microfibrillated cellulose

The physical characterisation techniques employed were chosen to understand the effects of chemical modification of MFC on the original properties of MFC. The different techniques adopted and details of the analysis are described in detail below.

2.2.8.1 Infrared Spectroscopy (FTIR)

Infrared spectra of dried unmodified and acetylated MFC (freeze dried over night) were recorded using a FTS 6000 spectrometer (Portmann Instruments AG, Biel-Benken, Switzerland). For each sample, the diamond crystal of an attenuated total reflectance (ATR) accessory was brought into contact with the area to be analyzed. The contact area was about 2 mm², and a torque of 10cN·m was used to ensure the same pressure on each sample. All spectra were recorded between 4000 and 400 cm⁻¹, with a resolution of 4 cm⁻¹ and 32 scans.

2.2.8.2 X-ray Diffraction Analysis

Wide-angle X-ray diffraction (WAXD) patterns were collected on a Panalytical X'Pert Pro Materials Research diffractometer working in reflection mode, from $2\Theta = 10^\circ$ to $2\Theta = 100^\circ$. Cu KR radiation (λ 0.15418 nm) was generated at a voltage of 45 kV and a current of 40 mA and was monochromated with a diffracted beam monochromator. Unmodified and acetylated MFC were pressed to form pellets and the surface was analysed. All spectra were normalized to the 004 lattice at $2\Theta = 34^\circ$, which was not affected by the chemical modification.

An index of crystallinity, CI, was calculated from a ratio of the area under the curve in Figure 2.1, using equation (1);

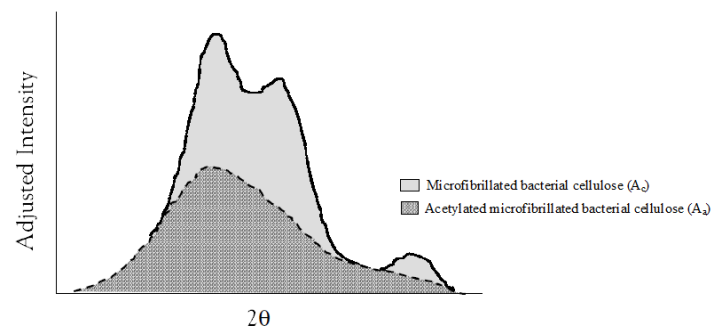


Figure 2.1 Schematic overlays of diffraction spectra for microfibrillated bacterial cellulose (MFC), (A_c) and acetylated microfibrillated bacterial cellulose (A_a)

$$CI = \frac{A_c}{A_c + A_a} \quad (1)$$

Where, A_c and A_a represent the integrated areas under the unmodified MFC and acetylated MFC WAXD patterns, respectively.

2.2.8.3 Scanning Electron Microscopy (SEM)

SEM experiments were conducted using a Jeol 6300F scanning electron microscope using an acceleration voltage (EHT) of 5 kV and a working distance of 16 mm. A 0.07% (w/w) suspension of unmodified and acetylated MFC in CHCl_3 was sonicated twice at room temperature for 15 min. One droplet of the suspension was then deposited on a freshly cleaved mica surface and then sputter coated with an 8 nm layer of platinum.

2.2.8.4 Dispersion Tests

The behaviour of unmodified and acetylated MFC in suspension was examined in CHCl_3 , a solvent for P(3HB). Dispersion tests were carried out with solvent exchanged and dried-redispersed nanofibres at a concentration of 0.07% (w/w). Unmodified MFC was first solvent exchanged from water to acetone and then to CHCl_3 . Acetylated MFC was directly solvent exchanged to CHCl_3 after completion of the reaction. In addition, the unmodified and acetylated MFC nanofibres were dried in a ventilated oven at 60°C , under continuous stirring and then redispersed in CHCl_3 . All suspensions were sonicated three times for 15 min at room temperature and allowed to stand for 24 h to ensure formation of a stable suspension.

2.3 P(3HB) Composite Preparation

2.3.1 P(3HB)/MFC Nanocomposite film Preparation

P(3HB) was first dissolved in CHCl_3 at room temperature and stirred for 24 h (2% w/w). The acetylated MFC suspensions in CHCl_3 were then prepared using solvent exchanged nanofibres. The desired amount of filler was added in the P(3HB) solution, and the mixture was homogenized for 2 min using a homogeniser (Ultra-Turrax T25 basic, Ika-Werke). The suspension was then degassed three times and poured into a glass petri-dish, where the films were obtained by solvent evaporation at room temperature. Nanocomposite films containing 0, 5, 10, 20, 30, 40 and 50 wt % of filler was prepared.

2.3.2 Preparation of Composite Scaffolds

The Compression moulding/Particulate leaching technique was employed in the preparation of all the biodegradable scaffolds samples produced in this work. Details of the methodology followed in the preparation of respective composite scaffolds are given below.

2.3.3 Preparation of P(3HB)/MFC Scaffold

P(3HB) and P(3HB)/MFC composite Scaffolds were prepared using the conventional compression moulding/particulate leaching technique developed and by employing sucrose grains as the porogen for porosity. For P(3HB) scaffold preparation, 1.0 g of P(3HB) was dissolved in 10 mL of chloroform and 20 g of sucrose grains of desired pore size was added. The resulting mixture was stirred to obtain a homogenous paste. The semi-solid paste formed was placed into a cylindrical syringe that was cut open at both ends. With the help of a plunger, the solid was moulded into shape by applying pressure up to 10 bars in the cylindrical syringe that was cut open at both ends. The moulded cylindrical solids were air dried at 30°C.

For P(3HB)/MFC scaffold preparation 1.0 g of P(3HB) was dissolved in 10 mL of chloroform and appropriate amounts of modified MFC (5, 10, 20, 30, 40, and 50%), were separately dissolved in chloroform and homogenised. Each of the appropriate amounts of homogenised MFC were later mixed with P(3HB) solution and sonicated

for 1 min (Ultrasonic Homogenizers US200, Philip Harris Scientific, UK) to improve the dispersion of the modified MFC in the P(3HB) solution. 20 g of sucrose grains of desired pore size was later added to the P(3HB) solution and stirred to form a semi-solid paste. The semi-solid paste formed was later moulded into shape as described above. The moulded cylindrical solids were air dried at 30°C for 6 h and later immersed in 500 mL of deionised water (which was occasionally changed) for 12 h to allow complete dissolution of sugar grains from the solid cylindrical body. After about 12 h, the porous scaffold were removed from the water and air dried at 30°C. The porous scaffolds were sectioned using sharp blades to cut foams in the size of 0.5 x 0.5 x 0.5 cm³ for further experiments.

2.3.4 Preparation of P(3HB)/Magnetic particles, and P(3HB)/Magnetic fluid Composite Scaffold

P(3HB)/Magnetic particles and P(3HB)/Magnetic fluid composite scaffolds were prepared using the same compression mould/particulate leaching technique and by employing sucrose grains as the porogen agent. For P(3HB)/Magnetic particles composite scaffold preparation, 1.0 g of P(3HB) was dissolved in 10 mL of chloroform. Appropriate amount of Magnetic particles were suspended in chloroform (0.5, 1.0, 1.5, and 5 mL), was added and the mixture sonicated (Ultrasonic Homogenizers US200, Philip Harris Scientific, UK) to improve the dispersion of magnetic particles in the P(3HB) solution. 20 g of sucrose grains (Sigma, Aldrich) of desired pore size was later added and the mixture was stirred to make a homogenous paste. The semi-solid paste formed was later moulded into shape by applying pressure up to 10 bars using a custom designed 10 mL syringe. The moulded cylindrical solids were air dried at 30°C for 6 h and subsequently immersed in 500 mL of deionised water (which was occasionally changed) for 12 h to allow complete dissolution of sugar grains from the solid cylindrical body. After 12 h, the porous scaffold was removed from the water and air dried at 30°C. P(3HB)/Magnetic fluid scaffold was prepared using the same protocol except that magnetic particles was replaced with magnetic fluid in chloroform. The Scaffolds fabricated were later sectioned using sharp blades to cut foams in the size of 0.5 x 0.5 x 0.5 cm³ for further experiments.

2. 4 P(3HB) Composite Characterization

2.4.1 Characterisation of P(3HB)/MFC films

The physical characterisation techniques employed were chosen to understand the effect of addition of modified MFC to P(3HB) in the composite films. The different techniques adopted and details of the analysis are described in detail below.

2.4.1.1 Dynamic Mechanical Analysis (DMA)

DMA experiments were carried out in tensile mode using a Perkin-Elmer Dynamic Mechanical Analyser (DMA 7e, Perkin-Elmer Instruments, USA) at room temperature. Tensile strength tests were conducted on flat specimens (width: 1.4 mm, length: 7-8 mm and thickness: ≈ 100 -120 μm) cut out from the solvent cast films. To erase any trace of solvent, samples were first heated from room temperature to 100°C at 10°C/min, 1 Hz frequency, and 0.01% of strain, and this temperature was kept for 10 min. Then dynamic cooling scans were conducted from 100 to 30°C at 2°C/min, 1 Hz, and 0.1% of strain. During the DMA experiment, the static load was kept at 1 mN and it was increased to 6000 mN at a rate of 200 mN min⁻¹. Four repeat specimens were tested for each sample and the average value was used.

2.4.1.2 Differential Scanning Calorimetry (DSC)

DSC measurements were performed with a differential scanning calorimeter (Perkin-Elmer Pyris Diamond DSC (Perkin-Elmer Instruments, USA)). The sample mass for this measurement, was in the range of 4-6 mg. To measure the thermal properties, each sample was encapsulated in standard aluminium pans and all tests were performed under nitrogen atmosphere. Samples were heated/cooled/heated at a rate of 20°C min⁻¹ between -50°C and 200°C. The glass transition temperature (T_g) was measured at half-height of the specific heat increment at the glass transition temperature. Measurements were carried out in triplicates.

2.4.1.3 Contact angle study

In order to evaluate the wettability of the composite samples, static contact angle measurements were carried out on each of the samples. The experiment was carried out on a KSV Cam 200 optical contact angle meter (KSV Instruments Ltd., Finland). An equal volume of water (<20 μ l) was placed on every sample by means of a gas tight micro-syringe forming a meniscus. Photos (frame intervals -1 s, number of frames-100) were taken to record the shape of the meniscus. The water contact angles on the specimens were measured by analysing the recorded drop images (four repeats for each sample) using the Windows based KSV-Cam software. Figure 2.2(a) shows the set up for the water contact analysis while Figure 2.2(b) shows the contact angle measurement on the drop images. The water contact angle was measured using Young's equation which defines the balance of forces caused by a wet drop on a dry surface and gives the following relation,

$$\gamma_{SL} + \gamma_{LV}, \cos \theta_c = \gamma_{SV} \quad (2)$$

Where, θ_c is the contact angle, and γ_{SL} , γ_{LV} , and γ_{SV} are the interfacial tensions between the solid and the liquid, the liquid and the vapor, and the solid and the vapor, respectively.

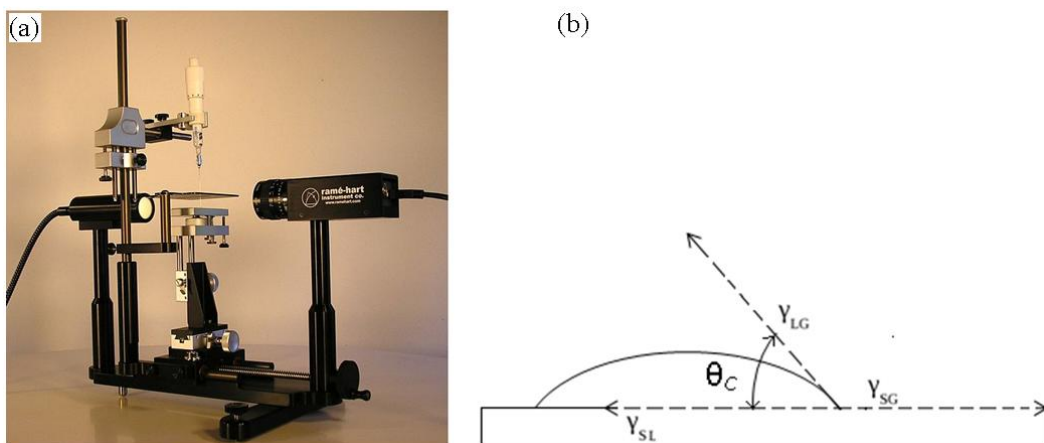


Figure 2.2 (a) Set up for goniometric measurement of contact angle of the P(3HB) composite materials, (b) an illustration of the sessile drop technique with a liquid droplet partially wetting a solid substrate (2D P(3HB) composite materials). θ_c is the contact angle, and γ_{SG} , γ_{LG} , γ_{SL} represent the solid-gas, gas-liquid, and liquid-solid interfaces, respectively.

2.4.1.4 Determination of surface charge

Surface charge was detected by staining the surfaces with a dilute solution of Toluidine blue, (PAANa) or Rose Bengal, (DMAPAAMe). Surfaces were incubated in 1 mL of 0.1 w/v% solution of Toluidine blue or 0.1 w/v% solution of Rose Bengal for 4 h at room temperature. Samples were rinsed thrice with deionized, distilled water for 5 min and dried overnight prior to imaging.

2.4.2 Characterization of P(3HB) Composite 3D scaffolds

The characterisation techniques employed for the entire constructs were chosen to understand the effect of addition of fillers on the properties of the resultant composite scaffolds. The different techniques adopted and details of the analysis are described in detail below. Table 8 shows the summary of the analyses done and the samples on which the analyses were performed.

2.4.2.1 Scanning electron microscopy (SEM)

Scanning electron microscopy (SEM) was used to examine the microstructure of the 2D and 3D scaffolds samples. Samples were sectioned using a sharp blade and placed on a freshly cleaved 8 mm diameter aluminium stubs and gold plated for 2 min. Images were taken at various magnifications and acceleration voltages (max. of 20 kV) to avoid beam damage to the polymer. For each image at least 20 pore throats were measured, taking the longer diameter in the cases where the throat appeared elliptical because of perspective.

2.4.2.2 Compression Modulus measurement

The compressive strength of P(3HB) and P(3HB)/MFC composite scaffolds was measured using a Perkin-Elmer Instruments, USA at room temperature as described elsewhere (Lebourg, 2008). Cylindrical samples of 2 mm diameter and around 2 mm height were cut with surgical scalpels, and then compressed. The initial load was set at 1 mN and it was increased to 6000 mN at a rate of 200 mN min⁻¹. Four repeat specimens were tested for each sample during this analysis and the results presented in this work are average of four

measurements. Elastic modulus of the scaffold was determined using a stress strain representation. Methodology for curve interpretation and modulus calculation was taken from ASTM D1621-04a standard ‘Compressive properties of rigid cellular plastics’.

2.4.2.3 Porosity measurements on the scaffolds

The gravimetric method was employed in measuring the porosity of the fabricated scaffolds. The samples were weighed dry, and then filled with distilled water under vacuum, and subsequently weighed again. Porosity was calculated as the quotient of the volume of pores (see below) and the total volume of the scaffold.

The volume of pores, V_{pore} , was deduced from the weight difference between dry (m_{dry}) and wet (m_{wet}) sample, according to equation (3) assuming that the amount of water absorbed by the scaffold composite phase is negligible due to its high hydrophobicity (Jones, 2005). Thus, the volume of pores equals the volume occupied by the absorbed water.

$$V_{pore} = \frac{m_{wet} - m_{dry}}{d_{water}} \quad (3)$$

Where, d_{water} is the density of water.

The volume of P(3HB) and P(3HB)/MFC was calculated from the dry weight of the scaffold assuming a density of P(3HB) about 1.135 gcm^{-3} , which corresponds to the average crystallinity measured by DSC about 63.6%. Density was calculated on the basis of amorphous phase and crystalline phase densities of 1.021 and 1.2 gcm^{-3} , respectively (Hayashi, 2002). For each sample type, at least five measurements were carried out and the obtained values were averaged.

2.4.2.4 *In vitro* degradation study

For the *in vitro* degradation assessment, a total of nine samples from each group were immersed in SBF for 1, 2, 3 and 4 weeks and 20 mL PBS was used for each sample. The pH-values of SBF were monitored every week by an electrolyte-type pH meter (PHS-2C, Jingke Leici Co., Shanghai, China). Three samples from each group were removed from the SBF at

the predetermined time point (1, 2, 3 and 4 weeks) and wiped with filter paper to remove surface water followed by measurement of the wet weight of the samples. These samples were then washed with deionised water, vacuum dried, and weighed to determine the mass of dried samples. The percentages of water absorption and mass loss were calculated using the following equations.

$$\text{Water absorption (\%)} = 100 \times \frac{(M_{t, \text{wet}} - M_{t, \text{dry}})}{M_{t, \text{dry}}} \quad (4)$$

$$\text{Water loss (\%)} = 100 \times \frac{(M_{0, \text{wet}} - M_{t, \text{dry}})}{M_{0, \text{dry}}} \quad (5)$$

Where, M_0 and M_t with subscript 0 and t are mass at the immersion time of 0 and t, respectively. All the values presented were average of three samples.

2.4.2.5 SQUID Analysis

A superconducting quantum interference device (SQUID, MPMS XL-7, Quantum Design) was used for the magnetic measurements. The hysteresis loops were collected at a temperature of 300 K in external magnetic fields from -1 T to $+1$ T. The analysis was performed at the Centre for Nanotechnology Research Centre, CNRC, by Dr. Jan Filip.

2.4.2.6 Protein adsorption study

Protein adsorption assay on 2D (films) and 3D scaffold was carried out using fetal bovine serum (FBS). All measurements were carried out in triplicates per sample. The samples were covered with 200 μL of undiluted FBS in 1.5 mL eppendorf and Incubated at 37°C for 24 h. The serum was then removed from the samples and the samples were washed three times with phosphate buffer saline (PBS). The proteins adsorbed on the samples were collected by incubating the samples with 1 mL of 2% sodium dodecyl sulfate (SDS) in PBS for 24 h at room temperature and under vigorous shaking. This was done to ensure the adsorbed proteins

were re-adsorbed in the PBS (with SDS). Amount of total protein adsorbed was measured using a commercial protein quantification kit (Qubit™ Protein Assay Kits). Fluorescence was measured at 485/590 nm against a calibration curve using bovine serum albumin (provided in the kit).

Calculating the Concentration of Sample

The Qubit® 2.0 Fluorometer gives values for the Qubit™ protein assay in µg/mL. This value corresponds to the concentration after sample was diluted into the assay tube. To calculate the concentration of sample, the following equation was used:

$$\text{Concentration of sample} = \text{QF value} \times \frac{200}{X} \quad (6)$$

Where, QF value = the value given by the Qubit® 2.0 Fluorometer, X = the number of microliters of sample added to the assay tube. This equation generates result in µg/mL.

2.4.2.7 Raman spectroscopy

All Raman spectra were recorded using Raman spectrometer (LabRAM HR, HORIBA JOBIN YVON Ltd., UK with Labspec software) with 633 nm laser, filter at 100%, hole at 300, slit at 150, grating at 1800, microscope objective x50, and acquisition properties of exposure time for 10s. Three spectra per location were recorded in the wave number interval of 400-1400 cm⁻¹.

Table 2.1 Summary of analysis carried out on specific experiments.

Properties Analyzed	P(3HB)/MFC composite film	P(3HB)/MFC composite scaffold	P(3HB)/magnetic particles composite scaffold	P(3HB)/Magnetic fluid composite scaffold
Tensile strength (DMA)	√		√	√
Compression modulus		√	√	√
Scanning Electron microscope (SEM)	√	√	√	√
X-ray Diffraction (XRD)	√	√	√	√
FTIR	√	√	√	√
Porosity measurements		√	√	√
In vitro degradation	√	√	√	√
SQUID Analysis			√	√
Differential Scanning Calorimetry (DSC)	√	√	√	√
Contact angle measurement	√		√	√
Water sorption	√	√	√	√
Protein adsorption	√	√	√	√

2.5 *In vitro* biocompatibility study

In vitro biocompatibility study were carried out on the different constructs to understand the response of human cell lines to the constructs in terms of cell adherence to the samples, cell proliferation as well as ability of the different constructs produced to support cell differentiation. Details of different approaches adopted for *in vitro* biocompatibility tests are described below.

2.5.1 Cell culture studies

All media including buffers, trypsin and dyes were filter-sterilised prior to use and warmed to 37°C. For the chondrogenic cell line, Murine ATDC-5 cell line was grown in chondrogenic media containing; low glucose Dulbecco's Modified Eagle Medium (DMEM), supplemented with 10% fetal calf serum, 1% (w/v) penicillin and 1% (w/v) streptomycin solution, 5 $\mu\text{g mL}^{-1}$ transformed growth factor Beta-3 (TGF β -3), 50 $\mu\text{g mL}^{-1}$ ascorbate-2-phosphate, 1 μM dexamethasone, 0.1 mM (100x) nonessential amino acids, and 5 $\mu\text{g mL}^{-1}$ Insulin.

For HOS cell line, MG-63 was grown in low glucose Dulbecco's Modified Eagle Medium (DMEM), supplemented with 10% fetal calf serum and 1% (w/v) penicillin and 1% (w/v) streptomycin solution.

The media for all the cell lines were changed every two days. The cell cultures were maintained at 37 °C, 5% CO₂ and passaged on confluence by adding 2 mL of trypsin and incubate for 5 mins. Following cell detachment, fresh medium was added to the cell suspension, which was then centrifuged at 1000 g for 5 minutes. The resulting cell pellet was resuspended in fresh medium and transferred to 75 cm² tissue culture flasks as required (Parshar *et al.*, 2002).

2.5.2 Culturing and Cyro-preservation of cell lines

The cell lines were resurrected from their frozen state by thawing them and transferring them quickly to centrifuge tubes containing 10 mL Low-glucose Dulbecco's Modified Eagle Medium (DMEM), supplemented with 10% fetal calf serum, 1% (w/v) penicillin and 1% (w/v) streptomycin solution, 5 µg mL⁻¹ transformed growth factor Beta-3 (TGF β-3), 50 µg mL⁻¹ ascorbate-2-phosphate, 1µM dexamethasone, 0.1 mM (100x) nonessential amino acids, and 5 µg mL⁻¹ Insulin for ATDC cells, and 10 mL Low-glucose Dulbecco's Modified Eagle Medium (DMEM), supplemented with 10% fetal calf serum, 1% (w/v) penicillin and 1% (w/v) streptomycin solution for MG-63 cell line.

The cell suspension was centrifuged at room temperature at 1000 rpm (3000 g) for 5 mins. The cell pellet was re-suspended using 5 mL of chondrogenic media and 2 mL of the resuspended cell suspension was added to the tissue culture flasks (gas permeable caps and a surface area of 80 cm²) followed by 8 mL of fresh chondrogenic media. The flasks were incubated in a humidified atmosphere, in 5% CO₂ and at 37°C. The spent medium of the flask was changed after every two days and the flasks were also checked for contamination using an optical microscope. Once the cells were grown to 70-90% confluency they were sub-cultured to maintain healthy growth.

For sub culturing, the spent medium was removed from the flask and washed with 5 mL of PBS followed by addition of 2 mL (1 mL cm⁻²) of trypsin /EDTA onto the washed cell monolayer and incubated at 37°C for 2 mins. The cells were examined under inverted phase microscope to observe the detachment of the cells. After cell detachment, 8 mL of fresh DMEM was added to the flask, to stop the action of the trypsin. The cell suspension was then centrifuged for 5 min at 1000 rpm (3, 000 g). The cell pellet was resuspended using 10 mL of fresh chondrogenic media. 3 mL of the resuspended cell suspension was further divided into three new flasks (3 mL) each and 7 mL of fresh chondrogenic media was added. The cells were then further allowed to grow

until the start of new experiments. The cells were not passaged for more than 3-4 times and they were frozen in ampules and stored in liquid nitrogen for further use.

For cyro-preservation the cell lines were preserved in liquid nitrogen for long term-storage. The cells were subjected to trypsinisation and centrifugation as mentioned earlier. After centrifugation the cell pellet was re-suspended in freezing medium (70% growth medium, 20% fetal calf serum and 10% dimethyl sulfoxide) at a concentration of $0.5-1 \times 10^6$ cells mL⁻¹. 1 mL aliquots were further pipetted into cyro-protective vials and stored at -80°C overnight. Frozen vials were then transferred to liquid nitrogen storage vessel and preserved until further use.

2.5.3 Sample preparation

2.5.3.1 Sterilization of P(3HB)/MFC film samples

All the samples were sterilised using ultra-violet (UV) light. The samples were kept in a 24-well microplate and placed under UV for 30 min, for each side of the sample. This form of sterilization was employed, as it has been shown to be more effective in killing bacteria. Also, it does not affect the chemical composition of the material being sterilized compared to washing with alcohol or autoclaving (Shishatskaya *et al.*, 2004).

2.5.3.2 Sterilization of composite scaffold samples (P(3HB)/MFC; P(3HB)/Magnetic particles and P(3HB)/Magnetic fluid

All the scaffold samples were sterilized by soaking them in 70% ethanol for 12 h followed by drying in sterilized hood until the samples were dried. Samples were kept in a 24-well microplate and placed under UV light for 30 minutes, for each side of the sample. This was done to ensure that the samples were well sterilized.

2.5.4 Seeding of cells on P(3HB) composites

2.5.4.1 Cell seeding on P(3HB)/MFC film substrates

The semi-confluent ATDC cells were released from the flasks by trypsinisation and centrifugation at 1000 rpm for 5 min. The supernatant containing trypsin was discarded and the cell pellet formed was resuspended with 1 mL of the chondrogenic media. Required cell density was calculated with the aid of a haemocytometer and microscope to count the cells. A cell seeding density of 20 000 cells cm⁻² was used for the films. The samples (5 cm in diameter) were placed in a polystyrene 24 well flat bottomed tissue culture plate with the film samples placed in the centre of the well and 50 µL of the cell suspended media was added for attachment of the ATDC cells. The plates were incubated in a humidified environment (37°C, 5% CO₂) for a period of 3 h to enable the cells to attach to the test material. After 3 h, 1 mL of chondrogenic media was added to each of the cells and the plates were replaced in the humidified incubator and maintained at 37°C, 5% CO₂. Standard tissue culture plastic was used as the control surface. The media in the wells were changed every 2 days.

2.5.4.2 Seeding of Maurine ATDC cell line on the P(3HB)/MFC composite scaffold samples

The semi-confluent ATDC cells were released from the flasks by trypsinisation and centrifugation at 1000 rpm (3000 g) for 5 min. The supernatant containing trypsin was discarded and the cell pellet formed was resuspended with 1 mL of the chondrogenic media. Required cell density was calculated with the aid of a haemocytometer and microscope to count the cells. A cell seeding density of 100 000 cells cm⁻² (based on the surface area of the sample) was used for all the 3D scaffold samples, respectively. The samples were placed in a polystyrene 24 well flat bottomed tissue culture plate with the scaffold samples placed in the centre of the well and 30 µL of the cell suspended media was added for attachment of the ATDC cells. The plates were incubated in a humidified environment (37°C, 5% CO₂) for a period of 3 h to enable the cells attached to the test material. After 3 h, 1 mL of chondrogenic media was added to each of the cells and the plates were replaced in the humidified incubator and maintained at 37°C, 5% CO₂. Standard tissue culture plastic was used as the control surface. The media in the wells were changed every 2 days. This protocol is the same with the experiment for MG-63 except the media and cell line used.

2.5.4.3 Seeding of MG-63 on the composite scaffold samples (P(3HB)/Magnetic particles, P(3HB)/Magnetic fluid

The same protocol employed in the seeding of Maurine ATDC cell line was followed except that Maurine ATDC cell line was change with MG-63. The same number of cells (100 000 cellscm⁻²) was seeded on to the scaffolds (size, 0.5 ×0.5×0.5cm³). The samples were also maintained under the same condition in growth medium containing low glucose Dulbecco's Modified Eagle Medium (DMEM), supplemented with 10% fetal calf serum and 1% (w/v) penicillin and 1% (w/v) streptomycin solution.

2.5.5 Cell Proliferation Assay

2.5.5.1 Alamar Blue assay of ATDC cell culture studies

The cell proliferation study was carried out using Alamar Blue assay (AbD Serotec, UK). On day 1, before Alamar Blue assay was performed, the samples were transferred into new 24-well plates and 1 mL of chondrogenic media was added. This was done to ensure that the fluorescence reading from the assay would be a true representation of cells attached on the samples as there are possibilities of having some cells attached on the walls of the wells in the tissue culture plate during cell seeding to the scaffolds. Alamar Blue assay (AbD Serotec, UK), was performed on the samples on day 1, 4, and 7 of the incubation periods in order to ascertain cell proliferation. The growth on the standard tissue culture plastic was used as control. Alamar Blue was added to the samples (10% v/v of the medium) and incubated at 37°C in an incubator (with 5% CO₂) for 4 h. Aliquots of 200µL from each sample well were transferred to a black 96-well plate and the fluorescence of Alamar blue was measured using a fluorescence plate reader (Fuoroskan, Lab Systems) at an excitation wavelength of 530 nm (A₅₃₀) and an emission wavelength of 590 nm (A₅₉₀). The experiment was performed in triplicates while readings were taken in duplicates. The results shown are average of the triplicate samples (n=3) and ANNOVA was adopted for the analysis of the results.

2.5.5.2. Measurement of total protein Production

For the measurement of total protein produced by the cell lines, osteogenic media was prepared by addition of dexamethasone solution to a final concentration of 0.1 μM and Ascorbic acid 2-phosphate solution to a final concentration of 0.2 mM to a low glucose Dulbecco's Modified Eagle Medium (DMEM), supplemented with 10% fetal calf serum and 1% (w/v) penicillin and 1% (w/v) streptomycin solution as described in section 2.5.1. The MG-63 cells were seeded to the scaffolds and grown as described in section 2.5.4.1 using freshly prepared osteogenic medium. Aliquots of supernatants were taken at day 1, 7, 14 and 21 days for the quantification of total protein produced by the cells using Qubit™ Protein Assay Kits and by following the protocols in the manufacturers' manual.

The Qubit® 2.0 Fluorometer gives values for the Qubit™ protein assay in $\mu\text{g/mL}$. This value corresponds to the concentration after sample was diluted into the assay tube. To calculate the concentration of sample, the following equation was used:

$$\text{Concentration of sample} = \text{QF value} \times \frac{200}{X} \quad (6)$$

Where, QF value = the value given by the Qubit® 2.0 Fluorometer, X = the number of microliters of sample added to the assay tube.

2.5.6 Microstructural Analysis

2.5.6.1 Fixing of materials for SEM examinations

Sample materials were examined under SEM to observe the cell line spreading and attachment on the surface of the samples. Day 1, 4 and 7 specimens were fixed in 3% glutaraldehyde in 0.1 M cacodylate buffer for 12 h at 4°C. Subsequent dehydration using a series of graded ethyl alcohols (50%, 70%, 90% and 100%) was performed. Samples were then critical point dried (cells were completely dried of alcohol) by immersion in hexamethyldisilane for 2 min and left in a fume cupboard for 2 h for subsequent drying. The dried samples were then attached to aluminium stubs, gold coated and examined under SEM (JEOL 5610LV, JEOL, USA) at the acceleration voltage of 10-15 kV.

2.5.6.2 Scanning electron microscopy (SEM)

Scanning electron microscopy (SEM) was used to examine cell adherence, and spreading in the microstructure of the scaffolds samples. Samples were sectioned using a sharp blade and placed on a freshly cleaved 8 mm diameter aluminium stubs and gold plated for 2 min. Images were taken at various magnifications and acceleration voltages (max. of 20 kV) to avoid beam damage to the polymer and cells. For each image at least 20 pore throats were examined.

2.6 Drug delivery system

2.6.1 Preparation of particulate carriers

2.6.1.1 Preparation of magnetic microspheres containing drug

For the production of magnetic microspheres containing drug, two different concentrations (0.8 and 0.1% w/v) of polyvinyl alcohol, PVA were prepared. First, 0.5 g of P(3HB) was dissolved in 10 mL of methylene chloride. After dissolution of the polymer in methylene chloride, appropriate amount of magnetic fluid was added and the resultant mixture was sonicated for 3 min (Ultrasonic Homogenizers US200, Philip Harris Scientific, UK) to ensure complete dispersion of magnetic fluid in the polymer solution. 2 mg mL⁻¹ of the desired drug was later added and the mixture was further sonicated for 3 min. Using a syringe and needle with specifications 26 G (0.45 mm) and ½” (13 mm) respectively, the polymer-drug solution was gradually dropped into 80 mL of 0.8% w/v aqueous PVA solution stirring with an overhead propeller (Electro Lab, UK) at 5000 rpm. The mixture was allowed to stir for 5 min followed by addition of 200 mL of 0.1% w/v aqueous PVA solution. The same rpm was maintained and the solution was allowed to stir for 4 h at room temperature to ensure complete evaporation of methylene chloride and stability of the microspheres formed. After 4 h, the microspheres formed were separated from the PVA solution using a magnet as shown in the figure below. The microspheres were later washed three times with deionised water, dried and stored in the fridge at -4°C until further needed.

Both the magnetic particles and magnetic fluid used in this experiment were generous donations from Dr. Mirka Safarikova of Institute of Nanobiotechnology and System Biology, Czech Republic. Figure 2.3 shows the schematic representation of the method used for the production of drug carrying magnetic particles.

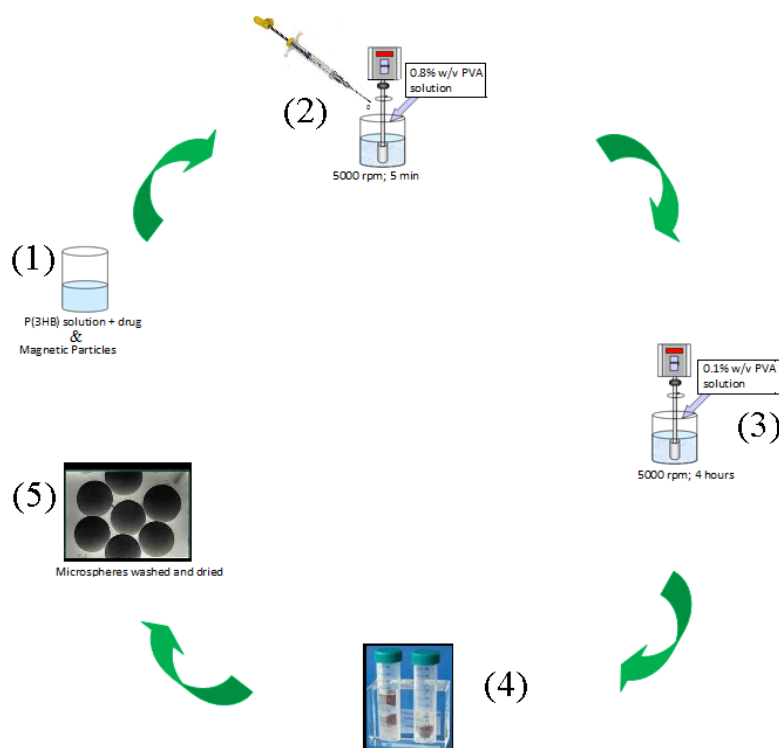


Figure 2.3 Schematic representation of preparation of drug containing magnetic microspheres; (1) Solution of P(3HB), drug and magnetic nanoparticles, (2) Addition of solution (1) into a stirring solution of 0.8% (w/v) PVA, (3) Addition of 40 mL of solution (2) into a stirring solution of 200 mL of 0.1% (w/v) PVA, (4) Separation of magnetic microspheres from the solution using bar magnet. (5) Dried drug encapsulated magnetic microspheres.

2.6.1.2 Preparation of Microspheres containing nanospheres

In the production of P(3HB) microspheres containing cellulose nanospheres, cellulose solution was first prepared by dissolving 8 g of cellulose in 200 mL of a solution containing NaOH/urea/H₂O in the ratio of 7:12:81 by weight and cooled to -12°C under vigorous stirring. The cellulose solution was then stirred over night using a magnetic stirrer (JENWAY 1203 Hotplate & Stirrer, UK) in a cold room in order to obtain a clear, transparent cellulose solution.

Gum arabic (sigma, Aldrich) solution (23%) was prepared by addition of 7.2 g of Gum arabic to 24.4 g of 6% aqueous solutions of sodium hydroxide while stirring at room temperature. The Gum arabic solution was stirred over night to obtain a solution. After preparation of cellulose and Gum arabic solutions, 450 mL of the Gum arabic solution was stirred using an overhead propeller (Electro Lab, UK) at 5000 rpm (15,000 g) for 30 min. 50 mL of prepared cellulose solution was later added to the stirring Gum arabic within a period of 1 h and the resultant solution was allowed to stir for further 4 h while maintaining the same condition of rotation speed and room temperature. A 2 N of sulphuric acid

was later added to the solution after 4 h until a pH of 7 was reached, to generate the cellulose nanospheres. The cellulose nanospheres obtained was separated by use of a glass filter and washed with water and freeze dried over night.

After drying, encapsulation of BSA in the cellulose nanospheres was carried out in PBS buffer (pH 7.4) at room temperature for 24 h. In brief, 100 mg of microspheres were immersed in 10 mL of PBS containing BSA (2 mg mL^{-1}). The mixture was gently shaken using a bench top incubator (Stuart orbital incubator 51500, UK) at 150 rpm (450 g) for 24 h. After 24 h, the microspheres were separated by filtering and dried at room temperature for 48 h.

To encapsulate the BSA-loaded cellulose nanospheres produced above with P(3HB), 0.5 g of P(3HB) was dissolved in 10 mL of chloroform. After dissolution of the polymer in chloroform, 2 mg mL^{-1} BSA was added and the resultant mixture was sonicated for 3 min (Ultrasonic Homogenizers US200, Philip Harris Scientific, UK) to ensure complete dissolution of BSA in the polymer solution. Later, 200 mg of BSA-encapsulated cellulose nanospheres was added to the P(3HB)-BSA mixture and the resultant mixture was vigorously vortexed for 3 min. Using a syringe and needle with specifications 20 G (0.9 mm) and 11/4" (32 mm), the P(3HB)-BSA-cellulose nanospheres mixture was gradually dropped into 80 mL of 1% w/v aqueous PVA solution stirred with an overhead propeller (Electro Lab, UK) at 5000 rpm (15, 000 g). The mixture was allowed to stir for 5 min followed by the addition of 200 mL of 0.1% w/v aqueous PVA solution. The same rpm was maintained and the solution was allowed to stir for 4 h at room temperature to ensure complete evaporation of chloroform and stability of the microspheres formed. After 4 h the microspheres formed were separated from the PVA solution using a glass filter. The microspheres were later washed three times with deionised water, dried and stored in the fridge at -4°C until further needed. Details of the processes followed are summarised in the Figure 2.4.

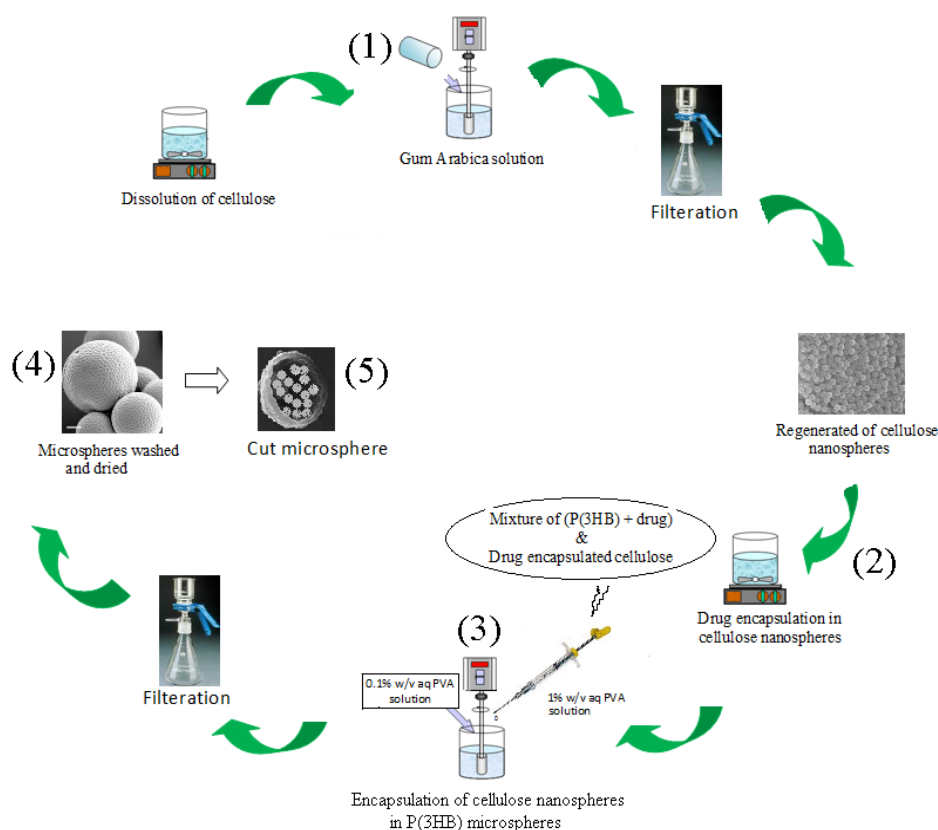


Figure 2.4 Schematic representations of processes of preparation of microsphere containing nanospheres; (1) Production of cellulose nanospheres, (2) Encapsulation of drug into the regenerated cellulose nanospheres, (3) Production of P(3HB) microspheres containing drug encapsulated cellulose nanospheres, (4) Dried P(3HB) microspheres containing cellulose nanospheres, (5) A cross section of the multipurpose microspheres highlighting the encapsulated cellulose nanospheres.

2.6.1.3 Preparation of Microspheric Scaffolds

P(3HB) composite scaffolds containing P(3HB) microspheres were prepared by first preparing the encapsulated microspheres using the protocols described 2.6.1.1 with a slight change for microsphere formation. The slight change made in the preparation of the microspheres was the replacement of the magnetic particles with TGF- β 3. The microspheres after preparation were dried and used to fabricate scaffolds as described here; 1g of P(3HB) was dissolved in 5 mL of chloroform. After dissolution of the P(3HB) in chloroform, appropriate amount of microspheres was added to the chloroform solution and homogeneously mixed together. Then, 20 g of sucrose grains was added as a porogen and the resultant mixture was homogeneously mixed together to form a solid paste. The resultant paste mixture was fabricated into scaffolds using the compression mould/particulate leaching method described in section 2.3.3.

2.6.2 Analysis and Assay

2.6.2.1 Determination of residual PVA content

The percentage residual PVA content present on the surface of the drug delivery microsphere constructs prepared were determined following method described by Yang *et al.*, 2008. The method depended on the formation of a complex between two adjacent hydroxyl groups of PVA solution and an iodine molecule. Briefly, 2 mg of the lyophilised microsphere samples prepared under different conditions were treated with 2 mL of 0.5 M sodium hydroxide for 15 min at 60°C. Each of the samples was then neutralized with 900 µL of 1N hydrochloric acid (HCl) and the volume was adjusted to 5 mL with distilled water. To each of the samples, 3 mL of 0.65 M solution of boric acid, 0.5 mL solution of (I₂)/Potassium iodide (KI) (0.05 M/0.15 M) and 1.5 mL of distilled water were added. Finally, the absorbance of the samples was measured at 690 nm (JENWAY 6305 spectrophotometer, UK) after 15 minutes of incubation. A standard plot of PVA was also prepared under identical conditions (Sahoo *et al.*, 2002).

2.6.3 Characterisation of Microspheres

2.6.3.1 Particle size analysis using Dynamic light Scattering, DLS

Particle size analysis was performed using dynamic light scattering (Malvern Zeta Sizer ZS 90). The samples were diluted 100 times to ensure reliability of the performed measurements. After ultrasonification for 5 minutes, it was discovered that the sample was sedimenting; hence, the analysis was performed using two methods. In the first method, the analysis was performed in “intensity mode” using the sedimenting part of the sample suspension while in the second method non-sedimenting part of the sample suspension was used. The results obtained in both methods were compared.

2.6.3.2 Surface morphology and microstructure characterization using SEM

The detailed morphological study of the solid microspheres was done on a field emission scanning electron microscope (SEM) Hitachi SU6600 with ultrahigh point-to-point resolution (1-2 nm) and equipped with electron-dispersive X-ray (EDX) spectroscopy. Samples were

prepared by placing small amounts of microspheres on a freshly cleaved carbon tape on an aluminium stub and then coated with a thin layer of gold. The cross-sections of single microspheres was analysed by transmission electron microscopy (TEM) using a JEOL JEM-2010 transmission electron microscope operated at 200 kV. Microspheres were cut using a sharp blade. Due to the micro size of the microsphere samples, they were difficult to handle. Therefore, random chopping of the samples with a sharp surgical blade was performed; the samples were later placed on a freshly cleaved carbon tape on an aluminium stub and thereafter coated with a thin layer of gold. Images were taken using SEM and analysed.

2.6.3.3 Determination of hydrophobicity of microspheres

The binding constant of Rose Bengal to the surface of the nanoparticles was used as a measure of hydrophobicity. Sample of various formulations of microspheres (1 mg) was incubated with different concentrations (5-40 $\mu\text{g/mL}$) of Rose Bengal dye for 3 h at room temperature. The samples were centrifuged at 14,000 g for 30 min in a microcentrifuge to spin down the microspheres. The supernatant from each sample was analyzed spectrophotometrically at 542.7 nm to determine the unbound dye. The dye solution without microspheres as a control was run each time under similar conditions to account for the dye that might bind to the centrifuge tubes. The binding constant was calculated using equation (7).

$$\frac{r}{a} = KN - Kr \quad (7)$$

Where, r is the amount of Rose Bengal adsorbed per mg microspheres ($\mu\text{g/mg}$); a is equilibrium concentration of Rose Bengal ($\mu\text{g/mL}$); K is the binding constant ($\text{mL}/\mu\text{g}$); and N is the maximum amount bound ($\mu\text{g/mg}$).

2.6.3.4. In vitro BSA release from multipurpose microsphere

Release of BSA from the microspheres formulated using either 0.1 or 1% as emulsifier was determined in phosphate buffer saline (PBS, 0.15 M, pH 7.4) at 37°C utilizing double chamber diffusion cells placed on a shaker at 100 rev min^{-1} . The donor chamber was filled

with 2.5 mL of microsphere suspension (2.5 mg/mL) and the receiver end was filled with buffer. A Millipore[®] hydrophilic low protein binding membrane with 0.1 μm pore size was placed between the two chambers. The protein is freely permeable across the membrane. At predetermined time intervals, the receiver chamber fluid was replaced with buffer and the BSA content was analyzed using Qubit[™] Protein Assay Kits and the amount of protein released was quantified using the same method described in details in section 2.2.4.7.

2.6.3.5 In vitro degradation of microsphere

The biodegradation study of the multipurpose microsphere was carried out by incubating the microsphere in lizozyme containing phosphate buffer saline (PBS) solution (pH 7.4) at 37°C. Egg-white lizozyme (Sigma–Aldrich) was used without further purification. The various weight ratios 200 mg of microspheres were immersed in 1 mL of lizozyme solution of stock concentration (0.2 mg/mL). The PBS solution was renewed every week. At predetermined time interval, the microspheres were taken out from the lizozyme solution, thoroughly rinsed with distilled water, freeze-dried, and examined with SEM.

Chapter 3

ENHANCED AND ECONOMIC PRODUCTION OF POLY(3- HYDROXYBUTYRATE), P(3HB) USING *BACILLUS CEREUS* SPV

Chapter 3

3.1.1 Introduction

PHAs are one of the relatively newer families of ‘green’ biodegradable and biocompatible polymers that have great potential in the future due to variability in their properties. They are linear polyesters of 3-, 4-, 5-, and 6-hydroxyalkanoic acids, accumulated as carbon and energy storage compounds by many microorganisms through bacterial fermentation of sugar and lipids (Halami, 2008; Lenz and Marchessault, 2005).

Normally PHAs are accumulated as a result of nutrient imbalance when the environment contains an excess of the carbon source and one or more limiting nutrients (Dawes, 1996). Under normal growth conditions, PHA content in the cells is usually not very high. Depending on bacterial strains, it is 2–10% weight of the dry cell mass. However, PHA content can reach up to 80% of the dry cell mass if growth is limited by the depletion of an essential nutritional compound such as nitrogen, phosphorus, sulphur, or magnesium (Du *et al.*, 2001). Nitrogen (N) or phosphate (P) limitation stimulates rapid PHA synthesis in most of the well-studied SCL (short chain-length)-PHA-synthesizing bacteria, such as *Ralstonia eutropha*. Therefore, most SCL-PHA production processes employ a stage of rapid cell growth followed by a PHA accumulation stage, which is almost always N-limited or P-limited. Apart from nitrogen and phosphorus, many other nutrients have served as limiting factors that can enhance PHA accumulations in organisms. Some of these limiting nutrients are; ammonia (*Alcaligenes eutrophus*), carbon (*Spirillum spp.*, *Hypomicrobium spp.*), iron, Mg (*Pseudomonas spp.*), Mn, O₂ (*Azospirillum*, *Rhodobacter spp.*), phosphate (*Rhodospirillum*, *Rhodobacter spp.*) and potassium (*Bacillus*, *Rhodospirillum*, *Rhodobacter*). PHAs can be synthesized and degraded *in vivo* to accumulate the excess carbon and energy sources and reutilize them when needed (Lenz and Marchessault, 2005).

P(3HB) is the most studied among the biodegradable polymers. Co-polymers of P(3HB) and P(3HV) (poly-3-hydroxyvalerate) can be obtained by co-feeding of glucose and a pentanoate (Anil-Kumar *et al.*, 2007; Full *et al.*, 2006). The production of copolymer of 3-hydroxybutyrate and 3-hydroxyvalerate was commercialized in the 1980s (Nikel *et al.*, 2006).

PHA producing bacteria are divided into two groups according to the culture conditions required for PHA synthesis. The first group requires the limitation of an essential nutrient(s) and bacteria in this group included *Cupriavidus necator*, *Protomonas oleovorans* and *Bacillus cereus*. The second group synthesises PHA alongside growth in the cultivation medium. Bacteria in this group included *Alcaligenes latus*, mutant strain of *Azotobacter vinelandii* and recombinant *E. coli* cloned with PHA synthesis genes.

The high cost of production has been the major setback in the production and utilization of PHAs produced from bacteria. The efficiency and economies of the production process of P(3HB) is mostly determined by the carbon source, fermentation process and the purification of the polymer. Hence, the development of fermentation strategies that would allow not only high PHA content but also increase the yield of the polymer through improvement in cell growth as well as utilization of cheap carbon sources are very important. Few bacteria, including *Alcaligenes latus* and *Azotobacter vinelandii* UWD are known to utilize sucrose as carbon source for PHA production up to 70-83 wt% of dry cell weight. This implies that inexpensive substrates such as raw sugars, beets and cane molasses can be utilized by these organisms to produce PHAs at a very high yield. It is therefore essential to explore alternative cheaper substrate for bacterial growth and P(3HB) production.

This chapter describe the investigations carried out on the use of sucrose as the main carbon source in both undefined medium (Kannan and Rehacek medium) and defined medium (modified G-medium) for P(3HB) production in *Bacillus cereus* SPV. Also, reported in this chapter is the use of cheap carbon sources for PHA production. In addition, details of the characterisation studies carried out on the isolated polymers from different fermentation studies are also given in this chapter.

SECTION I

P(3HB) production in *Bacillus cereus* SPV using Kannan and Rehacek medium and sucrose as carbon source

P(3HB) accumulation by *Bacillus cereus* SPV was carried out using the established Kannan and Rehacek production medium (Valappil *et al.*, 2007) and sucrose as the main carbon source. Sucrose was chosen as the main carbon source because of its ready availability from renewable agricultural feedstock. Yeast extract and ammonium phosphates were utilized as organic and inorganic nitrogen sources respectively. The study was carried out both at shaken flask (1L) and fermenter (2L) level in the batch mode.

3.1.2 Results

3.1.2.1 P(3HB) production at the shaken flask level, using sucrose as the main carbon source in Kannan and Rehacek medium

Investigations on P(3HB) production was first carried out at the shaken flask level. This was necessary to gain more information on the scaling up of production. At the shaken flask level, the agitation speed was kept constant at 250 rpm throughout the duration of the fermentation and the fermentation was continued until the optical density of the broth culture began to decrease. At this time, the maximal PHA accumulation was expected to have completed. The cultivation time was extended for a further six hours after death phase was attained (Figure 3.1). This was necessary to gain more understanding on the activities of the *Bacillus cereus* SPV towards the accumulated polyester. Increased cell growth was observed to have continued until 28 hours which was followed by a greatly reduced growth that was completed after 32 hours. At this time, the highest dcw accumulated was 5.98 g/L. PHA accumulation was found to have preceded cell growth with initial slow rate of accumulation. After 12 hours of fermentation, the rate of PHA accumulation improved substantially and reached a maximum at 32 hours. The maximum PHA accumulation achieved was 47.68 % dcw and the highest PHA yield was 2.85 g/L and both values were achieved at 32 hours.

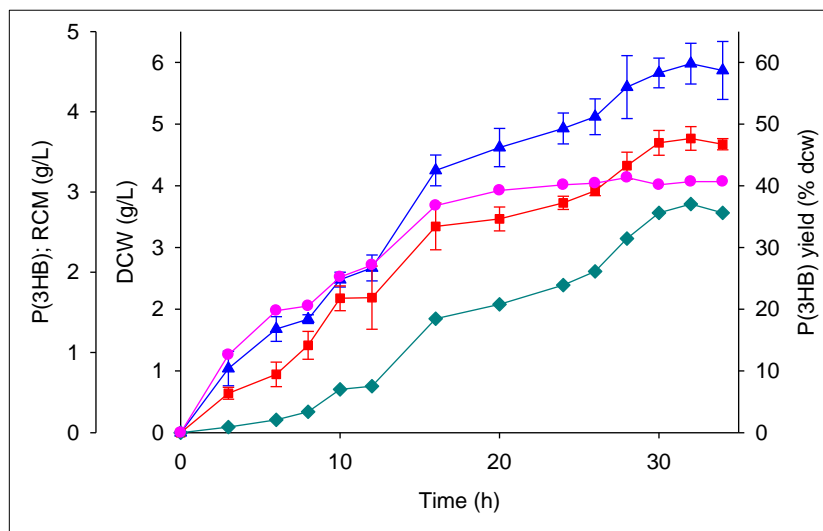


Figure 3.1 A temporal profile of DCW (g/L) (▲); P(3HB) yield (% dcw) (■); P(3HB) concentration (g/L) (◆) and RCM (g/L) (●) produced by *Bacillus cereus* SPV in Kannan and Rehacek medium containing sucrose as the main carbon source in shaken flask cultivation. Both experiments and sample analyses were done in triplicates (Error bars = \pm SD).

3.1.2.2 P(3HB) production at 2L fermenter level, using sucrose as the main carbon source in Kannan and Rehacek medium

PHA production studies using Kannan and Rehacek medium and sucrose as the main carbon source was further extended to fermenter scale (2L). Figure 3.2 shows the profile of the parameters measured during the study. It was observed that increase in cell growth continued until 10 hours, which was followed by stationary growth that lasted until 15 hours of the fermentation time. The maximum DCW (3.56g/L) was achieved during the end of stationary growth. Polymer accumulation was found to have continued simultaneously with increased cell growth and reached a maximum at 18 hours. At this time, the maximum PHA accumulation was found to be 32.87 % dcw. Also, PHA yield followed the same trend with polymer accumulation until 18 hours, after which reduction in PHA yield was noticed. The highest PHA yield achieved was 1.12 g/L.

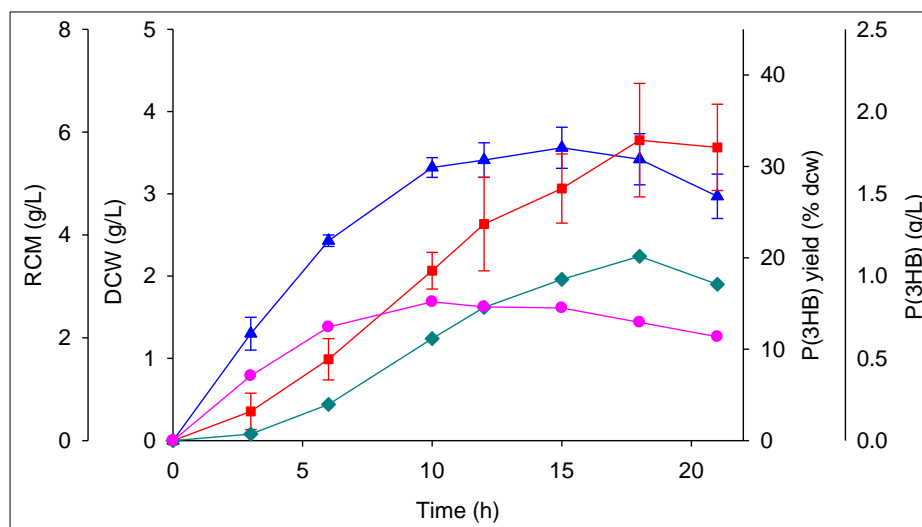


Figure 3.2 A temporal profile of DCW (g/L) (\blacktriangle); P(3HB) yield (% dcw) (\blacksquare); P(3HB) concentration (g/L) (\blacklozenge) and RCM (g/L) (\bullet) produced by *Bacillus cereus* SPV when sucrose was employed as the sole carbon source in batch fermentation using a 2L fermenter. Experiments were performed in duplicates while analyses of samples were done in triplicates (Error bars = \pm SD).

3.1.2.3 Comparison of dry cell weight, PHA concentration and PHA yield in shaken flask and 2L fermenter level.

Overall comparison of the values obtained in the parameters measured during the growth of *Bacillus cereus* SPV in Kannan and Rehacek medium containing sucrose as the main carbon source showed that more dry cell weight was accumulated by the organism in shaken flask (1L) than in fermenter (2L). Decrease in the values of both DCW, P(3HB) yield and P(3HB) content were found in the fermenter study. However, a shorter fermentation time of 21 hours for obtaining maximum (3HB) yield was achieved with the 2L fermenter as opposed to 34 hours observed in shaken flask investigations (Figure 3.3).

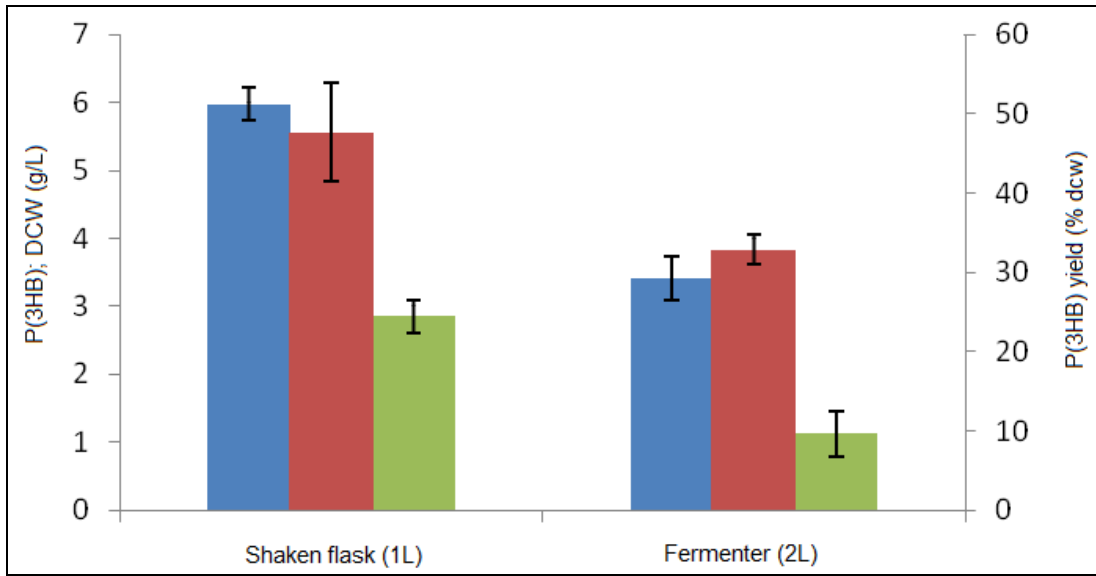


Figure 3.3 Comparison of DCW (g/L) ■, P(3HB) (g/L) ■, and P(3HB) yield (% dcw) ■, accumulated by *Bacillus cereus* SPV using sucrose as the main carbon source in shaken flask (1L) (at 32 hours fermentation) and fermenter (2L) levels (at 18 hours) (Error bars = \pm SD).

SECTION II

Production of Poly(3-hydroxyalkanoate), P(3HB) by *Bacillus cereus* SPV using Modified G-medium and sucrose as the main Carbon Source

Based on previous work related to P(3HB) production from glucose and the preliminary result in section 3.1, sucrose was chosen for further investigations on P(3HB) accumulation by *Bacillus cereus* SPV. To understand in details the role of the respective nutrient composition in the production medium towards cell growth and PHA accumulation, a defined medium was formulated. Studies were carried out in both shaken flask and fermenter level to assess the effects of different nutrients known to have serious effect on cell growth and PHA production in *Bacillus cereus* SPV. P(3HB) isolated during these studies were characterized using GC-MS, NMR, FTIR, and DSC.

3.2.1 Results

3.2.1.1 P(3HB) production by *Bacillus cereus* SPV using modified G-medium (MGM) supplemented with sucrose as the main carbon source in shaken flask

The profile of the parameters measured during the investigations is shown in Figure 3.4. As in the case of Kannan and Rehacek medium, no lag phase in cell growth was noticed after inoculation with 10% of the seed culture. The inoculation of the 1L shaken flask was followed by increased cell growth phase which continued until 12 hours, after which the rate of cell growth decreased. The highest dry cell weight achieved at this time was 4.66 g/L. With continued growth of the organism, until after 27 hours, the dry cell weight increase to 6.7 g/L (the maximum achieved). Further extension in the fermentation time resulted in decline in the accumulated dry cell weight. P(3HB) accumulation also followed the same trend as the cell growth with a P(3HB) yield of 42.80 % dcw observed after 30 hours of fermentation. Further extension in the fermentation time was noticed to have resulted to decrease in dry cell weight and

accumulated polyester. The highest residual cell mass (RCM) quantified was 3.56 g/L at the end of stationary phase, while the highest P(3HB) concentration achieved was 3.56 g/L.

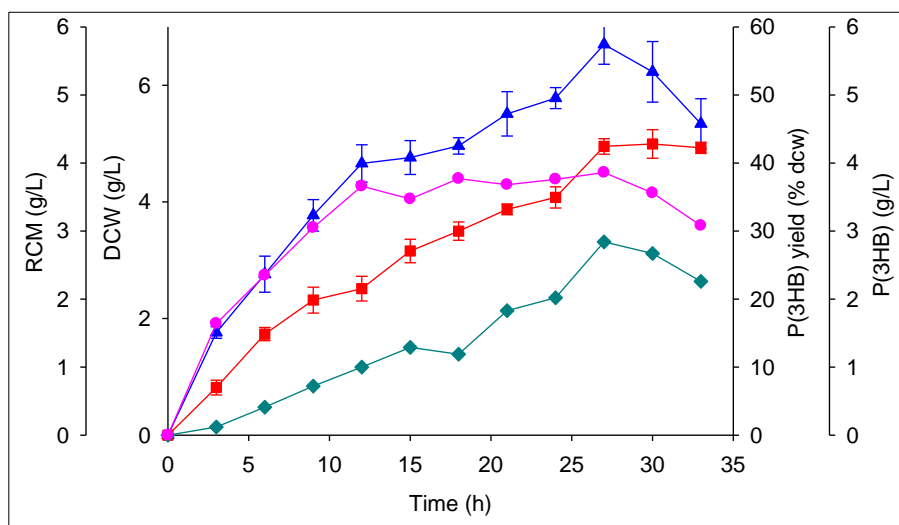


Figure 3.4 Temporal profile for DCW (g/L) (▲); P(3HB) yield (% dcw) (■); P(3HB) concentration (g/L) (◆) and RCM (g/L) (●) produced by *Bacillus cereus* SPV in MGM medium supplemented with sucrose in shake flask. Both experiments and sample analyses were done in triplicates (Error bars = \pm SD).

3.2.1.2 P(3HB) production by *Bacillus cereus* SPV using modified G-medium (MGM) supplemented with sucrose as the main carbon source in a 2L fermenter

Investigations on the effect of supplementing sucrose, as the main carbon source, in modified G-medium for PHA production were further extended to the fermenter level (2L). Figure 3.5 shows the profile of the result of the parameters evaluated during the study. Figure 3.6 shows the comparison of the parameters analysed during P(3HB) production using MGM medium supplemented with sucrose as the main carbon source in both shaken flask and 2L fermenter. As observed in the shaken flask study, no lag phase was noticed in cell growth after inoculation with 10% of the seed culture. Increased cell growth was noticed until 12 hours when the cell growth remained fairly stable. The stationary growth lasted until 21 hours and a decline in cell growth was noticed after 21 hours. The maximum dry cell weight and P(3HB) yield achieved were 3.29

g/L and 47.20 % dcw respectively. The residual cell mass observed during the maximum P(3HB) yield, at 24 hours, was 1.74 g/L.

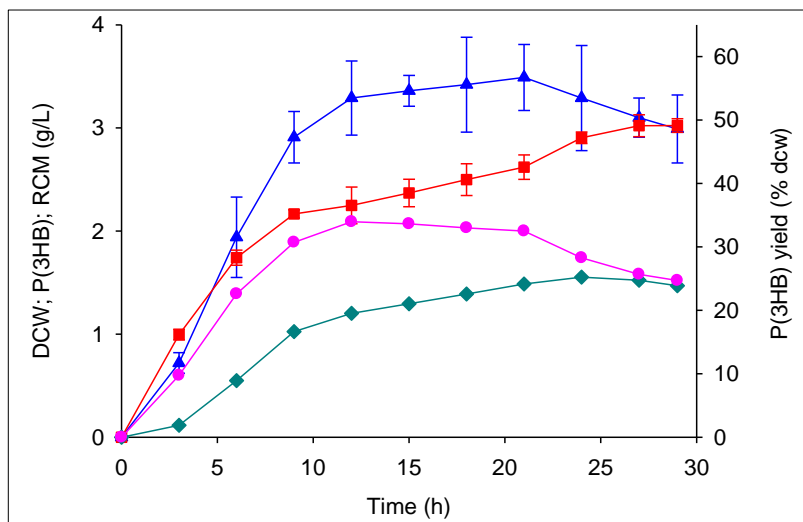


Figure 3.5 Temporal profile for DCW(g/L) (\blacktriangle);P(3HB) yield (% dcw) (\blacksquare); P(3HB) Concentration (g/L) (\blacklozenge) and RCM (g/L) (\bullet) produced by *Bacillus cereus* SPV in MGM medium supplemented with sucrose in 2 L fermenter. Experiments were performed in duplicates while analyses of samples were done in triplicates (Error bars = \pm SD).

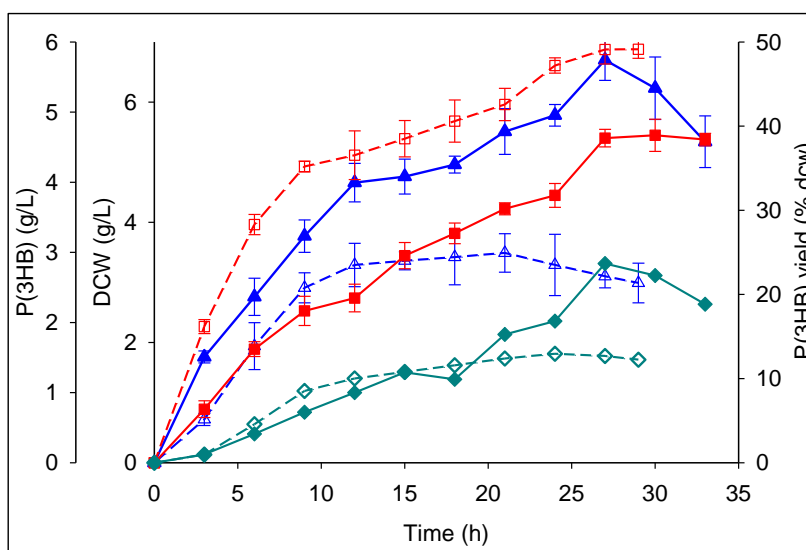


Figure 3.6 Temporal variation of DCW (g/L) (\blacktriangle); P(3HB) yield (\blacksquare); P(3HB) concentration (g/L) (\blacklozenge) produced by *Bacillus cereus* SPV using MGM and sucrose as the main carbon source in a 2L fermenter (dotted lines) and shake flask (solid lines).

3.2.1.3 Effect of increasing initial K_2HPO_4/KH_2PO_4 concentration in production medium on biomass and PHA accumulation by *Bacillus cereus* SPV.

The batch shaken flask (1L) and fermenter (2L) studies were used as the basis for further variation in the nutrient composition of the modified G-Medium in order to find an optimal balance of *B. cereus* SPV cell growth and P(3HB) accumulation. Investigation was started with variation in the concentration of K_2HPO_4/KH_2PO_4 buffer in the production medium. Potassium phosphate buffer was the source of potassium and phosphate used by the organism for cell growth. In addition, K_2HPO_4/KH_2PO_4 also provided a buffering effect. The potassium phosphate buffer concentration in the production medium was increased from the initial 0.1M K_2HPO_4/KH_2PO_4 to 0.25M K_2HPO_4/KH_2PO_4 and the effect was evaluated in a fermenter (2L) where pH was maintained at 6.8. The results of the study are shown in Figure 3.7 while Figure 3.8 shows the comparison of the results obtained in section 3.2.1.2 and 3.2.1.3 (i.e. addition of 0.1M K_2HPO_4/KH_2PO_4 and 0.25M K_2HPO_4/KH_2PO_4 in MGM). Contrary to what was observed in the conditions described in section 3.2.1.1, cell growth was found to be slightly slow during the first 5 hours of fermentation with 0.73 g/L dry cell weight accumulated. The organism entered into a rapid cell growth thereafter 5 hours with the increased cell growth lasting until 25 hours of fermentation. At this time point, the maximum dry cell weight accumulated was 6 g/L. The increased cell growth was preceded by a fairly stable cell growth which continued until 50 hours of fermentation with a maximum value of 7.13 g/L dry cell weight. Further extension in the fermentation time resulted in a decrease in cell growth. After 25 hours, at the end of increased cell growth, the P(3HB) yield (39.85 % dcw) was obtained. The maximum P(3HB) yield was 52.50 % dcw, obtained at 50 hours. However, this amount was found to be reduced to 49.63 % dcw with further extension in the fermentation time to 55 hours.

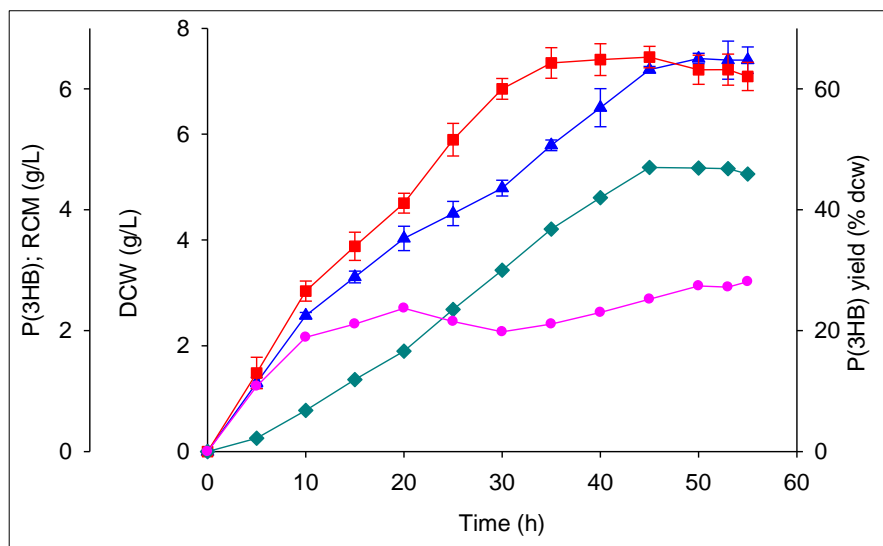


Figure 3.7 A temporal profile of growth of *Bacillus cereus* SPV in MGM medium buffered with 0.25M K_2HPO_4/KH_2PO_4 and supplemented with sucrose in 2 L fermenter and recording of DCW (▲) (g/L) ; P(3HB) yield (% dcw) (■) ;P(3HB) concentration (g/L) (◆) and RCM (g/L) (●) accumulated. Experiments were performed in duplicates while analyses of samples were done in triplicates (Error bars = \pm SD).

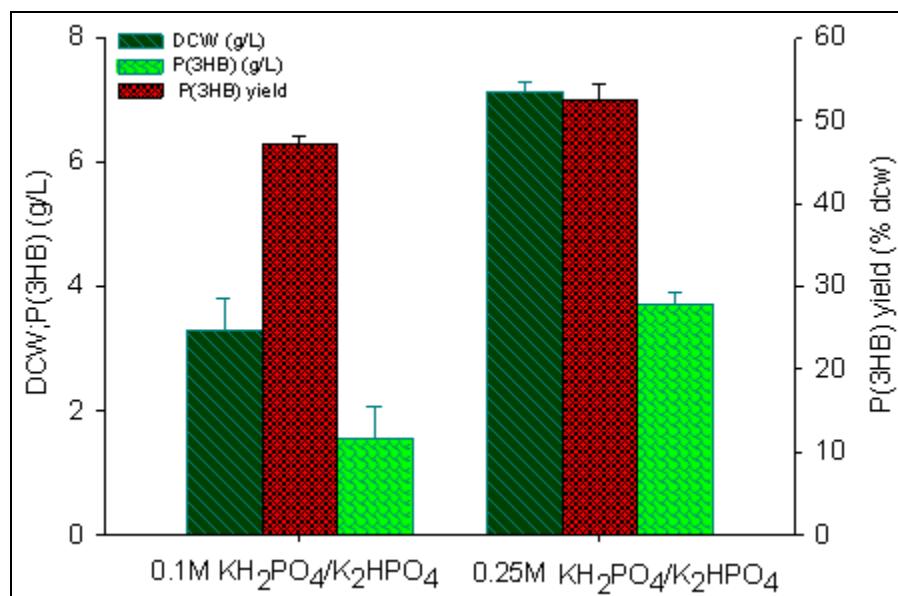


Figure 3.8 Comparison of DCW (g/L), P(3HB) yield and P(3HB) concentration (g/L) achieved with initial 0.1M KH_2PO_4/KH_2PO_4 (production time; 24 hours) and 0.25M KH_2PO_4/KH_2PO_4 (production time; 50 hours) present in the production medium (Error bars = \pm SD).

3.2.1.4 Effect of replacement of potassium phosphate with 1.0 g/L KH_2PO_4 in MGM on biomass and P(3HB) accumulation by *Bacillus cereus* SPV

Potassium has been found to be one of the major nutrients that effect PHA production in *Bacillus* strain (Valappil *et al.*, 2008). While some conditions can work effectively in organisms belonging to the same genus, it is expected that differences in the metabolic pathways of strains may cause variations in the response of individual strains towards a particular treatment. Hence, the effect of limiting potassium phosphate concentration in the production medium was initiated. In doing this, the potassium phosphate buffer was replaced with 1.0 g/L KH_2PO_4 . All other conditions were maintained as in the previous studies. Figure 3.9 shows the profile of the result obtained from the study. Increase in cell growth was observed until 40 hours before a stationary cell growth that lasted until 45 hours occurred. The maximum dry cell weight achieved at the end of stationary growth was 7.22 g/L and the maximum P(3HB) yield obtained was 65 % dcw. The highest P(3HB) concentration obtained was 4.7 g/L while the RCM value was found to be 2.74 g/L when the highest P(3HB) yield was achieved.

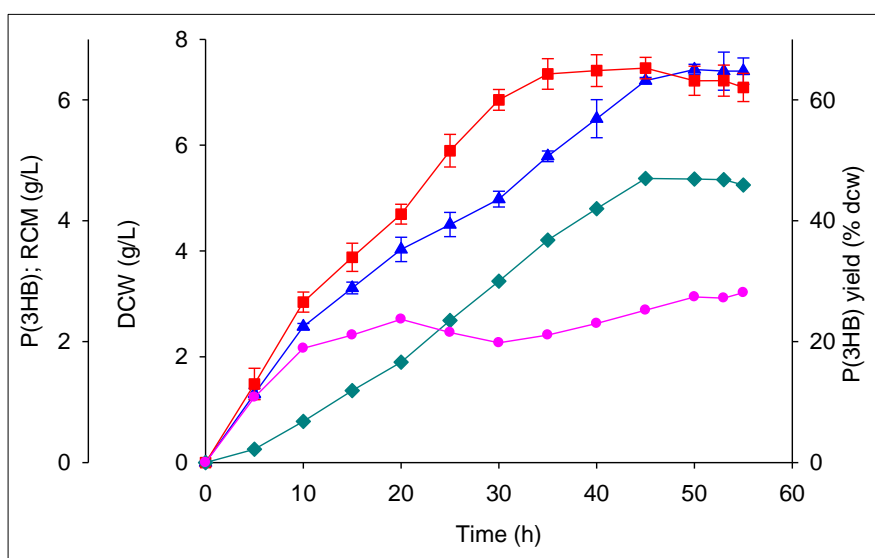


Figure 3.9 A temporal profile of DCW (g/L) (▲); P(3HB) yield (% dcw) (■); P(3HB) concentration (g/L) (◆) and RCM (g/L) (●) produced by *Bacillus cereus* SPV when potassium phosphate buffer was replaced with 1.0 g/L of KH_2PO_4 in MGM medium in 5L fermenter. Experiments were performed in duplicates while analyses of samples were done in triplicates (Error bars = \pm SD).

3.2.1.5 Effect of replacement of potassium phosphate buffer with 0.5 g/L KH_2PO_4 in MGM on biomass and P(3HB) accumulation by *Bacillus cereus* SPV

Following the result achieved above, investigations on the effect of potassium phosphate on P(3HB) accumulation was continued by reducing the amount of supplemented potassium phosphate in the MGM medium to 0.5 g/L KH_2PO_4 . The results on the parameters quantified are shown in Figure 3.10. Cell growth was found to have increased considerably after inoculation until 25 hours, after which the growth rate slowed down and the organism showed a stationary growth after 50 hours. The maximum dry cell weight accumulated after 55 hours was 7.21 g/L and the maximum P(3HB) yield obtained was 82.61 % dcw. The highest P(3HB) concentration achieved was 5.95 g/L. The residual cell mass (RCM) value was 1.26 g/L when the highest P(3HB) yield was achieved. The results on the parameters analysed on the replacement of potassium phosphate buffer with 1.0 g/L and 0.5 g/L are compared in Figure 3.11.

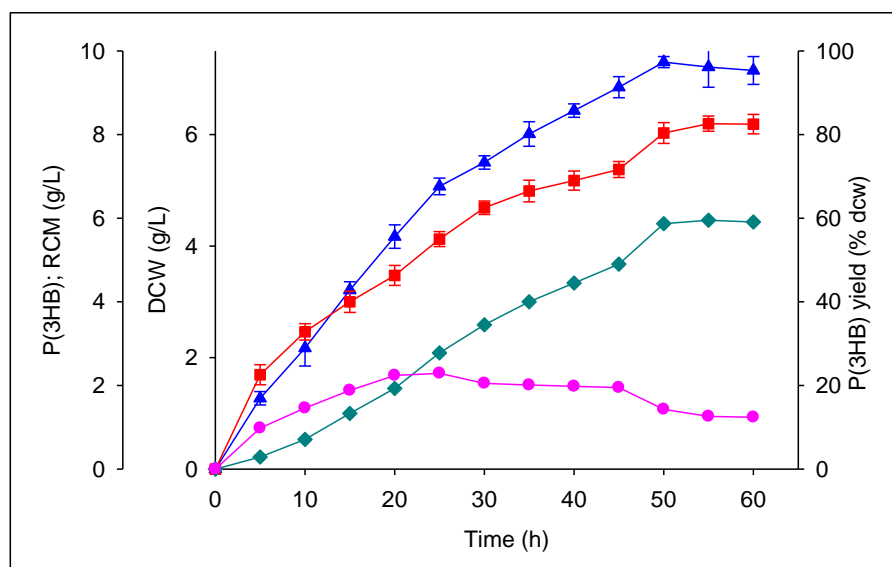


Figure 3.10 A temporal profile of DCW (▲); P(3HB) yield (■); P(3HB) concentration (g/L) (◆) and RCM (g/L) (●) produced by *Bacillus cereus* SPV when potassium phosphate buffer was replaced with 0.5g/L of KH_2PO_4 in MGM medium in 5L fermenter. Experiments were performed in duplicates while analyses of samples were done in triplicates (Error bars = \pm SD).

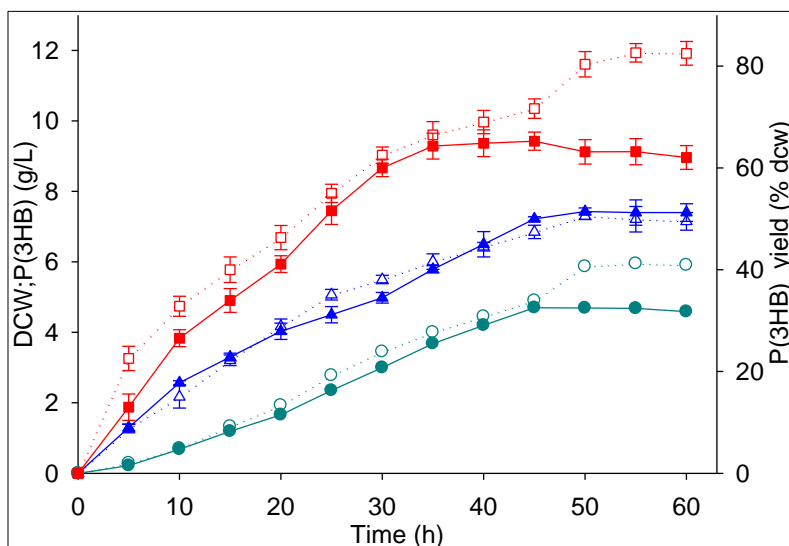


Figure 3.11 Comparison of DCW (g/L) (\blacktriangle); P(3HB) yield (% dcw) (\blacksquare); P(3HB) concentration (g/L) (\bullet) produced by *Bacillus cereus* SPV during batch fermentation with MGM media containing initial 1.0 g/L KH_2PO_4 (dotted lines) and 0.5 KH_2PO_4 (solid lines) in a 5L fermenter.

3.2.1.6 Effect of increasing yeast extract concentration in the MGM medium supplemented with sucrose as the main carbon source on *Bacillus cereus* SPV biomass and PHA accumulation.

Amino acids are very expensive and mostly required by *Bacillus cereus* for growth and biomass accumulations. Thus, to reduce the cost of providing amino acids for the growth of the organism, yeast extract (a complex amino acid source) was added to the production media. Apart from being a source of amino acids, yeast extract can be a source of carbon to *B. cereus* SPV. The effect of increasing the initial amount of yeast extract from 2.5 g/L to 4.5 g/L in the production medium on dry cell weight and P(3HB) production was investigated in a 2L fermenter. The temporal profile of the results obtained on the parameters investigated is shown in Figure 3.12. There was no lag phase noticed in the growth of the organism after inoculation with 10 % v/v of the inoculum rather the organism was found to have exhibited increase growth until 12 hours when it gradually entered into the stationary growth phase. The stationary growth lasted until 18 hours of cultivation when the pattern of growth proceeded with cessation of growth. The

maximum dry cell weight achieved was 5.71 g/L. The highest P(3HB) yield quantified was 44.81 % dcw. With further extension in the fermentation time, during the cessation growth phase, the P(3HB) yield was found to decrease to 42.30 % dcw. The maximum P(3HB) concentration was 2.56 g/L. The RCM was found to have increased progressively with increase in the dry cell weight with 3.16 g/L calculated at the end of exponential growth and remained constant during the stationary growth.

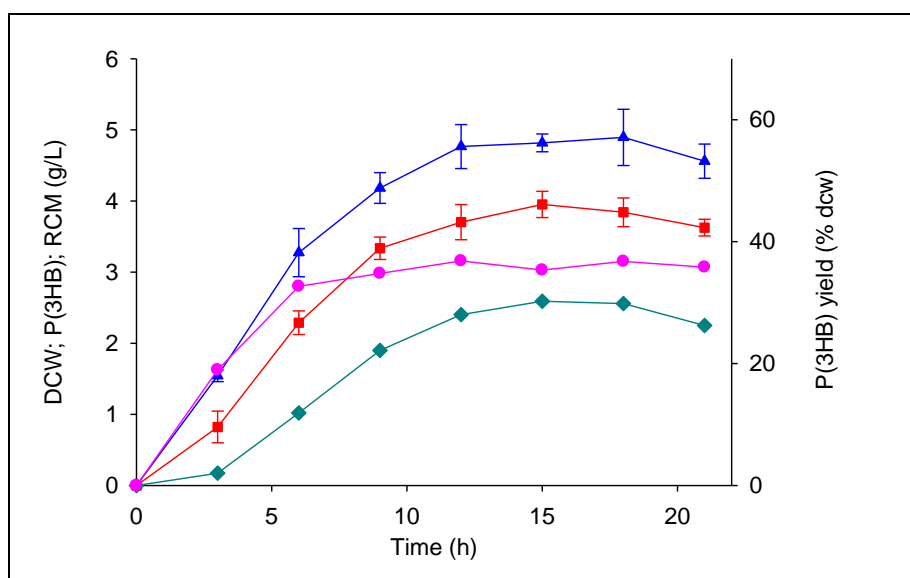


Figure 3.12 A temporal profile of DCW (g/L) (▲); P(3HB) yield (% dcw) (■); P(3HB) concentration (g/L) (◆) and RCM (g/L) (◆) produced by *Bacillus cereus* in a 2L Fermenter with an increased yeast extract concentration (4.5 g/L) in the production medium. Experiments were performed in duplicates while analyses of samples were done in triplicates (Error bars = \pm SD).

3.2.1.7 Effect of intermittent addition of sucrose solution to the growing *B. cereus* SPV culture in MGM production medium in a 2L fermenter (fed-batch fermentation).

Maximal PHA accumulations have been reported to occur in the presence of excess carbon source and limiting nutrient(s) in the production medium. Hence, studies were performed to investigate the effect of intermittent addition of aliquots (10 mL) of 100% sucrose to the growing culture in 2L fermenter. Sucrose solution were intermittently added to the growing culture after 9 hours, when a decrease in dissolve oxygen tension (DOT) from the initial set up (100%) was

noticed to have decreased to 20%. The details of the results obtained are shown in Figure 3.13. From the analysis conducted, it was found that exponential cell growth started at 3 hours and continued until 12 hours of fermentation time. The organism showed a stationary cell growth after 12 hours and this lasted until 17 hours of the total fermentation time. Further extension of the fermentation time beyond 17 hours led to decline in the growth of the organism. The highest dry cell weight achieved at the start of intermittent addition of sucrose (at 9 hours) was 2.97 g/L, while the highest dry cell weight achieved at the end of exponential and stationary growth were 4.1 g/L and 4.91 g/L respectively. The P(3HB) yield at the start of intermittent addition of sucrose was 25.2 % dcw. This value was found to have improved, at end of increased cell growth and stationary growth, to 36.86 % dcw and 50.5 % dcw respectively. The P(3HB) concentration achieved at the onset of intermittent addition of sucrose was 0.75 g/L. Again, this value was found to improve significantly to 2.48 g/L at the end of stationary growth. Further increase in the fermentation time led to a decrease in the P(3HB) accumulated during the stationary growth. At the start of intermittent addition of sucrose, 2.22 g/L of RCM was quantified which increased to 2.59 g/L at the end of exponential growth and the RCM was noticed to have decreased to 2.43 g/L during the stationary growth phase but rose significantly during the death phase.

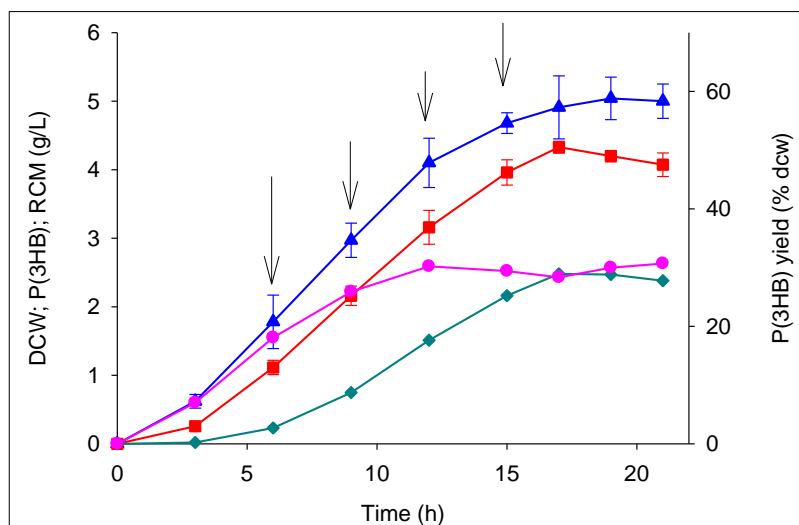


Figure 3.13 Temporal profile of DCW (g/L) (▲); P(3HB) yield (■); P(3HB) concentration (g/L) (◆); RCM (g/L) (●) produced by *Bacillus cereus* SPV during intermittent addition of sucrose in a 2L batch cultivation. Arrows indicates time points of addition of sucrose. Experiments were performed in duplicates while analyses of samples were done in triplicates (Error bars = \pm SD).

3.2.1.8 Production of P(3HB) by *Bacillus cereus* SPV using continuous feeding of sucrose as the main carbon source in modified G-medium in a 2L fermenter.

Fed-batch fermentation is one of the best methods of achieving a high cell density enriched with the highest possible amount of PHA (Akaraonye *et al.*, 2010). To improve the productivity achieved with the intermittent addition of aliquots of sucrose to the growing *Bacillus cereus* SPV culture, continuous feeding at the feeding rate of 0.71 ml/min, was investigated at two different conditions. Firstly, the fermentation was carried out with 1.0 g/L of KH_2PO_4 followed by investigations with 0.5 g/L KH_2PO_4 in the production medium.

3.2.1.8.1 Effect of replacement of potassium phosphate buffer in the production medium with 1.0 g/L KH_2PO_4 on the production of P(3HB) by *Bacillus cereus* SPV using a continuous feeding of sucrose as the main carbon source in a 2L fermenter.

The details of the experimental procedure followed in this study are described in Chapter 2.1, Section 2.1.2.3 while the results of the investigation are shown in Figure 3.14. The continuous feeding of nutrients was initiated based on the optical density measurement on the culture broth. This was started at 30 hours when the optical density was noticed to have dropped slightly, which was an indication of the depletion in the nutrient composition of the medium. The cell growth was found to have continuously increased until 40 hours, after which the growth rate slowed down and a stationary growth was later observed. The stationary growth lasted until 50 hours before a decrease in the dry cell weight was noticed. The maximum dry cell weight achieved before the initiation of the continuous feeding was 11.80 g/L. At the end of the exponential growth, the dry cell weight was found to have increased to 14.63 g/L while further extension of the fermentation time into the stationary growth phase led to further improvement in the dry cell weight to 15.22 g/L. The maximum P(3HB) yield before the initiation of fed-batch feeding was 51.01 % dcw. This value was found to have improved slightly to 54.8 % dcw at the end of the stationary growth. The P(3HB) concentration achieved before the initiation of continuous feeding was 6 g/L. At the end of the stationary growth, the P(3HB) concentration was found to have improved to 7.8 and 8.3 g/L respectively. The residual cell mass (RCM) was found to increase steadily throughout the fermentation with 5.8 g/L reached, before the initiation of continuous feeding, which increased to 6.9 g/L at the end of stationary growth.

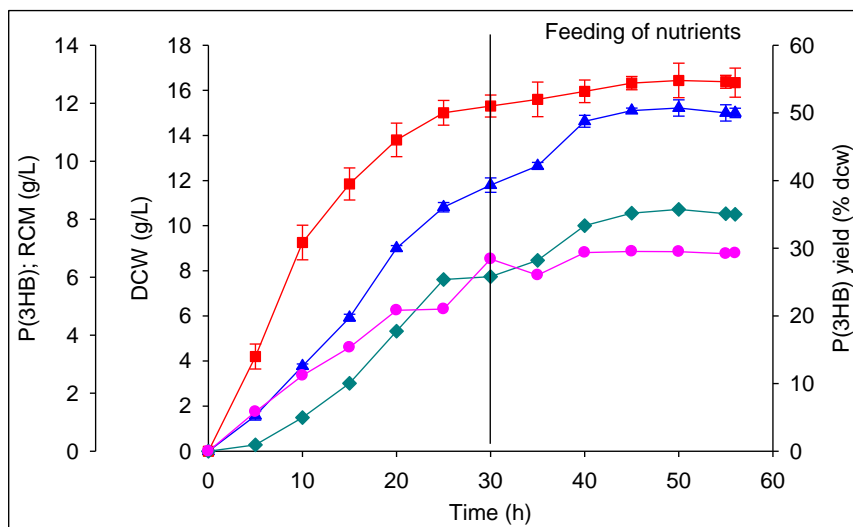


Figure 3.14 Temporal profile of DCW (g/L) (▲); P(3HB) yield (■); P(3HB) concentration (g/L) (◆) and RCM (g/L) (●) produced by *Bacillus cereus* SPV during a continuous feeding of sucrose rich nutrient in a 2L fermenter containing MGM supplemented with 1.0 g/L KH_2PO_4 . Experiments were performed in duplicates, while analyses of samples were done in triplicates (Error bars = \pm SD).

3.2.1.8.2 Effect of replacement of potassium phosphate buffer in the production medium with 0.5 g/L KH_2PO_4 on the production of P(3HB) by *Bacillus cereus* SPV using continuous feeding of sucrose in a 2L fermenter

The profile in Figure 3.15 shows the result obtained on the temporal modification of parameters investigated during the study. Following the same procedure as done above, continuous feeding of nutrients was initiated after 25 hours when the rate of increase in optical density of the nutrient broth reduced slightly. The exponential cell growth ended after 45 hours when the dry cell weight was found to be 7.6 g/L. The stationary cell growth ended 5 hours later with only a slight increase in the dry cell weight to 7.62 g/L and this was followed by a decrease in the dry cell weight. The P(3HB) yield obtained before the initiation of continuous feeding was 33.5 % dcw. At the end of the end of the fermentation, a P(3HB) yield 58.49% dcw was achieved. The P(3HB) concentration achieved before the initiation of continuous feeding was 1.57 g/L while P(3HB) concentration achieved at the end of the fermentation was 4.0 g/L. The RCM value at the

maximum P(3HB) yield was 2.85 g/L. Comparison of the results obtained by the addition of 1.0 g/L and 0.5 g/L KH_2PO_4 in MGM during fed-batch production of P(3HB) by *B. cereus* SPV in 5L fermenter is shown in Figure 3.16.

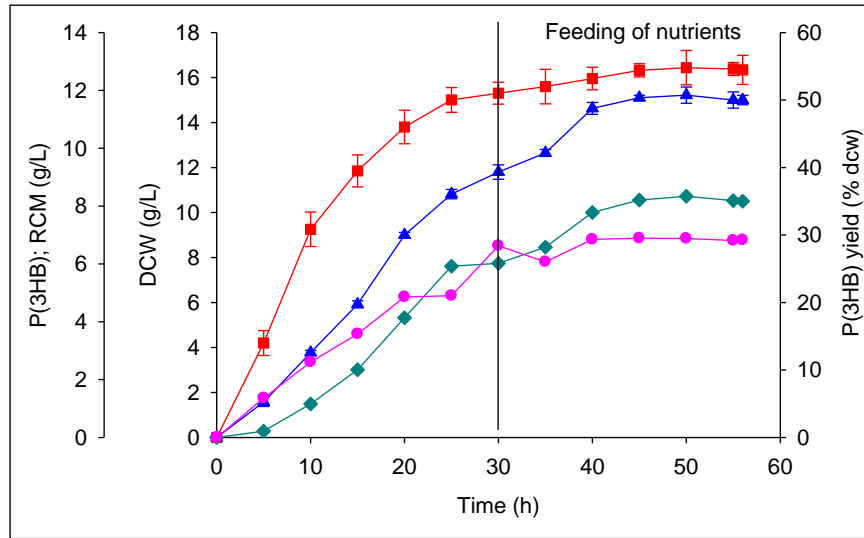


Figure 3.15 Temporal profile of DCW (g/L) (▲); P(3HB) yield (■); P(3HB) concentration (g/L) (◆) and (g/L) RCM (●) produced by *Bacillus cereus* SPV during a continuous feeding of sucrose rich nutrient in 2L fermenter containing MGM supplemented with 0.5 g/L KH_2PO_4 . Experiments were performed in duplicates while analyses of samples were done in triplicates (Error bars = \pm SD).

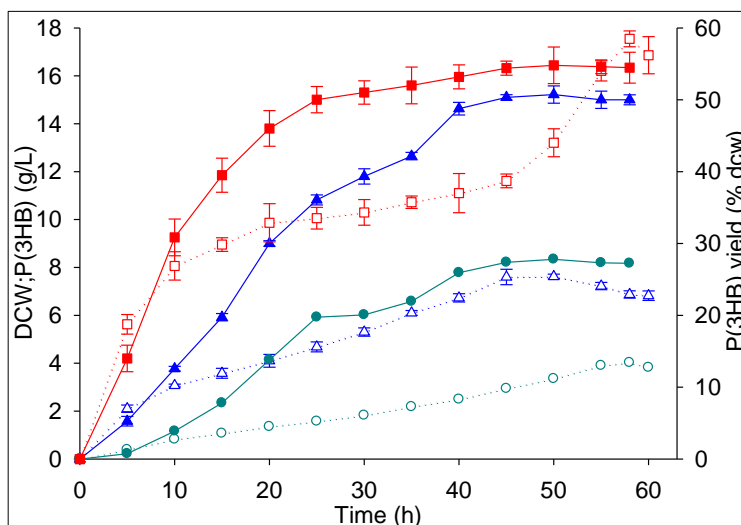


Figure 3.16 Temporal variation of DCW (g/L) (▲); P(3HB) yield (■); P(3HB) concentration (g/L) (●) produced by *Bacillus cereus* SPV during fed-batch fermentation with MGM media containing initial 1.0 g/L KH_2PO_4 (solid lines) and 0.5 KH_2PO_4 (dotted lines) a 2L fermenter.

3.2.1.9 Production of P(3HB) by *Bacillus cereus* SPV using Two-stage fermentation in 5L Fermenter.

Fermentation processes involving two or three stages have been widely used for the production of polyhydroxyalkanoates (PHAs) (Chen and Page 1997; Ruan *et al.* 2003; Rocha *et al.* 2008). In all those cases, the polyesters production has been improved, reaching up to 36 g/L of polymer in a 2.5 L fermenter (Chen and Page, 1997). In the case of *Bacillus*, there is no information about the application of a multistage fermentation system. Hence, a two-stage PHA production with *Bacillus cereus* SPV was investigated. The aim was to maximize further, PHA accumulation in the organism. The results obtained are represented in Figure 3.17. Based on the results of the previous studies, the first-stage of the fermentation was terminated after 30 hours. The second stage fermentation was initiated following the details of the protocol described in Chapter 2, section 2.1.2.4 with the MGM medium contained (in g/L) $(\text{NH}_4)_2\text{HPO}_4$, 1.0, yeast extract, 2.5 g, $\text{FeSO}_4 \cdot 7\text{H}_2\text{O}$, 0.0005, $\text{CuSO}_4 \cdot 5\text{H}_2\text{O}$, 0.005, $\text{ZnSO}_4 \cdot 7\text{H}_2\text{O}$, 0.005, $\text{MnSO}_4 \cdot 7\text{H}_2\text{O}$, 0.05, MgSO_4 , 0.2, CaCl_2 , 0.05, sucrose, 20.0, K_2HPO_4 , 0.5 and $6 \times 10^{-4}\text{M}$ α -Picolinic acid. The result obtained

shows that the highest dry cell weight (9.10 g/L) achieved before the termination of the first stage reduced to 8.30 g/L. In the second stage of fermentation the dry cell weight remained constant during the rest of the second phase until the 50th hour. The highest P(3HB) content achieved before the termination of first stage of fermentation was 63.9 % dcw. This valued increased to 80.3 % dcw P(3HB) yield at the end of the second stage. Further increase in the fermentation time resulted in a decrease in the P(3HB) content. The P(3HB) concentration achieved at the end first stage of fermentation was 5.8 g/L and the maximum value achieved at the end of stationary cell growth was 7.06 g/L. The RCM value at the end of first stage of the fermentation was 4 g/L and the RCM value at the maximum P(3HB) yield was 2 g/L.

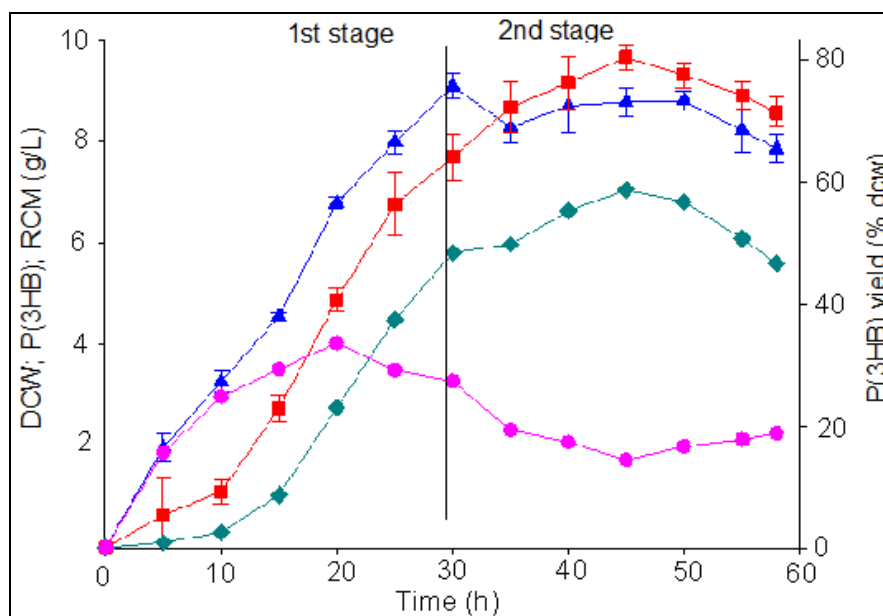


Figure 3.17 Temporal profile of DCW (g/L) (▲); P(3HB) yield (■); P(3HB) concentration (g/L) (◆) and RCM (g/L) (●) produced by *Bacillus cereus* SPV in a two- stage fermentation process in a 5L fermenter. Experiments were performed in duplicates while analyses of samples were done in triplicates (Error bars = ±SD).

Table 3.1 Summary of the fermentation studies on the use of MGM medium and sucrose as the main carbon source for P(3HB) production in *Bacillus cereus* SPV. The time column represents time points of maximum productions of the parameters quantified.

Condition	Time (h)	DCW (g/L)	% P(3HB) (% dcw)	P(3HB) (g/L)
^a Production using Kannan & Rehacek medium (Shaken flask)	32	5.98	47.7	2.85
Production using Kannan & Rehacek medium	18	3.42	32.87	1.12
^a Production using MGM medium (Shaken flask)	30	6.23	42.80	2.67
Production using MGM medium	24	3.29	47.20	1.55
^b Production in MGM medium (fed-batch)	17	4.91	50.50	2.48
Increase in initial KH ₂ PO ₄ /KH ₂ PO ₄ buffer conc. in MGM to 0.25M	50	7.13	52.50	3.72
Increase in Yeast extract conc. in MGM to 4.5 g/L	18	5.71	44.81	2.56
Replacement of potassium phosphate buffer with 0.5 g/L KH ₂ PO ₄ in MGM	55	7.21	82.61	5.95
Replacement of potassium phosphate buffer with 0.1 g/L KH ₂ PO ₄ in MGM	45	7.22	65.25	4.70
^b Replacement of potassium phosphate buffer with 0.5 g/L KH ₂ PO ₄ in MGM during fed-batch production	58	6.87	58.49	4.02
^b Replacement of potassium phosphate buffer with 1.0 g/L KH ₂ PO ₄ in MGM during fed-batch production	50	15.22	54.80	8.34
Two-Stage fermentation	50	8.79	80.30	7.06

^a indicate P(3HB) production in shaken flask scale

^b indicate P(3HB) production in fed-batch scale

3.2.2 Development of a novel wet cell extraction to facilitate continuous PHA production

One of the major factors that contribute to the high cost of PHA production is the recovery of PHAs from the host cells. Whilst some approaches in PHA extraction are effective in recovering high amounts of the polymer, many are only effective in recovering high purity PHAs with a large amount of the polymer left behind in the cell debris. Furthermore, in the use of PHAs for medical applications, it is very important that the purity of the PHAs is not sacrificed as this might illicit immunological effects when used in medical applications. For instance, PHAs from bacteria require special attention during recovery because of the presence of lipopolysaccharides (in Gram-negative bacteria) and teichoic acid (in Gram-positive bacteria) which are normally extracted alongside the polymers during isolation. Hence, a novel wet cell extraction technique described in detail in Section 2.1.3.3 was developed in this study which enabled the recovery of the polymer while still in a relatively more amorphous state and further enhanced purity and PHA recovery from the cells. It also saves the downstream processing time by removing the time consuming freeze drying step. Figure 3.18 shows the amount of polymer recovered at different time points. The amount of polymer recovered was highest with 2 hours incubation of the cells in solution of chloroform and hypochlorite and least with recovery after 1 hour incubation.

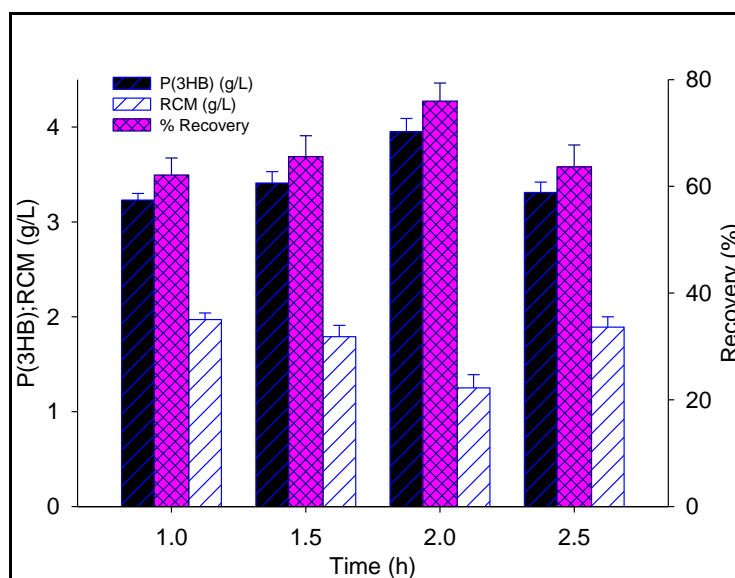


Figure 3.18 Graph showing the amount of P(3HB), residual cell mass and percentage recovery achieved during a wet cell polymer isolation from *Bacillus cereus* SPV (n=3; error bar = \pm SD).

3.2.3 Characterisation of P(3HB)

The polyesters isolated from the studies above using *Bacillus cereus* SPV in MGM production medium supplemented with sucrose as the main carbon source was characterised using GC-MS, NMR, FTIR and DSC for the identification of its chemical structure and thermal properties. All the parameters analysed were compared to the Standard P(3HB) purchased from Sigma.

3.2.3.1 Gas chromatography-Mass spectrometry

Gas chromatography is generally used to identify the constituents of the different polyhydroxyalkanoates and quantify the amount of PHA present in the cells. Thus, it was used to confirm that the polyester isolated from the *Bacillus cereus* SPV cells from various investigations described above was indeed the P(3HB) homopolymer. The profile of the GC chromatogram is shown in Figure 5.19a which confirmed the type of polymer to be a methyl ester of poly(3-hydroxybutyrate). The GC peaks obtained were further subjected to mass spectrometric analysis (Figure 5.19b). The molecular ion-related mass fragment occurred at m/z , 117 and this was due to the methyl ester of 3HB ($M_w = 118$). When compared to the ones reported in the literature, the result of the GC-MS analysis confirmed the presence of 3HB in the isolated polymer (Valappil *et al.*, 2007). Furthermore, both the GC chromatogram and the mass spectrum showed very pure and distinct peaks without impurities.

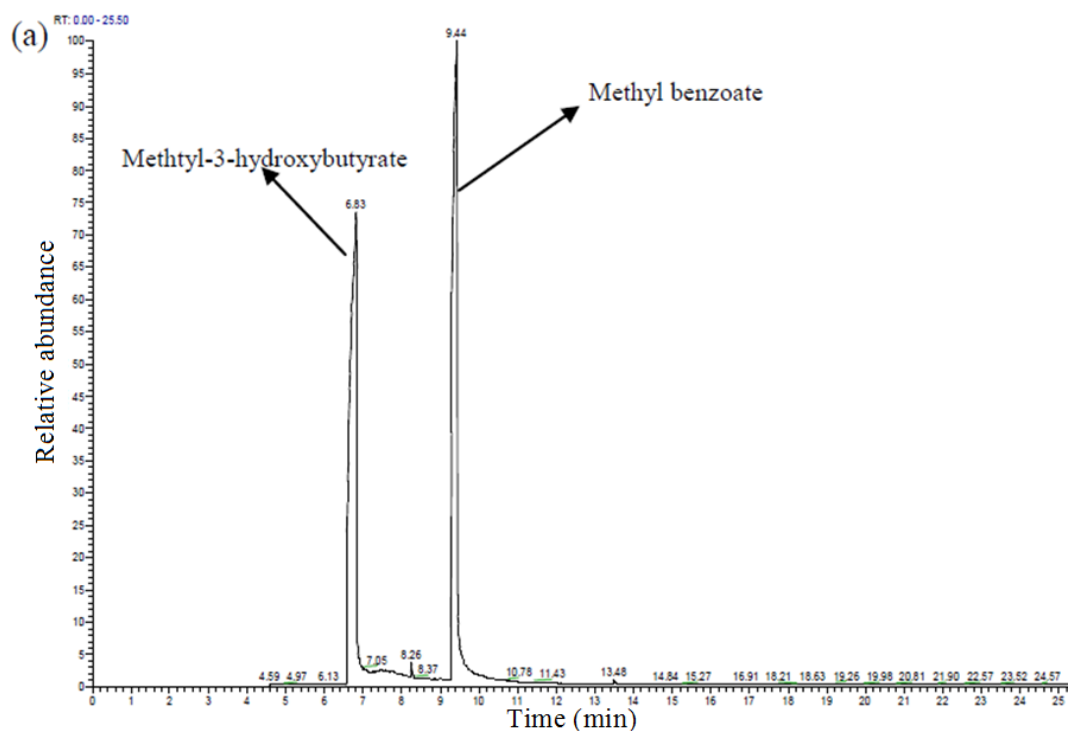


Figure 3.19 (a) The total ion chromatogram of the methanolysis products of the polymer isolated from *Bacillus cereus* SPV grown in MGM medium supplemented with sucrose as the main carbon substrate

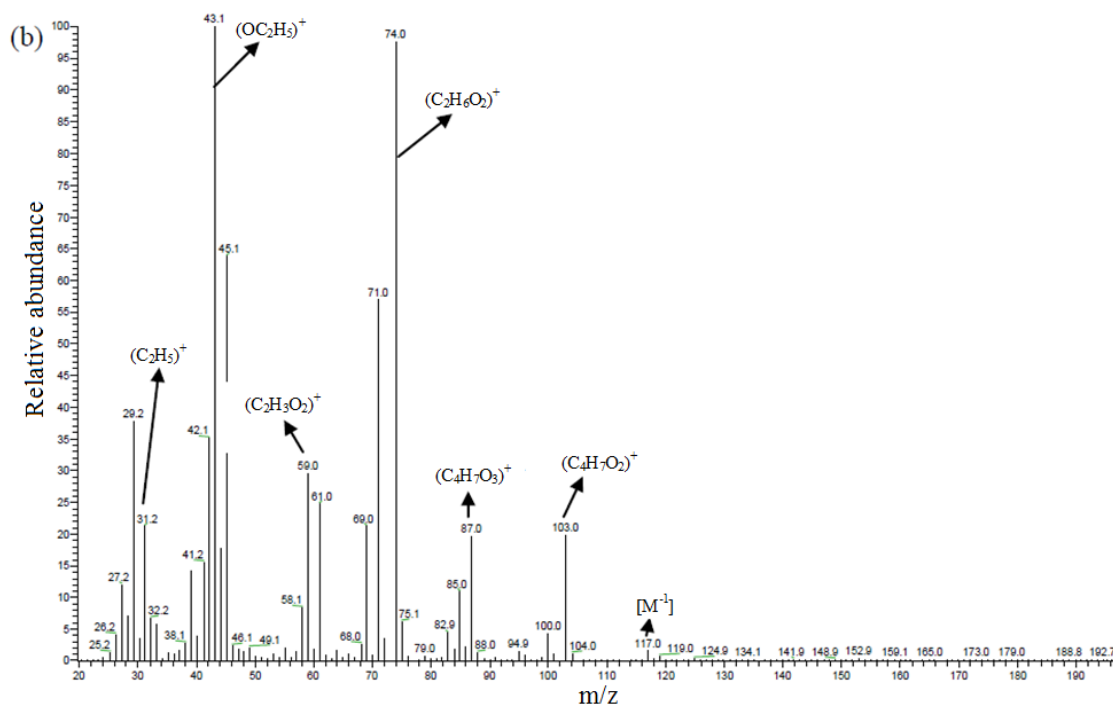


Figure 3.19 (b) Mass spectra of the methyl ester of 3-hydroxybutyrate.

3.2.3.2 Nuclear Magnetic Resonance Analysis, NMR

The structure of the extracted polymer was further examined with ^{13}C NMR analysis to confirm the result of the GC-MS analysis performed above. The chromatogram of the analysis is shown in Figure 3.20a. The very strong intensity lines obtained were identical to the ^{13}C NMR spectra of P(3HB) reported previously (Yoshie *et al.*, 2002). The four peaks were assigned to the methyl (CH_3 ; 21.1 ppm), methylene (CH_2 ; 41.7 ppm), methine (CH ; 68.3 ppm) and carbonyl ($\text{C}=\text{O}$; 169.3 ppm) carbon resonance of P(3HB). This result was found to be consistent with the findings of Doi and colleagues (Doi *et al.*, 1989). The ^1H NMR analysis is shown in Figure 3.20b. Signal at 5.3 ppm depicts the methine protons (CH) of the asymmetric carbons of 3HB. The signal observed at 2.27-2.3 PPM represent methylene protons (CH_2) of the main chain in the monomer units. The methyl 3 proton CH_3 of the monomer units are assigned with resonance at 1.3 ppm group of the side chain of all repeated units. Hence, the type of polyester produced from the studies with production medium (modified G-medium) supplemented with sucrose was confirmed to be a homopolymer of P(3HB).

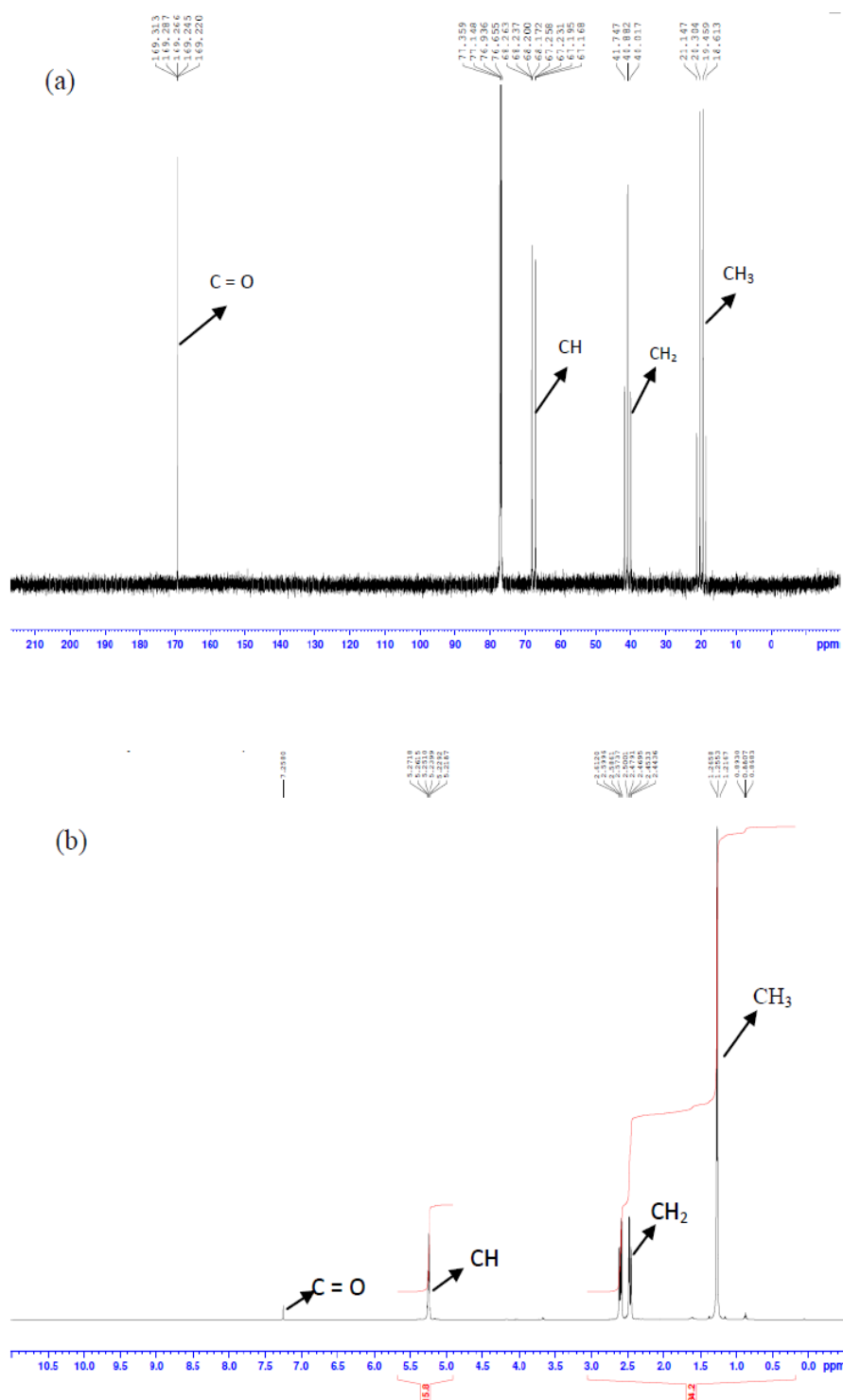


Figure 3.20 (a) ¹³C NMR spectrum of P(3HB), (b) ¹H NMR spectrum of isolated P(3HB) from *Bacillus cereus* SPV grown in MGM medium supplemented with sucrose as the main carbon source.

3.2.3.3 Fourier Transfer – Infra Red (FTIR) Analysis

The FTIR spectroscopy was further performed on the isolated polymer. This was done to establish the characteristic properties of the homopolymer of P(3HB) produced, which had already been confirmed using GC-MS and NMR analysis. The spectrum of the result compared to the commercial polymer is shown in Figure 3.21. Absorption bands at 1728 cm^{-1} corresponding to the ester carbonyl group and 1282 cm^{-1} corresponding to -CH group were observed (Figure 3.21). These absorption bands corresponded to the characteristic features of P(3HB) as reported in the work of Hong *et al.*, 1999.

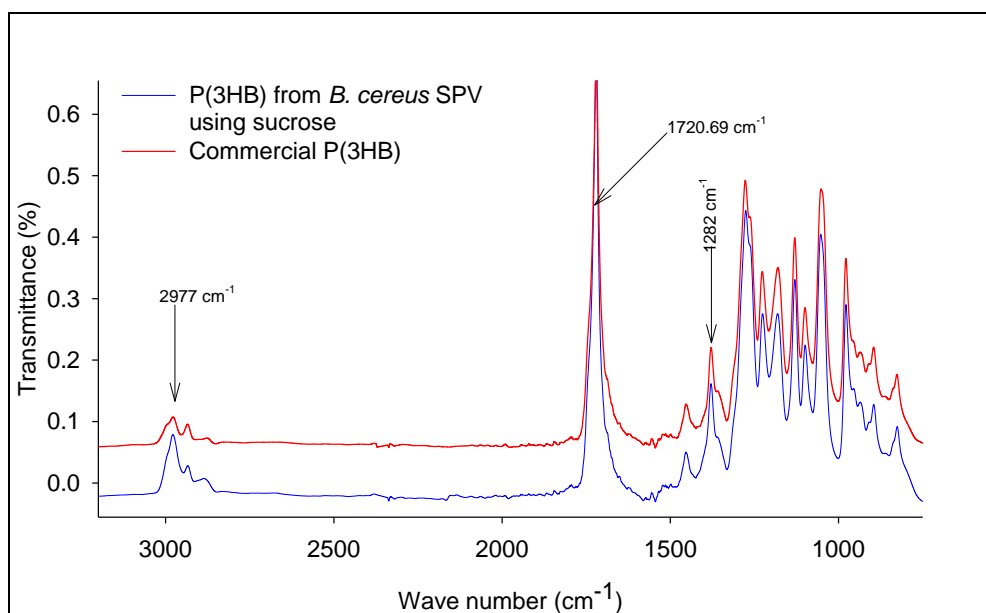


Figure 3.21 FT-IR spectrum of P(3HB) isolated from *B. cereus* SPV grown in MGM medium supplemented with sucrose (blue) and P(3HB) from Sigma-Aldrich (red). The absorption bands at 1282 cm^{-1} and 1728 cm^{-1} correspond to C=O and C-O of P(3HB) respectively.

3.2.3.4 Differential scanning calorimetry, DSC Analysis

DSC analysis was carried on the isolated P(3HB) to establish the thermal properties of the polymer. The results obtained were compared with the values of the commercial P(3HB) purchased from Sigma and the thermogram is shown in Figure 3.22. The differential scanning calorimetry (DSC) analysis performed on the isolated P(3HB) shows that the melting temperature, T_m (168.21°C), crystallization temperature, T_c (49.10°C), and glass transition temperature, T_g (3.61°C) of the isolated P(3HB) was slightly lower than the result obtained using the standard commercial polymer obtained from Sigma (T_m (173.11°C); T_c (59.45°C) and T_g (8.23°C) (Figure 3.22).

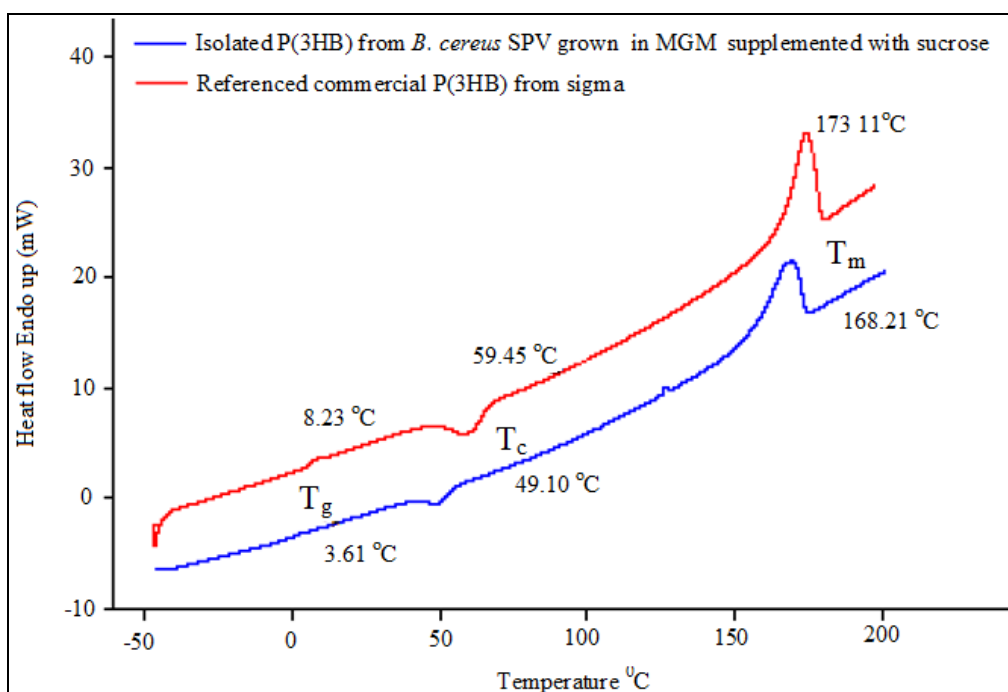


Figure 3.22 DSC thermograms of P(3HB) accumulated by *B. cereus* SPV in MGM medium supplemented with sucrose (blue line) and commercial P(3HB) purchased from Sigma-Aldrich (red line).

SECTION III

Bioconversion of agricultural raw materials and waste (sugarcane molasses) into the highly valued-green material, P(3HB) by *Bacillus cereus* SPV

3.3.1 Introduction

Recently, there has been increased scientific and commercial interest in the development of fermentation strategies to bio-convert renewable raw materials into biodegradable polymers such as PHAs. The economic evaluation of the cost of PHA production suggested that the cost of carbon sources alone accounts for 50% of the overall PHA production cost (Mudliar *et al.*, 2008). Hence, commercialization of PHAs would be enhanced if the full potential of agricultural raw materials and waste, as sources of carbon and nitrogen for PHA production can be exploited. Agricultural raw materials including wheat bran, corn steep liquor, rapeseed cake, starchy wastewater and molasses have been used as biorefinery feedstock for the industrial production of conventional chemicals and bioplastics (Akaraonye *et al.*, 2010). Sugar cane molasses have mostly been used in fermentation processes because of its low price and rich chemical composition (Berwanger *et al.*, 2007). Usually this includes the presence of sucrose, glucose and fructose as the main carbohydrates (Ali, 2004).

Different agricultural resources have been used as substrates in order to obtain reasonable levels of PHAs produced by different bacteria. This has demonstrated the possibility of employing sustainable cheap materials as carbon sources to reduce the production cost of PHAs. For instance, *Acinetobacter venetianus* has been shown to be able to utilize soy molasses as the carbon substrate for PHA production (Panilaitis *et al.*, 2007). On the other hand *Azotobacter vinelandii* has also been observed to accumulate high amounts of PHAs by utilizing sugar cane liquor as the main carbon source for growth and PHA production. Other organisms known to have the capacity of accumulating high amounts of PHAs from agricultural resources include *Pseudomonas fluorescens* (sugarcane molasses); *Azotobacter chroococcum* (beet molasses); *Burkholderia cepacia* and *B. sacchari* (starch); and *Pseudomonas hydrogenovora* (whey)

(Castilho *et al.*, 2009). Specifically in *Bacillus* sp, the utilization of mahua flowers as a carbon source produced high levels (51-54%) of the PHA copolymer, P(3HB-*co*-3HV) (Anil *et al.*, 2006). Vishnuvardhan and colleagues have also observed the accumulation of 60% dcw P(3HB-*co*-3HV) copolymer by *Bacillus megaterium* strain OU303A, when glycerol, a cheap by-product of the biodiesel industry, was employed as the main carbon source in the production medium (Vishnuvardhan *et al.*, 2009). These results confirm the potential of cheap agricultural resources and waste material to reduce the cost and hence enhance the commercialization of PHAs.

In this section, the use of the agricultural waste material, sugarcane molasses, as a low cost carbon source for the commercial production of the biodegradable polymer, poly(3-hydroxybutyrate) has been explored. This process, if developed well, would provide a sustainable means for agricultural waste management as well as reduction in the cost of carbon sources for P(3HB) production, leading to enhanced commercial viability.

3.3.2 Results

3.3.2.1 Poly(3-hydroxybutyrate) production by *Bacillus cereus* SPV using sugarcane molasses as the main carbon source in shaken flask

In order to evaluate the potential of sugarcane molasses as a replacement of the more expensive carbon sources in PHA production, *B. cereus* SPV was grown on modified G-medium, supplemented with 20 g/L sugarcane molasses in 1L shaken flasks. Figure 3.23 shows the temporal profile of growth and polymer accumulation. It was observed that polymer accumulation occurred alongside growth until 30 hours after which the rate of polymer accumulation became higher than the rate of biomass accumulation. The maximum polymer yield (61.07 % dcw) was achieved at 55 hours. Initially, the residual cell mass increased along with cell growth and P(3HB) accumulation. However, after 27 hours of growth, the increase in the RCM decreased and almost reached a constant value of 2.48 g/L.

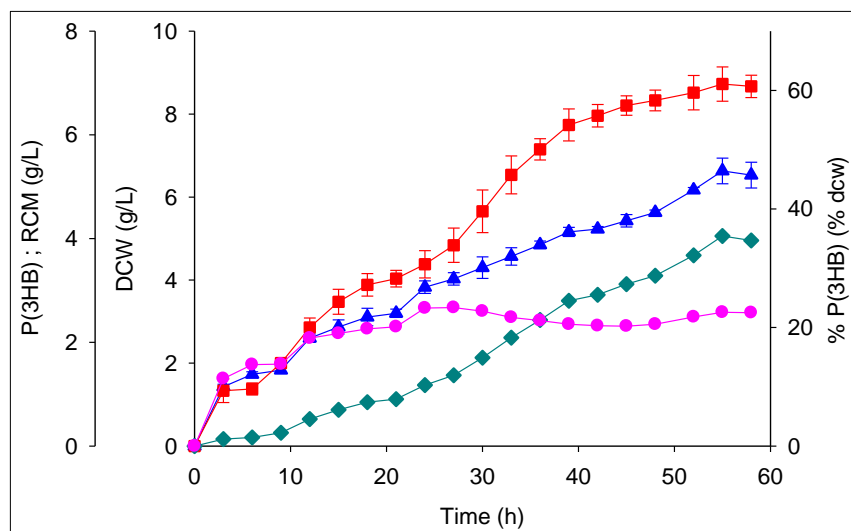


Figure 3.23 The temporal variation of DCW (g/L) (▲); P(3HB) yield, (■); P(3HB) concentration (g/L) (◆) and RCM (g/L) (●) produced by *Bacillus cereus* SPV in MGM medium supplemented with sugarcane molasses as the main carbon source in shaken flask culture. Experiments were performed in duplicates while analyses of samples were done in triplicates (Error bars = \pm SD).

3.3.2.2 Poly(3-hydroxybutyrate) production by *Bacillus cereus* SPV using sugarcane molasses as the main carbon source in a 2L fermenter

To further understand the potential of *Bacillus cereus* SPV in utilizing sugarcane molasses as an alternative carbon source for large scale PHA production, studies were extended to a 2L fermenter level. The results (Figure 3.24), showed initial exponential growth until 47 hours, with the maximal DCW value of 6.93 g/L observed at 55 hours. Polymer accumulation increased with cell growth until 47 hours where the maximum polymer yield of 51.37 % dcw was obtained, after which the yield decreased until the end of the fermentation. The residual cell mass increased along with the cell growth until 36 hours after which the value remained almost constant.

Comparison of the shaken flask and 2L fermenter studies show that comparable maximal values of dry cell weight (6.63 g/L) and P(3HB) concentration (3.45 g/L) were observed in the shaken flask investigations, and the 2L fermentation studies which yielded maximal values of

6.93 g/L and 4.05 g/L of dry cell weight and P(3HB) concentrations respectively. However, the maximum P(3HB) yield obtained was 61.07 % dcw in shaken flask studies as compared to a relatively lower value of 51.37 % dcw obtained in the 2L fermenter studies.

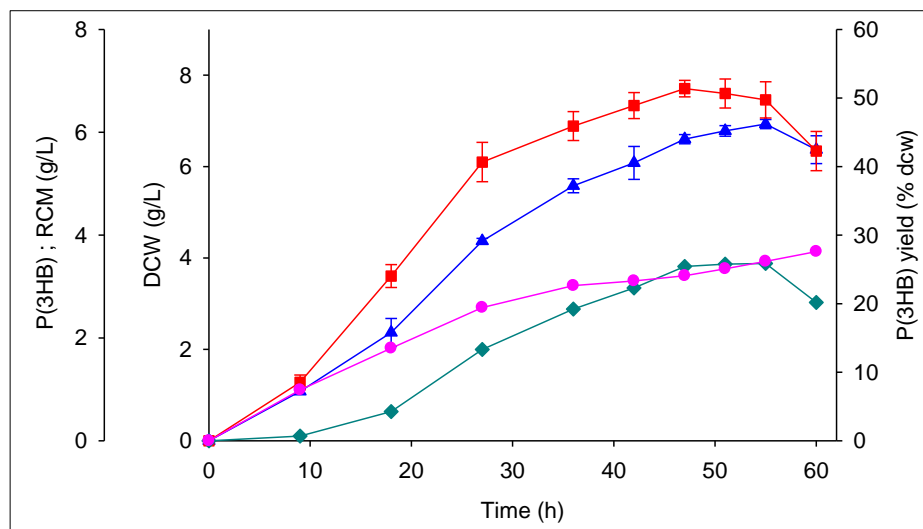


Figure 3.24 The temporal variation of DCW (g/L) (▲); P(3HB) yield (■); P(3HB) concentration (g/L) (◆) and RCM (g/L) (●) produced by *Bacillus cereus* SPV using sugarcane molasses as the sole carbon source in batch fermentation using 2L fermenters. Experiments were performed in duplicates while analyses of samples were done in triplicates (Error bars = \pm SD).

3.3.2.3 Effect of reduced $(\text{NH}_4)_2\text{PO}_4$ concentration on biomass and P(3HB) accumulation by *Bacillus cereus* SPV, using sugarcane molasses as the main carbon source.

In order to evaluate the effect of nutrients other than the carbon source on cell growth and polymer accumulation, the amount of $(\text{NH}_4)_2\text{PO}_4$ present in the production medium was reduced to half (1.0 g/L) the amount used in the above two sections (2.0 g/L). This investigation was carried out both at the shaken flask level and in 2L fermenter. Figure 3.25 shows the temporal variation of the parameters measured at shaken flask level. Simultaneous accumulation of polymer alongside growth was observed until 40 hours. However, the rate of polymer accumulation increased after 20 hours and the P(3HB) yield reached a maximum value of 52.27 % dcw at 55 hours. The P(3HB) concentration reached a maximum value of 3.64 g/L at 45 hours. The residual cell mass increased with the cell growth until 15 hours, after which the rate

of polymer accumulation increased with a simultaneous reduction in the rate of increase of RCM. Thus, maximal values of 4.30 g/L, 52.27 % dcw and 2.25 g/L of dry cell weight, P(3HB) yield and P(3HB) concentration, respectively were achieved in shaken flask studies.

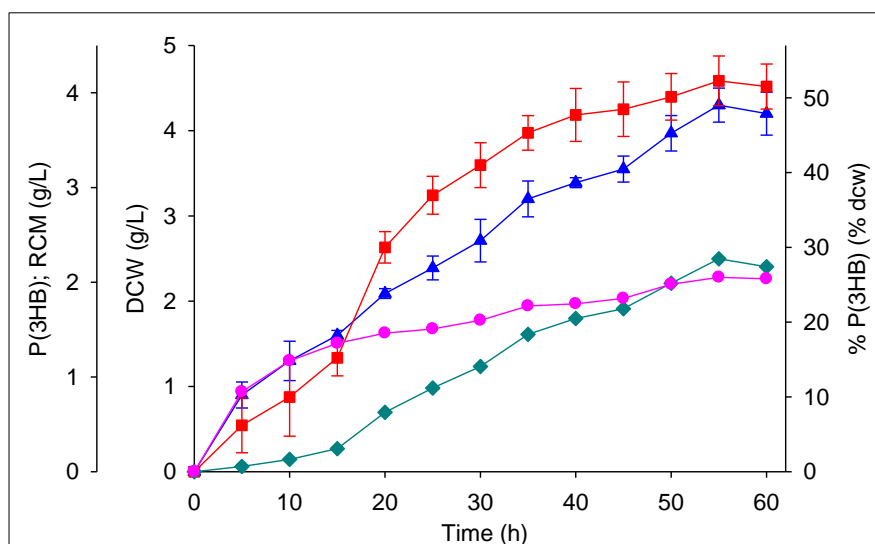


Figure 3.25 The temporal variation of DCW (g/L) (▲); P(3HB) yield (■); P(3HB) concentration (g/L) (◆) and RCM (g/L) (●) produced by *Bacillus cereus* SPV in shaken flasks supplemented with sugarcane molasses as the main carbon source in MGM medium containing 1.0 g/L $(\text{NH}_4)_2\text{PO}_4$. Both experiments and analyses of samples were performed in triplicates (Error bars = \pm SD).

A similar pattern of cell growth and polymer accumulation observed in shaken flask investigations was also observed in the study using the 2L fermenter (Figure 3.26). However, the stationary growth phase was achieved much earlier in the 2L fermentation (21 hrs vs 54 hrs in shaken flask), thereby resulting in an overall decrease in the fermentation time. Cell growth decreased after 28 hours while the highest polymer yield (47.43 % dcw) was achieved at 30 hours of fermentation and the maximum polymer concentration of 1.85 g/L was observed at 28 hours of fermentation. Thus, maximal values of 4.30 g/L, 47.43 % dcw and 1.85 g/L of dry cell weight, P(3HB) yield and P(3HB) concentrations respectively, were obtained in 2L fermenters.

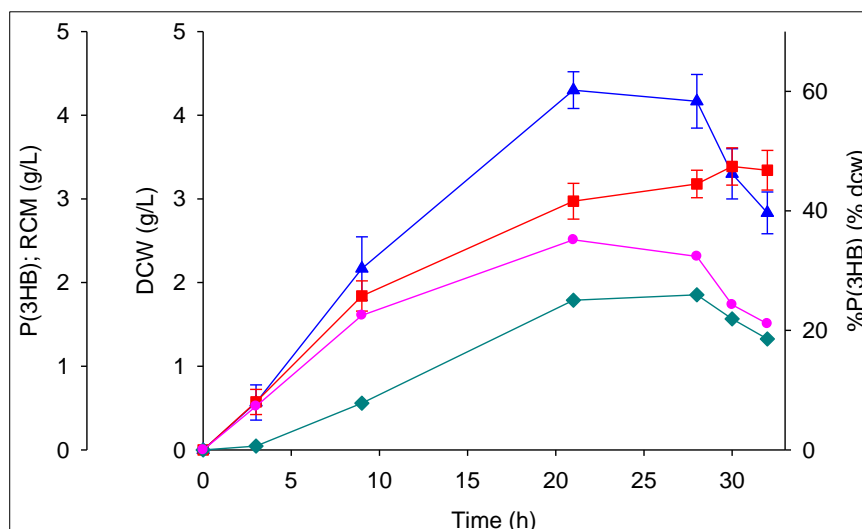


Figure 3.26 The temporal variation of DCW (g) (▲); P(3HB) yield (■); P(3HB) concentration (g/L) (◆) and RCM (g/L) (●) produced by *Bacillus cereus* SPV in a 2L fermenters with reduced $(\text{NH}_4)_2\text{PO}_4$. Experiments were performed in duplicates while analyses of samples were carried out in triplicates (Error bars = \pm SD).

3.3.2.4 Effect of continuous feeding of sugarcane molasses on biomass and P(3HB) accumulation by *Bacillus cereus* SPV

Since polymer accumulation occurs mostly in the presence of excess carbon source, the effects of a continuous supply of sugarcane molasses to the growing cultures of *Bacillus cereus* SPV were investigated. In the shaken flask study, the rate of increase of optical density decreased at 12 hours, indicating a decrease in cell growth; hence, continuous feeding of sugarcane molasses solution (1g/mL), at a feeding rate of 0.7 mL min^{-1} was initiated at this time point. A dry cell weight of 1.63 g/L and 15.37 % dcw PHA yield was achieved at this time point. Both dry cell weight and PHA yield were found to increase to a maximal value of 5.47 g/L and 57.13 % dcw respectively at 51 hours, after the introduction of continuous feeding of the sugarcane molasses solution (Figure 3.27).

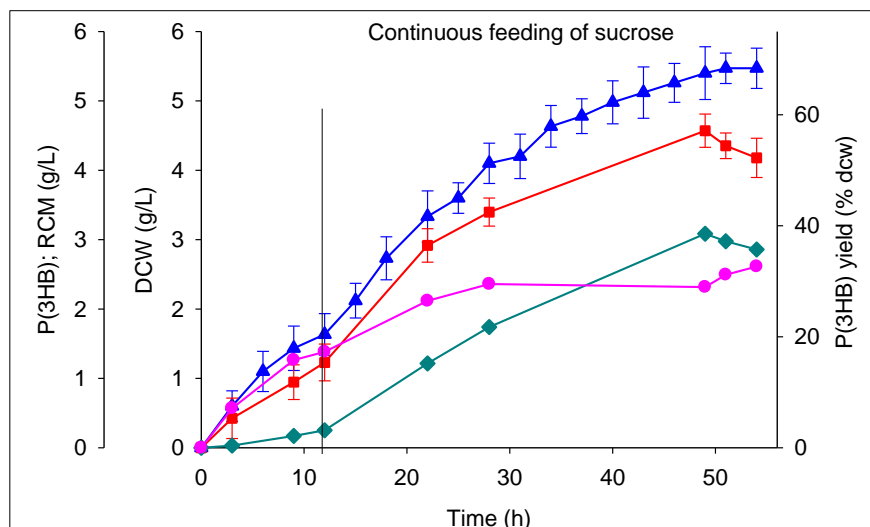


Figure 3.27 The temporal variation of DCW (g/L) (▲); P(3HB) yield (■); P(3HB) concentration (g/L) (◆) and RCM (g/L) (●) produced by *Bacillus cereus* SPV during a continuous feeding of sugarcane molasses solution in 1 L shaken flask cultures. Experiments were performed in duplicates while analyses of samples were done in triplicates (Error bars = \pm SD).

In the 2L fermenter study, continuous feeding of the sugarcane molasses solution (1g/mL) at a feeding rate of 0.7 mL min^{-1} was initiated after 23 hours of fermentation, when a decrease in the initial set value of 100% dissolved oxygen tension (DOT) to 20% DOT was noticed. This was carried out in order to enhance PHA accumulation. Contrary to what was expected, the continuous supply of the sugarcane molasses only increased cell growth with a reverse effect on polymer accumulation. Hence, the maximum polymer content (28.10 % dcw) achieved at 23 hours, before the continuous feeding of nutrient, reduced to 13.74 % dcw at 34 hours when the maximum dry cell weight of 6.83 g/L was achieved (Figure 3.28).

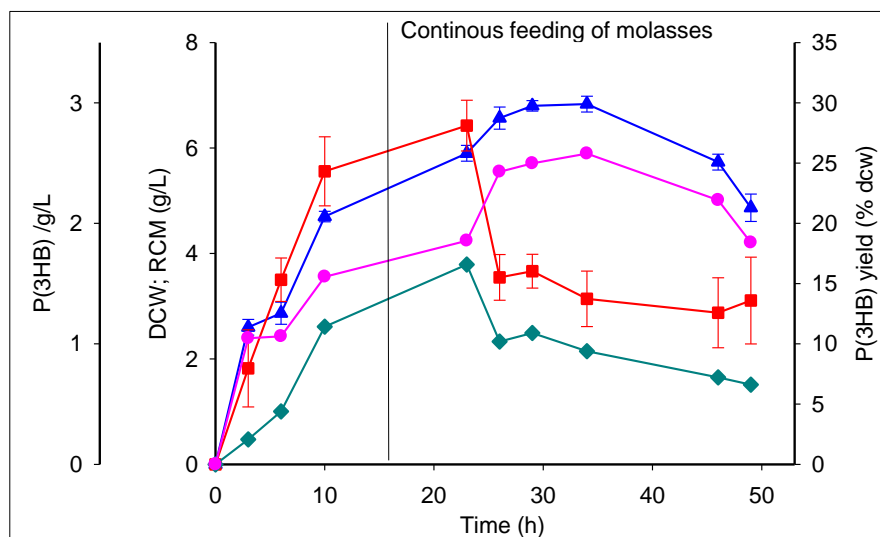


Figure 3.28 The temporal variation of DCW (g/L) (▲); P(3HB) Yield (% dcw) (■); P(3HB) concentration (g/L) (◆) and RCM g/L (●) produced by *Bacillus cereus* SPV during a continuous feeding of sugarcane molasses solution in a 2L fermenter. Experiments were performed in duplicates while analyses of samples were done in triplicates (Error bars = \pm SD).

Table 3.2 Summary of the fermentation studies on the use of sugarcane molasses as a cheap carbon source for P(3HB) production in *Bacillus cereus* SPV. The time column represents time points of maximum productions of the parameters quantified.

Process scale	Condition	Time (h)	DCW (g/L)	% P(3HB) (% dcw)	P(3HB) (g/L)
Shaken flask	Shaken flask (Batch)	55	6.63	61.7	4.06
	Shaken (Batch without yeast extract)	52	3.90	56.47	2.20
	Continuous feeding with molasses	48	5.30	54.60	2.89
	Continuous feeding with molasses and MGM	47	5.78	13.34	0.77
Fermenter	Batch	36	6.60	51.37	3.39
	Batch (without yeast extract)	23	2.43	49.55	1.20
	Continuous feeding with molasses	35	6.80	28.11	1.65
	Continuous feeding with molasses and MGM	53	7.83	45.24	3.54

3.3.3 Characterization of the isolated PHAs produced using sugarcane molasses

The PHA isolated from *B. cereus* SPV cells produced from each of the above mentioned conditions were identified by nuclear magnetic resonance. The ¹H-NMR confirmed the polymers isolated from all the conditions as the homopolymer of poly(3-hydroxybutyrate) (Figure 3.29).

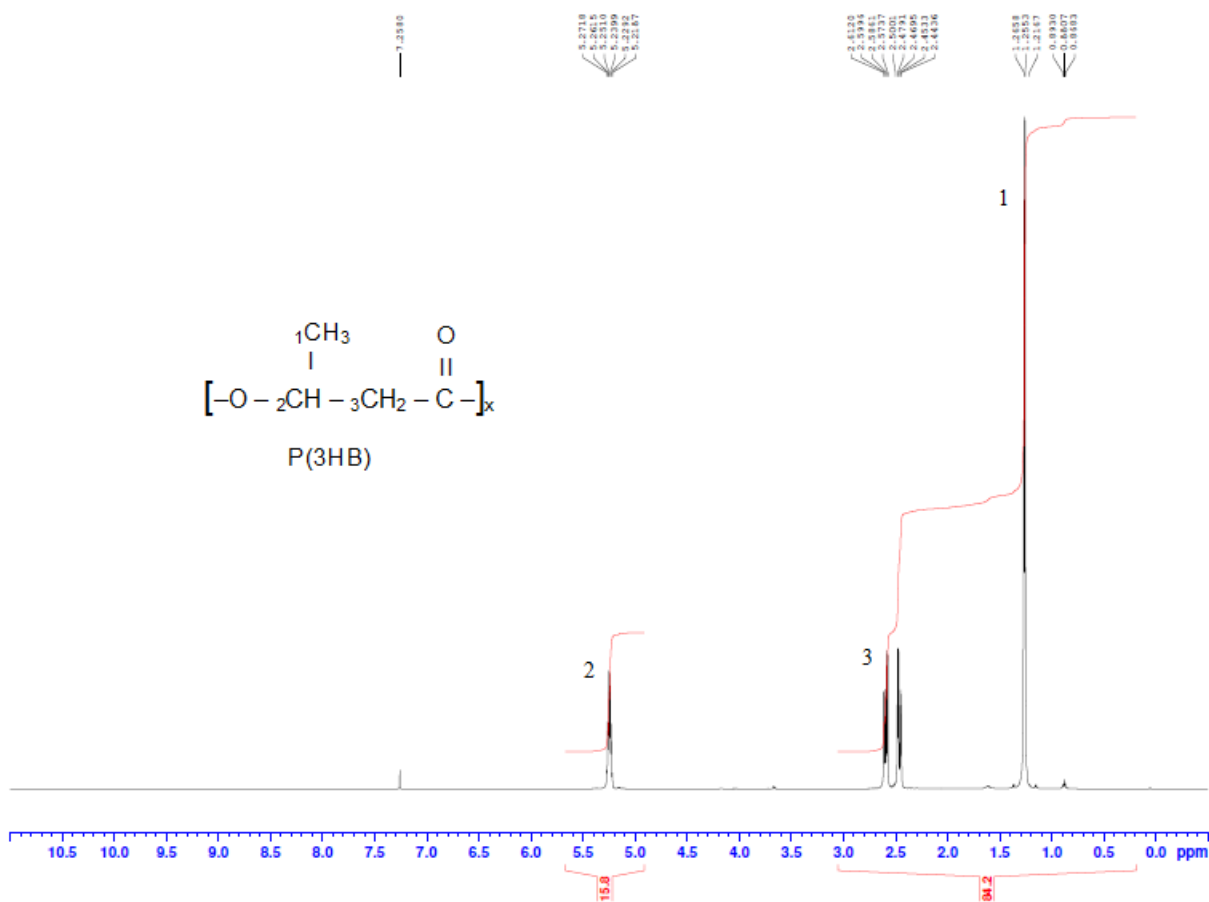


Figure 3.29 ¹H-NMR spectrum of P(3HB) isolated from *Bacillus cereus* SPV, when sugarcane molasses was used as the main carbon source.

The FT-IR analysis of the isolated polymers revealed absorption bands at 1720 cm^{-1} corresponding to the ester carbonyl group and 1282 cm^{-1} corresponding to the -CH group, characteristic features of P(3HB) (Figure 3.30).

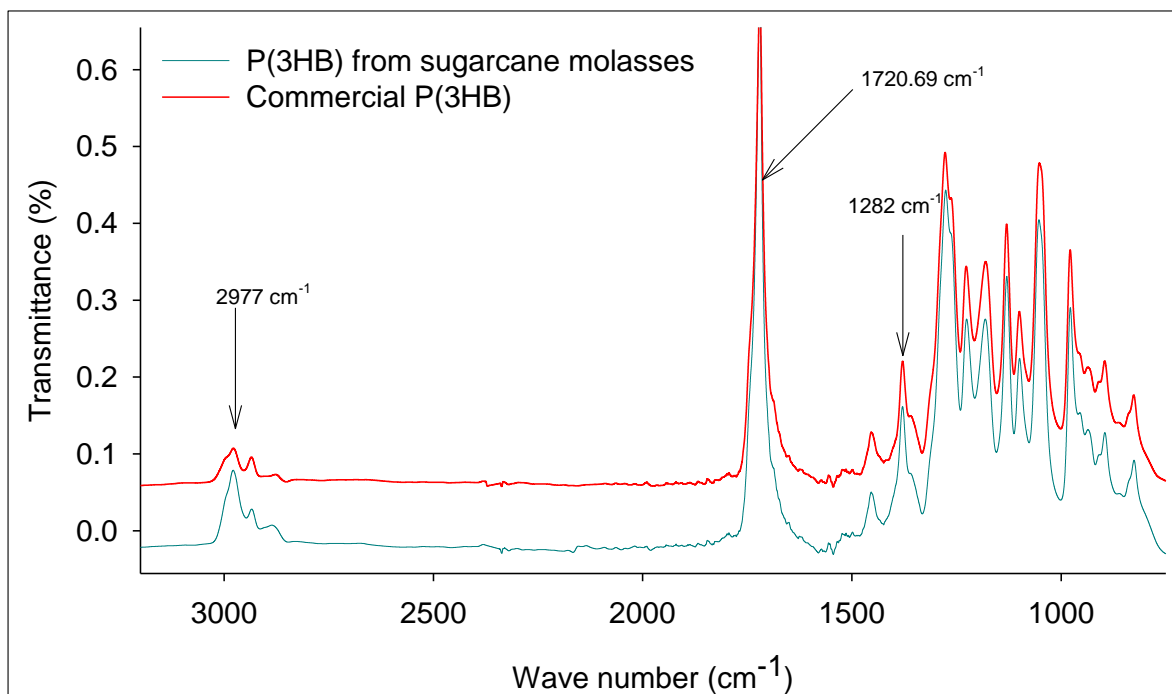


Figure 3.30 FT-IR spectrum of (a) P(3HB) produced using *B. cereus* SPV grown in modified MGM media supplemented with sugarcane molasses (blue) and (b) Standard P(3HB) from Sigma-Aldrich (red). The absorption bands at 1282 cm^{-1} and 1720 cm^{-1} correspond to C=O and C-O of P(3HB) respectively.

The differential scanning calorimetric (DSC) analysis performed on the isolated P(3HB) produced showed that the melting temperature, T_m (168.21°C), crystallization temperature, T_c (49.10°C), and glass transition temperature, T_g (3.61°C) of the isolated P(3HB) was slightly lower than the result obtained using the standard commercial polymer obtained from Sigma, T_m (173.11°C); T_c (59.45°C) and T_g (8.23°C) (Figure 3.31).

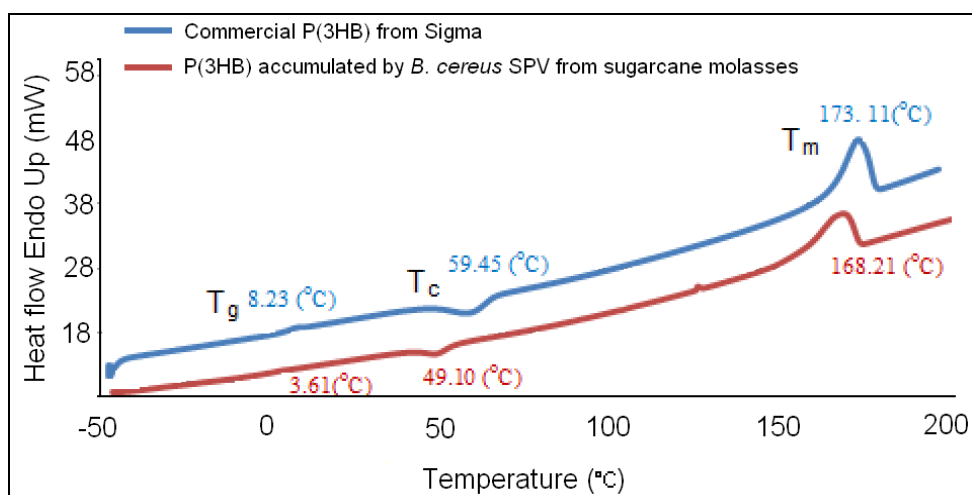


Figure 3.31 Comparison of DSC thermograms of P(3HB) accumulated by *B. cereus* SPV using sugar cane molasses (red) and commercial P(3HB) purchased from Sigma- Aldrich (blue).

3.4 Discussion

Investigations on PHA production by Gram positive bacteria have been recently reinitiated with detailed studies on *B. cereus* SPV, which is able to accumulate significant amounts of the polymer (38-42 % dcw), when grown on different carbon sources (Valappil *et al.*, 2007). In this work, effects of supplementing Kannan and Rehacek medium with sucrose as the main carbon source was investigated at both shaken flask (1L) and fermenter (2L) levels. To further enhance PHA production in the organism, a defined medium which allowed us to study (in detail) the effect of different nutritional components in the production medium on cell growth and PHA accumulation was formulated. Different nutritional components of the production media were studied in details for their effects on growth and PHA accumulation. Because of the abundance of agricultural raw materials and their inexpensiveness, attempts were made to make the production of PHAs by *Bacillus cereus* SPV more sustainable through the utilization of cheap and readily available carbon source (sugarcane molasses). The detailed results of these studies are discussed.

PHA accumulation occurred simultaneously with growth in all the investigations. The polymer accumulation occurring simultaneously with growth in both shaken flask and fermenter in all the

investigations, confirmed that *B. cereus* SPV is capable of producing polymer under normal growth conditions which was however enhanced during the stationary cell growth where some essential nutrients would be expected to have become limiting. In the stationary cell growth the medium could no longer support the growth of the organism; hence, there was a decline in the growth rate and a simultaneous increase in the polymer accumulation by the organism. At this stage, the amount of residual cell mass decreased because of the increased polymer accumulation without any simultaneous growth of the organism. A similar observation of growth-associated P(3HB) production has been reported for *Bacillus sp.* JMa5 by Wu *et al.*, 2001. Yamane *et al.*, 1996 also reported similar observations with *Alcaligenes latus* where they found that the maximal PHA production was achieved at the stationary growth phase. Maekawa *et al.*, 1993 attributed such growth associated P(3HB) production to a relatively lower k_{cat} value of the 3-ketothiolase for the reaction leading to the breakdown of acetoacetyl-CoA to acetyl-CoA. The growth associated P(3HB) production in this study is possibly due to the same reason. In addition, trace elements play an important role in the metabolic activity within a bacterial cell. It is possible that the growth conditions available to the organism at the start of fermentation may be lacking in one of the trace elements required by *Bacillus cereus* SPV. This could also result in early PHA accumulation. For instance, the rate of accumulation of PHA at the early stage of fermentation is slightly slower with Kannan and Rehacek medium than with MGM medium. Since Kannan and Rehacek medium is not chemically defined, it is possible that it has more of the trace elements that can inhibit polymer accumulation than the MGM medium. During the stationary growth phase, there is no growth, however, the amount and possibly the size of the PHA granules increases, occupying a large proportion of the space in the cytoplasm. This leads to an increase in PHA yield without a simultaneous increase in the dry cell weight during the stationary cell growth.

The use of sucrose as the main carbon source in the production medium resulted in a 3 fold increase in dry cell weight when compared to the maximum dry cell weight achieved with glucose as the main carbon source in Kannan and Rehacek medium (Valappil *et al.*, 2007). Also, under these conditions, higher P(3HB) content (47.7 % dcw) was obtained within 32 hours as compared to 38 % dcw of P(3HB) content achieved after 72 hours when glucose was employed

as the sole carbon source in Kannan and Rehacek medium in shaken flask (Valappil *et al.*, 2007). Furthermore, it has been reported elsewhere, that *Bacillus cereus* accumulates glucose-containing polysaccharide simultaneously with PHA (Slock and Stahly, 1974). Therefore, it is possible that the use of glucose as the main carbon source during PHA production would favour more the accumulation of glucose containing polysaccharide than PHA since less energy would be required for the conversion of glucose to the polysaccharide. Also, sucrose being a disaccharide releases two different monosaccharides (fructose and glucose), in the production medium on hydrolysis. Hence, with one mole of sucrose added, two moles of monosaccharide (glucose plus fructose) would be released after hydrolysis. This means that more carbon was available to the growing organism when the same amount of carbon equivalent to 2 % (w/v) glucose added by Valappil *et al.* Also, glucose is known to repress several genes which relate directly and indirectly to the metabolism of alternate carbon sources (Lee *et al.*, 2000). Per mole of sucrose supplemented in the production medium, half the amount of glucose was released, leading to reduced catabolic repression, resulting in reduced growth rate of the organism.

The maximal P(3HB) accumulation achieved during the stationary cell growth was most likely due to the nutrient limitation. Under nutrient limiting conditions, protein synthesis is reduced, leading to the building up of NADH, a universal electron carrier in biosynthesis. NADH inhibits citrate synthase and leads to the reduction in the rate of oxidation of acetyl-CoA in the tricarboxylic acid cycle, thus leading to the accumulation of acetyl-CoA. Although, the equilibrium constant of the reversible condensation reaction does not favour acetoacetyl-CoA formation under these conditions (i.e. high NADH and acetyl-CoA concentration, and low concentration of CoA). The equilibrium is displaced in favour of P(3HB) biosynthesis, leading to the accumulation of P(3HB) during stationary cell growth.

A gradual decrease in the amount of accumulated polymer was observed with further extension in the production time at the end of stationary cell growth. As pointed out in chapter 1, *Bacillus* is known to produce large amount of extracellular compounds. It is possible that the organism must have utilized the stored P(3HB) for the production of the extracellular compounds in the absence of alternative carbon source. Change in the colour of the culture broth during late fermentation was observed and the extracellular compound released by the organism is mostly

likely the source of the colour change in the culture broth. Further, it has been reported that pH above 7.0 enhances sporulation in *Bacillus cereus* (Nakata, 1963). Also Valappil *et al.*, have observed that pH below 5, prevented sporulation in *Bacillus cereus* SPV (Valappil *et al.*, 2007). The maintenance of pH below 5 during the PHA accumulation stage is expected to prevent sporulation. However, even when sporulation occurred, the organism is expected to preferentially utilize the accumulated glucose-containing polysaccharide (Slock and Stahly, 1974) before utilizing the accumulated PHA. The utilization of the accumulated polymer for sporulation therefore cannot hold under this condition. However, more analysis will need to be performed to identify the compounds that were produced which led to the colour change in the culture broth during the fermentation. A correlation between the accumulation of P(3HB) and production of the compound during the polymer accumulation stage in the organism could be made to further confirm the claim.

Yeast extract is a complex nutrient that could also serve as both nitrogen and carbon source to bacterial growth. Evaluations on the effect of increasing the amount of yeast extract in the production medium showed that yeast extract had minimal effect in increasing dry cell weight and PHA accumulation in the organism. However, extension in the production time most likely due to the additional nutrients (amino acids) provided by the yeast extract delayed the onset of the limitation in nutrient condition, known to lead to PHA accumulation.

The effect of the initial phosphate concentration in the medium was also investigated. Ward *et al.*, 2005 found an increase in PHA accumulation by *Pseudomonas putida* CA-3 when the amount of initial sodium ammonium phosphate concentration in the media was reduced from 134 mg/L to 67 mg/L. The results obtained in this study also demonstrated that changes in the amount of initial phosphate concentration in the production medium led to a significant effect on both dry cell weight and P(3HB) accumulation. However, in this study, both dcw and P(3HB) content (% dcw) were increased from 3.29 g/L and 47.2 % dcw respectively (Figure 3.7) to 7.13 g/L and 52.5 % dcw respectively (Figure 3.4), when the initial concentration of $\text{KH}_2\text{PO}_4/\text{K}_2\text{HPO}_4$ buffer was increased from 0.1M to 0.25M. However, a decreased in dry cell weight and P(3HB) content from 5.59 g/L and 82.61 % dcw to 4.7 g/L and 65 % dcw was observed when the initial KH_2PO_4 supplemented in the production media was increased from 0.5 to 1.0 g/L (Figure 3.11).

The decrease in dry cell weight and P(3HB) content with increase in KH_2PO_4 could be attributed to the effect of potassium ion, however, the details of mechanism of the effect of potassium ion concentration on PHA accumulation are not yet clear.

Also, during studies on the use of molasses as the carbon source for PHA production, both dry cell weight and P(3HB) content were found to have decreased from 6.63 g/L and 61.07 % dcw (Figure 3.23) to 4.30 g/L and 52.27 % dcw, respectively (Figure 3.25) when the initial ammonium phosphate concentration was reduced from 2.0 g/L to 1.0 g/L in the shaken flask study. Similarly, in the fermenter studies on sugarcane molasses, both dcw and P(3HB) production reduced from 6.93 g/L and 51.37 % dcw respectively, to 4.17 g/L and 47.43 % dcw when the amount of initial ammonium phosphate concentration was reduced from 2.0 g/L to 1.0 g/L. The reason for the decrease in the amount of accumulated dry cell weight and P(3HB) content could possibly be as a result of phosphate limitation. Since both $\text{KH}_2\text{PO}_4/\text{K}_2\text{HPO}_4$ buffer and ammonium phosphate are the main sources of phosphate in the production medium, reduction to half the amount available at the beginning of the study could have a direct effect on the growth of the organism. Furthermore, reducing the amount of phosphate buffer would also affect the pH balance in the media which could have effect on P(3HB) production and degradation.

A carbon source in the form of sugars or fatty acids is necessary during polymer accumulation in bacteria. Thus, the ability of bacteria to accumulate sufficient amounts of polymer is largely dependent on the amount of carbon source present in the production medium and its relative molar ratio with respect to the limiting nutrient during the polymer accumulation stage. In this study, the effect of supplying sufficient amount of carbon source to the growing organism was studied under two conditions; intermittent addition of aliquots of sucrose and continuous feeding of nutrient-limited medium with additional sucrose at a feed rate of 0.7 mL/min. Quantitative analysis carried out shows that addition of aliquots (10 mL) of 1 g/mL of sucrose intermittently, did not produce appreciable increase in biomass accumulation. Although, 4.91 g/L dry cell weight and 1.32 fold increase in P(3HB) (50.50 % dcw) were produced after 17 hours (Figure 3.13) as against DCW (3 g/L) and P(3HB) (38 % dcw) produced after 60 hours when glucose was intermittently added to the growing culture (Valappil *et al.*, 2007). The reason for the

increase in both biomass and P(3HB) produced could be due to reduced repression when sucrose is employed as the carbon source.

However, during continuous addition of media enriched with sucrose but deficient in other growth nutrients, the PHA accumulation was found to have improved significantly. The increase was more in the study with 0.5 g/L KH_2PO_4 initially present in the production medium than when 1.0 g/L KH_2PO_4 (Figure 3.16) was initially supplemented in the production media. The increase in production is possibly due to the presence of excess carbon source which the organism was able to convert to intracellular PHA. The difference in the yields obtained in the presence of initial 0.5 g/L and 1.0 g/L KH_2PO_4 is possibly due to the initial amount of KH_2PO_4 being lower in the former case than in the later.

In the investigation performed with the supply of additional amounts (1g/mL) of sugarcane molasses which contains a large percentage of carbon (80%), at a feed rate of 0.7 mL/min, throughout the fermentation; It was found that the organism utilized the additional sugarcane molasses mainly for growth resulting in 5.47 g/L dcw, achieved after 54 hours in shaken flask and 6.83 g/L dcw achieved in 2L fermenter. In the shaken flask study, a relative increase in P(3HB) concentration and yield was observed compared to a drastic decrease in P(3HB) concentration and yield obtained in the 2L fermenter. In shaken flask conditions it is difficult to control the dissolved oxygen level, hence, additional nutrients supplied by the feed possibly resulted in a decrease in oxygen concentration. This probably led to almost anaerobic conditions, leading to enhanced P(3HB) production. In contrast, controlled air supply in the fermenter would prevent the induction of anaerobic conditions. Also, the continuously fed nutrient might have led to a non-limiting nutrient condition thereby resulting in lower P(3HB) accumulation. Under the non-limiting nutrient conditions, bacteria would begin to grow again, leading to the breakdown of the previously accumulated P(3HB), to be utilized as a carbon source, thus leading to a reduction in P(3HB) yield.

In general, it is expected that polymer yields in fermenters should be greater than those achieved in shaken flask fermentation since the physical parameters can be well controlled in order to improve the performance of the organism. Nevertheless, the results obtained in this study showed maximum polymer yield in the shaken flask fermentation (Figure 3.6). Hence, the

conditions for polymer production using *Bacillus cereus* SPV in the fermenter needs optimization to further enhance the polymer yield.

Overall, reasonably high level of polymer accumulation and cell growth was achieved in this study; a maximal P(3HB) content of 61.07 % dcw and dcw of 6.63 g/L were achieved from shaken flask investigations while the 2L fermenter study yielded 51.37 % dcw and 6.60 g/L of PHA content and dry cell weight respectively with sugarcane molasses. With MGM supplemented with sucrose, as the main carbon source, maximal 82 % dcw and 7.21 g/L were achieved in P(3HB) yield and dry cell weight respectively in the presence of reduced initial KH_2PO_4 concentration in the production medium. These results are highly encouraging and confirm that both sucrose and sugarcane molasses are good sustainable carbon sources for P(3HB) production in *Bacillus cereus* SPV. Also, the outcome of this study confirmed that potassium phosphate plays a significant role in cell growth and PHA accumulation in *Bacillus cereus* SPV. The quantitative values obtained in this study are much higher than the values of 30% dcw P(3HB) yield and 3.5 g/L dry cell weight obtained by Albuquerque *et al.*, 2007 in their work on PHA production using sugarcane molasses as the sole carbon source in a sequencing batch reactor (SBR). Furthermore, the results obtained are comparable with those achieved by Santimano *et al.* 2010 with another strain of *Bacillus* (*Bacillus sp* COLI/A6), where a maximum PHA yield of 54.68 % dcw and a dry cell weight of 6.0 g/L was obtained using sugarcane molasses as the main carbon source contained in E2 mineral medium.

Two-stage fermentation was also conducted in this study to enhance dry cell weight accumulation prior to the initiation of polymer accumulation in *Bacillus cereus* SPV. Since PHAs are accumulated under conditions that inhibit growth, it was thought that by growing *Bacillus cereus* SPV in normal conditions that encourage high cell growth (first-stage) and subsequently introduce a condition that can induce stress (second-stage), both biomass and PHA accumulation would be improved. In this study, *Bacillus cereus* SPV was grown in a nutrient rich media during the first-stage and subsequently transferred to a nutrient limiting system during the second-stage to enhance PHA accumulation in the organism. As shown in Figure 3.17, there was a decrease in the accumulated dry cell weight in the profile. This was as a result of loss of cells during centrifugation and transfer of the organism to a second-stage system which lack

sufficient nutrient that can support active growth. Despite the problems encountered during cell recovery, this approach can be confirmed to have potential in improving polymer accumulation. The maximum amounts of P(3HB) accumulated was found to be 7 g/L and 80 % dcw much higher than those achieved in any other condition explored in this work. An improvement in cell recovery will further improve polymer yield, since PHA yield is dependent on the amount of dry cell weight and percentage PHA accumulation per cell.

The XRD analyses performed on the wet cell isolated PHA shows that the method has a significant effect on the crystallographic properties of the polymer. The reduction in the intensity of the diffraction peaks associated with the isolated polymer, for the same amount of the sample as compared to standard commercial P(3HB) confirmed that crystallinity of the polymer was reduced in the process. It is possible that relatively more of the isolated PHAs retained the amorphous state they had while still in the granules before extraction resulting in a decrease in the crystallinity of the isolated polymer. This is an advantage in the application of the polymer in medical use because of the higher immunological response to crystalline polymers. Furthermore, the technique allows the opportunity to recover most of the accumulated polymer as shown in Figure 3.18. The reductions in the residual cell mass shows that most of the polymers stored in the cells were extracted, leaving behind lower amount of cell debris. The treatment given to the cells before incubation ensured that the lipids were removed during the serial washing with solvents.

The chemical identity of the polymer produced using sucrose and sugarcane molasses was confirmed by ¹H-NMR and FT-IR in comparison with a standard reference poly(3-hydroxybutyrate) obtained from Sigma. The quality of the NMR spectrum indicated a high level of purity of the polymer due to the absence of background signals. The DSC results showed a slight decrease in the T_m, T_c and T_g values observed in the P(3HB) isolated from *B. cereus* SPV, as compared to that obtained from Sigma. This again indicates a slightly lower crystallinity of the sample. Generally, PHAs, including P(3HB), exist as amorphous granules within the bacteria cells. However, when the polymers are isolated from the bacteria, they form crystalline structures due to freeze-drying or the influence of the organic solvent treatment during recovery (Jacquel *et al.*, 2008). In this study, a unique wet cell extraction method was adopted in the isolation of the

polymer; leading to the recovery of relatively pure polymer. In addition, the decreased values of the thermal properties might also reflect lower molecular weight of the polymer isolated in this work as compared to that obtained from Sigma.

3.5 Conclusions

In conclusion, the observations recorded in this study suggested that, *Bacillus cereus* SPV was able to utilize sucrose as the carbon source for growth and PHA accumulation both in the Kannan and Rehacek medium and in MGM medium. Also, potassium phosphate is an important nutrient for growth and PHA accumulation in *B. cereus* SPV. The absence of reduction in P(3HB) accumulation even after increase in the amount of yeast extract in the production medium suggested that nitrogen limitation may not be the main reason for PHA accumulation in *Bacillus cereus* SPV. This led to a search for the other causes of PHA accumulation and it was found that potassium plays a significant role in PHA accumulation in *Bacillus cereus* SPV.

Also, this study shows, for the first time, that the biotechnological transformation of sugarcane molasses into the high-value green material, P(3HB), is possible using *Bacillus cereus* SPV. It is a suitable complex carbon source that can enhance both biomass and P(3HB) accumulations in *Bacillus cereus* SPV. The present study can form the basis of the development of a biotechnological process for the biotransformation of the renewable feedstock, sugarcane molasses, into P(3HB). This will decrease the cost of P(3HB) production substantially, leading to an enhancement in its widespread usage.

Finally, the novel wet cell extraction technique developed in this study is very significant not only in the isolation of PHAs from the cell but in the production of high purity PHA. It can also be very useful in the continuous production of PHAs, hence, saving time and energy.

Chapter 4

Bacterial Cellulose Production, Chemical modification and Characterisation

Chapter 4

4.1 Introduction

The abundance of polymeric cellulosic materials has provided a great potential for the utilisation of nanocellulose fibres in different applications ranging from medical, environmental and industrial applications. Apart from cellulose being the most abundant polymeric material, it is also renewable and serves as a multifunctional raw material capable of replacing many non-renewable materials in different applications (Wegner, 2006). Cellulose is the major component of plant biomass and also an extracellular polymer produced by microbes.

Bacterial cellulose is produced mainly by the non-pathogenic, Gram-negative bacteria known as *Gluconacetobacter xylinus* (formerly *Acetobacter xylinum* and *Acetobacter xylinus*) (Kerstens *et al.*, 2006). According to Jonas and Farah, 1998, this bacteria produces extracellular cellulose of pure, ultra-fine random fibre network known as pellicle, which possesses high crystallinity, water absorption capacity and, interestingly, with high tensile strength. The production of cellulose by bacteria is very interesting as it provides sustainability in the biomimetic production of pure cellulose for both organic and polymer chemists for different applications. Hence, by selecting the appropriate substrates, cultivation conditions and various additives as well as appropriate bacterial strain, cellulose with both high molecular weight and supramolecular structure can be produced.

As mentioned earlier, the nanocellulose fibres have a great potential in different applications. However, the difficulty in dispersing the highly polar nanocellulose fibres in non aqueous medium or in the formation of composites with hydrophobic polymers remains a challenge to overcome. Successful breakthrough in the homogenous dispersion of nanocellulose fibres in non aqueous media will provide advantages in the production of new biomaterials with enhanced physico-mechanical properties when incorporated in hydrophobic polymer matrix such as PHAs and PLAs. Nanocellulose fibres have high surface energy due to the polarity and hydrophilic properties. The hydrophilic property of cellulose is mainly as a result of the hydroxyl groups that are located on the surface of the cellulose fibres. Sassi and Chanzy, 1995 have observed in their studies on the features of fibrous modification of crystalline cellulose that the conversion of cellulose proceeds from the surface to internal regions. Thus,

partial chemical modification of cellulose fibres will only provide hydrophobic surfaces that can aid in the adhesion of the cellulose fibres with hydrophobic matrix without having much effect on the mechanical properties of the cellulose fibres. Replacement of the hydroxyl group on the surface of the cellulose fibres will result in a significant reduction in the hydrophilic properties of the cellulose fibres and make them more compatible with non polar media. Thus, the high tensile stress and modulus properties of bacterial cellulose can be utilized as reinforcing element for hydrophobic polymers such as PHAs. These composites will have improved physico-mechanical properties with new areas of applications, when compared to the original parent materials. Chemical modification through acetylation is one such treatment that is capable of modifying the hydroxyl groups present on the surface of the fibres. According to Sassi and Chanzy, 1995, acetylation of cellulose depends on the accessibility and susceptibility of the hydroxyl groups present in the amorphous and crystalline regions within the cellulose polymer chain. Hence, homogenisation of the cellulose pellicle to micro and nano-scale fibre sizes provides the opportunity to attain a high level of acetylation during chemical modifications.

In this chapter, the production, extraction and surface modification of bacterial cellulose produced from *Acetobacter xylinus* is discussed. Characterisations of the isolated cellulose to investigate the effects of surface modification on the physico-mechanical properties of the Bacterial cellulose are also discussed. This study was necessary for further applications of the modified bacterial cellulose in the production of bio-derived, P(3HB)-microfibrillated cellulose (P(3HB)/MFC) composites for cartilage tissue engineering.

4.2 Results

The flow chart in Figure 4.1, summarises the steps followed in the production, modification and characterisation of the bacterial cellulose produced from *Acetobacter xylinus*.

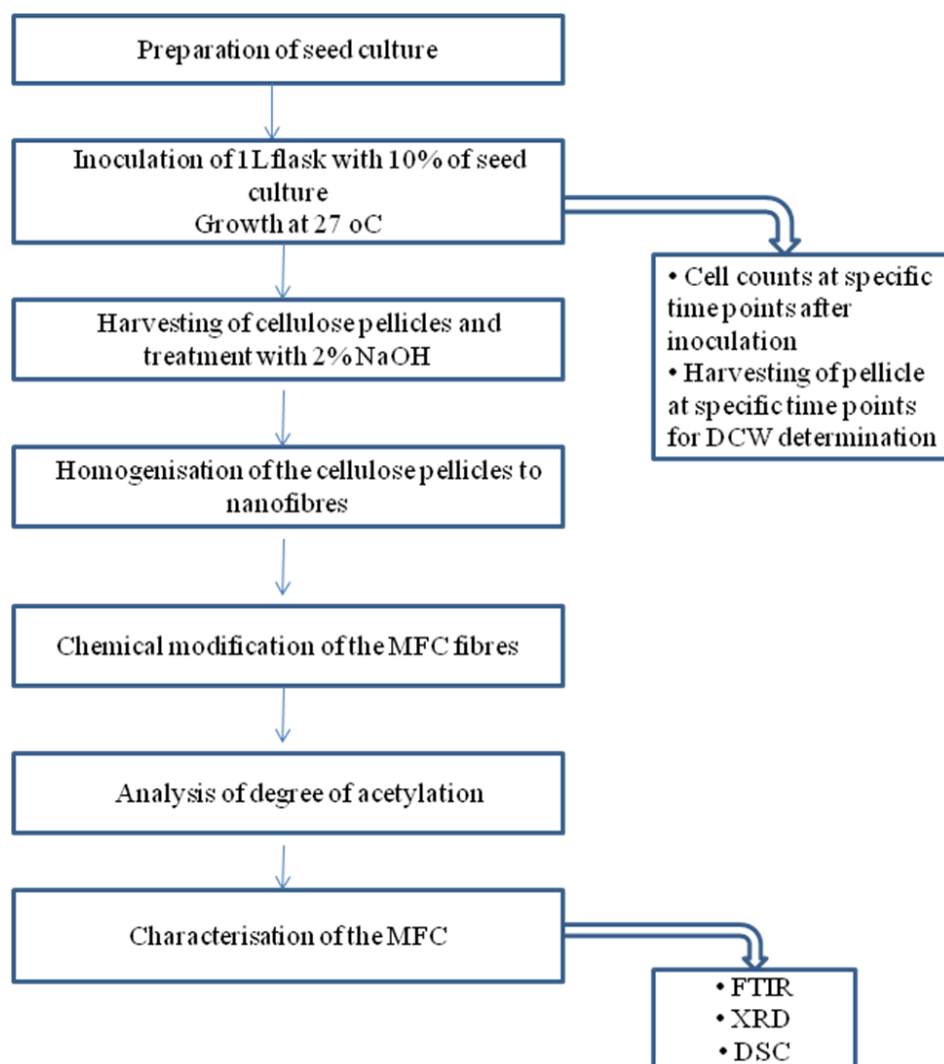


Figure 4.1 Flow chart of the production; chemical modification and characterisation of microfibrillated bacterial cellulose from *Acetobacter xylinus*

4.2.1 Production of bacterial cellulose from *Acetobacter xylinus*

The detail methodology used for the production of bacterial cellulose from *Acetobacter xylinus* are described in Chapter 2, Session 2.2.2. The profile of the time course of bacterial cellulose yield as a function of *Acetobacter xylinus* cell number and pH of the growing medium is highlighted in Figure 4.2. As can be seen from the graph, the bacterial cellulose yield increased with the fermentation time up to 72 hours. After 72 hours, the yield of native cellulose pellicle produced remained constant while cell growth continued, but at a reduced rate until 96 hours when the fermentation was stopped. The maximum cell count at 72 hours was 1.49×10^8 and the maximum cell count at 96 hours was 1.51×10^8 . Bacterial cellulose yield was determined under two different conditions. In one condition, the pellicle were harvested and washed with distilled water followed by freeze drying to a constant weight. In another condition, the cellulose pellicle was harvested, treated by boiling in 2 % NaOH solution at 96 °C for one hour, after which the cellulose pellicle was washed with running distilled water for 5 minutes to remove excess NaOH solution. From the dry weight analysis, it was found that the yield in both cases investigated increased with the cultivation time until after 72 hours when the rate of increase in dry weight reduced drastically. Furthermore, it was observed that the dry weight of the pellicle measured without treatment with NaOH was significantly high ($p < 0.05$) when compared to the dry weight measured after treatment with NaOH before freeze drying. However, there was no significant difference ($p > 0.01$) found in dry weight between time points 72 and 96 hours. The maximum dry weight obtained in both cases were 0.027 g/L for NaOH treated cellulose pellicle and 0.038 g/L for non treated cellulose pellicle.

The pH of the growing medium was found to increase slowly with the cultivation time. At the end of the cultivation period, the pH of the media was found to increase from the initial pH of 5.0 to a final pH of 5.63.

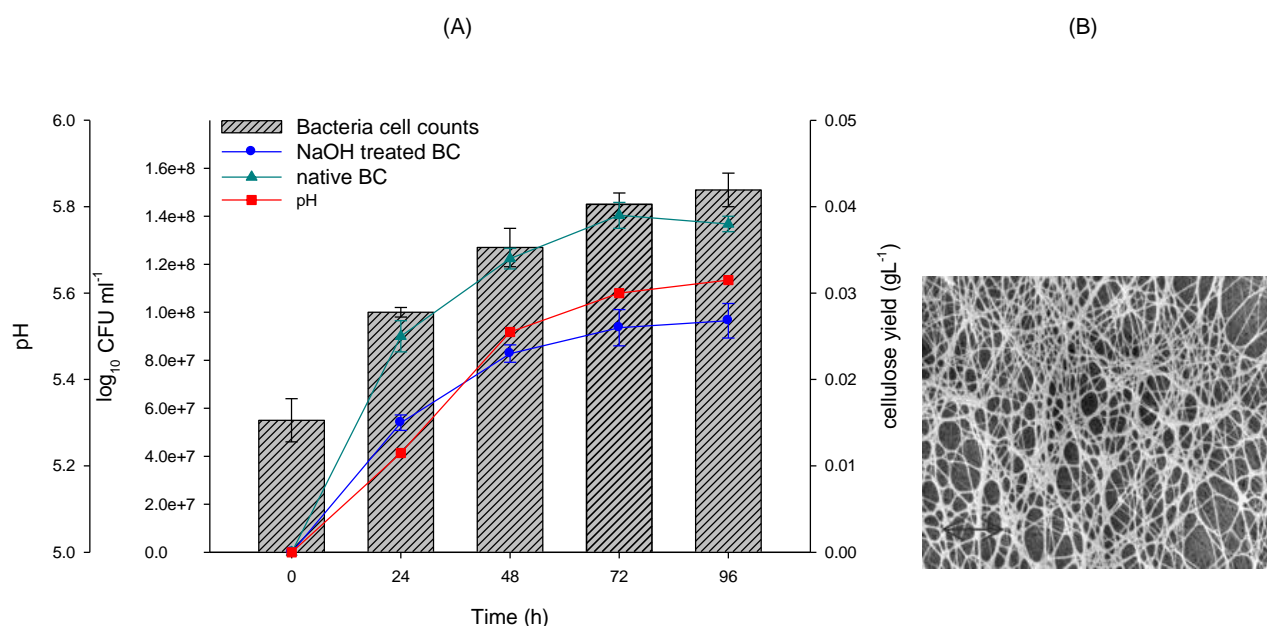


Figure 4.2 (A) Cell growth CFU mL⁻¹ (grey bars), pH (■), and bacterial cellulose yield (g/L) of native (▲) and NaOH treated (●) bacterial cellulose over different experimental time periods (B) SEM of cellulose pellicle highlighting the mass of fibres

4.2.2 Determination of the degree of acetylation of native cellulose

The harvested bacterial cellulose pellicle were homogenised into microfibrillated cellulose (MFC) fibres and chemically modified with acetic anhydride using pyridine as a catalyst. The chemical reaction involved the acetylation of the hydroxyl groups of the cellulose fibres as highlighted in Figure 4.3. The amount of intact cellulose fibres were found to decrease with the acetylation time (Table 4.1). Furthermore, the degree of acetylation (determined using the method described in Chapter 2, Section 2.2.6) of the bacterial cellulose microfibrils was found to increase with the reaction time, thus reaching the highest value at 96 hours.

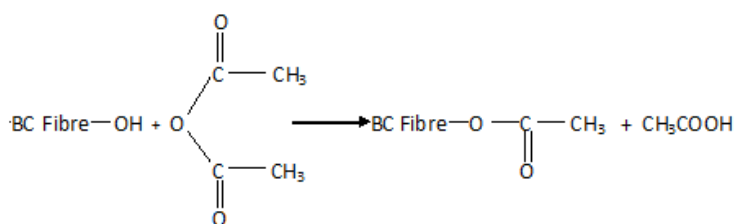


Figure 4.3 Chemical reaction of acetic anhydride with bacterial cellulose (Jonoobi *et al.*, 2010)

Table 4.1 Comparison of the degree of acetylation of microfibrillated bacterial cellulose treated at different time points (0, 24, 48, 72 and 96) hours with acetyl anhydride and pyridine as a catalyst.

Reaction Time (h)	Degree of Substitution
0	0.0
24	0.96 ± 0.1
48	1.71 ± 0.13
72	2.13 ± 0.06
96	2.43 ± 0.01

4.3 Characterisation of Bacterial Cellulose

4.3.1 Fourier transform infrared spectroscopy (FTIR)

FTIR spectroscopy was used to investigate the chemical characteristics of the bacterial cellulose fibres before and during the course of acetylation. The FTIR spectra obtained for the non acetylated bacterial cellulose and bacterial cellulose from different time points of acetylation are shown in Figure 4.4. As can be seen in the figure, there was new peak between the region 3000 and 2850 cm^{-1} . Also very prominent in the spectra is the shifting and degeneration of the absorption peak between 1310-1330 cm^{-1} . There was also reduction in intensity of the absorption peak between 1030 -1035 cm^{-1} which reduced from the spectrum of non-acetylated cellulose to cellulose acetylated for 72 hours. A new absorption peak was

observed in the region $1735\text{-}1742\text{ cm}^{-1}$. This absorption peak was not present in the non acetylated cellulose. Moreover, the intensity of the peak increased with duration of acetylation reaction. Another important observation was the disappearance of the absorption peak present at position 1632 cm^{-1} in the spectra of the non-acetylated cellulose. This particular peak was found to be completely absent in the spectra of the 72 hours acetylation time. There were also variations in the absorption peaks between the regions 1020 cm^{-1} and 1536 cm^{-1} of the non acetylated cellulose with shifting and disappearance of absorption peaks increasing towards the spectra obtained from the sample with 72 hours acetylation.

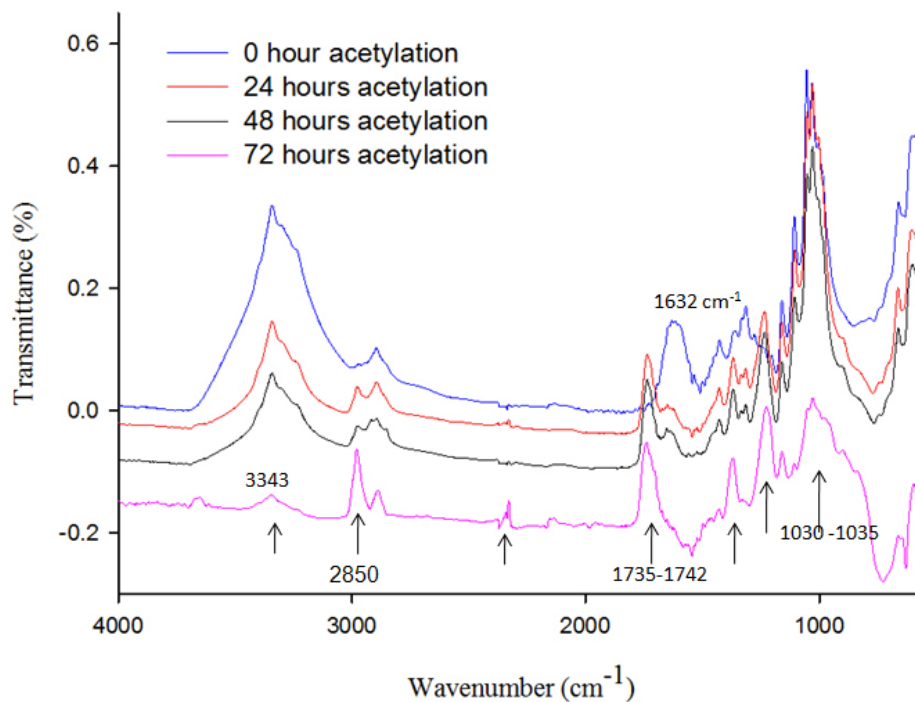


Figure 4.4 FTIR spectra of Bacterial Cellulose with different levels of acetylation

4.3.2 X-ray diffractometry

The effect of chemical modification of the microfibrillated cellulose on the crystallinity of the material was carried out as discussed in detail in Chapter 2, Section 2.6.3.5. Knowledge of the crystallinity of the modified bacterial cellulose was necessary since crystallinity influences the immune response in the application of the biomaterial in tissue engineering.

Hence, it is useful to determine the change in the level of crystallinity with variations in crystallinity of the cellulose microfibrils with duration of acetylation. The amount of crystalline cellulose was measured as a crystallinity index (CI) by applying the equation of Segal's empirical method (Segal *et al.*, 1959) specified in Chapter 2, Section 2.2.8.2. As can be seen in Figure 4.5, there is a significant difference ($p < 0.01$) in the crystallinity index between acetylated and non acetylated cellulose and also between homogenised and freeze dried bacterial cellulose pellicle ($p < 0.05$). The crystallinity of the native bacterial cellulose was found to decrease from 86.3 % to 82.7 % after homogenisation in to microfibrillated cellulose, MFC (Table 4.2). Also, the crystallinity decreased further to 72.9 % after 96 hours of chemical modification of the homogenised bacterial cellulose. There was also reduction in peak intensity in the spectrum. The XRD spectra of acetylated homogenised cellulose (acetylated for 72 hours) also showed an increase in the intensity of the peak at 29.5° when compared to the peak generated from the rest of the test materials.

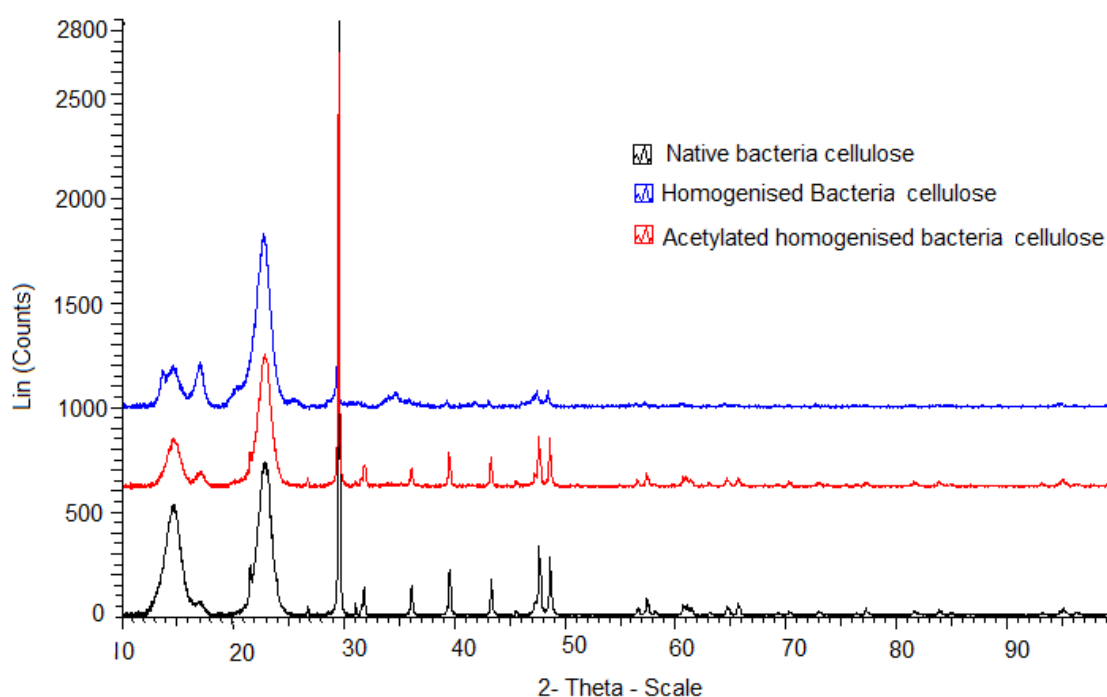


Figure 4.5 XRD patterns of native bacteria cellulose, homogenised cellulose and acetylated cellulose

Table 4.2 The crystallinity of native bacteria cellulose compared with the crystallinity of homogenised bacterial cellulose and acetylated bacteria cellulose.

Materials	Crystallinity (%)
Native Bacterial Cellulose	86.3
Homogenised Bacterial Cellulose	82.7
Acetylated Bacterial Cellulose	72.9

4.3.3 Dispersion of acetylated Bacterial Cellulose in Chloroform

The major reason for the chemical modification of cellulose was to provide microfibrillated cellulose (MFC) that would be compatible with non polar solvents to enable the incorporation of MFC into PHA matrix as a reinforcing element. However, the lesser the degree of acetylation, the higher would be the hydrophilicity effect of the MFC on the PHA polymer-MFC composite. This property is highly desirable in the more hydrophobic PHAs to further enhance cell attachment and proliferation when such materials are used in tissue engineering. Hence, a dispersion test was carried out with MFC acetylated for different time points (24, 48 and 72 h). The acetylated microfibrillated cellulose was dispersed in non polar organic solvent, chloroform. Figure 4.6 shows the stability of the microfibrillated cellulose (acetylated for 75 hours) dispersed in chloroform for one month. It was found that MFC acetylated for all the time points (24, 48, and 72 h) considered were soluble in chloroform. However, the stability of the 24 hours acetylated MFC solutions reduced after two weeks dissolution in chloroform while the 48 and 72 hours acetylated MFC remained homogeneously dispersed in the chloroform after one month (Figure not shown). As expected, the acetylated cellulose fibres did not mix well in water after acetylation, the fibres remained aggregated together. In the case of non acetylated MFC used as control, the fibres were immiscible with non polar chloroform but dispersed very well in water, even after one month (Figure not shown).



Figure 4.6 The stability of acetylated microfibrillated cellulose after one month of dissolution in chloroform.

4.7 Discussion

Recent advances in science and technology have made possible the utilization of abundant natural raw materials to the advantages of man-kind. Nanotechnology has rapidly developed into an interdisciplinary field of which the isolation of nanocellulose from bioresources using top-down technologies has become one major area of interest. Bacterial cellulose has a lot of potential ranging from its economic means of production to the provision of sustainable raw material for many applications. Hence, its production and modification for further utilization in the subsequent application was investigated in this chapter.

During production of the bacterial cellulose pellicle, it was observed that the dry weight obtained for native bacterial cellulose was higher than the dry weight obtained after treatment of the produced pellicle with NaOH. The reason behind this observation is possibly due to the removal of alkali –soluble non-cellulosic (bacterial) material by the NaOH treatment. *Nishi et al.* have made a similar observation during their study on the structure and mechanical properties of sheets prepared using bacterial cellulose and attributed the reason for their observation on the removal alkali soluble non-cellulosic material contained in the cellulose pellicle (*Nishi et al.*, 1990). *Mckenna et al.* have also made similar observation during their investigations on the mechanical and structural properties of native and alkali-treated bacterial cellulose; however, in addition to the suggestions giving by Nishi and co-workers, *Mckenna et al.* suggested that the difference in the dry weight can also be possible removal of some cellulose during the treatment (*Mckenna et al.*, 2009).

Because of the very strong hydrogen bonds between the hydroxyl groups, it is expected that the rate of acetylation would be slow. This could be the reason for the gradual increase in the degree of acetylation of the bacteria cellulose with time. With increase in the duration of the soaking of the cellulose fibres in the chemical reagent, the cellulose fibres swell and increase in size. The swelling of the cellulose fibres were thought to have provided opportunity for the acetyl anhydride to get into the cellulose fibres and gain accessibility to the hydroxyl groups. Furthermore, Hill and co-workers have reported in their work that in addition to speeding up the rate of reaction, the pyridine helped to disrupt the cellulose fibre cell wall during the acetylation reaction which provided accessibility to the hydroxyl site of the cellulose network (Hill *et al.*, 2000). Jonoobi *et al.* also made similar observations. In the FTIR spectra acquired from both non-acetylated bacterial cellulose (BC) (time 0) and acetylated BC for different durations of time (24, 48, 72, and 96) indicated formation of new peaks as the duration of acetylation increases. The broadening of the absorption peaks between 3000 and 2850 cm^{-1} was as a result of the stretching of CH group in the bacterial cellulose. This same observation has been reported by Khalil *et al.*, 2001. The absorption peaks observed in all the materials between 1320 -1330 cm^{-1} can be attributed to the bending vibration of C-H and C-O bonds in the polysaccharides as observed in the work of Troedec *et al.*, 2008. The characteristic vibrations of the acetyl groups added were easily identified in the sample with 24 hours acetylation to that with 96 hours acetylation. The characteristic vibrations included the carbonyl stretching vibration at 1740 cm^{-1} ($\nu_{\text{C=O}}$), the methyl in-plane bending at 1370 cm^{-1} ($\delta_{\text{C-H}}$), and the C-O stretching at 1231 cm^{-1} ($\nu_{\text{C-O}}$). The intensity of these peaks increased gradually with the duration of acetylation as shown Figure 4.4. Also, increase in the degree of acetylation with acetylation time confirmed that the MFC were increasingly modified as the reaction time was extended. The decrease in the absorption band between 3340 and 3342 cm^{-1} can be attributed to the loss of the stretching vibration related to the O-H bond, indicating partial acetylation of the MFC. As expected, the intensity of this band increasingly reduced as the acetylation time reached 96 hours confirming the maximum degree of acetylation found after 96 hours acetylation.

The x-ray diffraction spectrum was used to assess the crystallinity of the bacterial cellulose at different stages of treatments. In the XRD spectra in Figure 4.5, the intensity of the band at 14° when compared with the native bacterial cellulose, decreased in both the homogenised

and acetylated cellulose. This indicated a decrease in the crystallinity of the bacterial cellulose during acetylation. This was confirmed in the percentage crystallinity calculated which showed a significant difference ($p < 0.01$), in the calculated percentage crystallinity between native bacterial cellulose and the acetylated homogenised bacterial cellulose and a slight difference between the native bacterial cellulose and the homogenised microfibrillated cellulose. The shifting of the bands in the treated MFC indicated changes in the unit cell and the lattice. This can be due to the replacement of the OH groups on the surface of the fibres with the acetyl group.

The stability of the microfibrillated cellulose in non polar solvent is expected to depend on the degree of acetylation and the surface characteristics of the cellulose fibres. The higher the degree of acetylation, the more difficult it will be for the cellulose fibres to aggregate together in non polar solvents. Since the acetyl group is more hydrophobic, it would be expected that the acetylated cellulose fibres will remain well dispersed in the non polar organic solvent and would interact very well with another hydrophobic material such as PHA.

4.8 Conclusions

Bacterial cellulose was successfully produced from a non pathogenic *Acetobacter xylinus*. The isolated cellulose pellicle were homogenised to microfibrillated cellulose and chemically modified to a high degree of acetylation. This was necessary for further used of the acetylated microfibrillated cellulose in the production of P(3HB)/MFC composites for further application in hard tissue engineering. Since P(3HB) is hydrophobic and requires a hydrophobic solvent for its dissolution, it is therefore important that the material to be added as a filler should be made soluble in the organic solvent to allow efficient formation of a composite.

FTIR results confirmed the acetylation of the microfibrillated bacterial cellulose fibres and further demonstrated that the mechanical homogenisation of the cellulose pellicle to micro and nano-fibres provided additional accessibility of the hydroxyl group for the acetylation reagents. The displacement of the OH group by the acetyl group was further demonstrated in the broadening, disappearance and appearance of new peaks in the acquired spectra.

The XRD result further provided evidence of reduction of the crystallinity of the bacterial cellulose owing to the mechanical and chemical treatment during the process of acetylation. The decrease in crystallinity was necessary due to its intended application as filler for composite fabrication. Hence, the dispersion of the microfibrillated cellulose in chloroform was found to be stable which is essential for the production of composites with the PHAs. Hence, this study has led to the successful production of acetylated microfibrillated bacterial cellulose which can be used for varied applications in medicine, especially in the formation of composites with hydrophobic polymers such as PHAs.

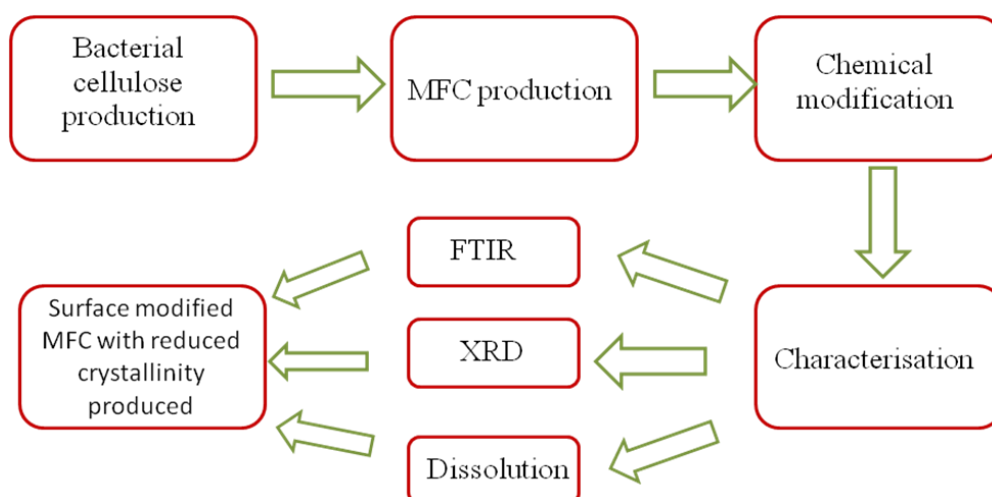


Figure 4.7 Schematic representation of summary of modified microfibrillated cellulose production

Chapter 5

POTENTIAL APPLICATION OF P(3HB)/MFC COMPOSITE IN CARTILAGE REGENERATION

Chapter 5

5.1 Introduction

Renewable polymeric materials from bacterial and plant origin such as cellulose, polyesters, polysaccharides and lignin are currently under-utilised due to the high cost and difficulties in their processing (i.e. further functionalisation). Currently researchers are aiming at the development of new technologies to introduce functionalities on the surface of polymer materials in order to design smart products with applications in medicine, cosmetics, and construction or technical textiles. The resulting functional products are proposed to be based on renewable materials and have a longer life time with benefits for both human and the environment. Cellulose and polyesters (PHAs) are among the most abundant biopolymers on Earth. They are found in both bacteria and plants. Both biopolymers serve as the structural element in the primary cell walls of wood and other land-based agricultural crops. They are also produced by many bacteria either, as intracellular energy reserve (PHAs) or as extracellular products (cellulose).

Although, there has been a long history of cellulose extraction and use in the paper and chemical industries dating back into the 19th century, recent decades have witnessed the development of cellulose-based composite materials by the material industry. The excellent properties of both bacterial and plant cellulose are now being exploited in the production of cellulose-reinforced polymeric materials. Furthermore, developments in composite materials have been driven by both technical and environmental factors. For example, plant fibres are both renewable and less aggressive to processing equipment than glass fibres. They also potentially provide mechanical properties that are comparable to or better than equivalent fibre glass-reinforced materials when employed as fillers in biomaterial composites. Despite the long history of cellulose applications which are stimulated by interest in the future bio-economy there are now many new and developing initiatives which are aimed at fully exploiting the fundamental properties of cellulose. These initiatives are, for example, aimed at new products for tissue engineering and drug delivery systems and composite for material industries.

Hence, this work focused mostly on the exploration of micro and nano-scale cellulose fibrils, microfibrillated cellulose (MFC), in the context of biopolymer reinforcement and further development of bionanocomposites for medical application in the tissue engineering

of cartilage. In this study, chemical modification of the microfibrils developed in the previous chapter (Chapter 4) and the P(3HB) produced in Chapter 3 have been employed in order to produce physico-mechanically improved, non toxic, homogenous biocompatible composite polymers for special application in tissue engineering. Firstly, 2D composite films of P(3HB)/MFC produced as described in Chapter 2 Section 2.3.1 were characterised to understand the physico-mechanical properties of the composite material containing different amount of MFC. This was necessary to understand the best suitable composition with the desired mechanical and physical properties for cartilage regeneration. The MFC was obtained from bacterial cellulose fibres after a two-step mechanical disintegration process consisting of an initial refining step followed by a high pressure homogenization step. This technology was first reported in 1983 in the work of Turbak *et al.* and allows the production of a network of interconnected cellulose microfibrils, with diameters ranging from 10 to 100 nm and aspect ratios from 50 to 100 (Turbak *et al.*, 1983; Zimmermann *et al.*, 2004; Gardner *et al.*, 2008).

The P(3HB)/MFC composite scaffold produced as described in Chapter 2, Section 2.3.2 were further characterised and tested for biodegradability, bioactivity and cytocompatibility with Murine ATDC-5 cell line to further understand the properties of the composite material that would suit the desired applications.

5.2 Results

P(3HB) was produced from *Bacillus cereus* SPV and chemically modified bacterial cellulose were combined with P(3HB) matrix to form P(3HB)/MFC composite 2D films and 3D scaffolds as described in Chapter 2, Section 2.3.1 and 2.3.2 respectively, using the conventional solvent casting technique and newly developed compression moulding/particulate leaching technique. Sucrose grains of sizes 80-100 μm were employed as the porogen materials. The composite film and scaffold (2D and 3D microstructures) of various MFC content were characterised following the experimental details described in Chapter 2 Section 2.4. The detailed results of the production and characterisation of the materials are given below.

5.2.1 Microstructural Characterisation of P(3HB)/MFC composite film (2D structure)

Scanning electron micrographic analysis was performed on both the neat P(3HB) and P(3HB) composite films by the method described in detail in Chapter 2, Session 2.2.8.3, to observe the surface morphology of the neat and composite polymeric materials. The results obtained are shown in Figure 5.1. Observation of the SEM image of the various composite shows that microfibrillated cellulose were not extensively present on the surface of the composites with 0, 10, 20, 30 and 40 wt% MFC (Figure 5.1a-e) but were observed more on the surface of the composites containing 50 wt% MFC (Figure 5.1f). Hence, as can be seen from the SEM microstructural analysis, the MFC fibres were not highly exposed on the films with 10, 30, and 40 wt% MFC rather, they were partially embedded in the polymer matrix. This was not the case with the 50 wt% composite where the MFC fibres are highly visible on the surface of the composite. When compared with the polymeric composite films, the microstructural appearance of the neat P(3HB) film was less rough (Figure 5.1a). Furthermore, slight difference was observed between the 10 wt% and 20 wt% MFC composites film. The composites with 30 and 40 wt% MFC had more of the MFC fibrils well dispersed, with the structures of the fibrils slightly visible.

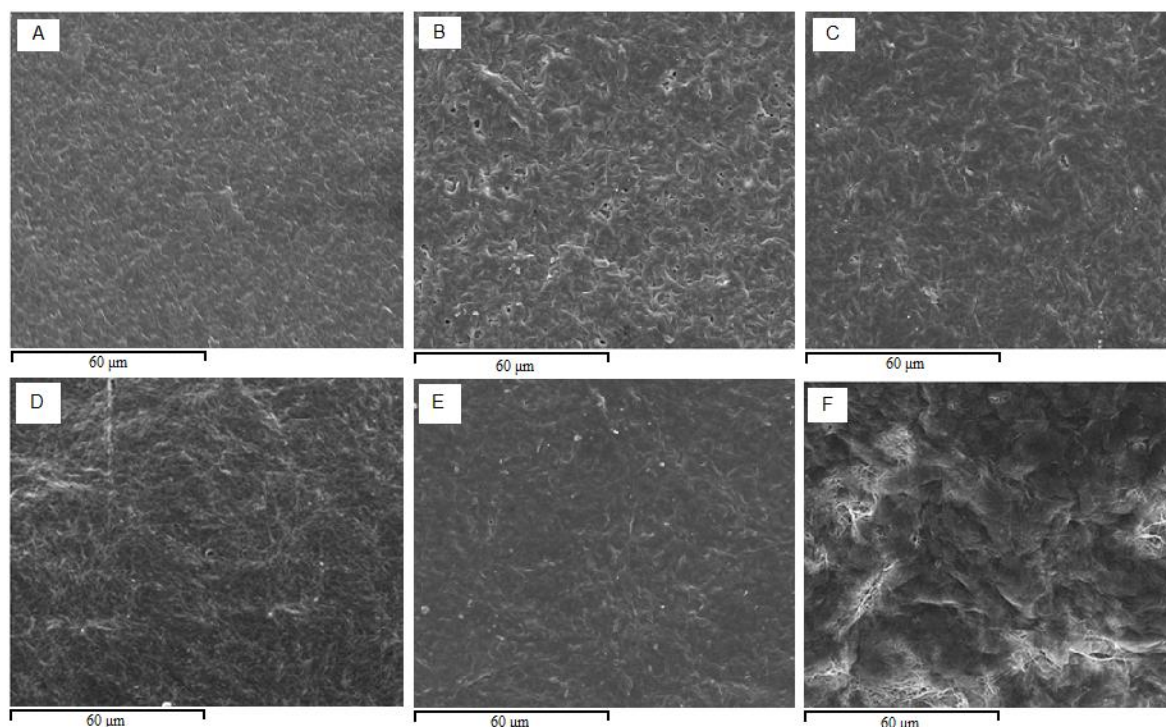


Figure 5.1 SEM micrographs of (a) Neat P(3HB) film, (b) 10 wt%, (c) 20 wt%, (d) 30 wt%, (e) 40 wt% and (f) 50 wt% MFC in P(3HB)/MFC Composite films.

5.2.2 Fourier Transform Infra Red (FT-IR) characterisation of P(3HB)/MFC composite

Figure 5.2 is the FTIR spectra of neat P(3HB) and acetylated MFC and the P(3HB)/MFC composite. As expected, the characteristic absorptions of the grafted acetyl groups were easily identified on the acetylated MFC and the P(3HB)/MFC composite but not on the neat P(3HB) film. The characteristic absorptions observed included the carbonyl stretching vibration at 1720 cm^{-1} ($\nu_{\text{C=O}}$), the methyl in-plane bending at 1378 cm^{-1} ($\delta_{\text{C-H}}$), and the C-O Stretching at 1226 cm^{-1} ($\nu_{\text{C-O}}$). Another easily observed feature of the P(3HB)/MFC composite was the increase and a slight shift in 2978 cm^{-1} band, representing the hydroxyl group, which was reduced in the neat P(3HB) and acetylated microfibrillated cellulose spectra. Also significant in the FTIR spectra of acetylated cellulose and the P(3HB)/MFC composite is the absorption band at 3335 cm^{-1} in the P(3HB)/MFC composite and 3343 cm^{-1} in the acetylated MFC. It can be observed that the band is almost completely absent in the neat P(3HB) spectrum and shifted to a slightly lower wave number in the P(3HB)/MFC composite

(a)

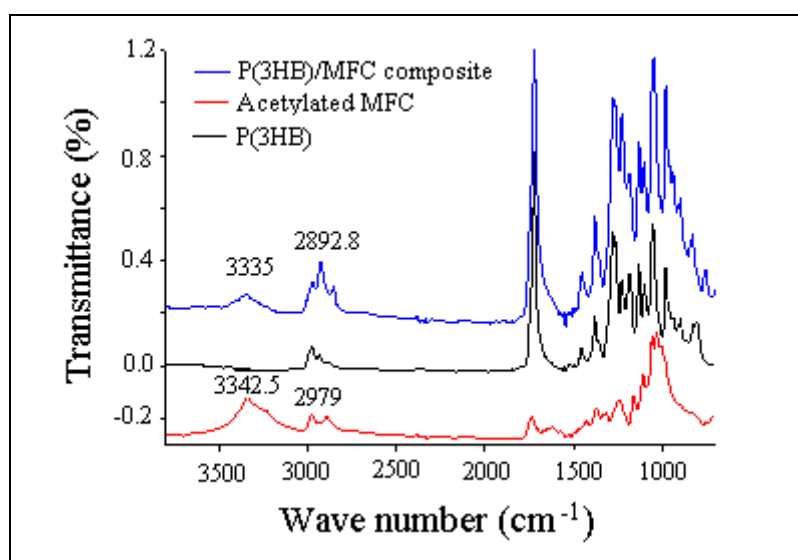


Figure 5.2 (a) FT-IR spectra of P(3HB)/MFC composite containing 40 wt% acetylated MFC (blue line); acetylated microfibrillated cellulose (red line), and FT-IR spectrum of P(3HB) (Black line)

(b)

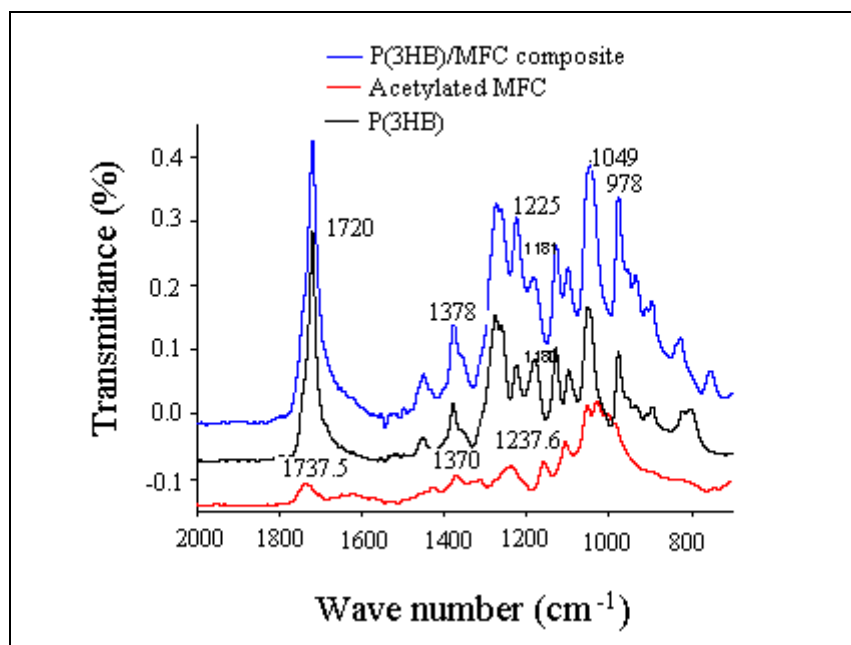


Figure 5.2(b) Magnification of the FTIR spectra within the 2000 and 750 cm^{-1} wave number

5.2.3 X-ray Diffraction Spectroscopy of P(3HB)/MFC composite

The impact of addition of acetylated microfibrillated cellulose to neat P(3HB) solution in the composite fabrication was further evaluated using X-ray diffraction analysis (Figure 5.3). The spectra collected was compared to the spectra of acetylated MFC and neat P(3HB) film. The neat P(3HB) materials were found to exhibit the typical spectrum of P(3HB) while the acetylated MFC displayed a typical X-ray diffraction pattern with characteristic diffractions peaks at 14.8, 17, 22.5, 39.5 2θ angles. The P(3HB)/MFC composite displayed characteristic peaks between 12.2 and 13.7 2θ angles. Also, characteristic peaks were observed at the 2θ angle positions of 28, 32 and 51. The intensity of the peaks were found to be shorter and slightly narrower in the spectra of the P(3HB)/MFC composite. Also, more peaks were observed on the spectra of the composite material. Overall the diffraction pattern of the P(3HB)/MFC composite differed significantly when compared to the diffraction patterns of neat P(3HB) and acetylated MFC which is an indication of changes in the crystallinity of the composite material.

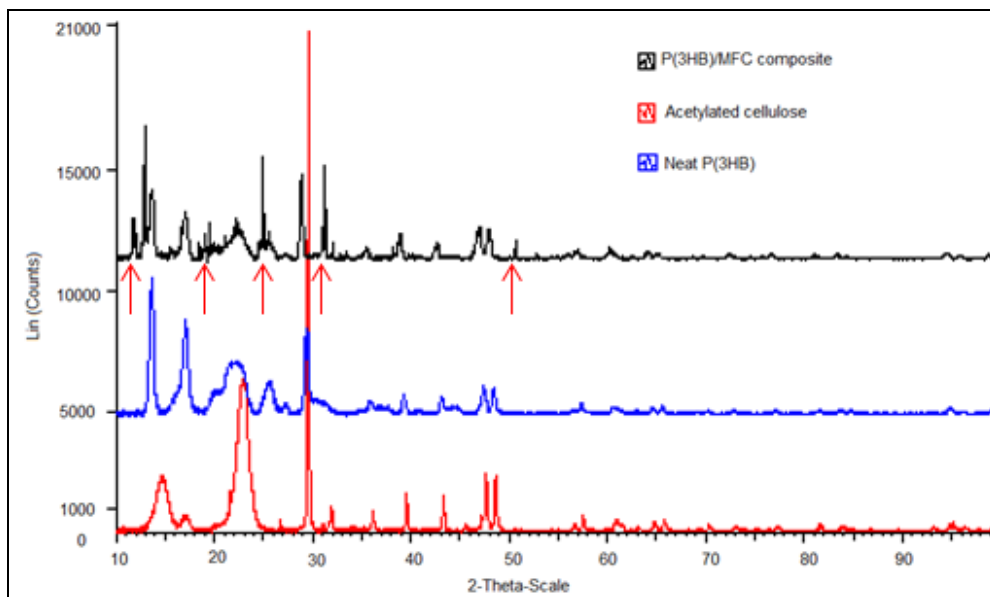


Figure 5.3 XRD spectra of (a) P(3HB)/MFC composite (black line), (b) acetylated cellulose (red line) and (c) Neat P(3HB) (blue line). The red arrows indicate significant peaks found in the P(3HB)/MFC composite.

5.2.4 Thermal Characterisation of P(3HB)/MFC composite

To further understand the changes caused as a result of the addition of MFC to the P(3HB) matrix, the composite material was characterised using Differential Scanning Calorimetry (DSC). The material was made to undergo a gradual heating and cooling process at a constant heating rate of (20 °C/min) as described in Chapter 2, Section 2.4.1.2. This was carried out to resolve the thermal transitions (melting and crystallization properties) in the neat P(3HB) and P(3HB)/MFC composite materials. Typical DSC thermograms of neat P(3HB) compared to the P(3HB)/MFC composite films is shown in Figure 5.4, which outlines the heating curves for the melting, T_m and crystallization temperatures, T_c of the polymer and the composites. Analysis of the results of the DSC showed no significant difference ($p > 0.01$) between the melting point of neat P(3HB) and the composites by the addition of the MFC. However, there was emergence of a secondary melting peak by the addition of the MFC in the first heat scan which was more prominent on increasing the amount of MFC in the composite as highlighted in Figure 5.4. The secondary melting peaks were found to disappear during the second heating of the composite material (figure not included). The crystallization temperature of the composite material was found to decrease with increase in the amount of MFC in the composite matrix. Furthermore, the heat of fusion for both the melting and crystallization

temperatures of the various composite samples fluctuated and did not follow the trend of decrease in value with increase in the wt % MFC content, as observed in T_m and T_c values (Table 5.1).

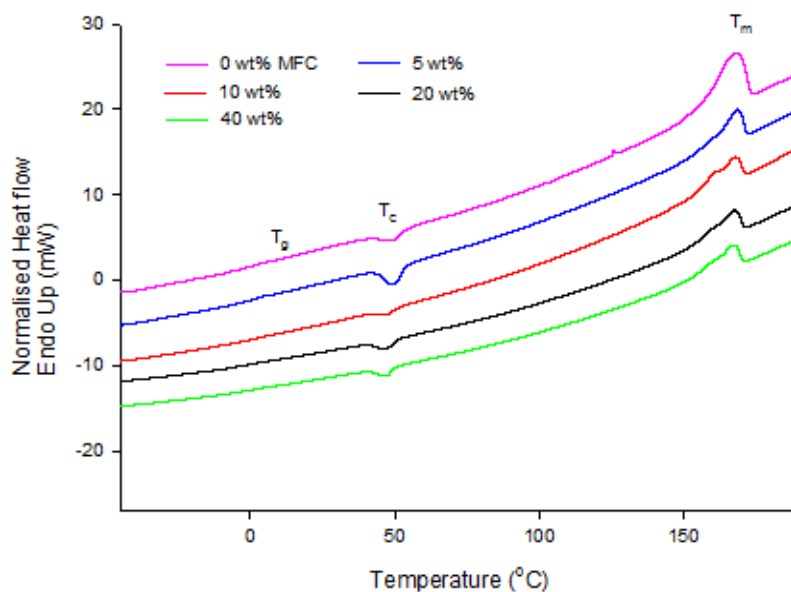


Figure 5.4 DSC thermographs of neat P(3HB) and P(3HB)/MFC composite films (0-40 wt%) showing the melting temperature, T_m , crystallization temperature, T_c and glass transition temperature T_g .

Table 5.1 Comparison of thermal properties for P(3HB)/MFC containing different amount of MFC per wt %

P(3HB)/MFC MFC content (wt %)	Melting Temperature		Crystallization temperature	
	T_m (°C)	ΔH_f (J/g)	T_c (°C)	ΔH_f (J/g)
0	169.81	40.32	59.43	-13.08
5	168.51	23.72	49.44	-18.74
10	166.79	35.86	48.48	-3.35
20	167.55	15.89	46.87	-7.29
40	167.68	20.20	43.81	-23.13

5.2.5 Dynamic mechanical analysis of P(3HB)/MFC composite films

Dynamic Mechanical Analysis, DMA has been used extensively in the characterisation of particulate reinforced polymer (Chen and Wang, 2002; Mukhopadhyay *et al.*, 1993). In this study, the mechanical properties of the composite film containing various amount of MFC were tested for their static tensile stress. Typical profiles of the curves generated in the DMA test are shown in Figure 5.5. The result of the static tensile tests showed that neat P(3HB) films achieved a Young's modulus of 0.22 ± 0.004 GPa. On the addition of MFC to the P(3HB) matrix, the Young's modulus of the resultant composites were found to increase significantly (Table 5.2). The addition of 10 wt% MFC increased the Young's modulus to 0.38 ± 0.003 GPa, further increase in the MFC content to 20 and 30 wt% significantly ($p < 0.05$) increased the Young's modulus to 1.29 ± 0.079 and 1.35 ± 0.116 GPa respectively. Additional increase in the MFC content to 40 and 50 wt% resulted in a gradual reduction in the measured Young's modulus to 1.26 ± 0.09 and 0.90 ± 0.002 respectively (Figure 5.6).

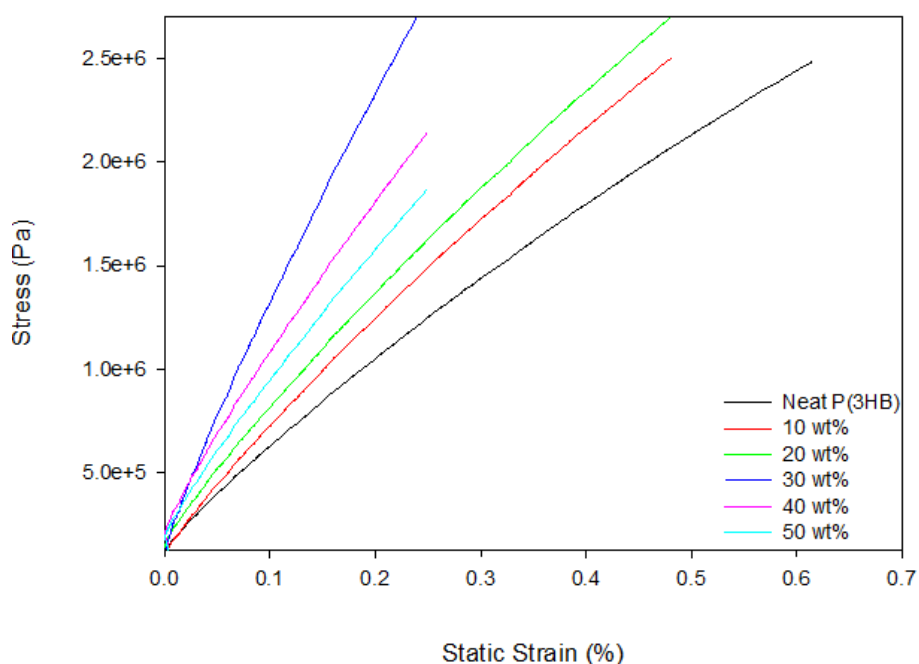


Figure 5.5 The Stress-Strain curve of neat P(3HB) and P(3HB)/MFC composite films highlighting differences in the measured Young moduli. Analyses were performed in triplicates. Only one representative curve for each sample has been shown for the purpose of clarity.

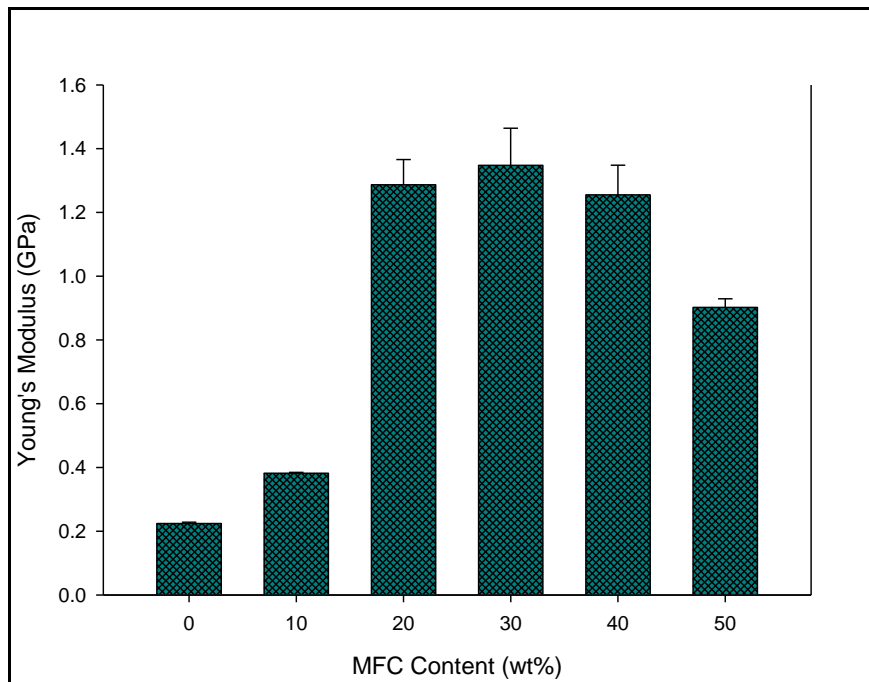


Figure 5.6 Moduli comparison of P(3HB)/MFC composite film containing different amounts of MFC

Table 5.2 Comparison of mechanical properties of fabricated P(3HB)/MFC film with the mechanical properties of some skeletal tissue.

Materials	E(GPa)
Neat P(3HB)	0.22±0.004
10 wt% MFC (P(3HB)/MFC)	0.38±0.003
20 wt% MFC (P(3HB)/MFC)	1.29±0.079
30 wt% MFC (P(3HB)/MFC)	1.35±0.116
40 wt% MFC (P(3HB)/MFC)	1.26±0.093
50 wt% MFC (P(3HB)/MFC)	0.90±0.002
Cancellous bone	0.02-0.5 (Yang <i>et al.</i> , 2001)
Cortical bone	3.30 ”
Cartilage	0.7-15.3 (MPa) ”
Ligament	0.06-0.54 ”
Tendon	0.14-2.31 ”

5.2.6 Surface Chemistry confirmation of P(3HB)/MFC Composite film.

In order to understand the influenced of the MFC on the surface chemistry of the composite materials, surface staining with a cationic and dianionic dye was performed on the different composites following the detailed staining protocols described in Chapter 2, Section 2.4.1.4. Both the colour staining and the intensity of the colours observed were compared with that of the neat P(3HB) films. It was observed that the P(3HB)/MFC composite films stained positively (red) with Rose Bengal, a dianionic dye (Figure 5.7). Also, it was found that the intensity of the Rose Bengal dye retained by the composite materials increased as the amount of MFC content in the composite increases. This was contrary to the case of staining with Toluidine blue, in which the colour of the retained dye decreased as the amount of the MFC content in the composite material increases. The neat P(3HB) stained negative with Rose Bengal dye. Comparison of the intensity of the retained dye on the materials showed that Rose Bengal was more retained by the material (Figure 5.8).

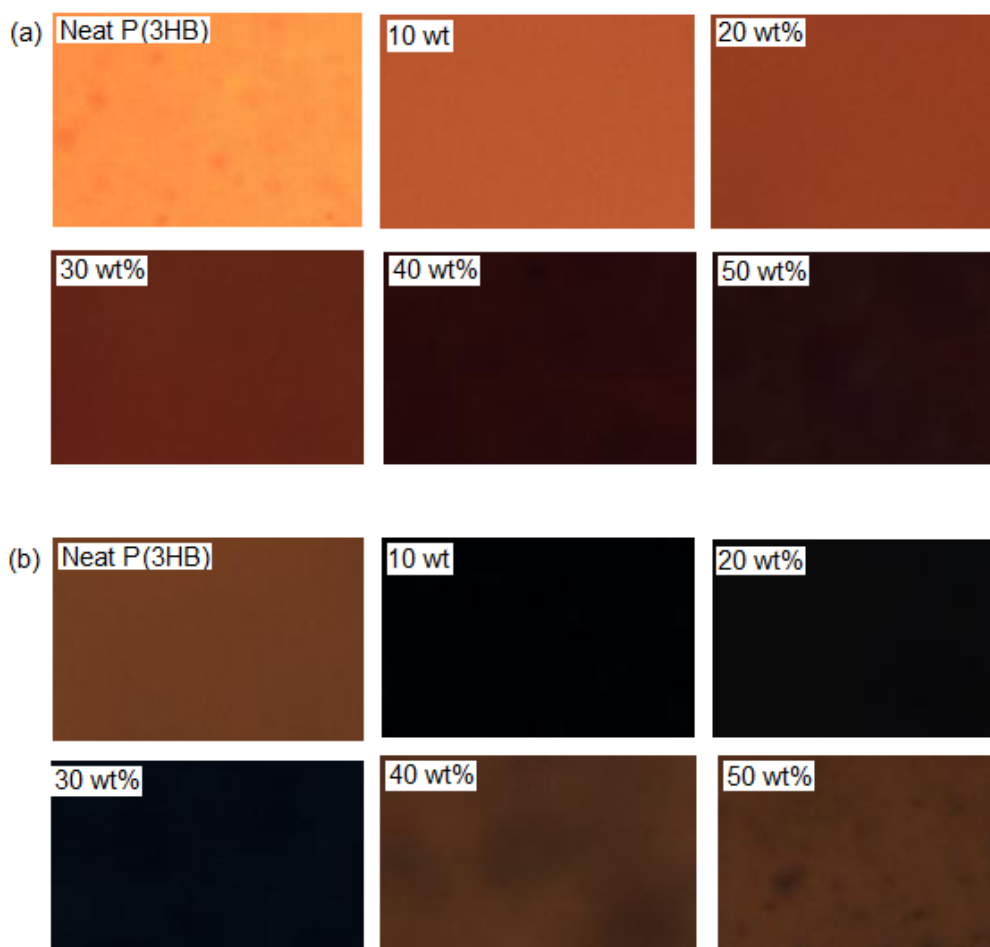


Figure 5.7 Images of neat P(3HB) and P(3HB)/MFC composite films with various MFC content stained with (a) Rose Bengal dye and (b) toluidine blue.

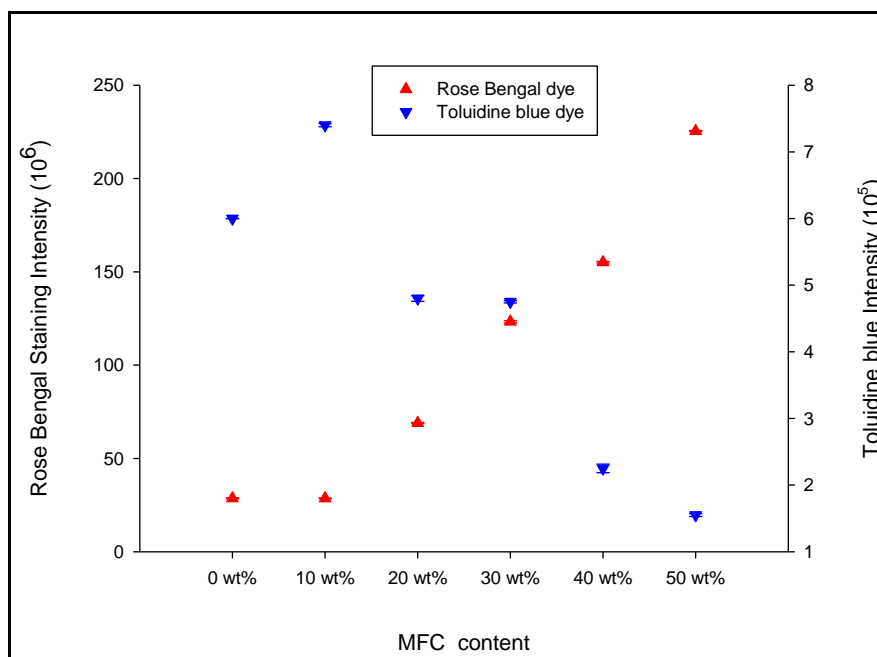


Figure 5.8 Colour intensity of neat P(3HB) and P(3HB)/MFC composite films of various MFC content measured after staining with Rose Bengal and Toluidine blue dyes for 4 hours ($n=3$, and error bars = \pm SD)

5.2.7 Aqueous Contact Angle Measurement

Aqueous contact angle is used to measure the degree of hydrophilicity/hydrophobicity of a biomaterial. Based on the differences in the surface chemistry of the composite film and the microstructure differences observed on the SEM images of the composite materials, static water contact angles were measured in order to determine the wettability of the surfaces. Typical water contact angle curve generated from the 50 wt% MFC content composite is shown in Figure 5.9. The aqueous contact angle measured on the neat P(3HB) film was 68 ± 6.7 . On the composite films, the aqueous contact angle measured on 10, 20, 30, 40 and 50 wt% were shown Figure 5.10. There was statistical difference ($n=3$, $p < 0.01$) found in the water contact angle between the neat P(3HB) and the composite polymeric materials. However, no significant differences ($n=3$, $p > 0.01$) was found between 10, 20, 30 and 40 wt% MFC content in P(3HB) matrix. The composite film with 50 wt% MFC content was found to exhibit the least aqueous contact angle with 26.9% less than the aqueous contact angle measured on the neat P(3HB) and 8.2% less than the aqueous contact angle measured on composite containing 10 wt% MFC.

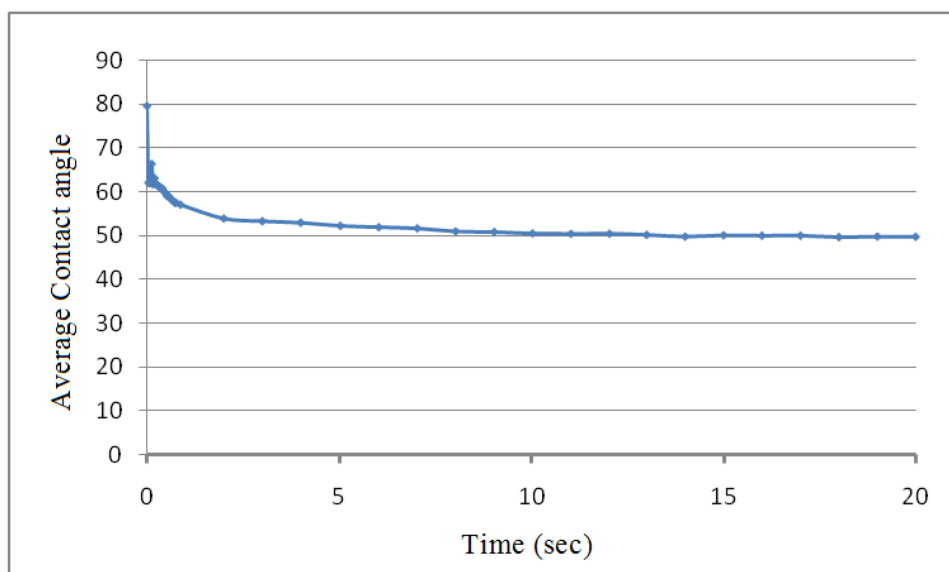


Figure 5.9 Typical aqueous contact angle plot for P(3HB)/MFC composite film containing 50 wt% MFC.

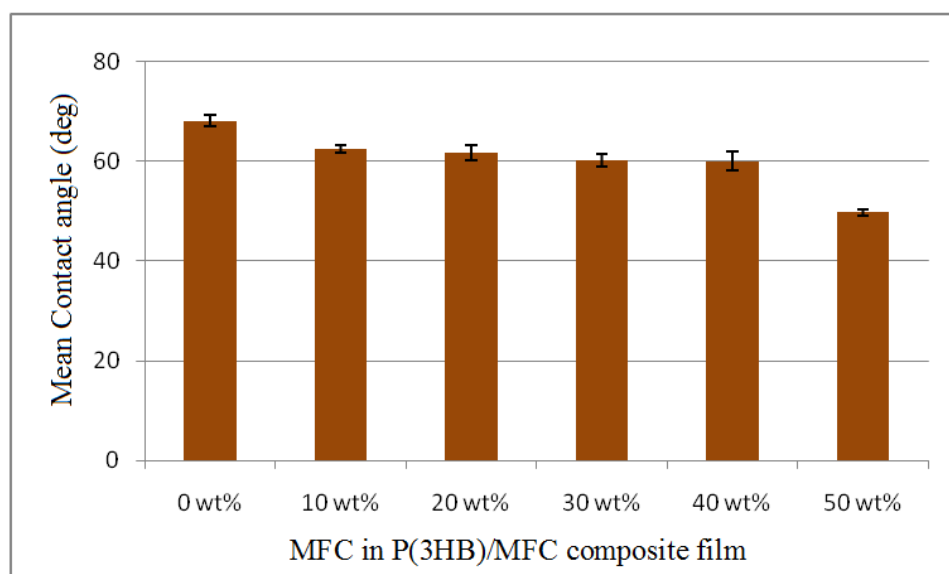


Figure 5.10 Relationship of aqueous contact Angles and the weight percentage content of MFC in P(3HB)/MFC composite films (n=3, error = \pm SD).

5.2.8 Water Absorption Test on neat P(3HB) and P(3HB)/MFC composite films

Water absorption analysis was specifically carried out on the composite material containing 40 wt% MFC and neat P(3HB) as the control. The 40 wt% MFC content composite was chosen based on the performance of the material in the physico-mechanical characterisation.

The result of the analysis illustrated in Figure 5.11 shows that the composite material absorbed water and reached a maximum value of water absorbed at the end of 28 days of incubation. However, no statistical difference ($p>0.01$) was found between the amount of water absorbed by the composite scaffold during the first 14 days. But, after 14 days of incubation in SBF (simulated body fluid), the percentage water absorption increased which was found to be significant ($p<0.05$) between 14, 21 and 28 days of incubation. Also, no significant difference ($p>0.01$) was observed in the water absorption by the neat P(3HB) film between day 7 and 14 of incubation time in SBF. After 14 days, the percentage water absorption increased significantly ($p<0.05$) between day 14 and 21 of the incubation period. The percentage water absorption by the neat P(3HB) decreased significantly ($p<0.05$) at the end of 28 days.

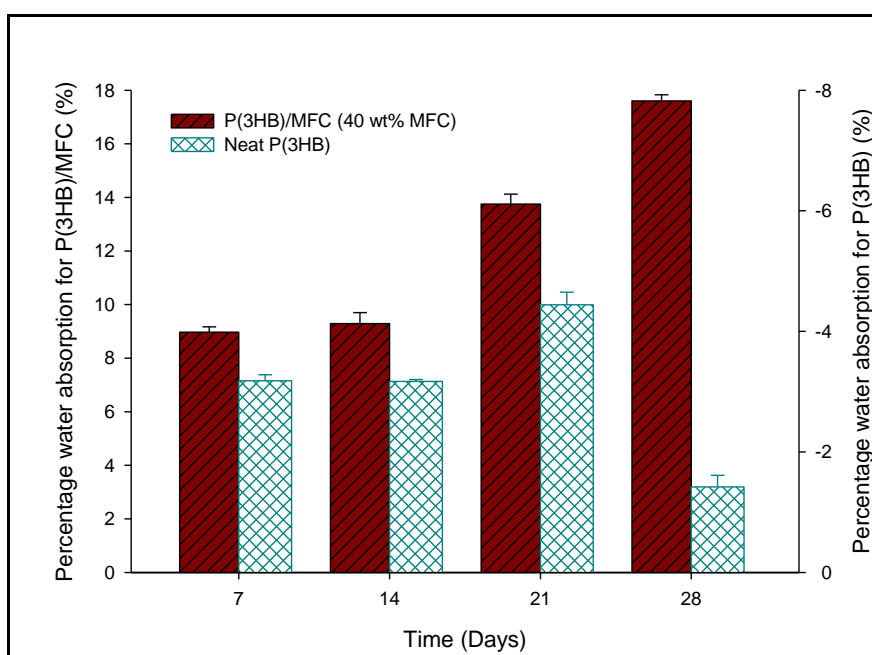


Figure 5.11 Comparison of percentage water absorption for neat P(3HB) and P(3HB)/MFC composite film (40 wt% MFC content) immersed in SBF for 28 days at 37°C. (n=3, error bar = \pm SD).

5.2.9 Weight loss of P(3HB)/MFC composite film during degradation studies in SBF

Figure 5.12 shows the percentage weight loss of the neat P(3HB) and polymeric composite material as a function of the incubation time. It can be seen from Figure 5.12 that the percentage weight loss of the composite material increased slightly at 14 days. After 14 days, the percentage weight loss decreased and reached a minimum at 28 days. The neat P(3HB)

showed a decrease in percentage weight loss after 7 days of immersion in SBF. The percentage weight loss of the neat P(3HB) film was found to be constant between 14 and 21 days and increased significantly at 28 days. Comparison of percentage weight loss by the neat P(3HB) and the P(3HB)/MFC composite showed that the neat P(3HB) lost more weight than the composite polymer.

Also shown in Figure 5.11 is the change in pH of the SBF after various time points. As can be seen in Figure 5.11, both the neat and composite polymer showed an increase in the pH of SBF from the initial value of 7.35 to a final value of 7.62. However, no significant difference ($p > 0.01$) was found in the change in pH of the immersed SBF during the incubation period.

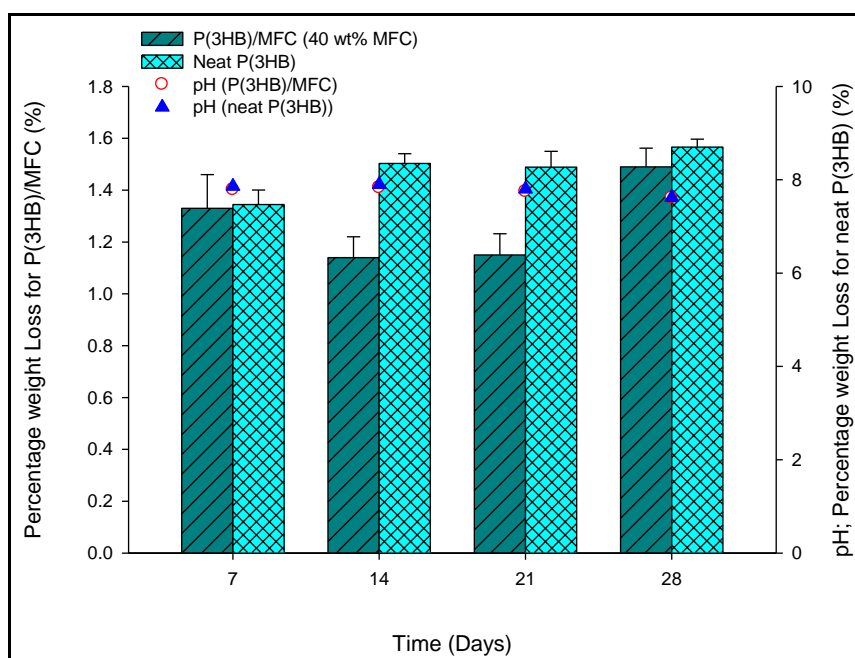


Figure 5.12 Comparison of percentage weight loss of neat P(3HB) and P(3HB)/MFC composite film (40 wt% MFC content) and pH value of the immersed SBF after incubation for 28 days at 37°C. (n=3, error bar = \pm SD).

5.2.10 Total Protein Absorption Analysis on the neat P(3HB) and P(3HB)/MFC composite films.

Protein absorption analysis was performed on both the neat P(3HB) and the composite scaffolds. This was necessary since it is known that most mammalian cells attach selectively on biocompatible protein rich surfaces for subsequent proliferation and differentiation to form new tissues (Wei *et al.*, 2004). On this note, the materials were tested for their ability to

absorb protein onto their surfaces. Fetal bovine serum (FBS) was used for this study and experimental details were explained in Chapter 2, Section 2.4.2.6. The protein adsorption study showed that the total amount of protein adsorbed on the surface of the P(3HB)/MFC was higher for the composites compared to neat P(3HB) films (which was measured to be $98 \pm 3.2 \mu\text{g}/\text{cm}^2$). The presence of MFC in the composite resulted in higher protein binding, as evident from the results shown in Figure 5.13. However, no statistical difference ($p > 0.05$) was found on the protein adsorption between 40 and 50 wt% MFC content composite film.

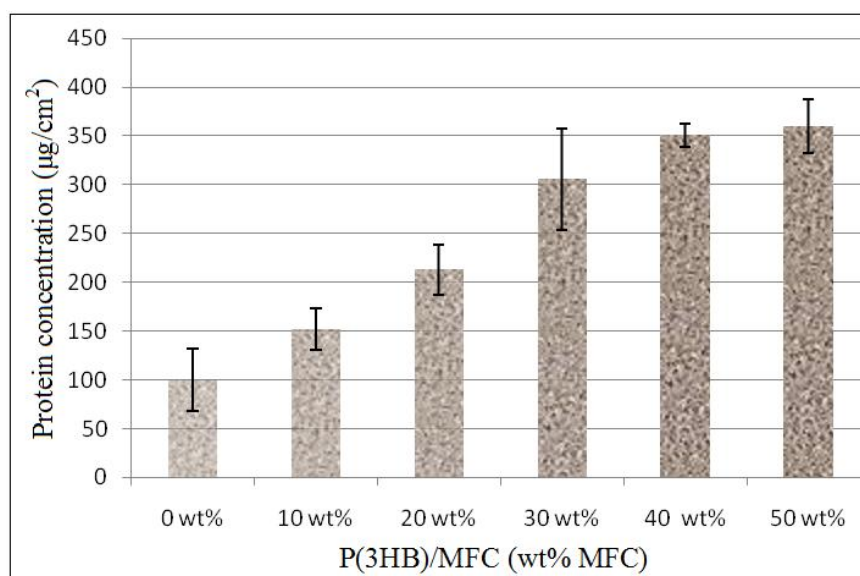


Figure 5.13 Total protein adsorption on P(3HB)/MFC composite films using foetal bovine serum. (n=3; error bars= \pm SD).

5.3 Characterisation of the P(3HB)/MFC Composite 3D Scaffolds

P(3HB) and P(3HB)/MFC composite scaffolds were prepared using a novel compression moulding/particulate leaching as described in Chapter 2, Section 2.3.3. This novel technique was developed for this study using an inexpensive technique which can be carried out at room temperature. Some of the important results obtained using this technique is described in this section.

- The dimension of the foams (P(3HB) and P(3HB)/MFC) produced using this technique is alterable as shown in Figure 5.14a,b and c. The porosity of the scaffolds can be controlled by adjusting the size and amount of porogen material (sucrose grain).

- The mechanical strength of the scaffold can be altered and controlled by adjusting the amount of P(3HB) and filler used in composite making.
- Both the proportion of the base polymeric matrix and the filler can be altered with ease to suit a particular need in tissue engineering. Also, the technique allows with ease the incorporation of known amount of other substances such as hydroxyapatite, Calcium triphosphate and Bioglass[®] during multifunctional scaffold fabrication as shown in Figure 5.14b and c.
- The shape of the pores in the scaffold can be varied which is dependent on the shape of the porogen material employed during scaffold fabrication.

The most important aspect of the technique used in the production of the scaffolds is that the technique is very simple, inexpensive and less time consuming unlike solvent casting/particulate leaching or electrospinning. Furthermore, the porous microstructure produced using this technique is comparable and in many cases better in the physico-mechanical properties than the ones achieved for other PHA scaffolds reported so far in literature like P(3HB-co-3HV)/BG scaffold prepared using compression moulding, thermal processing, and salt particulate leaching technique (Li *et al.*, 2005)

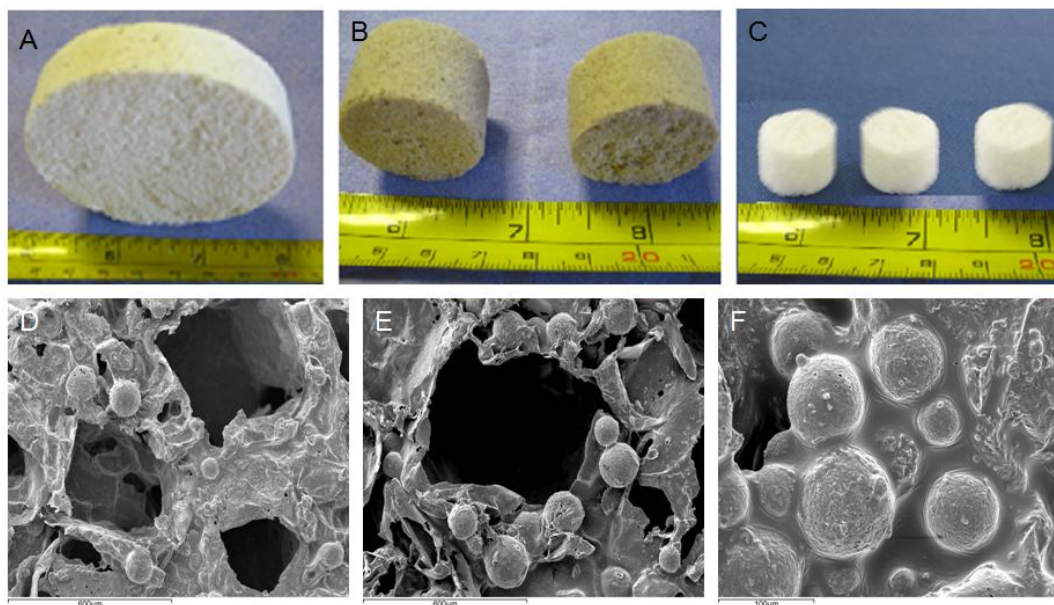


Figure 5.14 Digital images of different dimensions and type of scaffolds that can be produced using the compression moulding/particulate leaching techniques. (B) Shows a digital image of scaffold prepared by incorporation of vitamin E and magnetic particles for bone regeneration (C) Shows a digital image of scaffold prepared by incorporating cellulose microspheres in P(3HB) matrix (D) SEM image showing the incorporation of microspheres containing gentamicin and TFG- β 3 for sustainable

nutrient/drug (e.g. gentamicin, growth factors etc) release during tissue regeneration; (E) SEM image showing the arrangement of the microspheres around the pores of the scaffold for efficient content delivery; (F) SEM image of the tightly bound microspheres on the walls of the pores.

5.3.1 Microstructural characterisation of P(3HB)/MFC Composite 3D Scaffolds

Figure 5.15a shows a typical digital image of P(3HB) and P(3HB)/MFC foams produced using the novel compression moulding/particulate leaching technique. The SEM image of the surface of the foam highlights the interconnected pore network in the scaffold microstructure (Figure 5.15b). This is necessary for the infiltration of cells during bone and cartilage regeneration. Figure 5.15c displays the SEM image of the morphology of pores in the scaffold highlighting the nanotopography of the surface of the pore throat (inside pore).

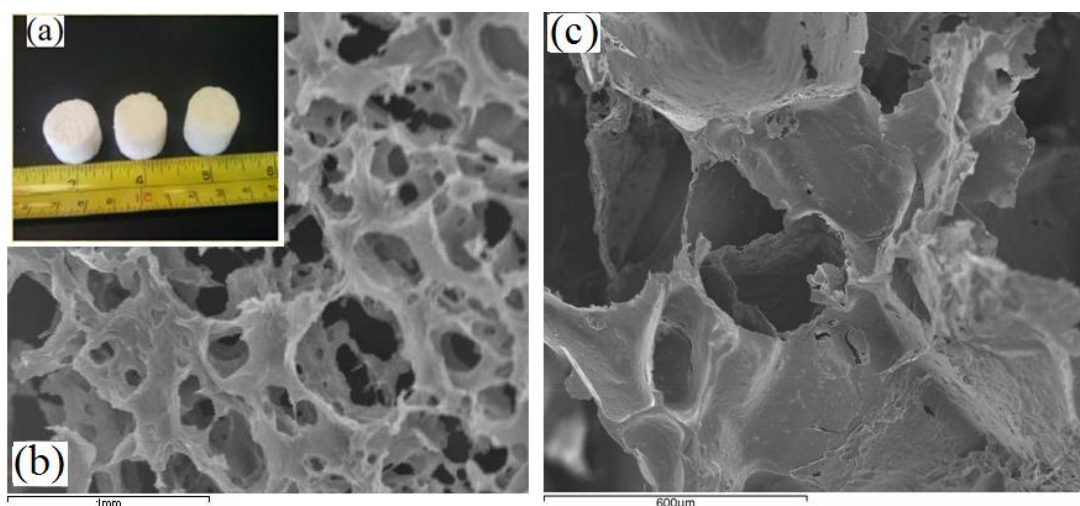


Figure 5.15 (a) Digital image of the P(3HB)/MFC scaffold after particulate leaching; (b) SEM image of P(3HB)/MFC composite foam at lower magnification showing the microstructural pores in P(3HB)/MFC scaffold; (c) SEM image of P(3HB)/MFC composite foam at higher magnification displaying the irregular pore structure with high interconnectivity.

5.3.2 Compression testing

Figure 5.16 shows a typical stress-strain curve of neat P(3HB) and P(3HB)/MFC composite of various MFC content (10, 20, 30, 40, and 50 wt%) tested in air. The curves demonstrate the typical behaviour of a scaffold undergoing deformation and comprise three distinct

regions: a linear-elastic region followed by a plateau of roughly constant stress leading into a final region of steeply rising stress.

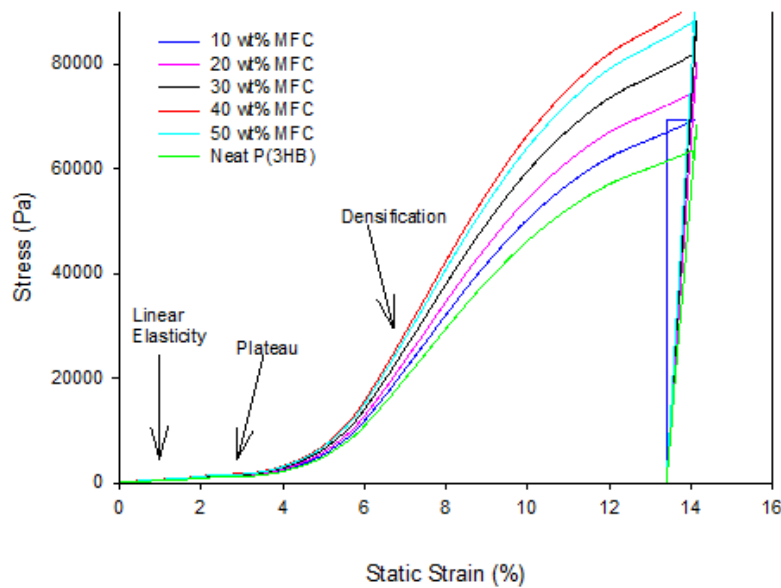


Figure 5.16 Typical stress-strain curves of neat P(3HB) and P(3HB)/MFC scaffolds of various MFC content under compression loading. The experiment was performed in triplicates. For clarity purpose, only the profiles for single analysis have been shown.

Figure 5.17 shows the compressive modulus and compressive yield strength of the neat P(3HB) and P(3HB)/MFC composite scaffold with varying wt% of MFC content. It can be deduced from Figure 5.17 that the incorporation of MFC into the polymer matrix significantly influenced the compressive modulus of the composites. Whilst, the compressive modulus of the neat P(3HB) was found to be 0.083 ± 0.006 MPa, the compressive modulus on addition of 10, 20, 30, and 40 wt% MFC were found to have increased to 0.112 ± 0.005 , 0.114 ± 0.016 , 0.136 ± 0.017 , and 0.186 ± 0.009 MPa respectively. From the statistical analysis performed on the result, statistical difference ($p < 0.05$) was found between the compression modulus of the neat P(3HB) and P(3HB)/MFC composite, and among the composites. However, compressive modulus of the P(3HB)/MFC composite was found to decrease to 0.161 ± 0.017 MPa on increasing the MFC content further to 50 wt%. On the other hand, the

compressive yield strength of the composite was found to increase progressively on the incorporation of MFC to the polymer matrix. Whilst, the compressive yield strength measured on the neat P(3HB) scaffold was 0.58 ± 0.06 KPa, this was found to have improved to 95, 97, 98, 102 and 109 % on addition of 10, 20, 30, 40 and 50 wt% MFC respectively. Besides, a statistical difference ($p < 0.05$) was calculated between the compressive yield strength of the neat P(3HB) scaffold and the P(3HB)/MFC composite scaffold. However, no significant difference ($p > 0.05$) was found on the yield strength among the composites containing different amounts of MFC.

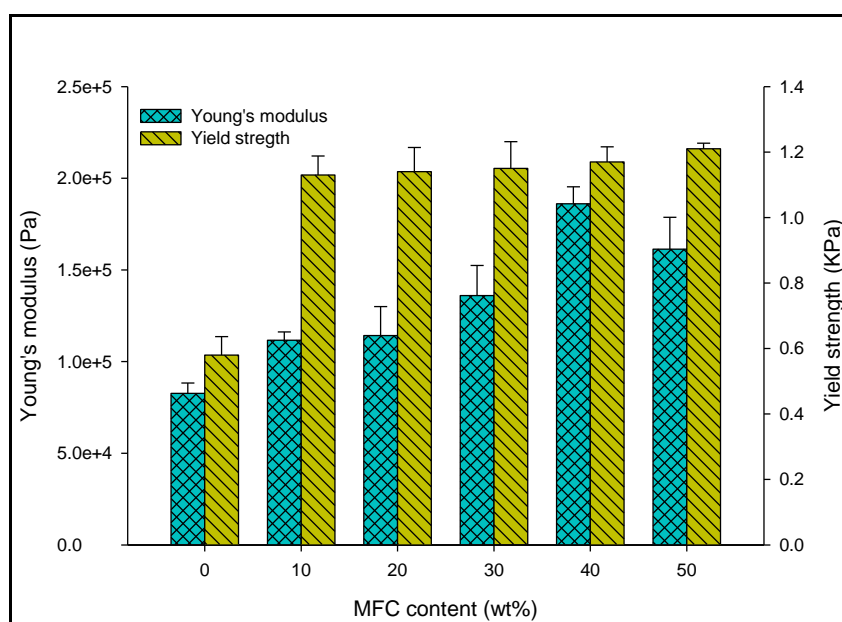


Figure 5.17 Compressive modulus and yield strength for P(3HB)/MFC scaffolds with various MFC (wt%) content measured in air ($n=4$, error = \pm SD).

5.3.3 Protein adsorption assay on P(3HB)/MFC composite 3D scaffold

Protein absorption was characterised on both the neat P(3HB) and P(3HB)/MFC 3D scaffold, as performed on the composite films to understand the effect of addition of cellulose microfibrils on protein adsorption. This was necessary in order to gain more understanding of the role of the added MFC in protein adsorption by the composite scaffolds, since the potential of biomaterial to function as a scaffold in tissue regeneration is partly based on their role in enhancing cell attachment, differentiation and subsequent tissue formation. The result of the protein adsorption test is shown in Figure 5.18. The result shows that the addition of MFC to the polymer matrix improved protein absorption by the composite material by 8, 15,

20, 22, 27% by the 10, 20, 30, 40 and 50 wt% MFC respectively when compared to 490 $\mu\text{g}/\text{cm}^2$ protein absorbed by the neat P(3HB) scaffold. Hence, the protein adsorbed by the composite material increased progressively as the amount of MFC added to the polymer matrix increased.

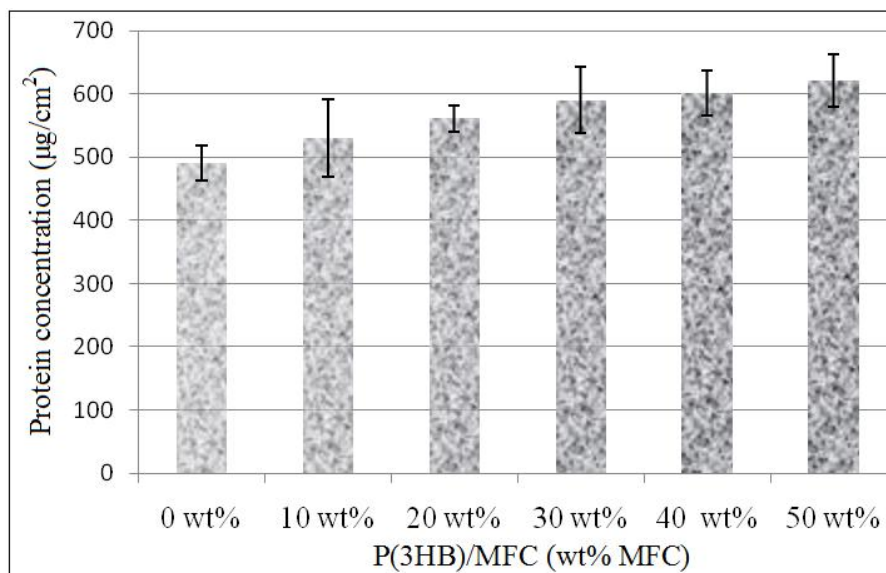


Figure 5.18 Total protein adsorption study on P(3HB)/MFC composite scaffold using foetal bovine serum ($n = 3$; error bars = \pm SD).

5.4 Biodegradation study

The biodegradability of PHAs in general is a major reason for their applications in medicine, environmental management and food processing. For instance, the biodegradability of PHAs is an important factor for their use as a biomaterial which eliminates the need for a second medical surgery in order to remove them from the body after performing their roles in tissue regeneration and drug delivery systems. Hence, the biodegradability of the P(3HB)/MFC composite material was assessed and the rate of degradation was compared to that of neat P(3HB). Nevertheless, it is absolutely necessary for a biomaterial for tissue engineering to degrade in a systematic manner that would not compromise the effective rehabilitation function for which it was employed. To carry out this test, the 40 wt% MFC content composite was chosen for the investigation. The reason for the choice of the 40 wt% MFC content was based on the performance of the protein absorption capability and the physico-

mechanical strength of the various composites. The detailed results of the parameters analysed are given below.

5.4.1 Weight loss measurement on P(3HB)/MFC composite 3D Scaffold

Initially, percentage weight loss by the neat P(3HB) and the P(3HB)/MFC composite scaffold was used to assess the rate of degradation of the materials. The result of the weight loss by the materials is shown in Figure 5.19. After analysis of the result achieved with the neat P(3HB) (control test) and the 40 wt% MFC composite, it was found that both control (neat P(3HB) and the test material (40 wt% MFC composite) were found to reduce in weight after immersion in SBF for 30 days. However, the addition of microfibrillated cellulose was found to have improved the degradation of the composite scaffolds. This was confirmed by the increase in weight loss of the composite scaffold as compared to the neat P(3HB) scaffold. No statistical difference ($p>0.05$) in percentage weight loss of the P(3HB) scaffold was found between 0 day and 14 days of incubation. But, after 30 days incubation in SBF, weight loss on the neat P(3HB) was found to increase significantly, up to $64\pm 4\%$ of the original weight. On the other hand, the percentage weight loss of the P(3HB)/MFC composite scaffold was found to increase to $43.7\pm 12\%$ of the original weight at 14 days of incubation. Further increase in the incubation time saw the weight loss in the composite material decreased to $34.4\pm 16\%$. Comparison of the weight loss of the neat P(3HB) and P(3HB)/MFC shows that there was a statistical difference ($p<0.05$) in the rate of degradation of both materials at all the time points considered (7, 14 and 30 days).

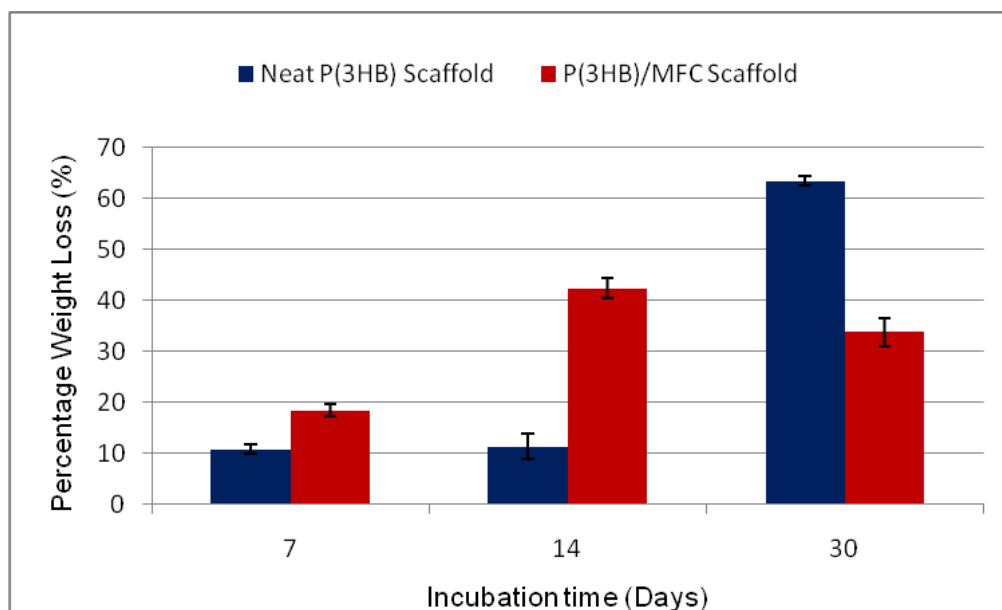


Figure 5.19 Typical plot of percentage weight loss of P(3HB)/MFC composite scaffold and neat P(3HB) scaffold immersed in SBF for 7 days, 14 days and 30 days (n=6, error, \pm SD).

5.4.2 Change in pH of the immersed SBF of the neat P(3HB) and P(3HB)/MFC 3D composite scaffolds.

It has been suggested that acidic degradation products of polymers such as PLA (polylactic acid) and P(3HB) result in a decrease in pH around the surrounding environment of degrading polymeric materials. Whilst, very low pH is not desirable during degradation of medical polymeric materials, very high pH is equally not desirable as this could affect the physiological functions of the surrounding cells and tissues. Hence, the change in the pH of the immersed SBF for the neat and composite P(3HB) materials was monitored over a period of time. The details of the variation in the pH of the SBF medium are shown in Figure 5.20. There was no rapid change in the pH of the immersed SBF on both the neat P(3HB) and the P(3HB) composite throughout the incubation period. However, it was found that the pH of the SBF for the composite samples increased slightly from the initial 7.35 to 7.47 at 7 days of immersion in SBF. The pH was found to remain constant until after 14 days and later gradually decreased to 6.4 after 30 days of incubation. For the control (neat P(3HB)), the pH was found to increase slightly from the initial 7.35 to 7.45 at 12 days and gradually decrease to a pH of 5.8. Comparison of pH of the immersed SBF for both samples shows that the pH

of the SBF immersed with neat P(3HB) decreased by 9% in relative to the pH of the SBF immersed with the P(3HB)/MFC composite material after 30 days.

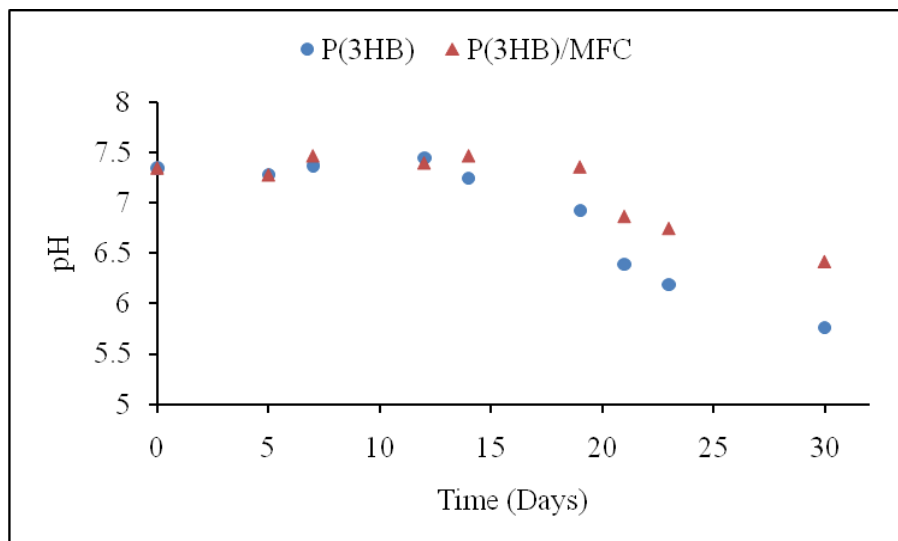


Figure 5.20 Change in pH of the SBF solution in which the neat P(3HB) (●) and P(3HB)/MFC (▲) 3D scaffold were incubated.

5.4.3 Raman shift spectroscopy

The Raman shift spectroscopy was employed to assess the formation of new compounds on the test samples during immersion in SBF at different time periods. Change in the intensity of the peaks was used to assess changes in the crystallographic properties of the polymeric composite material due to degradation of the samples. Figure 5.21 displays the Raman shift spectra of the P(3HB)/MFC composite at 0, 7, 14, 21 and 30 days. It was observed that there was formation of a new peak at position 770 cm^{-1} . Also evident in the spectra is the variation in the intensity of the peaks at different time points of immersion in SBF. The peak intensity was found to increase to the highest at 14 days of incubation and gradually decrease with further increase in the incubation time to 21 and 30 days. Another observable feature in the spectra is the broadening of the peaks which increases with increase in the incubation time.

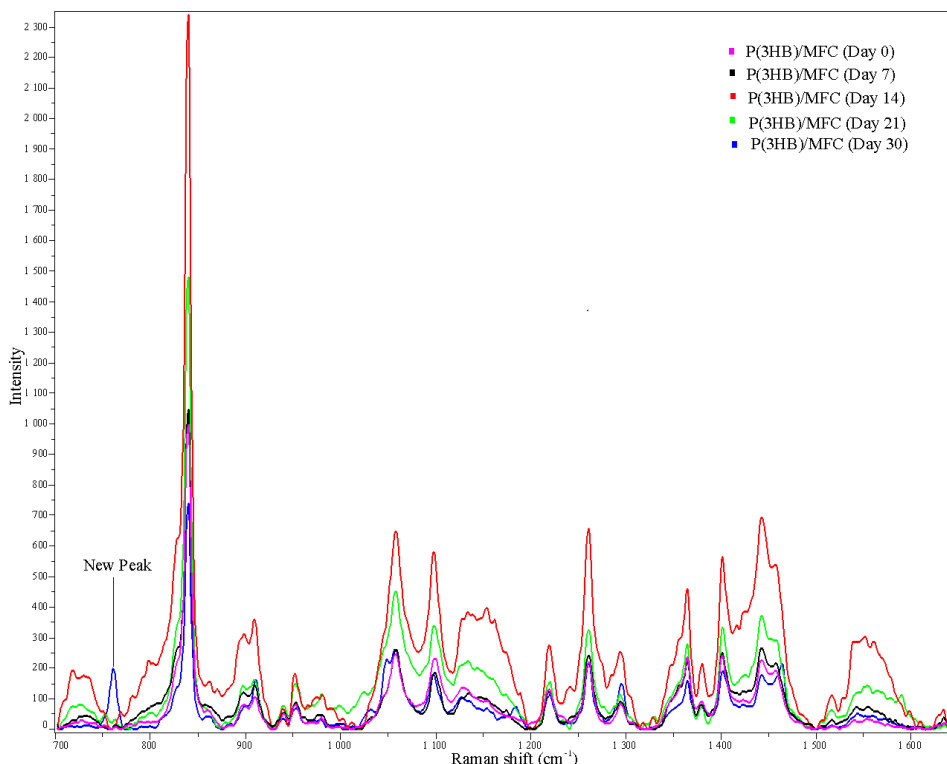


Figure 5.21 Raman Shift spectra performed on P(3HB)/MFC composite scaffold after immersion in SBF for 0 days, 7 days, 14 days, 21 days and 30 days.

5.4.4 X-ray diffraction (XRD) Analysis

X-ray diffraction analysis was further performed on the degraded samples to gain more understanding on the effect of degradation on the crystallographic properties of the composite. This was necessary since increase in the crystallinity of biomaterials can be an advantage in the attachment and differentiation of cells. Hence, understanding the crystallographic properties of the composite can help to tailor down the composition of the composite to suite a particular need. The X-ray diffraction patterns for both neat P(3HB) and P(3HB)/MFC composite scaffolds immersed in SBF highlighted an additional peak at 32° , (indicated with blue arrow in Figure 5.22) after immersion in SBF for 21 days. Also, there was additional peak found between position 45° and 47° (indicated with a green arrow in Figure 5.22) on both the spectra of neat P(3HB) and P(3HB)/MFC composite scaffolds immersed in SBF for 21 days. Furthermore, some bands present in the spectrum of original samples before immersion in SBF were lost after immersion in SBF for 21 days. Also obvious in the spectra are broadening and shifting of peak positions of both neat P(3HB) and

the composite after immersion in SBF. Furthermore, the intensity of the peaks related to the P(3HB)/MFC composite scaffolds became shorter after immersion in SBF.

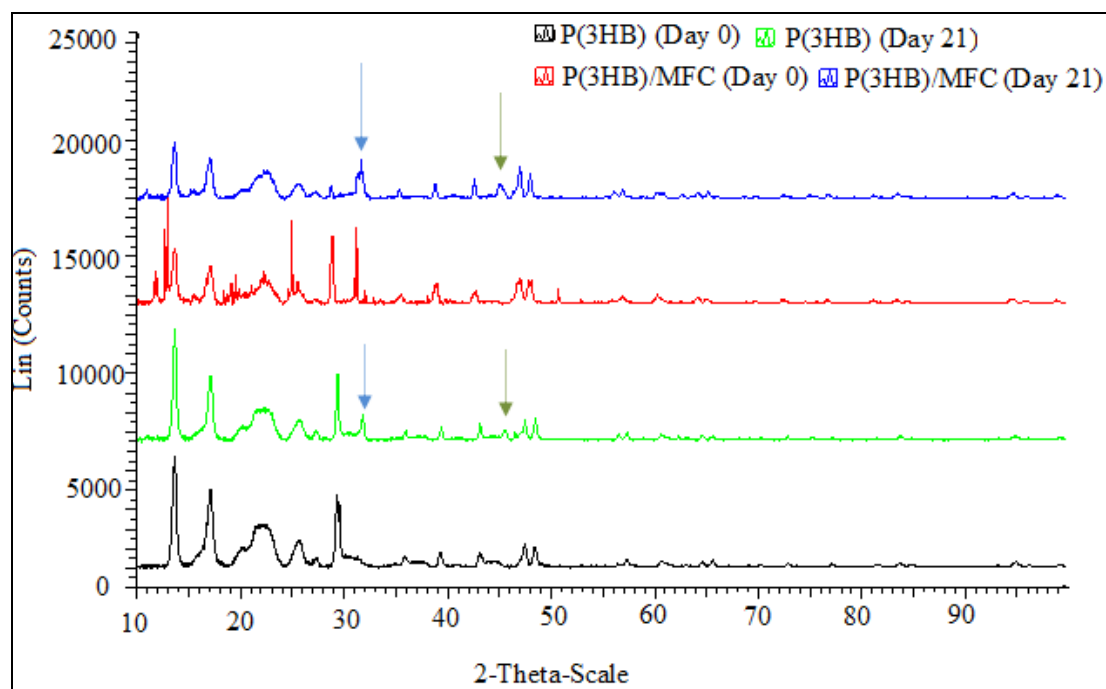


Figure 5.22 X-ray diffraction spectra of P(3HB)/MFC scaffolds immersed in SBF for a period of 21 days.

5.4.5 Differential Scanning Calorimetry (DSC)

Apart from additives influencing the thermal properties of pure materials, it is expected that degradation and bioactivity could also influence the thermal properties of composite materials over a period of time. Hence, the influence of bioactivity and degradation on the thermal properties of P(3HB)/MFC composite scaffold immersed in SBF for 30 days was investigated. The thermal analysis performed in this study was carried out under a constant heating rate of 20 °C/min to resolve the thermal transitions in P(3HB)/MFC composite scaffold before and after immersion in SBF over 30 days. Typical DSC thermograms of P(3HB)/MFC composite scaffolds is shown in Figure 5.23, which outline the first and second heat scan for the composite scaffolds as well as the crystallization temperatures at different time points during incubation in SBF. The results obtained showed the presence of an additional secondary melting temperature, T_m on the first heat scan of the composites after immersion in SBF. Also, obvious in Table 5.4 is the gradual increase with time in the T_m of

the additional secondary melting temperature in the first heat scan. However, no significant difference ($p>0.05$) was found in the melting temperature (during the first heat scan) of the composites material before and after incubation in SBF. But a slight gradual increase in the secondary melting temperature was observed after immersion in SBF. Statistical difference ($p<0.01$) was found between the crystallization temperature, T_c of the P(3HB)/MFC composite scaffold at different incubation times. There were also fluctuations in the heat of fusion in the DSC thermogram values for both T_m and T_c of the composite scaffold.

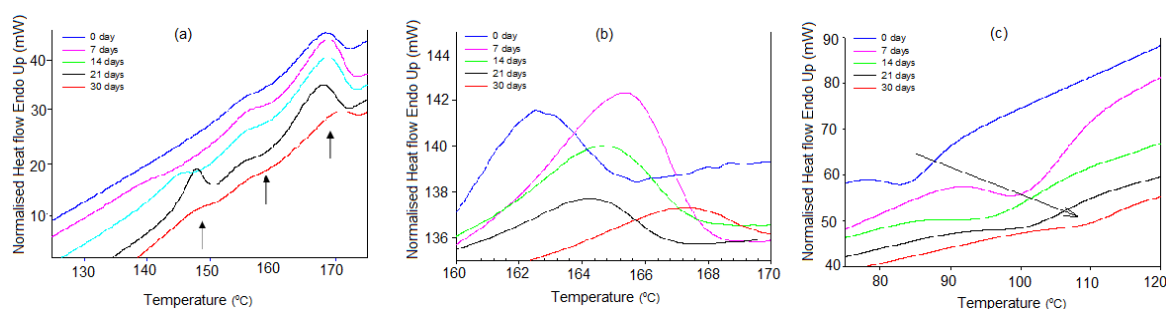


Figure 5.23 Normalised DSC (a) first heat scan (200 °C to -50°C) (b) second heating curve (200 °C to -50°C) (c) cooling curve (200°C to -50°C), obtained at a heating rate of 20°C for P(3HB)/MFC composite scaffold immersed in SBF for various time points (0, 7, 14, 21, 30). The arrows indicate the peaks observed in the heat scan profile

Table 5.4 Effect of degradation and bioactivity on the thermal properties of P(3HB)/MFC composite scaffold immersed in SBF for different time points

Time Points (Days)	1 st Heat Curve						2 nd Heat Curve, T_m		T_c	
	Primary Peak, T_m		1 st Secondary peak, T_m		2 nd secondary peak, T_m					
	T_m °C	ΔH_f (J/g)	T_m °C	ΔH_f (J/g)	T_m °C	ΔH_f (J/g)	T_m °C	ΔH_f (J/g)	T_c °C	ΔH_f (J/g)
0	167.68	20.20	155.38	1.31	-	-	162.51	17.99	83.81	-23.26
7	168.49	22.49	155.22	2.97	139.68	1.21	165.20	17.99	100.79	-41.28
14	168.77	22.10	155.49	2.17	144.80	2.34	164.54	31.34	95.89	-33.10
21	167.77	18.57	155.14	1.17	147.69	9.14	164.14	27.35	101.03	-30.18
30	169.36	20.22	156.41	1.84	147.67	4.035	166.76	23.49	109.15	-41.76

5.5 Cytocompatibility study of P(3HB)/MFC composite materials using Murine ATDC-5 cell lines

5.5.1 Cell Proliferation on P(3HB)/MFC composite material

The Murine ATDC-5 cell line has been well characterised and validated as an *in vitro* model of chondrogenesis (Challa *et al.*, 2010) and based on this fact, the cell line was chosen to gain more understanding on the biocompatibility of the P(3HB)/MFC composite on cartilaginous cell line. Cell proliferation study of ATDC-5 cell lines on P(3HB)/MFC composite films was measured using the Alamar blue assay. The detailed methods employed in the study are described in Chapter 2, Section 2.5.1. The result of the assay performed shows that the control (tissue culture plastic), neat P(3HB), 40 wt% and 50 wt% MFC showed increase in cell proliferation with time. The cell growth was found to be highest on the composite containing 40 wt% MFC when compared to the other composite samples. Furthermore, the pattern of progressive cell growth on the 40 wt% MFC with increase in culture time was comparable to that on the tissue culture plastic as shown in Figure 5.24 despite the fact that the rate of growth of ATDC cell lines on the tissue culture plastic was statistically more ($p < 0.05$) than growth on all the P(3HB)/MFC composite films. The P(3HB)/MFC composite films containing 10, 20 and 30 wt% MFC showed decreased cell proliferation at day 7 Figure 5.24.

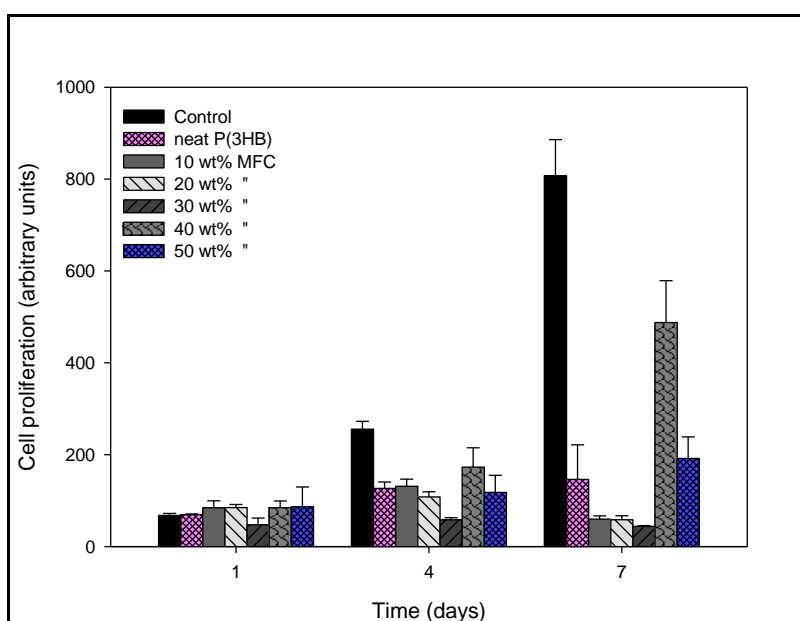


Figure 5.24 Cell proliferation study using Alamar blue assay for P(3HB) and P(3HB)/MFC composite films on day 1, 4 and 7 (n=3)

To further understand the behaviour of ATDC cell line on the P(3HB)/MFC composite materials, ATDC cell lines were grown on the composite 3D scaffolds. Figure 5.25 shows a different trend of growth pattern of the ATDC cell lines on the composite scaffold material than that observed on the composite films. No significant differences ($p>0.05$) were found between cell proliferations on all the samples analysed at day 1. However, on day 4 and 7, slight differences in cell proliferation were noticed on the tested samples. P(3HB)/MFC 3D composite scaffold with 40 wt% MFC content showed a slightly lower cell proliferation at day 4 when compared to other samples tested but at day 7, it was found that the cell proliferation on the 40 wt% MFC content composite sample was slightly higher than those found with the other samples. Also, cell proliferation on the composite samples was found to increase more than the control, i.e. neat P(3HB).

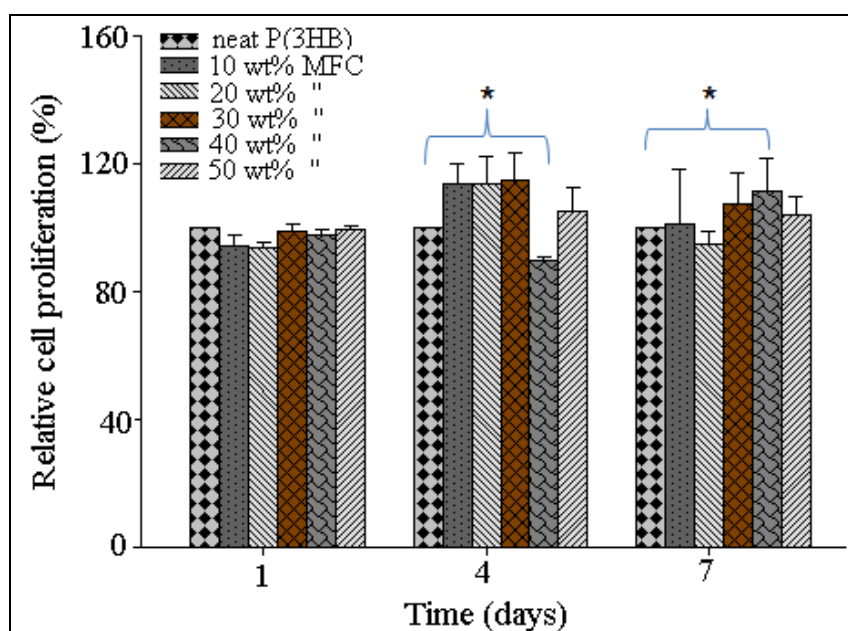


Figure 5.25 Cell proliferation relative to the control (neat P(3HB)) set at 100% for 1, 4 and 7 days growth, using Alamar Blue assay on P(3HB)/MFC composite 3D Scaffold with different amount of MFC contents. Data ($n=3$, error bars \pm SD, $p<0.01$, *) were compared using ANNOVA.

5.5.2 Cell Morphology

A detailed morphological study on cell adhesion and proliferation on the P(3HB)/MFC 2D and 3D composite scaffold was further performed on the composite scaffold containing 40 wt% MFC. The composite was chosen based on the call proliferation of the ATDC cell line

observed on the 2D and 3D scaffolds. The morphology of the ATDC cells culture on the 2D composite films at day 1 and 7 were examined by SEM and typical images are shown in Figure 5.26 and 5.27. The result of the SEM images shows that the ATDC cells attached more, at day 1, on the tissue culture plate (control) than they attached on the neat P(3HB) and P(3HB)/MFC composite (Figure 5.26). Furthermore, observation of the SEM image at day 7 showed that the ATDC cells proliferated more on the tissue culture plate. However, the ATDC cells spreaded out very well and almost assumed the shape of fibroblasts on the composite material while on the neat P(3HB) films, the ATDC cells were more elongated in shape (Figure 5.27).

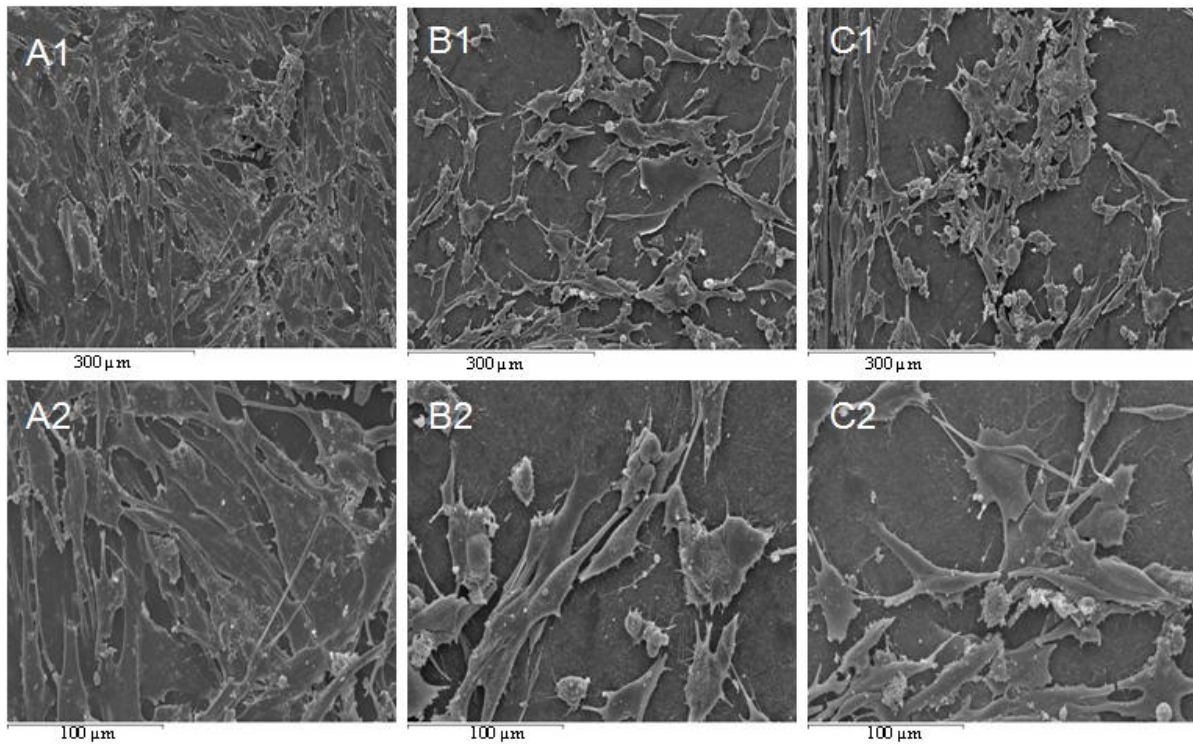


Figure 5.26 SEM images of ATDC cells growing at day 1 on (A) Tissue culture plastic, (B) neat P(3HB) and (C) P(3HB)/MFC composite films shown at lower (x150) and higher (x500) magnifications.

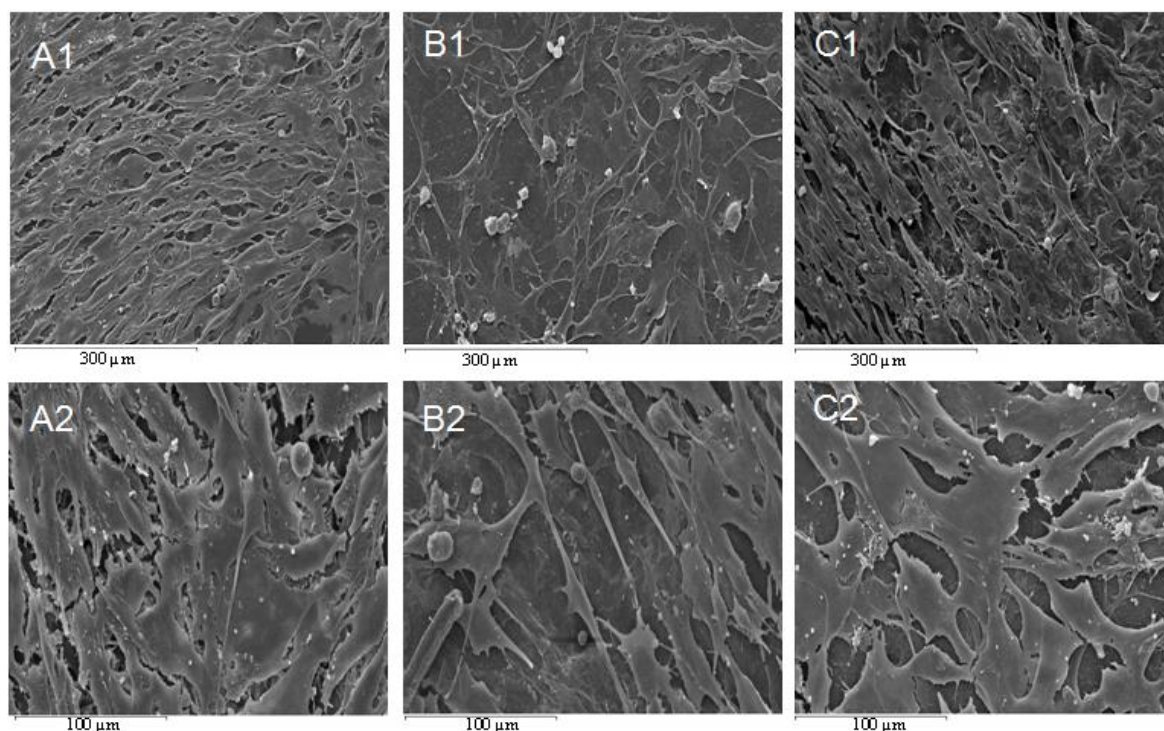


Figure 5.27 SEM images of ATDC cells growing at day 7 on (A) Tissue culture plastic, (B) Neat P(3HB) and (C) P(3HB)/MFC composite films shown at lower (x150) and higher (x500) magnifications.

The morphology of ATDC cells cultured on the P(3HB)/MFC composite scaffold at Day 1, 4 and 7 were examined by SEM and typical images are shown in Figures 5.28, 5.29 and 5.30. The morphology of the scaffold surface proved to provide favourable conditions for the attachment of the cells. This is evident from the cell adhesion, cell division, formation of long filopodia and proliferation depicted at day one in Figure 5.28b, c & e. At day 4, the cells were found to have a more flattened and stretched morphology, overlaying on each other and occupying and taking up the shape of the pore throat (inside the wall of pore opening) (Figure 5.29b, e & f). By day 7, the cells were found to have grown, bridging the pores in the scaffold and continuing overlaying on each other (Figure 5.30). Also, the intracellular communication of cells with one another was evident on all the examined samples as can be observed in Figure 5.28e, 5.29b, and 5.30a, where the cells were found to communicate with each other with their filopodia. In general, there was no evidence of cytotoxicity or verrucous necrosis on cells growing in the scaffolds at days 1, 4 and 7

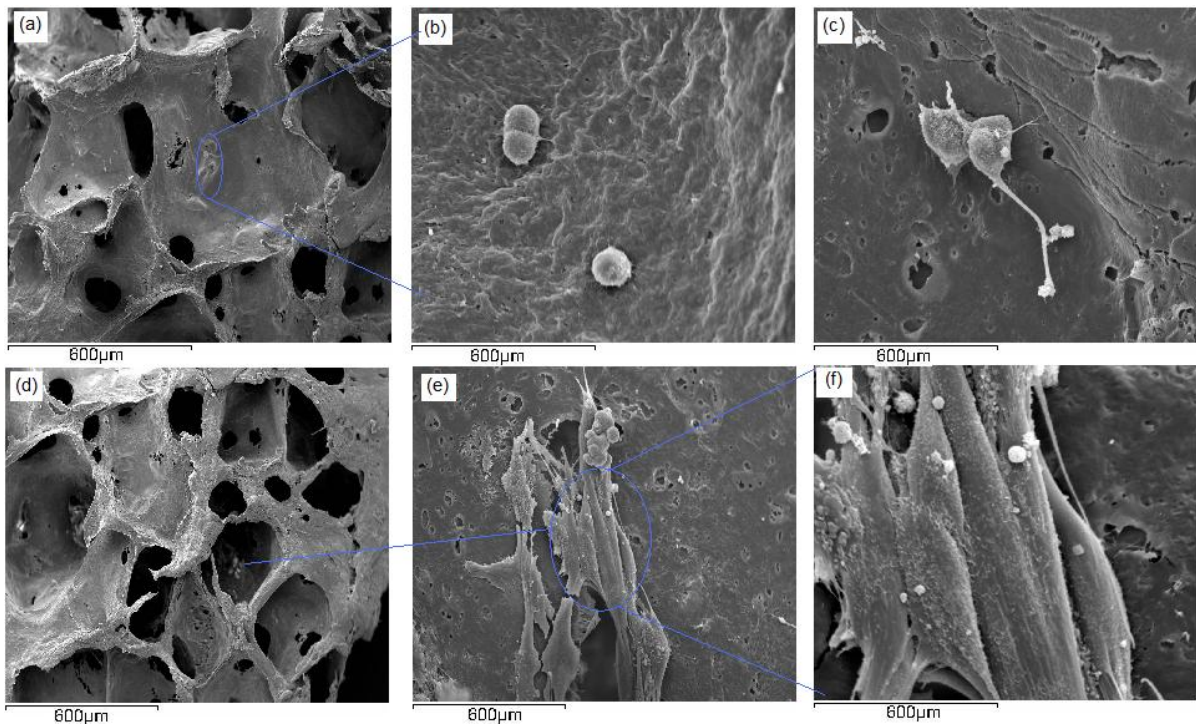


Figure 5.28 SEM micrographs of ATDC cells grown on P(3HB)/MFC composite scaffolds on Day 1; (a) ATDC cells growing on the pores in the scaffold; (b) ATDC cells still in round shape adhering to the nanotopography of the walls of the pores in the scaffold; (c) Cells growing filopodia after division and moving away for flattening; (d) Group of cells growing in the pore of the scaffold material (e) and (f) show a higher magnification of (d) for a clearer view of the cells adhering to one another and attaching themselves with their filopodia for communication.

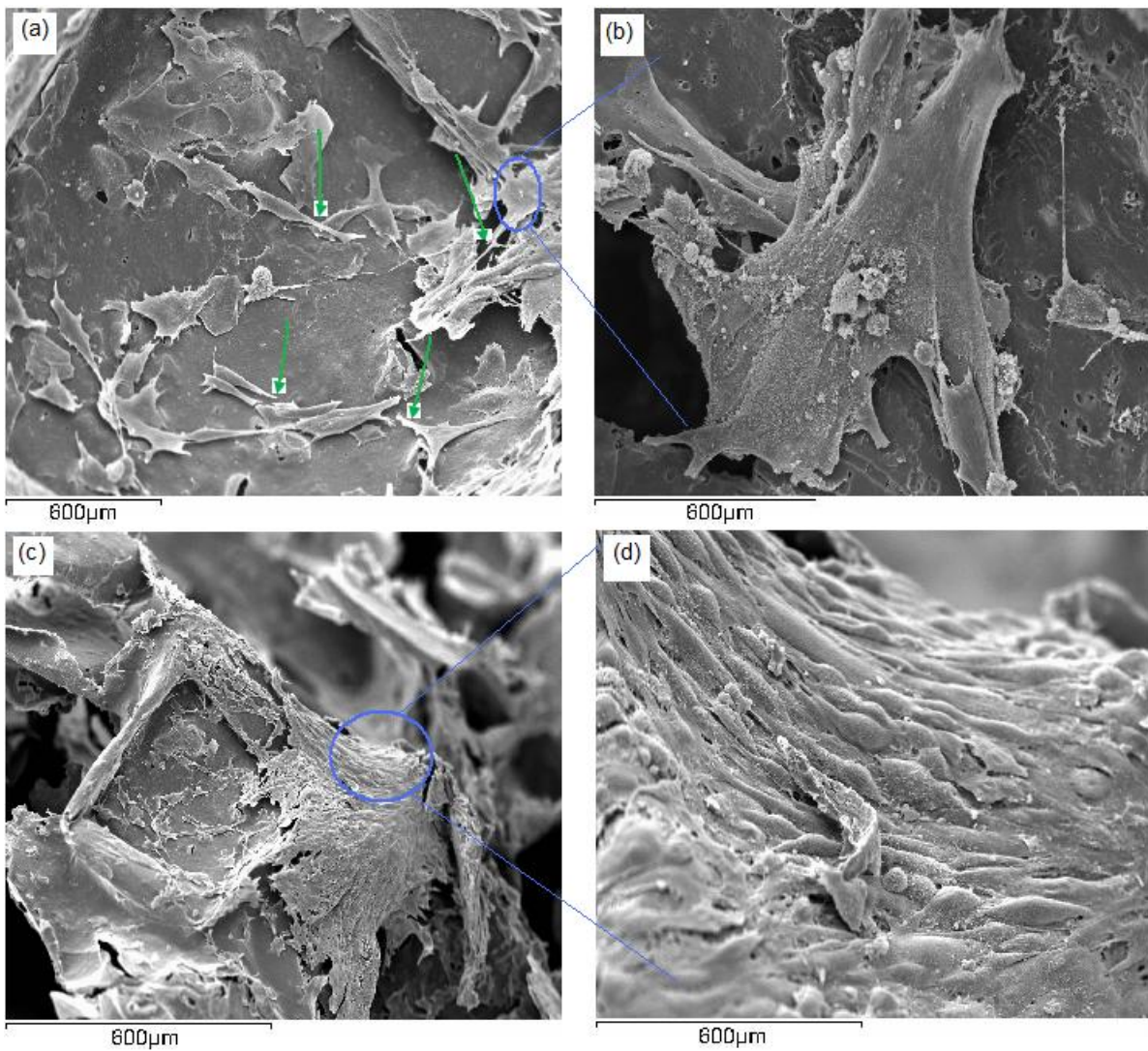


Figure 5.29 SEM micrographs of ATDC cells growing on the pores in the P(3HB)/MFC 3D composite scaffold at Day 4. (a) well spread ATDC cells extending their filopodia for cell-cell communications, (b) A higher magnification of (a) Flattening and layering of ATDC cells on the polymeric composite 3D substrate; (c) highlight the densely growing ATDC cells inside the pore (d) A higher magnification of (c) Rounding up of cells for dividing and higher cell proliferation.

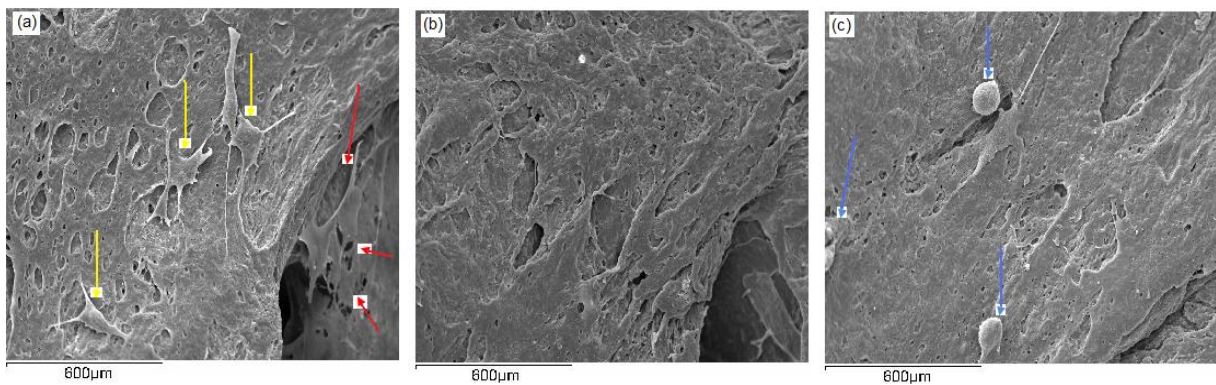


Figure 5.30 SEM micrographs of ATDC cells growing in the P(3HB)/MFC 3D composite scaffold at Day 7. The yellow arrows in (a) indicate the folding and withdrawal of filopodia, possibly for division and the red arrow highlights cells growing and bridging the pores. (b) Well flattened cells on the polymeric 3D composite substrate, while the blue arrows in Figure (c) highlight rounded ATDC cells ready for division.

5.5.3 Whole Protein Production by Murine ATDC-5 cell line grown on 3D P(3HB)/MFC composite

To further understand the capability of the composite material to support the growth of the ATDC cell line, in order to assess future cartilage formation, whole protein production was investigated. The hypothesis behind this investigation was that since cell activities including cartilage formation, can be correlated with the extracellular whole protein production, increase or decrease in the whole protein released into the surrounding medium is an indication of the ability of the test material to hinder or promote cartilage formation. The whole protein production is shown in Figure 5.31. The statistical analysis performed shows no significant difference ($p > 0.01$) among the test materials (neat P(3HB) and P(3HB)/MFC) and between the test material and the control (tissue culture plastic) at various time points investigated.

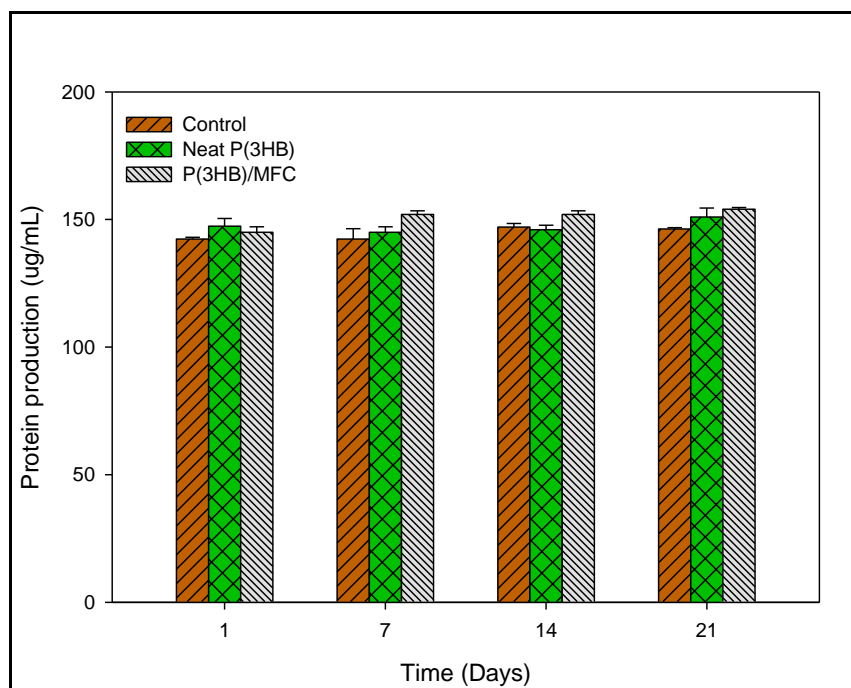


Figure 5.31 Whole protein production by the ATDC cell line grown on tissue culture plate (control), P(3HB) and P(3HB)/MFC composite (40 wt% MFC) for 21 days. Data (n=3, error bars = \pm SD) were compared using ANNOVA.

5.6 Discussions

The uniform distribution and exposure of the microfibrillated cellulose fibres is very important in achieving a mechanically reinforced and uniform surface chemistry on the P(3HB)/MFC composites. MFC microfibrils was observed in the SEM image of the composite material with various MFC content and hence confirmed the presence of microfibrils with diameters in the range of 10-100 nm. Agglomerates of the microfibrils were visible in the composite containing 50 wt% MFC. The presence of aggregates of microfibrils over the surface of the composite film containing 50 wt% MFC highlights the importance of maintaining a balance between the polymeric matrix and the filler (MFC). The reason for the absence of differences between composites containing 10 and 20 wt% MFC was most likely due to the domination of the P(3HB) properties with the MFC network structures being hidden within the large proportion of P(3HB). As the amount of the MFC content increased, the MFC fibrils aggregated and became more packed. This behaviour was due to the hydrophilic properties of the MFC, which led to the agglomeration of the fibrils in a relatively non polar environment comprising of a chloroform solution of P(3HB).

The FT-IR analysis performed on the composite sample confirmed that the process of composite formation did not introduce changes in the structure of P(3HB) and MFC. However, there was an increase and decrease in peak intensities as well as shifting and broadening of the bands which were expected to have an effect on the crystallographic properties of the composite materials as confirmed by the XRD analysis on the composite. Usually, the presence of absorption bands above 3000 cm^{-1} is due to the presence of a C-H \cdots O hydrogen bond (Sato *et al.*, 2004; Matsuura *et al.*, 2003). Thus, the weak band 3335 cm^{-1} can be attributed to the partial acetylation that took place during the modification of the microfibrillated cellulose. The absorption peak at 1226 cm^{-1} represents the characteristic vibrations of the C-O stretching ($\nu_{\text{C-O}}$) while the absorption peak at 1378 cm^{-1} is the methyl in plane bending ($\delta_{\text{C-H}}$) in the materials. The absorption peak at 1720 cm^{-1} represent the carbonyl stretching vibration ($\nu_{\text{C=O}}$). The overall increase in the absorption peaks is possibly due to the composite formed by the addition of MFC to P(3HB) matrix.

X-ray diffraction analysis performed on the composite material showed significant differences between the composite material and individual polymers before composite formation. The differences can be attributed to the change in the crystallographic properties of the composite materials. The increase in the number of peaks was expected as a result of the combined properties of both neat P(3HB) and MFC in the composite. This is expected to result in an overall increase in the crystallinity of the composite material as compared to the neat P(3HB) and cellulose. The narrowing of the peaks in the X-ray diffraction pattern of the composite is possibly due to a slight degradation of the polymers during composite fabrication or due to interactions of the two polymers at the interphase. Also, the slight shift in some of the bands observed in the spectrum of the composite material indicated changes in the unit cell leading to lattice changes in the structure of the composite material. These effects can be attributed to the effect of the chemical solvent employed during fabrication. The fact that the peaks of the X-ray diffraction pattern of the composite material were narrower than found in the individual polymeric materials confirmed less atomic rearrangement in the composite material due to the differences in physical properties (hydrophilicity-hydrophobicity) of individual polymers in the composite material.

The additional peaks found in the spectra of both neat P(3HB) and the P(3HB)/MFC composite, after immersion in SBF could be attributed to compound(s) deposition/formed on the surface of the materials. Misra *et al.* and Li *et al.* have reported the formation of

hydroxyapatite on the surface of the P(3HB)/BG surface after incubation in SBF (Misra *et al.*, 2007; Li *et al.*, 2004). According to Misra *et al.* the new peak at 32° was due to the formation of hydroxyapatite. The new peaks found in the spectra of both neat P(3HB) and the P(3HB)/MFC composite immersed in SBF was also found to be at 32° confirming the formation of hydroxyapatite. However, possibly due to the short period (21 days) of the degradation/bioactivity study and the small amount of compound formed it was not possible to observe a high intensity peak. Despite the low intensity of the peak at position 32 2 θ observed, the formation of hydroxyapatite confirmed that the composite material would exhibit some level of bioactivity when utilized as a biomaterial for cartilage regeneration. Another peak that was found at 47° was possibly due to the formation or deposition of another compound on the composite material. Further studies will be needed to verify the compounds formed during the bioactivity/biodegradation investigations. The loss of peaks by the test materials incubated in SBF can be attributed to the degradation processes taking place on the materials or due to loss of crystallinity. The broadening and shifting of bands found in the spectra of the SBF immersed composite material were due to the atomic rearrangement and unit cell changes in the crystal lattice of the material. Additives are known to influence the thermo-mechanical properties of composite materials as well as their degradation rate. This phenomenon has been reported in the work of Blaker *et al.*, 2005 and Buzarovska and Grosdanov, 2009. Blaker and co-worker found that addition of Bioglass® to polymeric material during composite fabrication led to a considerable change in the thermal properties of the resulted composite material. On the other hand, Buzarovska and Grozdanov investigated the effect of addition of different amounts of poly(dicyclohexylitaconate) (PDCHI) to poly(hydroxybutyrate-co-hydroxyvalerate), P(3HB-co-3HV) during P(3HB-co-3HV)/PDCHI composite fabrications on the thermal properties of the composite materials. The result of their investigation confirmed that addition of PDCHI to P(3HB-co-3HV) altered the thermal properties of the composite material. This phenomenon was investigated in this study and results showed that the melting and crystallization temperature of the composite material decreased proportionally to the amount of MFC added in the composite material. Though, the decrease in T_m was not significant, but the decrease in T_c of the composite material on addition of different amount of MFC was significant ($p < 0.001$). A similar observation has been observed in the work of Misra *et al.*, 2007 in their work on the P(3HB)/Bioglass® composite. Samir *et al.* have also observed a similar proportional decrease in T_m and T_c with increase in the amount of tunicin whiskers in tunicin

whiskers/poly(ethylene oxide) nanocomposite (Samir *et al.*, 2004). In PEO/tunicin whiskers the T_m and crystallinity index of PEO were significantly decreased by the presence of tunicin whiskers. Furthermore, changes in the morphological structure of the composite material like increased spherulitic growth with increase in the amount of MFC in the composite material could be the result of decrease in T_m and T_c of the material. In the presence of MFC, P(3HB) crystallization was hindered by the dispersion of cellulose nanofibres yielding smaller and less stable crystals. Apart from morphological effects, the slight decrease in the melting temperature may have also arisen from thermodynamic effects of miscibility of MFC and P(3HB) matrix (Kondo and Sawatari, 1994).

In addition to the slight decrease in T_m and T_c , there was emergence of a secondary melting peak. The emergence of the secondary melting peak suggested that addition of MFC may have cause the formation of crystals which melt at temperature lower than the melting temperature of P(3HB) matrix. The decrease in the crystallisation temperature of the composite material is possibly due to changes in the lattice structure due to the introduction of MFC within the P(3HB) crystalline lattice. The decrease in crystallinity of the composite material can also be confirmed by the loss of peaks observed in the X-ray diffraction spectrum of the composite material. As the concentration of the MFC in the composite material increases, the changes in the lattice structure increases and this reflected in further decrease in the crystallization temperature of the composite material as highlighted in Table 5.1.

The absence of secondary melting peaks in the second heat scan of the composite material with increase in MFC content from 5 to 40 wt% suggested that the spherulitic growth in the composite material degraded during the heating scan. Since the melting temperature of P(3HB) has been reported to be between 53-180 °C (Zinn and Hanny, 2005) and the composite material was heated at 200°C, it is also possible that the P(3HB) in the composite material may have degraded.

The combined effect of the surface charge, surface free energy and wettability is necessary in understanding the role of surface chemistry towards the applicability of the biomaterial as a scaffold to be used *in vivo*. In this study, a cationic surface charge was confirmed for the P(3HB)/MFC composite materials through a positive staining with Rose Bengal, a dianionic dye. It can be confirmed that the MFC was responsible for the cationic surface chemistry since the colour intensity of the materials stained with Rose Bengal increased with increase in

the amount of the MFC content in the composite. The neat P(3HB) possibly have a weak anionic surface charge since it stained positive with toluidine blue, a monocationic dye and not Rose Bengal.

The surface hydrophobicity/hydrophilicity of the composite materials was determined through the water contact angles measured using the sessile drop method described in detail in Chapter 2, Section 2.4.1.3. The water contact angle measured on the neat P(3HB) film was 68.1 ± 6.7 which is slightly lower than the $70 \pm 5^\circ$ reported by Wang *et al.*, 2003. As expected, the water contact angle of the composite films were slightly lower than the water contact angle of the neat P(3HB). This shows an increase in the hydrophilicity and decrease in hydrophobic properties of the composite polymeric matrix. As the amount of MFC content increased, the water contact angle decreased and reached a minimum value with the 50 wt% MFC content. The progressive decrease in the water contact angle of the composite material as the amount of MFC content increases can be attributed to the changes in the micro structural properties of the composite materials caused by increasing amount of the MFC content, which was confirmed by the SEM image of the films in Figure 5.1. As the amount of MFC content increases, the hydrophilic MFC fibrils become more exposed, hence, there are more tendencies of the exposed fibrils to hold and absorb more water than the fibrils embedded within the polymer matrix. The same observation has been made by Li *et al.*, 2004. They observed a decrease in the water contact angle of P(3HB-co-3HV) from $65^\circ \pm 1.3^\circ$ to $32^\circ \pm 1.5^\circ$ as the amount of Bioglass[®] filler increased from 0 to 20 wt%. As shown in Table 5.5 below, the water contact angle, surface charge and chemical properties of the materials correlated with the amount of MFC content in the polymer matrix.

Table 5.5 Surface chemistries of the neat P(3HB) and P(3HB)/MFC composite

Material	Rose Bengal stain	Toluidine blue stain	Chemical properties	Water Contact Angle (°)
P(3HB)	-	++	Hydrophobic	68.1 ± 6.7
10 wt% MFC	+	++	Hydrophilic	62.5 ± 3.5
20 wt% MFC	+	++	Hydrophilic	61.7 ± 6.1
30 wt% MFC	++	+	Hydrophilic	60.2 ± 3.2
40 wt% MFC	+++	+	Hydrophilic	60.1 ± 4.2
50 wt% MFC	+++	+	Hydrophilic	49.8 ± 2.7

The biodegradation of PHAs and its blends involves many aspects such as structural, mechanical, physical or chemical degradation. Usually all these forms of degradation are interrelated and a composite model can be built to mathematically equate and link the various forms through which biodegradation of PHAs can be ascertained (Wu *et al.*, 2004). The parameters measured in this study to assess the degradation behaviour of the P(3HB)/MFC composites were: water uptake, pH change, change in the Raman shift spectrum (i.e. change in chemical composition) of degrading samples, differences on the X-ray diffraction spectra of the original samples and degraded samples and differences in the measured thermographic properties of the degrading samples. The result of the degradation studies showed that the addition of MFC in the P(3HB) matrix increased the capacity of the composite to absorb water. Since cellulose is a hydrophilic polymeric material, it is expected that the microfibrillated cellulose fibrils will have more affinity to water and thus absorb more water than the neat P(3HB). As the incubation time increased, the rate of absorption of water increases. This phenomenon is possibly because during the early stage of immersion of the composite in SBF, only the fibrils present on the surface of the film absorbed water and somehow get saturated but the fibrils embedded inside the polymer matrix needed more time for the water to infiltrate and saturate them. Hence, the longer the incubation time, the greater the increase in the percentage water absorption. On the contrary, the neat P(3HB) absorbed less amount of water than the composite material. During the first 14 days of incubation in SBF, the amount of water absorbed was constant. This was as a result of the hydrophobic properties of the polymer which tends to repel water by the material. After 14 days of incubation, the rate of water absorption by the neat P(3HB) was found to have improved. This might have been due to an increased ionic deposition on the surface of the P(3HB) film which resulted in an increased affinity of water by the surface of the polymeric material. This ionic deposition may be responsible for the decreased weight loss observed between 21 and 28 days of incubation period.

The increase in percentage weight loss observed between 21 and 28 days of incubation of the composite is possibly the result of detachment of the microfibrils with prolonged increase in incubation time. Due to the deposition of ions onto the surface of the composite material, it is possible that the weak bond that bound the microfibrils together with the P(3HB) were weakened thereby leaving the microfibrils weakly bonded onto the polymer. With time, the microfibrils on the surface gradually detached thereby exposing the composite material to

further change in physical properties and degradation. Although, both the neat P(3HB) and the composite showed an increase in percentage weight loss which can confirm the degradation of the materials, the neat P(3HB) degraded faster than the composite material. Since the presence of additives in polymer matrix can affect the degradation rate of the material (Li *et al.*, 2004), it is possible that the presence of the MFC in the polymer matrix delayed/hindered the degradation of the composite due to formation of spherulitic growth during composite fabrication.

Gopferich has observed that pH is an important factor that influences the rate of hydrolysis during degradation in polymers (Gopferich, 1996). The pH of the SBF in which both types of samples were immersed rose a little above the initial pH of the buffer (7.35) and reached a maximum value of 7.90 after 14 days before decreasing to 7.62. The degradation product of P(3HB) is a hydroxy butyric acid, thus, with increase in degradation, the pH of the immersed SBF will be expected to decrease. Although, both the neat P(3HB) and composite polymer followed the same trend of initial rise and subsequent fall in pH, the composite polymeric materials were found to exhibit a slightly higher initial rate of increase in pH as shown in Figure 5.12. The initial rise in pH is obviously due to the leaching out of an unknown alkaline component from the composite material. Further study will be needed to confirm what the compound was and source of the compound in the composite material.

Surface nanotopography is very important for the adhesion of mammalian cells on biomaterials. This was investigated on the fabricated scaffold to ensure its efficiency in sustaining the proposed application in cartilage regeneration. The SEM image in Figure 5.15 displayed surface nanotopography on the throats of the pores in the scaffold. The surface nanotopography can be attributed mainly to the MFC filler. The surface structures of the sucrose grains which formed the pores would have also contributed to the nanotopography. The interconnected pore network in the scaffold was as a result of the amount of sucrose grains added and the homogenous mixture of the polymers and the sucrose grains during scaffold fabrication.

The stress-strain curves demonstrated the typical behaviour of a 3D scaffold undergoing deformation. The linear-elastic region represents the period of loading of the 3D scaffold with strain. At this stage, the 3D scaffold can still withstand the strain applied to it without much deformation. As the strain increases, the 3D scaffolds reached the offset yield strength and maintain a steady stress represented by the plateau in Figure 5.16. Further increase in the

strain led to the crushing of the 3D scaffold which resulted in a densification process in the 3D scaffold. This phenomenon caused the stress level to rise quickly which resulted in the steeply rising stress profile.

Incorporation of additives into a polymer matrix is an effective way of improving the physico-mechanical properties of biomaterial for a specific tissue engineering applications. Li *et al.*, 2004 observed the improvement of the compressive yield of P(3HB-co-3HV) by 156% of the initial strength of the polymer on addition of 20 wt% of Bioglass[®]. In the present study, the tensile strength, Young's modulus, compression modulus and compressive yield strength of the polymer have been improved significantly by the incorporation of varying amount of MFC in the polymer matrix. Since the MFC was modified to improve compatibility between the cellulose fibrils and the polymer matrix, it is expected that the P(3HB) will interact with the cellulose microfibrils using hydrophobic interaction on addition of the MFC and occupy the interfibrillar space. The presence of the MFC will restrain the movement of the P(3HB) on application of force resulting in increased Young's modulus. Also, it is possible that the microfibrils were able to withstand more stress and prevent the deformation of the microstructural scaffolds when strain was applied. Thus, increase in the amount of MFC, led to an increase in the compressive modulus and compressive yield strength of the composites. However, there is a limit to the amount of MFC that can be added to the polymer matrix to increase the compressive yield strength. This was proven by the decrease in the compression modulus of the composite containing 50 wt% MFC. The maximum compression modulus (0.186 ± 0.09 MPa) achieved with the 40 wt% MFC composite reduced to 0.161 ± 0.017 MPa with the addition of 50 wt% MFC. The cause of the reduction in the compressive modulus could be due to a weak interphase between P(3HB) and the cellulose fibrils beyond a certain wt%. As the amount of MFC increased, the weak interphase and shear forces between the polymer and MFC interphase continued to increase. This increase may have possibly resulted in the failure of the material when strain was applied to the composite materials beyond a certain limit.

Cell proliferation study of ATDC cell lines on P(3HB)/MFC 2D and 3D composites materials were carried out using Alamar blue assay. The proliferation assay performed on the P(3HB)/MFC composite films (2D material) showed the extent of cell growth to be highest on the composite containing 40 wt% MFC when compared to the other composite samples. The maximum value for the ATDC cell proliferation was 78% less than that of the control

surface. However, there was better ATDC cell proliferation on composites containing 10, 20 and 30 wt% MFC rather than the neat P(3HB) films. A possible reason for the lower cell number on the 2D composite films containing 10, 20, 30 wt% MFC at 7 days could be due to the non-optimal hydrophobic/hydrophilic surface chemistry of the composite materials. Also, interactions between the absorbed protein and hydrophobic surface can change the protein conformation of the absorbed protein thereby making ligand moieties needed for integrin binding and cellular adhesion inaccessible. In addition to the above mentioned factors, the slow growth seen on the P(3HB)/MFC composite film containing 50 wt% MFC at day 4 and 7 could result from the absorption of excess water by MFC which can create a barrier to protein adsorption resulting in inhibition of cellular adhesion. Upon exposure to serum-containing medium, albumin which is the most abundant serum protein preferentially adsorbs onto the surfaces of the P(3HB)/MFC composite during the early phase of formation of an adsorbed protein layer. Then, the adsorbed albumin is replaced by cell adhesive proteins such as fibronectin and vitronectin. The inability of the cell adhesive protein to replace albumin due to the affinity of the albumin to the surfaces, caused by high wettability or surface chemistry, may have resulted in lower cell proliferation during later stage of cell culture as observed in day 4 and 7 of the investigation. In addition, it is possible that the ATDC cells attached strongly to the surface of the composite material. Chondrocytes must adhere to a surface to be able to grow and proliferate but if the adhesion is too strong, growth and proliferation is prevented (Sieminski and Gooch, 2000). The more extended morphology of the ATDC cells growing on the P(3HB)/MFC composite (Figure 5.26c and 5.29b), is possibly due to the fact that chondrocytes adhered more strongly on the materials (2D film and 3D scaffold) due to surface charges. Svensson *et al.* had observed similar effect on chondrocytes growing on neat bacterial cellulose (Svensson *et al.*, 2004).

The results of the cell proliferation assay performed on the 2D and 3D composite material corresponded with the observations in SEM images of the ATDC cells growing on the samples. However, the cell proliferation results achieved with the 3D composite materials (neat P(3HB) and P(3HB)/MFC containing 40 wt% MFC) did not differ much. This can be attributed to the microstructure, the 3D topography and the presence of 3D pores where cells can infiltrate, resulted in better growth. Chondrocytes obtain a more extended morphology when growing on a two-dimensional surface, while a three-dimensional structure supports chondrocyte proliferation and differentiation (Hutmacher, 2000). In other words, rather than

the surface hydrophilicity, the 3D structure was the dominant factor in enhancing cell adhesion and proliferation. Hence, the ATDC cells were able to proliferate in both neat P(3HB) and the P(3HB)/MFC 3D composite scaffolds. A qualitative analysis of cell adhesion and distribution was further carried out by SEM observation of 2D samples at day 1 and, 7 and 3D samples at day 1, 4 and Day 7 of cell culture. The SEM study confirmed cell adhesion and proliferation on the 2D composite material at day 1 and day 7. The fact that the ATDC cells flattened out on the surface and proliferate proved that the 2D composite material provided a conducive environment for the cells to adhere, proliferate and differentiate. Also, The SEM study confirmed the infiltration and migration of ATDC cells deep into the porous network of the 3D composite structure. At Day 7, ATDC cells were found to have grown to a thick layer and flattened out indicating a favourable environment for their growth (Figure 5.30). On closer examination of the surface at higher magnification it was confirmed that the P(3HB)/MFC scaffold surface allowed ATDC cell attachment, cellular communication (indicated by the attachment of filopodia) as well as cell division (indicated by cell couplets) as shown in Figure 5.29. A flattened morphology of ATDC cells is also evident in the figure. Cells can obviously be seen attaching to the throat of the pores of P(3HB)/MFC scaffolds. A well highlighted feature is the alignment of the ATDC cells to the physical shape of the scaffold as observed in Figure 5.30. The cell attachment identified on the 3D composite structure further suggests the fact that the surface morphology and microstructure of the composite material played an important role in cell adhesion and spreading. The SEM results further prove the fact that P(3HB)/MFC scaffold is a cytocompatible substrate that can provide structural support for the cells to acquire the desired shape and morphology.

The investigation on the total protein production showed that both the control and the test materials did not hinder total protein production throughout the period of the investigation. However, Hardingham *et al.* have observed that chondrocytes grown on bacteria cellulose monolayer became fibroblastic and lost their characteristic pattern of matrix protein production (Hardingham *et al.*, 2002). Thus, the result of the total protein production indicated that the P(3HB)/MFC composite material is able to support growth of chondrocytes and possibly does not induce the cells to differentiate into fibroblasts. These results indicate that the composite material will be able to support cartilage regeneration better than bacterial cellulose.

The outcome of the experiments carried out in this Chapter was to demonstrate that the P(3HB) and P(3HB)/MFC scaffolds prepared using compression moulding/particulate leaching technique were appropriate supports for allowing cell adhesion and proliferation. The various characterization studies including biodegradation, bioactivity, cytocompatibility results have confirmed the P(3HB)/MFC composite scaffold to have excellent physico-mechanical properties; biocompatibility towards the Murine ATDC-5 cell line. Such cytocompatibility of another member of the PHA family such as (P(3HB-co-3HV) with respect to osteoblasts has also been observed by Kumarasuriyar *et al.*, 2005. Thus biodegradable polymers such as P(3HB) and cellulose are excellent green materials with biocompatible and biodegradable properties. Also, the credibility of the developed compression moulding/particulate leaching method of preparing biodegradable scaffold for tissue engineering has also been achieved. Finally, a new composite material of medical importance has been produced in this study. This technology could be used for the production of templates for *in vitro* and *in vivo* synthesis and regeneration of new tissues.

5.7 Conclusions

The mechanical and structural properties in combination with the degradation and detailed biocompatibility studies discussed in this chapter provided a better understanding of the effect of microfibrillated cellulose on the P(3HB)/MFC composite properties. The results obtained highlighted the advantages of incorporating microfibrillated cellulose in the P(3HB) polymeric matrix, which among other features, significantly enhanced mechanical strength of the scaffolds. The study further highlighted the role of MFC in inducing microtopography and hydrophilicity to the composite, which regulates the level of surface wettability (up to 12% decrease in water contact angle) and protein adsorption (up to 26.5% increase) on the surface of the composite. Furthermore, all the analyses carried out showed a considerable and significant difference ($p < 0.01$) in the properties between the neat P(3HB) and P(3HB)/MFC composite and among the P(3HB)/MFC 2D and 3D composites with varying MFC content. The bioactivity of the P(3HB)/MFC composites was confirmed by the formation of crystalline hydroxyapatite on the composites' surfaces after immersion in SBF for 21 days. *In vitro* degradation studies confirmed that the addition of MFC to the polymeric matrix significantly increased the water uptake.

Whilst, statistical differences were found in cell proliferation between the composite, neat P(3HB) films (2D) and the control surface (tissue culture plastic), no significant difference ($p>0.05$) in cell proliferation was found between the neat P(3HB) and the 3D P(3HB)/MFC composite scaffolds containing 40 wt% MFC. P(3HB) and P(3HB)/MFC scaffolds showed highly compatible surfaces for the adhesion and proliferation of the ATDC cells. The nanotopography of the throat of the pores in the scaffold was confirmed to have played a critical role in enhancing cell adhesion while the large pore sizes (60-83 μm) allowed infiltration and migration of ATDC cells deep into the porous network of the scaffold. Hence, in the 3D scaffolds the microstructure, pore architecture and size overruled the influence of the MFC on the hydrophilicity of the composite scaffold.

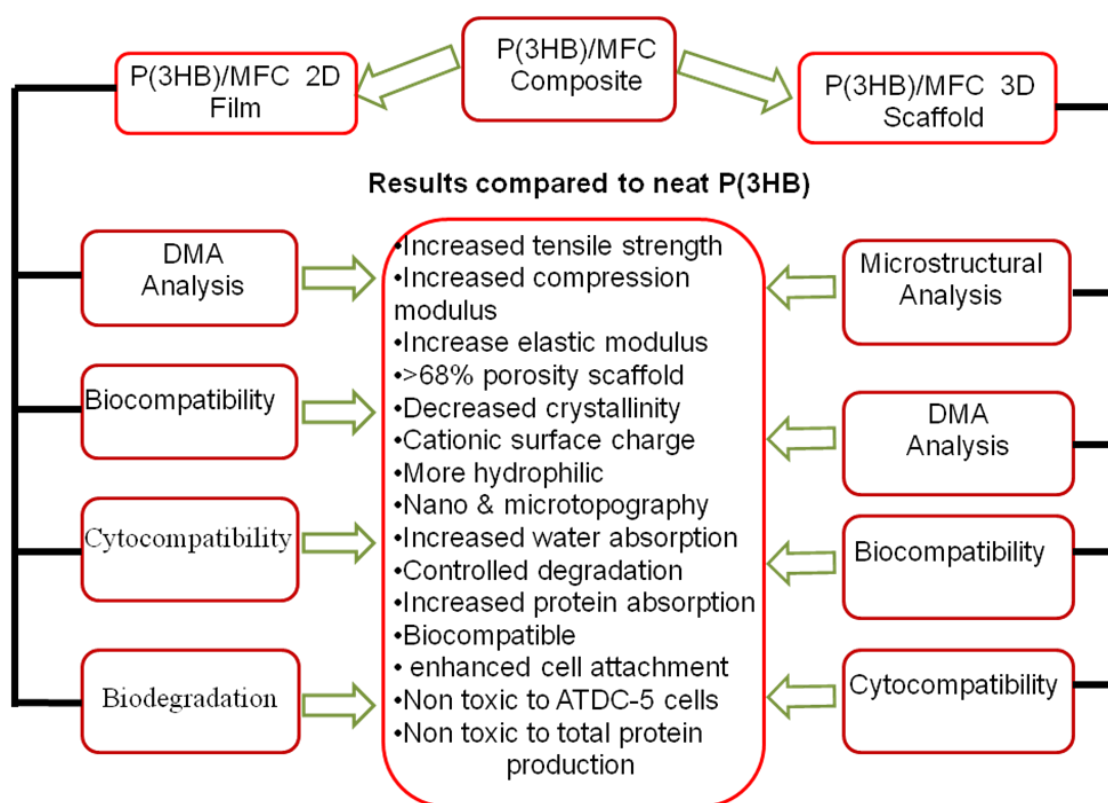


Figure 5.32 Schematic representation of investigations and results achieved compared to neat P(3HB) 2D and 3D structures

Chapter 6

POTENTIAL APPLICATION OF P(3HB)-BASED MAGNETIC NANOCOMPOSITES IN HARD TISSUE ENGINEERING

Chapter 6

6.1 Introduction

Recently, interest in tissue engineering and its solutions has increased significantly with bone and cartilage regeneration by autogenous cell delivery or tissue regeneration becoming one of the most promising modes of orthopaedic surgery. In particular, scaffolds have become fundamental tools in bone graft substitution and are used in combination with a variety of bio-agents (Bock *et al.*, 2010). Regenerative medicine benefits from biocompatible scaffolds on which stem cells can grow and differentiate, either under preliminary *ex vivo* conditions for further grafting into the injured organ, or as a result of direct *in vivo* implants. Tissue engineering scaffolds offer micro-structured 2D or 3D surfaces for cell attachment, differentiation and proliferation (Corchero *et al.*, 2010). In addition, scaffolds provide biomechanical properties that are suitable for supporting novel tissue structures and with no toxic effects. However, studies have demonstrated the need for stimulators of cell attachment, as many polymeric materials used for scaffold fabrication inhibit cell colonisation. Hence, to solve the problem of cell colonisation, growth factors and cell ligands are incorporated as biologically-active molecules to pattern the scaffold surfaces and thus facilitate cell attachment and expansion.

Current and future applications of magnetic nanoparticles in biology and medicine have been largely dependent on their nanometer-size particles (3-10 nm in diameter) which exhibit novel magnetic, chemical and bio-medical properties (Kim *et al.*, 2002). Maghemite, $\gamma\text{-Fe}_2\text{O}_3$, is a technologically important compound widely used for the production of magnetic materials and catalysts. As a confirmation of cytocompatibility of magnetic material in tissue engineering, an emerging tissue engineering strategy, magnetic force-based tissue engineering (Mag-TE), employs cells that have been magnetically labelled with magnetite cationic liposomes (MCLs). Such MCL-labelled cells can be manipulated and organised by magnetic force, and maintain their functionality. Thus MCLs are not toxic. Furthermore, the used of magnetic material to manipulate cells have been tested in many cell lines including mesenchymal stem cells, cardiomyocytes (Shimizu *et al.*, 2007), human umbilical vein endothelial cells (Akiyama *et al.*, 2009), retinal pigment epithelial cells (Ito *et al.*, 2005) and keratinocytes (Ito *et al.*, 2004).

In this study, polymeric P(3HB) based magnetic (maghemite) composite scaffolds were successfully developed using a simple and inexpensive compression moulding/particulate leaching technique. The two different types of magnetic composite scaffolds produced included P(3HB)/Magnetic nanoparticles, P(3HB)/MNP and P(3HB)/Ferro fluid, P(3HB)/FF. The developed magnetic scaffolds were further characterised for their magnetic properties as well as the effects of addition of magnetic materials (particles and fluid) on the thermo-mechanical properties of the composite scaffolds. FT-IR and XRD were employed to study the crystallographic properties of the scaffolds. *In vitro* degradation study of the composite scaffolds was performed in simulated body fluid (SBF) for a period of 30 days to understand the effect of introduced magnetic materials on the biodegradation of the composite scaffold. SBF was chosen because it has similar ionic concentration to human blood plasma (Kokubo *et al.*, 1991). Maghemite was used for the manipulation of the nano- and micro-environments on P(3HB) scaffolds in order to promote protein adsorption and subsequently, stimulate cell proliferation. Cytocompatibility studies on the magnetic scaffolds were carried out using Human Osteosarcoma MG-63 (MG-63) and cell proliferation was monitored using Alamar blue assay and SEM. The effect of the magnetic scaffold on the total protein production was further investigated using a commercial protein assay kit.

6.2 Result

6.2.1 Microstructural analysis of P(3HB)/MNP and P(3HB)/FF scaffolds

Microstructural analysis of the neat P(3HB) and the composite test materials were studied using SEM. The surface morphology of the films produced by solvent casting, as observed from the SEM imaging, is shown in Figure 6.1. The SEM image revealed nanotopography on the surfaces of the test materials. Nano scale crystals and sparsely distributed aggregates of nanoscale crystals were observed on the surface of the P(3HB)/MNP composite. These nanoscale crystals were more visible at a higher magnification (x500) image. As expected, the microstructural surfaces of the composite materials were slightly rougher than that of the neat P(3HB).

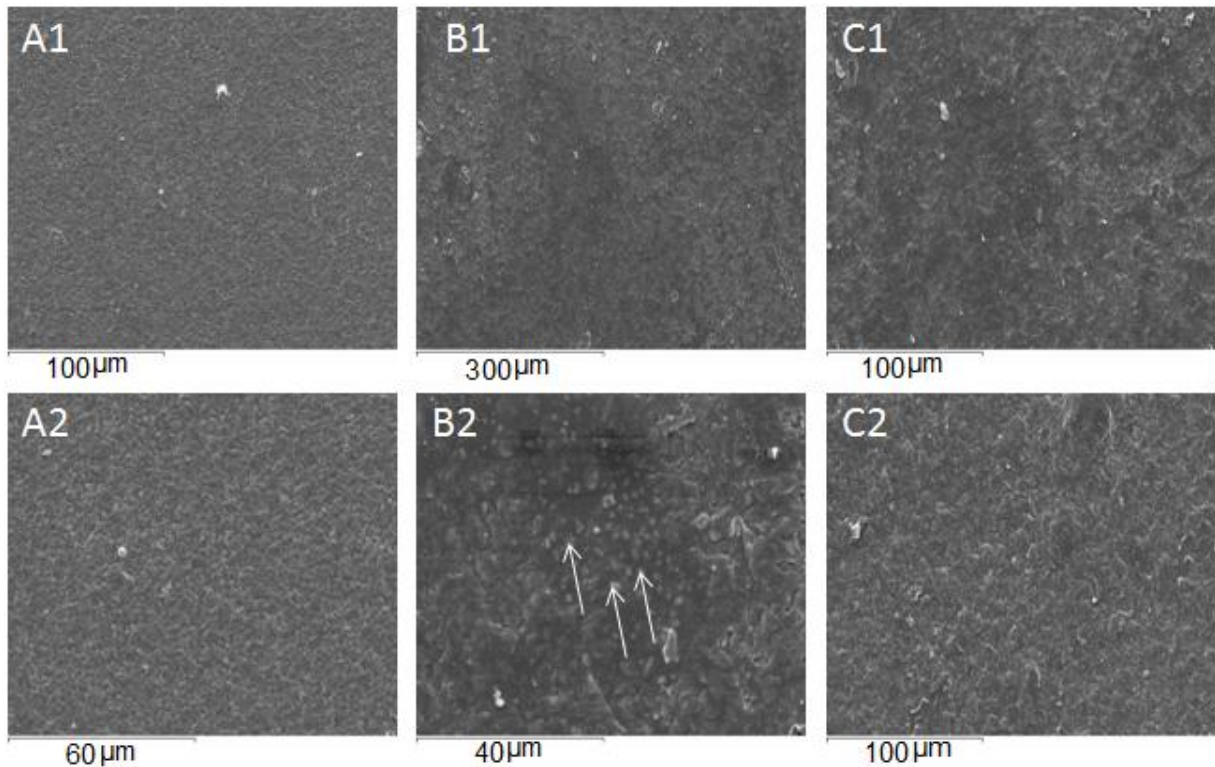


Figure 6.1 SEM image of (A1) neat P(3HB); (B1) P(3HB)/MNP; (C1) P(3HB)/FF at lower magnification (x150) and SEM Image of (A2) neat P(3HB); (B2) P(3HB)/MNP; P(3HB)/FF at higher magnification (x500). The arrows show the magnetic particles (Randomly distributed particles).

6.2.2 Morphology and structure of magnetic materials in the composite scaffolds

Transmission Electron Micrographs of the composite particles and their corresponding diffraction patterns are presented in Figure 6.2 and 6.3. The black spots in Figure 6.2a and 6.2b show the Fe_2O_3 nanoparticles while the grey spots reveals the P(3HB) fibres. Figure 6.2 also reveals agglomeration of the magnetic nano particles (MNPs). The MNPs were almost cube-like in shape and each side measured ranged between 80-100 nm.

Figure 6.2c shows a homogenous distribution of ferrofluid in the P(3HB) composite scaffold. Densely populated black spots with grey spaces, representing pores in the scaffold were observed. The electron diffraction patterns shown in Figure 6.3 shows a randomly oriented Fe_2O_3 in the P(3HB)/MNP and P(3HB)/FF composite scaffolds.

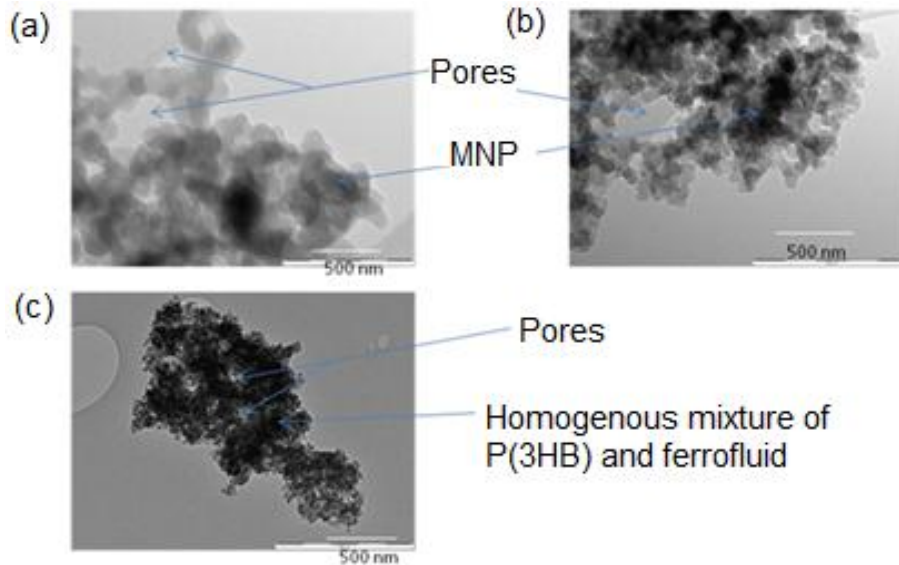


Figure 6.2 TEM micrographs of (a) P(3HB)/MNP at lower concentration (14 mg), P(3HB)/MNP at higher concentration (54 mg), and (c) TEM micrograph of P(3HB)/FF (14 mg) composite scaffolds

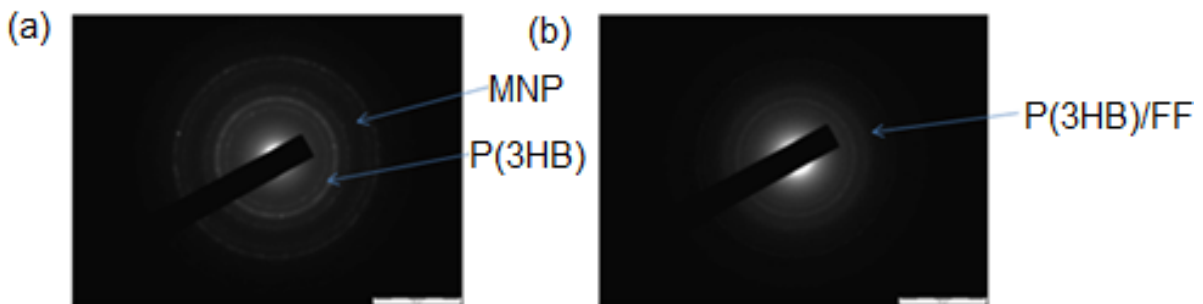


Figure 6.3 Electron diffraction patterns of (a) P(3HB)/MNP and (b) P(3HB)/FF composite scaffolds

6.2.3 Magnetic properties of P(3HB)/MNP and P(3HB)/FF composite material

Magnetic properties of the biodegradable nanocomposite scaffolds were investigated using superconducting quantum interference device (SQUID) as described in Chapter 2, Section 2.2.2.6. For each sample the magnetization at 300K was measured over a range of applied fields between -10,000 and +10,000 Oe. Figure 6.4b shows that, near ± 1 , the magnetization reached a saturation value roughly proportional to the MNP content (14, 27 and 54 mg) in the scaffolds. Figure 6.5a features the hysteresis loops of the composite scaffold produced by addition of ferrofluid (FF) (12.6 mg, $ca=10-15$ nm) while Figure 6.5b features the hysteresis loops of scaffold produced by the incorporation of magnetic nanoparticles (MNP). Figure 6.5a and 6.5b shows that the hysteresis loops of P(3HB)/FF and P(3HB)/MNP composites almost saturate at ± 1 Tesla without coercivity or remnant magnetization (i.e. ascending and

descending curves are almost the same). The details of the magnetic properties are as summarized in Table 6.1.

Table 6.1 Parameters of the hysteresis loops of neat P(3HB) and composite specimen containing different amount of MNP samples measured at a temperature of 300 K,

Sample	T (K)	$M_{\max+}$ (1 T) (emu/g)	$M_{\max-}$ (-1 T) (emu/g)	H_{C+} (Oe)	H_{C-} (Oe)	M_{R+} (emu/g)	M_{R-} (emu/g)
Neat P(3HB)	300	0.004	0.0014	---	---	---	---
14 mg (MNP)	''	0.6182	-0.6180	---	---	---	---
27 mg ''	''	0.6616	-0.6604	---	---	---	---
54 mg ''	''	0.8707	-0.8703	---	---	---	---

$M_{\max+}$ (1 T) is a maximum magnetization at 1 Tesla; $M_{\max-}$ (-1T) is a maximum magnetization at -1 Tesla, H_{C+} is a positive coercivity, H_{C-} is negative coercivity, M_{R+} is a positive remnent magnetization and M_{R-} is a negative remnant magnetization.

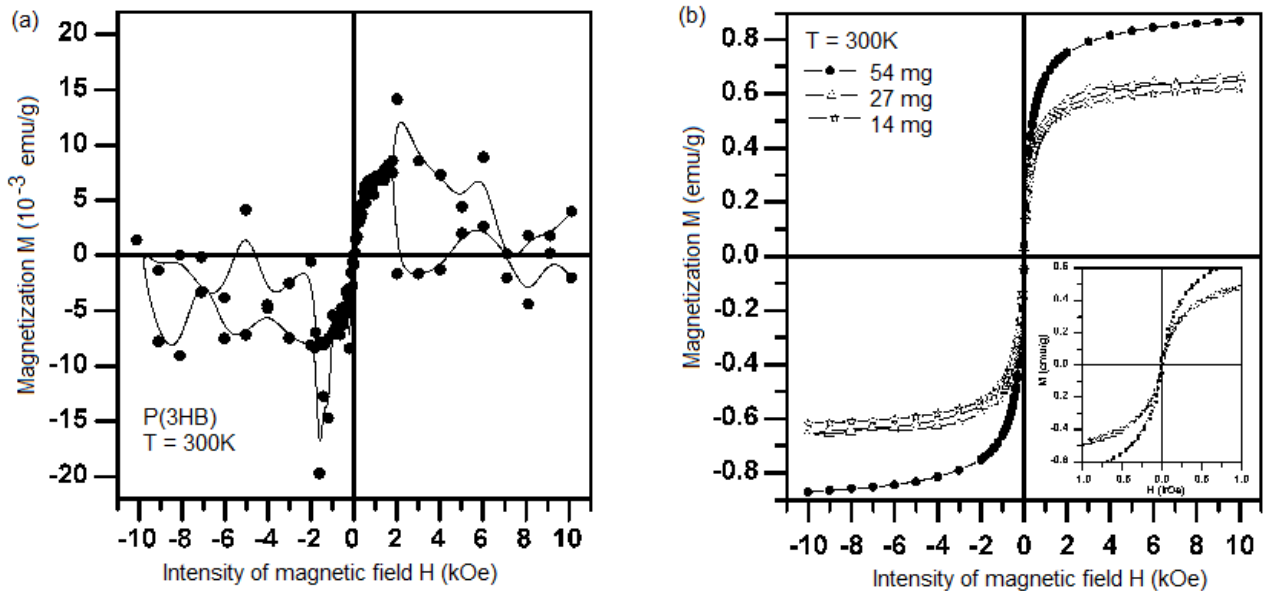


Figure 6.4 Comparison of SQUID data of saturation of specific magnetization with an applied field of approximately 5000 Oe at 300 K for (a) neat P(3HB) and (b) P(3HB)/MNP composite scaffold containing different amounts of MNP (14, 27 and 54mg)

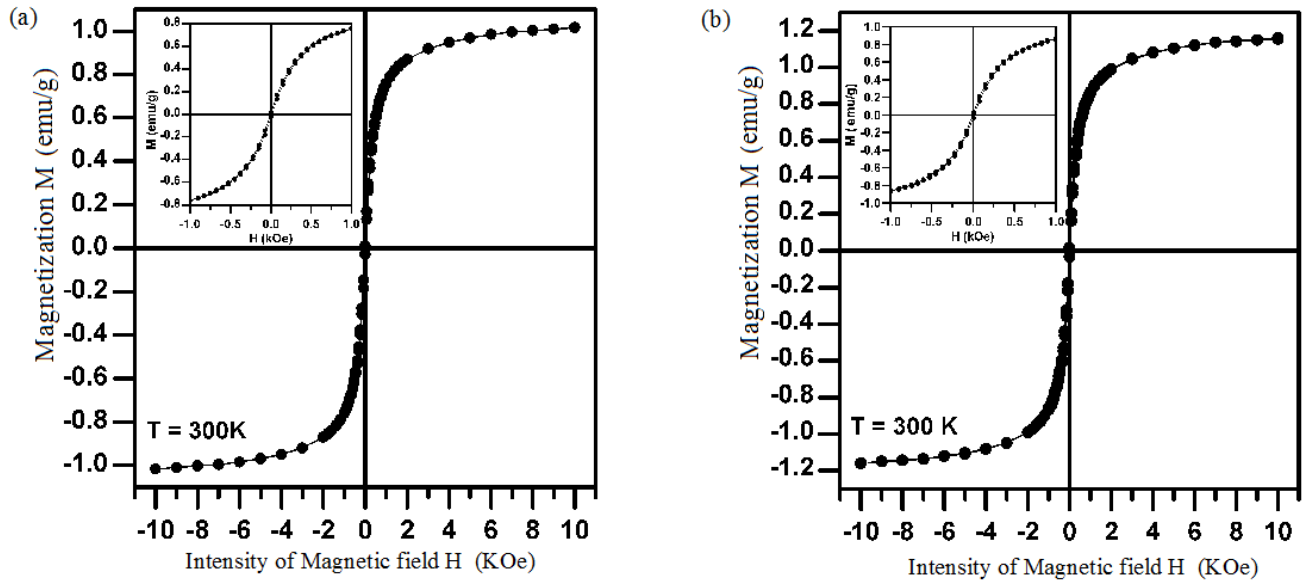


Figure 6.5 Comparison of SQUID data of saturation of specific magnetization with an applied field of approximately 5000 Oe at 300 K for (a) P(3HB)/FF composite scaffold (12.5mg, average particle size, $ca=10-15$ nm), and P(3HB)/MNP composite scaffold (14 mg, $ca=100$ nm).

6.2.4 Mechanical and thermo-mechanical properties of P(3HB)/MNP and P(3HB)/FF composite

Dynamic mechanical analysis, DMA has been demonstrated to be useful in evaluating the viscoelastic properties of polymers (Misra *et al.*, 2007; Rich *et al.*, 2002). For polymeric materials, the following equations hold (Ward, 1985).

$$E = \sigma/\varepsilon = E' + iE''$$

$$\tan \delta = E' / E''$$

Where E is the dynamic modulus, E' is termed storage modulus and E'' is the loss modulus and σ (sigma) is stress, ε (epsilon) is percentage change in strain and $\tan \delta$ (tan delta) is the ratio of the energy dissipated per cycle to the energy stored during the cycle).

Table 6.2 show the Young's modulus of the P(3HB)/MNP and P(3HB)/FF composites which were significantly influenced by the incorporation of magnetic maghemite either as nanoparticles or ferrofluid. The Young's modulus of the neat P(3HB) measured was 0.22 ± 0.04 GPa. This value increased to 0.83 ± 0.2 and 0.94 ± 0.4 GPa on addition of 14 mg of MNP and 14 mg of ferrofluid respectively to 1g of the P(3HB) matrix to form composites (Figure 6.5). The result of the static test thus showed that there was a 277 % and 327 % increase in the Young's modulus of the composite due to the incorporation of 14 mg of either

MNP or ferrofluid respectively. Besides, statistical difference ($p < 0.05$) in the elastic modulus between the P(3HB)/MNP and P(3HB)/FF composites were found.

Figure 6.6 highlights the result of dynamic modulus measured on both the neat P(3HB), P(3HB)/MNP and P(3HB)/FF composites. The dynamic storage and loss modulus were obtained in the temperature range of -20°C and 130°C and a typical profile of the data obtained is shown in Figure 6.7. A detailed set of data with standard deviations on the three set of analyses performed is shown in Table 6.2. The result shows that the storage modulus increased due to the incorporation of either magnetic nanoparticles or ferrofluid to the polymeric matrix. However, the storage modulus of the P(3HB)/MNP composite was found to be greater than the storage modulus measured for both neat P(3HB) and P(3HB)/FF composite. At -20°C , the storage modulus were found to be 0.97 ± 0.7 , 2.77 ± 0.7 , and 1.97 ± 0.5 GPa for the neat P(3HB), P(3HB)/MNP and P(3HB)/FF composites respectively. Moreover, both the storage modulus and loss modulus were found to decrease with increase in temperature. Apart from dynamic storage and Loss modulus, $\tan \delta$ (which is the ratio of the energy dissipated per cycle to the energy stored during the cycle) was used to quantify the internal friction existing in the material. The test performed explicitly, revealed that $\tan \delta$ increased with the addition of either magnetic nanoparticles or ferrofluid to the polymeric material. Also, $\tan \delta$ was noticed to have decreased with increase in temperature in both P(3HB)/MNP and P(3HB)/FF composite materials, but increased with increase in temperature above 20°C for the neat P(3HB) (Table 6.2).

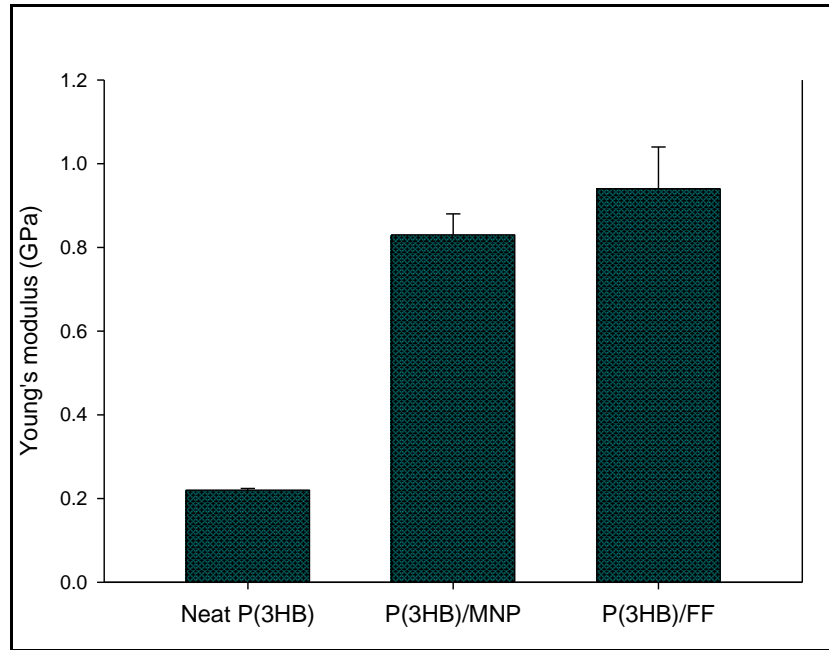


Figure 6.6 Young's modulus (E) measurement for neat P(3HB), P(3HB)/MNP, and P(3HB)/FF composite containing 14 mg of either MNP or ferrofluid solution in 1 g of P(3HB). (Error bars = \pm SD)

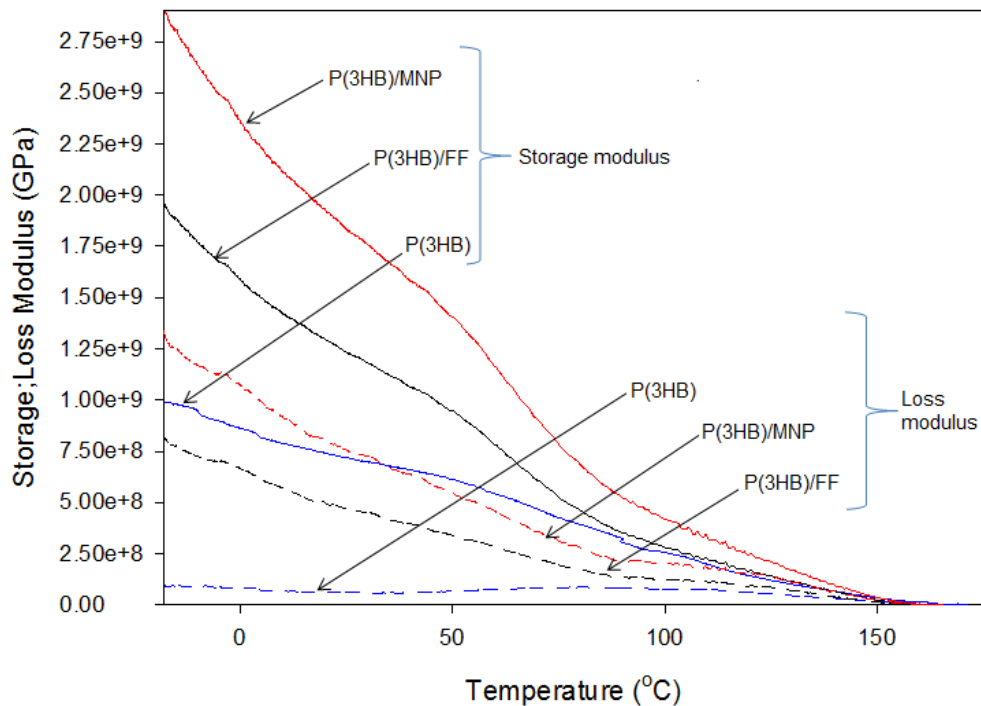


Figure 6.7 Typical plot of Storage modulus (solid lines) and Loss modulus (dotted lines) of neat P(3HB), P(3HB)/FF, and P(3HB)/MNP composite.

Table 6.2 Mean and standard deviation of storage modulus (E'), and loss modulus (E'') for neat P(3HB), P(3HB)/MNP and P(3HB)/FF composite at different temperatures

Measurement	Material	Temperature (°C)			
		-20	0	20	50
Storage Modulus (GPa)	Neat P(3HB)	0.98±0.7	0.86±0.4	0.74±0.6	0.61±0.4
	P(3HB)/MNP	2.77±0.7	2.28±0.5	1.87±0.30	1.36±0.5
	P(3HB)/FF	1.97±0.5	1.59±0.1	1.30±0.3	0.95±0.1
Loss Modulus (GPa)	Neat P(3HB)	0.09±0.02	0.08±0.02	0.06±0.01	0.06±0.04
	P(3HB)/MNP	0.76±0.3	0.68±0.1	0.06±0.01	0.05±0.01
	P(3HB)/FF	0.84±0.2	0.67±0.1	0.49±0.1	0.34±0.3
tan δ	Neat P(3HB)	0.09±0.02	0.09±0.04	0.08±0.03	0.10±0.07
	P(3HB)/MNP	0.27±0.04	0.29±0.09	0.26±0.02	0.37±0.02
	P(3HB)/FF	0.43±0.02	0.42±0.01	0.38±0.03	0.36±0.01

MNP (magnetic nanoparticle), FF (ferrofluid), tan δ (tan delta) (n=3, error = ±SD)

A typical DSC thermogram of P(3HB)/MNP composite is shown in Figure 6.8 and Figure 6.9. The thermogram is shown to illustrate the emergence of primary melting and crystallisation peak in P(3HB)/MNP during the heating and cooling cycles which was not observed during a heating and cooling cycle for P(3HB)/FF. In general, the DSC analysis was performed to study the melting and crystallisation behaviour of the composites and the crystallinity of the matrix polymer. The mass crystallinity of the test materials were approximated using the heat of fusion ($H_{100\%}$) of totally crystalline P(3HB), i.e., 146 J/g. This value, found for the P(3HB) homopolymer by Avella *et al.*, was considered as a reasonable approximation of the $H_{100\%}$ for P(3HB)/MNP and P(3HB)/FF, provided that the composite contained a low percentage of the fillers (magnetic nanoparticles and ferrofluid) as reported by Avella *et al.*, 2000. The area of the melting and crystallization peak endotherm was then directly equated to the heat of melting or crystallization, H_f in any case. The degree of crystallinity, $H^*(\%)$, of the composite can thus be estimated by using the following equation:

$$H^*(\%) = (H_f/H_{100\%}) \times 100,$$

Where, H_f is the apparent fusion enthalpy of the matrix polymer in the composite sample and $H_{100\%}$ is the theoretically 100% crystalline polymer.

The result of the crystallinity studies are summarised in Table 6.3. As can be seen in Table 6.3, both the melting and crystallisation temperatures of the composites (P(3HB)/MNP and P(3HB)/FF) increased on addition of either magnetic nanoparticles or ferrofluid. Also, the degree of increase in the melting and crystallisation temperatures of the composites depended on the amount of filler added to the polymer matrix. Whilst, primary and secondary melting and crystallisation peaks were observed in the P(3HB)/MNP thermograms, single melting and crystallization peaks were observed in both the neat P(3HB) and P(3HB)/FF composite thermograms. Besides, the heat of fusion for the melting and crystallization temperatures of both composites (P(3HB)/MNP and P(3HB)/FF) decreased as the amount of the fillers in the composite sample increased. The details of the values of the melting and crystallisation temperatures calculated are presented in Table 6.3.

Table 6.3 Thermal properties for P(3HB)/Magnetic material composite containing different amount of Magnetic materials (Particles or fluid)

Composite Material (amount of filler/1g of P(3HB))	Melting Temperature, T_m (°C)				Crystallization Temperature, T_c (°C)			
	Primary peak		Main peak		Primary peak		Main peak	
	°C	ΔH_f (J/g)	°C	ΔH_f (J/g)	°C	ΔH_f (J/g)	°C	ΔH_f (J/g)
Neat P(3HB)	-	-	169.81	40.32	-	-	59.43	-13.08
14 mg MNP	-	-	174.13	46.29	-	-	115.38	-60.92
40 mg “	163.85	0.17	174.02	37.84	94.94	-0.77	119.62	-58.59
54 mg “	169.26	75.97	179.05	17.53	164.17	-81.14	127.43	-42.53
14 mg Ferrofluid	-	-	174.06	24.60	-	-	118.94	-23.57
40 mg “	-	-	174.34	29.52	-	-	118.65	-49.92
54 mg “	-	-	173.72	24.70	-	-	117.38	-31.268

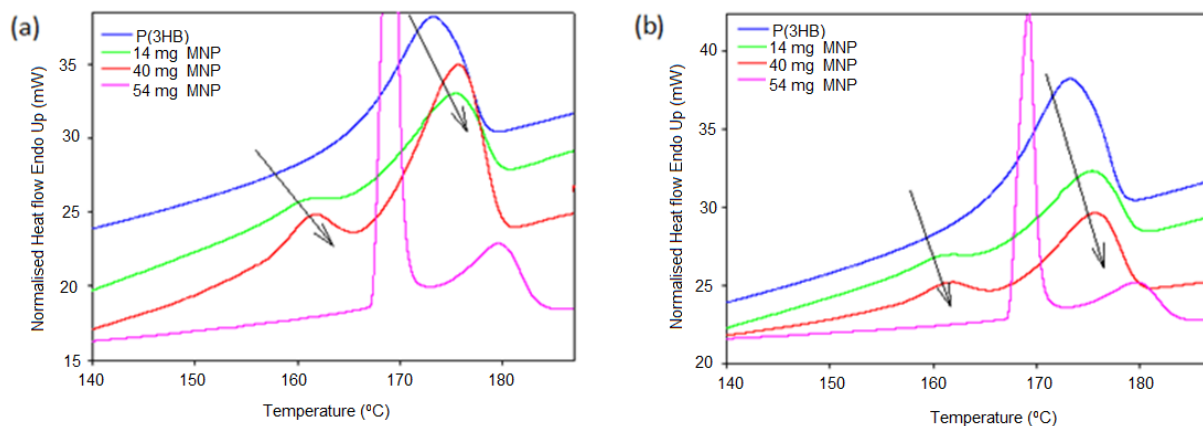


Figure 6.8 Typical heat flow thermograph for (a) the first heating curve (b) the second heating curve from DSC analysis for the neat P(3HB) and P(3HB)/MNP composites. Arrows indicate direction of increase of melting temperatures.

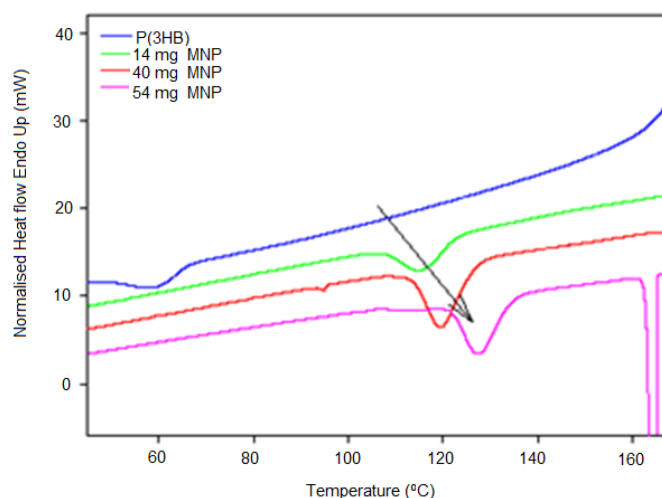


Figure 6.9 Typical heat flow thermograph for the cooling curve from DSC analysis for the neat P(3HB) and P(3HB)/MNP composites. Arrow indicates direction of increase in the crystallization temperature.

6.2.5 Fourier Transform-Infra Red, FT-IR Analysis

Fourier transform infrared (FTIR) spectroscopy was used to identify functional groups and obtain structural information of the P(3HB)/MNP and P(3HB)/FF composites. In any miscible composites, polymers containing the carbonyl group usually are involved in some interaction such as hydrogen bonds, and hence, a shift of the absorption wavelength corresponding to the C=O group is usually observed.

The FTIR spectra of P(3HB), P(3HB)/MNP and P(3HB)/FF composites is shown in Figure 6.10. The strong and sharp transmittance band at 1720 cm^{-1} can be assigned to the C=O stretching mode in both the neat P(3HB) and the composites specimens. The peaks at 1275

and 1226 cm^{-1} can be assigned to the C-O-C stretching modes in the composites. The peak at 1180 cm^{-1} is attributed to the C-O-C stretching band corresponding to the amorphous state (Sato *et al.*, 2004). Generally, the FTIR spectra of the composite specimens show modified bands in shape and intensity when compared to those characteristic of neat P(3HB). Most of the P(3HB) bands that are sensitive to the crystallinity of the sample became sharp and increased in intensity with the addition of either magnetic nanoparticles or ferrofluid. Furthermore, the intensity of these bands increased more with the addition of ferrofluid than on addition of MNP. For instance, the intensity of the peaks at positions 2978, 1720, 1378, 1275, 1129, 1050, 909 and 592 cm^{-1} increased in the order, (P(3HB)/FF > P(3HB)/MNP > P(3HB)). Also, conspicuous was the shift in bands with the addition of the fillers. The 591 cm^{-1} peak in the neat P(3HB) spectrum shifted to 592 cm^{-1} in P(3HB)/FF and 593 cm^{-1} in P(3HB)/MNP while the band at position 1451 cm^{-1} in the neat P(3HB) shifted to 1454 cm^{-1} on addition of either magnetic nanoparticles or ferrofluid. Besides, additional bands were also found at position 511 cm^{-1} in the P(3HB)/MNP composite and 1556 cm^{-1} in both composite specimens (P(3HB)/MNP and P(3HB)/FF).

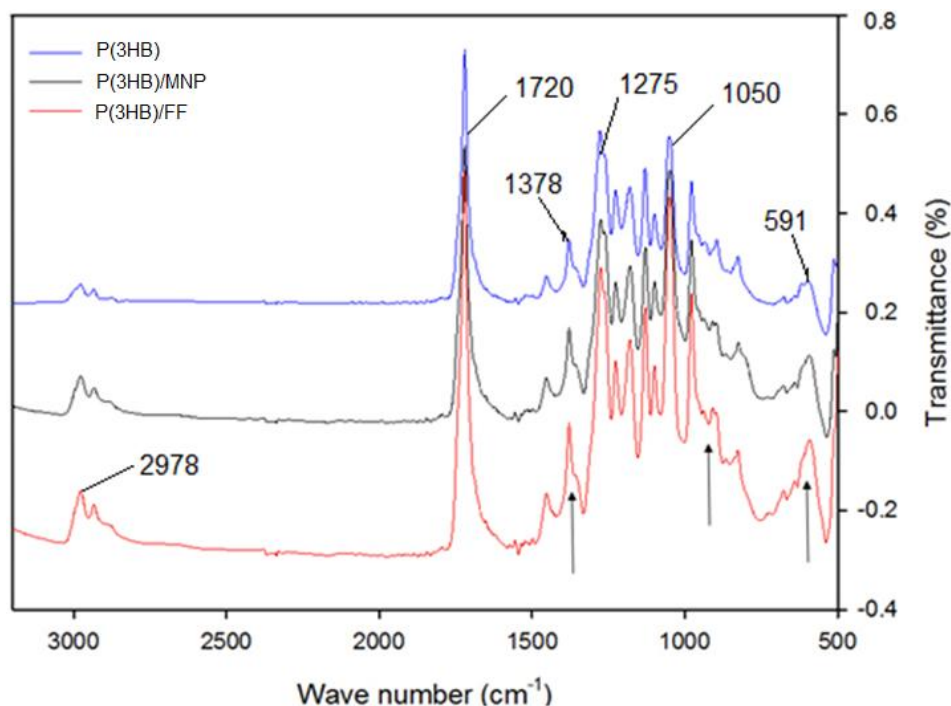


Figure 6.10 FT-IR spectra of neat P(3HB) (blue line), P(3HB)/MNP (black line), and P(3HB)/FF (red line).

6.2.6 Hydrophilicity Determination

The aqueous contact angle of the composites differed significantly from that of the neat P(3HB) as seen in Figure 6.11. Whilst, the aqueous contact angle measured on the neat P(3HB) specimen was 68.1 ± 7 , those measured on the P(3HB)/MNP and P(3HB)/FF were 59.7 ± 4.1 and 63.2 ± 6.4 respectively. Hence, the hydrophilicity of the composite specimens increased by 12% and 7% on addition of magnetic nanoparticles and ferrofluid, respectively.

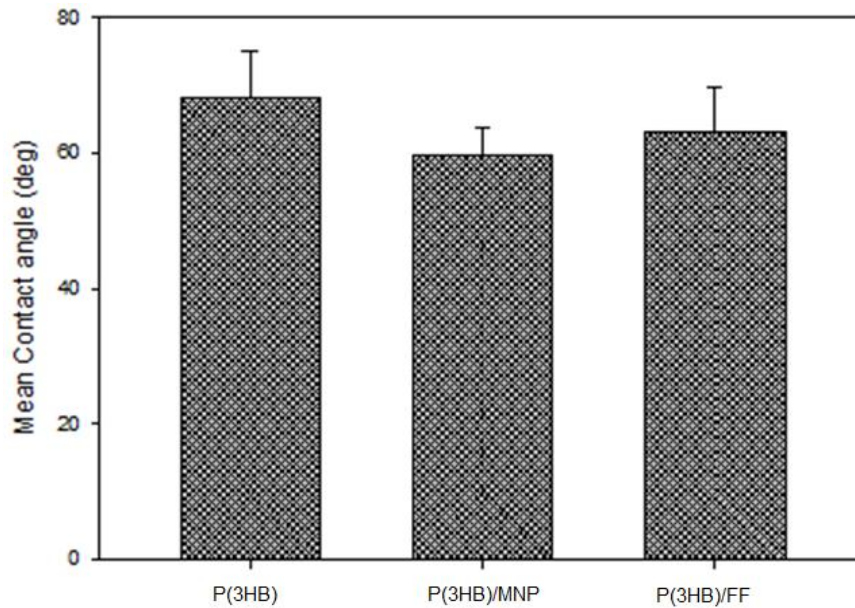


Figure 6.11 Aqueous contact angles for neat P(3HB), P(3HB)/MNP and P(3HB)/FF composite films (n=3, error = \pm SD).

6.2.7 Total Protein Absorption on the P(3HB)/MNP and P(3HB)/FF composite films.

The total amount of protein adsorbed onto the composite disc in $\mu\text{g}/\text{cm}^2$ is shown in Figure 6.12. For all the specimens, the total amount of adsorbed protein increased significantly with the addition of either magnetic nanoparticles or ferrofluid. The total amount of protein absorbed by the P(3HB)/FF and P(3HB)/MNP composite scaffolds increased by 83 and 91 % respectively. A statistical difference ($p < 0.05$) was found between total protein absorbed by either P(3HB)/MNP or P(3HB)/FF and the neat P(3HB). However, among the composite specimens, the extent of protein absorption did not differ significantly, though both composites followed the same trend of increase in total protein adsorption compared to the neat P(3HB).

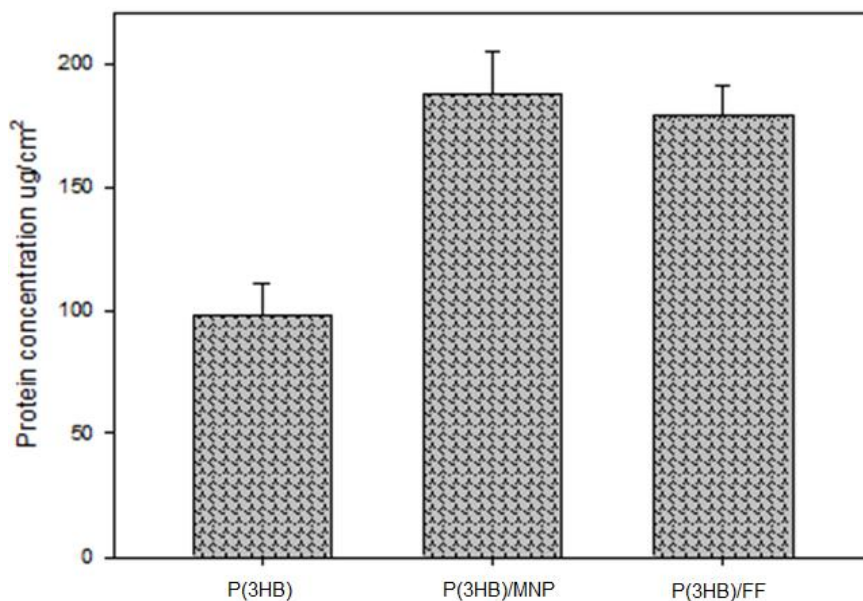


Figure 6.12 Total protein adsorption study on P(3HB)/MNP and P(3HB)/FF films using fetal bovine serum (FBS). (n=3; error bars= \pm SD).

6.3 Production of porous magnetic polymeric composite 3D scaffold for tissue engineering

6.3.1 Microstructure Analysis of P(3HB)/Magnetic material composite 3D scaffold

Figure 6.13(a) shows the digital images of the composite specimens produced using compression moulding/particulate leaching method, and Figure 6.13(b) shows the scanning electron micrograph of the cross sections of the composite scaffolds, highlighting the interconnected pores in the scaffold. Figure 6.13(c) & (d) shows the scanning electron micrographs of the cross section of the composite scaffolds highlighting the magnetic nanoparticles at lower and higher magnifications. The composite scaffolds exhibited microporous structure with well interconnected open pores, and the pore sizes varied from 70 to 100 μm (Figure 6.13b). The two composite scaffolds (P(3HB)/MNP and P(3HB)/FF) maintained their microporous structure and pore sizes which were comparable to the P(3HB)/MFC composite scaffold described in Chapter 5. The scaffolds maintained the same level of porosity (72%) and no statistical difference was found between the P(3HB)/MNP and P(3HB)/FF composite 3D scaffolds. Nanoparticles were identified on the polymeric matrix surface of the P(3HB)/MNP scaffold, more often assembled into aggregates. However, a

homogenous mixture of the polymeric P(3HB) and ferrofluid was observed on the P(3HB)/FF composite scaffold (image not shown).

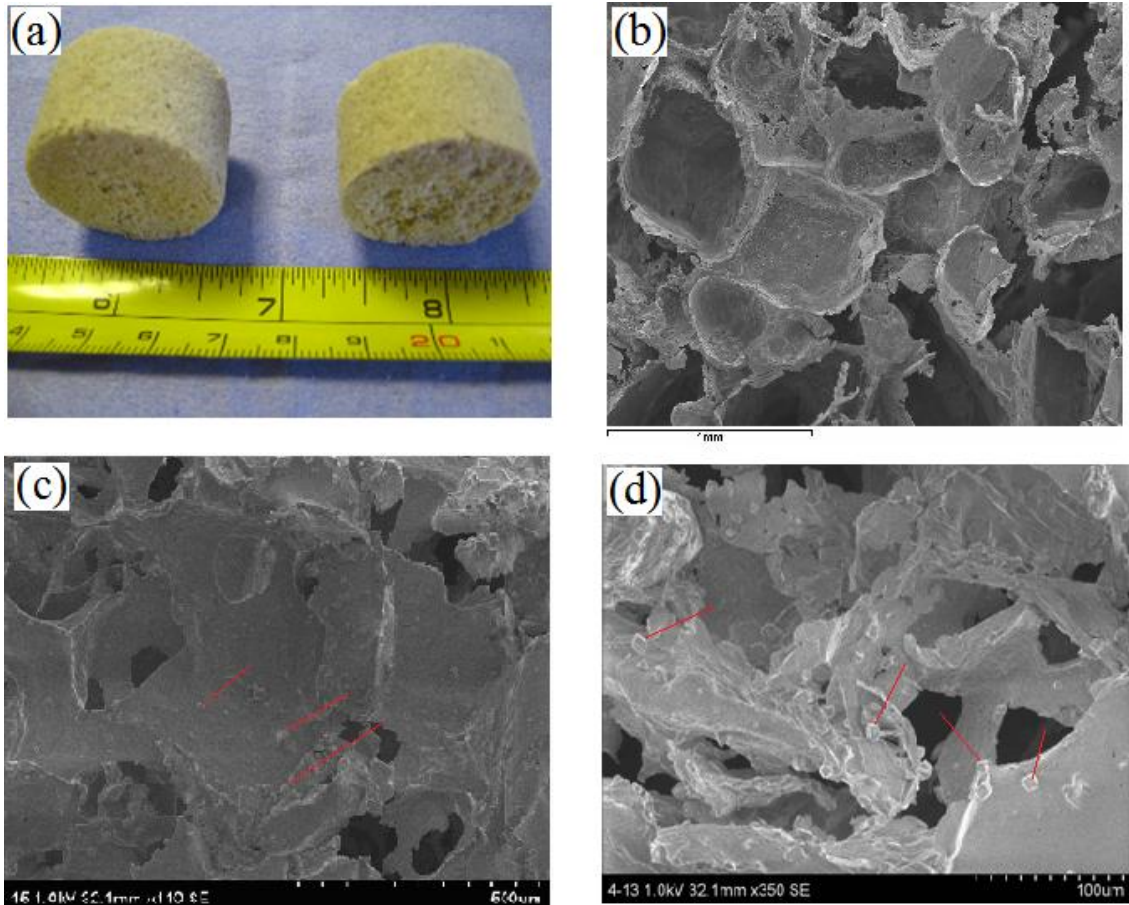


Figure 6.13: Typical (a) Digital image of P(3HB)/MNP composite scaffold, (b) SEM image of the composite scaffold revealing the interconnected pores, (c) SEM image of the pores reveal the magnetic nanoparticles (arrows) at lower magnification and at higher magnification

6.3.2 Compressive mechanical test

A typical stress-strain curve of the compressive modulus of the P(3HB)/MNP composite scaffolds is shown in Figure 6.14a, while a comparison of the typical stress-strain curve achieved from the dynamic analysis of the neat P(3HB), P(3HB)/MNP and P(3HB)/FF is shown in Figure 6.13b. The details of the compressive modulus and stress strength measured for different compositions of the P(3HB)/MNP and P(3HB)/FF composites are summarised in Table 6.4. The neat P(3HB) scaffold prepared using the compression moulding/particulate leaching techniques had a compressive modulus of 183.12 ± 2.1 KPa and a stress strength of 23.19 ± 1.2 KPa. Both the compression modulus and strength stress were found to have significantly reduced on addition of 14 mg of either MNP or FF. However, increase in the

amount of the fillers (MNP or FF) from 14 mg to 54 mg improved both the compression modulus and stress strength of the resultant composite. Furthermore, the result of the measurements showed that addition of the ferrofluid had a more positive effect on the compression modulus of the composite than the addition of magnetic nanoparticles. This is seen in Figure 6.14 which shows that the compression modulus increased significantly ($p < 0.05$) with the addition of 54 mg ferrofluid (i.e. 1g of P(3HB) to 54 mg of ferrofluid).

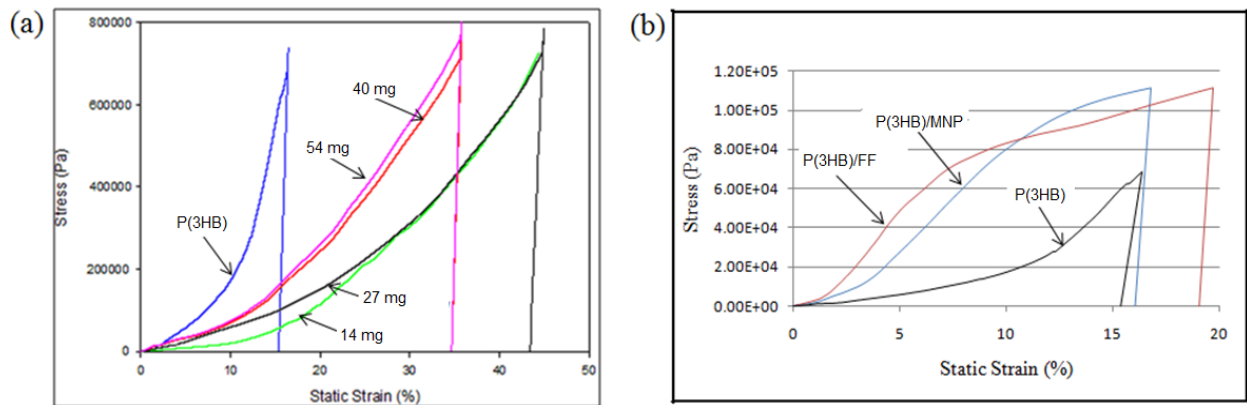


Figure 6.14 Typical stress-strain curves for (a) P(3HB)/MNP composites containing different amounts of MNP and (b) neat P(3HB) and P(3HB)/MNP and P(3HB)/FF composite scaffolds containing 14 mg of MNP or ferrofluid per 1g of P(3HB) under the same compression loading. The experiment was performed in triplicates. For clarity purpose, only the profiles for a single analysis was shown.

Table 6.4 Summary of the results obtained using Dynamic Mechanical Analysis (DMA) carried out on the neat P(3HB), P(3HB)/MNP and P(3HB)/FF composites

Composite Material (amount of filler)	Compression modulus (KPa)	Stress strength (KPa)
Neat P(3HB)	183.12±2.1	23.19±1.2
14 mg MNP	149.93±12.0	1.19±0.2
40 mg ”	122.56±9.9	1.25±0.3
54 mg ”	157.75±15.0	2.40±0.3
14 mg Ferrofluid	118.67±14.1	1.74±0.1
40 mg ”	214.39±11.1	2.74±0.6
54 mg ”	290.54±13.0	3.80±0.6

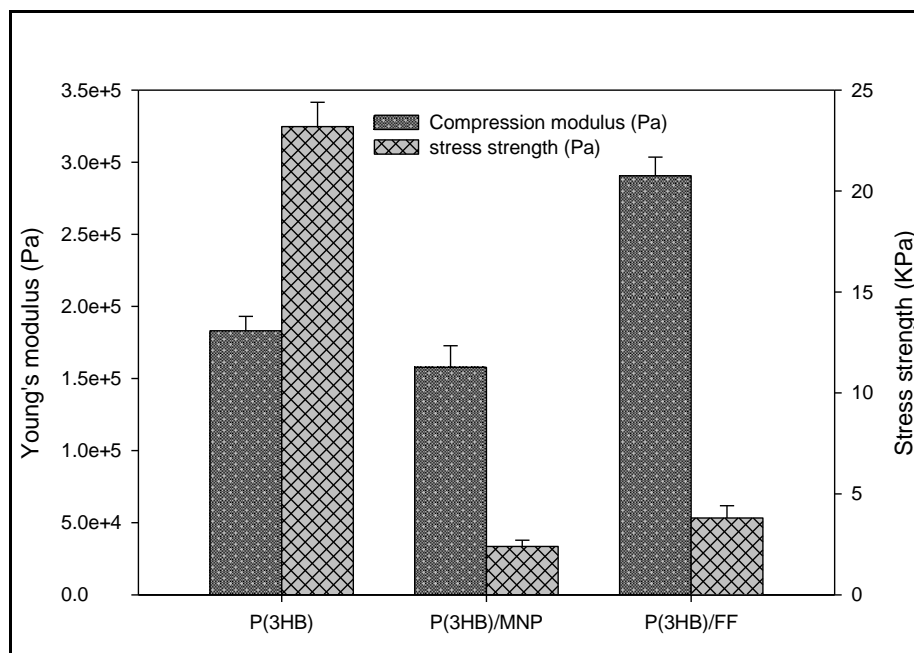


Figure 6.15 Compressive modulus and stress strength for neat P(3HB), P(3HB)/MNP, and P(3HB)/FF composite scaffold containing 54 mg MNP and 54g ferrofluid respectively per 1g P(3HB), measured in air. (n=3, Error = \pm SD).

6.4 *In vitro* Degradation Studies

6.4.1 Weight loss of the magnetic composite and pH change of the SBF solution

The percentage weight loss of the neat P(3HB), P(3HB)/MNP and P(3HB)/FF films measured at different time points for 30 days is shown in Figure 6.16. A statistical difference ($P < 0.05$) was found in percentage weight loss between the neat P(3HB) film and the composite films at all the time points considered during the degradation study. However, the percentage weight loss of the neat P(3HB) film decreased after reaching a maximum of 9.02 ± 0.61 % at 14 days. On the other hand, the percentage weight loss of the P(3HB)/FF film decreased from 4.67 ± 0.12 % on the 7th day to 1.16 ± 0.32 % on the 14th day of the degradation study. After 14 days, the percentage weight loss later increased to 4.34 ± 0.11 % on day 21 and remained fairly stable till the end of the study period. Degradation of P(3HB)/MNP films showed a different trend, with the percentage weight loss increasing to 4.55 ± 0.11 % on the 7th day and slightly further to 5.51 ± 0.39 % on the 14th day. The percentage weight loss later remained fairly stable throughout the study period after 14 days.

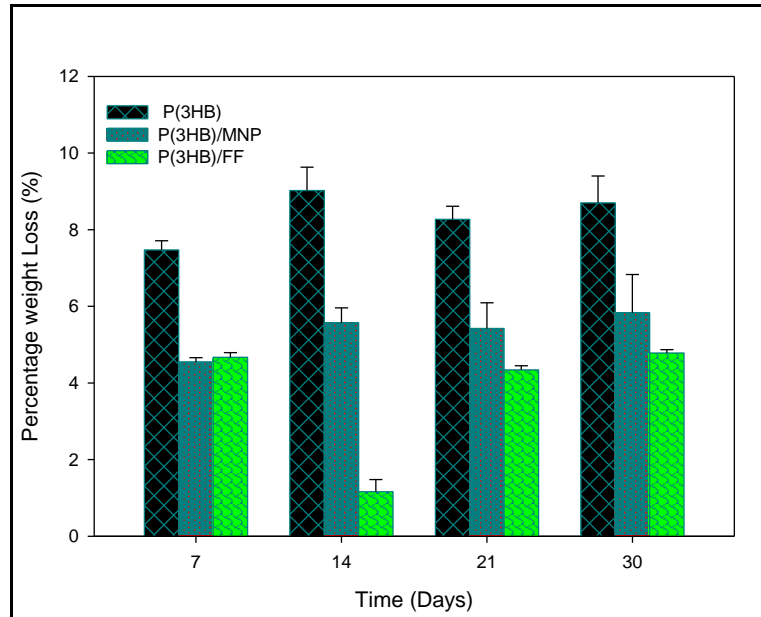


Figure 6.16 Percentage weight loss by neat P(3HB), P(3HB)/MNP, and P(3HB)/FF immersed in SBF for 30 days (n=3, Error bars = \pm SD).

The change in pH of the immersed SBF solution basically synchronized with the weight loss of the porous neat and composite films as shown in Figure 6.17. The pH of the immersed SBF for the composite material also exhibit initial increase in value and later decreased with increase in the incubation time. On the contrary, the pH of the neat P(3HB) film decreased to 7.62 on the 30th day of analysis, after an initial increase in value to 7.86 at day 7 of the study period.

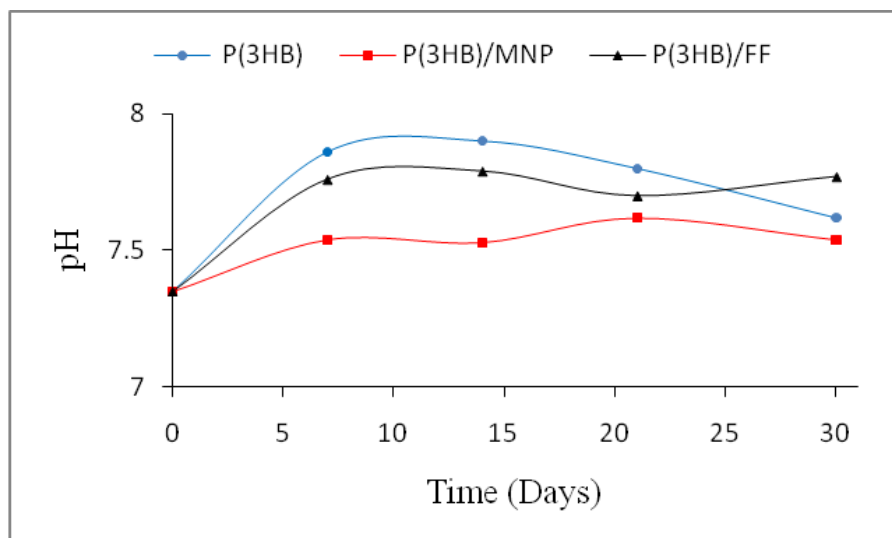


Figure 6.17 Change in pH of SBF with time of immersion of P(3HB), P(3HB)/MNP and P(3HB)/FF composite films

6.4.2 X-ray Diffraction analysis of P(3HB)/Magnetic nanoparticles immersed in SBF for 21 days

X-ray diffraction (XRD) has been extensively used in the study of crystallographic properties of biomaterials both in pure and composite forms. Hence, the magnetic composite materials were further investigated for changes in their crystallographic properties after undergoing degradation in SBF. The X-ray diffraction spectra of neat P(3HB), P(3HB)/ferrofluid before and after 21 days degradation in SBF solution are shown in Figure 6.18. Many bands in the XRD spectrum of the composite, before degradation, were lost after 21 days of degradation in SBF. Besides, there was an increase in the intensity of the bands sensitive to crystallinity. For instance, the intensity of the bands between 13 and 14, and between 15 and 17 degrees increased after 21 days of degradation. Nevertheless, the presence of new bands between position 31 and 33 degrees, and between 45 and 47 degrees was observed in both neat P(3HB) and the P(3HB)/ferrofluid composite after 21 days degradation.

Figure 6.19 displays the X-ray diffraction spectra of the neat P(3HB) and P(3HB)/Magnetic nanoparticles composite before and after subjection to degradation in SBF solution. In this case fewer bands were present in the P(3HB)/Magnetic nanoparticles composite. Moreover, the bands sensitive to crystallinity in the X-ray diffraction spectra of P(3HB)/Magnetic nanoparticles reduced in intensity after 21 days of degradation in SBF. Between 28 and 30 degrees, a sharp increase in the intensity of a peak was noticeable. Another important observation made was narrowing of the peak between 20 and 23 degrees and decrease in the peak intensity between 15 and 18 degrees. Furthermore, a new peak was observed between 31 and 33, and between 45 and 47 degrees in both neat the P(3HB) and P(3HB)/ferrofluid composite spectra.

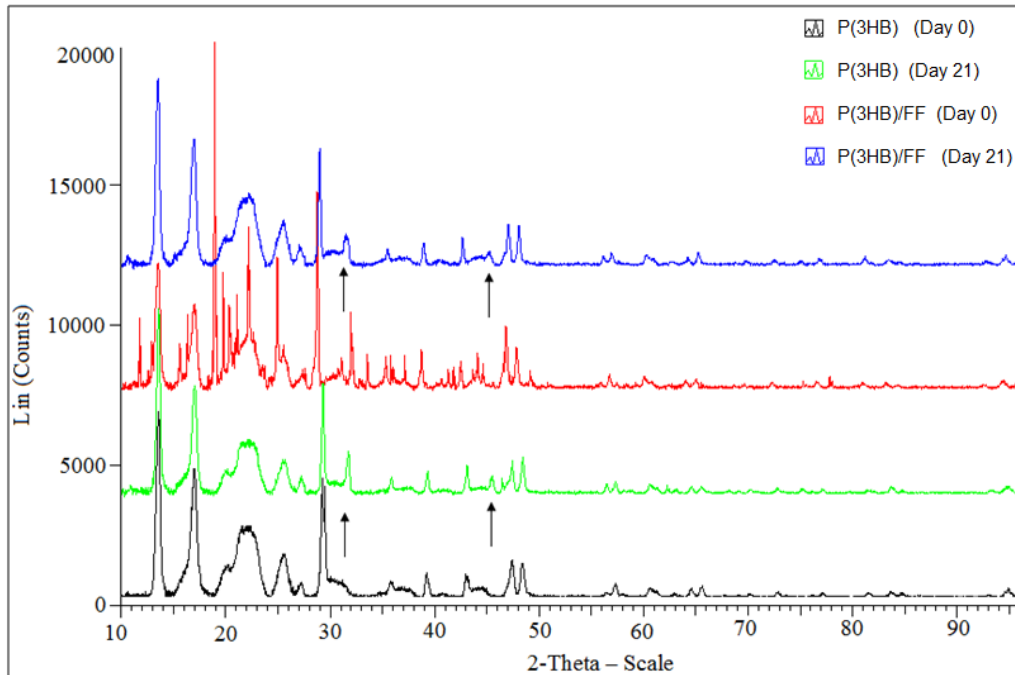


Figure 6.18 X-ray diffraction spectra for P(3HB), P(3HB)/FF composite scaffolds immersed in SBF for a period of 21 days. Arrows in the figure indicate new peak in the spectra.

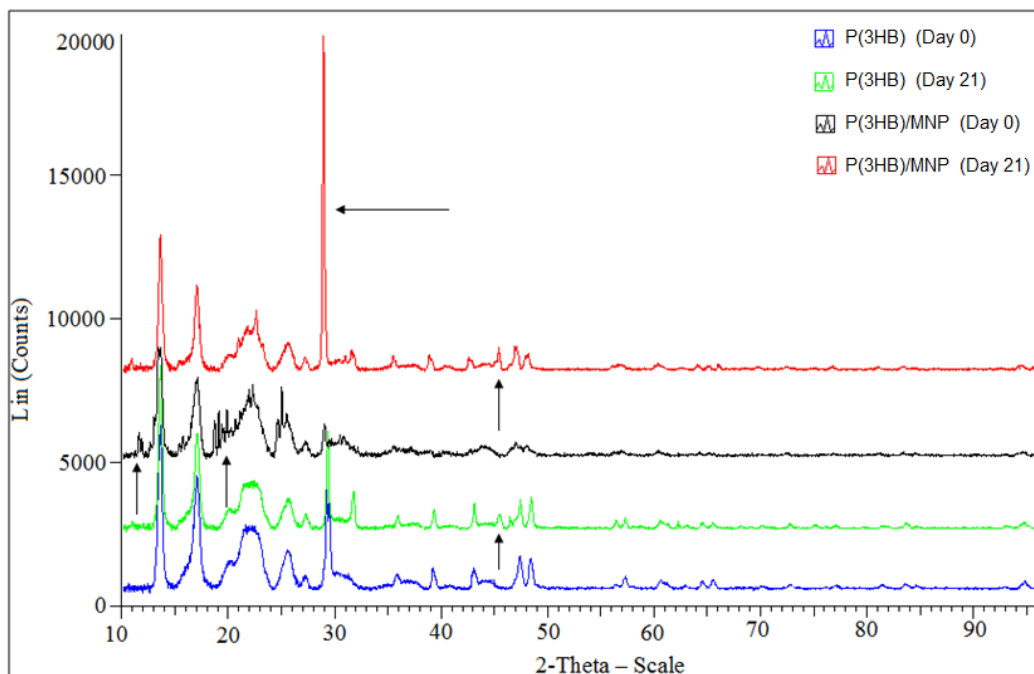


Figure 6.19 X-ray diffraction spectra for P(3HB), P(3HB)/MNP composite scaffolds immersed in SBF for a period of 21 days. Arrows in the figure indicate new peak in the spectra.

6.4.3 Raman Shift Analysis of the degraded composite specimen

Raman Shift was further employed to study the characteristics of the composite scaffolds subjected to degradation in SBF. Figure 6.20 and 6.21 shows the spectra of the Raman Shift of P(3HB)/MNP and P(3HB)/FF, respectively at different stages of degradation in SBF. As can be seen in the figures, the intensity of the bands decreases with increase in the immersion time in SBF in both P(3HB)/MNP and P(3HB)/FF composites.

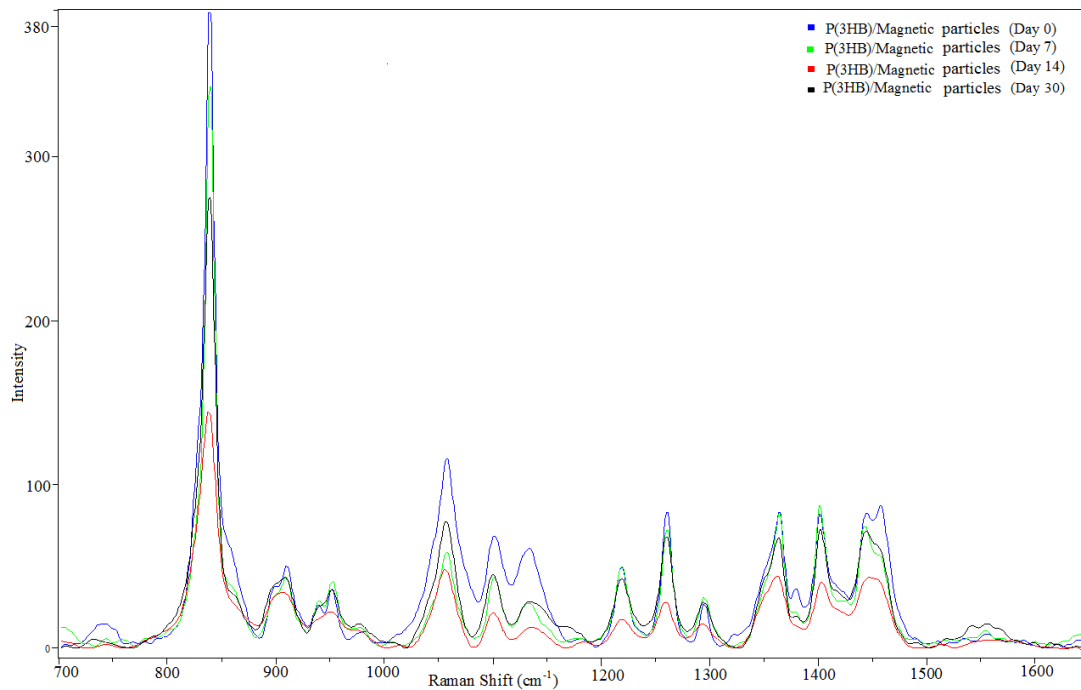


Figure 6.20 Raman Shift spectra performed on P(3HB)/MNP composite scaffold after immersion in SBF for 0 days, 7 days, 14 days, 21 days and 30 days.

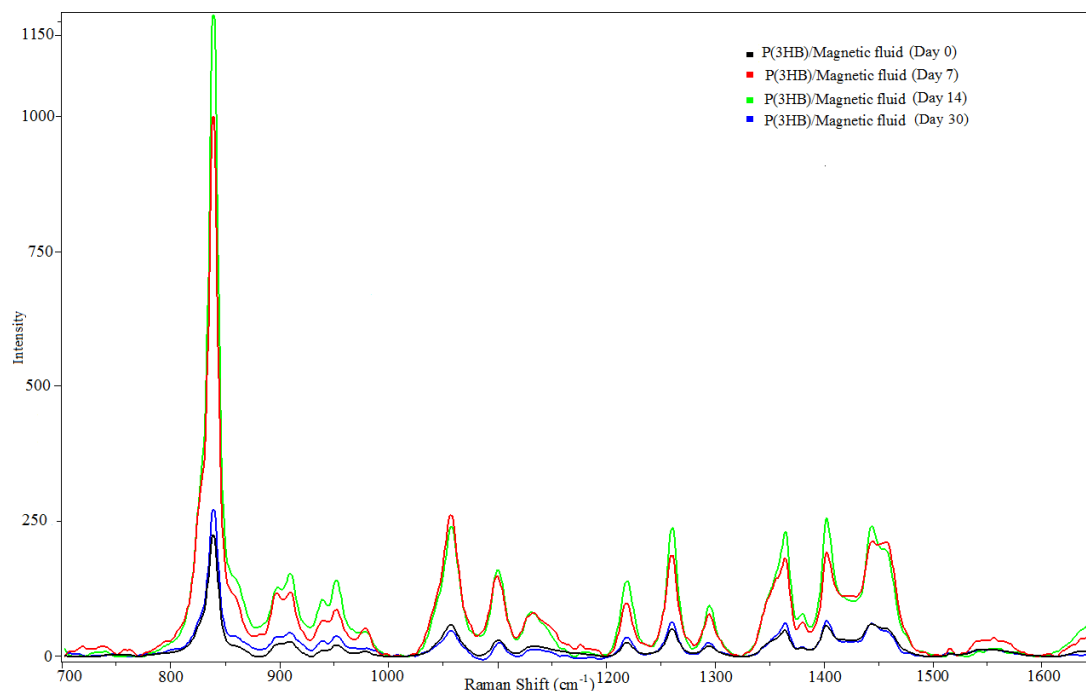


Figure 6.21 Raman Shift spectra performed on P(3HB)/FF composite scaffold after immersion in SBF for 0 days, 7 days, 14 days, 21 days and 30 days.

6.4.4 Thermal properties of the degrading composite

The thermal properties, as well as crystallisation kinetics, were investigated in order to obtain useful information for the potential medical application of the composite material in bone regeneration. The thermogram of the first and second heat scan for P(3HB)/MNP immersed in SBF at different time points are shown in Figure 6.22. The first heat scan thermogram revealed the presence of a third melting temperature after 21 and 30 days immersion of the composite scaffold in SBF. The second heat scan, however, did not have the third melting temperature. Moreover, among the three melting temperatures found in the first heat scan, only one had a high value of heat of fusion, ΔH_f which increased from 18.17 to 54.29 J/g with increase in the duration of immersion of the composite specimen in SBF. Also, the actual melting temperature (T_m value closest to the T_m value for P(3HB) and with distinct peak) in the first heat scan gradually increased from 167 °C (before immersion in SBF) to 169.6 °C after degrading in SBF for 30 days (Table 6.5). Observations on the second heat scan revealed a slight increase in the actual T_m and heat of fusion with increase in the immersion time. Unlike in the first heat scan, the third melting temperature was missing in the second heat scan. Figure 6.23 shows the DSC thermograms of the P(3HB)/MNP composite scaffold at a cooling rate of 10 °C/min. A single crystallization peak was highlighted on the

thermogram before degradation in SBF. After 7 days immersion in SBF, a primary crystallization peak was noticed which disappeared and reappeared at 21 and 30 days of immersion in SBF. Also, the crystallisation temperature, T_c increased significantly with degradation in SBF. However, the change of the crystallisation temperature, T_c did not follow the same trend with the change in the melting temperature, rather the T_c value fluctuated with increase in the immersion time (Table 6.6). Besides, the heat of fusion, ΔH_f of the crystallisation temperature decreased with increase in the immersion time of the scaffold samples in SBF.

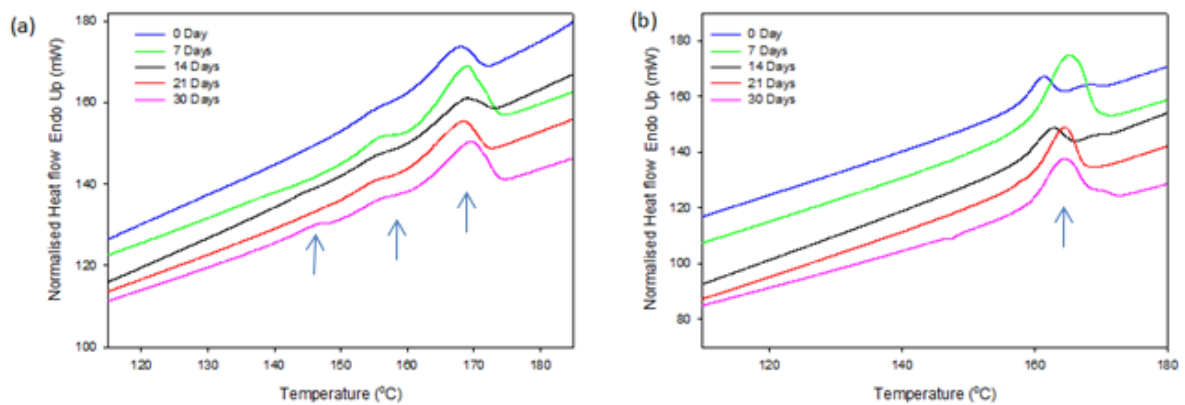


Figure 6.22 Melting endotherm (a) first run and (b) second run for P(3HB)/MNP composite scaffold degrading in SBF solution for 30 days (Scanning rate $10^{\circ}/\text{min}$). The arrows indicate the position of the peaks in the thermogram.

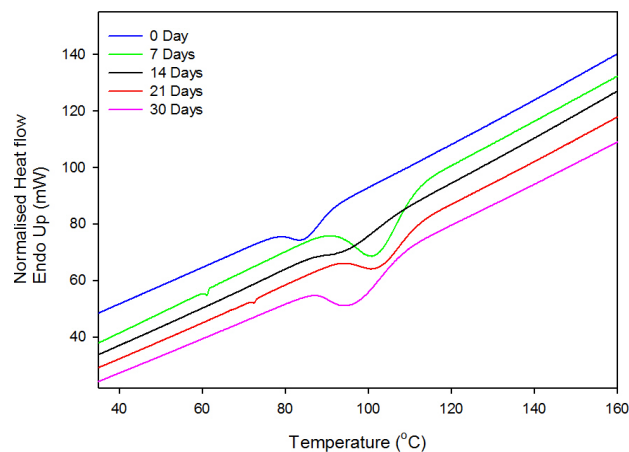


Figure 6.23 DSC cooling exotherms (cooling rate of $10^{\circ}\text{C}/\text{min}$) of P(3HB)/MNP at different time points of immersion in SBF solution

Figure 6.24 shows the thermogram of the first and second heat scan of P(3HB)/FF composite scaffold. As observed in the thermogram of the P(3HB)/MNP, emergence of a third melting temperature is observed in the thermogram of composite sample after immersion in SBF solution. However, the third melting temperature did not increase significantly as observed in the P(3HB)/MNP composite. Apart from that, a gradual increase in the heat of fusion of the melting temperatures, was observed in the P(3HB)/FF undergoing degradation.

The thermogram of the second heat scan shows a progressive increase in the T_m from 162.6 °C (T_m of the original composite before immersion in SBF) to 165.9 °C after 30 days immersion in SBF. Also, the change in the heat of fusion synchronized with that of the melting temperature, increasing from 15.8 to 53.7 J/g. Statistical differences ($p < 0.05$) were observed in the crystallisation temperature of the P(3HB)/FF before and after immersion in SBF. The crystallisation temperature, T_c of the original composite specimen increased from 84.2 to 101.76 °C after 30 days immersion in SBF. The heat of fusion of the crystallisation temperature synchronised with the crystallisation behaviour of the degrading specimen, decreasing from -23.7 to (-45.8 J/g) after 30 days degradation in SBF (Table 6.6). Primary crystallisation peak was not observed in the thermogram of the degrading composite as observed in the original composite material.

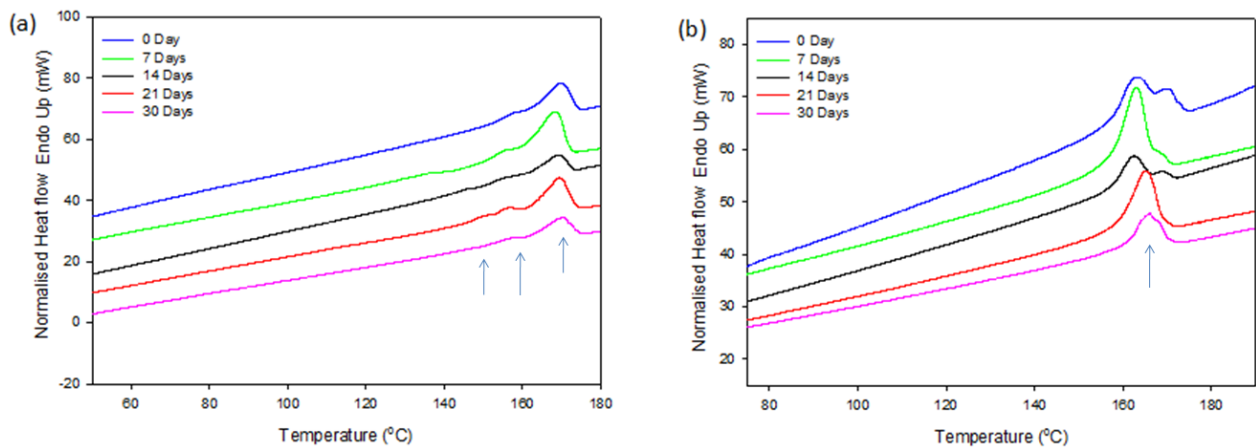


Figure 6.24 Melting endotherm (a) first run and (b) second run for P(3HB)/FF composite scaffold degrading in SBF solution for 30 days (Scanning rate 10°/min). Arrows indicate position of the peaks in the thermogram

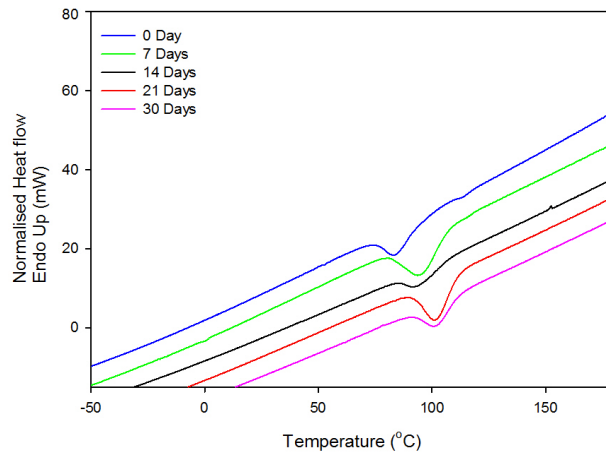


Figure 6.25 DSC cooling exotherms (cooling rate of 10°C/min) of P(3HB)/FF at different time points of immersion in SBF solution

Table 6.5 Comparison of thermal properties (Melting temperature, T_m) for P(3HB)/Magnetic material composite scaffold immersed in SBF for 30 days.

Material	T_m (°C) - 1 st Heat Scan						T_m (°C) - 2 nd Heat Scan			
	1 st T_m (°C)	ΔH_f (J/g)	2 nd T_m (°C)	ΔH_f (J/g)	3 rd T_m (°C)	ΔH_f (J/g)	1 st T_m (°C)	ΔH_f (J/g)	2 nd T_m (°C)	ΔH_f (J/g)
P(3HB)/MNP										
0 Day	167.00	18.17	157.03	0.13	-	-	161.15	13.37	167.96	1.42
7 "	168.94	39.79	156.00	2.22	-	-	164.92	52.50	-	-
14 "	168.87	35.73	155.28	2.72	-	-	162.72	39.80	168.87	1.06
21 "	169.61	54.29	156.35	1.57	145.98	2.12	164.38	56.31	-	-
30 "	169.61	54.29	156.35	1.57	145.98	2.12	164.41	78.95	168.95	-0.13
P(3HB)/FF										
0 Day	169.70	30.35	157.08	0.95	-	-	162.58	15.80	170.67	3.35
7 "	168.42	34.48	155.80	1.08	136.03	0.61	164.85	34.03	-	-
14 "	169.09	37.51	155.50	1.91	145.78	0.61	162.29	33.03	169.09	2.87
21 "	169.37	38.07	156.75	2.01	149.95	0.70	165.16	54.25	-	-
30 "	170.40	43.10	156.48	1.91	-	-	165.85	53.69	-	-

Table 6.6 Comparison of thermal properties (Crystallisation temperature, T_c) for P(3HB)/MNP and P(3HB)/FF material composite scaffold immersed in SBF for 30 days.

Material	Crystallisation Temperature, T_c			
	$1^{st} T_c$ ($^{\circ}C$)	ΔH_f (J/g)	$2^{nd} T_c$ ($^{\circ}C$)	ΔH_f (J/g)
P(3HB)/MNP				
0 Day	84.42	-23.77	-	-
7 "	101.86	-59.10	61.27	-0.59
14 "	94.75	-38.19	-	-
21 "	102.57	-59.22	72.40	-0.76
30 "	96.11	-72.22	-	-
P(3HB)/FF				
0 Day	84.20	-23.68	11.71	-1.30
7 "	95.24	-44.31	-	-
14 "	93.64	-42.76	-	-
21 "	101.71	-56.25	-	-
30 "	101.76	-45.79	-	-

6.5 Cytocompatibility study of P(3HB)/MNP and P(3HB)/FF 2D and 3D composite structure using Human osteosarcoma MG-63 cell line

Magnetic materials may serve as a substrate for propagation of cells expressing an osteoblast-like phenotype. These cells make an extracellular matrix, which has characteristics of bone. Hence, the hypothesis claimed in this chapter that magnetic materials (Magnetic fluid and magnetic nanoparticles) incorporated into the P(3HB) matrix can form a suitable substrate for supporting cell adhesion, proliferation and functioning of human osteoblasts was further tested. A human osteoblast-like cell line (MG-63) was used as the prototype for osteoblastic cells. This was based on the fact that human osteosarcoma MG-63 cells has been extensively characterized and validated as a model to test biocompatibility of various materials (Price *et al.*, 1997). Despite being a tumor cell line, MG-63 exhibits many osteoblastic traits, including high levels of 1, 25-dihydroxyvitamin D₃ (1, 25-(OH)₂D₃) responsive alkaline phosphatase activity and inhibition of cell proliferation after 1,25-(OH)₂D₃ treatment. Studies have also shown its ability to synthesize osteocalcin and collagen type 1, which are characteristic of bone-forming cells.

6.5.1 Cell proliferation study

The *in vitro* biocompatibility of the composite materials was investigated using the Human osteoblast MG-63 cell lines. The detailed experimental procedures are described in Chapter 2, Section 2.5.3. A histogram representing cell proliferation and growth on the composite film produced by incorporation of either 14 mg MNP or ferrofluid to the polymer matrix is shown in Figure 6.26. The result shows that the cells proliferated and grew well on all the samples. However, cell proliferation on the neat P(3HB) was lower than those of the control (tissue culture plate) and the composite materials. In contrast with the control, the MG-63 cells proliferated better on the P(3HB)/FF composite material. Thus, a significant difference ($p < 0.01$) was found in cell proliferation between the P(3HB)/MNP and P(3HB)/FF composite films. At day 6 of the cell proliferation study, the cell proliferation on the neat P(3HB) film did not improve compared to the high increase in cell proliferation on both P(3HB)/MNP and P(3HB)/FF composite specimens.

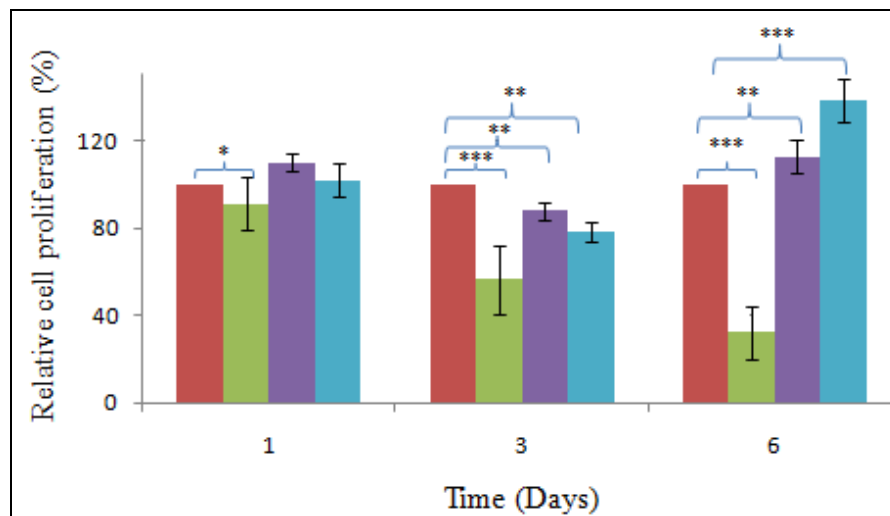


Figure 6.26 Cell proliferation study using Alamar blue assay for TCP (■), neat P(3HB) (■), P(3HB)/MNP (■) and P(3HB)/FF (■) composite film performed on day 1, 3 and 6. All samples are tested relative to the control set at 100% (n=3, error=±SD, ** $p < 0.01$, *** $p < 0.05$).

Histograms representing cell proliferation on and inside the 3D composite scaffolds are shown in Figure 6.27 and 6.28. Result of Alamar blue analysis shows that the MG-63 cells proliferated and grew in both the control (neat P(3HB)) and the composite samples containing different amount of either magnetic nanoparticles or ferrofluid composite. In spite of the differences in the materials, no statistical differences ($p < 0.05$) was found between the neat P(3HB); and the composite specimens containing different amounts of the fillers from

day 1 to day 7 of the investigation. Nevertheless, compared to cell proliferation on the neat P(3HB) scaffolds, a slightly higher level of cell proliferation was observed at day 7 of the study period for the composite specimens containing the highest amount of the incorporated materials (Magnetic nanoparticles or ferrofluid) Figure 6.27 and 6.28.

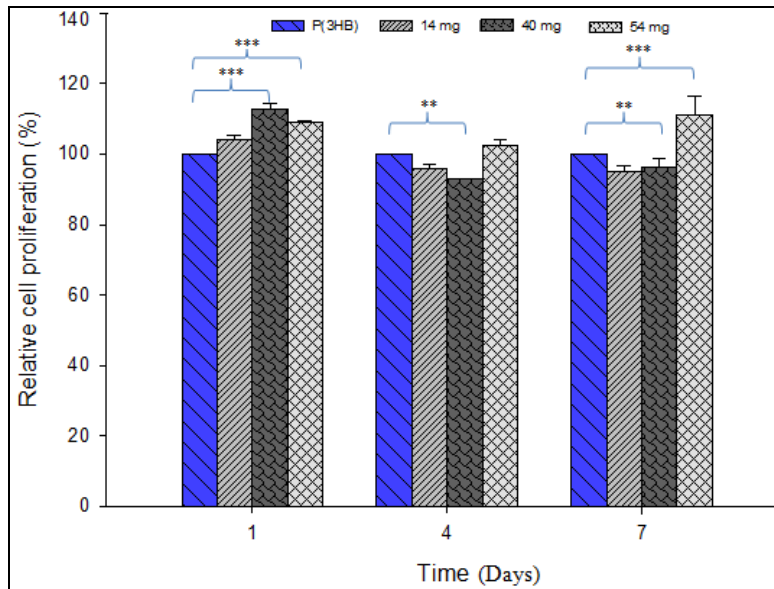


Figure 6.27 Cell proliferation study using Alamar blue assay for P(3HB) and P(3HB)/MNP composite scaffold containing different amount of magnetic particle suspension performed on day 1, 4 and 7. All samples are tested relative to the control set at 100% (n=3, error=±SD, ** $p < 0.01$, *** $p < 0.05$).

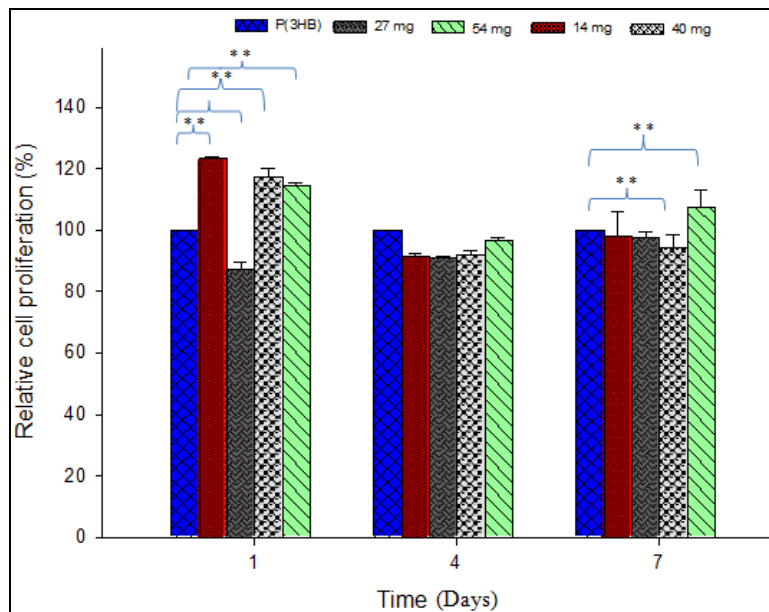


Figure 6.28 Cell proliferations using Alamar blue assay for P(3HB) and P(3HB)/FF composite scaffold containing different amounts of ferrofluid performed on day 1, 4 and 7. All tested samples was measured relative to the control set at 100% (n=3, error=±SD, ** $p < 0.01$, *** $p < 0.05$).

6.5.2 Total protein production by human osteosarcoma MG-63 cell lines on the P(3HB)/MNP and P(3HB)/FF composites

The total protein production by the MG-63 cell lines on the composite specimens were investigated from the supernatant of the cells grown in both osteogenic media and normal growth media at different time points. Since total protein production by the cells correlates with mineralisation by the growing cells, the protein produced by the growing MG-63 cells at day 1, 7, 14 and 21 were quantified using commercial Qubit™ Protein Assay Kits purchased from Invitrogen™. The detailed experimental procedures are described in Chapter 2, Section 2.5.5.2.

Figure 6.29 and 6.30 shows the histogram of the total protein produced by the growing cells at different time points investigated. Total protein produced was measured for MG-63 cells grown on both the tissue culture plastic, neat P(3HB) and the composite specimens grown in both osteogenic and normal growth media. However, a slight increase was found in the total protein produced by the MG-63 cells cultured in osteogenic media than that produced by the cells cultured in normal growth media. Furthermore, statistical difference ($p < 0.01$) was found between total protein produced by the MG-63 cells grown on P(3HB)/FF, and P(3HB)/MNP and the control.

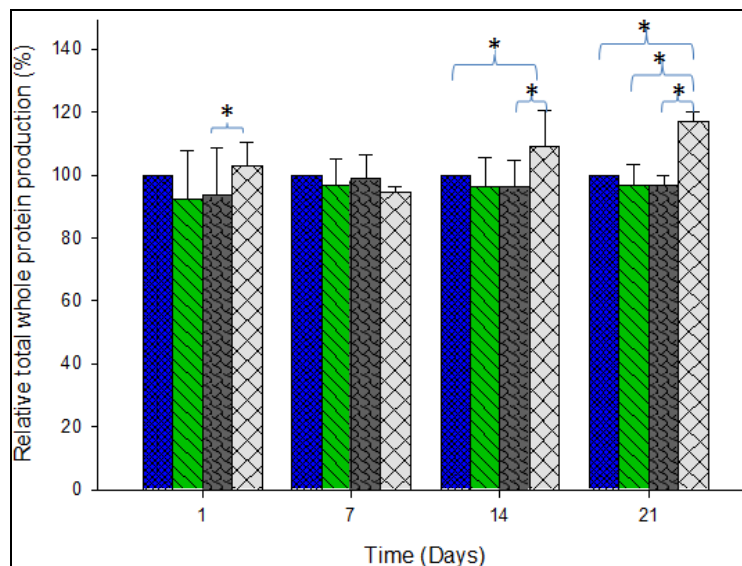


Figure 6.29 (a) Protein production by MG-63 cells on TCP (■), P(3HB) (■), P(3HB)/MNP (■) and P(3HB)/FF (■), grown in osteogenic media at different time points. Samples were measured relative to the control set at 100% (TCP) (n=3, error=±SD, * $p < 0.01$).

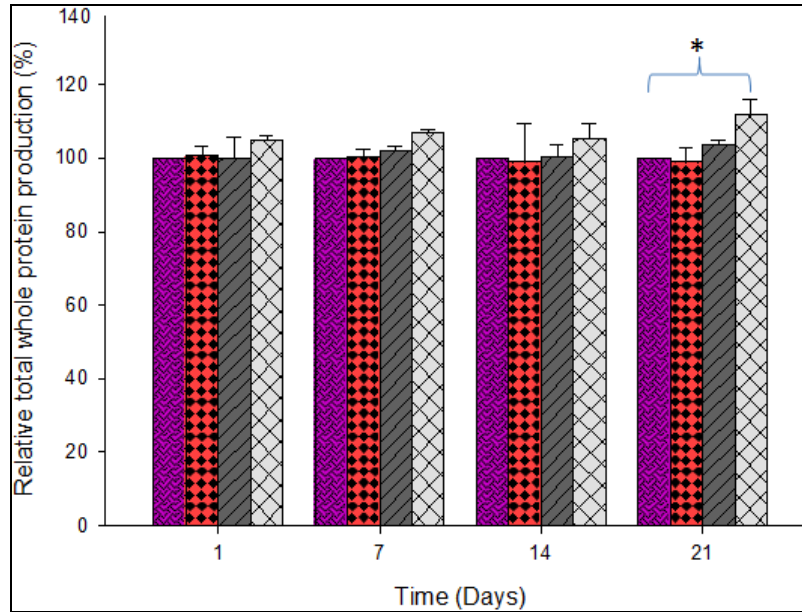


Figure 6.30 (a) Protein production by MG-63 cell lines on the control (■), P(3HB) (■), P(3HB)/MNP (■) and P(3HB)/FF (■), with normal growth media at different time points. Samples were measured relative to the control (TCP) set at 100 % (n=3, error bars=±SD, * $p<0.01$).

6.5.3 Cell Morphology

Figure 6.31 shows MG-63 cells grown on tissue culture plastic (control), neat P(3HB), P(3HB)/MNP and P(3HB)/FF films on day 1 and day 7. Both P(3HB)/MNP and P(3HB)/FF composite films contained 14 mg of either magnetic particles or magnetic fluid. The figure highlights the attachment of cells on the surface of the materials. Also, MG-63 cells flattened more on the magnetic composite films than observed on the tissue culture plastic and the P(3HB) films indicating that the composite materials were conducive for cell adhesion and proliferation. However MG-63 cells seem to have attached more on the tissue culture plastic than on the other test materials. At day 7, the MG-63 cells spread very well throughout the surface of both the control, TCP and the test materials forming a monolayer on the surfaces.

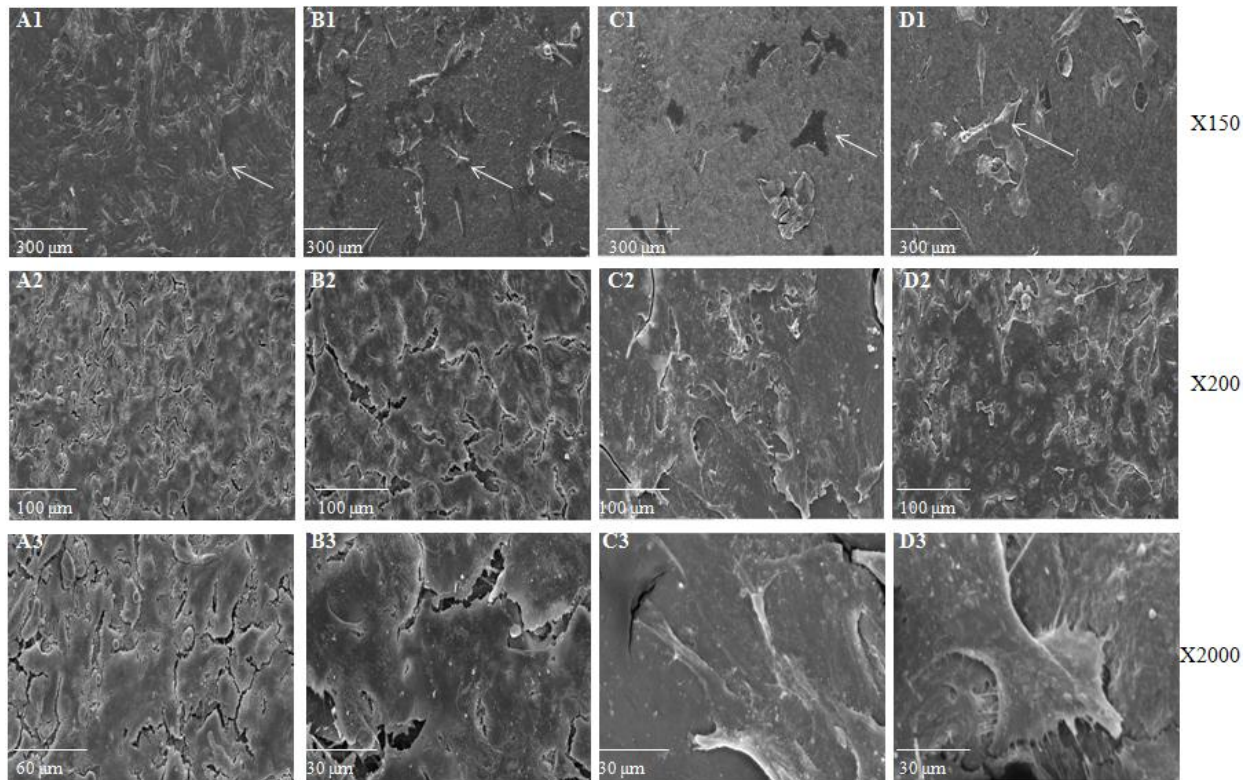


Figure 6.31 SEM images of MG-63 cells growing on (A1) Tissue culture plastic; (B1) neat P(3HB); (C1) P(3HB)/MNP; and (D1) P(3HB)/FF film at Day 1. SEM images of MG-63 cells growing on (A2) Tissue culture plastic; (B2) neat P(3HB); (C2) P(3HB)/MNP; and (D2) P(3HB)/FF film at Day 7. Higher magnification of MG-63 cells growing at Day 7 revealing healthy cells that flattened out and attached on the materials and on each other forming monolayer on (A3) Tissue culture plastic; (B3) neat P(3HB); (C3) P(3HB)/MNP; and (D3) P(3HB)/FF films. Arrows highlight cells attached on the materials.

Figure 6.32 features the MG-63 cells grown at day 1 of the cell proliferation investigations on both the neat P(3HB) scaffold and the composite scaffold of P(3HB)/MNP and P(3HB)/FF. The red circles with red lines indicate a section of each image that was magnified for a clearer view of the cells. The MG-63 cells attached very well on all the surfaces of the walls of the pores in the scaffolds attaching to each other and the walls of the throat in the scaffold with their filopodia. In addition, the cells were found to have started aligning on each other after making contacts with each other with their extended filopodia. No sign of necrosis or apoptosis was noticed on all the test materials. MG-63 cells on the composite materials exhibited variations in morphology that were surface-dependent. The shape of cells growing on the neat P(3HB) and the composite scaffolds depended on the roughness of the surfaces as well as the size of the cavity on which they were growing. Cells aggregated in cavities with narrow sizes and clusters of multilayered cells were found in some areas.

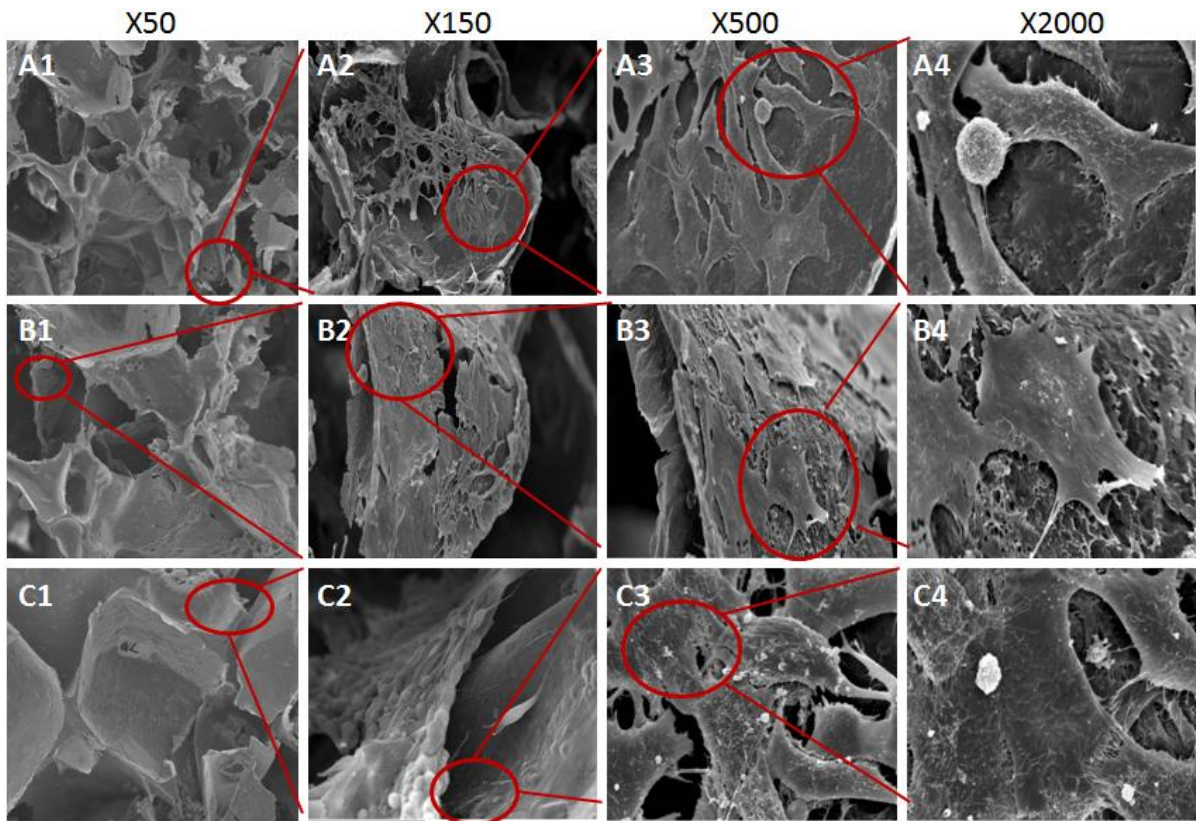


Figure 6.32 SEM images of MG-63 cells growing at day 1 on (A) neat P(3HB) scaffold; (B) P(3HB)/MNP and P(3HB)/FF composite scaffolds at different magnifications shown on the top of the figure.

Figure 6.33 shows the SEM images of MG-63 cells grown at Day 7 of the cell proliferation investigation. The cells were found to have proliferated well at a very high density on all the test materials forming a monolayer on the surface of the materials and connecting with neighboring cells with their filopodia on the nearby pore throats. The high magnified images revealed the extension of filopodia by the cells in preparation to connect to the neighboring monolayer of cells. There was no observable difference between the percentage cell proliferations as obvious by mere physical observations. However, the cells grown on the composite materials produced thread-like filopodia on their surface to reach neighboring cells in the nearby pores, while more of rounded cells were observed on the neat P(3HB) 3D scaffold.

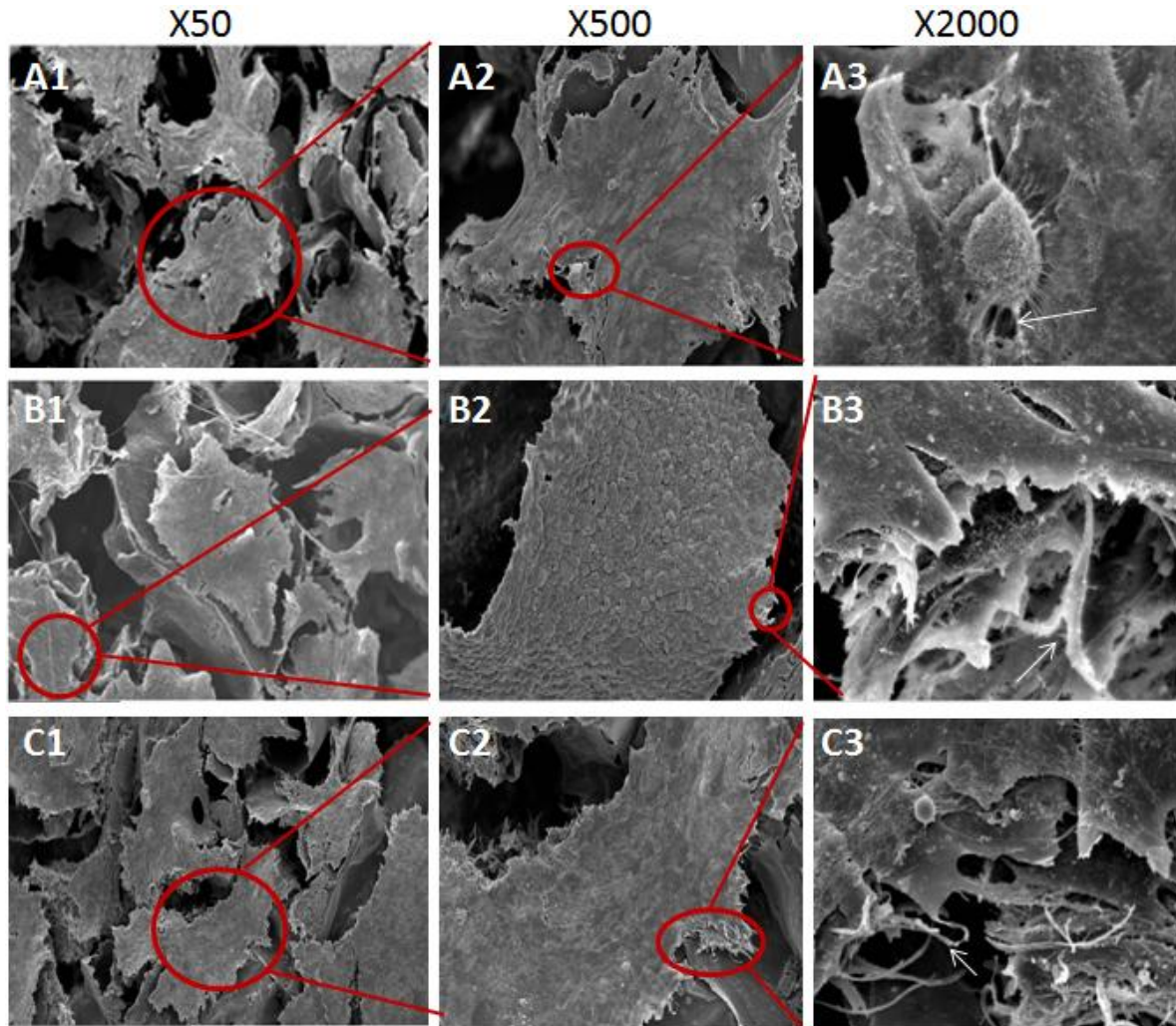


Figure 6.33 SEM images of MG-63 cells growing at day 7 on (A) neat P(3HB) scaffold; (B) P(3HB)/MNP and (C) P(3HB)/FF composite scaffolds at different magnifications shown on the top of the figure. Arrows in white indicate extension of filopodia by the cells to bridge the pores and form monolayer on the scaffold.

6.6 Discussion

Recently, much effort is being dedicated towards the development of sustainable technologies for the fabrication of customized tissue engineering scaffolds with reproducible internal morphology that can ensure enhanced oxygen and nutrient transport throughout the scaffold. Among the successfully developed scaffolds, there are still limitations and difficulties in controlling cell differentiation and angiogenesis as well as obtaining stable scaffold implantation in the pathological site. Hence, the conceptual provision of a scaffold that can not only provide architectural frame work and physico-mechanical support, but also enhance cell growth, proliferation and differentiation *in vivo* have been proposed in this study. Two

different forms of maghemite (nanoparticles and ferrofluid) were incorporated into polymeric P(3HB) in order to achieve these objectives. The SEM imaging confirmed the 2D composite materials to have nanotopography with microstructural pores. The crystals found on the surface of the P(3HB)/MNP composite were the incorporated magnetic particles, while the aggregates were agglomerates of nanomagnetic particles that came together due to magnetic attractions. Nevertheless, the well distributed nanoparticles are suggested to be very useful in the provision of large surface area for protein adsorption and cellular adhesions. Also, the presence of the highly distributed magnetic particles is expected to aid in reducing the hydrophobic properties of the polymer matrix. The micropores observed at higher magnification on the surfaces of both neat P(3HB) and composite materials were formed as a result of evaporation of solvent. During evaporation, the chloroform solvent leaves the surfaces of the materials in the form of vapours and as a result, micropores were created from the interior to the surfaces of the materials. These pores are suggested to be helpful during protein adsorption by the materials and consequent cell adhesions. Misra *et al.* have observed a similar nanotopography surface on the addition of nano-Bioglass[®] in P(3HB) matrix to produce P(3HB)/Bioglass 2D and 3D composites (Misra *et al.*, 2008). On the other hand, the agglomerated nanoparticles will be expected to influence both the static and dynamic mechanical properties of the materials. TEM micrographs of the composite materials confirmed the presence of the magnetic nanoparticles and ferrofluid as well as the homogenous distribution of the incorporated materials throughout the composite scaffold specimens. The homogenous distribution of the incorporated materials, as observed in the TEM and SEM images, emphasized that the magnetic nanoparticles and the ferrofluid were not lost during the particulate leaching employed for pore formation in the scaffold. This further strengthened the claim that the developed technique for tissue engineering scaffold production was ideal and can allow incorporation of bioactive materials like hydroxyapatite to further enhance bioactivity during bone regeneration. Also, homogenous distribution of the incorporated materials in the composites is necessary to obtain composites with high mechanical performance and similar degradation kinetics throughout the scaffold.

The agglomerated Fe₂O₃ observed in the P(3HB)/Magnetic nanoparticles composite scaffold can be attributed to the agglomeration of some of the Fe₂O₃ nanoparticles due to the magnetic influence in the nanoparticles. The diffraction rings of Fe₂O₃ and polymeric P(3HB) shown in Figure 6.3 indicated that Fe₂O₃ nanoparticles and ferrofluid were randomly distributed and oriented in the composite scaffolds (P(3HB)/MNP and P(3HB)/FF). This observation is in

agreement with the crystallographic features observed in the XRD spectra of the composite samples.

The hysteresis loops of the P(3HB)/Magnetic nanoparticles and P(3HB)/Magnetic fluid composites almost saturate at ± 1 T without any coercivity or remanent magnetization. This behaviour is typical for paramagnetic or superparamagnetic materials. As shown in Figure 6.2 and 6.3, all magnetic hysteresis loops passed through the grid origin. In addition, it was also shown in Table 6.1 that the residual magnetization (σ_r) of all the particles is completely zero. This shows that either the Fe_2O_3 particles or ferrofluid composite scaffold have good superparamagnetism. Also, comparing their saturation magnetization (σ_s) (Table 6.1), it is apparent that σ_s increased as the amount of maghemite nanoparticles in the scaffold increases. The absence of coerciveness at temperatures close to 300 K is characteristic of superparamagnetic material (Moment *et al.*, 2002) and therefore confirmed that both P(3HB)/MNP and P(3HB)/FF composites had superparamagnetic properties. The hysteresis loop of the neat P(3HB) is composed of two magnetic phases. First, corresponding to the paramagnetic or superparamagnetic material and second belonging to the diamagnetic phase as evident from the profile of the hysteresis curve at lower and higher applied fields, respectively. However, as expected the neat P(3HB) has a very low maximum magnetization $M_{\text{max+}}$ at 1 T (0.004emu/g) when compared to the composite material. Hence, the neat P(3HB) can be confirmed to have negligible magnetic properties.

According to Wang *et al.*, microhardness may be used as an indicator of Young's modulus of a biomaterial composite (Wang *et al.*, 1998). Thus, the increased in hardness achieved suggested that increasing MNP or ferrofluid content increases the Young's modulus of the composite materials. The result of the mechanical test performed confirmed that the addition of MNP or ferrofluid indeed increased the microhardness of the composite materials (Figure 6.6).

DMA has extensively been employed in characterizing polymer blends and fillers (Brahimi *et al.*, 1991; Mukhopadhyaya *et al.*, 1993; Chen and Wang, 2002). P(3HB) is a viscoelastic material and thus, has the ability to store mechanical energy without dissipation. Also, P(3HB) has the capability to dissipate energy instead of storing it in the presence of a filler. The stored mechanical energy can be expressed as storage modulus (E') while the dissipated energy can be termed as loss modulus (E''). The dissipation of energy can always manifest as internal friction or damping in a polymer matrix composite. The energy dissipation may also

come from the filler-matrix interface. In either cases, the friction can be quantified by $\tan \delta$ which is the ratio of the energy dissipated per cycle to the energy stored during the cycle (i.e., E''/E'). Furthermore, high damping in P(3HB) blends is always accompanied by a decrease in dimensional stability during loading. It therefore appeared that, within the temperature range of 20-50 °C, the addition of MNP limited the mobility of the amorphous phase in the polymer matrix and hence, damping in the composites was reduced. The degree of the damping process is expected to depend upon the amount of MNP or ferrofluid incorporated in the polymer matrix. This is true since the addition of the MNP or ferrofluid will reduce the volume ratio of the polymer matrix and thus, the overall damping in the composite. In the dissipation of energy during DMA stress cycling, a relatively large amount of the energy is assumed to be dissipated at the MNP –polymer interface due to the existence of interfacial mechanical bonds.

The dynamic modulus ($E'+E''$) of the P(3HB)/MNP and P(3HB)/FF showed a similar trend to that of the microhardness of the composite materials with the addition of the fillers (MNP or ferrofluid) and this decreased with increase in temperature. Similar effects have been reported on the addition of bioceramics to the polymer matrix by Wang *et al.*, 1997; Chen and Wang, 2002 and Misra *et al.*, 2007. Misra *et al.* achieved an increase in the hardness of the P(3HB)/Bioglass[®] composite when nano Bioglass[®] was added to form composite. In this study, the microhardness of the P(3HB)/MNP and P(3HB)/FF composites have increase significantly on the addition of magnetic particles.

Spherulites are spherical semicrystalline regions inside non-branched linear polymers. The formation of spherulites in polymeric materials affects many of their properties such as crystallinity, tensile strength and Young's modulus. These properties of polymers increase during spherulization and the increase is due to the lamellae fraction within the spherulites, where the molecules are more densely packed than in the amorphous phase. This phenomenon is made clear in Figure 6.34a. The addition of ferrofluid resulted in relatively large number of nucleation sites which led to the formation of numerous and small spherulites that interacted with each other upon growth. Stronger intermolecular interaction within the lamellae accounts for increased hardness. On the other hand, the amorphous regions between the lamellae within the spherulites give the material certain elasticity and impact resistance (Charles and Reymond, 2003).

Changes in mechanical properties of polymers upon formation of spherulites, however, strongly depend on the size and density of the spherulites. In the case of a few nucleation sites, a few larger spherulites are created (Linda *et al.*, 2008). The stress-strain curve and result shown in Figure 6.14a and Table 6.4, demonstrated that the compression modulus and stress strength of the composite materials initially decreased with the addition of either magnetic nanoparticles or ferrofluid but gradually increased with increase in the amount of magnetic nanoparticles and ferrofluid. At low amount of the fillers, the spherulite size formed in the polymer matrix increased but their number in the composite decreased. Similar trends have been observed for tensile strength, yield stress and toughness by Ehrenstein and Theriault on isotactic polypropylene (Ehrenstein and Theriault, 2001). Increase in the total volume of the spherulites results in their interaction as well as shrinkage of the polymer, which becomes brittle and easily cracks under load along the boundaries between the spherulites (Ehrenstein and Theriault, 2001). It can therefore be concluded that the addition of MNP and ferrofluid have a positive effect in enhancing the microhardness as well as improving the dynamic modulus of P(3HB).

The DSC analysis was carried out by subjecting the materials to heating rate of 10°C/min and within a temperature range of -50 to 200°C. During cooling from 200°C to -50°C, if the molten linear P(3HB) is cooled down rapidly, the orientation of its molecules, that were randomly aligned would be curved and entangled. The solid polymer matrix would therefore have a disordered structure. However, upon slow cooling, as in the case of this investigation, some polymer chains would be expected to take on a certain orderly configuration thereby aligning themselves in plates called crystalline lamellae (Charles and Reymond, 2003). However, in the presence of fillers in the polymer matrix (MNP or ferrofluid), spherulitic growth from the melted polymeric composite would follow the temperature gradient (as illustrated in Figure 6.34). If the thermal gradient is in the direction normal to the direction of molecular alignment, then the lamella will grow sideward into a planar crystallite. However, in the absence of thermal gradient, spherulitic growth can occur radially in all directions. The largest surfaces of the crystalline lamellae will be terminated by molecular bends and kinks, and growth of spherulites in this direction will result in disordered regions. Hence, spherulites have semicrystalline structure where highly ordered lamellae plates are interrupted by amorphous regions (Charles and Reymond, 2003). The same phenomenon has been observed in the thermal transition of the composite materials. Thus, DSC analysis showed that incorporation of either magnetic nanoparticles or ferrofluid

into the polymer matrix enhanced the crystallinity of the composite materials following the principles explained above. Since low crystallinity leads to high degradation rate of degradable biomaterials, (Chen and Wang, 2002), the increased crystallinity achieved in this study would help in the control of *in vivo* degradation rate of the composite materials. The melting temperature of the P(3HB) matrix was also found to be affected by the introduction of either magnetic nanoparticles or ferrofluid to the polymer matrix. The multiple melting peaks observed in this study can be due to the melting of the spherulites formed during sample preparations or melting of the magnetic nanoparticles. However, in this study, the melting temperature of the magnetic nanoparticles was not analysed. Further study will be needed to confirm the main source of the multiple peaks observed during thermal transition resolution in the composite. It was observed that the heat of fusion increased with increase in the amount of filler (MNP or ferrofluid). It is possible that the increase resulted from the increase in the spherulitic growth with increased in the amount of filler present in the composite materials, thus more energy was required for the spherulites to melt into amorphous state.

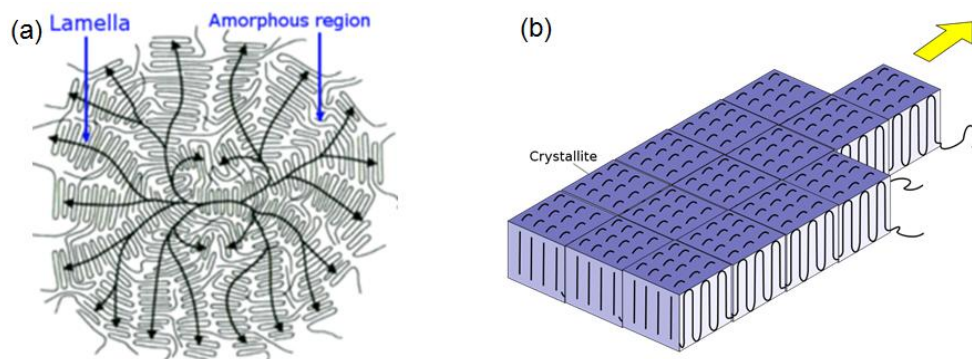


Figure 6.34 (a) Schematic model of a spherulite. Black arrows indicate direction of molecular alignment (b) Principle of lamellae formation during the crystallization of polymers. Arrow shows the direction of temperature gradient (adopted from Menges *et al.*, 2002).

The slight increase in the melting and crystallization temperature observed during the degradation study was possibly due to the formation of hydroxyapatite on the composite material. This was also observed as the appearance of a third melting temperature after 21 days immersion in SBF. The formation of new compound was further confirmed by the XRD spectroscopy and Raman Shift spectroscopy which indicated an increased crystallinity. The

loss in the second crystallization peak was possibly due to degradation of the small sized spherulites in the composite matrix (Table 6.6).

The FTIR spectra of the composite materials actually showed modified absorption peaks in shape and intensity when compared to the characteristic peaks of the neat P(3HB). This can possibly result from weak hydrogen and strong ionic bond interactions between the polymeric matrix and the maghemite. Millan *et al.* have observed similar weak hydrogen and strong ionic bonds during the preparation of maghemite polymer nanocomposite (Millan *et al.*, 2009). The result of the analysis indicated that the crystallisation of the polymer matrix was affected by the addition/introduction of the fillers which was confirmed by the result of the DSC analysis. This has therefore, further strengthened the claim that certain changes in the crystalline properties of the polymer structure occurred as a result of the crystallisation process of the nanocomposite material on the introduction of the fillers.

The surface property of biomaterials plays an important role in its performance in a biological environment. Much research has been conducted to analyze the effects of hydrophobicity and hydrophilicity on biological responses (i.e. protein adsorption and cell adhesion). Improved surface wettability generally improves the interactions between the composite materials and the cells and results in controlled cellular adhesion and maintenance of differentiated phenotypic expression (Gelego *et al.*, 2000). Many researchers including Li *et al.* have investigated the effect of addition of inorganic materials to biodegradable polymer matrix. Li *et al.* in their investigations with wollastonite composite scaffold observed that the incorporation of wollastonite to the P(3HB-co-3HV) polymer matrix improved the hydrophilicity of the composite (Li *et al.*, 2005). In this study, the introduction of the either magnetic nanoparticles or ferrofluid to the P(3HB) polymer matrix significantly improved the hydrophilicity of the composite material. Although, water contact angle measurement gives some information about the hydrophilicity of the composite material, Zhao *et al.* have suggested that investigation into the free energy of samples (Gibb's free energy) would give more information on the surface properties towards cell adhesion (Zhao *et al.*, 2005). Further study will be needed to investigate the contribution of wettability, surface chemistry and surface free energy towards cell attachment and mobility over the surface of the composite biomaterial.

Detailed knowledge of the relationship between the surface properties of a biomaterial and its ability to absorb protein when exposed to a protein-containing medium is very important in

the application of a specific biomaterial in tissue regeneration. Apart from the very important physico-mechanical properties, a biomaterial should be able to support cell adhesion, proliferation and differentiation and these can be achieved with the help of protein layers which provide support for the anchorage of cells onto a biomaterial. When a biomaterial is exposed to cells suspended in a culture medium supplemented with FBS, protein in the serum are rapidly adsorbed onto the surface of the biomaterial prior to cell adhesion. The adsorption of cell adhesive serum proteins, such as fibronectin and vitronectin, therefore plays a critical role in cell adhesion onto a biomaterial surface and subsequently determine cell adhesion behaviours (Grinnell and Feld, 1982). The adsorption of serum protein contained in FBS onto the surface of the 2D magnetic nanocomposite was investigated in this study. It was observed that the addition of magnetic nanoparticles or fluid improved protein adsorption on to the surface of the nanocomposite. This was possibly due to the combined effect of increased hydrophilicity, surface chemistry and surface charge provided by the incorporated magnetic materials. Also, the effect of the larger surface area provided by the magnetic nanoparticles could be another possible reason for the increased protein absorption observed on the composite material.

Previous research has shown that very hydrophobic materials such as polytetrafluoroethylene (PTFE) with a water contact angle between 105° – 116° inhibit cellular adsorption. In contrast, hydrophilic materials such as tissue culture polystyrene (TCPS) are well known to support cellular adhesion (Chen *et al.*, 2003). The observations made in this study using the Alamar blue assay showed that the cells were able to attach to the surface of the materials (i.e. TCPS, neat P(3HB), P(3HB)/MNP and P(3HB)/FF) on the first day of the assay. This was most likely due to the adsorbed protein layer which was able to provide anchorage for the cells during the first day. However, as the incubation time increased, it was found that cell proliferation on the neat P(3HB) film reduced when compared to the cell proliferation on the control and the composite materials. This could be explained based on the possibility that the adsorbed protein on the surface of the neat P(3HB) interacted with the hydrophobic surface of the neat P(3HB) in a manner that led to changes in the protein conformation and thus, resulted in reduced access of the cells to the ligand moieties needed for integrin binding and cell attachment. Cell proliferation were found to increase more on the magnetic nanocomposites than on the control (TCPS) and the neat P(3HB). This is probably due to the ability of the magnetic composite material to provide large surface area and good surface chemistry which enhanced hydration and protein adsorption onto the surface of the materials.

This result was in agreement with the result on the measurement of aqueous contact angle and protein adsorption and therefore confirms that the magnetic nanocomposites are excellent biomaterials for the cellular attachment and proliferation. However, there is need for a further investigation to confirm other factors that the magnetic materials contributed towards the growing cell, apart from nanostructured surfaces. There was no statistical difference between cell growth on the neat P(3HB) and nanocomposite 3D scaffolds containing different amount of nanoparticles and ferrofluid on day 1, 4 and 7. This shows that the magnetic nanocomposites are not toxic and can be safely used to improve mechanical properties as well as provide nanostructured surfaces for cell adhesion and proliferation in tissue regeneration.

It has been suggested that increased bone formation leads to increased total protein production by the bone cells. This was investigated on the magnetic nanocomposite to understand the influence of the magnetic materials on the bone formation activities of the MG-63 cells. The result of the investigation, depicted in Figure 6.27 and 6.28, shows that the magnetic nanoparticles and the ferrofluid did not have adverse effect towards proteins secreted by the cells. Also the protein produced in the osteogenic medium is slightly higher than those produced in the non-osteogenic medium and was also higher in the composite containing magnetic ferrofluid. It is possible that the cells grown on the P(3HB)/FF initiated greater expression of bone formation protein than those grown on the P(3HB)/MNP, TCPS and neat P(3HB) films.

Studies have shown that the degradation of polymers can lead to acidic conditions in the surroundings of the degrading polymers (Heinemann *et al.*, 2002; Lu *et al.*, 2000; Li *et al.*, 2005). This was observed in this study. The decrease in the pH of the SBF immersed with P(3HB) is due to 3-hydroxybutyric acid produced as a result of the degradation of P(3HB). The degradation results showed that the incorporation of MNP and ferrofluid led to reduced percentage weight loss when compared to the neat P(3HB), after immersion in SBF. The percentage weight loss of the P(3HB)/MNP composites was found to have occurred fairly slowly while those of the P(3HB)/FF decreased drastically from 4.67 ± 0.12 % (after 7 days) to 1.16 ± 0.32 % (after 14 days) with a sharp rise to 4.34 ± 0.11 % after 21 days. According to Gopferich, 1996, pH affects reaction rates through catalysis and ester hydrolysis can either be acid or base catalysed. In addition, Chu have observed that degradation of polymers such as poly(glycolic acid) and poly(lactic-co-glycolic acid) is mostly dependent on the pH of the

surrounding environment and therefore noted that degradation of the polymers were highest at neutral pH. However, when the polymers were placed in acidic or basic pH, fastest degradation was observed mostly at low and high pH. He further observed that the faster chain scission in heterogeneous erosion of poly(lactic acid) led to the generation of carboxylic acids which further accelerate the polymer degradation due to autocatalysis. Chu therefore suggested that by addition of acidic or basic additives to polymeric matrixes, the degradation rate of the polymer during hydrolysis can be controlled (Chu, 1982). Based on the above findings, it is possible that the initial degradation of the neat P(3HB) released hydroxyl acid (the degradation products of P(3HB)) which lowered the pH of the immersed SBF. Hence, the decrease in pH observed. On the other hand, the additives (MNP and ferrofluid) incorporated into the polymer matrix helped to control the degradation rate of the composite materials. Moreover, the ionic release, during degradation could further help to control the pH of the surrounding environment (SBF). Misra *et al.* have observed the control of the pH of SBF immersed with P(3HB)/Bioglass[®] by the ionic release from the incorporated nano-Bioglass[®] (Misra *et al.*, 2007).

In vivo, a biomaterial surfaces is usually coated by components present in the extracellular fluid. However, the adsorption of extracellular fluid to the biomaterial is largely dependent on the surface chemistry, charge, wettability and free energy of the biomaterial which is regulated by the microstructural features on the biomaterial surface. In this study, it was observed that cell attachment on the test materials (neat P(3HB) and composite materials films) were less on the first day. However, the attached cells spread and proliferated later as observed in SEM image at day 7, in Figure 6.31. The reason for the low cell attachment on the composite materials and neat P(3HB) compared to the higher attachment on the tissue culture plastic is most likely due to the effect of surface chemistry and free energy which might have affected the initial protein adsorption on the material surface. The spreading and proliferation after day 1 is possibly due to material surface-protein interactions. Further detailed studies will be needed to ascertain the effect of the magnetic component in the composite to the adsorption of fibronectin and other serum protein to the composite surfaces.

Cell responses to surface microtopography are expressed in their ability to attach, proliferate and differentiate. According to Boyan *et al.* cell adhesion and cell proliferation are sensitive to the microtopography of biomaterial surfaces (Boyan *et al.*, 1995). Ordinarily, it is difficult to determine which structures are responsible for individual phenotypic traits expressed by

cells grown on different materials. However, architectural designs have been proposed to be possibly responsible for the cell adhesion and proliferation observed on different biomaterial surfaces (Hutmacher, 2000). In this study, cells were found to have anchored to the surfaces of the different scaffold materials tested, with flattened morphology that were most often characterised by the extension of filopodia to reach the neighbouring cells. This is contrary to the observations made by Zinger *et al.* Zinger and co workers observed that osteoblasts do not extend filopodia while laid flattened and spread in a cavity (Zinger *et al.*, 2005). It is possible that favourable microstructural surfaces of the materials could have influenced the spreading of filopodia by the cells to reach the neighbouring cells. Furthermore, for the cells to bridge barriers such as crevices in the pore throat, they need to grow filopodia which helped them to form a monolayer and overcome the barriers in the crevices. Again, Boyal *et al.* have observed cells with cuboidal shape while attached on the surface of biomaterial. They suggested that architectural features present on the biomaterial surface could have influenced the morphological expression of the cells. Such architectural features included microrough surfaces and shorter peak-to-peak distances of pores in comparable to the length of the cell body. Boyal *et al.* later concluded that cells growing on biomaterial surfaces with these features are prone to exhibit cuboidal shape while anchoring to the surface with long dendritic filopodia (Boyan *et al.*, 2003). Brunette, 1986 & 1998 on the other hand observed that cells laid flat and spread, resulting in a fibroblastic appearance on the smoother surfaces. The cells seeded on to both the TCP and the 2D test materials conform to this characteristic behaviour of osteoblasts. It was also observed that the cells grown on the composite materials produced thread-like dendrites which they utilized to over lay on each other and spread to form monolayer. It is possible that the cells were induced by the magnetic properties of the composite material to produce fibronectin and other cell attachment protein. Hence, further investigation is necessary to understand the effect of the superparamagnetic properties of the composite materials to cells proliferating on them.

6.7 Conclusion

Both 2D and 3D magnetic polymeric composites were successfully prepared by incorporating either MNP or ferrofluid into the polymeric P(3HB) matrix using the novel compression moulding/particulate leaching techniques developed earlier in Chapter 5. The magnetic scaffolds were successfully characterised and the results of the characterisation confirmed

superparamagnetic properties on the composite materials. The introduction of MNP and ferrofluid were confirmed to have positively increased the crystallinity of the composite scaffolds. This has been suggested to be useful in bone regeneration. The result of the degradation study showed that the addition of magnetic nanoparticles or ferrofluid to P(3HB) matrix could help to maintain a gradual degradation of the composite material which would be useful during *in vivo* application of the materials in bone regeneration. Another important result achieved with the composite materials was improved thermo-mechanical properties. Furthermore, the cytocompatibility studies showed that neither MNP nor ferrofluid were toxic to the MG-63 cells. Rather, the cells were found to have grown more on the composite materials than on the neat P(3HB). Also, the result of the total protein production on the composite materials showed that the materials were neither toxic nor hindered total protein production, instead they were found to have an effect in improving the total protein production by the MG-63 cells in osteogenic media. This indicates the potential ability of the composite materials to support mineralisation and subsequent bone formation when employed in bone tissue engineering. In general, the results of this study contribute towards the establishment of magnetic particles and ferrofluid based scaffolds as the scaffold of choice for bone tissue engineering.

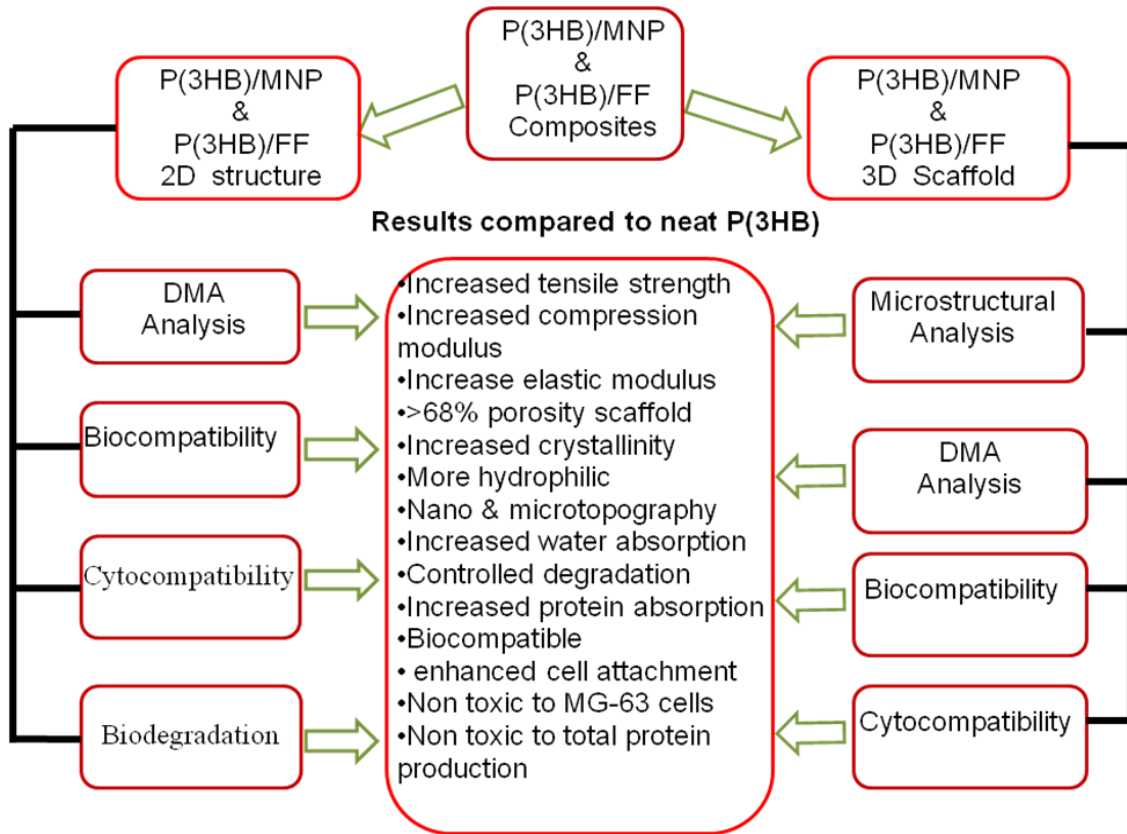


Figure 6.35 Schematic representation of summary of investigations and results achieved in this Chapter.

Chapter 7

POTENTIAL APPLICATION OF P(3HB) IN DRUG DELIVERY

Chapter 7

7.1 Introduction

The use of biodegradable polymeric systems for controlled drug delivery has attracted a lot of interest by scientists working in the medical fields. This is due to their spontaneous hydrolytic degradation in aqueous environment such as body fluids, which allows the removal of the applied materials from the human body after the delivery of loaded drug. PHAs in particular, are potential candidates for the delivery of drugs due to their unique and interesting physicochemical features. The variable properties of PHAs are highly conducive towards their use in the development of multicomponent delivery system that can allow delivering multiple drugs and active ingredients. This technology is based on the fabrication and encapsulation of nanospheres containing drugs or active ingredients into microspheres and allows the simultaneous release of the encapsulated materials in the body. The materials that could benefit from this technology include the water-soluble and fat-soluble drugs and ingredients which can be delivered at the same time using a single medium. This novel technology ensures not only the controlled delivery of drugs but also enhances the stability and bioavailability of a wide range of drugs and ingredients that control their release kinetics and prolong their residence time which is required for a long-term drug delivery.

The poor selectivity of drugs employed in chemotherapy and their associated damage to healthy tissues is a well-known fact. With magnetic polymer-immobilized drugs, it is possible to guide the release of drug molecules and place smart "chemical bombs" highly selective on individual biological targets. Consequently, the last five years have witnessed an exponential growth in activities associated with the potential use of magnetic nanoparticles in biology and biomedical applications (Goya *et al.*, 2008). Researchers are continuing efforts to develop targeted therapeutic systems that could be manipulated using external forces, including magnetic fields, ultrasound, electric fields, temperature, light, and mechanical forces to focus the drug action within diseased tissues (Kim and Lim, 2002). To achieve these technological applications, iron oxides such as magnetite (Fe_3O_4) and maghemite ($\gamma\text{-Fe}_2\text{O}_3$) have been proposed because of their biocompatibility, high magnetic transition temperatures and high saturation magnetization. Encapsulating drugs in these systems help to localize and activate drug molecules at a specific targeted area by externally generated forces such as magnetic field (Lubbe *et al.*, 2001). The drug molecules, on reaching the targeted site are gradually

released thereby improving their therapeutic efficiency and lower toxic side effects on the healthy cells or tissues (Lubbe *et al.*, 1999; Rugde 2000).

This chapter contains two sections; Section I deals with the application of P(3HB) in multiple drug delivery system. Cellulose nanospheres were produced and encapsulated within P(3HB) microspheres. By employing two polymers with different physicochemical properties, a novel hydrophobic P(3HB) microsphere with entrapped hydrophilic cellulose nanospheres was produced. The hydrophilic properties of the cellulose nanospheres will enhance the encapsulation efficiency of cellulose nanospheres for hydrophilic drugs/nutrients while the lipophilic properties of the P(3HB) will enhance the encapsulation efficiency of the P(3HB) for hydrophobic drugs/nutrients. Hence, it would be possible to deliver both hydrophobic and hydrophilic drugs into the body system. The microspheres produced were characterised and the detailed results of the characterisation analysis were described in the result section below. The constructs produced were subsequently tested for their *in-vitro* release of BSA, used as a model protein and the effect of lipase on the degradation and release of the entrapped cellulose nanospheres were also studied in detail.

Section II is divided into two categories comprising of (a) P(3HB)/magnetic particles (P(3HB)/MNP), composite and (b) P(3HB)/magnetic fluid (P(3HB)/FF), composite microspheres. The composite microspheres were characterised for their magnetic properties as well as the effect of the incorporated magnetic materials on the physicochemical properties of the composite microspheres.

SECTION I

Potential application of P(3HB)/cellulose composites in multiple drug delivery system (encapsulation of cellulose nanospheres in P(3HB) microspheres)

7.1.2 Results

7.1.2.1 SEM Examination

For the successful production of drug-loaded P(3HB) microspheres containing drug-loaded cellulose nanospheres, it is essential to produce the cellulose nanospheres loaded with hydrophilic drug before encapsulating the nanospheres with the P(3HB) solution containing the hydrophobic drug. Figure 7.1a and 7.1b shows a typical SEM image (at lower and higher magnifications) of the cellulose nanoparticles prepared using the method described in Chapter 2, Section 2.6.1. The image shows that the nanospheres exhibited almost uniform diameter of 6-9 nm, and average size of 10-15 nm. Figure 7.1c reveals a typical SEM image of a single P(3HB) microspheres containing cellulose nanospheres, while Figure 7.1d shows a cross section of P(3HB) microspheres highlighting the encapsulated cellulose spheres. Figure 7.2a and 7.2b shows the mono-dispersed hydrophobic P(3HB) microspheres containing hydrophilic cellulose nanospheres (at lower and higher magnifications). The average size of the microspheres was found to be 6 μm , using image J software. The size distribution of the multi-purpose microspheres is shown in Figure 7.4. Throughout the rest of this chapter, P(3HB) microspheres containing cellulose nanospheres will be referred to as multipurpose microspheres.

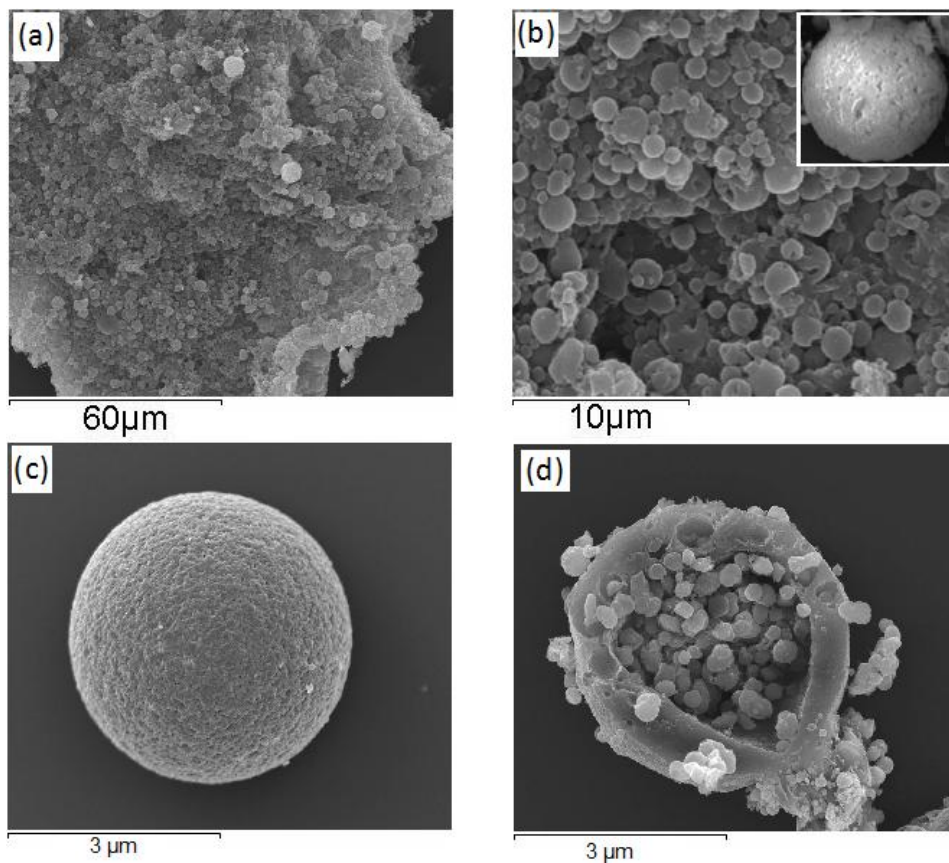


Figure 7.1 Typical SEM image of cellulose nanospheres (a) at lower magnification (b) at higher magnifications (inset, magnified image revealing the surface topography of the cellulose nanospheres; (c) typical SEM image of a single P(3HB) microspheres containing cellulose nanospheres; (d) SEM image of cross section of P(3HB) microsphere displaying the cellulose nanospheres encapsulated within it.

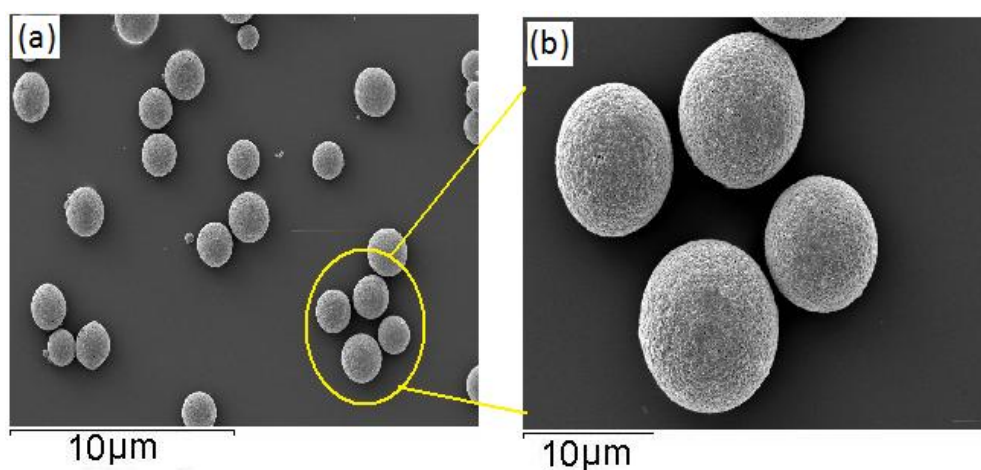


Figure 7.2 Typical SEM image displaying the, almost, monodisperse P(3HB) microspheres containing cellulose nanospheres (a) at lower magnification, (b) at higher magnification.

Figure 7.3a shows the SEM image of P(3HB) microspheres containing cellulose nanospheres prepared using 100 mg/mL of P(3HB), while Figure 7.3b reveals the SEM image of P(3HB) microspheres containing cellulose nanospheres prepared using 50 mg/mL of P(3HB). Large pores as well as rough surfaces are observed in the image in Figure 7.3b while Figure 7.3a depicts a smoother surface with nano scale indented pores.

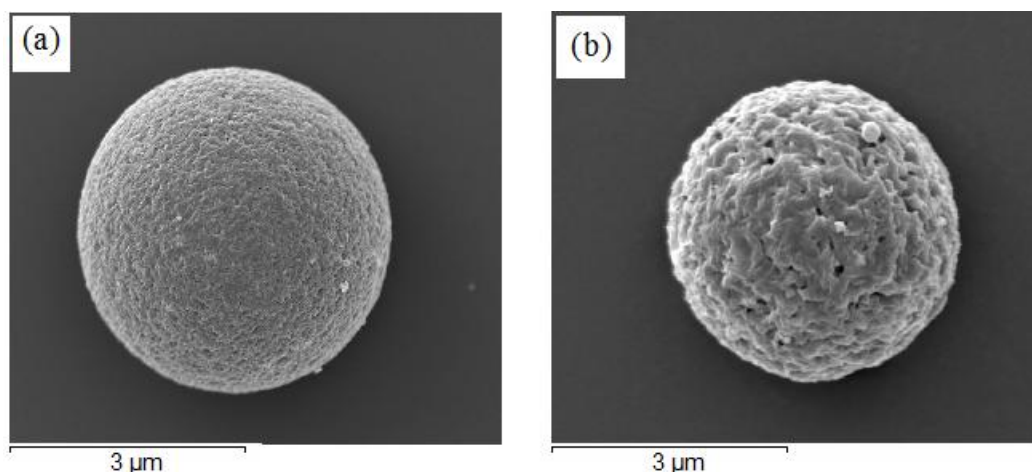


Figure 7.3 Typical SEM image of a P(3HB) microsphere prepared by dissolving 1g of P(3HB) in (a) 100 mg/mL and (b) 50 mg/mL chloroform.

7.1.2.2 Particle size measurements using Dynamic Light Scattering, DLS

A dynamic light scattering instrument (DLS) was used to measure the diameter distributions of the multipurpose microspheres produced. The operation of dynamic light scattering is based on the scattering of the light diffused by the particles suspended in a medium, due to brownian motion. This scattering is random and related to the translational diffusion coefficient D and also on the diameter of the particles. Figure 7.4 below shows the particle analysis performed on the multipurpose microsphere using DLS. The analysis in ‘intensity mode’ revealed particles in the diameter range of 1.04 μm to 6.40 μm . During the analysis, the sample exhibited partial sedimentation. Hence, the measurement was repeated using only the ‘non-sedimenting’ part of the sample. In the ‘intensity mode’ two diameter fractions were detected; 96.7 % particles with average diameter of 901.3 nm (this fraction involves particles in the diameter range of 712-1474 nm) and 3.3 % particles with the average diameter of 5.4 μm (this fraction involves particles in the range of 4145 – 6439 nm).

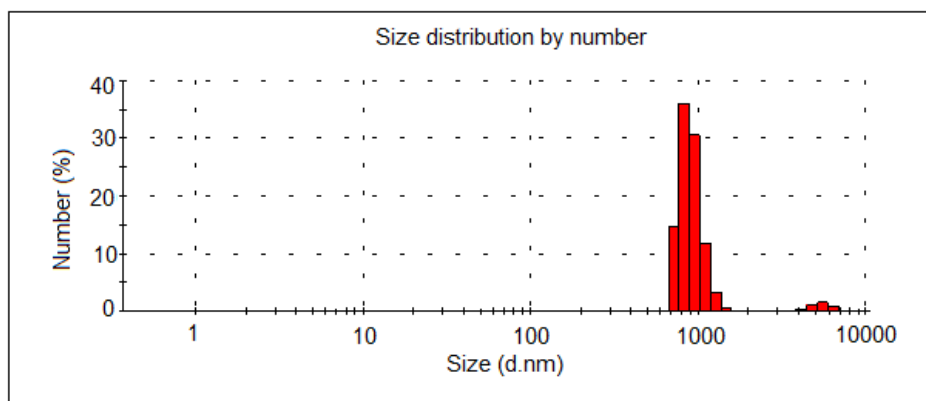


Figure 7.4 The histogram illustrates the particle size (nanometer scale) distribution of microspheres measured using Dynamic Light Scattering, DLS technique in number mode.

7.1.2.3 Surface Chemistry measurement

Figure 7.5 shows the surface chemistry measurement performed on the cellulose nanospheres, the multipurpose P(3HB) microspheres and pure P(3HB) microspheres. The cellulose nanospheres were found to be more hydrophilic when compared to multipurpose P(3HB) microspheres and pure P(3HB) microspheres. Statistical analysis on the result shows a highly significant difference ($p < 0.05$) of the binding constant of Rose Bengal dye between cellulose nanospheres and pure P(3HB) microspheres, and between multipurpose microspheres and pure P(3HB) microspheres.

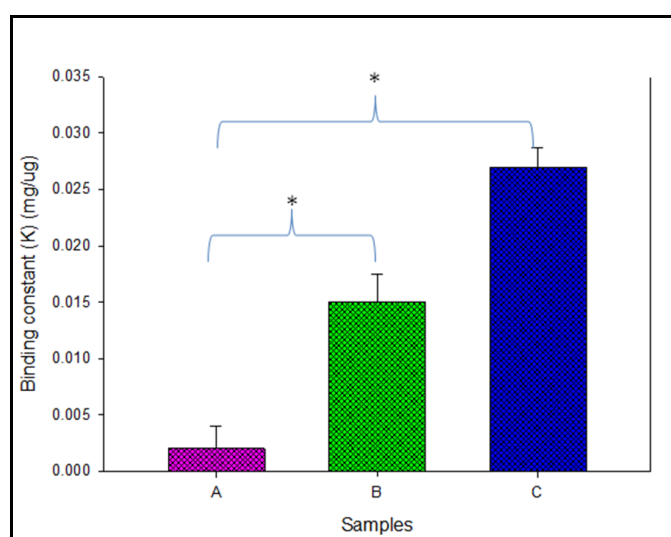


Figure 7.5 Surface chemistry measurement of (A) cellulose nanospheres (B) P(3HB) microspheres with cellulose nanospheres, (C) P(3HB) microspheres without cellulose nanospheres ($n=3$, error = \pm SD, $*p < 0.05$) using binding of Rose Bengal Blue.

7.1.2.4 Influence of organic solvent on the residual PVA on the microsphere surface

In the production of multipurpose P(3HB) microspheres, polyvinyl alcohol, PVA was employed as an emulsifier in the oil in water emulsion. Hence, chances of the PVA forming a stable network on the surface of the microspheres even after washing with distilled water is expected. P(3HB) dissolves easily in chloroform and dichloromethane, meaning that any of them can serve as solvent for microsphere production. The effect of these solvents were tested and the analysis performed showed that more PVA was detected on the microspheres prepared with dichloromethane than those prepared with chloroform as solvent (Figure 7.6).

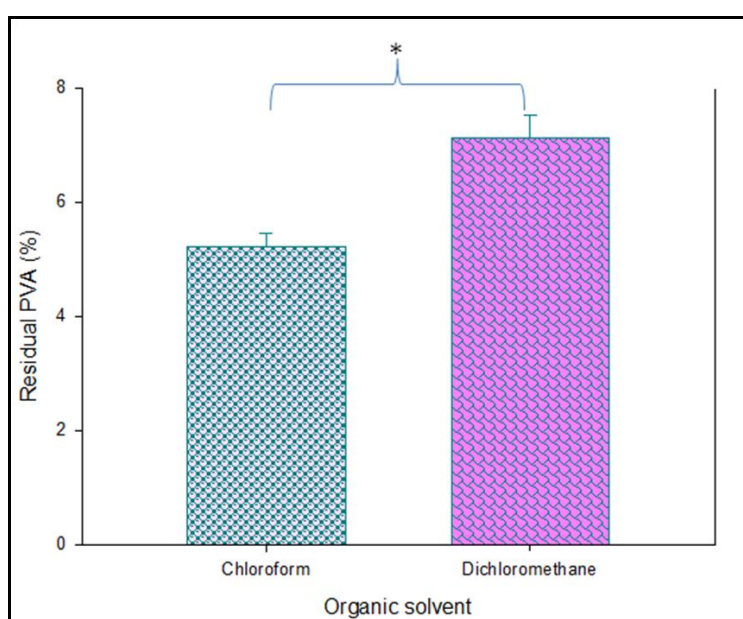


Figure 7.6 Effect of organic solvent on % residual PVA associated with P(3HB) microspheres (n=3; Error bars = \pm SD, $p < 0.05$).

7.1.2.5 Influence of PVA concentration in the oil in water emulsion on the residual PVA associated with P(3HB) microspheres.

Having confirmed with the analysis above that residual PVA is left on the surface of the microspheres during production, investigations were further extended on the effect of PVA concentrations in the oil in water emulsion on the capacity of the microspheres to retain PVA. This was performed to possibly reduce the amount of PVA associated surfaces of the microspheres. To perform this study, the microspheres were prepared using chloroform as an organic solvent and with oil in water emulsion containing different amount of PVA (0.5, 1.0,

1.5, 2.0 and 2.5%). Chloroform was chosen based on the minimal surface associated PVA found in the previous analysis. As shown in Figure 7.6, increase in PVA solution in the oil in water emulsion from 0.5 to 2.5% resulted in an increase in the percentage residual PVA associated surfaces of the microspheres after production.

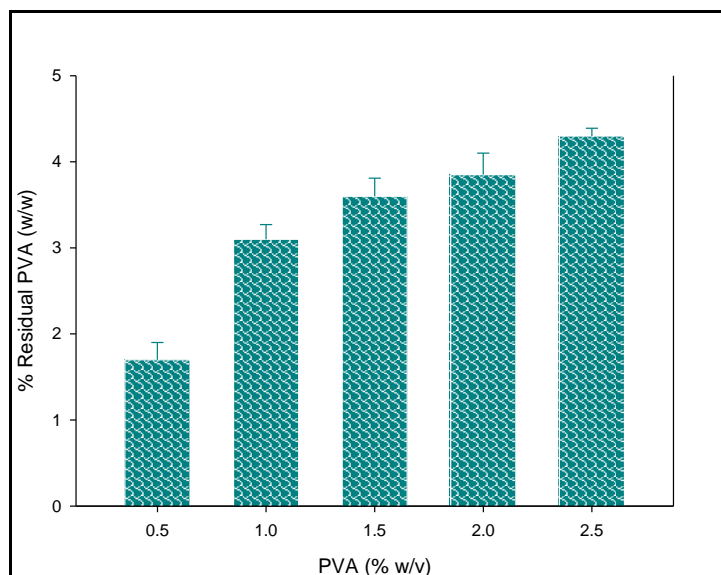


Figure 7.7 Determination of the effect of PVA concentration of the oil in water emulsion on the percentage residual PVA on the surface of microspheres.

7.1.2.6 *In vitro* BSA release analysis

Figure 7.8 shows the graph of a standard curve generated for the measurement of BSA concentration in the constructs. Figure 7.9 on the other hand, shows the percentage cumulative BSA released from the constructs when (a) only the cellulose nanospheres encapsulated inside the polymeric P(3HB) was loaded with BSA, (b) cellulose nanospheres loaded with BSA (c) when both the cellulose nanospheres and the surrounding P(3HB) microspheres were loaded with BSA. It can be seen from the release profile in Figure 7.9, that the BSA loaded cellulose nanospheres and the BSA loaded P(3HB) microsphere containing cellulose nanospheres loaded with BSA showed a biphasic behaviour (initial burst release and slower release phase) in the release of BSA protein. The BSA loaded cellulose nanospheres contained in non-BSA loaded P(3HB) microspheres shows a progressive BSA release with time with no associated burst release. In addition, a statistical difference ($p < 0.05$) in cumulative BSA release was found between the three sets of test spheres. BSA release was

lowest in the BSA loaded cellulose nanospheres entrapped within non-BSA loaded P(3HB) and the highest with the BSA loaded cellulose nanospheres entrapped within BSA loaded polymeric P(3HB). Furthermore, there was a lag phase observed in the drug release, as seen in Figure 7.9, for all the test spheres except for the BSA loaded cellulose nanospheres entrapped within non-BSA loaded P(3HB) which exhibited a uniform release.

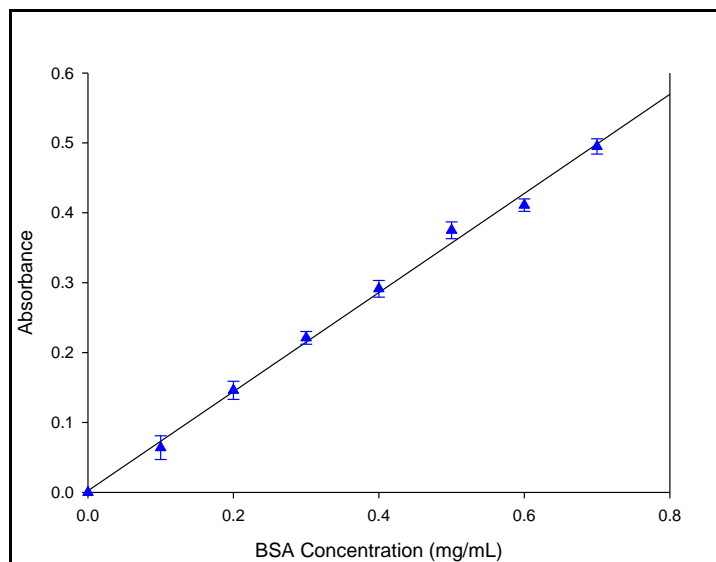


Figure 7.8 standard curves for BSA concentration measurements. UV-visible spectroscopy measurements were carried out for known concentrations of BSA at the absorbance maximum of 280 nm. The absorbance coefficient, ϵ was determined to be $0.7136 \text{ mg mL}^{-1} \text{ cm}^{-1}$.

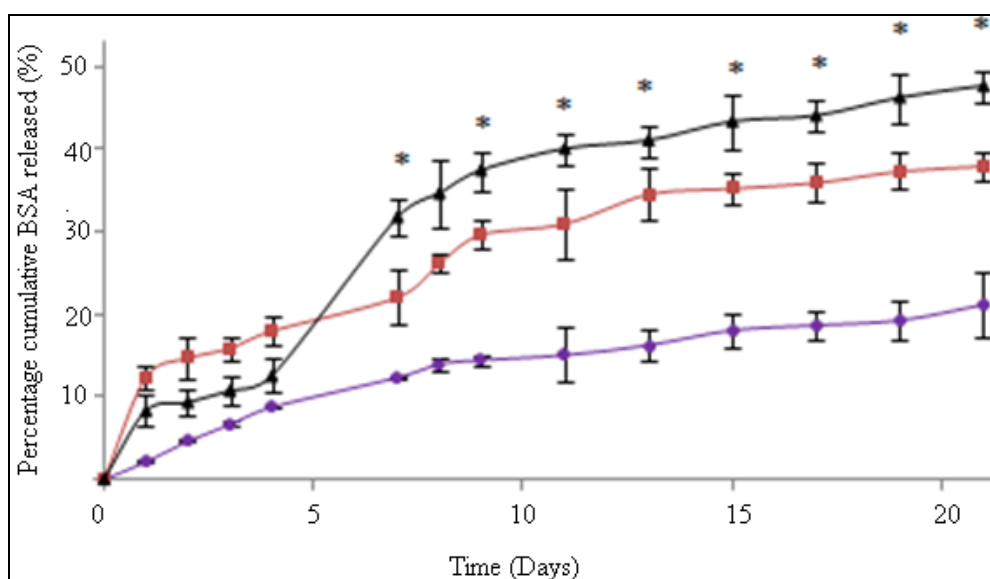


Figure 7.9 *In vitro* release of BSA for (A) Cellulose nanospheres loaded with BSA and encapsulated in P(3HB) microspheres, (—●—) (B) Cellulose nanospheres (—■—) and (C) cellulose nanospheres loaded with BSA and encapsulated by P(3HB) microspheres also loaded with BSA (—▲—).

7.1.2.7 *In-vitro* degradation studies

In-vitro degradation of the P(3HB) microspheres containing cellulose nanospheres was carried out in PBS buffer containing 0.2 mg/mL lipase at 37 °C. PBS buffer was chosen because of the buffering effect it shares with the human physiological conditions while lipase was chosen because of its action on esters. Also, lipase is found in the body and it is expected to aid in the hydrolytic degradation of the polymeric microspheres when employed as a drug delivery system in the body. The result of the investigations is shown in Figure 7.10. Hence, the P(3HB) microspheres were able to undergo degradation resulting in the release of the cellulose nanospheres.

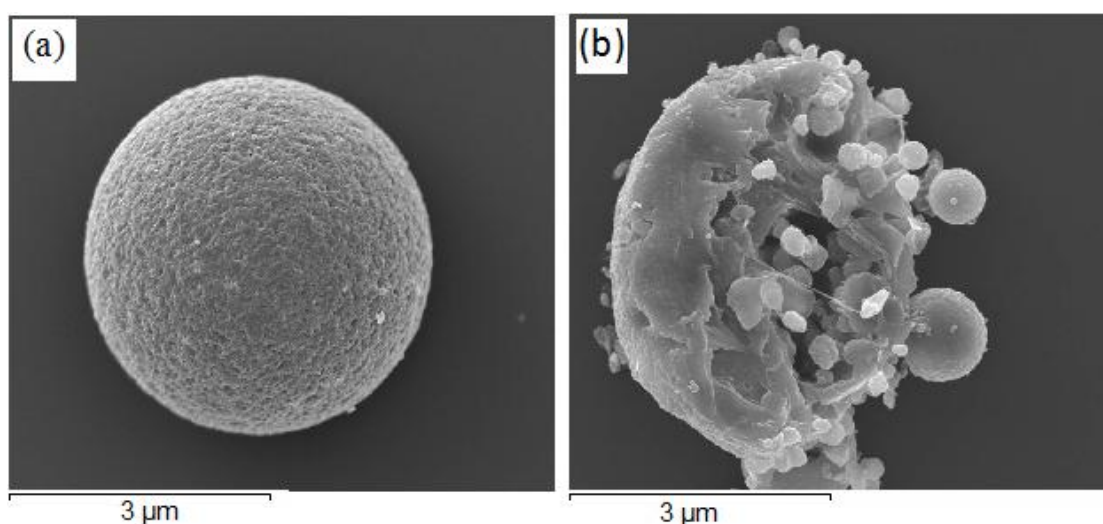


Figure 7.10 Typical SEM image of degrading P(3HB) microspheres containing cellulose nanospheres after incubation for 14 days in a PBS solution containing lipase at 37 °C

SECTION II

Potential Application of P(3HB) in targeted drug delivery system

Application of P(3HB) in the development of drug delivery systems was further extended to studies on targeted therapeutic drug delivery. Two different magnetic materials (magnetic nanoparticles and ferrofluid) were utilized to produce P(3HB) microspheres for intended applications in the delivery of cancer drugs. The composite microspheres (P(3HB)/MNP and P(3HB)/FF) produced were characterized. The details of the characterization are described below.

7.2 Results

7.2.1 SEM characterisation of the morphology of P(3HB)/FF and P(3HB)/MNP

The SEM image of the microspheres produced by incorporation of 14 mg of ferrofluid is shown in Figure 7.11, while Figure 7.12 shows the SEM image of roughly monodispersed P(3HB)/MNP composite microspheres prepared by addition of 14 mg of magnetic particles to 1g of P(3HB) in chloroform solution. The SEM images showed reasonably monodisperse microspheres of sizes 40 – 60 μm in diameter. It can be observed in Figure 7.13 that the P(3HB)/MNP composite microspheres have a rough surface with large pore size when compared to the microspheres produced by the addition of ferrofluid. However, all the microspheres prepared from both types of composite materials have almost spherical shapes.

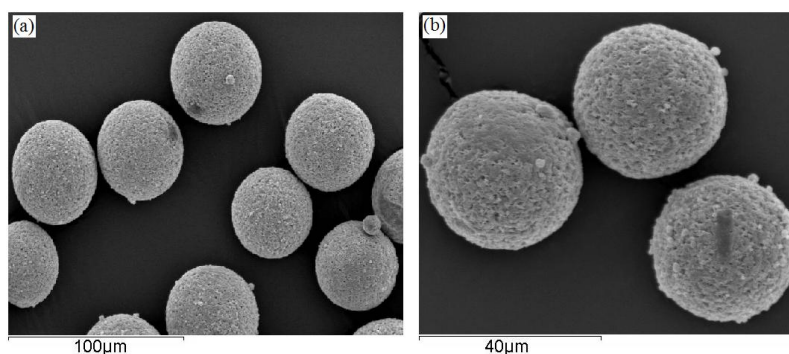


Figure 7.11 Typical SEM image of P(3HB)/FF microsphere (a) at lower magnification and (b) at higher magnification

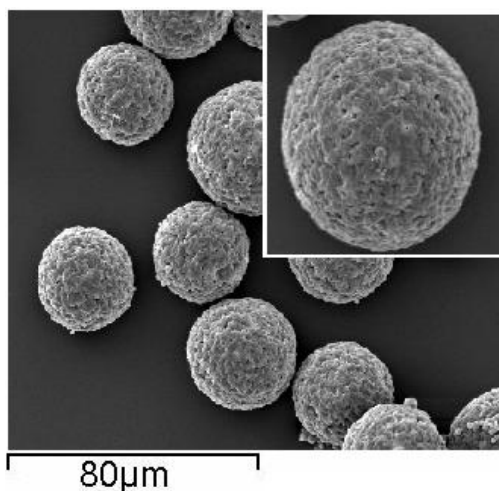


Figure 7.12 Typical SEM image of P(3HB)/MNP microsphere, inset is a magnified single microsphere highlighting the morphology of the microsphere

7.2.2 Effects of addition of different amounts of magnetic material on the shape and properties of microspheres produced

The effect of addition of different amounts of magnetic materials (MNP and ferrofluid) was investigated by incorporation of different amounts, 14, 27 and 40 mg of either magnetic particles or ferrofluid to 1 g of P(3HB) in chloroform solution. It was observed that the addition of 14, 27 or 40 mg of ferrofluid did not alter the shape and internal structure of the microspheres produced. The microspheres produced from the three different concentrations of ferrofluid look exactly the same (the image of only one concentration (14 mg) is shown in Figure 7.13a). Figure 7.13b depicts the SEM image of the cross section of the P(3HB)/FF composite microsphere by addition of 14 mg ferrofluid. As can be observed in the figure, the microspheres produced by incorporation of ferrofluid have a closely packed internal structure with well distributed pores throughout the entire microspheres.

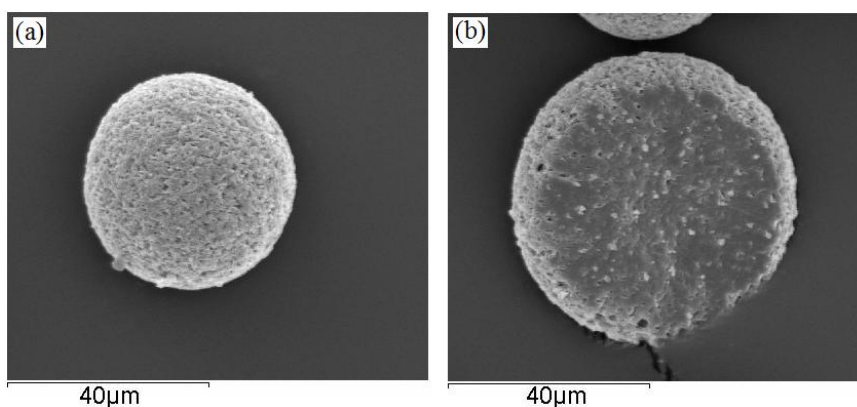


Figure 7.13 Typical SEM image of (a) single P(3HB)/FF microsphere (b) cross section of a P(3HB)/FF microsphere displaying the non hollow morphology of the microsphere

Figure 7.14 shows the SEM image of the cross section of microspheres produced by addition of different amount of magnetic particles to 1 g of P(3HB) in chloroform solutions. It was observed that addition of higher concentrations of magnetic particles led to the production of hollow microspheres with encapsulated microspheres. Furthermore, increase in the amount of magnetic particles led to the production of microspheres with different internal structures and morphological appearances.

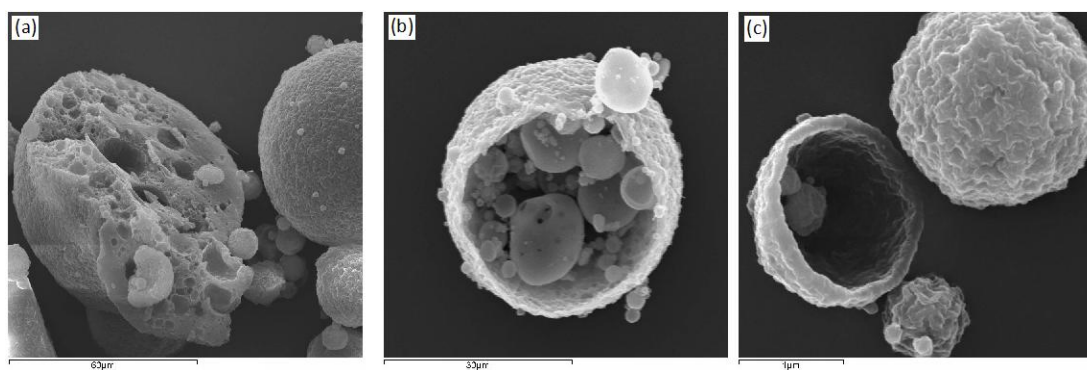


Figure 7.14 Typical SEM image of the P(3HB)/MNP microsphere revealing the internal structure of the microspheres at different amount of magnetic particles (a) 14 mg (b) 27 mg and (c) 40 mg of magnetic particles

7.2.3 TEM characterisation of the internal structure of P(3HB)/FF and P(3HB)/MNP composite microspheres

The TEM image of the neat P(3HB) and P(3HB)/FF composite microspheres is shown in Figure 7.15a and 7.15b respectively while Figure 7.15c and 7.15d display TEM image of P(3HB)/MNP composite microsphere at lower concentration (14 mg MNP) and at higher

concentration (27 mg MNP). It can be seen from the figures that whilst the TEM image of the neat P(3HB) microsphere and the composite P(3HB)/FF microsphere look similar without any crystals or particles observed inside the microspheres, the TEM image of the P(3HB)/MNP shows agglomeration of particles inside the microspheres. Also, the TEM image of the P(3HB)/MNP microspheres have more randomly distributed nanoparticles inside at lower concentration of MNP than at higher concentration of MNP.

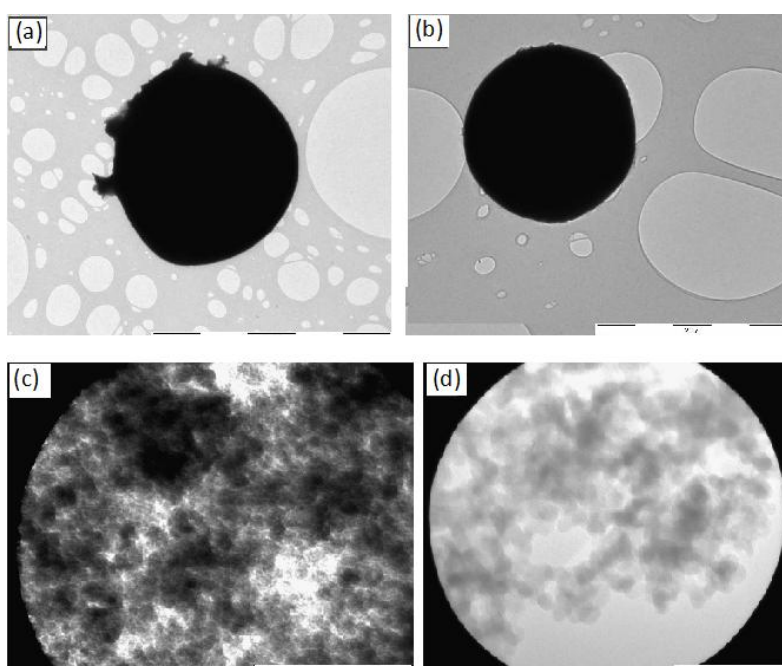


Figure 7.15 Transmission electron micrograph (TEM) of (a) P(3HB) microsphere (b) P(3HB)/FF microsphere, (c) P(3HB)/MNF composite microsphere containing lower concentration of MNP (14 mg MNP) and (d) P(3HB)/MNP composite microsphere containing higher concentration of MNP (27 mg MNP).

Figure 7.16a displays the electron diffraction pattern of P(3HB)/FF while Figure 7.16b displays the electron diffraction pattern of P(3HB)/MNP composite microspheres. It can be observed from the figures that electron diffraction pattern of P(3HB)/FF composite microspheres have less randomly oriented crystalline structure than the electron diffraction patterns of P(3HB)/MNP which have more randomly oriented crystalline structure.

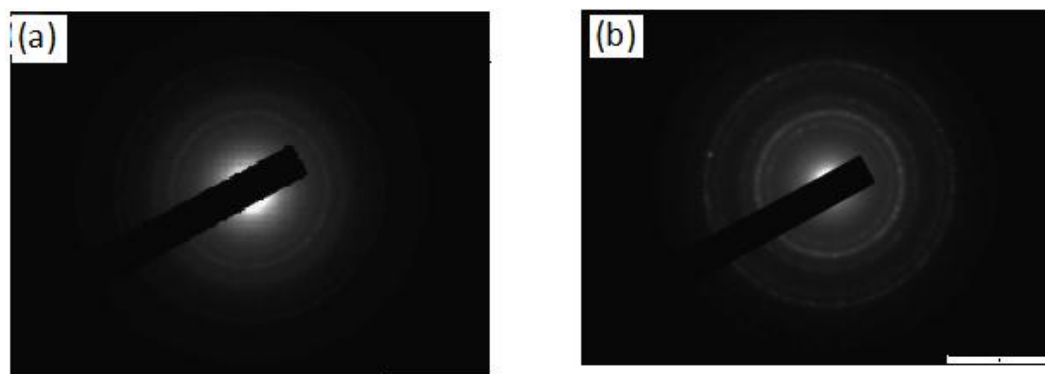


Figure 7.16 Randomly oriented crystalline structure of (a) P(3HB)/FF and (b) P(3HB)/MNP composite microspheres.

7.2.4 Characterisation of the magnetic properties of P(3HB)/FF and P(3HB)/MNP composite microspheres

The magnetic P(3HB) microspheres produced by introduction of magnetic nanoparticles and ferrofluid in the P(3HB) matrix were characterised for their magnetic properties. Superconducting quantum interference device (SQUID) was used to measure the magnetic properties of the microspheres. The detailed results of the SQUID analysis and the hysteresis loops of neat P(3HB), P(3HB)/FF and P(3HB)/MNP composite microspheres are shown in Figure 7.17, while Table 7.2 summarises the saturation magnetization measured on the samples at different concentrations of MNP and ferrofluid. The observations made show that the hysteresis loops of P(3HB)/FF and P(3HB)/MNP composite microspheres saturate at ± 1 Tesla without any coercivity and remnant magnetization. The hysteresis loop of P(3HB) microspheres were found to be composed of two magnetic phases; paramagnetic or superparamagnetic and the diamagnetic phase which is very clear from the hysteresis curve at lower and higher applied fields respectively. Furthermore, the results summarised in Table 7.2 shows that the maximum magnetization of both composite microspheres increased as the amount of MNP or ferrofluid incorporated increased.

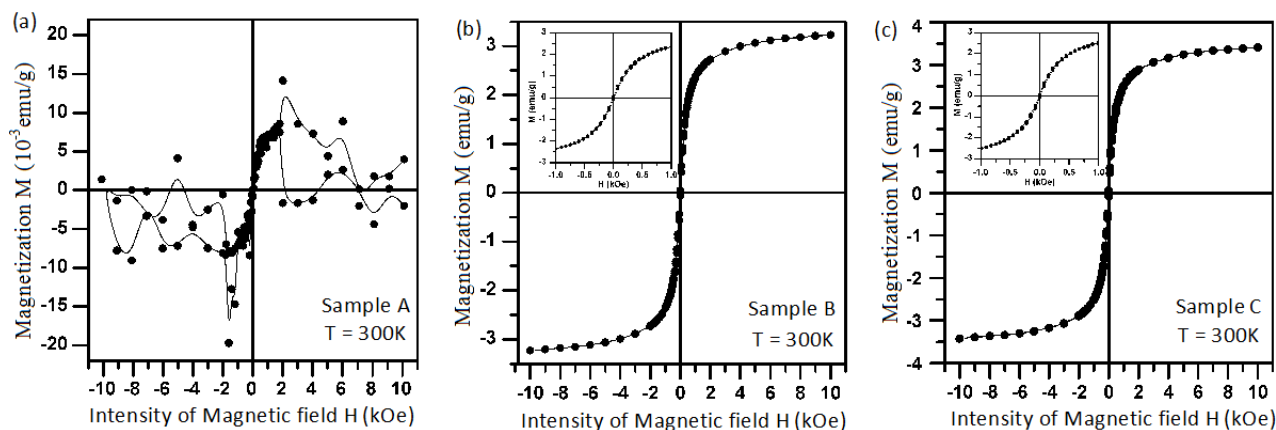


Figure 7.17 Comparison of SQUID data for (a) P(3HB), (b) P(3HB)/FF and (c) P(3HB)/MNP microspheres. Specific saturation of magnetization measured with an applied field of approximately 5 000 Oe at 300K.

Table 7.2 Parameters of the hysteresis loops of samples neat P(3HB) microsphere, P(3HB)/Magnetic particles composite microspheres containing 0.5, 1.0, and 1.5 mL magnetic particle suspension measured at a temperature of 300 K.

Sample,	T	$M_{\max+}$ (1 T)	$M_{\max-}$ (-1 T)	H_{C+}	H_{C-}	M_{R+}	M_{R-}
P(3HB)/Magnetic particles	(K)	(emu/g)	(emu/g)	(Oe)	(Oe)	(emu/g)	(emu/g)
Neat P(3HB)	300	0.0040	0.0014	---	---	---	---
14 mg Ferrofluid	"	2.0147	-2.0144	---	---	---	---
27 mg "	"	3.4152	-3.4145	---	---	---	---
40 mg "	"	4.0272	-4.0259	---	---	---	---
14 mg MNP	"	1.0155	-1.0157	---	---	---	---
27 mg "	"	1.1594	-1.1591	---	---	---	---
40 mg "	"	3.2331	-3.2326	---	---	---	---

$M_{\max+}$ (1 T) is a maximum magnetization at 1 T. $M_{\max-}$ (-1T) is a maximum magnetization at -1 T. H_{C+} is a positive coercivity. H_{C-} is negative coercivity. M_{R+} is a positive remanent magnetization and M_{R-} is a negative remanent magnetization

7.3 Discussion

For a successful long term delivery of drugs, it is essential to develop a conventional carrier system which can achieve long term delivery as well as controlled release of drugs. This is necessary since burst release of drugs may be detrimental to health. Hence, the development of a zero-order release system is necessary in order to achieve a controlled and extended period of drug delivery in biological systems. In this study, a multiple drug delivery system consisting of P(3HB) microspheres encapsulating cellulose nanospheres was produced and investigated for their ability to release BSA, a model protein. SEM observation in Figure 7.1b (inset) and 7.1c shows that the both the cellulose nanospheres and the P(3HB) microspheres produced have roughly spherical shape and surfaces with well distributed regular pores. This is in contrast with most of P(3HB) microspheres in the literature which have been shown to have smooth surfaces. This is an advantage in drug delivery as the rough surfaces will enhance both the attachment of the spheres and release of loaded drug. It is possible that the rough surfaces could have resulted from rapid evaporation of solvent (chloroform) from the microspheres. The SEM image of the cross section of the microspheres confirmed the encapsulation of the cellulose nanospheres by the P(3HB) microspheres. The particles size analysis performed showed that approximately 96 % of the microspheres have diameters in the range of 712-1474 nm ($\sim 0.7 - 1.5 \mu\text{m}$). The course of the Dynamic light scattering, DLS measurement (image not shown) shows that the P(3HB) microspheres were probably formed by the smaller nanospheres which were however, stuck together as one microsphere. Moreover, the SEM image of the cross section of the multipurpose microsphere shown in Figure 7.1d further confirm the observation made during DLS measurement. The result of variation in the concentration of P(3HB) in chloroform solution as shown in Figure 7.4 confirmed that the concentration of P(3HB) in chloroform solution had important effects on the morphology, shape and structure of pores on the microspheres produced.

The surface chemistry test performed showed that cellulose nanospheres were more hydrophilic with the least binding constant to Rose Bengal dye compared to P(3HB) microspheres containing cellulose nanospheres and the P(3HB) microspheres alone. This can possibly be due to the fact that PVA being a hydrophilic polymer had more affinity to a hydrophilic surface and therefore, bound more on to the surface of the cellulose nanospheres than to the hydrophobic P(3HB) microspheres. This possibly resulted in the observed decrease in the binding constant of Rose Bengal dye to the surface of the cellulose

nanospheres. Also, because of the rough surface and porosity of the microspheres produced, it is possible that the Rose Bengal dye was able to pass through the pores and attached to the more hydrophilic cellulose nanospheres than on the surface of the hydrophobic P(3HB) microspheres. Sahool *et al.* have also made similar observations on poly(D,L-lactide-co-glycolide) (PLGA) nanoparticles. They observed that residual PVA were left on the surface of PLGA nanospheres even after washing with distilled water. By employing X-ray photoelectron spectroscopy, Shakesheff and colleagues also demonstrated that PVA was adsorbed on the surface of PLA and PLGA microspheres during preparation of the microspheres (Shakesheff *et al.*, 1997).

The mechanism of PVA binding to the surface of the P(3HB) microspheres is possibly due to the interpenetration of PVA and P(3HB) molecules during microsphere production. The hydrophobic segments of PVA solution will be expected to penetrate into the organic phase of the oil in water (o/w) and remain entrapped in the polymeric matrix of the microspheres. Because of the chemical interactions between hydrophobic molecules, most of the PVA molecules will be entrapped into the P(3HB) microspheres after solvent evaporation. Besides, partially hydrolyzed PVA is a copolymer of poly(vinyl acetate) and poly(vinyl alcohol) with considerable block copolymer character. The hydrophobic vinyl acetate part serves as an anchor polymer at the oil interface for binding to the surface of P(3HB) polymer during the formulation. Thus, the higher PVA concentration in the continuous phase (PVA solution) could lead to an increase in PVA molecule density at the o/w interface of the emulsion droplet which would increase the amount of PVA content per weight of microspheres. Hence, higher the amount of PVA in the o/w emulsion, the increase in the residual PVA attached to the surface. On the other hand, the mechanism of attachment of PVA to the hydrophilic cellulose nanospheres is possibly by adsorption and this is likely to happen when the organic solvent is removed from the interface between entrapped PVA solution and the cellulose nanospheres in the P(3HB) microsphere. Lea *et al.* have demonstrated that the amount of residual PVA attached to the surface of particles is inversely proportional to the specific surface area of the particles. Hence, the decrease in microsphere size would lead to an increase in the attached residual PVA (Lee *et al.*, 1999).

Furthermore, due to the polarity of the organic solvent employed in the dissolution of the polymeric P(3HB), it was observed that the spheres produced with dichloromethane had more residual PVA on their surface compared to the spheres prepared with chloroform. As

explained above, partially hydrolyzed PVA is a copolymer of poly(vinyl acetate) and poly(vinyl alcohol). There are more possibilities for the dichloromethane to introduce more polarity to the oil in water emulsion and because of the affinity of PVA to a hydrophilic surface, the entrapped PVA solution will be adsorbed more onto the surface of the cellulose nanospheres than it would adsorb when a more hydrophobic solvent is employed in the oil in water emulsion. Also, during the production of the microspheres, a complex of polymer-organic solvent-water interface is formed. Therefore, increase in the miscibility of the organic solvent with water will tend to increase the attraction of the hydrophilic PVA to the organic solvent in which the polymer was dissolved and thus increase in the overall PVA attachment to the microspheres.

Residual PVA attached to the surface of the microspheres was suspected to have the possibilities of influencing the surface chemistry of the spheres. This was verified by testing with Rose Bengal dye and observations showed that, with increase in the concentration of PVA in the oil in water emulsion, the attachment of Rose Bengal dye increased. It is possible that the attached PVA formed a stable complex after interpenetrating into the microspheres. This might have changed the surface chemistry of the microspheres and with increase in the amount of PVA in the oil in water emulsion; the more the interpenetration of PVA, the more stable complexes were formed.

The drug release investigations carried out on the spheres, using BSA as a model protein, shows a biphasic protein release from the BSA loaded cellulose nanospheres and the BSA loaded cellulose nanospheres encapsulated in BSA loaded P(3HB) microspheres. The first phase of the burst release can be attributed to the protein associated with the spheres surface which was first released in the PBS buffer solution during the first day of the release studies. The release mechanism in this case can either be by dissolution of the encapsulated protein from the spheres into the hydrophilic PBS, or by diffusion of the BSA protein through the pores in the spheres into the surrounding PBS buffer. In either case, concentration gradient played an important role (Asmatulu *et al.*, 2009). The remaining drug remained entrapped within the spheres and was only released when the PBS solution actually penetrated enough into the spheres through the pores and due to the concentration gradient, the protein was released. In addition, the entrapped protein can be released when the polymeric material starts degrading. Thus BSA release can be by degradation of the polymeric materials and dissolution and diffusion through the pores. However, protein release can still be observed

during the lag phase (after burst release) which can be attributed to the small scale diffusion of the protein that had taken place during this time.

The BSA release from the cellulose nanospheres were higher during the initial burst release than the burst release observed from the BSA loaded cellulose nanospheres encapsulated within BSA loaded P(3HB) microspheres. It will be expected that since diffusion and dissolution lead to burst release as compared to degradation, the cellulose nanospheres will most likely release more of its entrapped drug/protein during the initial burst release than the larger sized microspheres. However, the cumulative protein release was higher in the BSA-loaded cellulose nanospheres encapsulated in the BSA-loaded P(3HB) microspheres. Thus after penetration of PBS into the microspheres, the hydrophilic BSA-loaded cellulose nanospheres will have more affinity for the hydrophilic PBS and hence, the entrapped BSA can easily dissolve and diffuse out of the nanospheres leading to a higher amount of protein release. Because of the concentration gradient, the protein would easily diffuse out of the microspheres. In addition, the BSA protein entrapped within the P(3HB) matrix that encapsulated the cellulose nanospheres would also be released at the same time. Hence, the accumulation of BSA release from the cellulose nanospheres and those from the P(3HB) matrix is expected to increase the total BSA released from the construct.

The BSA-loaded cellulose nanospheres encapsulated in unloaded P(3HB) microspheres behaved very differently in the release of its content. A highly controlled release rate was observed with a slightly linear BSA release at the beginning of the release studies until after 8 days when the amount of BSA release from the construct became almost constant. This can be explained, considering the fact that after penetration of PBS solution into the microspheres, the BSA entrapped on the cellulose nanospheres will first dissolve and diffuse out in to the space within the microspheres. Following this, due to the concentration gradient between the inside and outside of the microspheres, the BSA released by the nanospheres would diffuse out of the P(3HB) microspheres. Besides, the porosity of the microspheres will control the release of the dissolved/diffused BSA outside the microspheres, thereby avoiding burst release. The initial higher release was due to the surface entrapped BSA on the surface of the cellulose nanospheres which has more chances of being released first than the entrapped BSA that would be released during the degradation of the polymer.

The main aim of this study was to prove the concept that the unique construct of microspheres with encapsulated nanospheres would function both in the simultaneous

delivery of hydrophilic and hydrophobic drugs in addition to the controlled release of the encapsulated drugs. Hence, degradation study was performed with lipase to test the ability of the construct to degrade and release its contents for further degradation. The result of two weeks degradation in PBS showed that the lipase was able to degrade P(3HB) and release the encapsulated cellulose nanospheres as shown in Figure 7.14. This can be attributed to the hydrolytic action of the lipase (Zhao *et al.*, 2002). Ordinarily, it is difficult for lipase to degrade P(3HB) because of the side chains which makes it difficult for the enzyme to attack the polymer, however, the action of the enzyme can be attributed to the hydrophilicity provided by the residual PVA during microsphere fabrication. Since lipase is a water-soluble enzyme and would prefer a hydrophilic surface (Yu *et al.*, 2007), it is possible that the lipase was able to attach itself to the polymer with the help of the attached residual PVA which further enhanced the degradation of the polymer.

To further extend the scope of application of the biodegradable P(3HB) in drug delivery, magnetic P(3HB) was produced by addition of magnetic nanoparticles and ferrofluid. The purpose for the fabrication of this construct was for its medical application in the delivery of drug to target sites in the body, such as cancer using externally manipulated magnetic field. The SEM image of the microspheres showed that a uniformly distributed rough surfaces was formed on the surface of the microspheres produced by the incorporation of ferrofluid to the P(3HB) solution. The rough surfaces can be attributed to the method of production which enhanced faster evaporation of the solvent, with the resultant pores created by the evaporating solvents. Hollow spheres were formed when magnetic nanoparticles was introduced as confirmed by the SEM image of the cross section of the P(3HB)/MNP microsphere. And the tendency of producing hollow spheres increased as the amount of magnetic particles introduced into the polymer solution increased. The mechanism of hollow sphere production in the microspheres is not yet confirmed, but it is possible that magnetic attractions on the nanoparticles might have played a significant role in the process. During the introduction of drops of P(3HB)/MNP solution in the oil in water solution, the magnetic particles can aggregate inside the drop. As the chloroform solvent evaporated, the P(3HB)/MNP solution would gradually solidify and the opening created by the nanoparticle that pulled out of position to attract to another nanoparticles might remain unfilled. The aggregates formed resulted in smaller spheres found within the larger hollow spheres. Thus, empty spaces were created inside the microspheres which were seen as hollows in the SEM image. The tendency

of having bigger spaces inside the microspheres with increase in the amount of magnetic particles is thus expected due to increased magnetic attractions in the magnetic particles.

Aggregates of nanoparticles were observed in both the SEM and TEM images as well as formation of hollow microspheres in the P(3HB)/MNP microspheres. Asmatulu *et al.* have made similar observations (using TEM) of magnetic nanoparticles forming clusters in PLGA microspheres, but they attributed the phenomenon to be due to a large surface area to volume ratio, and intermolecular interactions, such as electrostatic, hydrophobic, and van der Waals interaction (Asmatulu *et al.*, 2009). Hence, it is possible that the same effect could be responsible for the similar observation made in this study in addition the molecular attraction explained above. The detail mechanism of the hollow sphere formation will need to be confirmed in the future study as this is important in the encapsulation and release of drugs during applications.

The electron diffraction pattern in Figure 7.16 confirmed random orientation of the crystal lattices in the two different composite microspheres (P(3HB)/MNP and P(3HB)/FF). The random orientation of the crystal lattices in the magnetic composite samples is expected to influence the degradation of the polymeric microspheres and subsequent release of its contents.

The observations using SQUID analysis indicated that the composite constructs were superparamagnetic. Hence, the method of preparation of the composite microspheres did not affect the magnetic properties of both magnetic nanoparticles and ferrofluid. This would allow the manipulation of the composite microspheres using a higher magnetic field. The advantage of this property is that the construct can be effectively utilized in the delivery of drug to a specific site in the body using an external magnetic field. Increase in maximum magnetization was observed with an increase in the concentration of added MNP or ferrofluid however, the increase in the maximum magnetization of the P(3HB)/FF was more than that observed in P(3HB)/MNP composite microspheres. This is possibly due to the formation of clusters of smaller spheres inside the P(3HB)/MNP microsphere.

7.4 Conclusion

A multiple drug delivery system based on P(3HB) microspheres carrying cellulose nanospheres (P(3HB)/cellulose nanospheres) was successfully produced. Microspheres of average sizes of 1.5-6 μm were produced. The various characterisations confirmed that the produced microspheres have residual PVA left on the surfaces which was influenced by the concentration of the PVA solution. BSA was used as a model protein to understand the drug release kinetics and the result obtained confirmed that the construct led to controlled release of BSA into the surrounding environment. Furthermore, the degradation studies confirmed that microspheres produced were able to undergo hydrolytic degradation to release the encapsulated cellulose nanospheres through the action of lipase.

The areas of application of P(3HB) in drug delivery was further extended to the production of carriers for site-directed delivery of drugs. The production was successful as the magnetic materials were successfully introduced into the microspheres. SQUID analysis on the composite microspheres confirmed that the spheres produced were superparamagnetic. Also in the study, the effect of addition of different amount of magnetic particles to P(3HB) was investigated and results confirmed clusters or aggregates of particles inside the microspheres. The electron diffraction pattern confirmed the presence of randomly oriented crystalline lattice in the microspheres produced by the introduction of magnetic nanoparticles and ferrofluid. This was expected to further aid in the degradation of the polymer. Further study would need the investigation of the drug encapsulation efficiency of the construct using real drug molecules as well as the release kinetics of the specific drug *in vitro* and *in vivo* using animal models.

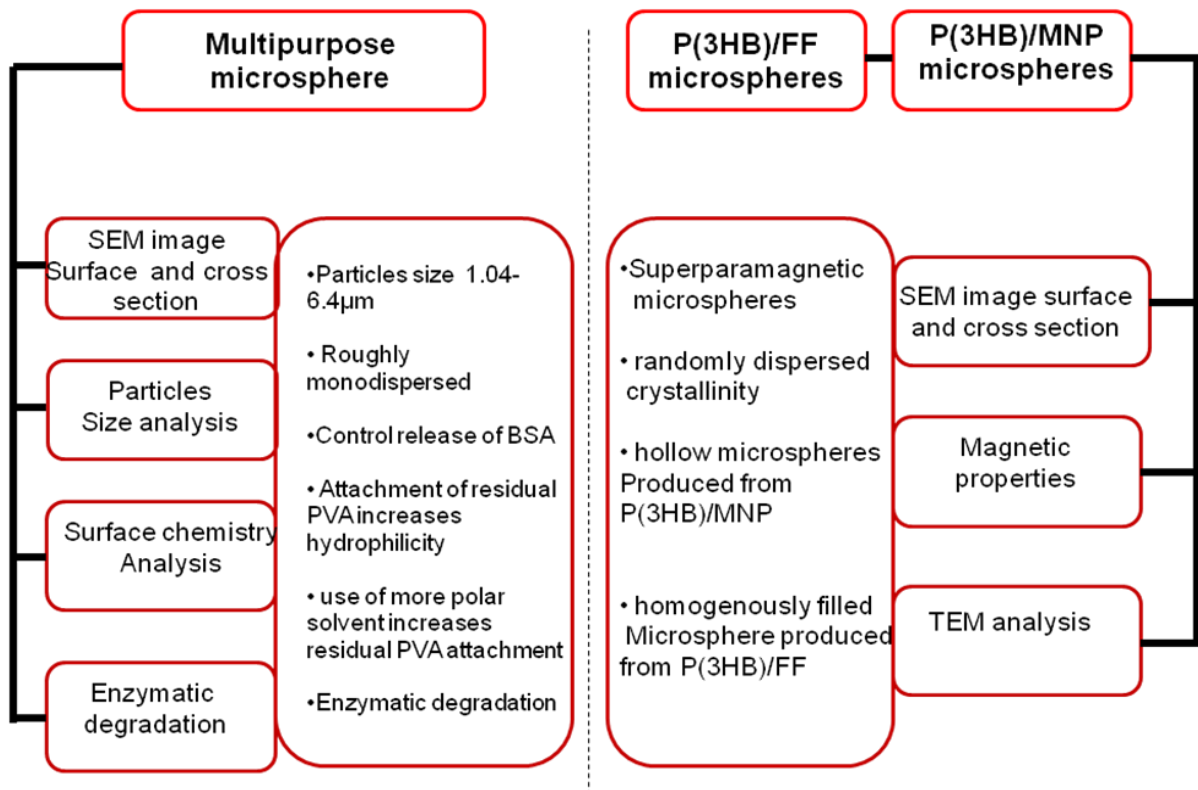


Figure 7.18 Schematic representation of summary of analysis and results achieved

Chapter 8

CONCLUSIONS AND FUTURE WORK

Chapter 8

8.1 Conclusions

This multidisciplinary project encompassed a wide range of techniques ranging from microbiology, biotechnology, material sciences to cell culture. The various results achieved at different stages in the research highlighted the potential of developing multifunctional scaffolds capable of providing chemical and physical signals to guide cell attachment and spreading as well as providing growth factors and antibacterial agents that can protect the regenerating site against infections by potential pathogens. Also, the potential of developing unique drug delivery systems were explored in this research.

Initially, enhancement of P(3HB) production using a Gram positive *Bacillus cereus* SPV and sucrose as the main carbon source was achieved. *Bacillus cereus* SPV is able to efficiently utilize sucrose as the main carbon source for growth and PHA accumulation both in the Kannan and Rehacek medium and in MGM medium. Also, potassium phosphate was found to be an important nutrient for growth and PHA accumulation in *B. cereus* SPV. The absence of reduction in P(3HB) accumulation even after increase in the amount of yeast extract in the production medium suggested that nitrogen limitation may not be the main condition leading to PHA accumulation. This led to the search for the main limiting condition that can enhance PHA accumulation in *Bacillus cereus* SPV. In the search for the limiting condition, different investigations were performed and it was found that potassium and sulphate limitation were the main limiting nutrients that can enhance accumulation of PHAs in *Bacillus cereus*. By addition of 0.5 g/L K_2HPO_4 in modified G-medium containing sucrose as the main carbon source, a total amount of 7.21 g/L dry cell weight, P(3HB) yield of 82.61 wt% dcw and P(3HB) concentration of 5.95 g/L were achieved in a 2 L fermenter. The result achieved in this study is significantly high when compared to 2.14 g/L dry cell weight, 38 wt% dcw P(3HB) yield and P(3HB) concentration of 0.81 g/L previously achieved by Valappil *et al.*, 2007 with the same organism and by employing glucose as the main carbon substrate.

In addition, economic production of P(3HB) using agricultural/industrial waste (molasses) as the main carbon substrate was also achieved. The results obtained showed that a high yield of polymer was obtained, 61.07 % dcw in 1L shaken flask and 51.37 % dcw in 2L fermenter,

using *Bacillus cereus* SPV with sugarcane molasses as the main carbon source. These yields are much higher than previously reported yield of 35 wt% dcw achieved by Wu *et al.*, in their investigation on P(3HB) production by *Bacillus sp* JMA5 using molasses as the main carbon substrate (Wu *et al.*, 2001). The results are encouraging and show that sugarcane molasses is a promising carbon source for an economical and commercially viable production of P(3HB). This study can form the basis of the development of a biotechnological process for the biotransformation of the renewable feedstock, sugarcane molasses, into P(3HB). This will decrease the cost of P(3HB) production substantially, leading to an enhancement in its widespread usage.

Furthermore, in the quest to improve PHA recovery and further reduce the cost of production of PHAs, a novel wet cell PHA extraction was developed which resulted in efficient isolation of PHA from *Bacillus cereus* SPV. In addition this novel method resulted in the production of high purity and less crystalline polymers, with excellent applications in medicine. Most importantly the technique will also be very useful in continuous production of PHAs resulting in saving time and energy.

In order to make useful composites for a variety of applications, bacterial cellulose was produced using *Acetobacter xylinus*. The isolated cellulose pellicle were homogenised to fine fibres of microfibrillated cellulose and chemically modified to a high degree of acetylation which was necessary for further application as a reinforcing element in P(3HB)/MFC composite fabrications. The FTIR analysis confirmed the partial acetylation of the MFC while XRD analysis confirmed the production of modified microfibrillated cellulose with reduced crystallinity. The decrease in the crystallinity was necessary due to its intended applications as a reinforcement element for composite fabrication. Hence, this study has led to the successful production of acetylated microfibrillated bacterial cellulose which can be used for varied applications in medicine, especially in the formation of composites with hydrophobic polymers such as PHAs.

The polymer produced was then used for the production of a variety of tissue engineering scaffolds. A novel inexpensive and sustainable ‘compression moulding/particulate leaching’ technique for tissue engineering scaffold fabrications was developed. The novel technique enabled the production of degradable composite scaffolds of P(3HB)/MFC for potential applications in cartilage regeneration.

Both 2D and 3D composite scaffolds of P(3HB)/MFC were successfully produced using the P(3HB) and the bacterial cellulose produced. The characterisation of the composites with respect to their mechanical and structural properties in combination with the degradation and detailed biocompatibility studies provided a better understanding of the effect of microfibrillated cellulose on the P(3HB)/MFC composite properties. The results obtained highlighted the advantages of incorporating microfibrillated cellulose in the P(3HB) polymeric matrix, which among other features, significantly enhanced mechanical strength of the scaffolds. The study further highlighted the role of MFC in inducing nanotopography and hydrophilicity to the composite, which regulates the level of surface wettability (up to 12% decrease in water contact angle) and protein adsorption (up to 26.5% increase) on the surface of the composite. The bioactivity of the P(3HB)/MFC composites was confirmed by the formation of crystalline hydroxyapatite on the composites' surfaces after immersion in SBF for 21 days. *In vitro* degradation studies confirmed that the addition of MFC to the polymeric matrix significantly increased the water uptake. Considerable differences were found in cell proliferation between the composite films, neat P(3HB) films and the control surface (tissue culture plastic). However, no difference ($p>0.05$) in cell proliferation was found between the neat 3D P(3HB) scaffold and the 3D composite scaffold indicating the dominance of the 3D structure over the material properties. Both the P(3HB) and P(3HB)/MFC films and 3D scaffolds were found to be highly compatible surfaces for the adhesion and proliferation of the ATDC cells. The nanotopography of the throat of the pores in the scaffold was confirmed to have played a critical role in enhancing cell adhesion while the large pore sizes (60-83 μm) allowed infiltration and migration of ATDC cells deep into the porous network of the scaffold.

In addition, magnetic composite scaffolds of P(3HB)/MNP and P(3HB)/FF were produced for application in bone regeneration. The addition of magnetic particles and ferrofluid into the P(3HB) matrix played a significant role in increasing the microhardness, introduction of nanotopographic features as well as enhancing hydrophilicity on the 2D and 3D composite materials. Both 2D and 3D magnetic polymeric composites were successfully prepared by incorporating either magnetic nanoparticles (MNP) or ferrofluid (FF) into the polymeric P(3HB) matrix using the novel compression moulding/particulate leaching technique. Detailed characterisation of the magnetic scaffolds confirmed superparamagnetic properties on the composite materials. The introduction of MNP and ferrofluid resulted in increased

crystallinity of the composite scaffolds which would be useful in bone regeneration. This study also provided preliminary evidence that the addition of MNP or ferrofluid resulted in the enhancement of both thermal and physico-mechanical properties of the composite materials compared with the neat P(3HB) material.

Furthermore, the cytocompatibility studies showed that neither MNP nor ferrofluid were toxic to the MG-63 cells. Rather, the cells were found to have grown more on the composite materials than on the neat P(3HB). Also, the result of the total protein production on the composite materials showed that the materials were neither toxic nor hindered total protein production, instead they were found to have effect in improving the total protein production by the MG-63 cells in osteogenic media. This indicated the potential ability of the composite materials to support mineralisation and subsequent bone formation when employed in bone tissue engineering. In general, the results of this study can contribute towards the establishment of magnetic particles and ferrofluid based scaffolds as the scaffold of choice for bone tissue engineering.

Finally, a unique multipurpose delivery system to be used for the delivery of multiple drugs was successfully developed. A biodegradable P(3HB) drug carrier system with bacterial cellulose nanospheres and P(3HB) microspheres were successfully produced. Microspheres of average sizes of 1.5-6 μm were produced. The produced microspheres had residual PVA on the surfaces. BSA was used as a model protein to understand the drug release kinetics and the result obtained confirmed that the construct led to controlled release of BSA into the surrounding environment. Furthermore, the degradation studies confirmed that microspheres produced were able to undergo enzymatic degradation in the presence of lipase. The areas of application of P(3HB) in drug delivery was further extended to the production of carriers for site-directed delivery of drugs. The magnetic materials were successfully introduced into the microspheres. SQUID analysis on the composite microspheres confirmed that the spheres produced were superparamagnetic while the electron diffraction pattern image confirmed the presence of randomly oriented crystallinity in the microspheres produced due to the introduction of magnetic nanoparticles and ferrofluid. This would aid in increasing the degradation rate of the polymer as well as in the release of its content.

8.2 Further Study

This study on biodegradable poly(3-hydroxybutyrate) production and its biomedical applications has led to highly innovative and interesting results. Nevertheless, there are many potential areas that could be the subject of future research to gain more understanding on the different constructs produced in this research. Some potential experiments that would need to be performed are:

8.2.1 P(3HB) production:- It would be interesting to carry out more research in the utilization of other cheaper carbon sources that could enhance P(3HB) yield and further reduce the cost of production of the polymer. Further optimization of the physical parameters for P(3HB) production in the fermenter would need to be performed as this is a prerequisite towards understanding the real potential of the organism in producing P(3HB) from different cheap carbon sources. The production of copolymers and block polymer using *Bacillus cereus* SPV would be very interesting because of the lack of lipopolysaccharides, which is a major toxin that causes immunogenic reaction in the use of PHAs from Gram-negative bacteria for medical applications.

8.2.2 P(3HB)/MFC characterisation:- Surface energy measurements of P(3HB)/MFC and its potential role in cell attachment would need further investigation. The porosity of the scaffolds and its relationship with the mechanical properties of the scaffold would need to be further investigated. Also, it would be interesting to gain more understanding of the effects of using microfibrillated cellulose with different degrees of acetylation on the physico-mechanical properties of the composite scaffolds of P(3HB)/MFC. *In vivo* implantation of P(3HB)/MFC scaffold directly in animal model and measuring the cartilage formation and effect on angiogenesis and vascularisation of tissue/scaffold construct would be the next step forward.

8.2.3 P(3HB)/MNP and P(3HB)/FF Characterisation:- The effect of the magnetic properties of MNP and ferrofluid added to the composite scaffold on the biochemical activities in the MG-63 cell line would be an interesting future area of investigation. Since P(3HB) is hydrophobic and lacks signal molecules for cell attachment, as most pure polymers do, the effect of the magnetic materials on bone formation, especially as a signal molecule for

cell attachment, will need to be investigated further. Also, the effect of the magnetic materials on hemocompatibility and endothelialization of the P(3HB) composite scaffold material will be investigated. Further investigation of the bioactive materials formed on the composite material after immersion in SBF which resulted in an additional melting peak in the DSC analysis and also additional peaks in the XRD spectra would be of interest.

8.2.4 Biocompatibility study:- Histological assessment of the different scaffold materials produced will be performed to evaluate immune response to the composite scaffolds after implantation for different time points in animal (mouse). To avoid bias in the assessment, evidence of endotoxin or bacteria associated with the scaffolds during implantation in animal model would be assessed from either limulus assays or Gram staining of sections. Further cellular immune response and serological reactions will be determined by lymphocyte proliferation assays and antibody responses. The cellular immune response would be evaluated by determining significant increase (SI) for lymphocyte proliferation on the 2D composite materials while antibody binding to the 2D P(3HB) composite materials would be evaluated using ELISA techniques. Evaluation of more biological markers (Collagen I and IGF II gene expression using real time quantitative PCR) need to be performed in order to gain a complete understanding of cell behaviour on the different composites P(3HB) MFC, P(3HB)/MNP and P(3HB)/FF surfaces.

8.2.5 Drug Release kinetics:- In future it would be interesting to investigate drug encapsulation efficiency of the constructs as well as the release of specific drugs *in vitro* and *in vivo* using animal models.

REFERENCES

References

- Abe, H., Doi, Y. and Yamamoto, Y. (1992) Controlled release of lastet, an anticancer drug, from poly(3-hydroxybutyrate) microspheres containing acyl-glycerols, *Macromol. Rep.* **A29**:229-235
- Abe, H., Yamamoto, Y. and Doi, Y. (1992) Preparation of poly(3-hydroxybutyrate) microspheres containing lastet an anticancer drug and its application to drug delivery system, *Kobunshi Ron-bunshu* **49**:61-67
- Adebajo, M.O., Frost, R.I., Kloprogge, J.T.K. and Kokot, S. (2006) Raman spectroscopic investigation of acetylation of raw cotton. *Spectrochim Acta Part A Mol Biomol Spectrosc* **64(2)**:448-453
- Aebischer, P., Valentini, R.F. and Galletti, P.M. (1988) Piezoelectric nerve guidance channels, PCT Patent Application No. WO 88/06866
- Agrawal, C.M. and Athanasiou, K.A. (1997) Techniques to control pH in vicinity of biodegrading PLA-PGA implants. *J Biomed Mater Res Appl Biomater.* **38(2)**:105-14
- Aigner, J., Tegeler, J., Hutzler, P., Campoccia, D., Pavesio, A., Hammer, C., Kastenbauer E. and Naumann, A. (1998) Cartilage tissue engineering with novel non-woven structured biomaterial based on hyaluronic acid benzyl ester. *J Biomed Mater Res.* **42**:172-81
- Akaraonye, E., Keshavarz, T. and Roy, I. (2010) Production of Polyhydroxyalkanoates: the future green materials of choice. *J chem Tech Biotech.* **85(6)**:732-743
- Akiyama, H., Ito, A., Sato, M., Kawabe, Y. and Kamihira, M. (2010) Construction of Cardiac Tissue Rings Using a Magnetic Tissue Fabrication Technique. *Int J Mol Sci.* **11**:2910-2920
- Albuquerque, M.G.E., Eiro., M, Torres, C., Nunes, B.R., Reis, M.A.M. (2007) Strategies for the development of a side stream process for polyhydroxyalkanoate (PHA) production from sugar cane molasses. *J. Biotechnol* **130**: 411-421

- Alemdar, A. and Sain, M. (2007) Isolation and characterization of nanofibres from agricultural residues-Wheat straw and soy hulls. *Bioresour Technol.* **99(6)**:1664-1671
- Alemdar, A., Oksman, K. and Sain M (2009) Effect of decreased fiber size in wheat straw/polyvinyl alcohol composites. *J Biobased Mater Bioenerg* **3**:75-80
- Alexio, C., Arnold, W., Klein, R.J., Parak, F.G., Hulin, P, Bergemann, C, *et al.* (2000) Locoregional cancer treatment with magnetic drug targeting. *Cancer Res.* **60**:6641-8
- Anderson, A.J. and Dawes, E.A. (1990) Occurrence, metabolism, metabolic role, and industrial use of bacteria polyhydroxyalkanoates. *J. Microbiol. Rev.* **54**:450-472
- Ashby, R.D., Solaiman, D.K.Y. and Foglia, T.A. (2002) The synthesis of short and medium-chain-length poly(hydroxyalkanoates) mixtures from glucose or alkanolic acid-grown *Pseudomonas oleovorans*. *J Ind Microbiol Biotechnol* **28**:147–153
- Asmatulu, R., Fakhari, A., Wamocho, H.L., Chu, H.Y., Chen, Y.Y. and Eltabey, M.M. (2009) Drug-carrying Magnetic Nanocomposite Particles for Potential Drug Delivery Systems. *J Nanotech.* Doi: 10.1155/2009/238536.
- Avella, M., La Rota G., Martuscelli, E, Raimo, M., Sadocco, P., Elegir, G and Riva, G. (2000) Poly(3-hydroxybutyrate-co-3-hydroxyvalerate) and wheat straw fibre composites: thermal, mechanical properties and biodegradable behaviour. *J Mater Sci.* **35**:829-36.
- Avella, M., Martuscelli, E. and Raimo, M. (2000) Properties of Blends and Composite based on Poly(3-hydroxybutyrate) and Poly(3-hydroxybutyrate-co-3-hydroxyvalerate) (PHBV) Copolymers, *J Mater Sci.* **35**:523-545.
- Backdahl, H., Helenius, G., Bodin A., Nannmark, U., Johansson, B.R., Risberg B. and Gatenholm, P. (2006) Mechanical properties of bacterial cellulose and interactions with smooth muscle cells. *Biomaterials*, **27**:2141-2149.
- Baptist, J.N., Ziegler, J.B. (1965) Method of making absorbable surgical sutures from poly beta hydroxy acids, U. S. Patent No. 3,225,766

- Behrend, D., Lootz, D., Schmitz, K. P., Schywalsky, M., Labahn, D., Hartwig, S., Schaldach, M., Unverdorben, M., Vallbracht, C. and Laenger, F. (1998) PHB as a bioresorbable material for intravascular stents, *Am. CardioL, Tenth Annual Symposium Transcatheter Cardiovascular Therapeutics, Abstract TCT-8*, 48
- Behrend, D., Nischan, C., Kunze, C., Sass, M., Schmitz, K.P. (1999) Resorbable scaffolds for tissue engineering, Proc. European Medical and Biological Engineering Conference, *Med Biol Eng Comput.* **37**(Suppl.). 1510-1511
- Behrend, D., Schmitz, K.P., Haubold, A. (2000) Bioresorbable polymer materials for implant technology. *Adv Eng Mater.* **2**:123-125
- Bengtsson, S., Hallquist, J., Werker, A. and Welander, T.(2007) Acidogenic fermentation of industrial wastewaters: Effects of chemostat retention time and pH on volatile fatty acids production. *J Biochem Eng* **40**:492-499
- Benya, P.D. and Shaffer, J.D. (1982) Dedifferentiated chondrocytes express the differentiated collagen phenotype when cultured in agarose gels. *Cell.* **30**:215-224.
- Bergsma, E.J., Brujn, W., Rozema, F.R., Bos, R.M., Boering, G. (1995) Late tissue response to poly(L-lactide) bone plates and screws. *Biomat.* **16**(1):25-31
- Berlanga, M., Montero, M., Fernandez-Borrell, J. and Guerrero, R. (2006) Rapid spectrofluorometric screening of poly-hydroxyalkanoate-producing bacteria from microbial mats, *Int Microbiol* **9**:95–102
- Bhubalan, K., Lee, W.H., Loo, C.Y., Yamamoto, T., Doi, Y. and Sudesh, K. (2008) Controlled biosynthesis and characterization of poly(3-hydroxybutyrate-co-3-hydroxyvalerate-co-3-hydroxyhexanoate) from mixtures of palm kernel oil and 3HV-precursors. *Polymer Degrad Stab* **93**:17-23
- Bissery, M.C., Puisieux, F. and Thies, C. (1983) A study of process parameters in the making of microspheres by the solvent evaporation procedure, *Third Expo. Congr. Int. Technol. Pharm.* **3**:233-239
- Bissery, M.C., Valeriote, F. and Thies, C. (1984) *In vitro* and *in vivo* evaluation of CCNU-loaded microspheres prepared from poly(L)-lactide and poly(p-

- hydroxybutyrate), in: *Microspheres and Drug Therapy, Pharmaceutical, Immunological and Medical Aspects* (Davis, S.S., Ilium, L, McVie, J.G., Tomlinson, E., Eds), Amsterdam: Elsevier. 217 - 227.
- Bissery, M.C., Valeriote, F. and Thies, C. (1985) Fate and effect of CCNU-loaded microspheres made of poly(D,L)lactide (PLA) or poly- β -hydroxybutyrate (PHB) in mice. *Proc. Int. Symp. Controlled Release Bioact. Mater.* **12**:181-182
- Bissery, M.C., Valeriote, F. and Thies, C. (1984) *In vitro* lomustine release from small poly(β -hydroxybutyrate) and poly(D,L-lactide) microspheres, Proc Int Symp. *Controlled Release Bioact. Mater.* **11**:25-26
- Boccaccini, A.R., Rother, J.A., Hench, L.L., Maquet, V. and Jerome, R. (2002) A Composite Approach to Tissue Engineering, *Ceramic. Eng. Sci. Proc.*, **23**: 805-816
- Bock, N., Riminucci, A., Dionigi, C., Russo, A., Tampieri, A., Landi, E., Goranov, V.A., Marcacci, M., and Dediu, V., (2010) A novel route in bone tissue engineering: magnetic biomimetic scaffolds. *Acta Biomater.* **6(3)**:786-96.
- Borah. B., Thakur, P.S. and Nigam (2002) The influence of nutritional and environmental conditions on the accumulation of poly-beta-hydroxybutyrate in *Bacillus mycoides* RLJ B-017. *J Appl Microbiol* **92**:776-783
- Borkenhagen, M., Stoll, R.C., Neuenschwander P, Suter, U.W. and Aebischer, P. (1998) In vivo performance of a new biodegradable polyester urethane system used as a nerve guidance channel. *Biomater* **19**:2155-2165
- Bostmann, O., Hirvensalo, E., Makinen, J. and Rokkanen, P. (1990) Foreign body reactions to fracture fixation implants of biodegradable synthetic polymers. *J Bone Jt Surg. B* **72**:529
- Bourque, D., Ouellette, B., Andre, G. and Groleau, D. (1992) Production of poly- β -hydroxybutyrate from methanol: characterization of a new isolate of *Methylobacterium extorquens*. *Appl Microbiol Biotechnol* **37**:7-12
- Bowald, S. F. and Johansson-Ruden, G. (1997) A novel surgical material. European Patent Application No. 0754 467

- Bowald, S. F., Johansson, E. G. (1990) A novel surgical material, European Patent Application No. 0349 505
- Boyan, B.D., Hummert, T.W., Kieswetter, K., Schraub, D., Dean, D.D. and Schwartz, Z. (1995) Effect of titanium surface characteristics on chondrocytes and osteoblasts in vitro. *Cells Mater.* **5**:323-335
- Boyan, B.D., Lossdorfer, S., Wang, L., Zhao, G., Lohmann, C.H., Cochran, D.L. and Schwartz, Z. (2003) Osteoblasts generate an osteogenic microenvironment when grown on surfaces with rough microtopographies. *Eur Cell Mater.* **6**:22-27
- Bozell, J.J. and Landucco, R. (1993) Alternative Feed stocks Program Technical and Economic Assessment: Thermal/Chemical and Bioprocessing Component U.S. Department of Energy, Office of Industrial Technologies. Washington DC, pp 11-126
- Brandl, H., Gross, R.A., Lenz, R.W. and Fuller, R.C. (1988) *Pseudomonas oleovorans* as a source of poly(β -hydroxyalkanoates) for potential applications as biodegradable polyesters. *Appl Environ Microbiol* **54(8)**:1977–1982
- Braunegg, G., Lefebvre, G., Renner, G., Zeiser, A., Haage, G. and Loidl-Lanthaler, K. (1995) Kinetics as a tool for polyhydroxyalkanoate production optimization. *J Microbiol* **41(Suppl.1)**:239-248
- Brophy, M.R. and Deasy, P.B. (1986) *In vitro* and *in vivo* studies on biodegradable polyester microparticles containing sulphamethizole, *Int. J. Pharm.* **29**:223-231
- Bruenette, D.M. (1986) Spreading and orientation of epithelial cells on grooved substrata, *Exp Cell Res.* **167: Implants Res.** **6**:1-13
- Brune, H. and Niemann, E. (1973) Use and compatibility of bacterial protein (*Hydrogenomonas*) with various contents of poly-beta-hydroxybutyric acid in animal nutrition, Weight development and N balance in growing rats, *Z. Tierphysiol. Tier-ernahr. Futtermittelkd* **38**:13-22
- Brune, H. and Niemann, E. (1977) Value and compatibility in animal nutrition of bacterial protein (*Hydrogenomonas*) containing various amounts of poly-beta-hydroxybutyric acid. 2. Body weight, nitrogen balance and fatty acid pattern of

- liver, muscle and kidney depot fat of growing swine, *Z. Tierphysiol. Tierernahr. Futtermittelkd* **38**:81-93
- Brunette D.M. (1988) The effects on implant surface topography on the behaviour of cells. *Int J Oral Maxillofac Implants*. **3**:231-246
- Buzarovska, A. and Grozdanov, A (2009) Crystallization kinetics of poly(hydroxybutyrate-co-hydroxyvalerate) and poly(dicyclohexylitaconate) PHBV/PDCHI blends: thermal properties and hydrolytic degradation. *J. Mater Sci.* **44**:1844-1850
- Byrom, D. (1994) Polyhydroxyalkanoate, In: Mobley DP, editor, *Plastics from microbes: microbial synthesis of polymers and polymer precursors*, Hanser, Munich, pp5–33
- Caballero, K.P., Karel, S.F., and Register, R.A. (1995) Biosynthesis and characterization of hydroxybutyrate-hydroxycaproate copolymers. *Int J Biol Macromol.* **17**:86-92
- Carlozzi, P. And Sacchi, A. (2001) Biomass production and studies on *Rhodospseudomonas, palustris* grown in an outdoor, temperature controlled, underwater tubular photobioreactor. *J Biotech.* **88**:239-249
- Chaipinyo, K., Oakes, B.W. and Van Damme, M.P. (2004) The use of debrided human articular cartilage for autologous chondrocyte implantation: Maintenance of chondrocyte differentiation and proliferation in type I collagen gels. *J Orthop Res.* **22**:446–455.
- Charles, E.C. and Raymond B.S. (2003). *Crystallisation of Polymers*. Seymour/Carraher's polymer chemistry. *CRC Press*. pp. 44–45. ISBN 0824708067.
- Charlton, S., Moir, A.J.G., Baillie, L. and Moir, A. (1999). Characterization of the exosporium of *Bacillus cereus*. *J Appl. Microbiol.* **87**:241–245
- Chen, C.W., Don, T.M. and Yen, H.F. (2006) Enzymatic extruded starch as a carbon source for the production of poly(3-hydroxybutyrate-co-3-hydroxyvalerate) by *Haloferax mediterranei*. *Process Biochem* **41**:2289-2296
- Chen, G.Q. (2005) *Polyhydroxyalkanoates in Biodegradable Polymers for Industrial Applications*, ed. Smith R. CRC, FL, USA pp 32-56

- Chen, G.Q., Konig, K.H., Lafferty, R.M. (1991) Occurrences of poly-D(-)-3-hydroxyalkanoates in the genus *Bacillus*. *FEMS Microbiol Lett* **84**:173-176
- Chen, J.H., Chen, Z.L, Hou, L.B. and Liu, S.T. (2000) Preparation and characterization of di-azepam-polyhydroxybutyrate microspheres, *Gongneng Gaofenzi Xuebao* **13**:61-64.
- Chen, L.J. and Wang, M. (2002) Production and Evaluation of Biodegradable Composites based on PHB-PHV Copolymer, *Biomaterials*. **23**:2631-2639
- Chen, M., Zamora, P.O., Som, P., Pena, L.A., and Osaki S. (2003) Cell attachment and biocompatibility of polytetra uoroethylene (PTFE) treated with glow-discharge plasma of mixed ammonia and oxygen. *J. Biomater. Sci. Polymer. Edn.* **14(9)**:917–35
- Chen, U. and Wang, M. (2002) Production and evaluation of biodegradable composite based on PHB-PHV copolymer. *Biomaterials*. **23**:2631.
- Choi, J.I. and Lee, S.Y. (1999) High-level production of poly(3-hydroxybutyrate-co-3-hydroxyvalerate) by fed-batch culture of recombinant *Escherichia coli*. *Appl Environ Microbiol* **65**:4363-4368
- Chu, C.C. (1982) A comparison of the effect of pH on the biodegradation of two synthetic absorbable sutures. *Arch Surg*. **195**: 55-59.
- Chu, C.R., Douchis, J.S., Yoshioka, M., Sah, R.L., Coutts, R.D. and Amiel, D. (1997) Osteochondral repair using perichondrial cells. A 1-year study in rabbits. *Clin Orthop*. **340**:220-9
- Chua, A.S.M., Takabatake, H., Satoh, H., Mino, T. (2003) Production of polyhydroxyalkanoates (PHA) by activated sludge treating municipal wastewater: Effect of pH, sludge retention time (SRT) and acetate concentration in influent. *Water Res* **37**:3602-3611
- Corchero, J.L., Seras, J., García-Fruitós, E., Vazquez, E., and Villaverde, A. (2010) Nanoparticle-assisted tissue engineering. *Nanobiotech*. Pp13-15
- Cydzik-Kwiatkowska, A., Pokoj, T. and Klimiuk, E. (2006) Molecular detection and diversity of medium-chain-length polyhydroxyalkanoates-producing bacteria enriched from activated sludge, *J Appl Microbiol* **101**:190–199

- Czaja, W., Krystynowicz, A., Bielecki, S. and Brown, R.M. Jr. (2006) Microbial cellulose-the natural power to heal wounds. *Biomater.* **27**:145-51.
- Czaja, W., Young, D.J., Kawechi, M. and Brown, R.M. Jr. (2007) The future prospects of microbial cellulose in biomedical applications, *Biomacromol.* **8**:1-12.
- Davies, J.E. (2003) Understanding peri-implant endosseous healing. *J Dent Educ.* **67**:932-49.
- Davies, S. and Tighe, B. (1995) Cell attachment to gel-spun polyhydroxybutyrate fibers, *Poly. Prepr. (Am. Chem. Soc., Div. Polym. Chem.)* **36**:103-104.
- de Groot, J.H., Zijlstra, F.M., Kuipers, H.W., Pennings, A.J., Klompmaker, J., Veth, R.P., and Jansen, H.W. (1997) Meniscal tissue regeneration in porous 50/50 copoly(l-lactide/e-caprolactone) implants. *Biomater.* **18**:613-622
- Di Donato, P., Anzelmo, G., Tommonaro, G., Fiorentino, G., Nicolaus, B. and Poli, A. (2009) Vegetable wastes as suitable biomass feedstock for biorefineries. *New Biotechnol* **25(1)**:S257
- Doi, Y 'microbial Polyesters', VCH publishers, New York, 1990
- Doyle, C., Tanner, E.T. and Bonfield, W. (1991) *In vitro* and *in vivo* evaluation of polyhydroxybutyrate and of polyhydroxybutyrate reinforced with hydroxyapatite. *Biomater.* **12**:841-847
- Duvernoy, O., Malm, T., Ramstrom, J. and Bowald, S. (1995) A biodegradable patch used as a pericardial substitute after cardiac surgery: 6- and 24-month evaluation with CT, *Thorac Cardiovasc Surg.* **43**:271-274
- Ehrenstein, G.W. and Theriault, R.P. (2001) Polymeric materials: structure, properties, applications, Hanser Verlag, Munich. pp 84
- Eldridge, J.H., Hammond, C.J., Meulbroek, J.A., Staas, J.R., Gilley, R.M. and Tice, T.R. (1990) Controlled vaccine release in the gut-associated lymphoid tissues. I. Orally administered biodegradable microspheres target the Peyer's patches, *Controlled Release.* 205-214.
- FAO will be the world's wheat production for 2009/10 is raised to 678 million tons.
[http:// Fao.org](http://Fao.org) [accessed 12 Nov; 2009]

- Fidler, S. and Dennis, D. (1992) Polyhydroxyalkanoate production in recombinant *Escherichia coli*. *FEMS Microbiol Rev* **103**:231–236
- Fine, E.G., Magari, S.R., Rousseau, S., Orndorff, K.A., Heath, C.A. and Rosen, J.M. (April 1994) Proceedings of the 20th Annual Meeting of the Society for Biomaterials, Boston, USA, pp.279
- Freed, L., Vunjak-Novakovic, G., Biron, R.J., Eagles, D.B., Lesnoy, D.C., Barlow, S.K., Langer, R. (1994) Biodegradable polymer scaffolds for tissue engineering. *Biotechnol.* **12**:689-93
- Freed, L.E., Hollander, A.P., Martin, I., Barry, J.R., Langer, R. and Vunjak-Novakovic G. (1998) Chondrogenesis in a cell-polymer-bioreactor system. *Exp Cell Res* **240**:58-65
- Freed, L.E., Marquis, J.C., Nohria, A., Emmanuel, J., Mikos, A.G. and Langer, R. (1993) Neocartilage formation in vitro and in vivo using cells cultured on synthetic biodegradable polymers. *J Biomed Mater Res* **27**:11–23
- Fukui, T. and Doi, Y. (1998) Efficient production of polyhydroxyalkanoates from plant oils by *Alcaligenes eutrophus* and its recombinant strain. *Appl Microbiol Biotechnol* **49**:333-336 (1998)
- Futui, T., Kichise, T., Yoshida, Y. and Doi, Y. (1997) Biosynthesis of poly(3-hydroxybutyrate-co-3-hydroxyvalerate-co-3-hydroxyheptanoate) terpolymers by recombinant *Alcaligenes eutrophus*. *Biotechnol Lett* **19**:1093-1097
- Galego, N., Rozsa, C., Sanchez, R., Fung, J., Vazquez, A. and Tomas, J.S. (2000) Characterization and application of poly(β -hydroxyalkanoates) family as a composite biomaterials. *Polym Test* **19**:485-492
- Galgut, P., Pitrola, R., Waite, I., Doyle, C. and Smith, R. (1991) Histological evaluation of biodegradable and non-degradable membranes placed trans-cutaneously in rats. *Clin. Periodontol.* **18**:581-586.
- Gangrade, N. and Price, J.C. (1991) Poly(3-hydroxybutyrate-3-hydroxyvalerate) microspheres containing progesterone: preparation, morphology and release properties. *Microencapsulation* **8**:185-202

- Gerard, C., Catuogno, C., Amargier-Huin, C., Grossin, L., Hubert, P., Gillet, P., Netter, P., Dellacherie, E. and Payan, E. (2005) The effect of alginate, hyaluronate and hyaluronate derivatives biomaterials on synthesis of non-articular chondrocyte extracellular matrix. *J Mater Sci Mater Med.* **16**:541–551.
- Gerhardt, P., and Ribí, E. (1964) Ultrastructure of the exosporium enveloping spores of *Bacillus cereus*. *J Bacteriol.* **88**:1774–1789.
- Gerngross, T.U., and Martin, D.P., (1995). Enzyme-catalyzed synthesis of poly[(R)-(-)-3-hydroxybutyrate]: formation of macroscopic granules *in vitro*. Proc. Natl. Acad. Sci. USA **92**:6279–6283.
- Gerngross, T.U., Snell, K.D., Peoples, O.P., Sinskey, A.J., Csuhai, E., Masamune, S and Stubbe, J. (1994) Overexpression and purification of the soluble polyhydroxyalkanoate synthase from *Alcaligenes eutrophus*: evidence for a required post translational modification for catalytic activity. *Biochem.* **33**:9311–9320
- Gopferich, A. (1996) Mechanisms of Polymer Degradation and Erosion. *Biomater.* **17**:103-114
- Greg, B., Uwe, L and Kazuteru, Y. (2006) Biodegradable polymers. *Chem Ind Lett.* 3659-3668
- Grinnell, F. and Feld, M.K. (1982) Fibronectin Adsorption on Hydrophilic and Hydrophobic Surfaces detected by antibody binding and analyzed during cell adhesion in serum-containing medium. *J Bio Chem.* **257(9)**:4888-1893
- Grothe, E., Moo-Young, M. and Chisti, Y. (1999) Fermentation optimization for the production of poly(β hydroxybutyric acid) microbial thermoplastic. *Enzyme Microb Technol* **25**:132–41
- Guo-Qiang C, Jun X, Qiong W, Zengming Z and Kwok-Ping H, Synthesis of copolyesters consisting of medium-chain-length hydroxyalkanoates by *Pseudomonas stutzeri* 1317. *React Funct Polym* **48**:107–112 (2001)
- Gursel, I., Korkusuz, F., Turesin, F., Alaeddinogiu, N.G. and Hasirci, V. (2001) *In vivo* Application of Biodegradable Controlled Antibiotic Release Systems for the Treatment of Implant-related Osteomyelitis, *Biomaterials.* **22**:73-80

- Guzmán, G., Van-Thuoc, D., Martín, J., Hatti-Kaul, R., Quillaguamán, J. (2009) A process for the production of ectoine and poly(3-hydroxybutyrate) by *Halomonas boliviensis*. *Appl Microbiol Biotechnol.* **84**:1069–1077
- Haas, R., Jin, B. and Zepf, F.T. (2008) Production of poly(3-hydroxybutyrate) from waste potato starch. *Biosci Biotechnol Biochem* **72(1)**: 253-256
- Hahn, S.K., Chang, Y.K. and Lee, S.Y. (1995) Recovery and characterization of poly(3-hydroxybutyric acid) synthesized in *Alcaligenes eutrophus* and recombinant *Escherichia coli*. *Appl Environ Microbiol* **61**:34–39
- Halami, P.M. (2008) Production of polyhydroxyalkanoate from starch by the native isolates *Bacillus cereus* CFR06 *World J Microbiol. Biotechnol* **24**:805-812
- Hanley, S.Z., Pappin, D.J, Rahman, D., White, A.J, Elborough, K.M. and Slabas, A.R. (1999) Re-evaluation of the primary structure of *Ralstonia eutropha* phasin and implication for polyhydroxyalkanoic acid granule binding. *FEBS Lett.* **447**:99-105
- Hardingham, T. Tew, S. and Murdoch, A. (2002) Tissue engineering: chondrocytes and cartilage. *Arthritis res.* **4(Suppl 3)**: 63-8
- Hartmann, R., Hanny, R., Pletscher, E., Ritter, A., Witholt, B. and Zinn, M. (2005) Tailor-made olefinic medium-chain-length poly[(R)-3-hydroxyalkanoates] by *Pseudomonas putida* GPo1: Batch versus chemostat production. *Biotech and Bioeng* **93**:737-746
- Hasirci, V, Gursel, I., Turesin, F., Yigitel, G., Korkusuz, F. and Alaeddinoglu, G. (1998) Microbial polyhydroxyalkanoates as biodegradable drug release materials, in: *Biomedical Science and Technology* (Hincal, A. A. and Kas, H. S., Eds), New York, Plenum Press, 183-187
- Hazari, A., Johansson-Ruden, G., Junemo-Bos-trom, K., Ljungberg, C., Terenghi, G., Green, C. and Wiberg, M. (1993) A new resorbable wraparound implant as an alternative nerve repair technique. *Hand Surg.* **248**:291-295.
- Heller, J. 1993) Poly(ortho esters) In: Peppas N, Langer R, eds. *Advances in Polymer Science* (Vol 107). Berlin: Springer Verlag: 41-93. Hiemenz PC. *Polymer Chemistry*

- Herrick, F.W, Casebier, R.L., Hamilton, J.K. and Sandberg, K.R. (1983) Microfibrillated cellulose: Morphology and accessibility, journal of Applied Polymer Science: *Appl Polymer Symp.* **37**:797-813.
- Hill, C.A.S., Cetin, N.S. and Ozmen, N. (2000) Potential catalysts for the acetylation of wood. *Holzforschung.* **54**:269-272
- Hirokazu, A., Akira Ito, Masanori, S., Yoshinori, K. and Masamichi, K. (2007) Construction of Cardiac Tissue Rings Using a Magnetic Tissue Fabrication Technique. *J Biomed Mater Res B Appl Biomater.* **82**(2):471-480.
- Hocking and Marchessault (1994) "Biopolyesters" in Chemistry and Technology of Biodegradable Polymers, Griffin GJL, editor, Chapman and Hall, London pp 48-96
- Holmes, P.A. (1985) Sterilised powders of poly(3-hydroxybutyrate), UK Patent Application No. 2 160 208A
- Holmes, P.A. (1988) Biologically produced [5-3-hydroxyalkanoate polymers and copolymers, in: *Developments in Crystalline Polymers* (Bassett, D.C., Ed.), London: Elsevier, 1-65, Vol. 2
- Huang, T.Y., Duan, K.J., Huang, S.Y., Chen, C.W. (2006) Production of polyhydroxyalkanoates from inexpensive extruded rice bran and starch by *Haloferax mediterranei* *J Ind Microbiol Biotechnol* **33**:701-706
- Huijberts, H.N., de Rijk, T.C., de Waard, P. and Eggink, G. (1994) ¹³C nuclear magnetic resonance studies of *pseudomonas putida* fatty acid metabolic routes involved in poly(3-hydroxyalkanoate) synthesis. *J Bacteriol.* **176**(6):1661-1666
- Huisman, G.W., Leeuwde, O. And Witholt, B. (1989) Synthesis of poly-3-hydroxyalkanoates is a common feature of fluorescent *pseudomonads*. *Appl Environ Microbiol.* **55**:1949-1954
- Hutmacher, D.W. (2000) Scaffolds in tissue engineering bone and cartilage. *Biomater.* **21**:2529-2543
- Ibusuki, S., Fujii, Y., Iwamoto, Y., and Matsuda, T. (2003) Tissue-engineered cartilage using an injectable and in situ gelable thermo responsive gelatin: Fabrication and in vitro performance. *Tissue Eng.* **9**:371-384.

- Ishikawa, K. (1996) Flexible member for use as a medical bag, US Patent No. 5,480,394
- Ishizaki, A., Tanaka, K. and Taga, N. (2001) Microbial production of poly- β -3-hydroxybutyrate from CO₂. *Appl Microbiol Biotech* **57(1-2)**:6-12
- Ito A, Hibino E, Kobayashi, C *et al.*, (2005) Delivery of Tissue-Engineered Human Retinal Pigment Epithelial Cell Sheets, Using Magnetite Nanoparticles and Magnetic Force. *Tissue Eng.* **11(3-4)**: 489 -496
- Ito, A., Hayashida, M., Honda, H., Hata, K, Kagami, H., Ueda, M., Kobayashi, T. (2004) Construction and harvest of multilayered keratinocytes sheets using magnetite nanoparticles and magnetic force. *Tissue Eng.* **10(5-6)**: 873-880.
- Ito, A., Shinkai, M., Honda, H. and Kobayashi, T. (2005) Medical application of functionalized magnetic nanoparticles. *J Biosci Bioeng.* **100**:1-11
- Jackson, D.E. and Srienc, F. (1994) Novel methods to synthesize polyhydroxyalkanoates. *Biochemical Engineering VIII*. Volume 745 of the Annals of the New York Academy of Sciences. **745**:134-148
- Johannsen, M., Gneveckow, U., Eckelt, I., Feussner, A., Waldofner, N., Scholz, R., et al., (2005) Clinical hyperthermia of prostate cancer using magnetic nanoparticles; presentation of a new interstitial technique. *Int J Hyperthermia.* **21**:637-647
- Jonas, R. and Farah, L.F. (1998) Production and application of microbial cellulose. *Polym Degra Stabil* **59**:101-106. Doi: 10.1016/S0141-3910(97)00197-3
- Jonoobi, M., Harun, J., Mathew, A.P., Zobir, M.B., Hussein and Oksman, K. (2010) Reparation of cellulose nanofibres with hydrophobic surface characteristics. *Cellulose.* **17**:299-307
- Jonoobi, M., Harun, J., Shakeri, A., Misra, M. and Oksman, K. (2009) Chemical composition, crystallinity and thermal degradation of bleached and unbleached kenaf bast (*Hibiscus cannabinus*) pulp and nanofibres. *BioResources* **4(2)**:626-639
- Jung, K., Hazenberg, W., Prieto, M. and Witholt, B. (2001) Two-stage continuous process development for the production of medium-chain-length poly(3-hydroxyalkanoates). *Biotechnol Bioeng* **72**:19-24

- Juni, K. and Nakano, M. (1987) Poly(hydroxy acids) in drug delivery, *CRC Crit. Rev. Ther. Drug Carrier Systems* **3**:209-232
- Juni, K., Nakano, M., Kubota, M., Matsui, N., Ichihara, T., Beppu, T, Mori, K. And Akagi, M. (1985) Controlled release of aclarubicin from poly(beta-3-hydroxybutyric acid) microspheres, *Igaku no Ayumi* **132**:735-736
- Jurasek, L. and Marchessault, R.H. (2004) Polyhydroxyalkanoate (PHA) granule formation in *Ralstonia eutropha* cells: a computer simulation. *Appl Microbiol Biotechnol.* **64**:611-617
- Kahar, P., Agus, J., Kikkawa, Y., taguchi, K., Doi, Y. and Tsuge, T. (2005) Effective production and kinetic characterization of ultra-high-molecular-weight poly[(R)-3-hydroxybutyrate] in recombinant *Escherichia coli*. *Polym Degrad Stabil* **87**:161-169
- Kang, I.K., Choi, S.H., Shin, D.S., Yoon, S.C. (2001) Surface modification of polyhydroxyalkanoate films and their interaction with human fibroblasts. *Inter J Biomacromol* **28(3)**:205-212
- Katirciog˘lu, H., Aslim, B., Y˘uksekd˘ađ, Z.N., Mercan, N. and Beyatli, Y. (2003) Production of poly-beta-hydroxybutyrate (PHB) and differentiation of putative *Bacillus* mutant strains by SDS-PAGE of total cell protein. *African J Biotechnol* **2**:147–149
- Kawaguchi, T., Tsugane, A., Higashide, K., Endoh, H., Hasegawa, T., Kanno, H., Seki, T., Juni, K., Fukushima, S. and Nakano, M. (1992) Control of drug release with a combination of prodrug and polymer matrix: Antitumor activity and release profiles of 2',3'-diacyl-5-fluoro-2'-deoxyuridine from poly(3-hydroxybutyrate) microspheres. *Pharm Sci.* **81**:508-512
- Kawaguchi, Y. and Doi, Y. (1992) Kinetics and mechanism of synthesis and degradation of poly(3-hydroxybutyrate) in *Alcaligenes eutrophus*. *Macromol.* **25 (9)**:2324–2329
- Kerstens, K., Lisdiyanti, P., Komagata, K. and Swings, J. (2006) The Family Acetobacteraceae: the Genera *Acetobacter*, *Aci-domonas*, *Asaia*, *Gluconacetobacter*, *Gluconobacter*, and *Kozakia*. In *The Prokaryotes*. Springer, New York, pp163-200
- Kessel, R. (1998) Connective Tissue: Cartilage. In: *Basic Medical Histology*. New York: Oxford university press. PP 128–137.

- Khalil, H.P.A., Ismail, H., Rozman, H.D. and Ahmad, M.N. (2001) The effect of acetylation on interfacial shear strength between plant fiber and various matrices. *Eur Polym J.* **37(5)**:1037-1045
- Khanna, S. and Srivastava, A.K. (2005) Recent Advances in microbial polyhydroxyalkanoates, *Process Biochemistry* **40**:607-619
- Kharenko, A.V. and Iordanskii, A.L. (1999) Diltiazem release from matrices based on polyhydroxybutyrate, *Proc. Int. Symp. Controlled Release Bioact Mater.* **26**:919-920
- Kim, B.S. (2000) Production of PHB from inexpensive substrates. *Enzyme Microb Technol.* **27**:774-777
- Kim, B.S., Lee, S.C., Lee, S.Y., Chang, H.N., Chang, Y.K. and Woo, S.I. (1994) Production of poly(3-hydroxybutyric-co-hydroxyvaleric acid) by fed-batch culture of *Alcaligenes eutrophus* with substrate control using on-line glucose analyzer. *Enzyme Microb Technol.* **16**:556-561
- Kim, B.S., Lee, S.Y. and Chang, H.N. (1992) Production of poly-beta-hydroxybutyrate by fed-batch culture of recombinant *Escherichia coli*. *Biotechnol Lett* **14**:811-816
- Kim, B.S., Lee, S.Y. and Chang, H.N. (1995) Control of glucose feeding using exit gas data and its application to the production of PHB from tapioca hydrolysate by *Alcaligenes eutrophus*. *Biotechnol Tech* **9**:311-314
- Kim, D.K., Toprak, M., Mikhailova, M., Zhang, Y., Bjelke, B., Kehr, J. and Muhammed, M. (2002) Surface modification of superparamagnetic nanoparticles for *in-vivo* biomedical applications". *Mat.Res. Soc. Symp. Proc.* **704**:W11.2.1-W11.2.6.
- Kim, S.W., Kim, P., Lee, H.S. and Kim, J.H. (1996) High production of poly- β -hydroxybutyrate (PHB) from, *Methylobacterium organophilum* under potassium limitation. *Biotechnol Lett* **18**:25-30
- Knowles, J.C. and Hastings, G.W. (1991) In vitro degradation of a PHB/PHV copolymer and a new technique for monitoring early surface changes. *Biomater.* **12 (2)**:210-214
- Knowles, J.C., Mahmud, F. A. and Hastings, G.W. (1991) Piezoelectric characteristics of a polyhydroxybutyrate-based composite, *Clin. Mater.* **8**:155-158.

- Koller, M., Bona, R., Chiellini, E., Fernandes, E.G., Horvat, P., Kutschera, C., Hesse, P., Braunegg, G. (2008) Polyhydroxyalkanoate production from whey by *Pseudomonas hydrogenovora*. *Bioresource Technol* **99(11)**:4854-63
- Kokubo, T., Hata, K., Nakamura, T. and Yamamura, T. (1991) Apatite formation on ceramics, metals and polymers induced by CaO-SiO₂-based glass in simulated body fluid. *Bioceramics*. (eds.) Bonfield W, Hastings GW, Tanner KE. Butterworth-Heinemann, Oxford.
- Kondo, T. and Sawatari, C. (1994). Intermolecular Hydrogen-Bonding in Cellulose Poly(Ethylene Oxide) Blends - Thermodynamic Examination Using 2,3-Di-O-Methylcelluloses and 6-OMethylcelluloses as Cellulose Model Compounds. *Polymer*. **35**:4423-4428.
- Korsatko, W., Wabnegg, B., Tillran, H.M., Braunegg, G. and Lafferty, R.M. (1983) A biodegradable carrier for long term medication dosage, 2nd communication: The biodegradation in animal organism and *in vitro-in vivo* correction of the liberation of pharmaceuticals from parenteral matrix retard tablets, *Pharm Ind.* **45**:1004-1007
- Kostopoulos, L. and Karring, T. (1994) Augmentation of the rat mandible using guided tissue regeneration, *Clin Oral Impl Res.* **5**:75-82.
- Kostopoulos, L. and Karring, T. (1994) Guided bone regeneration in mandibular defects in rats using 3 bioresorbable polymer, *Clin. Oral Impl Res.* **5**:66-74.
- Krans, R.G., Gabbert, K.K., Locke, T.A. and Madigan, M.T. (1997) Polyhydroxyalkanoate production in *Rhodobacter capsulatus*: Genes, mutants, expression, and physiology, *Appl Environ Microbiol.* **63**:3003-3009
- Kubota, M., Nakano, M., Juni, K. (1988) Mechanism of enhancement of the release rate of adarubicin from poly-3-hydroxybutyric acid microspheres by fatty acid esters, *Chem. Pharm Bull.* **36**:333-337
- Kumar, P.R.A., Varma, H.K., and Kumary, T.V., (2007) Cell patch seeding and functional analysis of cellularized scaffolds for tissue engineering. *Biomed. Mater.* **2(1)**:48
- Labuzek, S. and Radeck, I. (2001) Biosynthesis of PHB tercopolymer by *Bacillus cereus* UW85. *J Appl Microbiol* **90**:353-357

- Lapointe, R., Lambert, A. and Savard, L. (2002) Process for production of biopolymer. U.S. Patent No. WO 0222841
- Lauzier, C.A., Monastererios, C.J., Saracovan, I., Marchessault, R.H. and Ramsay, B.A. (1993) Film Formation and paper coating with poly(β -hydroxyalkanoates), a Biodegradable Latex. *J Tappi*. **76(5)**:71-77
- Lee, S.Y. (1995) Bacterial Polyhydroxyalkanoates. *Biotechnol Bioeng* **49**:1-14
- Lee, S.Y. (1996) Plastic bacteria? Progress and prospects for polyhydroxyalkanoate production in bacteria. *Trends Biotechnol.* **14**:431-438.
- Lee, S.Y., Choi, K. and Song, J.Y. (1999) Removal of Endotoxin during Purification of Poly(3-Hydroxybutyrate) from Gram-Negative Bacteria. *Appl Environ Microbiol.* **65(6)**:2762-2764
- Leenstra, T.S., Maltha, J.C. and Kuijpers-Jagtman, A.M. (1995) Biodegradation of non-porous films after submucoperiosteal implantation on the palate of Beagle dogs. *Mater. Sci. Mater. Med.* **6**:445-450.
- Lemos, P.C., Serafim, L.S. and Reis, M.A.M. (2006) Synthesis of polyhydroxyalkanoates from different short-chain fatty acids by mixed cultures submitted to aerobic dynamic feeding. *J Biotech.* **122**:226-238
- Lenz, R.W. and Marchessault, R.H. (2005) Bacterial polyesters: Biosynthesis, biodegradable plastics and biotechnology. *Biomacromol* **6**:1-8
- Li, R., Hanxing, Z. and Qingsheng, Q. (2007) The Production of polyhydroxyalkanoates in recombinant *Escherichia coli*. *Biores Tech* **98(12)**:2313-2320
- Li, S., Garreau, H. and Vert, M. (1990) Structure-property relationships in the case of the degradation of massive aliphatic poly(α -hydroxy-acids) in aqueous media. Part: Poly(D,L-lactic acid). *J Mater Sci: Mater med.* **1**:131
- Li J, Yun H, Gong Y, Zhao N and Zhang X (2005) Effects of surface modification of poly (3-hydroxybutyrate- co-3-hydroxyhexanoate) (PHBHHx) on physicochemical properties and on interactions with MC3T3-E1 cells. *J Biomed Mater Res. A* **75**:985.

- Lin, K.Y., Ogle, R.C., Jane, J.A. (2002). *Craniofacial surgery: science and surgical technique*. Philadelphia, Pennsylvania: W.B. Saunders
- Linda, C.S., David, T.G. and Gregory, F.M. (2008) Polymer microscopy. Springer. p. 5.
ISBN 0387726276
- Liu, F., Li, W., Ridgway, D. and Gu, T. (1998) Production of poly-beta-hydroxybutyrate on molasses by recombinant *Escherichia coli*. *Biotechnol Lett* **20**:345–348
- Liu, H.Y., Hall, P.V., Darby, J.L., Coats, E.R, Green, P.G., Thompson, D.E. and Loge, F.J. (2008) Production of polyhydroxyalkanoate during treatment of tomato cannery wastewater. *Water Environ Res* **80**:367-372
- Ljungberg, C., Johansson-Ruden, G., Bostrom, K.J., Novikov, L. and Wiberg, M. (1999) Neuronal survival using a resorbable synthetic conduit as an alternative to primary nerve repair, *Microsurgery* **19**:259-264
- Lu, L., Zhu, X., Valenzuela, R.G., Currier, B.L. and Yaszemski, M.J. (2001) Biodegradable polymer scaffolds for cartilage tissue engineering. *Clin Orthop. suppl* **291**:S251–S270.
- Lubbe, A.S., Bergemann, C., Riess, H., Schriever, F., Reichardt, P., Possinger, K., et al. (1996) Clinical experiences with magnetic drug targeting: a phase 1 study with 4'-epidoxorubicin in 14 patients with advance solid tumors. *Cancer Res.* **56**:4686-93.
- Madison, L.L. and Huisman, G.W. (1999) Metabolic engineering of poly(3-hydroxyalkanoates): From DNA to plastic. *Microbiol Mol Biol Rev* **63**:21-53
- Malm, T., Bowald, S., Bylock, A., Busch, C. and Saldeen, T. (1994) Enlargement of the right ventricular outflow tract and the pulmonary artery with a new biodegradable patch in trans-annular position, *Eur. Surg. Res.* **26**:298-308.
- Maquet, V., Boccaccini, A.R., Pravata, L., Notingher, I. and Jerome, R. (2003). Preparation, Characterization, and *in vitro* Degradation of Bioresorbable and Bioactive Composites based on Bioglass®-filled polylactide Foams, *J Biomed Mater Res.* **66**:335-346
- Marangoni, C., Furigo, A. and De Aragdo, G.M.F. (2002) Production of poly(3-hydroxyvalerate) by *Ralstonia eutropha* in whey and inverted sugar with propionic acid feeding. *Process Biochem* **38**:137-141

- Martin, D.P., Peoples, O.P. and Williams, S.F. (2000) Nutritional and therapeutic uses of 3-hydroxy-alkanoate oligomers, PCT Patent Application No. WO 00/04895
- Martin, D.P., Rizk, S., Ho, K. and Williams, S.F. (2007) Medical Devices Containing Melt-Blown Non-Wovens of Poly-4-Hydroxybutyrate and Copolymers. U S. Patent. 61/014,906
- Martin, D.P., Williams, S.F. (2003) Medical applications of poly 4-hydroxybutyrate: a strong flexible absorbable biomaterial, *J Biochem Eng* **16**:97–105
- Mathew, A.P., Chakraborty, A., Oksman, K. And Sain, M. (2006) Cellulose nanocomposite Processing, Characterization and properties, American Chemical Society, Washington, D C. **938**:114-131.
- Matsusaki, H., Manji, S., Taguchi, K, Kato, M., Fukui, T. and Doi, Y. (1998) Cloning and molecular analysis of the Poly(3-hydroxybutyrate) and Poly(3-hydroxybutyrate-co-3-hydroxyalkanoate) biosynthesis genes in *Pseudomonas sp.* strain 61-3. *J Bacteriol* **180**:6459–6467.
- Matz, L.L., Beaman, T.C. and Gerhardt, P. (1970). Chemical composition of exosporium from spores of *Bacillus cereus*. *J Bacteriol.* **101**:196–201
- McCool, G.J. and Cannon, M.C. (1999) Polyhydroxyalkanoate inclusion body-associated proteins and coding regions in *Bacillus megaterium*. *J Bacteriol.* **181**:585–592
- Mckenna, B.A., Mikkelse, D., Wehr, J.B., Gidley, M.J. and Menzies, N.W. (2009) Mechanical and structural properties of native and alkali-treated bacterial cellulose produced by *Gluconacetobacter xylinus* strain ATCC 53524. *Cellulose.* **16**:1047-1055
- Menges, G., Haberstroh, E., Michaeli, W. and Schmachtenberg, E. (200) *Plastics Materials Science*. Hanser Verlag. ISBN 3-446-21257-4
- Millan, A., Palacio, F., Falqui, A., Snoeck, E., Serin, V., Bhattacharjee, V., Ksenofontov, V., Gutlich, P. and Gilbert, I. (2009) Maghemite polymer nanocomposites with modulated magnetic properties. *Acta Materialia.* **55**:2201–2209
- Miller, N.D. and Williams, D.F. (1987) On the biodegradation of poly- β -hydroxybutyrate (PHB) homopolymer and poly- β -hydroxybutyrate-hydroxyvalerate copolymers. *Biomat.* **8(2)**:129-137

- Misra, S.K., Ansari, S.K, Mohn, D., Valappil, S.P., Brunner, A.J., Stark, W.J., Roy, I., Knowles, J.C., Sibbons, P.D., Jones, E.V., Boccaccini, A.R. and Salih, V., Effect of nanoparticulate bioactivity and cytocompatibility of poly(3-hydroxybutyrate) composites. *J Royal Soc Interface*. Doi: 10:1098/rsif.2009.0255.
- Misra, S.K., Watts, P.C.P., Valappil, S.P., Silva, S.R.P., Roy, I., Boccaccini, A.R. (2007). Poly(3-hydroxybutyrate)/Bioglass composite films containing carbon nanotubes. *Nanotechnol.***18**:075701
- Mohanty, A.K., Misra, M and Drzal, L.T. (2002) Sustainable Bio-Composites from Renewable Resources: Opportunities and Challenges in the Green Materials World. *J Polymers & Environ.* **10**:1-2
- Mudliar, S.N., Vaidya, A.N., Suresh Kumar, M., Dahikar, S. and Chakrabarti, T. (2008) Techno economic evaluation of PHB production from activated sludge. *Clean Technologies and Environmental Policy.* **10 (3)**:255–262.
- Mukhopadhyay, K., Tripathy, D.K. and De, S.K. (1993) Dynamic mechanical properties of silica-filled ethylene vinyl acetate rubber. *J Appl Polym Sci.* **48**:1089-1103
- Müller, B. and Jendrossek, D. (1993) Purification and properties of poly(3-hydroxyvaleric acid) depolymerase from *Pseudomonas lemoignei*. *Appl Microbiol Biotechnol.* **38**:487–492
- Murphy, W.L. and Mooney, D.J. (1999) Controlled delivery of inductive proteins, plasmid DNA, and cells from tissue engineering matrices. *J Periodont Res.* **34**: 413.
- Nakagaito, A.N. and Yano, H. (2004) Effect of morphological changes from pulp fiber towards nano-scale fibrillated cellulose on the mechanical properties of high-strength plant fiber based composites. *Applied Physics A.* **78**:547-552
- Naughton, G.K, Tolbert W.R., and Grillo T.M. (1995) Emerging developments in tissue engineering and cell technology. *Tissue Eng.* **1(2)**:211-9
- Navarro, M., Aparicio, C., Harris, C.M, Ginebra, MP, Engel, E, Planell, J.A. (2006) Development of biodegradable composite scaffold for bone tissue engineering: physiochemical, topographical, mechanical, degradation and biological properties. *Adv Polym Sci.* **200**:209-31

- Nehrer, S., Breinan, H.A., Ramappa, A., Shortkro, S., Young, G., Minas, T., Sledge, C.B., Yannas, I.V. and Spector, M. (1997) Canine chondrocytes seeded in type I and type II collagen implants investigated in vitro. *J Biomed Mater Res* 38: 95–104 (erratum in *J Biomed Mater Res* **38(4)**:288)
- Nikel, P.I., Almeida, A.D., Melillo, E.C., Galvagno, M.A. and Pettinari, M.J. (2006) New recombinant *Escherichia coli* strain tailored for the production of poly(3-hydroxybutyrate) from agro-industrial by-products. *Appl Environ Microbiol.* **72(6)**:3949-3954
- Nishi, Y., Uryu, M., Yamanaka, S., Watanabe, K., Kitamura, N., Iguchi, M., Mitsunashi, S. (1990) The structure and mechanical properties of sheets prepared from bacterial cellulose 2. Improvement of the mechanical properties of sheets and their applicability to diaphragms of electroacoustic transducers. *J Mat Sci.* **25**:2997-3002
Dio:10.1007/BF00584917.
- Nishioka, M., Nakai, K., Miyake, M., Asada, Y. and Taya M. (2001) Production of the poly-3-hydroxyalkanoate by thermophilic cyanobacterium, *S'echococcus* sp. MA19, under phosphate-limited condition. *Biotechnol Lett.* **23**:1095-1099
- Nkere, U.U., Whawell, S.A., Sarraf, C.E., Schofield, J.B. and O'Keefe, P.A. (1998) pericardial substitution after cardiopulmonary bypass surgery: A trial of an absorbable patch, *Thome. Cardiovasc Surg.* **46**:77-83
- Noisshiki, Y. and Komatsuzaki, S. (1995) Medical materials for soft tissue use, Japanese Patent Application No. 07275342
- Ohye, D.F., and Murrell, W.G. (1973) Exosporium and spore coat formation in *Bacillus cereus* T. *J Bacteriol.* **115**:1179–1190
- Ojumu, T.V., Yu, J. and Solomon, B.O. (2004) Production of polyhydroxyalkanoate, a bacterial biodegradable polymer. *African J Biotech* **3(1)**:18-24
- Omar, S., Rayes, A., Eqaab, A., Viss, I. and Steinbuechel (2001) Optimization of cell growth and poly(3-hydroxybutyrate) accumulation on date syrup by a *Bacillus megaterium* strain. *Biotechnol Lett.* **23**:1119-1123

- Park, S.J., Ahn, W.S., Green, P.R., Lee, S.Y. (2001) Biosynthesis of Polyhydroxybutyrate-co-3-Hydroxyvalerate-co-3-Hydroxyhexanoate) by Metabolically Engineered *Escherichia coli* strains. *Biotechnol Bioeng* **74**:81-86
- Patnaik, P.R. (2005) Perspectives in the modelling and optimization of PHB production by pure and mixed cultures. *Critical Reviews in Biotechnol.* **25**:153–171
- Patrick Jr, C.W., Mikos, A.G. and McIntire, (1998) Prospectus of tissue engineering. In: Patrick Jr, C.W., Mikos, A.G. McIntire, L.V., editors, *Frontiers in tissue engineering*. New York, USA: Elsevier Science, pp 3-14
- Peoples, O.P., Saunders, C., Nichols, S. and Beach, L. (1999) Animal nutrition compositions, PCT. Patent Application No. WO 99/34687
- Philip, S., Keshavarz, T., Roy, I., (2007) Polyhydroxyalkanoates: biodegradable polymers with a range of applications. *J Chem Technol Biotechnol* **82**:233-247.
- Pitt CG, Chasalow, F.I., Hibionada, Y.M., Klimas, D.M. and Schindler A. (1981) Aliphatic polyesters. I. The degradation of poly(*s*-caprolactone) *in vivo*. *J App Polym Sci*: **26**:3779-787.
- Poirier, Y., Nawrath, C. and Somerville, C. (1995) Production of polyhydroxyalkanoates, a family of biodegradable plastics and elastomers, in bacteria and plants. *Biotechnol* **13**:142–150
- Potter, M., Muller, H. and Steinbuchel, A. (2005) Influence of homologous phasins (phaP) on PHA accumulation and regulation of their expression by the transcriptional repressor phaR in *Ralstonia eutropha* H16. *Microbiology*. **151**:825-833
- Pouton, C.W. and Akhtar, S. (1996) Biosynthetic polyhydroxyalkanoates and their potential in drug delivery. *Adv Drug Deliv Rev.* **18**:133–162
- Pozo, C., Martinez-Toledo, M.V., Rodelas, B. and Gonzalez-Lopez, J. (2002) Effects of culture conditions on the production of polyhydroxyalkanoates by *Azotobacter chroococcum* H23 in media containing a high concentration of alpechin (wastewater from olive oil mills). *J Biotech.* **97**:125-131

- Pramanik N, Bhargava, P., Alam, S. and Pramanik, P. (2006) Processing and properties of nano- and macro-hydroxyapatite/poly(ethylene-co-acrylic acid) composites. *Polym Compos.* **27**:633
- Preusting, H., Van, Houten, R., Hoefs, A., Kool, van Langenberghe, E., Favre-Bulle, O. and Witholt, B. (1993) High cell density cultivation of *Pseudomonas oleovorans*: growth and production of poly (3-hydroxyalkanoates) in two-liquid phase batch and fed-batch systems. *Biotechnol Bioeng* **41**:550–556
- Price, N., Bendall, S.P., Frondoza, C., Jinnah, R.H. and Hungerford, D.S. (1997) Human osteoblast-like cells (MG63) proliferate on a bioactive glass surface. *J Biomed Mater Res.* **37**:394-400.
- Quillaguamán, J, Van-Thouc, D., Guzmán, H., Guzmán, D., Martín, J., Everest, A., Hatti-Kaul, R. (2008) Poly(3-hydroxybutyrate) production by *Halomonas boliviensis* in fed batch culture. *Appl Microbiol Biotechnol.* **78**:227–232
- Quillaguaman, J., Hashim, S., Bento, F., Mattiasson, B. and Hatti-Kaul, R. (2005) Poly(β -hydroxybutyrate) production by a moderate halophile, *Halomonas boliviensis* LC1 using starch hydrolysate as substrate. *J Appl Microbiol.* **99**:151-157
- Radnedge, L., Agron, P.G., Hill, K.K., Jackson, P.J., Ticknor, L.O., Keim, P. and Andersen, G.L. (2003) Genome differences that distinguish *Bacillus anthracis* from *Bacillus cereus* and *Bacillus thuringiensis*. *Appl Environ Microbiol.* **69**:2755–2764
- Ramadas, N.V., Singh, S.K., Soccol, C.R. and Pandey, A. (2009) Polyhydroxybutyrate Production using Agro-industrial Residue as Substrate by *Bacillus sphaericus* NCIM5149. *Brazilian Archives of Biology & Technol* **52(1)**:17-23
- Reddy, C.S.K., Ghai, R., Rashmi, Lalia, V.C. (2003) Polyhydroxyalkanoates: an overview. *Bioresour Technol* **87**:137-146
- Rehm, B.H. (2003) Polyester synthases: natural catalysts for plastics. *Biochem J.* **376**:15–33
- Rehm, K.E., Claes, L., Helling, H.J. and Hutmacher, D. (1994) Application of a polylactide pin. An open clinical prospective study. In: Leung, K.S., Hung, L.K., Leung, P.C., editors. Biodegradable implants in fracture fixation. Hong Kong: World Scientific. Pp54

- Rehm, R.H.A. (2006) Genetics and biochemistry of polyhydroxyalkanoate granule self-assembly: the key role of poly-ester synthases. *Biotechnol Lett* **28**:207-213
- Rein, B.H.A. (2007) Biogenesis of Microbial Polyhydroxyalkanoate Granules: a Platform Technology for the Production of Tailor-made Bioparticles *Curr. Issues Mol Biol.* **9**:41-62
- Ren, Q., Grubelnik, A., Hoerler, M., Ruth, K., Hartmann, R., Felber, H. and Zinn, M. (2005) Bacterial Poly(hydroxyalkanoates) as a Source of Chiral Hydroxyalkanoic Acids. *Biomacromol* **6**(4):2290-2298
- Ribera, R.G., Monteoliva-Sanchez, M. and Ramos-Cormenzana, A. (2001) Production of polyhydroxyalkanoates by *Pseudomonas putida* KT2442 harboring pSK2665 in wastewater from olive oil mills (alpechin). *J Biotech* **4**(2):116-119
- Rice policy-IRRI world Rice statistics (WRS). Trends in Rice economy. <http://beta.irri.org/statistics> [accessed 12 Nov; 2009]
- Rich, J., Tuominen, J., Kylma J., Seppala J., Nazhat, S.N et al. (2002) Lactic acid based PEU/HA and PEU/BCP composites: dynamic mechanical characterisation of hydrolysis. *J Biomed Mater Res Part B App Biomater.* **63**:346.
- Rivard, C.H., Chaput, C., Rhalmi, S. and Selmani, A. (1996) Bio-absorbable Synthetic Polyesters and Tissue Regeneration. A Study of Three-dimensional Proliferation of Ovine Chondrocytes and Osteoblasts, *Ann. Chir.* **50**:651-658.
- Ron, E., Turek, T., Mathiowitz, E., (1993) Controlled release of polypeptides from polyanhydrides. *Proc Nat Acad Sci USA:* **90**: 4176-4180.
- Ryu, H.W., Hahn, S.K., Chang, Y.K. and Chang, H.N. (1997) Production of poly(3-hydroxybutyrate) by high cell density fed-batch culture of *Alcaligenes eutrophus* with phosphate limitation. *Biotechnol Bioeng* **55**:28-32
- Saito, T., Tomita, K., Juni, K. and Ooba, K. (1991) *In vivo* and *in vitro* degradation of poly(3-hydroxybutyrate) in rat. *Biomater* **12**:309-312

- Samir, M.A.S., Alloin, F., Sanchez, J.Y., El Kissi, N. and Dufresne, A. (2004) Preparation of cellulose whiskers reinforced nanocomposites from an organic medium suspension. *Macromol.* **37(4)**:1386-93.
- Santimano, M.C., Prabhu, N.N. and Garg, S. (2009) PHA Production Using Low-Cost Agro-Industrial Wastes by *Bacillus sp.* Strain COL1/A6. *J Microbiol* **4(3)**:89-96
- Sassi, J.F. and Chanzy, H. (1995) Ultrastructural aspects of the acetylation of cellulose. *Cellulose.* **2**:111-127
- Satoh, H., Mino, T. and Matsuo, T. (1992) Uptake of organic substrates and accumulation of polyhydroxyalkanoates linked with glycolysis of intracellular carbohydrates under anaerobic conditions in the biological excess phosphate removal processes. *Wat Sci Technol* **26(5-6)**: 933-942
- Satoh, Y., Minamoto, N, Tajima, K. and Munekata, M. (2002) Polyhydroxyalkanoate synthase from *Bacillus sp.* INT005 is composed of PhaC and PhaR. *J Biosci Bioeng* **94**:343–350
- Scandola, M., Focarete, M.L., Adamus, G., Sikorska, W., Baranowska, I., Swierczek, S., Gnatowski, M., Kowalczyk, M., Jedlinski, Z. (1997) Polymer blends of natural poly(3-hydroxybutyrate-co-3-hydroxyvalerate) and a synthetic poly(3-hydroxybutyrate). Characterization and biodegradation studies. *Macromol.* **30**:2568-2574
- Scherer, F., Anton, M., Schillinger, U., Henke, J., Bergemann, C., Kruger, A *et al.*, (2002) Magnetofection: enhancing and targeting gene delivery by magnetic force *in vitro* and *in vivo*. *Gene Ther.* **9**:102-109.
- Schirmer A, Jendrossek D, Schlegel HG. Degradation of poly(3-hydroxyoctanoic acid) [P(3HO)] by bacteria: purification and properties of a P(3HO) depolymerase from *Pseudomonas fluorescens* GK13. *Appl Environ Microbiol.* April; **59(4)**: 1220–1227 (1993).
- Schmitz, K.P. and Behrend, D. (1997) Method of manufacturing intraluminal stents made of polymer material. European Patent Application No. 0770 401 A2

- Scholz, C. (2000) Poly(β -hydroxyalkanoates) as potential biomedical materials: an overview, In: (Ed.) Scholz C, Gross RA. *Polymers from renewable resources-biopolymers and biocatalysis*. ACS series **764**:328-334
- Seal, B.L., Otero, T.C. and Panitch, A. (2001) Polymeric biomaterials for tissue and organ regeneration. *Mater Sci Eng.* **34**:147-230
- Segal, L., Creely, L., Martin, A.E. and Conrad, C.M. (1959) An empirical method for estimating the degree of crystallinity of native cellulose using X-ray diffractometer. *Text Res J.* **29**:786-794
- Seydibeyoglu, M.O. and Oksman, K. (2008) Novel nanocomposites based on polyurethane and micro fibrillated cellulose. *Compos Sci Technol* **68(3-4)**:908-914
- Shamala, T.R., Chandrashekar, A., Vijayendra, S.V. and Sharma, L. (2003) Identification of polyhydroxyalkanoate (PHA)-producing *Bacillus spp.* using the polymerase chain reaction (PCR). *J Appl Microbiol.* **94**:369-374
- Shimizu, K., Ito, A., Lee, J.K., Yoshida, T., Miwa, K., Ishiguro, H., Numaguchi, Y., Murohara, T., Kodama, I. and Honda, H. (2007) Construction of multi-layered cardiomyocyte sheets using magnetite nanoparticles and magnetic force. *Biotechnol Bioeng.* **96**:803-809.
- Sieminski, A.L. and Gooch, K.J. (2000) Biomaterial-microvasculature interactions. *Biomat.* **21**:2233-41
- Simon-Colin, C., Raguene, G., Crassous, P., Moppert, X. and Guezennec, J. (2008) A novel mcl-PHA produced on coprah oil by *Pseudomonas guezennei biovar*. Tikehau, isolated from a 'kopara' mat of French Polynesia. *Int J Biol Macromol* **43(2)**:176-181
- Sittinger, M., Reitzel, D., Dauner, M., Hierlemann, H., Hammer, C., Kastenbauer, E., Planck, H., Burmester, G.R and Bujia, J. (1996) Resorbable polyesters in cartilage engineering: affinity and biocompatibility of polymer fiber structures to chondrocytes. *J Biomed Mater Res* **33**:57-63
- Sodian, R., Hoerstrup, S.P., Sperling, J.S., Daebritz, S., Martin, D.P., Moran, A.M., Kim, B.S., Schoen, F.J., Vazcanti, J.P. and Mayer, J.E. Jr. (2000) Early *in vivo* experience

- with tissue-engineered trileaflet heart valves. *Circulation* **102(Suppl.3):III22-29**
- Solaiman, D., Ashby, R., Hotchkiss, A. and Foglia, T. (2006) Biosynthesis of medium-chain-length poly(hydroxyalkanoates) from soy molasses. *Biotechnol Lett* **28:57-162**
- Stamboulis, A.G., Hench, L.L. and Boccaccini, A.R. (2002). Mechanical Properties of Biodegradable Polymer Sutures Coated with BG, *J Mat Sci: Mat. Med.* **13:843-848**
- Steel, M.L. and Norton-Berry, P. (1986) Non-woven fibrous material. U.S. Patent 4,603,070
- Steinbüchel, A. (1991) Polyhydroxyalkanoic acids, In: Byron D, editor, *Biomaterials: Novel-Materials from Biological Sources*. Stockton Press, New York, pp 124-213
- Steinbüchel, A. (2001) Perspectives for biotechnological production and utilization of biopolymers: Metabolic engineering of polyhydroxyalkanoate biosynthesis pathway as a successful example. *Macromol Biosci* **1:1-24**
- Steinbüchel, A. and Valentin, H. (1995) Diversity of bacterial polyhydroxyalkanoic acids. *FEMS Microbiol Lett.* **128:219-228**
- Stevens, M.M., Qanadilo, H.F., Langer, R., and Prasad Shastri, V. (2004) A rapid-curing alginate gel system: Utility in periosteum-derived cartilage tissue engineering. *Biomat.* **25:887– 894.**
- Stock, U.A, Sakamoto, T., Hatsuoka, S., Martin, D.P., Nagashima, M., Moran, A.M., Moses, M.A., Khalil, P.N., Schoen, F.J., Vacanti, J.P. and Mayer, J.E. (2000) Patch augmentation of the pulmonary artery with bioabsorbable polymers and autologous cell seeding. *J Thorac Cardiovasc Surg.* **120:1158-1168**
- Sudesh, K., Abe, H. and Doi, Y. (2000) Synthesis, structure and properties of Polyhydroxyalkanoates: Biological polyesters. *J Prog Polymer Sc.* **25:1503-1555**
- Sugiyama, J., Vuong, R. and Chanzy, H. (1991) Electron-diffraction study on the 2 crystalline phases occurring in native cellulose from an algal cell-wall. *Macromol.* **24:4168-4175.**
- Sun, X.F., Sun, R.C (2002) Comparative study of acetylation of rise straw fibre with or without catalysts. *Wood Fiber Sci.* **34(2):306-317**

- Sun, Z., Ramsay, J.A., Guay, M. and Ramsay, B.A. (2007) Carbon-limited fed-batch production of medium-chain length polyhydroxyalkanoates from nonanoic acid by *Pseudomonas putida* KT2440. *Appl Microbiol Biotechnol* **74**:69–77
- Svensson, A., Nicklasson, E., Harrah, T., Panilaitis, B., Kaplan, D.L., Brittberg, M. and Gatenholm, P. (2005) Bacteria cellulose as a potential scaffold for tissue engineering of cartilage. *Biomater.* **26**:419-431
- Tajima, K., Igari, T., Nishimura, D., Nakamura, M., Satoh, Y. and Munekata, M. (2003) Isolation and characterization of *Bacillus* sp. INT005 accumulating polyhydroxyalkanoate (PHA) from gas field soil. *J Biosci Bioeng* **95**:77-81
- Tanaka, K., Katamune, K., Ishizaki, A. (1995) Fermentative production of poly-(β -hydroxybutyric acid) from xylose via L-lactate by a two-stage culture method employing *Lactococcus lactis* IO-1 and *Alcaligenes eutrophus*. *Can J Microbiol.* **41**:257–261
- Taniguchi, T. and Okamura, K. (1998) Novel nanocomposites based on polyurethane and micro fibrillated natural fibres. *Polym Int.* **47**(3):291-294.
- Tasaki, O., Hiraide, A., Shiozaki, T., Yamamura, H., Ninomiya, N. and Sugimoto, H. (1998) The dimer and trimer of 3-hydroxybutyrate oligomer as a precursor of ketone bodies for nutritional care, *JPENJ Parenter. Enteral Nutr.* **23**:321-325
- Tian, J., Sinskey, A.J. and Stubbe, J. (2005) Kinetic studies of polyhydroxybutyrate granule formation in *Wautersia eutropha* H16 by transmission electron microscopy. *J Bacteriol.* **187**:3814-3824
- Ting, V., Sims, C.D., Brecht, L.E., McCarthy, J.G., Kasabian, A.K., Connelly, P.R., Elisseeff, J., Gittes, G.K., Longaker, M.T. (1998) In vitro prefabrication of human cartilage shapes using fibrin glue and human chondrocytes. *Ann Plast Surg.* **40**:413– 420.
- Todd, S.J., Moir, A.J.G, Johnson, M.J., and Moir, A. (2003) Genes of *Bacillus cereus* and *Bacillus anthracis* encoding proteins of the exosporium. *J Bacteriol.* **185**:3373–3378

- Tohyama, M. and Shimizu, K. (1999) Control of a mixed culture of *Lactobacillus delbrueckii* and *Ralstonia eutropha* for the production of PHB from glucose via lactate. *J Biochem Eng* **4**:45–53
- Tohyama, M., Patarinska, T., Qiang, Z. and Shimizu, K. (2002) Modelling of the mixed culture and periodic control for PHB production. *J Biochem Eng* **10**:157-173
- Tohyama, M., Takagi, S. and Shimizu, K. (2000) Effect of controlling lactate concentration and periodic change in DO concentration on fermentation characteristics of a mixed culture of *Lactobacillus delbrueckii* and *Ralstonia eutropha* for PHB production. *J Biosci Bioeng* **89**:323-328
- Troedec, M., Sedan, D., Peyratout, C., Bonnet, J., Smith, A., Guinebretiere, R., Gloaguen, V., Krausz, P. (2008) Influence of various chemical treatments on the composition and structure of hemp fibres. *Composites: Part A*. **39(3)**:514-522
- Turbak, A.F., Snyder, F.W. and Sandberg, K.R. (1983) Microfibrillated cellulose, a new cellulose product: Properties, uses and commercial potential. *J Appl Polym Sci*. **37**:815–827.
- Ueno, T., Satoh, H., Mino, T. and Matsuo, T. (1993) Production of biodegradable plastics. *Polym Preprints Jpn* **42(9)**:3673-3675
- Unverdorben, M., Schywalsky, M., Labahn, D., Hartwig, S., Laenger, F., Lootz, D., Behrend, D., Schmitz, K., Schaldach, M. and Vallbracht, C. (1998) Polyhydroxybutyrate (PHB) stent-experience in the rabbit, *Am. J. Card. Transcatheter Cardiovascular Therapeutics, Abstract TCT-n*, 58
- Vainionpaa, S., Vihtonen, K., Mero, M., Patiala, H., Rokkanen, P., Kilpikari, and Tbrmala, P. (1986) Biodegradable fixation of rabbit osteotomies, *Acta Orthopaed. Scand*. **57**:237-239
- Valappil, S., Misra, S.K., Boccaccini, A.R. and Roy, I. (2006) Biomedical applications of polyhydroxyalkanoates, an overview of animal testing and in-vivo responses. *Expert Rev Med Devices* **3**:853– 868
- Valappil, S.P., Boccaccini, A.R., Bucke, C. and Roy, I. (2007) Polyhydroxyalkanoates in Gram-positive bacteria: insights from the genera *Bacillus* and *Streptomyces*. *Antonie Van Leeuwenhoek* **91**:1–17

- Valappil, S.P., Peiris, D., Langley, G.J., Herniman, J.M., Boccaccini, A.R., Bucke, C. and Roy, I. (2007) Polyhydroxyalkanoates (PHA) biosynthesis from structurally unrelated carbon sources by a newly characterised *Bacillus spp.* *J Biotechnol* **127**:475-487
- Valappil, S.P., Rai, R., Bucke, C., and Roy, I. (2008) Polyhydroxyalkanoate biosynthesis in *Bacillus cereus* SPV under varied limiting conditions and an insight into the biosynthetic genes involved. *J Appl Microbiol.* 104(6):1624-35.
- Van-Thuoc, D., Quillaguaman, J., Mamo, G., Mattiasson, B. (2008) Utilization of agricultural residues for poly(3-hydroxybutyrate) production by *Halomonas boliviensis* LC1. *J Appl Microbiol* **104**:420-428
- Veech, R.L. (1998) Therapeutic compositions, PCT Patent Application Nos. WO 98/41200 and WO 98/41201
- Veech, R.L. (2000) Therapeutic compositions, PCT Patent Application No. WO 00/15216
- Verlinden, R.A., Hill, D.J., Kenward, C.D. and Radecka, I. (2007) Bacterial synthesis of Biodegradable polyhydroxyalkanoates. *J Appl Microbiol.* **102(6)**:1437-49
- Volova, T. (2004) *Polyhydroxyalkanoates Plastic Material of the 21st Century*; Nova Science Publishers: Hauppauge, NY
- Volova, T.C., Shishatskaya, E.I., Sevastianov, V.I., Efremov, S. and Mogilnaya, O. (2003) Results of biomedical investigations of PHB and PHB/PHV fibres. *J Biochem Eng* **16**:125-133.
- von der Mark, K., Gauss, V., von der Mark, H., Muller, P. (1977) Relationship between cell shape and type of collagen synthesised as chondrocytes lose their cartilage phenotype in culture. *Nature.* **267**:531-532.
- Wallen, L.L. and Rohwedder, W.K. (1974) Poly- β -hydroxyalkanoate from activated sludge. *Environ Sci Technol* **8**:576-579
- Wan, W.K. and Millon, L.E. (2005) Poly(vinylalcohol)-bacterial cellulose nanocomposite. *U.S. Pat. Appl.*, Publ. US 2005037082 A1, 16.

- Wang, B. and Sain, M. (2006) Dispersion of soybean stock-based nanofibre in plastic matrix. ACS Symposium Series, 229th National Meeting of the American Chemical Society, 187-2008.
- Wang, B., Sain, M. (2007) Effect of chemically coated nanofibre reinforcement on biopolymer based nanocomposites. *Bioresources*. **2(3)**:371-388.
- Wang, D.W. and Lehmann, L.T. (1991) Bioabsorbable coating for a surgical device, US Patent No. 5,032,638
- Wang, F. and Lee, S.Y. (1997) Poly(3-hydroxybutyrate) production with high productivity and high polymer content by a fed-batch culture of *Alcaligenes latus* under nitrogen limitation. *Appl Environ Microbiol* **63**:3703–3706
- Wang, H.Y., Cooney, C.L. and Wang, D.I.C. (1979) Computer control of baker's yeast production. *Biotechnol Bioeng* **21**:975-995
- Wang, M. Joseph, R. and Bonfield, W. (1997) Influence of hydroxyapatite particle size and morphology on HAPEX TM. In: Sedel L, Rey C, editors. *Bioceramics*. Vol. 10. Oxford: Pergamon. Pp 15-18
- Wang, M., Hench, L.L. and Bonfield, W (1998) Bioglass[®]/high density polyethelen composites for soft tissue applications: preparation and evaluation. *J Biomed Mater Res*. **42**:577-586
- Wang, Y.W., Wu, Q. and Chen, G.Q. (2004) Attachment, Proliferation and Differentiation of Osteoblasts on Random Biopolyester Poly(3-hydroxybuty-y rate-co-3hydroxyvalerate) Scaffolds, *Biomater*. **25**:669-675
- Ward, I.M. (1985) Mechanical properties of solid polymers. New York: Wiley.
- Webb, A. and Adsetts, J. R. (1986) Wound dressings, UK Patent Application No. 2,166,354
- Wegner, T.H. and Jones, P.E. (2006) Advancing cellulose-based nanotechnology. *Cellulose* **13**:115-118
- Williams, S.F. and Martin, D.P. (2001) Therapeutic uses of polymers and oligomers comprising gamma-hydroxybutyrate. PCT Patent Application No. WO 01/19361A2

- Williams, S.F. and Martin, D.P. (2002) In: Series of Biopolymers, Volume 4, A. Steinbuechel and Y. Doi (Eds), p.91. Wiley-VCH, Weinheim)
- Williams, S.F. and Peoples, O.P. (1996) Biodegradable plastics from plants. *Chemtech* **26**:38-44
- Williams, S.F., Martin, D.P., Horowitz, D.M. and Peoples, O.P. (1999) Mirel applications: addressing the price performance issue. I: Tissue Engineering. *Int. J Biol Macromol.* **25**:11
- Wong, H.H. and Lee, S.Y. (1998) Poly(3-hydroxybutyrate) production from whey by high density cultivation of recombinant *Escherichia coli*. *App Microbiol Biotechnol.* **50**:30-33
- Wu, Q., Huang, H., Hu, G.H., Chen, J., Ho, K.P. and Chen, G.Q. (2001) Production of poly-3-hydroxybutyrate by *Bacillus* sp. JMa5 cultivated in molasses media. *Antonie van Leeuwenhoek.* **80**:111-118
- Wu, L., Chen, S., Li, Z., Xu, K and Chen, G. (2008) Synthesis, characterization and biocompatibility of novel biodegradable poly[*((R)*-3-hydroxybutyrate)-*block*-(D,Llactide)- *block*-(ϵ -caprolactone)] triblock copolymers. *Polym Int.* **57**:939–949
- Xi, J., Zhang, L., Zheng, Z., Chen, G., Gong, Y., Zhao, N., and Zhang, X., (2008) Preparation and Evaluation of Porous poly(3-hydroxybutyrate-co-3-hydroxyhexanoate) -- Hydroxyapatite Composite Scaffolds. *J Biomater Appl.* **22**:293. DOI: 10.1177/0885328207075425
- Yamane, T., Fukunaga, M. and Lee, Y.W. (1996) Increased PHB productivity by high cell-density fed-batch culture of *Alcaligenes latus*, a growth-associated PHB producer. *Biotechnol Bioeng* **50**:197-202
- Yan, S., Tyagi, R.D. and Surampalli, R.Y. (2006) Polyhydroxyalkanoates (PHA) production using wastewater as carbon source and activated sludge as microorganisms. *Water Sci Technol.* **53**(6):175-80
- Yang, S., Leong, K.F., Du, Z. and Chua, C.K. (2001) The design of scaffolds for use in Tissue engineering. Part I. Traditional Factors. *Tissue Eng.* **7**:679.

- Yeza, A., Fournier, D., Halasz, A. and Hawari, J. (2006) Production of polyhydroxyalkanoates from methanol by a new methylotrophic bacterium *Methylobacterium sp. GW2*. *Appl Microbiol Biotechnol* **73**:211-218
- Yu G., Zhang Y., Shi, X., Li, Z. and Gan, Z. (2007) Surface property and *in vitro* biodegradation of microspheres fabricated by poly(e-caprolactone-b-ethylene oxide) diblock copolymers. *J Biomed Materials Research Part A*. DOI:10.1002/jbm.a.31325
- Zhao, K., Yang, X., Chem, G.Q and Chem, J.C. (2002) Effect of Lipase treatment on the biocompatibility of microbial PHA. *J material Sciences: Material in medicine*. **13**:849-854.
- Zimmermann, T., Pohler, E. and Schwaller, P. (2005) Mechanical and morphological properties of cellulose fibril reinforced nanocomposites. *Adv Eng Res* **7**:1156-1161
- Zinger, O., Zhao, G., Schwartz, Z., Simpson, J., Wieland, M., Landolt, D. and Boyan, B. (2005) Differential regulation of osteoblasts by substrate microstructural feature. *Biomater*. **26**:1837-1847
- Zinn, M. and Hany, R. (2005) Tailored Material Properties of Polyhydroxyalkanoates through Biosynthesis and Chemical Modification. *Adv Eng Materials* **7(5)**:408-411
- Zinn, M., Hartmann, R., Noger, D., Pletscher, E., Ren, Q., Wüthrich, J. and Hany, R. (2004) Tailor-made synthesis of polyhydroxyalkanoate. *Bioworld*. **3**:4-5
- Zinn, M., Weilenmann, H.U., Hany, R., Schmid, M. and Egli, T. (2003) Tailored Synthesis of Poly[R]-3-hydroxybutyrate-co-3hydroxyvalerate (PHB/PHV) in *Ralstonia eutropha DSM 428*. *Acta Biotechnologica*. **23(2-3)**:309-316
- Zinn, M., Witholt, B. and Egli, T. (2001) Occurrence, synthesis and medical application of bacterial polyhydroxyalkanoate. *Adv Drug Deliv Rev*. **53(1)**: 5–21
- Zinn, M., Witholt, B. and Egli, T. (2004) Dual nutrient limited growth: models, experimental observations, and applications. *J Biotechnol*. **113**:263–279

Production of polyhydroxyalkanoates: the future green materials of choice

Everest Akaraonye, Tajalli Keshavarz and Ipsita Roy*

Abstract

Polyhydroxyalkanoates (PHAs) have recently been the focus of attention as a biodegradable and biocompatible substitute for conventional non degradable plastics. The cost of large-scale production of these polymers has inhibited its widespread use. Thus, economical, large-scale production of PHAs is currently being studied intensively. Various bacterial strains, either wild-type or recombinant have been utilized with a wide spectrum of utilizable carbon sources. New fermentation strategies have been developed for the efficient production of PHAs at high concentration and productivity. With the current advances, PHAs can now be produced to a concentration of 80 g L^{-1} with productivities greater than $4 \text{ g PHA L}^{-1} \text{ h}^{-1}$. These advances will further lower the production cost of PHAs and allow this family of polymers to become a leading biodegradable polymer in the near future. This review describes the properties of PHAs, their uses, the various attempts towards the production of PHAs, focusing on the utilization of cheap substrates and the development of different fermentation strategies for the production of these polymers, an essential step forward towards their widespread use.

© 2010 Society of Chemical Industry

Keywords: polyhydroxyalkanoates; cheap carbon sources; bacteria; batch culture; fed-batch culture; continuous culture; mixed culture

INTRODUCTION

The current emphasis on sustainability, eco-efficiency and green chemistry has led to intensive search for renewable and environmentally friendly resources. Thus, sustainable development is recognized to be essential for the growth of the economy and industrial productivity. Since global petroleum reserves are finite, there is a need for additional new sources of durable materials. Renewable materials from microorganisms can provide a source of sustainable alternative to petroleum derived chemicals including polymers. According to Bozell and Landucco, integrating renewable feedstocks into the economy could lower crude oil demand, thus limiting economic downturns in the chemical industry due to oil price volatility.¹ It would also expand the options of the chemical industry by increasing feedstock flexibility and broadening the spectrum of potential chemical products. Hence, this would provide an acceptable answer to the current problems with petroleum-based chemicals.

The total demand for biodegradable polymers in North America, Western Europe and Asia reached 85 000 metric tons which was valued at approximately \$280 million in 2005. It has been estimated that consumption of biodegradable polymers in the three regions will increase to 230 000 metric tons this year. This increase will represent an average annual growth rate of 22% over 5 years from 2005 to 2010.² The production of petroleum-based plastics results in the generation of toxic and recalcitrant waste whereas the production of biodegradable polymers involves aqueous processing environments during microbial cultivation, generation of non-toxic waste and the use of renewable non-fossil feedstocks. Biodegradable polymers release carbon dioxide and water vapour into the air while undergoing biological decomposition and growing biomass during photosynthesis subsequently absorb the released carbon dioxide. Hence, the problems associated with conventional

petroleum-based plastics have brought biodegradable polymers to the forefront.

Currently, different types of biodegradable polymers are being studied for different applications ranging from the production of everyday used products to medical applications. Numerous biodegradable polymers are being studied including polyhydroxyalkanoates (PHAs), polylactide (PLA), poly(ϵ -caprolactone) (PCL), poly(*p*-dioxanone) (PPDO) and poly(butylene succinate) (PBS). Other natural renewable polymers include porous sponges (from cellulose wood fibres), fibres (made from natural fibres), hydrogels, starch, cellulose, chitin, chitosan, lignin and proteins.

PHAs are one of the relatively newer families of biodegradable polymers that have great potential in the future due to their variability in properties. This review describes the properties of these polymers, their use and focuses on various attempts to optimize the production of these polymers using different cheap carbon substrates and a range of different fermentation strategies.

PHAS, THEIR STRUCTURE, BIODEGRADABILITY AND BIOCOMPATIBILITY

PHAs are polyesters of hydroxyalkanoic acids with the general structure shown in Fig. 1. The structure of PHAs produced by bacteria can be manipulated by genetic or physiological strategies.³ The pendant group (R in Fig. 1) varies from methyl (C_1) to tridecyl

* Correspondence to: Ipsita Roy, School of Life Sciences, University of Westminster, 115 New Cavendish Street, London W1W 6UW, UK. E-mail: roy@wmin.ac.uk

Applied Biotechnology Research Cluster, Department of Molecular and Applied Biosciences, School of Life Sciences, University of Westminster, London W1W 6UW, UK

Research Article

Poly(3-hydroxybutyrate) production by *Bacillus cereus* SPV using sugarcane molasses as the main carbon source

Akaraonye E.¹, Moreno C.¹, Knowles J. C.^{2,3}, Keshavarz T.¹ and Roy I.^{1*}

¹Applied Biotechnology Research Cluster, Department of Molecular and Applied Biosciences, School of Life Sciences, University of Westminster, London, UK

²Department of Biomaterial & Tissue Engineering, Eastman Dental Institute, University College London, UK

³WCU Research Centre of Nanobiomedical Science, Dankook University, San#29, Anseo-dong, Dongnam-gu, Cheonan-si, Chungnam, South Korea

***corresponding author**

Address for corresponding author:

School of Life Sciences, University of Westminster,
115 New Cavendish Street, London W1W 6UW, UK

Phone: +44-207-995000

Fax: +44-207-995800

Email: royi@wmin.ac.uk

Keywords: Bacillus cereus SPV, Sugar cane molasses, Polyhydroxyalkanoates, Poly(3-hydroxybutyrate)

This article has been accepted for publication and undergone full peer review but has not been through the copyediting, typesetting, pagination and proofreading process which may lead to differences between this version and the Version of Record. Please cite this article as an 'Accepted Article', doi: 10.1002/biot.201100122.

Submitted: 12-Apr-2011
Revised: 06-Jun-2011
Accepted: 18-Jun-2011

Abstract

The main hindrance in the use of PHAs as a replacement for the existing petroleum based plastics is their high cost of production. Reducing the cost of production and increasing the yield and productivity of PHAs is an important challenge for biotechnologists, since this would enhance the commercialization and applications of these polymers. The carbon source alone has been found to account for 50% of the cost of PHA production. Hence, in this study, the use of the agricultural raw material, sugarcane molasses was investigated as the main carbon source for P(3HB) production by *Bacillus cereus* SPV. These studies were carried out in both shaken flasks and 2L bioreactors. Various conditions were evaluated for their effects on biomass and P(3HB) accumulation. The results obtained showed that a high yield of polymer was obtained, 61.07 % dcw, in 1L shaken flask study and 51.37 % dcw in 2L fermenter study, using *Bacillus cereus* SPV with sugarcane molasses as the main carbon source. These yields are much higher than previously observed yields using *Bacillus cereus* SPV. Hence, the results are encouraging and show that sugarcane molasses is a promising carbon source for an economical and commercially viable production of P(3HB).